Integrating *in situ* Geochronology and Metamorphic Petrology: An Example from the Gruf Complex, European Central Alps

By

Jeffrey Oalmann
M.S., Texas Tech University, 2010
B.S., Kansas State University, 2009

Submitted to the graduate degree program in Geology and the Graduate Faculty of the University of Kansas in partial fulfillment of the requirements for the degree of Doctor of Philosophy.

_____

Chair: Dr. Andreas Möller

_____

Dr. J. Douglas Walker

_____

Dr. Daniel Stockli

_____

Dr. David Fowle

_____

Dr. Stephen Egbert

Date Defended: 10 May 2017

The dissertation committee for Jeffrey Oalmann certifies that this is the approved version of the following dissertation:

Integrating *in situ* Geochronology and Metamorphic Petrology: An Example from the Gruf Complex, European Central Alps

_____

Chair: Dr. Andreas Möller

Date Approved: 10 May 2017

ABSTRACT

Understanding the thermal evolution (i.e. the timing, rate, duration, and magnitude of thermal events) within mountain belts has important implications for the geodynamic evolution of both ancient and modern orogenies. Ultra-high temperature (UHT) metamorphism requires geodynamic or tectonic processes that bring excess heat to the lower crust. Therefore, dating UHT metamorphism can shed light on the geodynamic evolution of the geological settings in which UHT rocks are exposed. In recent years, many researchers have used accessory mineral U-Pb geochronology to date (U)HT metamorphic events. However, it is not always clear to what part of the pressure-temperature (P-T) path the ages relate.

Using an *in situ* approach, this study combines accessory mineral U-Pb geochronology with single mineral thermometry, thermobarometric modeling, and trace element geochemistry to elucidate the P-T-time (P-T-t) evolution of sapphirine-bearing granulites from the Gruf Complex in the Central Alps. Two main questions are addressed: (1) When did the Gruf Complex experience UHT metamorphism? (2) What parts of the P-T evolution of high-grade metamorphic rocks can be dated using U-Pb geochronology of different accessory phases?

Equilibrium phase diagrams calculated from whole rock and microdomain compositions and Zr-in-rutile thermometry indicate that the Gruf granulites underwent UHT metamorphism at 900–1000°C and 7.0–9.5 kbar after decompressing from ca. 800°C and 9–12 kbar. This decompression-heating event resulted in the breakdown of garnet to form orthopyroxene, sapphirine, and cordierite. A lack of inherited monazite and presence of young (34–30 Ma) monazite within UHT textures is interpreted to indicate that UHT metamorphism was the last main metamorphic event the Gruf granulites experienced, thus precluding a Permian UHT event followed by a lower temperature (700–750°C) Alpine event. Textural observations and Ti-in-

zircon thermometry reveal that minor zircon growth occurred in equilibrium with garnet at 34.8 ± 1.1 Ma, and zircon was not growing, but resorbing during UHT metamorphism. Therefore, the youngest zircon rims can only be used to date post-UHT melt crystallization and cooling at 32.7 ± 0.7 Ma. The U-Pb zircon ages of variable deformed felsic dikes indicate that the lower crustal UHT rocks were juxtaposed against the midcrustal migmatites between 30 and 27 Ma and contractional deformation ceased by 25.6 ± 0.3 Ma in the Gruf Complex. Finally, U-Pb rutile ages indicate that the amalgamated Gruf Complex cooled from 700–420°C over an 11 m.y. period from 30 to 19 Ma.

These results indicate that different accessory minerals can be used to date different stages of the evolution of UHT rocks. However, depending on the reactions in the rock volume, dateable accessory minerals may be crystallizing, resorbing, or not reacting at a given P-T condition. Therefore, combining accessory mineral ages with textural, geochemical, and petrological information is necessary to elucidate the P-T-t evolution of a particular rock package.

ACKNOWLEDGEMENTS

This research was supported by grants from the National Science Foundation, the Geochemical Society, the Geological Society of America, the National Academy of Sciences, and the University of Kansas Doctoral Research Fund. Other support came from the Department of Geology at the University of Kansas came in the form of Summer Field Research Grants, the Angino and Angino-Ferry Geochemical Scholarships, and two Patterson Scholarships.

I am grateful to Peter Lippert who carried lots of heavy granulites around Val Codera and drove us safely on the Autobahn. The Biavaschi Famiglia were wonderful hosts at Rifugio Brasca and made our stays very pleasant. Thanks go to the pilots and crews at Elitellina and Eliwork for flying us safely in the steep terrain, transporting my rocks to the road, and not leaving us on the mountain! I am indebted to Andrea Galli for taking us up to Valle del Conco to see some of the extremely important field relationships, even when though he doesn't quite agree with us on the timing of the UHT event ;). Thanks to the Bousquet and Wilke families who let me stay at their respective homes while doing research in Potsdam.

Many thanks go to all the geologists who helped me develop my interpretation of the complicated Gruf Complex through numerous discussions on various continents. These people include but are not limited to Andrea Galli, Victor Guevara, Mark Caddick, Kyle Samperton, Andy Smye, and others. I am grateful for my fellow grad students at the Universities of Kansas, Potsdam, and Kiel for being my cohorts and teaching me about their cultures.

I am grateful to my dissertation committee members for their patience and making this work possible. In particular, I am thankful to my committee chair Andreas for his great mentorship and understanding the ups and downs of life in general. He has taught me more than I ever

expected. Thanks also go to my other coauthors Romain, Erik, and Jessica for their hard work. They have made the manuscripts better than I could have ever done on my own.

Perhaps most of all, I am grateful to my family for their support, understanding, and encouragement through my long journey through graduate school. Without them, this would be for naught. I am grateful for the loving God with whom I have developed a personal relationship over the past couple of years, for my support groups in the Lawrence community, and my Velocity family. They have showed me how to live life in a way I never thought possible.

TABLE OF CONTENTS

LIST OF FIGURES

LIST OF TABLES

CHAPTER 1

Introduction

Background and Significance

Determining the ages of metamorphic and igneous events preserved in the exposed roots of orogens has important implications for the thermal and tectonic evolutions of mountain belts. In the past 15 to 20 years, advances have been made in U-Pb geochronology and trace element thermometry of accessory minerals (e.g. Spear and Pyle, 2002; Hanchar and Hoskin, 2003; Harley and Kelly, 2007; Meinhold, 2010). However, tying the ages of accessory minerals to a specific pressure-temperature (P-T) stage can be ambiguous, especially in high-grade metamorphic rocks from terranes that have experienced multiple high-temperature events (e.g. Degeling et al., 2001; Rubatto, 2002; Kelly et al., 2006; Kelsey et al., 2008).

Ultra-high temperature (UHT) metamorphism is defined as metamorphism occurring in excess of 900°C at 7–13 kbar pressure (Harley, 1998; Brown, 2006; Harley, 2008). Attaining UHT conditions requires tectonic or geodynamic processes that provide excess heat to the lower crust (Collins, 2002; Kelsey, 2008; Clark et al., 2011). Therefore, the timing of UHT metamorphism has important implications for the timing of important processes within the regions UHT rocks are found.

The sapphirine-bearing granulites of the Gruf Complex of the Central Alps are the primary subjects of this study. Although these rocks are quite scarce, they have well-preserved reaction textures that are useful in constraining P-T conditions at different stages in their history. These rocks are also unique in that they are the only known UHT rocks within the Central Alps. Therefore, constraining the pressure-temperature-time (P-T-t) history of these rocks has important implications for the geodynamic evolution of the Central Alps.

By combining U-Pb ages of rutile, zircon, and monazite with pressure-temperature estimates determined by accessory phase thermometry and equilibrium phase diagram modeling, this study addresses two main questions: (1) What was the P-T-t path taken by the sapphirine-bearing granulites and related charnockites from the Gruf Compex? In particular, when did UHT metamorphism occur? (2) What geologic processes can be dated by accessory mineral U-Pb geochronology in high-grade metamorphic rocks? Do the ages constrain the timing of prograde, peak, or retrograde metamorphism or other events?

Summary of Chapters

This dissertation comprises four studies on the UHT rocks from the Gruf Complex that will be published in peer-review journals. Chapters 2, 3, and 4 each focus on a different accessory mineral. In Chapter 5, the major minerals are the main concern.

Chapter 2, which was submitted to the journal *Chemical Geology*, focuses on U-Pb dating and trace element geochemistry of rutile. The main conclusion of this chapter is that rutile U-Pb ages and Zr-in-rutile temperatures are decoupled. The ages indicate that the Gruf complex underwent cooling from 700°C to 420°C between 30 and 19 Ma. The temperatures, which are strongly correlated with textural setting, record the conditions during prograde (500–890°C), peak (840–1000°C), and retrograde metamorphism (650–850°C).

Zircon U-Pb dating and trace element geochemistry is the focus of Chapter 3. Based on zircon textures and Ti-in-zircon thermometry, we conclude that zircon was not growing but resorbing during UHT metamorphism. Therefore, the zircon dates that are preserved constrain the timing of three main events: (1) Permian protolith crystallization, (2) a Jurassic to Cretaceous magmatic or thermal event, and (3) cooling and melt crystallization after UHT metamorphism at ca. 32.7 ± 0.7 Ma. The U-Pb zircon ages of variably deformed felsic dikes constrain the timing of

amalgamation of the lower crustal and mid crustal units of the Gruf Complex to between 30 and 27 Ma.

Monazite U-Pb ages are the focus of Chapter 4. All monazite grains and domains have U-Pb dates between 34 and 31 Ma, and inherited monazite was not observed. Numerous studies have shown that monazite can record multiple high-temperature metamorphic events unless near complete recrystallization occurs, and diffusional resetting of U-Pb monazite ages is unlikely at even the highest grades of metamorphism. Therfore, we conclude that UHT metamorphism must have completely recrystallized the monazite (and most of the other minerals) in the granulites, and the UHT event occurred during Cenozoic Alpine orogenesis. This conclusion is supported by the UHT P-T estimates of monazite-bearing textures that is presented in Chapter 5.

In Chapter 5, we present the results from thermobarometric modeling of microdomains and whole rock compositions to constrain the P-T evolution of the Gruf granulites and migmatitic paragneisses. The Gruf granulites and charnockites underwent decompression from ca. 800°C and 10–13 kbar to UHT conditions of 900–1000°C and 7.0–9.5 kbar followed by exhumation into the midcrustal migmatites, which equilibrated at 675–750°C and 5–7 kbar. This P-T path and the timing constraints presented in the other chapters indicates that UHT metamorphism occurred after exhumation of (U)HP units in the Central Alps and was most likely driven by slab breakoff.

References

Brown, M., 2006. Duality of thermal regimes is the distinctive characteristic of plate tectonics since the Neoarchean. Geology, 34(11): 961-964.

Clark, C., Fitzsimons, I.C., Healy, D., Harley, S.L., 2011. How does the continental crust get really hot? Elements, 7(4): 235-240.

Collins, W., 2002. Hot orogens, tectonic switching, and creation of continental crust. Geology, 30(6): 535-538.

Degeling, H., Eggins, S., Ellis, D., 2001. Zr budgets for metamorphic reactions, and the formation of zircon from garnet breakdown. Mineralogical Magazine, 65(6): 749-758.

Hanchar, J.M., Hoskin, P.W., 2003. Zircon. Reviews in Mineralogy and Geochemistry, 153. The Mineralogical Society of America, Washington, DC.

Harley, S., 2008. Refining the P–T records of UHT crustal metamorphism. Journal of Metamorphic Geology, 26(2): 125-154.

Harley, S.L., 1998. On the occurrence and characterization of ultrahigh-temperature crustal metamorphism. Geological Society, London, Special Publications, 138(1): 81-107.

Harley, S.L., Kelly, N.M., 2007. Zircon tiny but timely. Elements, 3(1): 13-18.

Kelly, N.M., Clarke, G.L., Harley, S.L., 2006. Monazite behaviour and age significance in poly-metamorphic high-grade terrains: a case study from the western Musgrave Block, central Australia. Lithos, 88(1): 100-134.

Kelsey, D., Clark, C., Hand, M., 2008. Thermobarometric modelling of zircon and monazite growth in melt-bearing systems: Examples using model metapelitic and metapsammitic granulites. Journal of Metamorphic Geology, 26(2): 199-212.

Kelsey, D.E., 2008. On ultrahigh-temperature crustal metamorphism. Gondwana Research, 13(1): 1-29.

Meinhold, G., 2010. Rutile and its applications in earth sciences. Earth-Science Reviews, 102(1–2): 1-28.

Rubatto, D., 2002. Zircon trace element geochemistry: partitioning with garnet and the link between U-Pb ages and metamorphism. Chemical Geology, 184(1-2): 123-138.

Spear, F.S., Pyle, J.M., 2002. Apatite, monazite, and xenotime in metamorphic rocks. Reviews in Mineralogy and Geochemistry, 48(1): 293-335.

CHAPTER 2

Decoupling of Zr-thermometry and U-Pb thermochronology in rutile from the UHT granulites and charnockites of the Gruf Complex (Central Alps)

Jeffrey Oalmann[1]

Andreas Möller[1]

Romain Bousquet[2]

[1]*The University of Kansas, Department of Geology, 1475 Jayhawk Blvd., Rm. 120, Lawrence, KS 66045, USA.*

[2]*Christian-Albrechts-Universität zu Kiel, Institute of Geosciences, Ludewig-Meyn-Strasse 10, 24098 Kiel, Germany.*

Abstract

In situ U-Pb dating and trace element analysis of rutile is used to constrain the thermal history of UHT granulites and charnockites in the Gruf Complex, European Central Alps. Zirconium-in-rutile temperatures are coupled with textural settings providing temperature estimates for prograde (495–895°C), peak (840–1000°C), and retrograde (610–890°C) metamorphism. Even at the highest temperatures, Zr concentrations are not affected by diffusion unless a Zr sink (e.g. zircon) is present or nucleates at or near the rutile grain boundary. Zr and Hf concentrations are strongly correlated, but other high field strength elements (HFSE) are not correlated, indicating that Zr and Hf are more robust to modification during retrograde metamorphism and cooling. Some trace elements (e.g. W) may provide constraints on fluid compositions during retrograde metamorphism. U-Pb cooling dates are decoupled from Zr-in-rutile temperatures and textural settings, indicating that Pb diffusion is controlled by the presence or absence of localized fast diffusion pathways. Dispersion of concordant $^{206}Pb/^{238}U$ dates between

30 Ma and 19 Ma is interpreted to record ca. 11 m.y. of crustal processes in the range of 420–700°C, constraining the average cooling rate to ca. 25°C/m.y. for this time period. Assuming that UHT metamorphism in the Gruf Complex occurred at ca. 34 Ma, these rocks initially cooled at ca. 63°C/m.y. between 34 and 30 Ma. These results are consistent with a tectonic model in which asthenospheric upwelling after slab breakoff provided heat for magmatism, migmatization, and UHT metamorphism in the Central Alps.

Introduction

Ultra-high temperature (UHT) rocks are defined as metamorphic rocks that experienced peak temperatures in excess of 900°C within the sillimanite stability field (Harley, 1998; Brown, 2007; Harley, 2008). These extreme crustal conditions require an elevated geothermal gradient >>20°C/km (e.g. Kelsey, 2008). Therefore, thermal studies of UHT terranes are important in understanding lower crustal rheology, mantle to crust heat flow, and geodynamic processes in the tectonic settings where they are found.

Determining peak pressure and temperature conditions in UHT granulites and polymetamorphic terranes presents a major challenge. Peak mineral assemblages and phase compositions commonly become overprinted during retrogression or subsequent metamorphic events (e.g. Carswell and O'Brien, 1993; Fitzsimons and Harley, 1994; Harley, 1998; Pattison et al., 2003). Due to their resistance to recrystallization and diffusional loss of certain trace elements, accessory phases such as rutile can record metamorphic conditions that major minerals do not preserve (e.g. Zack et al., 2004; Luvizotto and Zack, 2009; Meinhold, 2010; Kooijman et al., 2012). Zirconium-in-rutile thermometry is particularly robust to resetting even in slowly cooled terranes (e.g. Kooijman et al., 2012; Pape et al., 2016), and thus rutile has the ability to record the temperatures of different metamorphic reactions and recrystallization events. Other trace elements

(e.g., Nb, Ta, U, W) can record the fluid composition and degree of elemental fractionation at different temperatures (e.g. Meyer et al., 2011). The high U and low common-Pb concentrations in rutile make it a useful chronometer (e.g. Mezger et al., 1989; Mezger et al., 1991), and it is well established that rutile records cooling in upper amphibolite to granulite facies rocks (e.g. Mezger et al., 1989; Möller et al., 2000; Vry and Baker, 2006). Other studies have used rutile U-Pb thermochronology to constrain the timing of cooling and cooling rates in UHT rocks (Zack et al., 2004; Jiao et al., 2011; Meyer et al., 2011; Kooijman et al., 2012). These characteristics make rutile a useful mineral for determining thermal histories of complex metamorphic terranes from prograde metamorphism through cooling at upper crustal conditions.

This study presents rutile trace element and U-Pb isotopic data collected *in situ* (i.e. directly from thin sections) by laser ablation inductively coupled plasma mass spectrometry (LA-ICP-MS). The goal is to constrain the temperature conditions and cooling ages recorded by different textural domains within the UHT granulites and charnockites of the Gruf Complex in the Central Alps. This provides a thermal history used to interpret the specific geodynamic setting and evolution of UHT metamorphism during continental collision.

Geological Setting

The Central Alps consist of nappes derived from the European paleomargin and the Penninic Units (the Valais and Piemont-Liguria oceans plus the Briançonais microcontinent) that were thrust together during the late stages of the Cenozoic Alpine orogeny (Stampfli et al., 1998; Figure 2.1; Bousquet et al., 2012b). Prior to amalgamation, some of these units experienced various degrees of (ultra) high-pressure metamorphism related to south-directed subduction of Europe beneath the Adriatic microplate, which is now represented by the Austroalpine nappes and the Southern Alps (Becker, 1993; Gebauer, 1996; Brouwer et al., 2005; Hermann et al., 2006). A

large part of the Central Alps, known as the Lepontine Dome, is characterized by a Barrovian metamorphic field gradient in which metamorphic grade increases from greenschist facies in the north to upper amphibolite facies in the south toward the Insubric fault zone (Frey and Ferreiro Mählmann, 1999; Rubatto et al., 2009; Berger et al., 2011). Isotherms and mineral isograds crosscut nappe boundaries, indicating that temperature-dominated metamorphism occurred after nappe amalgamation (Niggli and Niggli, 1965; Trommsdorff, 1966; Todd and Engi, 1997; Frey and Ferreiro Mählmann, 1999). Burri et al. (2005) divided the Lepontine dome into three zones of migmatites based on the style of melting. The most northern zone consists of rocks intruded by pegmatitic and aplitic dikes and did not undergo *in situ* melting. Migmatites in the intermediate zone underwent *in situ*, fluid induced, anatexis. The southernmost migmatite zone, the Southern Steep Belt (SSB) was formed by muscovite dehydration melting. Rubatto et al. (2009) interpreted the SSB to have undergone protracted or repeated migmatization between 32 and 22 Ma.

The Gruf Complex is bounded by Penninic Units (the Chiavenna ophiolite and the Tambo Nappe) to the north, structurally overlain by the 32–30 Ma (von Blanckenburg, 1992; Samperton et al., 2015) Bergell intrusion in the east (Berger et al., 1996; Davidson et al., 1996), intruded by the 24 ± 1 Ma (Liati et al., 2000) Novate S-type leucogranite (Chappell and White, 1974) in the south, and bordered by the European plate-derived (Schmid et al., 2004) Adula Nappe to the west (Figure 2.1). The northern and western contacts are covered by valley fill. The Adula Nappe consists of rock packages with distinct P-T histories and has been interpreted as a lithospheric mélange (Trommsdorff, 1990) that formed by tectonic accretion in a subduction channel (e.g. Engi et al., 2001). Some researchers (e.g. Frey and Ferreiro Mählmann, 1999; Liati and Gebauer, 2003) have interpreted the Gruf Complex as part of the Adula Nappe, which contains rocks that experienced ultrahigh pressure metamorphism, but lack evidence for UHT metamorphism. In

contrast, Galli et al. (2013) proposed that the Gruf Complex is not equivalent to the Adula Nappe, but is a separate migmatitic unit exhumed to the middle crust together with the Bergell intrusion. This interpretation is based in part on the lack of evidence for ultrahigh pressure metamorphism in the Gruf Complex. Some researchers (e.g., Ciancaleoni and Marquer, 2006; Galli., 2010) have concluded that the Gruf Complex and the Adula Nappe are separated by the normal-sense Forcola fault (Figure 2.1) and represent distinct pieces of European lower crust with different metamorphic histories.

Migmatitic ortho- and paragneisses are the volumetrically dominant rock types in the Gruf Complex (Galli, 2010; Galli et al., 2011; Figure 2.2). The migmatitic layering defines the main NE-SW striking foliation (Figure 2.2), and the changing dip direction from predominately SE in the south to NW in the north gives the Gruf Complex a dome-like shape. Mineral lineations, defined by aligned biotite or sillimanite, plunge moderately to the E-NE. The migmatites underwent peak metamorphism at 700–750°C and 7 kbar (Oalmann et al., in preparation-a).

Two large charnockite bodies occur within a narrow, east-west striking zone in the center of the Gruf Complex (Figure 2.2) at the highest elevations, and smaller charnockitic boudins are present within the lower grade migmatitic gneisses. Scarce sapphirine-bearing granulites preserve UHT mineral assemblages and occur as enclaves and schollen within charnockite and less commonly within orthogneiss (Galli, 2010; Galli et al., 2011). These are the only known UHT rocks in the Central Alps (Bousquet et al., 2012a). In the charnockite bodies, foliation and lineation orientations vary significantly from the main foliation in the other units. Mylonites along the charnockite–migmatite contacts consist of a zone of <50 cm-wide mylonitic layers that anastomose around the less deformed charnockitic sheets and schollen (Figure 2.3F). Galli *et al.* (2011; 2012) concluded that the charnockites and granulites underwent peak metamorphism at 920–940°C and

8.5–9.5 kbar during Permian rifting at 282–260 Ma. They interpreted orthopyroxene-, sapphirine-, cordierite-, and spinel-bearing symplectites and coronae to have formed at 720–740°C and 7.0–7.5 kbar subsequently during the Alpine orogeny 34–29 Ma (Galli et al., 2011; 2012). In contrast, evidence from a U-Pb zircon rim age of 32.7 ± 0.5 Ma (Liati and Gebauer, 2003) and a texturally controlled monazite U-Th-Pb chemical age of 33 ± 4 Ma (Schmitz et al., 2009) from the sapphirine-bearing granulites indicates that UHT metamorphism occurred during the Alpine orogeny. Thus, the timing of UHT metamorphism in the Gruf Complex is still a matter of debate. Regardless of the timing of UHT metamorphism, the sapphirine-bearing granulites as well as the charnockites were subjected to upper amphibolite facies conditions, equivalent to the peak conditions in the migmatitic units, at some point after the UHT event. This indicates that the juxtaposition of the UHT and lower grade units occurred prior to or coevally with the upper amphibolite facies metamorphism.

Abundant felsic dikes, ranging from hornblende-bearing granitoids to biotite ± muscovite ± garnet ± tourmaline ± beryl pegmatites, occur throughout the Gruf Complex. The least evolved dikes are commonly ductily deformed whereas the most evolved dikes crosscut migmatitic foliations. Some of these dikes are deformed within the mylonitic shear zones separating the UHT units from the lower grade migmatites (Galli et al., 2013). The youngest zircon populations from the deformed dikes have U-Pb ages between ca. 30 and 27 Ma. (Oalmann et al., in preparation-c) constraining the timing of amalgamation of these units to 30–27 Ma. The crosscutting, most evolved pegmatites have an age 25.6 ± 0.3 Ma (Oalmann et al., in preparation-c).

Petrographic Descriptions and Major Mineral Compositions

Residual Granulite

Sample G1A-2009 (Figure 2.3A) is a massive, nonfoliated, mafic, residual granulite that was collected from a talus slope east of Bresciadega village (Figure 2.2). The peak metamorphic assemblage consists of garnet + orthopyroxene + sapphirine + biotite + sillimanite porphyroblasts. Leucosomes containing intergrown quartz + plagioclase + K-feldspar occur as discrete pods. Anhedral garnet porphyroblasts (up to 1 cm diameter) have multiphase embayments that consist of orthopyroxene ± sapphirine ± rutile ± cordierite ± minor biotite (Figure 2.5A). Garnet-replacing symplectites, which consist of consist of elongate orthopyroxene and scarce sapphirine grains as well as blocky plagioclase, are also present (Figure 2.5A, B). Prismatic to bladed sapphirine porphyroblasts are 0.4-0.7 mm long. Orthopyroxene porphyroblasts forms subhedral to anhedral porphyroblasts, some of which are intergrown with sapphirine porphyroblasts. Primary porphyroblasts are invariably surrounded by cordierite coronae or multiphase symplectites. Fine-grained sapphirine grains are the dominant mineral within fine-grained, polymineralic aggregates that also contain sillimanite, spinel, cordierite, and/or quartz (Figure 2.5B). Some of these aggregates surround or emanate from the larger sapphirine porphyroblasts and are commonly surrounded by cordierite moats (Figure 2.5B). Biotite primarily forms subrounded aggregates of bladed to tabular grains that also contain scarce sapphirine and rutile (Figure 2.5B). Biotite also occurs as discrete grains (up to 1 mm diameter), within symplectites, and replacing orthopyroxene prophyroblasts. Prismatic sillimanite porphyroblasts (0.4 mm long on average) are commonly surrounded by cordierite moats, leucosomes, or fine-grained, sapphirine-dominated aggregates.

Anhedral rutile grains (0.02-0.80 mm) mostly occur as part of the multiphase embyaments in garnet (Figure 2.5A). Outside of garnet, rutile grains are only found within biotite-dominated aggregates where they are commonly in contact with sapphirine (Figure 2.5B). These textures

suggest that rutile was stable during prograde and peak metamorphism but was consumed by retrograde reactions.

Stromatic Granulites

Samples Bras10-5 and Bras10-6 are stromatic, migmatitic granulites that consist of charnockitic leucosomes and garnet- + orthopyroxene- + sapphirine- ± cordierite- ± sillimanite bearing melanosomes. Alternating leucosomes and melanosomes give this rock type its layered (gneissic) appearance. In one thin section (Bras10-5b-1), coarse-grained and fine-grained textural domains with similar mineralogies can be distinguished (Figure 2.4A). Quartzofeldspathic layers, which are interpreted to represent crystallized melt, consist of subhedral quartz + mesoperthitic alkali feldspar + plagioclase + minor orthopyroxene (Figure 2.5C). Subhedral garnet porphyroblasts (0.8-1.2 mm) contain small proportions of fine-grained rutile, quartz, spinel + plagioclase, and opaque inclusions and are commonly rimmed by fine-grained orthopyroxene + sapphirine symplectites, which contain minor biotite and rutile (Figure 2.5D). Subhedral to anhedral orthopyroxene grains (1-3 mm on average) commonly contain embayments filled with cordierite and/or biotite (Figure 2.5E). In some cases, coarse-grained orthopyroxene + sapphirine intergrowths and minor plagioclase fill embayments in garnet (Figure 2.5F). In addition to the symplectites and intergrowths with orthopyroxene, sapphirine occurs as distinct prismatic to bladed porphyroblasts (Figure 2.5D). Sample Bras10-6 has a higher proportion of cordierite and lower proportion of sapphirine compared to sample Bras10-5. Anhedral to tabular biotite grains (0.1-1.8 mm) are primarily intergrown with and in contact with orthopyroxene, suggesting that much of the biotite is secondary. Bladed biotite is the dominant mineral in some mafic layers (Figure 2.5G).

Subhedral to euhedral rutile grains (0.01-0.22 mm) occur primarily in the more mafic layers of the granulites and as single-phase inclusions in garnet. Rutile is also present in sapphirine + orthopyroxene symplectites and multi-phase, coarse grained embayments around garnet (Figure 2.5A, D, F, 7E). In the quartzofeldspathic layers, rutile grains have similar shapes and sizes as those in the mafic layers but are less abundant. Rarely, rutile also occurs as fine-grained needles within orthopyroxene porphyroblasts (Figure5E). In some cases, there are small zircon grains along the edges of rutile (Figure 2.5C, G).

Leucogranulite

Sample GR11-35 is felsic, sapphirine-bearing granulite schlieren that was collected from one of the large charnockite bodies (Figure 2.2). It consists of ≤ 4 mm-long quartz ribbons, subhedral plagioclase and mesoperthite, subhedral to anhedral, inclusion-poor garnet porphyroblasts (0.1-0.7 mm), bladed to tabular biotite, and orthopyroxene. Minor, prismatitic sillimanite and aggregates of fine-grained sapphirine are also present. Aggregates of green spinel ± opaque minerals ± plagioclase ± biotite ± orthopyroxene + sillimanite ± sapphirine commonly surround or fill embayments in garnet (Figure 2.5H). Compositional layering and shape-preferred orientations of quartz ribbons, biotite grains, and sapphirine aggregates define a weakly developed foliation.

Subhedral to anhedral rutile grains mostly occur within the matrix of this sample and range from 0.05 to 0.5 mm in size. Some rutile grains are included in garnet, and others are in contact with sapphirine aggregates (Figure 2.7F).

Charnockite

Sample GR11-43 is a garnet-biotite-alkali feldspar granitic gneiss (retrogressed charnockite) collected from a small charnockite body near Val Codera (Figure 2.2). A hypidiomorphic granular matrix consists mainly of quartz + mesoperthitic, alkali feldspar. Scarce, blocky plagioclase grains (≤0.1 mm) occur mainly as inclusions in and adjacent to garnet and, more rarely, within the matrix. Anhedral to subhedral garnet porphyroblasts (0.4-1.75 mm) contain embayments filled with quartz, plagioclase, alkali feldspar, biotite, and spinel (Figure 2.5I) and form atoll structures in some cases. Tabular biotite grains (≤1.75 mm) most commonly occur adjacent to garnet porphyroblasts and form finger-like intergrowths with plagioclase, quartz, and opaque minerals in some cases. Bladed biotite grains (≤1.5 mm long) are restricted to fractures and microschlieren.

Subhedral to euhedral rutile grains (0.05-0.15 mm) occur mainly within the matrix and as inclusions in quartz and K-feldspar (Figure 2.5I). Rare rutile inclusions in garnet are also present.

Retrogressed Granulites

Two samples (GR11-1A and GR11-1C) of retrogressed granulite were collected from a large boulder in Val Codera near the village of Bresciadega (Figure 2.2). These samples have the assemblage quartz + feldspar + biotite + pinnitized cordierite + orthopyroxene + garnet + minor sillimanite + abundant rutile (Figure 2.5J, K). Cordierite + orthopyroxene symplectites (Figure 2.5J, K) commonly surround garnet. Within garnet embayments, sample GR11-1C contains some relict sapphirine porphyroblasts, which are rimmed by cordierite coronae (Figure 2.5L). Most of the orthopyroxene in these samples is surrounded by fine-grained masses of chlorite + cordierite (Figure 2.5K).

Sample GR11-1A contains two textural domains, based on grain size, that have similar mineralogy (Figure 2.4B), and both domains contain rutile. The majority of rutile grains in sample GR11-1C are included in garnet (Figure 2.5L).

Analytical Methods

Trace element compositions and U-Pb isotopic data were collected by laser ablation inductively coupled plasma mass spectrometry (LA-ICP-MS) using a Thermo Scientific Element 2 ICP-MS coupled with a Photon Machines 193 nm ArF excimer laser at The University of Kansas, Isotope Geochemistry Laboratories (IGL). Rutile grains were ablated directly in 40μm-thick, polished section to preserved textural context. Trace element and U-Pb data were collected in separate analytical sessions. See Table 2.1 for details on the analytical set-up, procedures, and data reduction.

Zirconium-in-rutile temperatures were calculated with the calibration of (Tomkins et al., 2007) using the equation for the β-quartz field and a pressure of 9 kbar. This corresponds to the maximum pressure of UHT metamorphism (Oalmann et al., in preparation-a). Therefore, the reported temperatures are maximum estimates. Decreasing the pressure to 7 kbar, which is the minimum pressure estimated for the UHT assemblages, decreases the apparent temperature by ca. 5–10°C. The analytical uncertainty of Zr compositions is 2–7%, corresponding to a maximum temperature uncertainty of 63°C at 900°C and 49°C at 700°C. Therefore, the temperature difference due to a pressure difference of 2 kbar is well within analytical uncertainty.

The legacy mode of ET_Redux (McLean et al., 2016) was used to plot concordia diagrams and calculate ages. Because high Hg backgrounds made it impossible to perform a ^{204}Pb-based common Pb correction, lower intercept ages are the preferred ages, but weighted mean ^{206}Pb/^{238}U ages of concordant analyses are also reported in some cases.

U-Pb Ages

Regardless of rock type, textural setting, and grain size, many of the U-Pb rutile ages are similar, but there is a high degree of dispersion in $^{206}Pb/^{238}U$ dates within the populations of each sample. All analyzed samples contain rutile grains with observable amounts of common Pb as seen on the concordia diagrams (Figure 2.6). Combining all analyses from all samples yields a lower intercept age of 22.79 ± 0.05 Ma (MSWD = 32, n = 358) and a common-Pb upper intercept. The $^{206}Pb/^{238}U$ dates of concordant analyses range from 18.8 ± 1.5 to 32.2 ± 1.5 Ma (Figure 2.6 and Table 2.2). Lower intercept ages from individual samples range from 20.8 ± 0.2 to 25.8 ± 0.3 Ma, and all have common-Pb upper intercepts (Figure 2.6). Spot analyses along traverses in the largest rutile grains do not show any detectable core to rim age variation (Figure 2.7).

Residual granulite sample G1A-2009 (Figure 2.6B) contains rutile inclusions in garnet (Figure 2.7A) with scarce matrix rutile (Figure 2.7B). All analyses combined yield a lower intercept age of 23.7 ± 0.6 Ma (MSWD = 3.5, n = 28). A single rutile inclusion in garnet yields the only two concordant analyses with $^{206}Pb/^{238}U$ dates of 20.2 ± 2 and 22.1 ± 2 Ma. Excluding these two concordant analyses results in a lower intercept age of 24.6 ± 0.7 Ma (MSWD = 2.4, n = 26).

Sample GR11-1A (Figure 2.6C) is a retrogressed residual granulite that contains abundant rutile as inclusions in garnet and as matrix grains. The analyzed grains yield a lower intercept age of 25.9 ± 0.3 Ma (MSWD = 6.3, n = 27). The $^{206}Pb/^{238}U$ dates of concordant grains included in the age calculation range from 23.0 ± 1.0 to 27.8 ± 1.3 Ma. Two matrix grains, which are not included in the age calculation but are concordant, yield $^{206}Pb/^{238}U$ dates of 18.8 ± 1.5 and 19.8 ± 0.9 Ma.

Another retrogressed residual granulite (sample GR11-1C, Figure 2.6D) contains rutile inclusions in garnet that yield a lower intercept age of 24.0 ± 0.5 Ma (MSWD = 1.8, n = 18). Concordant analyses have $^{206}Pb/^{238}U$ dates between 22.4 ± 2.6 and 25.7 ± 2.6 Ma.

Rutile grains are restricted to the matrix of charnockite sample GR11-43 (Figure 2.6E). The lower intercept age calculated for this sample is 23.5 ± 0.5 Ma (MSWD = 0.95, n = 12). Concordant analyses have $^{206}Pb/^{238}U$ dates ranging from 22.2 ± 2.2 to 25.9 ± 3.1 Ma.

Leucogranulite sample GR11-35 (Figure 2.6F) contains only matrix rutile grains. Two different common-Pb discordia can be interpreted from the analyses. The younger group, which includes more analyses, yields a lower intercept age of 25.5 ± 0.4 Ma (MSWD = 2.0, n = 11), and the older group yields a lower intercept age of 27.6 ± 0.6 Ma (MSWD = 0.42, n = 4). One discordant analysis ($^{206}Pb/^{238}U$ date = 21.9 ± 1.4 Ma) was not included in either of the calculations.

The following stromatic granulite samples (Figure 2.6G–J) contain rutile included in garnet and within the UHT matrix assemblages except where otherwise noted. These samples are the most texturally complex, and they all show excessive dispersion of concordant dates and complex patterns of discordant results.

Sample Bras10-5b-1 (Figure 2.6G) is a stromatic granulite sample that yields a lower intercept rutile age of 20.5 ± 0.2 Ma (MSWD = 3.4, n = 15). The $^{206}Pb/^{238}U$ dates of concordant analyses range from 19.8 ± 0.7 to 23.9 ± 1.2 Ma. Two nearly concordant analyses ($^{206}Pb/^{238}U$ dates = 23.5 ± 0.9 and 23.9 ± 1.2 Ma) were excluded from the age calculation.

Stromatic granulite sample Bras10-5b-2 (Figure 2.6H) contains only matrix rutile and yields the largest dispersion of concordant analyses with $^{206}Pb/^{238}U$ dates ranging from 21.3 ± 0.6 Ma to 32.2 ± 1.5 Ma. Constructing a discordia through all analyses results in a lower intercept at 24.4 ± 0.2 Ma (MSWD = 42, n = 24) coinciding with a cluster of concordant analyses (weighted

mean $^{206}Pb/^{238}U$ age = 24.6 ± 0.3 Ma, MSWD = 1.2, n = 4). The youngest group of concordant analyses from this sample has a weighted mean $^{206}Pb/^{238}U$ age of 22.2 ± 0.2 Ma (MSWD = 5.4, n = 7).

The rutile dates obtained from stromatic granulite sample Bras10-6-1 (Figure 2.6I) also exhibit a high degree of dispersion along concordia, with $^{206}Pb/^{238}U$ dates ranging from 18.7 ± 0.7 to 28.2 ± 0.7 Ma. A lower intercept age calculated for this sample is 22.2 ± 0.1 Ma (MSWD = 32, n = 131), but the discordant results do not lie on the same common Pb array. The implications of such U-Pb patterns for age interpretation are discussed below.

Stromatic granulite sample Bras10-6-2 (Figure 2.6J) yields a lower intercept age of 25.0 ± 0.2 Ma (MSWD = 13, n = 57). Concordant analyses have $^{206}Pb/^{238}U$ dates between 21.2 ± 1.5 and 28.3 ± 1.0 Ma.

Figure 2.7 shows the dates of rutile grains from various textures in different rock types. The dates of rutile grains within a single microdomain vary in some cases, but these variations do not correlate with grain size, and typical intragrain diffusion profiles are not observed (Figure 2.7).

Rutile Trace Element Compositions

Most samples display a wide range of compositional variation in trace elements from grain to grain (Figure 2.8). There is a higher degree of correlation between trace element content and textural setting than for rock type. In general, matrix rutile grains have higher trace element abundances than inclusions in garnet. Matrix grains from peak and lower temperature assemblages in all samples show similar concentration ranges for most trace elements (Figure 2.8). However, grains from peak assemblages contain higher concentrations of Zr, Hf, and U than grains from lower temperature domains (Figure 2.8A–B). Retrogressed granulite sample GR11-1A and the finer-grained parts of stromatic granulite samples Bras105b-1 and Bras10-5b-2 contain matrix

rutile grains with elevated concentrations of W (Figure 2.8C). The two grains with the highest Nb concentrations (ca. 5.0 and 6.8 wt. %) are from a sapphirine-bearing domain in residual granulite sample G1A_2009, and several grains from all textural domains have Nb concentrations between 2.7 and 4.0 wt. % (Figure 2.8D).

Only two pairs of elements show strong correlations, Zr-Hf (Figure 2.8A) and Nb-Ta (Figure 2.8E). Zirconium and Hf are positively correlated, with an average Zr-Hf ratio of 29.2 ($y = 0.034x + 6.26$) and a correlation factor r of 0.97 (Figure8A). Niobium and Ta are also positively correlated, but show a wider range of trends (Figure8E) than Zr and Hf. Figures 8F, G, and H show that, on ratio plots, there is a high degree of scatter for the high field strength elements (HFSE). Grains with high Ta concentrations tend to have less scatter in the Nb-Ta ratio (Figure 2.8F), but this may be a result of higher analytical uncertainties for lower concentrations. Figure 2.8G shows that there is a higher degree of scatter in the Zr-Hf ratios of grains included in garnet (blue symbols) and from retrogressed domains (green symbols) than for rutile grains from UHT domains (red symbols). The Nb/Ta vs. Zr/Hf plot (Figure 2.8H) shows that there is high degree of variability, but no correlation with granulite type or textural setting.

Zr-in-rutile Thermometry

Zirconium concentrations of rutile grains and thus calculated temperatures are highly correlated with their textural setting in all investigated samples (Figure 2.7). Intragrain Zr concentration profiles are not observed (Figure 2.7). There is considerable overlap of temperature ranges obtained from similar textural settings in the different rock types. The details of these intrasample variations are discussed in this section (see also Table 2.3).

Massive, Mg- and Al-rich Granulite (Residual Granulite)

Rutile grains occur mostly within multiphase embayments (e.g. orthopyroxene + sapphirine + rutile; Figure 2.7A) and as single phase inclusions in the large garnet porphyroblasts of the residual granulite sample (G1A-2009) and record a wide range of temperatures ranging from 588–880°C (Figure 2.7A). Scarce grains outside of the garnet porphyroblasts occur primarily within large biotite clots and in contact with sapphirine (Figure 2.7B). These grains record UHT conditions (950–1000°C).

Stromatic Granulites

Rutile inclusions in garnet have the lowest trace element abundances and record the lowest Zr-in-rutile temperatures, ranging from 540–640°C and 490–700°C for samples Bras10-5b-1(Figure 2.7C) and Bras10-6, respectively. Rutile, which records UHT temperatures (900–1000°C), occurs within some multiphase embayments in garnet that contain plagioclase + orthopyroxene + biotite + sapphirine (Figure 2.7D).

Outside of garnet, within the matrix domains of the stromatic granulite samples Bras10-6 (Figure 2.7E) and in the coarser-grained domain of sample Bras10-5b-1 (Figure 2.4A), rutile grains record mainly UHT conditions, ranging from 870–1070°C; however, only a few grains record temperatures higher than 1000°C. Rutile grains within orthopyroxene + sapphirine symplectites surrounding garnet porphyroblasts invariably record UHT conditions (Figure 2.7C). Rutile grains with small (<10 μm) zircon grains at their boundaries (Figure 2.5G) as well as rutile in contact with larger zircon grains (Figure 2.5C) record temperatures between 710 and 750°C. Rutile grains within the finer-grained matrix domain (Domain B) of sample Bras10-5b-1 (Figure 2.4A) record intermediate temperatures, ranging from 710–850°C.

Leucocratic Granulite

In the leucocratic granulite sample (GR11-35), matrix rutile grains (Figure 2.7F) record temperatures of 790–1040°, and ruitle inclusions in garnet were too small to be analyzed. Seven of the 45 rutile grains that were analyzed record extremely low temperatures (435–570°C). This is possibly the result of analyzing exsolution lamellae of ilmenite or inclusions of another Zr-poor phase, and thus these temperatures are not considered to be geologically relevant.

Charnockite

Matrix rutile grains within the charnockite sample (GR11-43) are commonly surrounded by qurtz + mesoperthite, which represents crystallized melt. These grains record temperatures between 715 and 960°C (Figure 2.5I). Two grains from this sample record very low temperatures (402 and 545°C), probably related to ablation of micro inclusions or exsolution lamellae, and are therefore not considered for discussion.

Retrogressed Granulites

Rutile grains were analyzed from three textural domains in samples GR11-1A and GR11-1C, which came from the same boulder: grains in the 1) coarse- and 2) fine-grained matrix domains of sample GR11-1A (Figure 2.5K) and 3) inclusions within garnet from sample GR11-1C (Figure 2.5J). Zr-in-rutile temperatures are similar in all three domains. The coarse-grained (Domain A) and fine-grained (Domain B) matrix domains of sample GR11-1A contain rutile grains recording temperatures ranging from 510–890°C and 650–890°C, respectively. Four matrix grains have Zr concentrations corresponding to Zr-in-rutile temperatures ≤460°C, likely caused by ablating micro inclusions or exsolution lamellae. Rutile inclusions in garnet (sample GR11-1C) record temperatures between 610 and 895°C.

Discussion

Significance of Trace Element Compositions

The trace element patterns presented here are similar to those discussed by Meyer et al. (2011), who studied rutile from UHT granulites in NW South Africa. The good positive correlation between Zr and Hf (Figure 2.8A) indicates that these elements were strongly coupled throughout peak metamorphism and lower temperature retrogression and cooling. The correlation is not as good for Nb and Ta (Figure 2.8B), and in agreement with Meyer et al. (2011), we conclude that Zr and Hf are decoupled from the other HFSE. The high degree of correlation between Zr and Hf indicate that these elements exhibited similar behavior during the lower temperature overprint and cooling. The high degree of scatter in the Zr-Hf ratios for rutile grains included in garnet and from the retrogressed domains (Figure 2.8G) indicates that Zr and Hf are more easily fractionated at lower temperatures and during recrystallization. The wide scatter between concentrations and ratios of other elements (e.g. Zr/Hf vs. Hf and Nb/Ta vs. Hf; Figure 2.8) indicates that the primary concentrations of these elements were modified during recrystallization. Scatter in some elements is also possibly due to diffusional loss. The elevated W concentrations in rutile grains from low temperature domains (Figure 2.8C) of the retrogressed and stromatic granulite samples (GR11-1A, Bras105b-1, and -2) is interpreted to be the result of recrystallization in the presence of a W-rich fluid, which was likely sourced from the abundant pegmatitic dikes (Graham and Morris, 1973) within the Gruf Complex.

Zr-in-rutile Thermometry

Temperatures estimated by Zr-in-rutile thermometry are well correlated with textural setting within the samples (inclusions, matrix, recrystallized domains) indicating that Zr diffusion is negligible in most cases, and thus the temperatures represent crystallization temperatures, supporting the results of previous studies (Cherniak et al., 2007; Luvizotto and Zack, 2009;

Kooijman et al., 2012). This allows estimation of temperature at different stages in the metamorphic history of the Gruf granulites. Because the Zr-in-rutile temperatures are better correlated with textural setting than rock type, the results from all samples are combined and organized based on textural setting for this discussion. Mean temperatures of rutile from the different textural domains were estimated using histograms (Figure 2.9), and uncertainties are given as 2 SE.

Rutile included in garnet shows the widest range of temperatures (ca. 495–895°C) and the most non-Gaussian histogram (Figure 2.9), which is skewed toward higher temperatures. Because of the wide temperature range and the highest temperatures being slightly lower than the peak temperatures (see below), rutile inclusions in garnet are interpreted to have formed during prograde metamorphism. These grains likely crystallized continuously along the prograde path and were subsequently included in garnet. However, a detailed account of the garnet growth history is outside the scope of this study.

The highest average Zr-in-rutile temperatures were obtained from grains within matrix assemblages indicative of the metamorphic peak temperature in the granulites and charnockites. Temperature estimates for all except 9 analyses range from ca. 715–1075°C. The majority of these grains (219 of 282) record UHT conditions, and the mean temperature is 908 ± 83°C (Figure 2.9). This mean temperature from the peak assemblages corresponds well with peak temperature estimates of 900–1000°C at 7.5–9.5 kbar (Oalmann et al., in preparation-a) obtained by thermodynamic modeling techniques. The occurrence of UHT rutile grains within multiphase embayments and symplectites around garnet porphyroblasts indicates that garnet breakdown, likely due to decompression, began at temperatures in excess of 900°C. This is consistent with textural evidence for UHT decompression (e.g., sapphirine-bearing symplectites around garnet in

stromatic granulites and spinel- and sapphirine-bearing garnet breakdown textures in the leucogranulites). The absence of UHT rutile inclusions in garnet and presence of UHT rutile within garnet-breakdown textures suggests that the UHT conditions occurred late in the garnet-growth history of the granulites or after garnet growth.

Some rutile grains are part of multiphase embayments in garnet consisting of orthopyroxene + sapphirine + rutile in the residual granulite sample G1A_2009 (Figure 2.7A). We interpret these embayments to have formed as the result of garnet breakdown at UHT conditions based on the presence of orthopyroxene and sapphirine. However, the apparent Zr-in-rutile temperature estimates from these grains are quite low, at ca. 750°C (Figure 2.7A), which is likely the result of low Zr activity in the local reaction environment (i.e. absence of zircon and melt/fluid to transport Zr). In contrast, a sapphirine-bearing embayment in garnet from the stromatic granulite sample Bras10-6-2 (Figure 2.7C) contains rutile grains that record UHT conditions (900–1000°C). This embayment also contains biotite and an apatite grain with a zircon inclusion, indicating that fluid was present and Zr activity was high. Therefore, we interpret the temperatures recorded by rutile in this texture to accurately represent the conditions of garnet breakdown.

Experimental studies (e.g. Cherniak et al., 2007) indicate that primary Zr concentrations should not be preserved in UHT rutile unless very rapid cooling (>100°C/m.y.) occurred. The majority of the rutile grains analyzed in this study preserve Zr concentrations corresponding to UHT conditions, but lack intragrain diffusion profiles or grain size–temperature relationships. (Figure 2.7). Some rutile grains within UHT assemblages record temperatures between ca. 700–750°C, which corresponds to the closure temperature of Zr diffusion in a 200μm rutile grain cooling from a peak temperature of 900°C at 10°C/m.y. (Cherniak et al., 2007). These grains are commonly in contact with zircon grains (Figure 2.5C, G). Based on the position and size of the

small (<10µm) zircon grains (Figure 2.5G), we interpret that they formed as a result of Zr-exsolution from the UHT rutile during cooling. Therefore, we propose that grain boundary diffusion of Zr from rutile occurs only if a Zr-rich sink (e.g., zircon) is already present (Figure 2.5C) or can nucleate along the rutile grain boundary (Figure 2.5G). This is in good agreement with Taylor-Jones and Powell (2014) and Pape et al. (2016), who suggested that grain boundary diffusion of Zr from rutile is sluggish under the dry conditions experienced by many UHT rocks.

Within matrix domains that contain major mineral assemblages indicative of recrystallization at lower than peak temperatures (stromatic granulite samples Bras10-5b-1 and -2 and retrogressed granulite sample GR11-1A), rutile grains record temperatures ranging from ca. 610–890°C with a mean of 740 ± 72°C. The Gaussian distribution of this population (Figure 2.9) can possibly be explained by (re)crystallization of rutile in response to a single thermal event and over a limited temperature range. The recrystallization of these domains was likely driven by fluid or melt influx, supported by the abundance of biotite relative to orthopyroxene in these assemblages and the elevated W concentrations of some of these rutile grains (Figure 2.8C). The mean temperature corresponds to the upper range of peak temperature estimates of 700–750°C at ≤ 7.5 kbar (Oalmann et al., in preparation-a) for migmatitic paragneisses, which lack textural evidence for ever experiencing UHT metamorphism. Therefore, we interpret it to be likely that this recrystallization occurred within the granulites after they were juxtaposed against the lower grade units (Galli et al., 2013; Oalmann et al., in preparation-c). This temperature range is also consistent with temperatures recorded by migmatites elsewhere in the southern part of the Leopontine Dome (e.g., Todd and Engi, 1997; Engi et al., 2004; Burri et al., 2005).

In summary, the crystallization temperatures of rutile from different textural settings record three stages of the metamorphic evolution of the Gruf granulites and charnockites (Figure 2.10):

1) prograde metamorphism, which was accompanied by garnet growth and did not exceed 900°C; 2) peak metamorphism and garnet breakdown at UHT conditions; 3) retrograde (Lepontine) metamorphism and/or cooling in the range of ca. 700–750°C during amalgamation of the UHT and migmatitic units in the Gruf complex. The good agreement between the results presented here and those of other studies, which utilized other techniques to estimate temperature, indicate that Zr-in-rutile thermometry is a robust method for constraining the thermal evolution of high-grade crustal rocks that experienced multiple high temperature events.

Rutile U-Pb Cooling Ages

The most striking result from *in situ* rutile dating in these samples is that there is no evident correlation between the obtained U-Pb ages and the textural setting or specific trace element characteristics. This decoupling indicates that textural setting has no bearing on Pb diffusivity in rutile here. The analyzed grains do not exhibit intragrain age zoning, and there is not a clear correlation between grain size and age. We therefore interpret that Pb diffusivity is most likely controlled by the presence or absence of localized fast diffusion pathways such as grain boundary melts or fluids, exsolution lamellae, and intragrain fractures (e.g. Kooijman et al., 2010).

Some samples are characterized by clusters of concordant analyses and common Pb arrays with different trajectories. These clusters and arrays may represent distinct events that affected some grains but not others. For example, the vast majority of analyses from samples G1A_2009 (residual granulite) and GR11-1A (retrogressed granulite) lie along common Pb arrays with similar lower intercept ages (24.6 ± 0.7 and 25.8 ± 0.3 Ma, respectively). These samples also contain scarce grains with concordant $^{206}Pb/^{238}U$ dates of 19–22 Ma. Assuming that most of the grains were closed to Pb diffusion by ca. 25 Ma (i.e. the sample was below the Dodson closure

temperature of Pb diffusion in rutile), the grains that give younger dates may have been subjected to melts or fluids that allowed Pb to diffuse out at lower temperatures.

Core to rim age variations have been observed in rutile grains from other (ultra)high temperature granulites (e.g. Kooijman et al., 2010), which cooled slowly (on the order of 0.1°C/m.y.). Because no intragrain age variations along traverses of large rutile grains were observed in this study (Figure 2.7), the Gruf granulites and charnockites must have cooled faster than 0.1°C/m.y. as a first order approximation.

The large range in concordant dates and common Pb arrays is interpreted to represent ca. 11 m.y. of low- to mid-crustal processes (e.g. melt crystallization, fluid flow, cooling, and deformation) between the onset of retrograde metamorphism and final closure to Pb diffusion. Assuming that peak metamorphic conditions (ca. 950°C and 8 kbar) occurred by ca. 34 Ma (oldest U-Pb rutile dates; interpretation of earliest Alpine U-Pb zircon ages (Liati and Gebauer, 2003; Oalmann et al., in preparation-c); U-Pb monazite ages (Oalmann et al., in preparation-b); model of (Beltrando et al., 2010)) and the Gruf Complex reached the upper limit of the Pb closure temperature range for rutile (ca. 700°C, e.g. Cherniak, 2000) by ca. 30 Ma, we estimate the cooling rate to have been ca. 63°C/m.y. between 34 and 30 Ma (Figure 2.10). Based on the range of concordant U-Pb rutile dates, we interpret that the Gruf Complex remained in the temperature window of Pb partial retention in rutile (700–420°C, e.g. Mezger et al., 1989; Cherniak, 2000) from 30–19 Ma, which yields an average cooling rate of ca. 25°C/m.y. for this time period (Figure 2.10). However, the temperature-time path for the Gruf Complex after juxtaposition of the UHT and lower grade units (between 30 and 19 Ma) may have been more complex. The crystallization ages of underformed dikes (ca. 25 Ma; Oalmann et al., in preparation-c) and the Novate granite (ca. 24 Ma; Liati et al., 2000) indicate that the Gruf Complex was above 650°C until at least 24

Ma. Therefore, a likely scenario involves slow cooling (ca. 8°C/m.y.) between 30 and 24 Ma followed by more rapid cooling (ca. 46°C/m.y.) between 24 and 19 Ma (Figure 2.10). This scenario is in good agreement with the conclusions of Berger et al. (2011) who used lower temperature thermochronology (zircon and apatite fission track ages) to constrain the cooling history of the Central Alps.

Decoupling of Zr-in-rutile temperatures and U-Pb ages

Figures 7 and 11 and Table 2.4 show that U-Pb ages and Zr-in-rutile temperatures are strongly decoupled. Grains with Zr concentrations indicating UHT crystallization have $^{206}Pb/^{238}U$ dates anywhere from 19 to 30 Ma, and lower temperature (700–900°C) grains also span this age range. We interpret these results to indicate that Pb and Zr behave significantly different during retrograde metamorphism and cooling.

We interpret that zirconium concentrations represent crystallization temperatures in most cases, and that Zr is only mobilized by recrystallization or diffusion if there is a transport medium and pathway (see *Zr-in-rutile Thermometry* section above). The lowest Zr-in-rutile temperatures recorded by matrix rutile grains are ca. 700°C. Lower temperatures are recorded by rutile grains included in garnet, but these grains likely formed during prograde metamorphism (see *Zr-in-rutile Thermometry* section above). We interpret these results to indicate that rutile does not release Zr by diffusion below ca. 700°C, which is consistent with empirical and experimental studies (e.g. Cherniak et al., 2007; Kooijman et al., 2012). Based on the lack of correlation between ages and temperatures, we conclude that Pb is completely lost from rutile at temperatures above 700°C, and Pb is retained only below 700°C at the high cooling rates experienced by the UHT rocks of the Gruf complex. This is consistent with results of other studies that determined the closure temperature for Pb diffusion in rutile to be between ca. 420 and 700°C (Mezger et al., 1989;

Mezger et al., 1991; Cherniak, 2000; Möller et al., 2000; Vry and Baker, 2006). In summary, these results support the notion that the temperature range for Zr retention is higher than that for Pb retention. Diffusion behavior is controlled by availability of fluids/melts as transport media and grain boundaries as diffusion pathways.

Regional significance of Zr-in-rutile thermometry and U-Pb thermochronology

The results from texturally controlled Zr-in-rutile thermometry of this study indicate that the UHT event occurred late in the evolution of the granulites and charnockites. However, from this study alone, the precise timing of this event cannot be constrained. Our interpretation that initial decompression leading to garnet breakdown and symplectite formation occurred at UHT conditions is in contrast to the results of Galli et al. (2011), who estimated that symplectite formation occurred at ca. 740°C and 6.5–7.5 kbar. However, the results of Galli et al. (2011) are inconsistent with the first-order petrographic observation of UHT assemblages in the garnet breakdown textures (Figure 2.5A, D, F) and the Zr-in-rutile temperatures presented here. Therefore, we argue that this short-lived UHT event occurred during Alpine orogenesis. The lack of Zr-diffusion profiles in rutile grains supports the hypothesis that UHT metamorphism and the subsequent upper amphibolite to lower granulite facies overprint occurred within a very short timeframe (ca. 5–6 Ma), during a single metamorphic cycle.

There is good agreement between the mean Zr-in-rutile temperature from lower temperature matrix domains in the UHT granulites and peak temperature estimates of the paragneisses of 700–750 °C (Oalmann et al., in preparation-a). We interpret this as evidence for coeval recrystallization of some granulite domains and peak metamorphism of the paragneisses in the Gruf Complex at the same crustal level. We conclude that this happened after the Alpine juxtaposition of the granulite/charnockite and lower grade gneiss units as documented by Galli et

al. (2013). The juxtaposition and exhumation of the composite Gruf Complex likely occurred during and as a result of emplacement of the Bergell intrusion at ca. 30 Ma as discussed by (Galli et al., 2013).

The range of rutile ages (30–19 Ma) from all samples centers broadly on the crystallization age of the Novate leucogranite at 24 ±1 Ma (Liati et al., 2000) and the latest crosscutting dikes within the Gruf Complex at 25.6 ± 0.3 Ma (Oalmann et al., in preparation-c). These combined results indicate that the Gruf granulites and charnockites cooled to below the closure temperature of Pb diffusion in rutile coevally with the latest magmatic crystallization events in the immediate vicinity (Figure 2.10, 12). The rutile cooling ages also coincide with the latest crystallization of zircon in migmatites throughout the Lepontine Dome at ca. 22 Ma (Figure 2.12; Rubatto et al., 2009). It can therefore be proposed that after the UHT rocks of the Gruf Complex were exhumed to mid-crustal levels, upper amphibolite facies conditions persisted between ca. 30 and 24 Ma in the Southern Central Alps, and rapid cooling ensued between 24 and 19 Ma (Figure 2.10, 12).

Conclusions

The results presented in this study have some general implications for the use of rutile as a geothermochronometer in high-grade metamorphic rocks. Hafnium is the only HFSE that is strongly correlated with Zr. Concentrations of the other HSFEs do not appear to be a function of crystallization temperature and have most likely been modified during retrogression and cooling. Some trace elements (e.g. W) may be used to constrain fluid compositions. Zirconium-in-rutile thermometry is a robust method for determining prograde, peak, and retrograde temperatures in UHT rocks when specific attention is given to the textural setting of rutile. However, diffusional loss of Zr from rutile may occur if a Zr sink is present at or near the grain boundary. In the case of a short-lived UHT event with a very high cooling rate as in the Gruf Complex, Zr-in-rutile

temperatures generally represent crystallization temperatures. However, in terranes with slow post-peak metamorphic cooling, some modification of Zr-in-rutile temperatures may occur, and retrieving peak-T conditions can be difficult (e.g. Kooijman et al., 2012; Pape et al., 2016).

U-Pb rutile cooling ages are not correlated with texture or Zr-in-rutile temperatures. This indicates that Pb diffusion is controlled by the presence or absence of localized fast diffusion pathways such as fluids, melts, or intragrain defects. Above 700°C rutile does not effectively retain Pb, whereas Zr is fully retained by rutile below ca. 700°C. The temperature range for Pb-retention is likely cooling rate dependent.

The granulites of the Gruf Complex most likely reached UHT conditions during Alpine orogenesis, and some recrystallization of the granulites occurred during and after juxtaposition of these lower-crustal rocks with mid-crustal migmatites. The Gruf complex underwent fast cooling on the order of 63°C/m.y. between 34 and 30 Ma; cooling rates slowed to ca. 8°C/m.y. between 30 and 24 Ma and then accelerated to ca. 46°C/m.y. between 24 and 19 Ma. The U-Pb rutile age range of 30–19 Ma coincides with emplacement of the Novate leucogranite at 24 ± 1 Ma (Liati et al., 2000) and migmatization within the Southern Steep Belt between 32 and 22 Ma (e.g. Rubatto et al., 2009). The most likely geodynamic scenario for UHT conditions being reached during decompression is considered to be slab breakoff, which resulted in heat transfer from asthenospheric upwelling to the crust by ca. 34 Ma.

Acknowledgements

This research is supported by the American National Science Foundation under Grant No. EAR 0911633 to A. Möller. We would like to thank A. Galli for guiding us in the field area, the Biavaschi family at Rifugio Brasca for their hospitality and logistical help, P.G. Lippert for field

assistance, and C. Fischer at the University of Potsdam and W.C. Dickerson at the University of Kansas for preparing thin sections.

Figure Captions

Figure 2.1. Tectonic map of the Central Alps showing the location of the Gruf Complex and surrounding units (color coded by paleogeographic affinity) and major faults (modified from Bousquet et al., 2012b). SSB = Southern Steep Belt. Inset shows location of map area within Europe. Ages of Bergell and Novate Intrusions are from von Blanckenburg (1992) and Liati et al. (2000), respectively.

Figure2. Geologic map of the Gruf Complex and surrounding units with strike and dip of foliations and locations of samples used in this study (modified from Galli et al., 2013). Inset shows location of map area within Europe. Ages of Bergell and Novate Intrusions are from von Blanckenburg (1992) and Liati et al. (2000), respectively.

Figure 2.3. Photos of rock types. (A) Residual granulite (sample G1A_2009). (B) Stromatic granulite (sample Bras10-5). (C) Leucogranulite (upper part of photo; sample GR11-35). (D) Charnockite (sample GR11-43). (E) Large granulite boulder from Val Codera with multiple mineralogical/textural domains; 1 and 2 refer to samples GR11-1A and GR11-1C, which are retrogressed granulites. (F) Example of mylonite zone separating charnokite from orthogneiss.

Figure 2.4. Scans of thin sections of selected granulites showing Zr-in-rutile temperature ranges for different texural domains. (A) Stromatic granulite sample BRAS10-5b showing coarser-

grained Domain A and finer-grained Domain B. (B) Retrogressed granulite GR11-1C showing coarser-grained Domain A and finer-grained Domain B.

Figure 2.5. Photomicrographs with Zr-in-rutile temperatures (in red). (A) Residual granulite (sample G1A_2009): Embayments in large garnet porphyroblast filled with orthopyroxene + sapphirine + rutile + minor biotite. Also note the orthopyroxene + cordiertite sillimanite + sapphirine symplectite, which surrounds biotite, on the left side of the image. (B) Residual granulite (sample G1A_2009): Large biotite clot with inclusions of sapphirine + rutile. Left side of photo shows a relict garnet porphyroblast with sapphirine + cordierite + orthopyroxene-filled embayments and orthopyroxene + cordierite + sapphirine symplectites between the garnet and the biotite clot. Right side of photo shows quartz + K-feldspar leucosome with fine-grained sapphirine aggregates and biotite. (C) Stromatic granulite (sample Bras10-5b-2): Quartz + K-feldspar + plagioclase leucosome surrounding orthopyroxene + several rutile grains. Note the low apparent temperature for the rutile grain in contact with zircon compared. (D) Stromatic granulite (sample Bras10-5b-1): Sapphirine + orthopyroxene + biotite + rutile intergrowths and symplectites at the edge of a large garnet porphyroblasts. Quartz + K-feldspar + plagioclase leucosomes and large orthopyroxene porphyroblasts surround the garnet and its finer-grained reaction products. (E) Stromatic granulite (Bras10-6-2): Large orthopyroxene porphyroblasts surrounded by cordierite + biotite with minor quartz and plagioclase Note the very fine-grained needles (red arrow) and small grains (green arrow) of rutile within the orthopyroxene. (F) Stromatic granulite (Bras10-6-2): Orthopyroxene + sapphirine intergrowths, rutile, biotite, and plagioclase within an embayment in garnet. (G) Stromatic granulite (Bras10-6-1): Rutile with small zircon grains along grain boundaries within a biotite rich layer. (H) Leucogranulite (sample GR11-35): Relict garnet

porphyroblast breaking down to plagioclase + spinel + opaques surrounded by quartz + K-feldspar + minor plagioclase leucosome. A small garnet porphyroblast is intergrown with orthopyroxene. (I) Charnockite (sample GR11-43): Anhedral garnet + biotite + rutile within quartz + K-feldspar + plagioclase leucosome. (J) Retrogressed granulite (sample GR11-1A): Large garnet porphyroblast with a rutile inclusion surrounded by orthopyroxene + cordierite symplectite. Biotite (with exsolved rutile needles) + orthopyroxene + sillimanite + cordierite occurs outside of the symplectite. (K) Retrogressed granulite (sample GR11-1A): Garnet porphyroblast with orthopyroxene + cordierite symplectite surrounded by orthopyroxene + biotite + cordierite + rutile. (L) Retrogressed granulite (sample GR11-1C): Garnet porphyroblast with chlorite-filled fractures and spinel, rutile, opaque, and bioitite inclusions. Sillimanite and cordierite are present between the garnet and an orthopyroxene porphyroblast. Relict sapphirine grains fringed by spinel aggregates are also present. Black boxes in panels A, B, and D denote areas shown in Figure 2.7 where Zr-in-rutile temperatures are shown. Mineral abbreviations after Whitney and Evans (2010).

Figure 2.6. Concordia plots: (A) All samples combined. (B)–(J) Individual plots for each sample. Gray ellipses represent analyses not used in age calculations. L.I. = lower intercept age. In panel (F), the two lower intercept ages shown are calculated for the yellow and purple ellipses, respectively. In panel (H), ages near the inset refer to weighted mean $^{206}Pb/^{238}U$ ages for each group of ellipses (blue and purple).

Figure 2.7. Photomicrographs with plots of $^{206}Pb/^{238}U$ dates (upper), and Zr-in-Rt temperatures (lower) for selected textures from different granulite types. (A) Rutile within garnet breakdown texture in garnet embayment from residual granulite sample G1A_2009. (B) UHT rutile +

sapphirine with biotite-rich clot from residual granulite sample G1A_2009. (C) UHT rutile-bearing sapphirine + orthopyroxene symplectite around garnet with lower temperature rutile inclusions in garnet from stromatic granulite sample Bras10-5b-1. (D) UHT rutile from stromatic granulite sample Bras10-6-2. (E) UHT rutile from stromatic granulite sample Bras10-6-1. (F) Near UHT rutile with sapphirine + spinel aggregate in leucogranulite sample GR11-35. Error bars on date plots represent 2SE internal plus propogated uncertainty. Error bars on temperature plots represent 2SE internal uncertainty. Mineral abbreviations after Whitney and Evans (2010). See Figure 2.5 for locations of photos A, B, and C.

Figure 2.8. Rutile trace element concentrations for granulites and charnockites. Points represent individual spot analyses. Symbol colors represent textural domains (blue: inclusions in garnet; red: peak matrix domains; green: retrogressed matrix domains), and symbol shapes represent sample. (A) Hf versus Zr with calculated linear regression line. (B) U versus Zr. (C) W versus Zr. (D) Nb versus Zr. (E) Ta versus Nb. (F) Nb/Ta versus Ta. (G) Zr/Hf versus Hf. (H) Nb/Ta versus Zr/Hf.

Figure 2.9. Composite histogram showing Zr-in-rutile temperatures color coded by textural setting (blue: inclusions in garnet; green: retrogressed matrix domains; red: peak matrix domains). Temperatures given in the figure are means calculated from each histogram. Rextal. = recrystallized.

Figure 2.10. Schematic temperature versus time diagram for evolution of Gruf granulites. Boxes represent time/temperature ranges for the ages listed in the figure. U-Pb zircon ages for granulites and dikes are from (Oalmann et al., in preparation-c). Cooling rates are also shown for various

segments of the temperature-time path. For the time period between 30 and 19 Ma, both a continuous and two-stage cooling path are shown. The diagrams across the top of the Figure 2.are schematic cross sections showing stages of dike emplacement and deformation at given times. The pluton symbols across the bottom are scaled to show U-Pb crystallization ages of the Bergell intrusion (von Blanckenburg, 1992) and Novate leucogranite (Liati et al., 2000).

Figure 2.11. Zr-in-rutile temperature versu $^{206}Pb/^{238}U$ date for rutile analyses from representative stromatic and retrogressed granulite samples. Rutile from all textural domains are included. Error bars are 2SE internal plus propogated uncertainties on the $^{206}Pb/^{238}U$ date. Uncertainty of the Zr-in-rutile temperatures are less than or equal to the height of the symbols.

Figure 2.12. Summary of metamorphic and plutonic ages in the Central Alps (going from north to south) roughly color coded for temperature of event. Numbers refer to the following ages: 1) U-Pb staurolite: ca. 28 Ma (Nagel, 2002); 2) U-Pb zircon (rims): 33–32 Ma (Liati et al., 2009); 3) Ar-Ar phengite: 33–30 Ma (Talerico, 2000); 4) U-Pb zircon: 37.1 ± 0.9 (Liati et al., 2003); 5) U-Pb zircon: undeformed dikes = 25.6 ± 0.3 Ma; deformed dikes = 30–27; zircon rims in UHT rocks = 32.9 ± 0.5 Ma (Oalmann et al., in preparation-c); 6) U-Pb monazite in UHT rocks: 34–31 Ma (Oalmann et al., in preparation-b); 7) U-Pb zircon: 24.0 ± 1.2 Ma (Liati et al., 2000); 8) U-Pb zircon (tonalite): 31.88 ± 0.09 Ma, U-Pb allanite (granodiorite): 30.1 ± 0.25 Ma (von Blanckenburg, 1992); 9) U-Pb zircon: 32–22 Ma (Rubatto et al., 2009); 10) U-Pb zircon: 34.2 ± 0.2 and 32.9 ± 0.3 Ma (Hermann et al., 2006); 11) Lu-Hf garnet: 70–36 Ma (Brouwer et al., 2005); 12) U-Pb zircon: 43 ± 2 and 35.4 ± 0.5 Ma (Gebauer, 1996). Height of black boxes is scaled to age plus uncertainty or age range. SSB = Southern Steep Belt.

References

Becker, H., 1993. Garnet peridotite and eclogite Sm-Nd mineral ages from the Lepontine dome (Swiss Alps): New evidence for Eocene high-pressure metamorphism in the central Alps. Geology, 21(7): 599-602.

Beltrando, M., Lister, G.S., Rosenbaum, G., Richards, S., Forster, M.A., 2010. Recognizing episodic lithospheric thinning along a convergent plate margin: The example of the Early Oligocene Alps. Earth-Science Reviews, 103(3): 81-98.

Berger, A., Rosenberg, C., Schmid, S., 1996. Ascent, emplacement and exhumation of the Bergell pluton within the Southern Steep Belt of the Central Alps. Schweizerische mineralogische und petrographische Mitteilungen, 76(3): 357-382.

Berger, A., Schmid, S.M., Engi, M., Bousquet, R., Wiederkehr, M., 2011. Mechanisms of mass and heat transport during Barrovian metamorphism: A discussion based on field evidence from the Central Alps (Switzerland/northern Italy). Tectonics, 30(1): TC1007.

Bousquet, R. et al., 2012a. Metamorphic Framework of the Alps, Commission for the Geological Map of the World, CCGM/CGMW.

Bousquet, R. et al., 2012b. Tectonic framework of the Alps, Commission for the Geological Map of the World, CCGM/CGMW.

Brouwer, F., Burri, T., Engi, M., Berger, A., 2005. Eclogite relics in the Central Alps: PT-evolution, Lu-Hf ages, and implications for formation of tectonic mélange zones. Schweizerische mineralogische und petrographische Mitteilungen, 85: 147-174.

Brown, M., 2007. Metamorphic conditions in orogenic belts: a record of secular change. International Geology Review, 49(3): 193-234.

Burri, T., Berger, A., Engi, M., 2005. Tertiary migmatites in the Central Alps: Regional distribution, field relations, conditions of formation, and tectonic implications. Schweizerische mineralogische und petrographische Mitteilungen, 85(2-3): 215-232.

Carswell, D., O'Brien, P., 1993. Thermobarometry and geotectonic significance of high-pressure granulites: examples from the Moldanubian Zone of the Bohemian Massif in Lower Austria. Journal of Petrology, 34(3): 427-459.

Chappell, B., White, A., 1974. Two contrasting granite types. Pacific geology, 8(2): 173-174.

Cherniak, D., 2000. Pb diffusion in rutile. Contributions to Mineralogy and Petrology, 139(2): 198-207.

Cherniak, D., Manchester, J., Watson, E., 2007. Zr and Hf diffusion in rutile. Earth and Planetary Science Letters, 261(1-2): 267-279.

Ciancaleoni, L., Marquer, D., 2006. Syn-extension leucogranite deformation during convergence in the Eastern Central Alps: example of the Novate intrusion. Terra Nova, 18(3): 170-180.

Davidson, C., Rosenberg, C., Schmid, S., 1996. Symmagmatic folding of the base of the Bergell pluton, Central Alps. Tectonophysics, 265(3): 213-238.

Engi, M., Berger, A., Roselle, G.T., 2001. Role of the tectonic accretion channel in collisional orogeny. Geology, 29(12): 1143-1146.

Engi, M., Bousquet, R., Berger, A., 2004. Metamorphic structure of the alps: Central alps. Explanatory notes to the map of metamorphic structures of the Alps. Mitteilungen der Österreichischen Mineralogischen Gesellschaft, 149: 157-173.

Fitzsimons, I., Harley, S., 1994. The influence of retrograde cation exchange on granulite PT estimates and a convergence technique for the recovery of peak metamorphic conditions. Journal of Petrology, 35(2): 543-576.

Frey, M., Ferreiro Mählmann, R., 1999. Alpine metamorphism of the Central Alps. Schweizerische mineralogische und petrographische Mitteilungen, 79(1): 135-154.

Galli, A., 2010. Tectonometamorphic evolution of the Gruf Complex (Swiss and Italian Central Alps). PhD Thesis Thesis, ETH Zürich, Zürich, 164 pp.

Galli, A. et al., 2011. Granulites and charnockites of the Gruf Complex: Evidence for Permian ultra-high temperature metamorphism in the Central Alps. Lithos, 124(1-2): 17-45.

Galli, A. et al., 2012. U–Pb zircon dating of the Gruf Complex: disclosing the late Variscan granulitic lower crust of Europe stranded in the Central Alps. Contributions to Mineralogy and Petrology, 163: 353-378.

Galli, A., Le Bayon, B., Schmidt, M.W., Burg, J.-P., Reusser, E., 2013. Tectonometamorphic history of the Gruf complex (Central Alps): exhumation of a granulite–migmatite complex with the Bergell pluton. Swiss Journal of Geosciences, 106(1): 33-62.

Galli., A., 2010. Tectonometamorphic evolution of the Gruf Complex (Swiss and Italian Central Alps). PhD Thesis Thesis, ETH Zurich, 164 pp.

Gebauer, D., 1996. A P-T-t path for an (Ultra?-) High-pressure ultramafic/mafic rock-association and its felsic country-rocks based on SHRIMP-dating of magmatic and metamorphic zircon domains. Example: Alpe Arami (Central Swiss Alps), Earth Processes: Reading the Isotopic Code. Geophys. Monogr. Ser. AGU, Washington, DC, pp. 307-329.

Graham, J., Morris, R., 1973. Tungsten-and antimony-substituted rutile. Mineralogical Magazine, 39(304): 470-473.

Harley, S., 2008. Refining the P–T records of UHT crustal metamorphism. Journal of Metamorphic Geology, 26(2): 125-154.

Harley, S.L., 1998. On the occurrence and characterization of ultrahigh-temperature crustal metamorphism. Geological Society, London, Special Publications, 138(1): 81-107.

Hermann, J., Rubatto, D., Trommsdorff, V., 2006. Sub-solidus Oligocene zircon formation in garnet peridotite during fast decompression and fluid infiltration (Duria, Central Alps). Mineralogy and Petrology, 88(1): 181-206.

Jiao, S., Guo, J., Mao, Q., Zhao, R., 2011. Application of Zr-in-rutile thermometry: a case study from ultrahigh-temperature granulites of the Khondalite belt, North China Craton. Contributions to Mineralogy and Petrology, 162(2): 379-393.

Kelsey, D.E., 2008. On ultrahigh-temperature crustal metamorphism. Gondwana Research, 13(1): 1-29.

Kooijman, E., Mezger, K., Berndt, J., 2010. Constraints on the U–Pb systematics of metamorphic rutile from in situ LA-ICP-MS analysis. Earth and Planetary Science Letters, 293(3): 321-330.

Kooijman, E., Smit, M., Mezger, K., Berndt, J., 2012. Trace element systematics in granulite facies rutile: implications for Zr geothermometry and provenance studies. Journal of Metamorphic Geology.

Liati, A., Gebauer, D., 2003. Geochronological constraints for the time of metamorphism in the Gruf Complex (Central Alps) and implications for the Adula-Cima Lunga nappe system. Swiss Bulletin of Mineralogy and Petrology, 83(2): 159-172.

Liati, A., Gebauer, D., Fanning, C.M., 2003. The youngest basic oceanic magmatism in the Alps (Late Cretaceous; Chiavenna unit, Central Alps): geochronological constraints and geodynamic significance. Contributions to Mineralogy and Petrology, 146(2): 144-158.

Liati, A., Gebauer, D., Fanning, C.M., 2009. Geochronological evolution of HP metamorphic rocks of the Adula nappe, Central Alps, in pre-Alpine and Alpine subduction cycles. Journal of the Geological Society, 166(4): 797-810.

Liati, A., Gebauer, D., Fanning, M., 2000. U-PbSHRIMP dating of zircon from the Novate granite (Bergell, Central Alps): evidence for Oligocene-Miocene magmatism, Jurassic/Cretaceous continental rifting and opening of the Valais trough. Schweizerische mineralogische und petrographische Mitteilungen, 80(3): 305-316.

Luvizotto, G., Zack, T., 2009. Nb and Zr behavior in rutile during high-grade metamorphism and retrogression: an example from the Ivrea-Verbano Zone. Chemical Geology, 261(3-4): 303-317.

McLean, N., Bowring, J., Gehrels, G., 2016. Algorithms and software for U-Pb geochronology by LA-ICPMS. Geochemistry, Geophysics, Geosystems.

Meinhold, G., 2010. Rutile and its applications in earth sciences. Earth-Science Reviews, 102(1–2): 1-28.

Meyer, M., John, T., Brandt, S., Klemd, R., 2011. Trace element composition of rutile and the application of Zr-in-rutile thermometry to UHT metamorphism (Epupa Complex, NW Namibia). Lithos, 126(3): 388-401.

Mezger, K., Hanson, G., Bohlen, S., 1989. High-precision UPb ages of metamorphic rutile: application to the cooling history of high-grade terranes. Earth and Planetary Science Letters, 96(1-2): 106-118.

Mezger, K., Rawnsley, C., Bohlen, S., Hanson, G., 1991. U-Pb garnet, sphene, monazite, and rutile ages: implications for the duration of high-grade metamorphism and cooling histories, Adirondack Mts., New York. The Journal of Geology, 99(3): 415-428.

Möller, A., Mezger, K., Schenk, V., 2000. U–Pb dating of metamorphic minerals: Pan-African metamorphism and prolonged slow cooling of high pressure granulites in Tanzania, East Africa. Precambrian Research, 104(3): 123-146.

Nagel, T., 2002. Metamorphic and structural history of the southern Adula Nappe (Grabünden, Switzerland), University of Basel, Basel.

Niggli, E., Niggli, C., 1965. Karten der Verbreitung einiger Mineralien der alpidischen Metamorphose in den Schweizer Alpen (Stilpnomelan, Alkali-Amphibol, Chloritoid, Staurolith, Disthen, Sillimanit). Eclogae Geologicae Helvetiae, 58: 335-368.

Oalmann, J., Düsterhöft, E., Möller, A., Bousquet, R., in preparation-a. Constraining the pressure-temperature evolution and geodynamic setting of UHT granulites and migmatitic paragneisses of the Gruf Complex, Central Alps.

Oalmann, J., Möller, A., Bousquet, R., in preparation-b. Texturally controlled U-Pb monazite dating of sapphirine granulites from the Gruf Complex, Central Alps: Evidence for UHT metamorphism in a Cenozoic continent-continent collision.

Oalmann, J., Möller, A., Bousquet, R., Savage, J., in preparation-c. Constraining the timing of UHT metamorphism, melt crystallization, and deformation with zircon geochronology and trace element geochemistry: The Gruf Complex, Central Alps.

Pape, J., Mezger, K., Robyr, M., 2016. A systematic evaluation of the Zr-in-rutile thermometer in ultra-high temperature (UHT) rocks. Contributions to mineralogy and petrology, 171(5): 1-20.

Pattison, D.R., Chacko, T., Farquhar, J., McFarlane, C.R., 2003. Temperatures of granulite-facies metamorphism: constraints from experimental phase equilibria and thermobarometry corrected for retrograde exchange. Journal of Petrology, 44(5): 867-900.

Rubatto, D., Hermann, J., Berger, A., Engi, M., 2009. Protracted fluid-induced melting during Barrovian metamorphism in the Central Alps. Contributions to Mineralogy and Petrology, 158(6): 703-722.

Samperton, K.M. et al., 2015. Magma emplacement, differentiation and cooling in the middle crust: Integrated zircon geochronological–geochemical constraints from the Bergell Intrusion, Central Alps. Chemical Geology, 417: 322-340.

Schmid, S.M., Fügenschuh, B., Kissling, E., Schuster, R., 2004. Tectonic map and overall architecture of the Alpine orogen. Eclogae Geologicae Helvetiae, 97(1): 93-117.

Schmitz, S. et al., 2009. Chemical U-Th-Pb dating of monazite by 3D-Micro X-ray fluorescence analysis with synchrotron radiation. European Journal of Mineralogy, 21(5): 927-945.

Stampfli, G. et al., 1998. Subduction and obduction processes in the Swiss Alps. Tectonophysics, 296(1): 159-204.

Talerico, C., 2000. Petrological and chemical investigation of a metamorphosed oceanic crust-mantle section (Chiavenna, Bergell Alps), ETH Zürich, Zürich.

Taylor-Jones, K., Powell, R., 2014. Understanding Zirconium-in-Rutile Thermometric Results in High Metamorphic Grade Rocks. Mineralogical Magazine, 77(5): 2457.

Todd, C.S., Engi, M., 1997. Metamorphic field gradients in the Central Alps. Journal of Metamorphic Geology, 15(4): 513-530.

Tomkins, H., Powell, R., Ellis, D., 2007. The pressure dependence of the zirconium-in-rutile thermometer. Journal of Metamorphic Geology, 25(6): 703-713.

Trommsdorff, V., 1966. Progressive Metamorphose kieseliger Karbonatgesteine in den Zentralalpen zwischen bernina und Simplon. Schweizerische mineralogische und petrographische Mitteilungen, 46: 431-460.

Trommsdorff, V., 1990. Metamorphism and tectonics in the Central Alps: The Alpine lithospheric mélange of Cima Lunga and Adula. Memorie della Società Geologica Italiana, 45: 39-49.

von Blanckenburg, F., 1992. Combined high-precision chronometry and geochemical tracing using accessory minerals: applied to the Central-Alpine Bergell intrusion (central Europe). Chemical Geology, 100(1-2): 19-40.

Vry, J.K., Baker, J.A., 2006. LA-MC-ICPMS Pb-Pb dating of rutile from slowly cooled granulites: Confirmation of the high closure temperature for Pb diffusion in rutile. Geochimica et Cosmochimica Acta, 70(7): 1807-1820.

Whitney, D.L., Evans, B.W., 2010. Abbreviations for names of rock-forming minerals. American mineralogist, 95(1): 185.

Zack, T., Moraes, R., Kronz, A., 2004. Temperature dependence of Zr in rutile: empirical calibration of a rutile thermometer. Contributions to Mineralogy and Petrology, 148(4): 471-488.

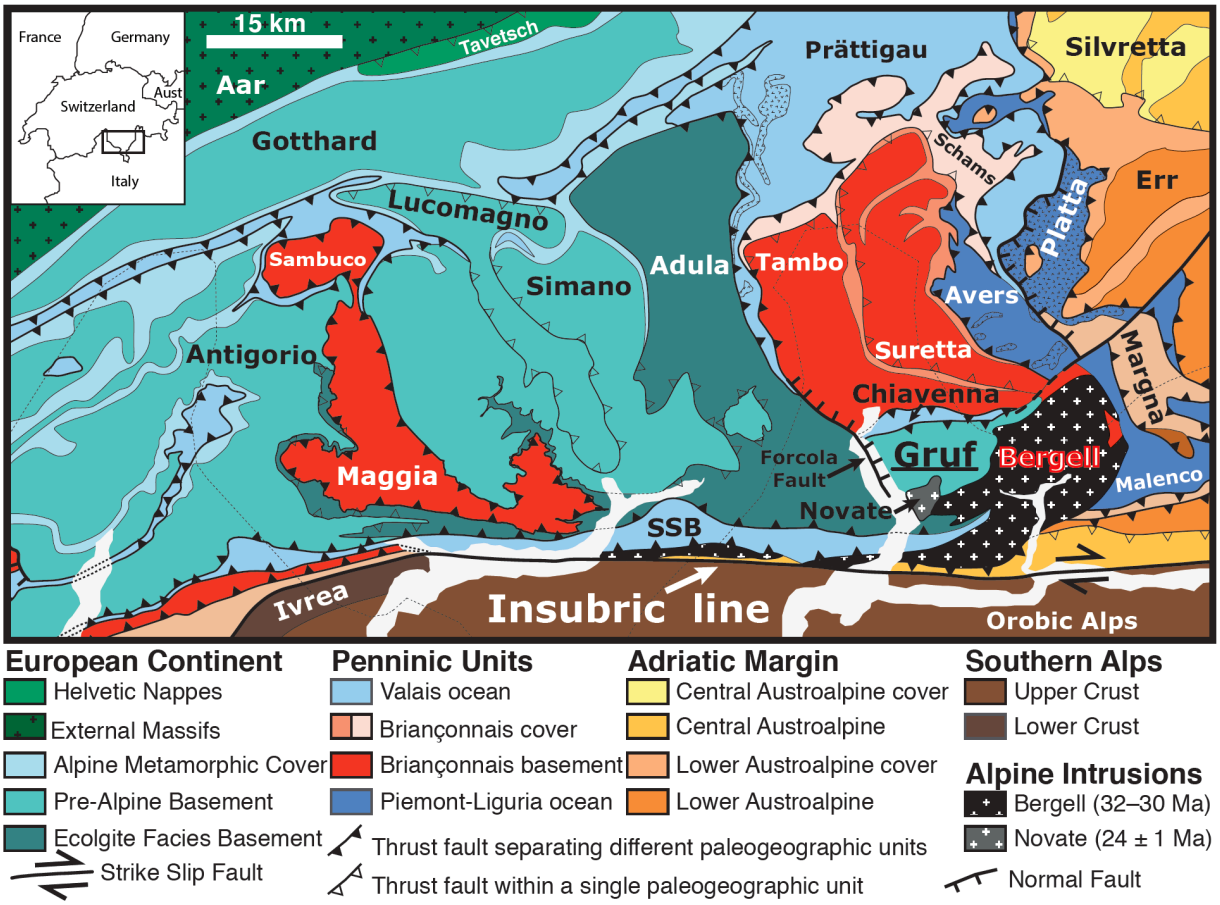
France
Germany
Switzerland
Aust
Italy
15 km
Tavetsch
Aar
Gotthard
Lucomagno
Sambuco
Simano
Adula
Prättigau
Silvretta
Schams
Err
Platta
Tambo
Avers
Suretta
Margna
Chiavenna
Antigorio
Maggia
Forcola Fault
Gruf
Bergell
Malenco
Novate
SSB
Ivrea
Insubric line
Orobic Alps
European Continent
Helvetic Nappes
External Massifs
Alpine Metamorphic Cover
Pre-Alpine Basement
Ecolgite Facies Basement
Strike Slip Fault
Penninic Units
Valais ocean
Briançonnais cover
Briançonnais basement
Piemont-Liguria ocean
Thrust fault separating different paleogeographic units
Thrust fault within a single paleogeographic unit
Adriatic Margin
Central Austroalpine cover
Central Austroalpine
Lower Austroalpine cover
Lower Austroalpine
Southern Alps
Upper Crust
Lower Crust
Alpine Intrusions
Bergell (32–30 Ma)
Novate (24 ± 1 Ma)
Normal Fault

Figure 2.1

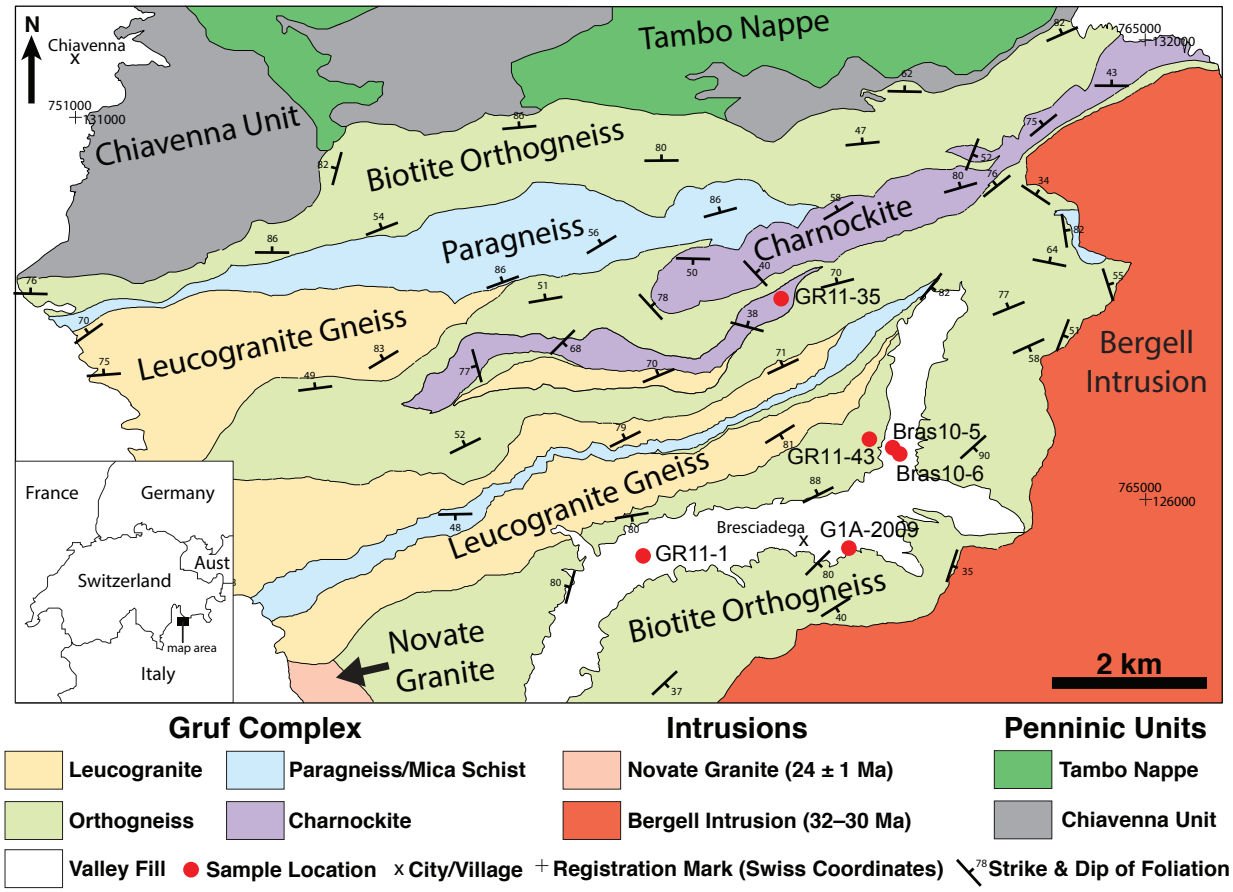
N
Chiavenna
751000
131000
765000
132000
Tambo Nappe
Chiavenna Unit
Biotite Orthogneiss
Paragneiss
Charnockite
GR11-35
Leucogranite Gneiss
Bergell Intrusion
Bras10-5
GR11-43
Bras10-6
765000
126000
Leucogranite Gneiss
Bresciadega
G1A-2009
GR11-1
Biotite Orthogneiss
Novate Granite
2 km
France
Germany
Switzerland
Aust
map area
Italy
Gruf Complex
Leucogranite
Paragneiss/Mica Schist
Orthogneiss
Charnockite
Valley Fill
Sample Location
City/Village
Intrusions
Novate Granite (24 ± 1 Ma)
Bergell Intrusion (32–30 Ma)
Registration Mark (Swiss Coordinates)
Penninic Units
Tambo Nappe
Chiavenna Unit
Strike & Dip of Foliation

Figure 2.2

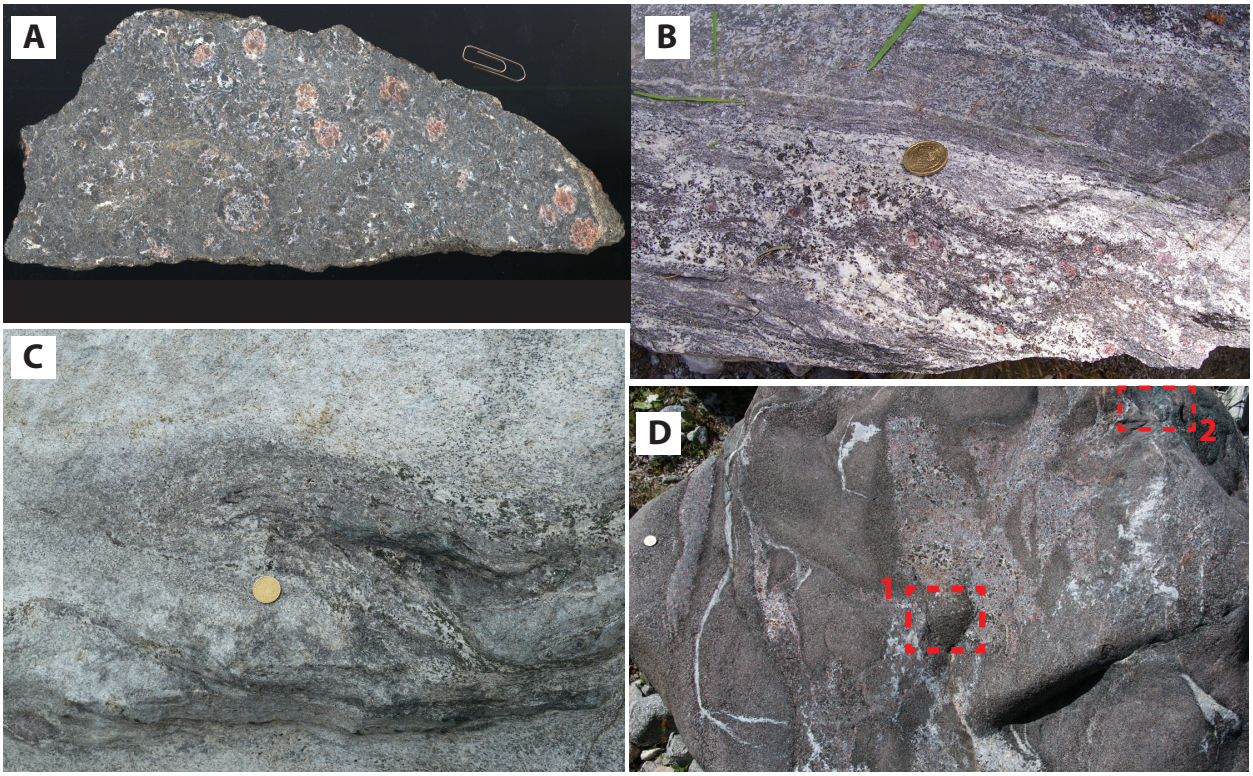

Figure 2.3

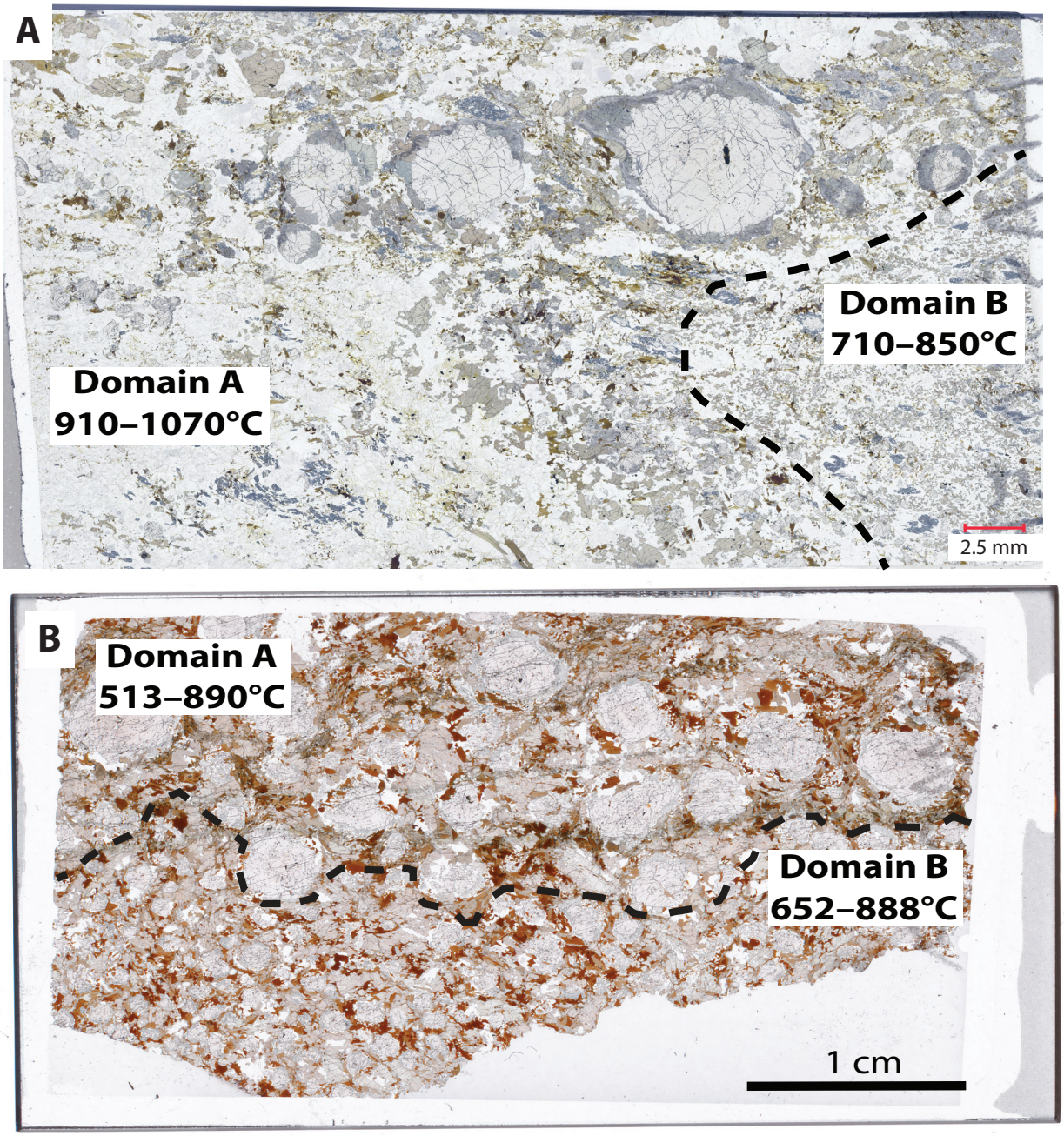
A
Domain A
910–1070°C
Domain B
710–850°C
2.5 mm
B
Domain A
513–890°C
Domain B
652–888°C
1 cm

Figure 2.4

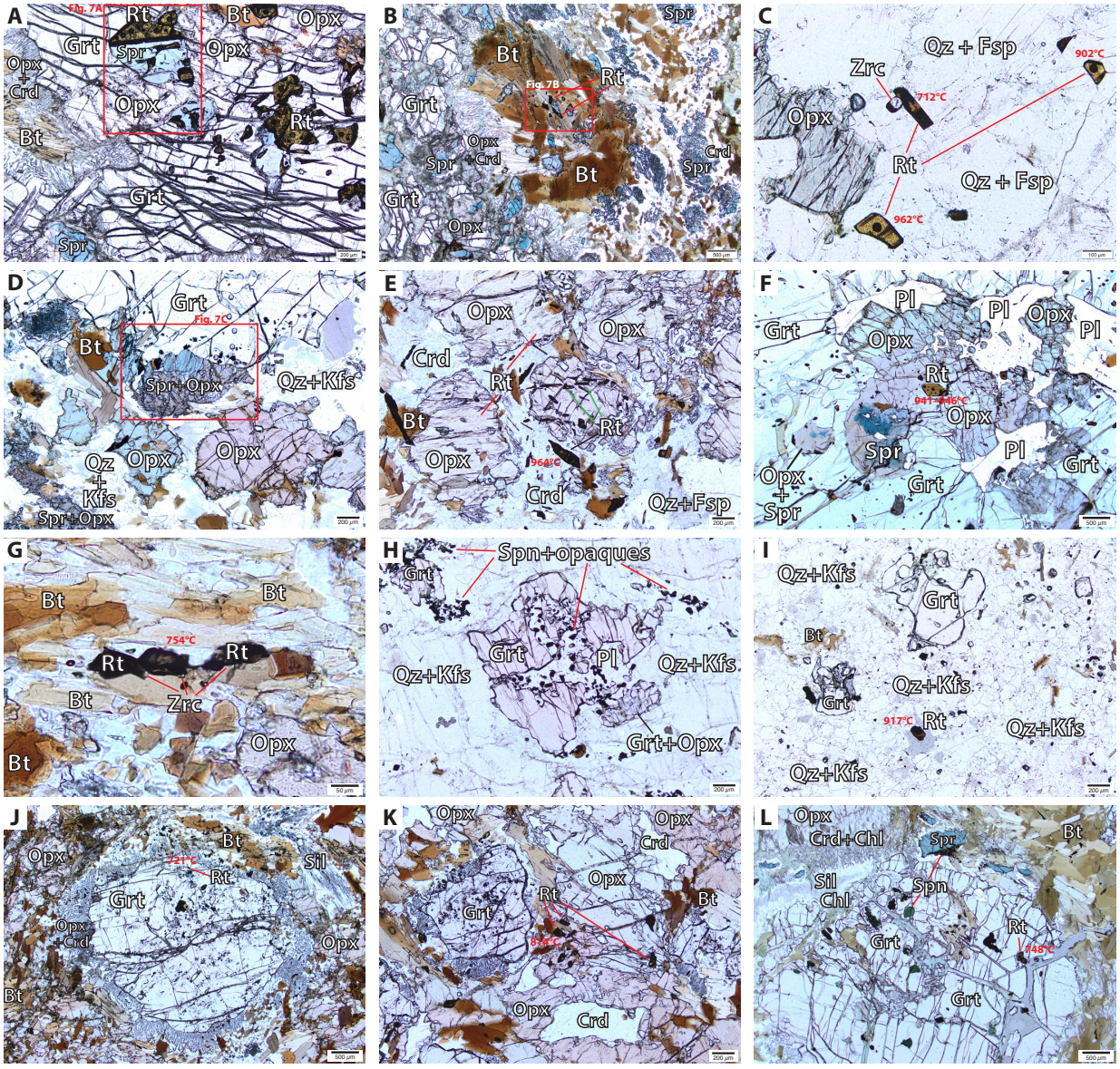
A
Fig. 7A
Rt
Bt
Opx
Grt
Spr
Opx
+
Crd
Opx
Opx
Rt
Bt
Grt
Spr
B
Spr
Bt
Rt
Fig. 7B
Grt
Opx
+
Crd
Spr
Crd
Spr
Bt
Grt
Opx
C
Qz + Fsp
902°C
Zrc
712°C
Opx
Rt
Qz + Fsp
962°C
D
Grt
Fig. 7C
Bt
Spr+Opx
Qz+Kfs
Qz
+
Kfs
Opx
Opx
Spr+Opx
E
Opx
Opx
Crd
Rt
Bt
Rt
Opx
964°C
Crd
Qz+Fsp
F
Pl
Pl
Opx
Pl
Grt
Opx
Rt
941–946°C
Opx
Spr
Pl
Grt
Opx
+
Spr
Grt
G
Bt
Bt
754°C
Rt
Rt
Bt
Zrc
Opx
Bt
H
Spn+opaques
Grt
Qz+Kfs
Grt
Pl
Qz+Kfs
Grt+Opx
I
Qz+Kfs
Grt
Bt
Grt
Qz+Kfs
917°C
Rt
Qz+Kfs
Qz+Kfs
J
Opx
Bt
721°C
Rt
Sil
Grt
Opx
Crd
Opx
Bt
K
Opx
Opx
Crd
Opx
Rt
Bt
Grt
814°C
Opx
Crd
L
Opx
Crd+Chl
Spr
Bt
Sil
Chl
Spn
Rt
Grt
748°C
Grt

Figure 2.5

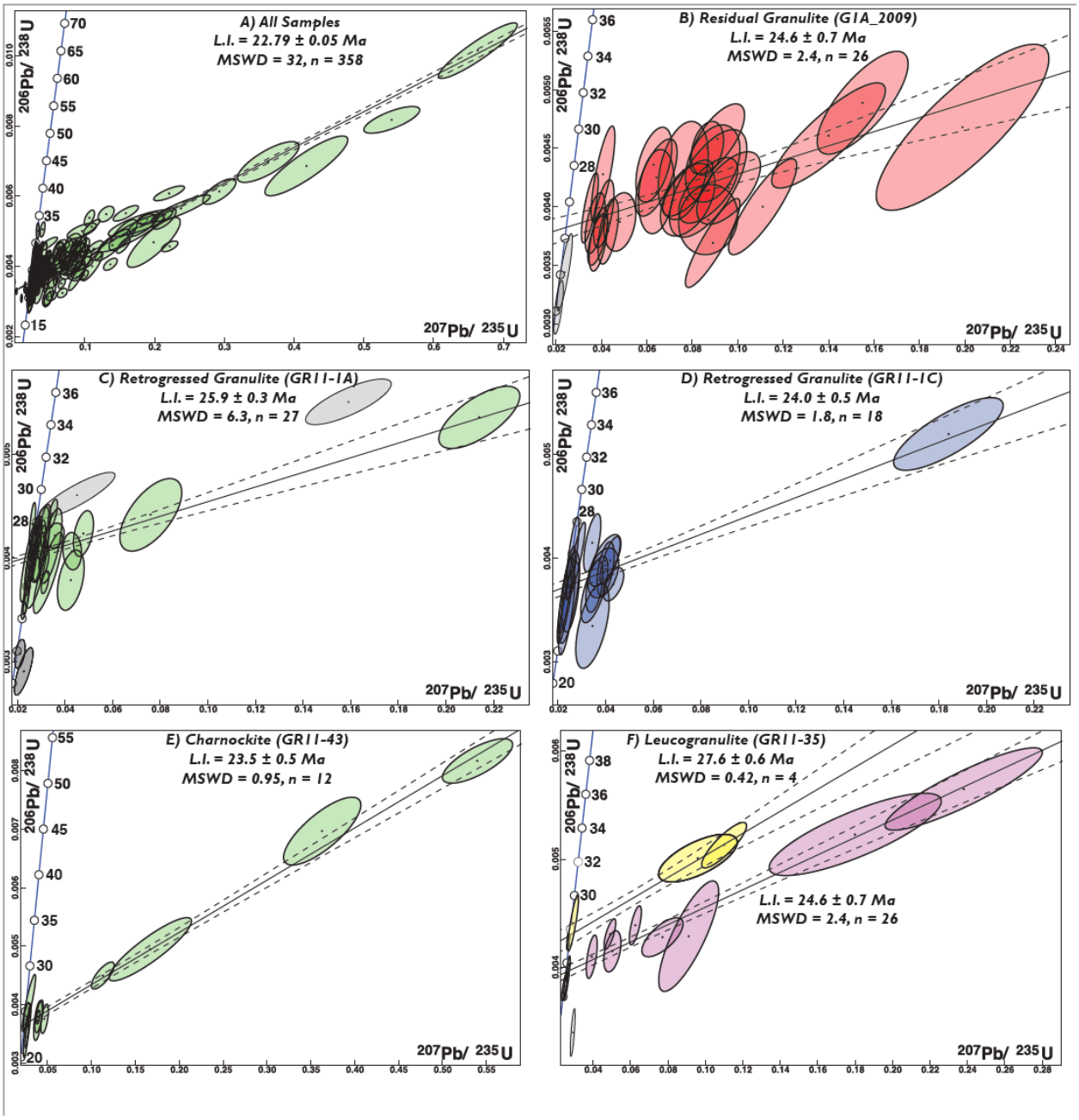
A) All Samples
L.I. = 22.79 ± 0.05 Ma
MSWD = 32, n = 358
B) Residual Granulite (G1A_2009)
L.I. = 24.6 ± 0.7 Ma
MSWD = 2.4, n = 26
C) Retrogressed Granulite (GR11-1A)
L.I. = 25.9 ± 0.3 Ma
MSWD = 6.3, n = 27
D) Retrogressed Granulite (GR11-1C)
L.I. = 24.0 ± 0.5 Ma
MSWD = 1.8, n = 18
E) Charnockite (GR11-43)
L.I. = 23.5 ± 0.5 Ma
MSWD = 0.95, n = 12
F) Leucogranulite (GR11-35)
L.I. = 27.6 ± 0.6 Ma
MSWD = 0.42, n = 4
L.I. = 24.6 ± 0.7 Ma
MSWD = 2.4, n = 26
206Pb/ 238U
207Pb/ 235U

Figure 2.6

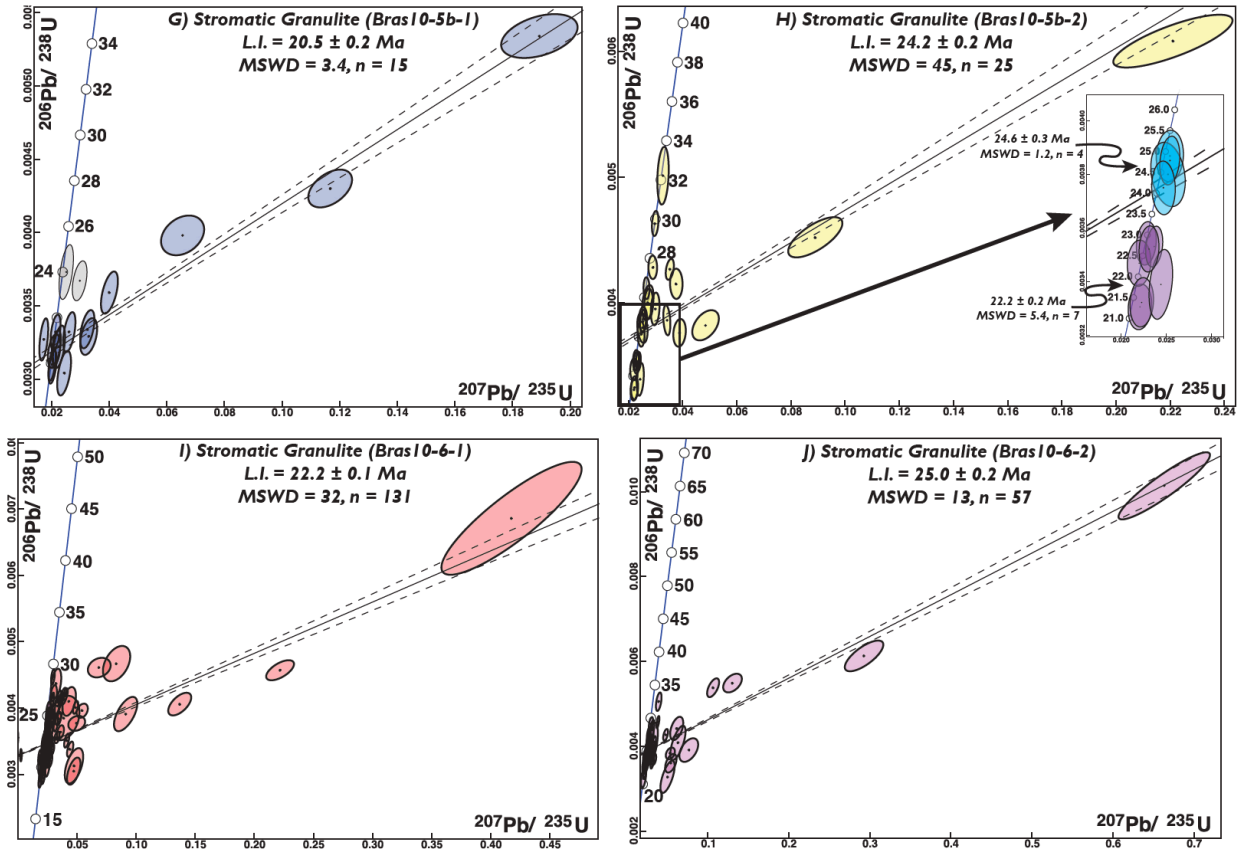

Figure 2.6 (continued)

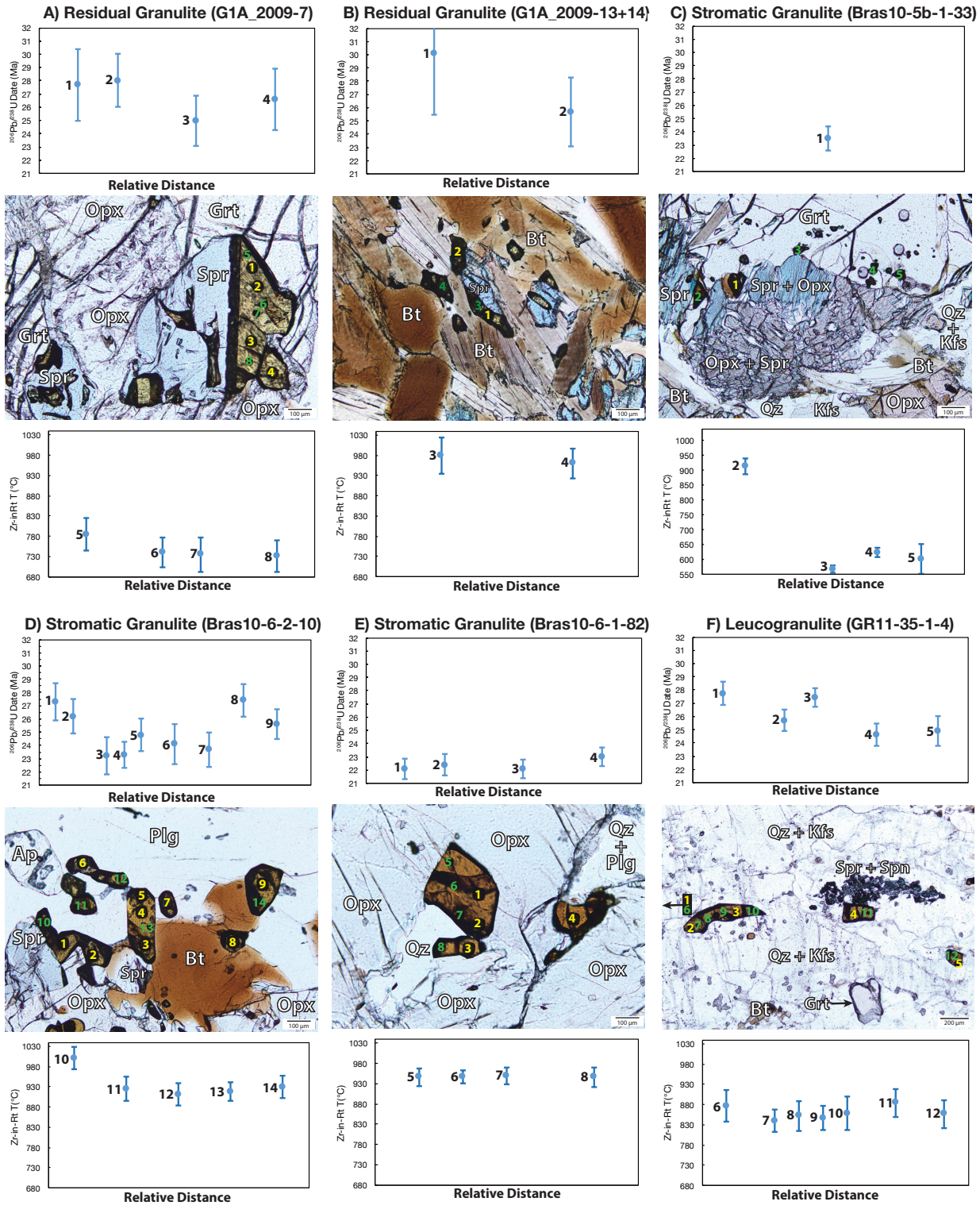
A) Residual Granulite (G1A_2009-7)
B) Residual Granulite (G1A_2009-13+14)
C) Stromatic Granulite (Bras10-5b-1-33)
D) Stromatic Granulite (Bras10-6-2-10)
E) Stromatic Granulite (Bras10-6-1-82)
F) Leucogranulite (GR11-35-1-4)
Relative Distance
Zr-in-Rt T (°C)
Opx
Grt
Spr
Bt
Plg
Ap
Qz
Kfs
Spr + Opx
Opx + Spr
Qz + Kfs
Spr + Spn

Figure 2.7

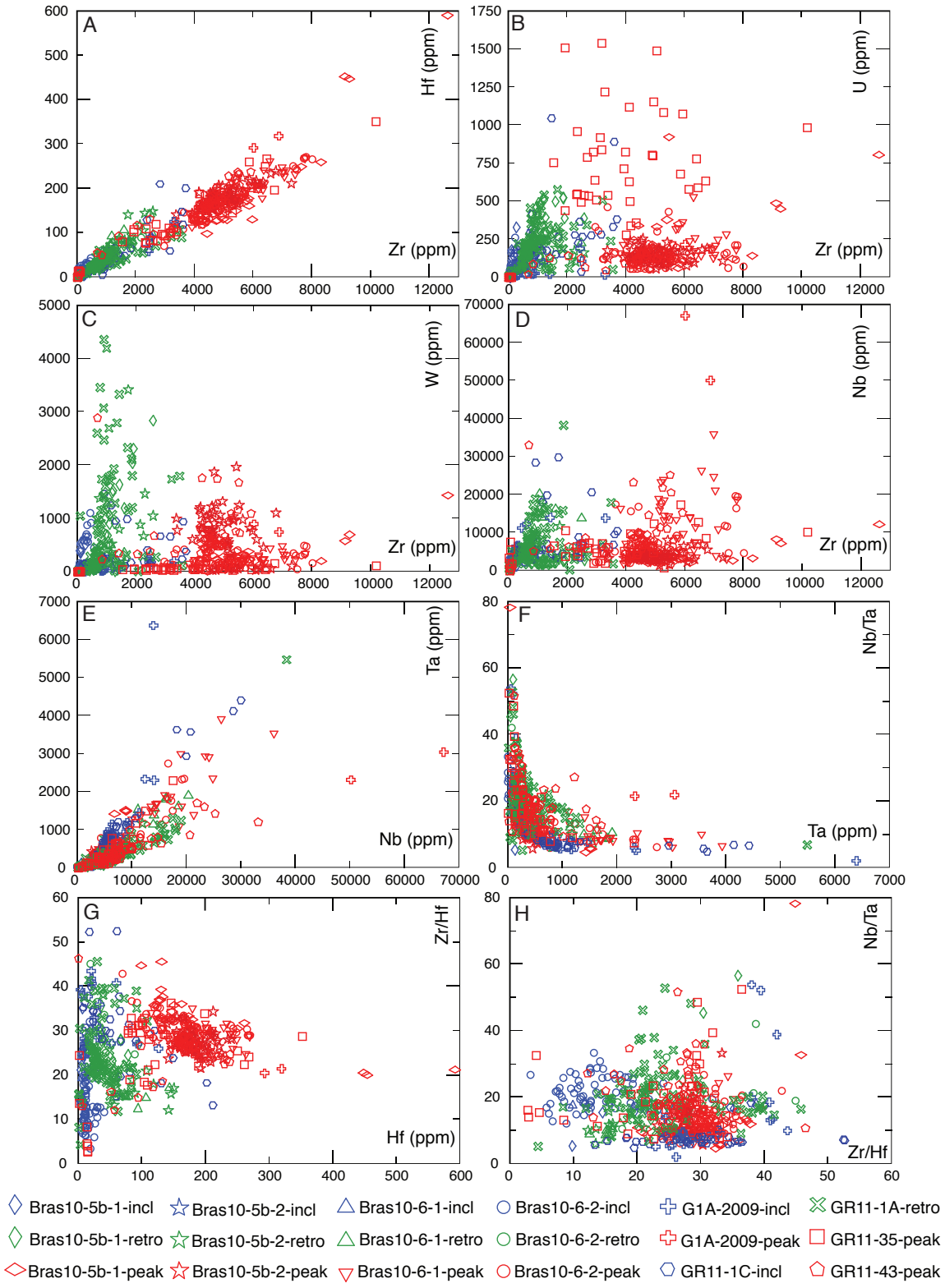
A
Hf (ppm)
Zr (ppm)
B
U (ppm)
Zr (ppm)
C
W (ppm)
Zr (ppm)
D
Nb (ppm)
Zr (ppm)
E
Ta (ppm)
Nb (ppm)
F
Nb/Ta
Ta (ppm)
G
Zr/Hf
Hf (ppm)
H
Nb/Ta
Zr/Hf
Bras10-5b-1-incl
Bras10-5b-2-incl
Bras10-6-1-incl
Bras10-6-2-incl
G1A-2009-incl
GR11-1A-retro
Bras10-5b-1-retro
Bras10-5b-2-retro
Bras10-6-1-retro
Bras10-6-2-retro
G1A-2009-peak
GR11-35-peak
Bras10-5b-1-peak
Bras10-5b-2-peak
Bras10-6-1-peak
Bras10-6-2-peak
GR11-1C-incl
GR11-43-peak

Figure 2.8

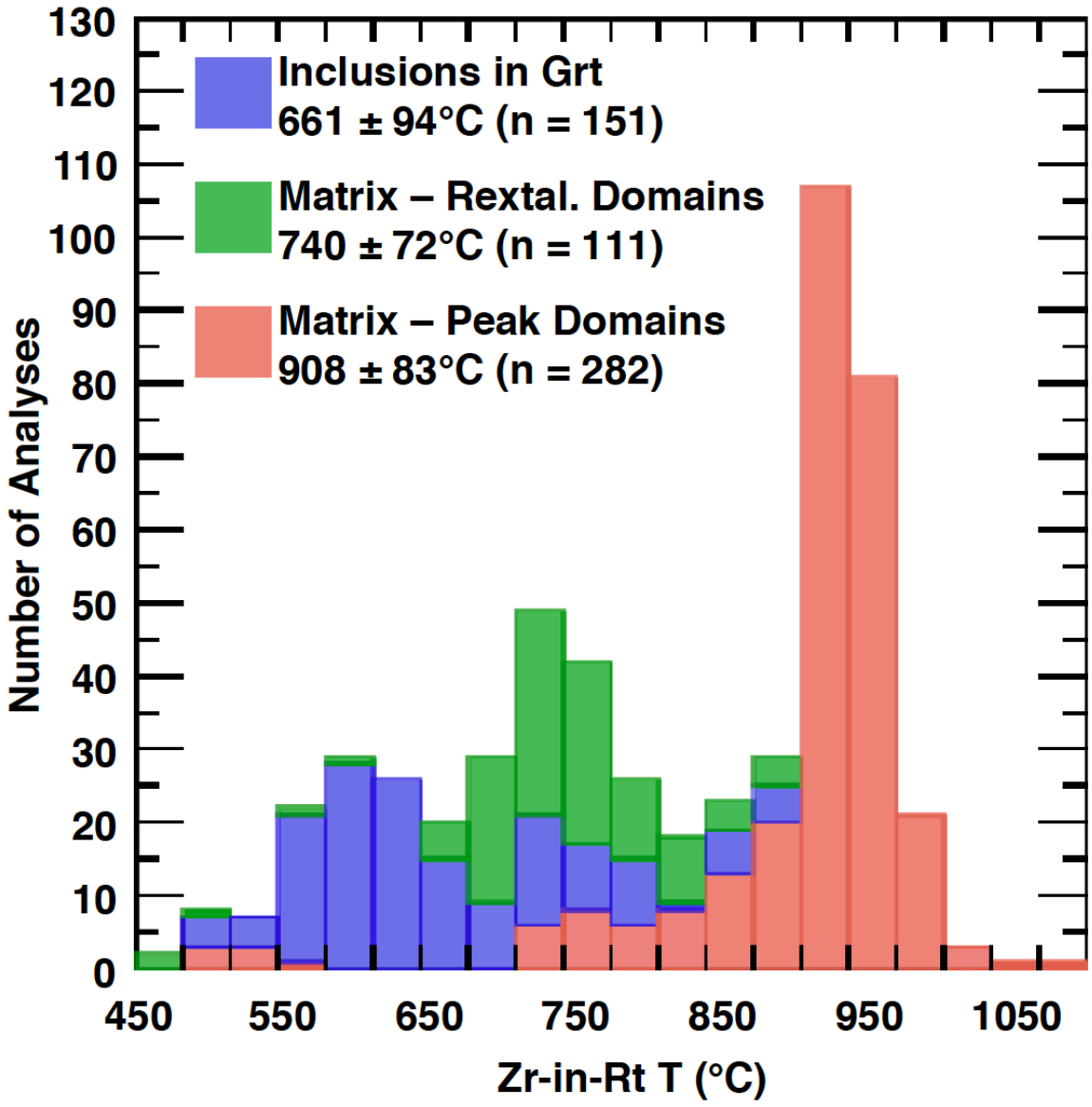
Inclusions in Grt
661 ± 94°C (n = 151)
Matrix – Rextal. Domains
740 ± 72°C (n = 111)
Matrix – Peak Domains
908 ± 83°C (n = 282)
Number of Analyses
0
10
20
30
40
50
60
70
80
90
100
110
120
130
450
550
650
750
850
950
1050
Zr-in-Rt T (°C)

Figure 2.9

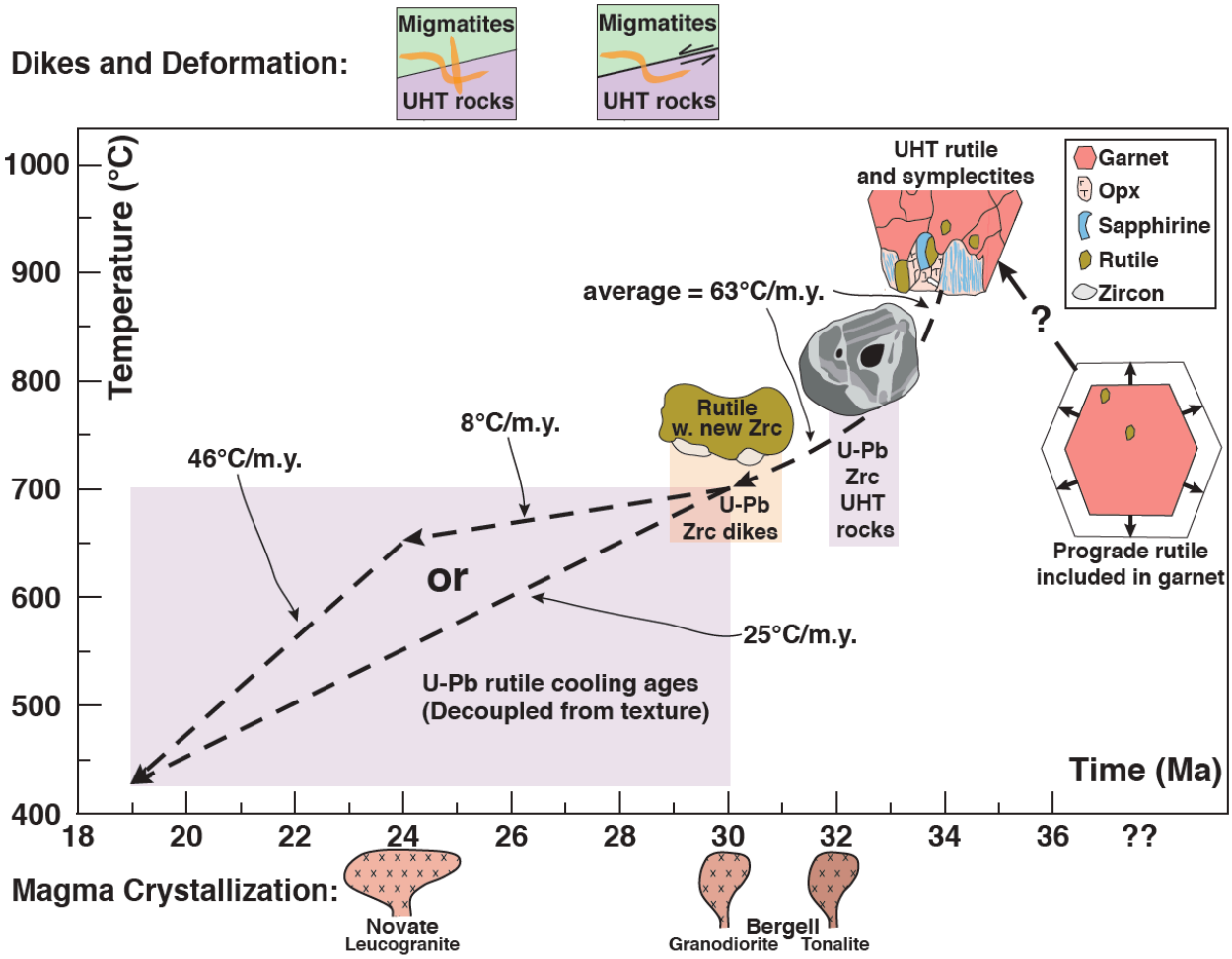
Dikes and Deformation:
Migmatites
UHT rocks
Migmatites
UHT rocks
Temperature (°C)
1000
900
800
700
600
500
400
18
20
22
24
26
28
30
32
34
36
??
Time (Ma)
UHT rutile
and symplectites
Garnet
Opx
Sapphirine
Rutile
Zircon
average = 63°C/m.y.
?
Rutile
w. new Zrc
U-Pb
Zrc
UHT
rocks
U-Pb
Zrc dikes
8°C/m.y.
46°C/m.y.
or
25°C/m.y.
U-Pb rutile cooling ages
(Decoupled from texture)
Prograde rutile
included in garnet
Magma Crystallization:
Novate
Leucogranite
Granodiorite
Bergell
Tonalite

Figure 2.10

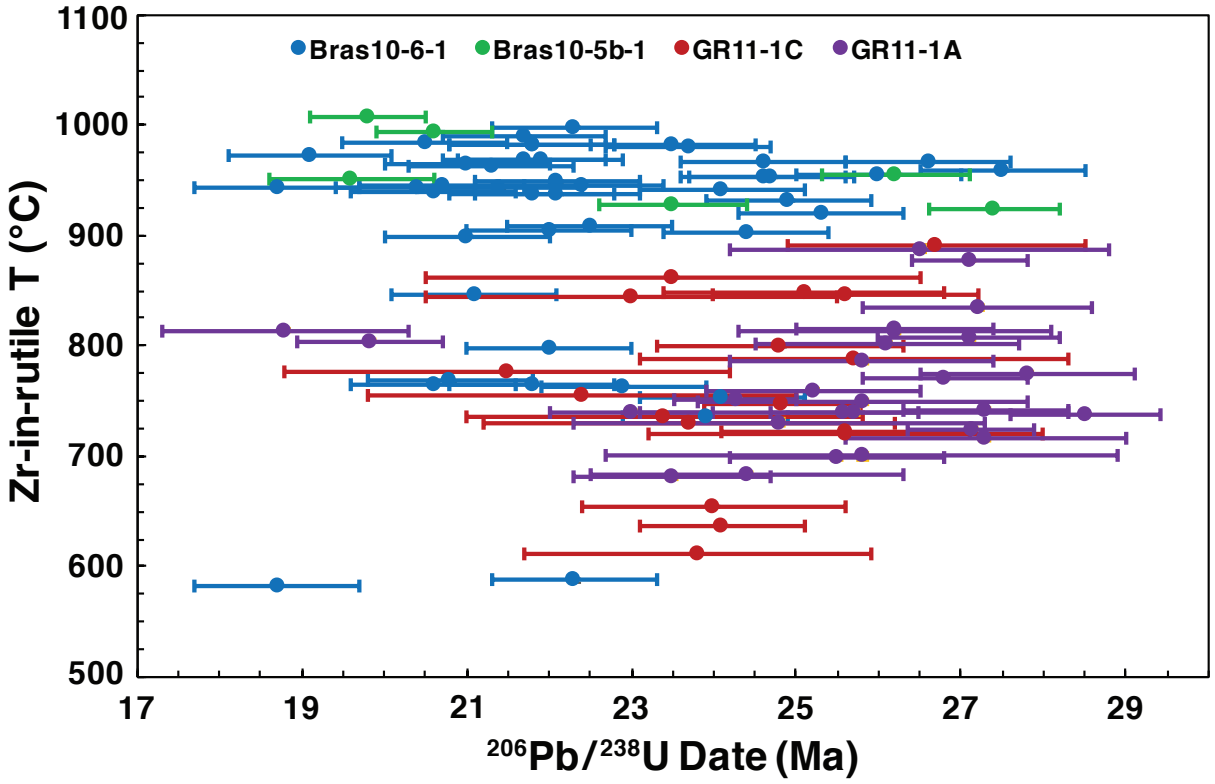
Bras10-6-1
Bras10-5b-1
GR11-1C
GR11-1A
Zr-in-rutile T (°C)
1100
1000
900
800
700
600
500
17
19
21
23
25
27
29
206Pb/238U Date (Ma)

Figure 2.11

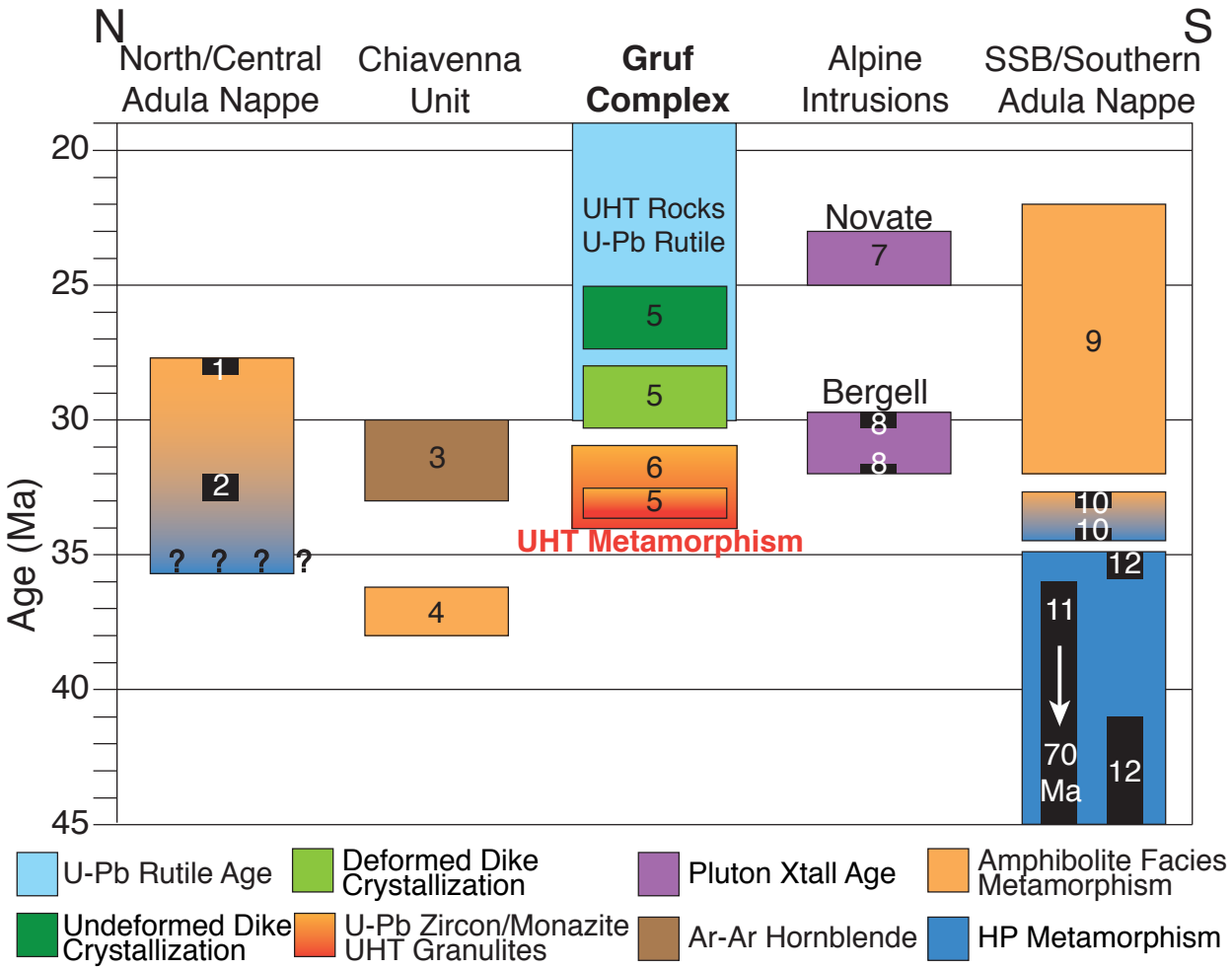
N
S
North/Central Adula Nappe
Chiavenna Unit
Gruf Complex
Alpine Intrusions
SSB/Southern Adula Nappe
Age (Ma)
20
25
30
35
40
45
UHT Rocks U-Pb Rutile
5
5
6
5
UHT Metamorphism
Novate
7
Bergell
8
8
9
10
10
12
11
70 Ma
12
1
2
? ? ? ?
3
4
U-Pb Rutile Age
Deformed Dike Crystallization
Undeformed Dike Crystallization
U-Pb Zircon/Monazite UHT Granulites
Pluton Xtall Age
Ar-Ar Hornblende
Amphibolite Facies Metamorphism
HP Metamorphism

Figure 2.12

Table 2.1. LA-ICP-MS Analytical Methods

Laboratory & Sample Preparation	
Laboratory name	The University of Kansas, Dept. of Geology, Isotope Geochemistry Lab
Sample type/mineral	Rutile
Sample preparation	40 µm-thick, polished sections
Imaging	Petrographic microscope
Laser ablation system	
Make, model & type	ATL Arf excimer laser (193 nm), Photon Machines Analyte
Ablation cell & volume	Large volume 'Frames Cell' with teardrop-shaped insert
Laser wavelength	193 nm
Pulse width (ns)	5 ns
Fluence	3.7 J/cm^2
Repetition rate	10 Hz
Spot size (um)	Trace elements: 22 µm; U-Pb: 36 µm
Sampling mode / pattern	Single spots
Carrier gas	He, 0.4 l/min, Ar, 1.2 l/min
Ablation duration	30 s
Cell carrier gas flow	He, 0.4 l/min
ICP-MS Instrument	
Make, Model & type	Thermo Element2 magnetic sector field ICP-MS (single collector)
Sample introduction	Aerosol with sample + He was mixed with Ar using a Y-connector 15 cm upstream from torch. For some samples, a cyclonic spray chamber was attached at the inlet of the torch (downstream from the T-connector to improve stability of the aerosol introduction.
RF power	1100–1350 W
Make-up gas flow	Ar, 1.2 l/min
Sampling depth	20 µm
Detection system	single detector (SEM), counting & analog modes
Elements/ isotopes analyzed	Trace elements: 29Si, 49Ti, 51V, 53Cr, 90Zr, 93Nb, 95Mo, 118Sn, 120Sn, 121Sb, 178Hf, 181Ta, 184W, 206Pb, 208Pb, 232Th, 238U; U-Pb: 202Hg, 204Pb, 206Pb, 207Pb, 208Pb, 232Th, 235U, 238U
Integration time per peak (Sample Time)	Trace elemets: 5 ms for all isotopes; U-Pb: 202=1 ms, 204=1 ms, 206=4 ms, 207=4 ms, 208=2 ms, 232=2 ms, 235=3 ms, 238=1 ms
Total integration time (Segment Duration)	Trace elements: 4 ms for all isotopes; U-Pb: 202Hg=4 ms, 204Hg/Pb=4 ms, 206Pb=16 ms, 207Pb=16 ms, 208Pb=8 ms, 232Th=8 ms, 235U=12 ms, 238U=4 ms

Table 2.1

Total method time	Trace elements: 1:31 (300 runs, 1 pass); U-Pb: 1:33 (230 runs, 5 passes)
Sensitvity (cps/ppm)	Si=464cps/ppm, Ti=1151cps/ppm, V=1390cps/ppm, Cr=bdl, Zr=1050cps/ppm, Nb=1391cps/ppm, Mo=2186cps/ppm, Sn=6048cps/ppm, Sb=2228cps/ppm, Hf= 2063cps/ppm, Ta=1743cps/ppm, W=2515cps/ppm, Pb=4228cps/ppm, Th=2278cps/ppm, 238U=5136cps/ppm
ICP Dead time	22 ns
UO+/U+	≤0.5%
238U+/232Th+	≤1.7
Data Processing	
Gas blank	Trace elements: 30 s, U-Pb: 10 s
Calibration strategy	Trace elements: standard-sampling bracketing + internal standardization assuming 100% TiO2; U-Pb: standard-sampling bracketing
Reference material info	Trace elements: GSD-1G (Guillong et al., 2005; Jochum et al., 2005); U-Pb: R10 (Luvizotto et al., 2009)
Internal std for trace elements	49Ti
Data processing package used / Correction for LIEF	IGOR PRO, Iolite 2.5 (Patton et al. 2011): Trace elements: TraceElmentsIS data reduction scheme; U-Pb: U_Pb_Geochronology (Paton, et al. 2010) and VizualAge data reduction schemes (Petrus & Kamber, 2011), exponential LIEF correction for U-Pb ratios.
Common-Pb correction, composition and uncertainty	Not performed because of high Hg backgrounds
Uncertainty level & propagation	Trace elements: 2se internal uncertainty; U:Pb: 2se propogated uncertainty from VizualAge data reduction scheme. Concordia diagrams were plotted using ET_Redux (McLean et al. 2016) with 2s uncertainty ellipses.
Reproducibility	Trace elements: 5–7%. U-Pb ratios: 2–4%
Quality control / Validation	Trace elements: R10 and R19 (Luvizotto et al., 2009); U-Pb: R19

Table 2.2. Rutile U-Pb Data

	Isotopic Ratios							Dates (Ma)								Compositions		
Sample and Analysis Number	207Pb/ 235U	±2σ %	206Pb/ 238U	±2σ %	Rho 6/38-7/35	207Pb/ 206Pb	±2σ %	206Pb/ 238U	±2σ abs	207Pb/ 235U	±2σ abs	207Pb/ 206Pb	±2σ abs	% disc a 6/38-7/35	% disc b 6/38-7/6	U (ppm)	Th (ppm)	Th/U
Residual Granulite (G1A_2009)																		
G1A_2009-1a.FIN2	0.043	10.5	0.00379	7.4	0.55	0.0848	9.4	24.4	1.8	42.6	4.4	1300	120	42.7	98.1	50.9	0.000	6.1E-06
G1A_2009-1b.FIN2	0.0481	14.6	0.00387	6.5	0.27	0.09	12.2	24.9	1.6	47.4	6.7	1350	160	47.5	98.2	52.8	0.000	6.1E-06
G1A_2009-1c.FIN2	0.0387	10.6	0.00372	7.3	0.55	0.0746	7.5	24	1.8	38.5	3.9	1049	97	37.7	97.7	65.5	0.001	9.3E-06
G1A_2009-1d.FIN2	0.0383	11.2	0.00372	5.9	0.64	0.0728	9.1	23.9	1.4	38	4.2	1030	110	37.1	97.7	64.3	0.000	3.0E-06
G1A_2009-2.FIN2	0.0867	8.2	0.0045	5.1	0.30	0.141	7.8	28.9	1.5	84.1	6.6	2260	110	65.6	98.7	58.9	0.029	5.0E-04
G1A_2009-3.FIN2	0.155	12.9	0.00489	9.0	0.75	0.222	9.0	31.5	2.8	144	18	3010	110	78.1	99.0	17.2	0.006	3.6E-04
G1A_2009-4a.FIN2	0.091	13.2	0.00458	6.6	0.68	0.148	10.1	29.5	1.9	88	11	2340	150	66.5	98.7	18.9	0.068	3.6E-03
G1A_2009-4b.FIN2	0.078	14.1	0.00416	5.8	0.72	0.131	13.0	26.8	1.5	76	11	2060	160	64.7	98.7	18.9	0.020	1.0E-03
G1A_2009-4c.FIN2	0.087	14.9	0.00414	6.8	0.64	0.146	11.6	26.6	1.8	83	12	2280	130	68.0	98.8	19.1	0.009	4.8E-04
G1A_2009-4d.FIN2	0.089	13.5	0.00437	7.6	0.36	0.146	13.0	28.1	2.1	86	11	2370	150	67.3	98.8	18.6	0.000	5.9E-06
G1A_2009-5.FIN2	0.096	14.6	0.00416	7.5	0.61	0.157	12.1	26.8	2	92	13	2330	130	70.9	98.8	20.5	0.000	2.1E-05
G1A_2009-6.FIN2	0.087	19.5	0.0042	11.0	0.65	0.143	14.7	27	3	83	16	2350	200	67.5	98.9	22.5	0.001	3.6E-05
G1A_2009-7a.FIN2	0.076	14.5	0.00431	9.7	0.34	0.132	12.1	27.7	2.7	73	10	2030	150	62.1	98.6	27.5	0.003	1.2E-04
G1A_2009-7b.FIN2	0.0631	12.5	0.00436	7.3	0.49	0.114	11.4	28	2	61.7	7.4	1790	150	54.6	98.4	29.4	0.003	9.7E-05
G1A_2009-7c.FIN2	0.087	14.9	0.00389	7.7	0.10	0.168	19.0	25	1.9	84	12	2380	170	70.2	98.9	28.4	bdl	-
G1A_2009-7d.FIN2	0.0642	12.3	0.00413	8.7	0.24	0.127	12.6	26.6	2.3	62.8	7.4	2070	190	57.6	98.7	32.6	0.001	3.6E-05
G1A_2009-8.FIN2	0.078	15.4	0.00406	7.6	0.46	0.13	14.6	26.1	2	75	11	2190	190	65.2	98.8	27.4	0.003	1.2E-04
G1A_2009-9a.FIN2	0.0407	12.8	0.00428	9.6	0.78	0.0675	7.4	27.5	2.6	40.4	5.1	909	86	31.9	97.0	76.9	bdl	-
G1A_2009-9b.FIN2	0.0372	11.8	0.00386	6.7	0.55	0.0675	9.2	24.8	1.6	36.9	4.3	883	75	32.8	97.2	71.1	bdl	-
G1A_2009-10.FIN2	0.0642	14.2	0.00425	7.8	0.65	0.102	10.8	27.3	2.1	62.6	8.5	1670	120	56.4	98.4	73.9	bdl	-
G1A_2009-11.FIN2	0.041	11.0	0.00394	7.4	0.59	0.0737	7.1	25.4	1.8	40.6	4.3	1016	92	37.4	97.5	132.3	5.080	3.8E-02
G1A_2009-12.FIN2	0.0349	10.6	0.00399	7.5	0.75	0.0605	6.6	25.7	1.9	34.7	3.6	722	96	25.9	96.4	144.0	1.283	8.9E-03
G1A_2009-13.FIN2	0.199	19.1	0.00468	15.2	0.82	0.286	11.5	30.1	4.6	181	32	3382	77	83.4	99.1	308.0	0.026	8.4E-05
G1A_2009-14.FIN2	0.111	13.5	0.004	10.3	0.86	0.194	7.2	25.7	2.6	106	14	2758	99	75.8	99.1	408.0	0.009	2.2E-05
G1A_2009-15a.FIN2	0.0211	10.0	0.00314	7.3	0.69	0.0484	7.9	20.2	1.5	21.2	2.1	380	70	4.7	94.7	232.0	0.517	2.2E-03
G1A_2009-15b.FIN2	0.0238	14.3	0.00344	9.6	0.85	0.0471	7.6	22.1	2.1	23.8	3.3	298	71	7.1	92.6	231.0	0.098	4.2E-04
G1A_2009-16.FIN2	0.14	17.9	0.00461	9.8	0.86	0.196	10.2	29.6	2.9	133	22	2840	160	77.7	99.0	140.0	10.400	7.4E-02
G1A_2009-17.FIN2	0.089	13.5	0.00369	10.3	0.89	0.184	7.1	23.7	2.4	86	11	2673	92	72.4	99.1	316.0	38.900	1.2E-01
Retrogressed Granulite (GR11-1A)																		
GR111A-1.FIN2	0.0316	5.1	0.00377	2.9	0.57	0.0607	4.3	24.27	0.74	31.6	1.6	583	60	23.2	95.8	573.0	1.890	3.3E-03
GR111A-2.FIN2	0.0309	3.2	0.00421	2.6	0.34	0.0536	3.4	27.1	0.7	30.9	1	344	50	12.3	92.1	646.0	0.780	1.2E-03
GR111A-8.FIN2	0.0348	5.7	0.00443	3.2	0.66	0.0566	4.6	28.52	0.91	34.7	2	456	55	17.8	93.7	291.0	1.170	4.0E-03
GR111A-17.FIN2	0.0239	6.3	0.00365	5.2	0.79	0.0468	3.8	23.5	1.2	24	1.5	114	35	2.1	79.4	1000.0	bdl	-
GR111A-18.FIN2	0.029	3.8	0.00425	3.8	0.50	0.049	4.1	27.3	1	29.2	1.1	238	54	6.5	88.5	198.0	2.010	1.0E-02
GR111A-22.FIN2	0.0424	13.2	0.00379	7.7	0.41	0.084	14.3	24.4	1.9	42.1	5.5	1260	270	42.0	98.1	126.1	0.003	2.8E-05
GR111A-23a.FIN2	0.0274	5.1	0.00416	3.8	0.71	0.0482	3.5	26.8	1	27.4	1.4	133	27	2.2	79.8	335.0	bdl	-
GR111A-23b.FIN2	0.0232	6.5	0.00357	4.5	0.76	0.0471	4.9	23	1	23.3	1.5	140	43	1.3	83.6	486.0	bdl	-
GR111A-24.FIN2	0.0312	8.7	0.00425	6.4	0.62	0.0512	6.8	27.3	1.7	31.2	2.7	342	88	12.5	92.0	186.4	bdl	-
GR111A-25.FIN2	0.0247	6.1	0.00391	5.1	0.83	0.0463	3.0	25.2	1.3	24.8	1.4	140	33	-1.6	82.0	654.0	bdl	-
GR111A-27.FIN2	0.0288	4.9	0.00421	4.0	0.73	0.0503	3.6	27.1	1.1	28.8	1.4	258	49	5.9	89.5	299.0	bdl	-
GR111A-28.FIN2	0.0262	5.7	0.00396	5.1	0.61	0.0485	4.5	25.5	1.3	26.3	1.4	229	44	3.0	88.9	256.0	bdl	-
GR111A-28.FIN2	0.0283	7.8	0.00442	5.2	0.42	0.0468	7.1	28.5	1.5	28.3	2.2	175	52	-0.7	83.7	365.0	bdl	-
GR111A-28.FIN2	0.0226	17.3	0.00291	7.9	0.76	0.0558	12.7	18.8	1.5	22.7	3.9	440	110	17.2	95.7	128.0	bdl	-
GR111A-32.FIN2	0.0292	9.6	0.00407	7.4	0.57	0.0527	8.2	26.2	1.9	29.2	2.8	374	93	10.3	93.0	231.0	bdl	-
GR111A-35.FIN2	0.0477	8.8	0.00424	5.2	0.41	0.085	8.5	27.2	1.4	47.2	4.1	1190	170	42.4	97.7	392.0	bdl	-
GR111A-37a.FIN2	0.0311	6.8	0.00398	3.5	0.41	0.0571	5.6	25.58	0.9	31.1	2	496	70	17.7	94.8	244.8	bdl	-
GR111A-37b.FIN2	0.159	11.3	0.00551	4.0	0.78	0.206	8.7	35.4	1.4	148	15	2870	130	76.1	98.8	226.0	bdl	-

	Isotopic Ratios							Dates (Ma)								Compositions		
Sample and Analysis Number	207Pb/ 235U	±2σ %	206Pb/ 238U	±2σ %	Rho 6/38-7/35	207Pb/ 206Pb	±2σ %	206Pb/ 238U	±2σ abs	207Pb/ 235U	±2σ abs	207Pb/ 206Pb	±2σ abs	% disc a 6/38-7/35	% disc b 6/38-7/6	U (ppm)	Th (ppm)	Th/U
GR111A-38.FIN2	0.045	35.6	0.00461	4.8	0.87	0.061	21.3	29.7	1.4	44	14	480	180	32.5	93.8	226.0	bdl	-
GR111A-39.FIN2	0.034	13.8	0.00412	8.7	0.68	0.0583	8.1	26.5	2.3	33.9	4.6	620	110	21.8	95.7	303.0	bdl	-
GR111A-40.FIN2	0.0263	4.9	0.00433	4.8	0.65	0.0449	4.5	27.8	1.3	26.3	1.3	123	35	-5.7	77.4	303.0	bdl	-
GR111A-41.FIN2	0.0328	18.6	0.00386	10.1	0.84	0.0597	10.2	24.8	2.5	32.7	5.9	600	180	24.2	95.9	198.0	bdl	-
GR111A-42.FIN2	0.214	7.9	0.00536	5.6	0.69	0.302	6.0	34.5	1.9	198	15	3465	83	82.6	99.0	231.0	bdl	-
GR111A-43a.FIN2	0.0261	6.5	0.00406	6.4	0.94	0.04695	2.0	26.1	1.6	26.1	1.7	84	18	0.0	68.9	691.0	bdl	-
GR111A-50.FIN2	0.0282	18.8	0.00401	12.2	0.69	0.0513	13.8	25.8	3.1	28.2	5.2	320	140	8.5	91.9	237.0	bdl	-
GR111A-52.FIN2	0.0286	9.1	0.00401	6.0	0.67	0.0533	6.9	25.8	1.6	28.5	2.5	402	82	9.5	93.6	165.0	bdl	-
GR111A-57.FIN2	0.0265	6.4	0.00397	5.0	0.70	0.0486	4.1	25.5	1.3	26.5	1.7	207	42	3.8	87.7	253.0	bdl	-
GR111A-59a.FIN2	0.0358	10.6	0.00422	2.8	0.22	0.0615	10.6	27.12	0.76	35.7	3.7	740	210	24.0	96.3	367.0	bdl	-
GR111A-59b.FIN2	0.0253	16.2	0.00399	10.3	0.84	0.0457	9.8	25.7	2.6	25.4	4	159	74	-1.2	83.8	580.0	bdl	-
GR111A-59c.FIN2	0.0258	8.9	0.00401	7.7	0.81	0.0484	4.8	25.8	2	25.9	2.3	167	31	0.4	84.6	505.0	bdl	-
GR111A-60.FIN2	0.076	17.1	0.00442	7.9	0.61	0.124	12.9	28.4	2.2	73	12	1960	210	61.1	98.6	106.6	bdl	-
GR111A-79b.FIN2	0.043	9.1	0.00407	4.4	-0.08	0.0792	11.1	26.2	1.2	42.7	3.7	1140	200	38.6	97.7	129.0	bdl	-
GR111A-81.FIN2	0.0287	3.8	0.00456	4.2	0.39	0.0467	4.3	29.4	1.2	28.8	1.1	126	53	-2.1	76.7	361.0	bdl	-
GR111A-81.FIN2	0.026	5.4	0.004	5.0	0.73	0.0468	3.6	25.7	1.3	26.1	1.4	179	42	1.5	85.6	266.0	bdl	-
GR111A-81.FIN2	0.021	10.5	0.00308	4.5	0.44	0.0517	10.3	19.83	0.88	21.1	2.2	330	110	6.0	94.0	164.3	bdl	-
Retrogressed Granulite (GR11-1C)																		
GR11-1C36-1.FIN2	0.0235	16.2	0.00365	12.9	0.86	0.0469	8.3	23.5	3	23.5	3.8	293	64	0.0	92.0	435.0	0.000	8.3E-07
GR11-1C36-3.FIN2	0.0254	5.9	0.00386	3.9	0.29	0.0481	4.8	24.83	0.94	25.4	1.4	210	46	2.2	88.2	247.0	0.015	6.2E-05
GR11-1C36-6a.FIN2	0.0248	16.1	0.00357	10.9	0.78	0.0478	11.7	23	2.5	24.8	4	411	79	7.3	94.4	373.0	0.029	7.8E-05
GR11-1C36-9.FIN2	0.0419	10.0	0.00398	5.8	0.72	0.0739	7.0	25.6	1.5	41.5	4.1	1030	120	38.3	97.5	193.0	0.334	1.7E-03
GR11-1C36-11.FIN2	0.0433	9.9	0.00375	4.3	0.54	0.0828	8.2	24.1	1	42.9	4.1	1220	110	43.8	98.0	253.0	0.015	6.0E-05
GR11-1C36-12.FIN2	0.0398	16.6	0.00398	6.3	0.65	0.07	15.7	25.6	1.6	39.5	6.4	1020	160	35.2	97.5	55.3	0.449	8.1E-03
GR11-1C36-13.FIN2	0.184	12.5	0.0052	6.7	0.78	0.248	8.9	33.4	2.2	169	19	3230	100	80.2	99.0	174.0	1.570	9.0E-03
GR11-1C36-15.FIN2	0.0353	10.2	0.00373	6.7	0.45	0.0687	9.9	24	1.6	35.1	3.5	950	180	31.6	97.5	166.0	0.090	5.4E-04
GR11-1C36-16a.FIN2	0.039	16.7	0.00386	6.2	0.40	0.073	15.1	24.8	1.5	38.6	6.2	1080	260	35.8	97.7	227.0	0.003	1.5E-05
GR11-1C36-17a.FIN2	0.0237	14.3	0.00348	11.8	0.76	0.0525	10.3	22.4	2.6	23.7	3.4	352	78	5.5	93.6	313.0	0.082	2.6E-04
GR11-1C36-17b.FIN2	0.0353	16.1	0.0037	8.6	0.66	0.0685	10.1	23.8	2.1	35	5.5	920	160	32.0	97.4	176.0	0.218	1.2E-03
GR11-1C36-18d.FIN2	0.0345	20.3	0.00335	12.2	0.56	0.0619	12.8	21.5	2.7	34.2	6.8	950	260	37.1	97.7	370.0	0.070	1.9E-04
GR11-1C36-22.FIN2	0.026	10.8	0.004	10.0	0.80	0.048	6.3	25.7	2.6	26.1	2.8	236	44	1.5	89.1	1434.0	0.000	1.5E-07
GR11-1C36-23.FIN2	0.0231	12.6	0.00364	10.2	0.83	0.0487	7.2	23.4	2.4	23.1	2.9	310	51	-1.3	92.5	373.0	0.089	2.4E-04
GR11-1C36-24.FIN2	0.0276	14.1	0.00398	9.3	0.89	0.0476	7.1	25.6	2.4	27.6	3.8	282	52	7.2	90.9	413.0	0.129	3.1E-04
GR11-1C36-25.FIN2	0.0254	14.6	0.00368	10.6	0.51	0.0531	13.2	23.7	2.5	25.4	3.7	410	110	6.7	94.2	638.0	0.014	2.1E-05
GR11-1C36-26.FIN2	0.04	9.0	0.0039	6.7	0.51	0.0735	7.9	25.1	1.7	39.7	3.5	1055	60	36.8	97.6	190.0	0.672	3.5E-03
GR11-1C36-27.FIN2	0.0344	10.5	0.00415	6.7	0.64	0.0568	6.3	26.7	1.8	34.2	3.6	514	75	21.9	94.8	1103.0	0.028	2.5E-05
Leucogranulite (GR11-35)																		
GR11-35-1.FIN2	0.0489	6.3	0.00431	3.2	0.73	0.0801	3.9	27.75	0.88	47.7	2.7	1188	63	41.8	97.7	1063.0	0.367	3.5E-04
GR11-35-2A.FIN2	0.0266	4.1	0.00399	3.0	0.75	0.0482	2.7	25.7	0.79	26.7	1.1	139	27	3.7	81.5	740.0	0.000	6.5E-08
GR11-35-2B.FIN2	0.11	10.9	0.00513	4.1	0.85	0.152	7.9	33	1.4	105	11	2290	130	68.6	98.6	745.0	0.434	5.8E-04
GR11-35-2C.FIN2	0.0268	3.4	0.00427	2.6	0.73	0.0464	2.4	27.45	0.7	26.85	0.89	106	26	-2.2	74.1	745.0	0.001	1.9E-06
GR11-35-3.FIN2	0.0247	6.1	0.00383	3.4	0.81	0.0465	3.7	24.62	0.86	24.7	1.5	137	24	0.3	82.0	1022.0	0.000	2.5E-07
GR11-35-4.FIN2	0.0257	6.2	0.00387	4.4	0.83	0.0466	3.0	24.9	1.1	25.7	1.6	113	20	3.1	78.0	1269.0	0.000	8.0E-08
GR11-35-6.FIN2	0.0502	9.2	0.00415	4.6	0.42	0.0872	7.8	26.7	1.2	49.6	4.4	1390	140	46.2	98.1	1007.0	1.080	1.1E-03
GR11-35-15.FIN2	0.0392	7.4	0.0041	4.9	0.57	0.0679	5.7	26.4	1.3	39	2.8	804	80	32.3	96.7	1181.0	bdl	-
GR11-35-16.FIN2	0.096	21.9	0.00501	4.4	0.67	0.127	18.9	32.2	1.4	91	18	1880	300	64.6	98.3	1415.0	bdl	-
GR11-35-18.FIN2	0.0291	4.5	0.0034	6.5	0.71	0.0633	4.1	21.9	1.4	29.1	1.3	744	49	24.7	97.1	1164.0	1.090	9.4E-04
GR11-35-22.FIN2	0.238	17.6	0.00565	6.7	0.89	0.302	12.9	36.3	2.4	212	34	3420	210	82.9	98.9	737.0	35.400	4.8E-02
GR11-35-25.FIN2	0.0625	5.1	0.00439	4.1	0.69	0.1039	4.0	28.3	1.2	62	3.2	1709	60	54.4	98.3	1462.0	bdl	-

	Isotopic Ratios							Dates (Ma)								Compositions		
Sample and Analysis Number	207Pb/ 235U	±2σ %	206Pb/ 238U	±2σ %	Rho 6/38-7/35	207Pb/ 206Pb	±2σ %	206Pb/ 238U	±2σ abs	207Pb/ 235U	±2σ abs	207Pb/ 206Pb	±2σ abs	% disc a 6/38-7/35	% disc b 6/38-7/6	U (ppm)	Th (ppm)	Th/U
GR11-35-38.FIN2	0.18	25.6	0.00523	7.3	0.81	0.236	20.8	33.6	2.4	168	40	2740	420	80.0	98.8	1116.0	10.700	9.6E-03
GR11-35-40.FIN2	0.0293	9.9	0.00441	5.9	0.86	0.047	6.0	28.4	1.7	29.3	2.9	162	44	3.1	82.5	1169.0	0.000	2.5E-07
GR11-35-41.FIN2	0.077	14.3	0.00428	4.2	0.69	0.137	12.4	27.5	1.1	75	10	1970	230	63.3	98.6	2145.0	2.820	1.3E-03
GR11-35-50.FIN2	0.091	17.6	0.00429	11.9	0.81	0.157	12.1	27.6	3.2	88	15	2410	130	68.6	98.9	1380.0	1.960	1.4E-03
Charnockite (GR11-43)																		
GR11-43-1	0.113	11.5	0.0045	5.1	0.76	0.182	8.8	28.9	1.5	110	12	2690	120	73.7	98.9	193.0	0.010	5.0E-05
GR11-43-8	0.0279	12.2	0.00364	10.4	0.85	0.0558	7.0	23.4	2.4	27.9	3.4	545	89	16.1	95.7	166.0	0.000	-4.0E-08
GR11-43-12	0.0391	12.5	0.00373	9.1	0.57	0.0789	10.3	24	2.2	38.8	4.7	1213	96	38.1	98.0	268.0	0.000	2.6E-07
GR11-43-29	0.0393	4.8	0.00379	3.2	0.49	0.0762	4.7	24.38	0.79	39.1	1.9	1096	68	37.6	97.8	172.1	0.000	3.4E-07
GR11-43-30	0.0404	11.6	0.0038	7.4	0.66	0.0729	8.6	24.5	1.8	40.1	4.6	970	110	38.9	97.5	175.1	0.000	1.4E-07
GR11-43-31	0.54	7.4	0.00817	4.7	0.74	0.484	5.0	52.5	2.4	438	27	4233	35	88.0	98.8	174.9	bdl	-
GR11-43-34a	0.0255	11.8	0.00345	10.1	0.73	0.0548	7.7	22.2	2.2	25.5	3	473	51	12.9	95.3	183.0	0.000	1.0E-08
GR11-43-36	0.0263	14.1	0.0038	6.3	0.63	0.0536	12.5	24.4	1.5	26.3	3.7	400	100	7.2	93.9	105.2	0.001	4.9E-06
GR11-43-40	0.0467	9.2	0.00376	6.6	0.56	0.0963	8.9	24.2	1.6	46.2	4.2	1530	120	47.6	98.4	196.3	0.000	5.6E-07
GR11-43-41b	0.167	28.1	0.00495	10.9	0.89	0.204	18.6	31.8	3.5	139	34	2600	300	77.1	98.8	200.0	0.000	5.0E-07
GR11-43-49	0.363	12.1	0.00697	8.3	0.77	0.357	8.4	44.8	3.7	307	33	3792	82	85.4	98.8	179.0	0.004	2.2E-05
GR11-43-50	0.0288	26.4	0.00403	12.2	0.89	0.0469	15.6	25.9	3.1	28.7	7.5	290	110	9.8	91.1	131.0	bdl	-
Bras10-5a-1 (Stromatic Granulite)																		
Bras105a1-1	0.06039	7.7	0.00366	5.1	0.66	0.11966	5.8	23.6	1.2	59.6	4.5	1951.1	107.4	60.4	98.8	121.7	nd	-
Bras105a1-2	0.06793	10.3	0.00324	4.1	0.40	0.15207	9.5	20.8	0.9	66.7	6.7	2369.4	171.9	68.8	99.1	135.7	nd	-
Bras105a1-3	0.02716	8.9	0.00308	4.4	0.49	0.06396	7.7	20.3	0.9	27.9	2.5	740.2	171.9	27.2	97.3	148.9	nd	-
Bras105a1-4	0.07868	15.0	0.00258	8.7	0.58	0.22117	12.2	16.6	1.4	76.6	11.1	2989.3	211.3	78.3	99.4	120.4	nd	-
Bras105a1-5	0.05246	13.9	0.00316	4.3	0.31	0.1204	13.2	19.8	0.9	50.7	6.9	1962.2	256.5	60.9	99.0	126.3	nd	-
Bras105a1-6	0.09454	7.0	0.00462	4.5	0.64	0.14841	5.4	34.2	1.5	104.8	7	2327.7	95.6	67.4	98.5	112.9	nd	-
Bras105a1-7	0.09891	6.5	0.00375	3.7	0.57	0.1913	5.3	23.8	0.9	94.6	5.9	2753.4	89.8	74.8	99.1	159.7	nd	-
Bras105a1-8	0.10007	6.5	0.00441	4.2	0.65	0.16457	5.0	28.9	1.2	98.7	6.1	2503.2	86.7	70.7	98.8	114.9	nd	-
Bras105a1-9	0.02344	7.4	0.00321	3.4	0.46	0.05296	6.6	20.5	0.7	23.3	1.7	327	157.1	12.0	93.7	204.0	nd	-
Bras105a1-10	0.02825	8.4	0.00349	3.6	0.43	0.05871	7.6	23.2	0.8	29.2	2.4	556.3	175	20.5	95.8	174.3	nd	-
Bras105a1-11	0.05122	5.8	0.00388	2.8	0.48	0.09575	5.1	24.6	0.7	50.1	2.8	1542.9	99	50.9	98.4	277.1	nd	-
Bras105a1-12	0.01955	7.9	0.00298	4.0	0.51	0.04759	6.8	19.9	0.8	20.3	1.6	78.9	78.8	2.0	74.8	196.2	nd	-
Bras105a1-13	0.04667	7.8	0.00409	3.2	0.41	0.08276	7.1	26.1	0.8	46	3.5	1263.7	145.4	43.3	97.9	157.1	nd	-
Bras105a1-14	0.08857	26.0	0.00411	4.9	0.19	0.15629	25.5	26.4	1.3	86.2	21.7	2416	513.7	69.4	98.9	231.8	nd	-
Bras105a1-15	0.03043	6.7	0.00334	2.9	0.43	0.06607	6.0	21.8	0.6	30.9	2	808.7	130.8	29.4	97.3	191.7	nd	-
Bras105a1-16	0.07162	7.1	0.00392	3.8	0.54	0.13251	6.0	25.7	1	71.6	4.9	2131.5	108.9	64.1	98.8	195.9	nd	-
Bras105a1-17	0.15536	6.2	0.00459	4.8	0.77	0.24549	4.0	30.3	1.4	150.1	8.7	3156	65	79.8	99.0	161.8	nd	-
Bras105a1-18	0.06733	7.3	0.00351	4.0	0.55	0.13913	6.1	22.4	0.9	65.5	4.6	2216.4	109.8	65.8	99.0	217.7	nd	-
Bras105a1-19	0.00959	11.9	0.00309	3.8	0.32	0.02251	11.3	20.1	0.8	9.8	1.2	0.1	0	-105.1	-20000.0	231.2	nd	-
Bras105a1-20	0.01447	9.8	0.0034	4.7	0.48	0.03086	8.6	21.2	1	14.1	1.4	0.1	0	-50.4	-21100.0	255.1	nd	-
Bras10-5b-1 (Stromatic Granulite)																		
009_Bras10-5b_4b.txt	0.02979	8.5	0.00367	3.7	0.44	0.05888	7.6	23.5	0.9	29.7	2.5	562.6	174.8	20.9	95.8	136.9	nd	-
010_Bras10-5b_5.txt	0.02262	9.3	0.00322	4.5	0.48	0.05095	8.1	20.6	0.9	22.6	2.1	238.5	198.4	8.8	91.4	115.1	nd	-
012_Bras10-5b_6.txt	0.11672	6.5	0.0043	3.0	0.46	0.19686	5.8	27.4	0.8	111.2	6.9	2800.4	98.2	75.4	99.0	182.1	nd	-
013_Bras10-5b_7.txt	0.02039	6.8	0.00308	3.6	0.53	0.04802	5.8	20.1	0.7	20.8	1.4	100.3	100.2	3.4	80.0	194.8	nd	-
015_Bras10-5b_8a.txt	0.03244	7.6	0.00334	3.9	0.51	0.07044	6.5	21.3	0.8	32.1	2.4	941.2	139.2	33.6	97.7	115.2	nd	-
016_Bras10-5b_8b.txt	0.03292	8.9	0.00329	3.8	0.43	0.07257	8.0	21.2	0.8	32.9	2.9	1001.9	171.5	35.6	97.9	114.1	nd	-
018_Bras10-5b_8c.txt	0.04012	7.3	0.00359	4.0	0.55	0.08105	6.1	23.1	0.9	39.9	2.9	1222.6	124.8	42.1	98.1	114.2	nd	-
019_Bras10-5b-9a.txt	0.02439	9.8	0.00304	5.0	0.51	0.0582	8.4	19.6	1	24.5	2.4	537.4	195.3	20.0	96.4	109.9	nd	-
021_Bras10-5b-9b.txt	0.02619	8.1	0.00332	4.1	0.51	0.05722	7.0	21.1	0.9	25.9	2.1	500	162	18.5	95.8	110.0	nd	-
022_Bras10-5b-10.txt	0.02513	9.9	0.00373	5.0	0.51	0.04886	8.6	23.9	1.2	25.1	2.5	141.3	141.2	4.8	83.1	80.1	nd	-

Isotopic Ratios								Dates (Ma)								Compositions		
Sample and Analysis Number	207Pb/ 235U	±2σ %	206Pb/ 238U	±2σ %	Rho 6/38-7/35	207Pb/ 206Pb	±2σ %	206Pb/ 238U	±2σ abs	207Pb/ 235U	±2σ abs	207Pb/ 206Pb	±2σ abs	% disc a 6/38-7/35	% disc b 6/38-7/6	U (ppm)	Th (ppm)	Th/U
024_Bras10-5b-11.txt	0.06551	11.4	0.00398	3.4	0.30	0.11937	10.9	26.2	0.9	65.9	7.3	1946.9	208.9	60.2	98.7	80.0	nd	-
025_Bras10-5b-12.txt	0.01734	8.8	0.00327	4.4	0.50	0.03845	7.6	20.9	0.9	17.3	1.5	0.1	0	-20.8	-20800.0	120.3	nd	-
027_Bras10-5b-13.txt	0.02168	7.3	0.00322	3.5	0.48	0.04883	6.4	20.7	0.7	21.8	1.6	139.7	139.6	5.0	85.2	182.3	nd	-
028_Bras10-5b-14.txt	0.02023	6.3	0.0031	3.6	0.57	0.04734	5.2	19.8	0.7	20.1	1.3	66.3	66.2	1.5	70.1	201.9	nd	-
030_Bras10-5b-15.txt	0.02143	8.0	0.00332	3.6	0.45	0.04682	7.2	20.7	0.7	20.9	1.7	40	39.9	1.0	48.3	149.9	nd	-
031_Bras10-5b-16.txt	0.02092	10.3	0.00319	3.6	0.35	0.04757	9.7	20.6	0.7	21.1	2.1	78.2	78.1	2.4	73.7	135.6	nd	-
033_Bras10-5b-17.txt	0.18932	7.0	0.00534	2.8	0.40	0.25713	6.4	34.6	1	177.2	11.4	3229.2	104.7	80.5	98.9	144.9	nd	-
Bras10-5b-2 (Stromatic Granulite)																		
Bras105b2-1	0.0328	6.4	0.00501	4.6	0.22	0.0475	7.2	32.2	1.5	32.8	2	194	66	1.8	83.4	280.1	0.000	1.5E-06
Bras105b2-2	0.0299	4.0	0.00463	2.2	0.25	0.0465	4.1	29.75	0.65	29.9	1.2	197	42	0.5	84.9	293.2	0.000	5.1E-07
Bras105b2-3	0.0353	4.2	0.004265	1.9	0.37	0.0606	4.0	27.43	0.54	35.2	1.5	605	56	22.1	95.5	232.7	0.000	5.2E-07
Bras105b2-4	0.029	5.5	0.004281	2.2	-0.03	0.0475	5.9	27.54	0.6	29	1.6	438	68	5.0	93.7	138.9	0.000	2.2E-07
Bras105b2-5	0.221	10.0	0.00608	3.5	0.78	0.256	7.8	39	1.3	200	18	3130	140	80.5	98.8	140.6	0.001	4.0E-06
Bras105b2-6	0.0254	5.9	0.003869	2.5	0.07	0.0489	7.0	24.89	0.62	25.4	1.4	331	68	2.0	92.5	181.8	0.000	6.1E-07
Bras105b2-7	0.0252	7.5	0.0038	3.2	-0.22	0.0469	8.3	24.46	0.77	25.2	1.9	265	57	2.9	90.8	222.3	0.000	2.2E-06
Bras105b2-8	0.089	11.2	0.00452	3.5	0.70	0.138	8.7	29.1	1	86.1	9.3	2120	150	66.2	98.6	191.4	0.004	2.0E-05
Bras105b2-9	0.0254	4.3	0.003852	2.4	0.20	0.0478	4.8	24.78	0.59	25.5	1.1	195	43	2.8	87.3	150.7	0.001	5.8E-06
Bras105b2-10	0.0228	4.8	0.003543	2.3	0.16	0.0461	5.2	22.8	0.52	22.8	1.1	222	53	0.0	89.7	195.2	0.001	3.8E-06
Bras105b2-11	0.0221	5.9	0.003306	2.6	0.12	0.0498	6.0	21.27	0.55	22.1	1.3	354	60	3.8	94.0	211.8	0.000	1.7E-06
Bras105b2-12	0.0485	10.1	0.00382	3.1	0.44	0.0922	9.0	24.56	0.76	47.9	4.7	1450	160	48.7	98.3	189.6	0.001	4.7E-06
Bras105b2-13	0.022	5.9	0.003469	2.5	0.08	0.0468	6.2	22.32	0.55	22.1	1.3	219	54	-1.0	89.8	285.1	0.002	7.7E-06
Bras105b2-14	0.02367	4.0	0.003531	2.2	0.24	0.0491	3.9	22.72	0.49	23.75	0.93	234	39	4.3	90.3	353.7	0.003	9.0E-06
Bras105b2-15	0.0275	5.8	0.00399	3.0	0.08	0.0504	6.2	25.64	0.78	27.6	1.6	362	73	7.1	92.9	150.8	0.004	2.9E-05
Bras105b2-16	0.0389	5.9	0.00376	2.9	0.16	0.0737	5.6	24.16	0.69	39	2.2	1048	62	38.1	97.7	171.9	0.002	1.2E-05
Bras105b2-17	0.0223	5.8	0.003323	2.8	0.12	0.049	5.9	21.39	0.59	22.4	1.3	368	63	4.5	94.2	182.0	0.004	2.4E-05
Bras105b2-18	0.0244	5.3	0.00339	3.8	0.31	0.0515	6.6	21.83	0.86	24.5	1.3	311	73	10.9	93.0	322.2	0.001	3.4E-06
Bras105b2-19	0.0231	4.8	0.003522	2.4	0.11	0.0478	5.0	22.66	0.55	23.2	1.1	292	65	2.3	92.2	310.0	0.005	1.7E-05
Bras105b2-20	0.0247	5.3	0.00375	2.7	-0.04	0.0486	5.3	24.12	0.66	24.8	1.2	274	71	2.7	91.2	332.7	0.004	1.1E-05
Bras105b2-21	0.0342	3.8	0.00386	3.1	-0.27	0.0638	6.4	24.82	0.78	34.1	1.3	769	91	27.2	96.8	254.9	bdl	-
Bras105b2-22	0.0267	4.1	0.004115	2.1	-0.04	0.0467	4.3	26.47	0.56	26.8	1.1	162	36	1.2	83.7	301.2	bdl	-
Bras105b2-23	0.0377	6.1	0.00415	2.9	-0.02	0.0628	6.8	26.72	0.79	37.5	2.3	788	69	28.7	96.6	232.2	0.025	1.1E-04
Bras105b2-24	0.0299	5.4	0.00395	3.3	0.18	0.0566	6.2	25.39	0.82	29.9	1.5	490	81	15.1	94.8	305.8	0.001	2.9E-06
Bras105b2-25	0.0272	7.7	0.004	3.5	0.33	0.0493	7.3	25.73	0.93	27.2	2.1	202	88	5.4	87.3	505.0	bdl	-
Bras10-6-1 (Stromatic Granulite)																		
003Br_1c.txt	0.01877	7.5	0.00291	3.8	0.51	0.04678	6.5	18.7	0.7	18.8	1.4	37.8	37.7	0.5	50.5	263.4	nd	-
004Br_1i.txt	0.0217	5.8	0.00314	3.3	0.57	0.05013	4.8	20.6	0.7	22.2	1.3	201.1	115.4	7.2	89.8	262.2	nd	-
006Br_1r.txt	0.02003	6.5	0.00313	3.7	0.57	0.04641	5.3	20.7	0.8	20.7	1.3	18.8	18.7	0.0	-10.1	261.5	nd	-
007Br_2c.txt	0.02615	5.7	0.00345	3.1	0.54	0.05497	4.8	22	0.7	26	1.5	411	111.1	15.4	94.6	266.1	nd	-
009Br_2r.txt	0.02678	5.7	0.00339	3.1	0.54	0.05729	4.8	22.4	0.7	27.6	1.6	502.9	109.3	18.8	95.5	256.3	nd	-
010Br_2b.txt	0.02784	4.6	0.00342	2.9	0.63	0.05903	3.6	22.1	0.6	28	1.3	568.1	80.3	21.1	96.1	281.4	nd	-
012Br_3a.txt	0.01981	6.5	0.00299	3.4	0.52	0.04805	5.5	19.1	0.6	19.8	1.3	101.9	101.8	3.5	81.3	245.2	nd	-
013Br_3b.txt	0.01915	6.6	0.00302	3.4	0.52	0.04598	5.7	20.1	0.7	19.9	1.3	0.1	0	-1.0	-20000.0	217.1	nd	-
015Br_4c.txt	0.021	5.0	0.00326	2.9	0.58	0.04672	4.1	21.3	0.6	21.4	1.1	35	34.9	0.5	39.1	335.2	nd	-
016Br_4r1.txt	0.02055	5.0	0.00307	2.8	0.56	0.04855	4.1	20.4	0.6	21.4	1.1	126.4	99.5	4.7	83.9	428.7	nd	-
018Br_4r2.txt	0.02063	5.2	0.00322	2.7	0.52	0.04646	4.5	20.4	0.5	20.4	1.1	21.7	21.6	0.0	6.0	396.0	nd	-
019Br_5a.txt	0.0206	4.5	0.00318	2.6	0.58	0.04699	3.7	20.8	0.5	21.1	0.9	48.9	48.8	1.4	57.5	468.7	nd	-
021Br_5b.txt	0.02373	4.7	0.00341	2.6	0.55	0.05048	3.9	22	0.6	23.8	1.1	217.2	92.9	7.6	89.9	439.8	nd	-
022Br_5c.txt	0.02095	4.5	0.00318	2.6	0.58	0.04779	3.7	20.6	0.5	21.2	0.9	88.7	88.6	2.8	76.8	521.9	nd	-
024Br_6.txt	0.0292	4.5	0.00411	3.0	0.67	0.05152	3.3	23.9	0.7	26.4	1.2	264.3	77.5	9.5	91.0	442.1	nd	-

	Isotopic Ratios							Dates (Ma)							Compositions		
Sample and Analysis Number	207Pb/ 235U	±2σ %	206Pb/ 238U	±2σ %	Rho 6/38-7/35	207Pb/ 206Pb	±2σ %	206Pb/ 238U	±2σ abs	207Pb/ 235U	±2σ abs	207Pb/ 206Pb	±2σ abs	% disc a 6/38-7/35	% disc b 6/38-7/6	U (ppm)	Th (ppm)	Th/U
025Br_7.txt	0.02566	3.8	0.00381	2.3	0.61	0.04884	3.0	24.6	0.6	25.8	1	140.1	72	4.7	82.4	637.3	nd	-
027Br_8.txt	0.02087	4.3	0.00323	2.4	0.56	0.04687	3.6	20.6	0.5	20.8	0.9	42.4	42.3	1.0	51.4	525.5	nd	-
028Br_9.txt	0.02161	4.5	0.00322	2.4	0.53	0.04868	3.8	20.8	0.5	21.8	1	132.5	91.9	4.6	84.3	439.0	nd	-
030Br_10.txt	0.02339	4.8	0.00338	2.7	0.56	0.0502	4.0	21.9	0.6	23.6	1.1	204.4	95.5	7.2	89.3	437.9	nd	-
031Br_12.txt	0.05437	8.7	0.00396	2.7	0.31	0.09958	8.3	26.4	0.7	55.7	4.7	1616.2	163.1	52.6	98.4	243.3	nd	-
033Br_13a.txt	0.03577	5.6	0.00392	3.6	0.64	0.06618	4.3	25.3	0.9	35.8	2	812.2	92.6	29.3	96.9	208.1	nd	-
034Br_13b.txt	0.02719	5.8	0.0033	2.3	0.40	0.05975	5.3	21.2	0.5	27.2	1.6	594.6	119.2	22.1	96.4	427.4	nd	-
037Br_14.txt	0.02235	7.1	0.00342	3.4	0.48	0.0474	6.2	22.9	0.8	23.3	1.6	69.5	69.4	1.7	67.1	257.0	nd	-
039Br_15.txt	0.02878	6.5	0.00338	2.7	0.42	0.06176	5.9	21.7	0.6	28.7	1.8	665.7	131.6	24.4	96.7	443.8	nd	-
040Br_16.txt	0.0204	5.3	0.00313	3.3	0.62	0.04728	4.2	20.1	0.7	20.4	1.1	63.5	63.4	1.5	68.3	345.9	nd	-
042Br_17.txt	0.03004	9.6	0.00418	4.0	0.42	0.05212	8.7	26.6	1.1	29.7	2.8	290.8	212	10.4	90.9	142.4	nd	-
043Br_18a.txt	0.02585	8.4	0.00395	3.8	0.45	0.04746	7.5	25.7	1	26.2	2.2	72.7	72.6	1.9	64.6	147.3	nd	-
044Br_18b.txt	0.02818	7.3	0.00385	3.7	0.51	0.05308	6.3	24.7	0.9	28.1	2	332.5	149.6	12.1	92.6	150.9	nd	-
046Br_19.txt	0.02314	4.4	0.0036	2.3	0.52	0.04661	3.7	23.1	0.5	23.2	1	29.5	29.4	0.4	21.7	541.9	nd	-
047Br_20a.txt	0.02209	6.3	0.00329	3.0	0.48	0.0487	5.5	21.3	0.6	22.3	1.4	133.3	133.2	4.5	84.0	285.4	nd	-
048Br_20b.txt	0.02232	6.1	0.00326	2.5	0.41	0.04966	5.6	24.1	0.6	25.7	1.5	179.1	136	6.2	86.5	293.5	nd	-
050Br_21.txt	0.02281	6.3	0.00348	2.4	0.38	0.04753	5.8	22.3	0.5	22.8	1.4	75.8	75.7	2.2	70.6	261.8	nd	-
051Br_22.txt	0.02451	6.4	0.00333	2.5	0.39	0.05338	5.9	21.1	0.5	24.3	1.5	344.9	139.3	13.2	93.9	325.4	nd	-
052Br_23.txt	0.02148	5.0	0.00311	2.5	0.50	0.0501	4.3	20.5	0.5	22.1	1.1	199.8	103	7.2	89.7	353.5	nd	-
054Br_24.txt	0.02095	4.3	0.00329	2.4	0.56	0.04619	3.6	21.3	0.5	21.1	0.9	7.4	7.3	-0.9	-187.8	391.1	nd	-
055Br_25.txt	0.02158	6.4	0.00334	3.2	0.50	0.04687	5.5	21.6	0.7	21.8	1.4	42.6	42.5	0.9	49.3	272.5	nd	-
056Br_26.txt	0.02172	4.2	0.00327	2.1	0.50	0.04818	3.6	21	0.4	21.8	0.9	108.2	87.3	3.7	80.6	357.9	nd	-
058Br_27a.txt	0.02416	4.9	0.00337	2.6	0.53	0.05199	4.1	21.8	0.6	24.4	1.2	285	96.6	10.7	92.4	354.8	nd	-
059Br_27b.txt	0.02958	5.4	0.00447	2.6	0.48	0.04799	4.7	28.2	0.7	29	1.5	98.9	98.8	2.8	71.5	310.8	nd	-
061Br_28.txt	0.02324	5.3	0.00332	2.2	0.42	0.05077	4.8	21.8	0.5	23.8	1.2	230.4	114.9	8.4	90.5	431.7	nd	-
062Br_29a.txt	0.02725	6.4	0.00321	3.1	0.48	0.06156	5.6	21	0.6	27.7	1.7	658.9	124.9	24.2	96.8	236.5	nd	-
063Br_29b.txt	0.03199	5.7	0.00376	3.0	0.53	0.06171	4.8	24.1	0.7	31.9	1.8	664.1	106.3	24.5	96.4	300.9	nd	-
065Br_30.txt	0.023	6.5	0.00335	3.0	0.46	0.0498	5.8	22.3	0.7	23.9	1.5	185.6	140.9	6.7	88.0	243.9	nd	-
066Br_31.txt	0.02291	7.2	0.00338	3.0	0.42	0.04915	6.5	21.7	0.7	23	1.6	154.9	154.8	5.7	86.0	247.4	nd	-
067Br_32.txt	0.02219	6.1	0.00332	3.2	0.52	0.04848	5.2	21	0.7	21.9	1.3	122.6	122.5	4.1	82.9	215.5	nd	-
069Br_33.txt	0.04121	5.2	0.00351	3.0	0.58	0.08515	4.2	21.7	0.6	39.4	2	1319	83.7	44.9	98.4	203.4	nd	-
070Br_34.txt	0.02112	5.8	0.00335	3.2	0.55	0.04572	4.8	21.4	0.7	21	1.2	0.1	0	-1.9	-21300.0	220.3	nd	-
071Br_34b.txt	0.02225	7.4	0.00331	2.9	0.39	0.04876	6.8	21.8	0.6	22.9	1.7	136.3	136.2	4.8	84.0	239.2	nd	-
073Br_35r.txt	0.02258	7.1	0.00331	3.6	0.51	0.04947	6.1	21.6	0.8	23	1.6	170.3	149.1	6.1	87.3	152.0	nd	-
074Br_35c.txt	0.02141	7.1	0.00339	3.6	0.51	0.04581	6.1	21.8	0.8	21.5	1.5	0.1	0	-1.4	-21700.0	152.0	nd	-
075Br_36.txt	0.02555	5.8	0.00367	3.0	0.52	0.0505	5.0	23.5	0.7	25.5	1.5	218.3	120	7.8	89.2	191.2	nd	-
077Br_37.txt	0.02083	8.1	0.00295	3.4	0.42	0.05121	7.3	19.6	0.7	21.6	1.7	250.2	177.3	9.3	92.2	185.8	nd	-
078Br_38a.txt	0.01842	7.3	0.00326	3.4	0.47	0.04097	6.5	20.5	0.7	18.1	1.3	0.1	0	-13.3	-20400.0	183.2	nd	-
079Br_38b.txt	0.02006	6.4	0.00318	2.6	0.41	0.04576	5.9	20.6	0.5	20.3	1.3	0.1	0	-1.5	-20500.0	246.0	nd	-
081Br_39a.txt	0.02762	6.8	0.00344	3.8	0.56	0.05823	5.6	22.8	0.9	28.5	1.9	538.6	127.5	20.0	95.8	167.8	nd	-
082Br_39b.txt	0.02121	8.4	0.00299	4.4	0.52	0.05146	7.1	19.7	0.9	21.8	1.8	261.5	171.8	9.6	92.5	160.9	nd	-
083Br_42.txt	0.02143	6.5	0.0032	3.2	0.49	0.04856	5.7	20.3	0.6	21.2	1.4	126.8	126.7	4.2	84.0	224.9	nd	-
085Br_43a.txt	0.02514	8.5	0.0034	4.7	0.55	0.05363	7.1	22	1	25.4	2.1	355.4	168.9	13.4	93.8	170.1	nd	-
086Br_43b.txt	0.0214	6.3	0.00318	3.6	0.57	0.0488	5.2	20.4	0.7	21.5	1.3	138.5	126.9	5.1	85.3	233.9	nd	-
087Br_44a.txt	0.02479	6.5	0.00378	2.8	0.43	0.04756	5.9	24.1	0.7	24.7	1.6	77.6	77.5	2.4	68.9	239.6	nd	-
089Br_44b.txt	0.02135	5.5	0.00323	2.9	0.53	0.04793	4.7	20.8	0.6	21.5	1.2	96.1	96	3.3	78.4	311.8	nd	-
090Br_45.txt	0.02179	5.0	0.00337	2.8	0.56	0.0469	4.2	21.7	0.6	21.9	1.1	44.3	44.2	0.9	51.0	400.3	nd	-
091Br_46.txt	0.02809	3.9	0.00395	2.3	0.59	0.05158	3.1	25.3	0.6	28	1.1	267	72.7	9.6	90.5	891.9	nd	-
093Br_47.txt	0.02946	5.3	0.00386	2.3	0.43	0.05536	4.8	25.1	0.6	29.8	1.6	426.9	110.7	15.8	94.1	652.1	nd	-

	Isotopic Ratios							Dates (Ma)							Compositions		
Sample and Analysis Number	207Pb/ 235U	±2σ %	206Pb/ 238U	±2σ %	Rho 6/38-7/35	207Pb/ 206Pb	±2σ %	206Pb/ 238U	±2σ abs	207Pb/ 235U	±2σ abs	207Pb/ 206Pb	±2σ abs	% disc a 6/38-7/35	% disc b 6/38-7/6	U (ppm)	Th (ppm)	Th/U
094Br_48a.txt	0.0403	4.5	0.00421	2.1	0.47	0.06943	4.0	27.5	0.6	40.8	1.8	911.7	84.6	32.6	97.0	489.1	nd	-
095Br_48b.txt	0.0388	6.7	0.00418	3.0	0.45	0.06733	6.0	26.3	0.8	37.8	2.5	848.1	130	30.4	96.9	470.8	nd	-
097Br_48c.txt	0.03421	6.5	0.00384	2.7	0.42	0.06462	5.9	25	0.7	34.5	2.2	761.9	129.6	27.5	96.7	538.0	nd	-
098Br_48d.txt	0.0332	5.9	0.00403	3.0	0.51	0.05975	5.1	26	0.8	33.3	1.9	594.8	114.6	21.9	95.6	503.3	nd	-
099Br_49.txt	0.04877	4.5	0.00401	2.4	0.53	0.08821	3.8	26.1	0.6	48.9	2.1	1387.1	74.8	46.6	98.1	511.5	nd	-
101Br_50a.txt	0.03619	4.5	0.00413	2.5	0.56	0.06356	3.7	27.1	0.7	36.8	1.6	726.9	80.5	26.4	96.3	589.2	nd	-
102Br_50b.txt	0.03499	4.9	0.00417	2.3	0.47	0.06085	4.3	27.1	0.6	35.3	1.7	634	95.4	23.2	95.7	586.1	nd	-
103Br_50c.txt	0.04968	14.3	0.00377	3.0	0.21	0.09557	14.0	24	0.7	48.8	6.8	1539.4	289.3	50.8	98.4	189.3	nd	-
104Br_51.txt	0.06877	14.0	0.00461	3.2	0.23	0.10819	13.6	34	1.1	77	10.4	1769.2	271.6	55.8	98.1	190.3	nd	-
106Br_52.txt	0.03601	7.9	0.00364	2.8	0.35	0.07175	7.4	24.6	0.7	37.7	2.9	978.8	158.5	34.7	97.5	433.5	nd	-
107Br_54.txt	0.03299	6.4	0.00356	2.5	0.39	0.06721	5.9	22.7	0.6	32.7	2.1	844.2	127.8	30.6	97.3	255.2	nd	-
108Br_55a.txt	0.02678	5.3	0.00337	2.9	0.55	0.05764	4.4	21.8	0.6	27	1.4	516	99.7	19.3	95.8	375.5	nd	-
109Br_55b.txt	0.02603	6.2	0.00343	2.6	0.42	0.05505	5.6	22.1	0.6	26.2	1.6	414.3	130.3	15.6	94.7	341.3	nd	-
111Br_56.txt	0.02749	3.8	0.00393	2.4	0.63	0.05073	3.0	24.9	0.6	27.1	1	228.7	70.9	8.1	89.1	784.7	nd	-
112Br_57a.txt	0.02456	8.4	0.00357	2.4	0.29	0.0499	8.1	22.5	0.5	24.2	2	190.3	190.2	7.0	88.2	273.0	nd	-
113Br_57b.txt	0.02571	6.6	0.00365	2.8	0.42	0.05108	6.0	23.7	0.7	26	1.7	244.6	144.4	8.8	90.3	254.3	nd	-
114Br_58.txt	0.02156	5.8	0.00328	3.1	0.53	0.04768	4.9	21.5	0.7	22.1	1.3	83.7	83.6	2.7	74.3	301.9	nd	-
116Br_59c.txt	0.02304	7.2	0.00338	3.4	0.47	0.04944	6.4	20.6	0.7	21.9	1.6	168.8	156.7	5.9	87.8	197.6	nd	-
117Br_59r.txt	0.07117	12.8	0.00225	6.4	0.50	0.22941	11.1	15.1	1	72.8	9	3048	189.9	79.3	99.5	176.1	nd	-
118Br_59i.txt	0.04414	6.0	0.00338	3.4	0.57	0.09472	4.9	22.6	0.8	45.5	2.7	1522.6	95.3	50.3	98.5	189.9	nd	-
119Br_60.txt	0.02307	5.6	0.00352	2.8	0.50	0.04753	4.9	22.4	0.6	22.9	1.3	75.8	75.7	2.2	70.4	283.2	nd	-
121Br_61.txt	0.02483	6.0	0.00342	3.3	0.55	0.05266	5.0	21.7	0.7	24.5	1.5	314.2	117.9	11.4	93.1	222.1	nd	-
122Br_62a.txt	0.02597	4.5	0.00394	1.9	0.42	0.04781	4.1	25.4	0.5	26.1	1.2	89.8	89.7	2.7	71.7	558.4	nd	-
123Br_62b.txt	0.02491	4.3	0.00384	2.8	0.65	0.04705	3.3	25.3	0.7	25.5	1.1	51.7	51.6	0.8	51.1	498.5	nd	-
124Br_63.txt	0.0256	5.1	0.00357	2.7	0.53	0.05201	4.3	23.2	0.6	25.9	1.3	285.9	101.4	10.4	91.9	409.4	nd	-
126Br_64a.txt	0.02356	5.8	0.00328	3.1	0.53	0.05209	4.9	21.8	0.7	24.4	1.4	289.5	116.1	10.7	92.5	372.2	nd	-
127Br_64b.txt	0.00246	30.2	0.00329	2.8	0.09	0.00542	30.1	21.4	0.6	2.5	0.8	0.1	0	-756.0	-21300.0	376.7	nd	-
128Br_65.txt	0.02402	3.4	0.00382	2.2	0.65	0.04561	2.6	24.6	0.5	24.2	0.8	0.1	0	-1.7	-24500.0	931.5	nd	-
129Br_66.txt	0.02517	7.5	0.00356	3.1	0.41	0.05128	6.8	22.8	0.7	25.2	1.9	253.5	164.4	9.5	91.0	171.0	nd	-
131Br_67a.txt	0.02955	7.2	0.00386	2.1	0.29	0.05552	6.9	24.2	0.5	28.9	2.1	433.3	161.5	16.3	94.4	546.2	nd	-
132Br_67b.txt	0.13689	7.1	0.00406	4.2	0.59	0.24453	5.7	24.5	1	122.6	8.2	3149.7	93.5	80.0	99.2	248.5	nd	-
133Br_67c.txt	0.22182	5.3	0.00457	3.3	0.62	0.35204	4.2	29.8	1	206	9.9	3715.9	65.5	85.5	99.2	403.1	nd	-
134Br_68a.txt	0.08344	13.8	0.00467	5.7	0.41	0.12958	12.6	30.9	1.8	83.6	11.1	2092.4	240	63.0	98.5	38.9	nd	-
136Br_68b.txt	0.04739	16.4	0.00313	8.5	0.52	0.10982	14.0	20.5	1.7	47.9	7.7	1796.4	279.4	57.2	98.9	50.1	nd	-
137Br_68c.txt	0.04325	13.3	0.0041	5.3	0.40	0.0765	12.2	26	1.4	42.3	5.5	1108.2	265.2	38.5	97.7	43.5	nd	-
138Br_68d.txt	0.41768	14.2	0.00686	12.4	0.87	0.44159	7.0	44.3	5.5	356	43.6	4057.2	108.5	87.6	98.9	41.3	nd	-
146Br_69f.txt	0.04718	12.0	0.00305	6.7	0.56	0.11218	12.0	19.4	1.3	46.2	5.4	1835.1	193.1	58.0	98.9	74.1	nd	-
147Br_70a.txt	0.0229	4.5	0.00351	2.3	0.51	0.04731	4.5	23.2	0.5	23.6	1	64.8	64.7	1.7	64.2	499.1	nd	-
148Br_70b.txt	0.02723	7.0	0.00356	5.0	0.71	0.05548	7.0	23.6	1.2	28.1	1.9	431.7	113.1	16.0	94.5	266.0	nd	-
158Br_71.txt	0.09112	10.8	0.00391	6.6	0.61	0.16902	10.8	25.1	1.7	88.4	9.2	2548	149.9	71.6	99.0	32.3	nd	-
166Br_72f.txt	0.01925	11.1	0.00316	5.2	0.47	0.04418	11.1	18.7	1	17.8	2	0.1	0	-5.1	-18600.0	156.0	nd	-
167Br_72g.txt	0.02516	13.3	0.00341	6.1	0.46	0.05351	13.3	22.3	1.4	25.7	3.4	350.7	291.3	13.2	93.6	72.9	nd	-
178Br_73a.txt	0.03889	33.7	0.00385	8.7	0.26	0.07326	33.7	24.3	2.1	38.1	12.7	1021.2	855.4	36.2	97.6	40.9	nd	-
179Br_73b.txt	0.0249	9.1	0.00348	4.3	0.47	0.0519	9.1	22.6	1	25.2	2.3	281.3	194.2	10.3	92.0	103.0	nd	-
181Br_74a.txt	0.02382	13.2	0.00325	5.1	0.39	0.05316	13.2	20.5	1	23.4	3.1	335.7	303.1	12.4	93.9	80.9	nd	-
182Br_74b.txt	0.03227	13.4	0.00437	5.1	0.38	0.05355	13.4	27	1.4	30.9	4.1	352.3	307.6	12.6	92.3	88.8	nd	-
183Br_75.txt	0.02132	5.6	0.00336	3.0	0.54	0.04603	5.6	21.8	0.7	21.6	1.2	0.1	0	-0.9	-21700.0	353.4	nd	-
184Br_76.txt	0.0223	5.4	0.00353	3.2	0.59	0.04581	5.4	26.7	0.9	26.2	1.4	0.1	0	-1.9	-26600.0	446.0	nd	-
186Br_77.txt	0.02101	6.3	0.00333	3.0	0.48	0.04575	6.3	21.9	0.7	21.6	1.3	0.1	0	-1.4	-21800.0	254.0	nd	-

	Isotopic Ratios							Dates (Ma)								Compositions		
Sample and Analysis Number	207Pb/ 235U	±2σ %	206Pb/ 238U	±2σ %	Rho 6/38-7/35	207Pb/ 206Pb	±2σ %	206Pb/ 238U	±2σ abs	207Pb/ 235U	±2σ abs	207Pb/ 206Pb	±2σ abs	% disc a 6/38-7/35	% disc b 6/38-7/6	U (ppm)	Th (ppm)	Th/U
187Br_78.txt	0.02373	6.4	0.00348	3.2	0.50	0.04945	6.4	22.2	0.7	23.6	1.5	169.3	136.3	5.9	86.9	240.4	nd	-
188Br_79a.txt	0.02424	6.9	0.00365	3.3	0.48	0.04816	6.9	23.2	0.8	24	1.6	107.1	107	3.3	78.3	199.8	nd	-
191Br_79c.txt	0.02578	6.6	0.00373	3.4	0.52	0.05013	6.6	23.3	0.8	25.1	1.6	201.3	138	7.2	88.4	568.6	nd	-
192Br_80r.txt	0.02191	7.1	0.0033	3.4	0.48	0.04816	7.1	21.3	0.7	22	1.5	107.2	107.1	3.2	80.1	224.4	nd	-
193Br_80c.txt	0.02495	7.4	0.00352	4.0	0.54	0.0514	7.4	22	0.9	24.3	1.8	258.9	149.1	9.5	91.5	214.4	nd	-
194Br_81.txt	0.02317	5.2	0.00361	3.0	0.58	0.04655	5.2	23.1	0.7	23.2	1.2	26	25.9	0.4	11.2	334.0	nd	-
196Br_82a.txt	0.02271	6.6	0.00337	3.7	0.56	0.04888	6.6	22.1	0.8	23.2	1.5	142.3	134.4	4.7	84.5	254.6	nd	-
197Br_82b.txt	0.02208	6.3	0.00349	3.5	0.56	0.04589	6.3	22.4	0.8	22.2	1.4	0.1	0	-0.9	-22300.0	325.3	nd	-
198Br_82c.txt	0.02279	5.9	0.00339	3.2	0.54	0.04876	5.9	22.1	0.7	23.2	1.4	136.6	119.4	4.7	83.8	388.5	nd	-
199Br_83.txt	0.02316	5.9	0.00358	3.1	0.53	0.04691	5.9	23	0.7	23.2	1.4	44.6	44.5	0.9	48.4	463.3	nd	-
201Br_84.txt	0.02439	6.0	0.00375	3.1	0.52	0.04717	6.0	24.4	0.8	24.8	1.5	57.9	57.8	1.6	57.9	302.4	nd	-
202Br_85.txt	0.02128	6.6	0.00347	4.0	0.61	0.04448	6.6	22	0.9	21	1.4	0.1	0	-4.8	-21900.0	295.3	nd	-
203Br_86.txt	0.02888	6.4	0.00376	3.9	0.61	0.0557	6.4	24.9	1	29.7	1.9	440.4	117.7	16.2	94.3	307.4	nd	-
204Br_87a.txt	0.02251	6.4	0.00354	3.8	0.59	0.04611	6.4	22.5	0.9	22.3	1.4	3.3	3.2	-0.9	-581.8	226.0	nd	-
206Br_87b.txt	0.02166	4.9	0.00335	2.7	0.55	0.0469	4.9	21.7	0.6	21.9	1.1	44.3	44.2	0.9	51.0	405.0	nd	-
207Br_87c.txt	0.02504	7.7	0.00311	4.6	0.60	0.05839	7.7	20.4	0.9	25.5	1.9	544.4	141.5	20.0	96.3	223.3	nd	-
208Br_87d.txt	0.02168	6.5	0.00329	3.3	0.51	0.0478	6.5	21.1	0.7	21.7	1.4	89.2	89.1	2.8	76.3	326.2	nd	-
209Br_87e.txt	0.02081	5.1	0.0033	2.9	0.57	0.04573	5.1	21.1	0.6	20.7	1	0.1	0	-1.9	-21000.0	453.4	nd	-
Bras10-6-2 (Stromatic Granulite)																		
003Br_1.txt	0.02589	9.2	0.00392	4.5	0.49	0.0479	8.0	25.4	1.1	26.2	2.4	94.3	94.2	3.1	73.1	81.8	nd	-
004Br_1b.txt	0.02281	8.1	0.00339	4.8	0.59	0.0488	6.5	22.2	1.1	23.3	1.9	138.2	138.1	4.7	83.9	78.4	nd	-
006Br_2a.txt	0.02474	8.0	0.00382	4.4	0.55	0.04697	6.7	24.2	1.1	24.4	1.9	47.8	47.7	0.8	49.4	104.7	nd	-
007Br_2b.txt	0.02768	7.4	0.00396	3.6	0.49	0.05069	6.5	25.4	0.9	27.6	2	226.7	157.6	8.0	88.8	117.2	nd	-
009Br_2c.txt	0.02288	7.6	0.00352	3.9	0.51	0.04714	6.5	23.1	0.9	23.4	1.8	56.4	56.3	1.3	59.0	112.9	nd	-
010Br_2d.txt	0.02576	7.7	0.00398	3.9	0.51	0.04694	6.6	25.8	1	26	2	46.4	46.3	0.8	44.4	112.9	nd	-
012Br_2e.txt	0.02834	6.9	0.00418	3.8	0.55	0.04918	5.7	26.9	1	28.4	1.9	156.4	139.2	5.3	82.8	114.5	nd	-
013Br_2f.txt	0.02663	6.8	0.004	3.5	0.51	0.04828	5.8	25.1	0.9	26.1	1.8	113	112.9	3.8	77.8	127.1	nd	-
015Br_2g.txt	0.02469	6.2	0.00388	3.6	0.58	0.04616	5.1	24.6	0.9	24.4	1.5	5.9	5.8	-0.8	-316.9	133.7	nd	-
016Br_2h.txt	0.03364	8.9	0.00369	3.7	0.42	0.06611	8.1	23.6	0.9	33.4	2.9	810	179.3	29.3	97.1	108.5	nd	-
022Br_2l.txt	0.02612	6.7	0.00367	3.5	0.52	0.05161	5.7	23.6	0.8	26.2	1.7	268.4	136.3	9.9	91.2	116.7	nd	-
028Br_2p.txt	0.03417	6.3	0.0041	3.4	0.54	0.06045	5.3	26.6	0.9	34.5	2.1	619.8	118.7	22.9	95.7	139.7	nd	-
030Br_2q.txt	0.03094	7.2	0.00393	3.4	0.47	0.0571	6.4	24.8	0.8	30.4	2.2	495.5	147.6	18.4	95.0	122.8	nd	-
031Br_2r.txt	0.02367	9.2	0.00362	4.3	0.47	0.04742	8.1	22.2	1	22.6	2.1	70.5	70.4	1.8	68.5	128.1	nd	-
033Br_2s.txt	0.12369	16.0	0.00231	14.6	0.91	0.38835	6.5	10.6	1.5	85.5	13.2	3864.6	101.6	87.6	99.7	85.7	nd	-
034Br_3a.txt	0.03122	23.8	0.00407	12.0	0.50	0.05564	20.6	26.2	3.1	31.2	7.3	438.2	438.1	16.0	94.0	83.7	nd	-
036Br_3b.txt	0.05062	17.3	0.00328	11.6	0.67	0.11193	12.9	20.8	2.4	49.4	8.4	1831	254.3	57.9	98.9	16.8	nd	-
037Br_3c.txt	0.02926	9.6	0.00372	3.6	0.38	0.05705	8.9	23	0.8	28.2	2.7	493.4	209.2	18.4	95.3	80.8	nd	-
039Br_3d.txt	0.0302	8.8	0.00452	3.7	0.42	0.04846	8.0	28.3	1	29.5	2.6	121.9	121.8	4.1	76.8	68.7	nd	-
040Br_3e.txt	0.02675	8.0	0.00375	3.6	0.45	0.05173	7.2	24.4	0.9	27.1	2.1	273.7	174	10.0	91.1	79.8	nd	-
042Br_3f.txt	0.0264	9.2	0.00398	4.2	0.46	0.04811	8.2	25.5	1.1	26.3	2.4	104.6	104.5	3.0	75.6	87.5	nd	-
043Br_3g.txt	0.05408	10.4	0.00383	3.6	0.35	0.1024	9.8	24.1	0.9	52.4	5.3	1668.1	193.1	54.0	98.6	99.4	nd	-
044Br_3h.txt	0.06342	14.8	0.00408	9.9	0.67	0.11273	11.0	26.4	2.6	62.8	9.1	1843.9	213.7	58.0	98.6	94.5	nd	-
046Br_3i.txt	0.02814	10.3	0.00373	4.6	0.45	0.05472	9.2	24.6	1.1	28.9	2.9	400.9	220.5	14.9	93.9	47.0	nd	-
047Br_3j.txt	0.0272	11.9	0.00376	5.3	0.45	0.05247	10.6	24.1	1.3	27.2	3.2	305.9	261.4	11.4	92.1	51.6	nd	-
048Br_4a.txt	0.02703	7.4	0.00401	4.0	0.54	0.04889	6.2	30.2	1.2	31.6	2.3	142.7	142.6	4.4	78.8	114.6	nd	-
050Br_4b.txt	0.02514	9.5	0.0036	4.8	0.51	0.05064	8.2	23.5	1.1	25.6	2.4	224.6	201.5	8.2	89.5	193.7	nd	-
055Br_4f.txt	0.02562	15.3	0.00381	7.1	0.46	0.04877	13.5	24.8	1.8	26	3.9	136.7	136.6	4.6	81.9	53.3	nd	-
058Br_5.txt	0.04828	6.2	0.00427	3.2	0.52	0.08201	5.3	27.5	0.9	47.9	2.9	1245.7	107.4	42.6	97.8	170.2	nd	-
059Br_6a.txt	0.027	8.5	0.00408	4.1	0.48	0.04799	7.5	26.2	1.1	27	2.3	98.7	98.6	3.0	73.5	63.5	nd	-

	Isotopic Ratios							Dates (Ma)							Compositions		
Sample and Analysis Number	207Pb/ 235U	±2σ %	206Pb/ 238U	±2σ %	Rho 6/38-7/35	207Pb/ 206Pb	±2σ %	206Pb/ 238U	±2σ abs	207Pb/ 235U	±2σ abs	207Pb/ 206Pb	±2σ abs	% disc a 6/38-7/35	% disc b 6/38-7/6	U (ppm)	Th (ppm)	Th/U
060Br_6b.txt	0.29301	8.1	0.00613	5.9	0.73	0.34667	5.6	38.9	2.3	257.7	18.6	3692.5	88.2	84.9	98.9	29.6	nd	-
062Br_6c.txt	0.0274	9.6	0.00381	4.3	0.45	0.05216	8.6	25.7	1.1	28.8	2.7	292.5	209.3	10.8	91.2	60.1	nd	-
063Br_6d.txt	0.02533	6.1	0.00396	3.3	0.54	0.04639	5.1	25.6	0.8	25.5	1.5	17.9	17.8	-0.4	-43.0	153.6	nd	-
064Br_6e.txt	0.03138	9.0	0.00385	4.4	0.49	0.05911	7.8	25.5	1.1	32.3	2.9	571.2	179.4	21.1	95.5	77.5	nd	-
066Br_6f.txt	0.03194	7.4	0.00365	4.8	0.65	0.06346	5.6	24.4	1.2	33.1	2.4	723.8	123.5	26.3	96.6	89.9	nd	-
067Br_6g.txt	0.10682	6.9	0.00538	4.1	0.59	0.144	5.5	34.2	1.4	102.1	6.7	2276	98	66.5	98.5	74.7	nd	-
068Br_6h.txt	0.03871	4.8	0.00457	3.1	0.65	0.06144	3.6	29.3	0.9	38.5	1.8	654.6	79.2	23.9	95.5	248.8	nd	-
070Br_7a.txt	0.02674	7.1	0.00396	3.7	0.52	0.04897	6.1	25.1	0.9	26.4	1.9	146.5	146.4	4.9	82.9	105.0	nd	-
071Br_7b.txt	0.06192	13.0	0.00442	6.2	0.48	0.10161	11.4	28.7	1.8	61.6	7.8	1653.8	227.6	53.4	98.3	29.8	nd	-
072Br_8a.txt	0.0768	15.1	0.00391	7.1	0.47	0.14245	13.3	21.9	1.6	65.8	9.7	2257.3	249.8	66.7	99.0	50.5	nd	-
074Br_8b.txt	0.66327	8.5	0.01014	7.8	0.92	0.47441	3.5	67.5	5.2	531.6	35.8	4163.6	52.8	87.3	98.4	34.0	nd	-
075Br_9.txt	0.02569	9.0	0.00398	4.3	0.48	0.04681	7.9	25.6	1.1	25.7	2.3	39.6	39.5	0.4	35.4	62.4	nd	-
076Br_10a.txt	0.02266	10.0	0.00376	4.1	0.41	0.0437	9.1	23.3	1	21.9	2.2	0.1	0	-6.4	-23200.0	69.3	nd	-
078Br_10b.txt	0.02496	9.5	0.00379	4.9	0.52	0.04776	8.1	24.8	1.2	25.5	2.4	87.5	87.4	2.7	71.7	66.8	nd	-
079Br_10c.txt	0.05472	12.8	0.0036	6.1	0.48	0.11024	11.2	23.2	1.4	54.1	6.8	1803.5	219	57.1	98.7	72.5	nd	-
080Br_10d.txt	0.02809	9.9	0.00409	5.0	0.51	0.04982	8.5	26.2	1.3	28	2.7	186.5	186.4	6.4	86.0	73.8	nd	-
082Br_10e.txt	0.03067	9.1	0.0042	5.0	0.55	0.05297	7.6	27.3	1.4	30.9	2.8	327.7	182.4	11.7	91.7	71.4	nd	-
083Br_10f.txt	0.02292	15.0	0.00357	6.1	0.41	0.04657	13.7	24.1	1.5	24.1	3.6	27.1	27	0.0	11.1	78.5	nd	-
084Br_10g.txt	0.02666	12.7	0.00373	5.4	0.43	0.05183	11.5	23.7	1.3	26.4	3.3	277.8	277.7	10.2	91.5	62.7	nd	-
086Br_10h.txt	0.02752	8.9	0.00427	4.2	0.47	0.04675	7.9	27.4	1.2	27.5	2.4	36.3	36.2	0.4	24.5	73.9	nd	-
087Br_10i.txt	0.02685	8.5	0.00413	4.6	0.54	0.04715	7.1	26.7	1.2	27	2.3	57	56.9	1.1	53.2	75.5	nd	-
088Br_10j.txt	0.0325	8.5	0.00394	4.4	0.52	0.05982	7.3	26.2	1.2	33.6	2.8	597.1	166.6	22.0	95.6	76.5	nd	-
090Br_10k.txt	0.03977	8.7	0.00505	4.3	0.49	0.05712	7.6	33.4	1.4	40.7	3.5	496.2	176.8	17.9	93.3	79.3	nd	-
091Br_10l.txt	0.021	15.1	0.00326	7.3	0.48	0.04671	13.2	21.2	1.5	21.3	3.2	34.4	34.3	0.5	38.4	86.9	nd	-
092Br_10m.txt	0.02852	8.2	0.00407	4.3	0.52	0.05083	7.0	26.1	1.1	28.5	2.3	233.3	170.1	8.4	88.8	98.6	nd	-
094Br_10n.txt	0.02828	8.2	0.00401	4.5	0.55	0.05115	6.9	25.2	1.1	27.7	2.2	247.7	167.2	9.0	89.8	86.0	nd	-
095Br_10o.txt	0.03161	8.7	0.00441	4.7	0.54	0.05198	7.3	28.4	1.3	31.7	2.7	284.7	176.2	10.4	90.0	83.0	nd	-
096Br_10p.txt	0.13077	8.8	0.00549	4.0	0.45	0.17276	7.8	35.4	1.4	125.2	10.4	2584.6	136.5	71.7	98.6	93.7	nd	-

Notes:

Rho = correlation coeffecient between 206Pb/238U and 207Pb/235U ratios

a % discordance = 100 - (100 * (206Pb/238U date) / (207Pb/235U date))

b % discordance = 100 - (100 * (206Pb/238U date) / (207Pb/206Pb date))

bdl = below detection limit

nd = not determined

Table 2.3. Rutile trace element data.

Sample and Analysis Number	Texture	Ti (cps)	± 2SE (cps)	V (ppm)	± 2SE (ppm)	Zr (ppm)	± 2SE (ppm)	± 2SE %	Zr-in-Rt T (°C)	± 2SE (°C)	Nb (ppm)	± 2SE (ppm)	Mo (ppm)	± 2SE (ppm)	Sn (ppm)	± 2SE (ppm)	Sb (ppm)	± 2SE (ppm)	Hf (ppm)	± 2SE (ppm)	Ta (ppm)	± 2SE (ppm)	W (ppm)	± 2SE (ppm)	206Pb (ppm)	± 2SE (ppm)	208Pb (ppm)	± 2SE (ppm)	Th (ppm)	± 2SE (ppm)	U (ppm)	± 2SE (ppm)
Residual Granulite (G1A_2009)																																
G1A_3.FIN2	Grt	2.5E+07	2.0E+06	698	33	134.6	6.5	4.8	**588**	**28**	4210	200	26	4	193	10	0.264	0.089	3.42	0.44	80.5	6.2	2.5	0.32	0.8	0.1	0.40	0.08	0.0	0.0	14.2	1.3
G1A_10.FIN2	Grt	2.8E+07	2.4E+06	624	21	174.9	9.3	5.3	**606**	**32**	4140	220	34.1	5	220	15	0.183	0.075	7.16	0.7	300	21	10.1	1	1.3	0.2	0.21	0.05	0.0	0.0	58.1	5.3
G1A_6.FIN2	Grt	3.7E+07	4.0E+06	576	26	207	13	6.3	**618**	**39**	5620	390	43.5	6.7	296	23	0.34	0.1	8.5	1.1	659	71	47	5.3	1.1	0.2	0.35	0.08	0.2	0.1	34.7	4
G1A_1b.FIN2	Grt	3.0E+07	2.6E+06	668	28	232	13	5.6	**626**	**35**	5100	290	36.2	5.2	277	16	0.175	0.071	8.55	0.88	547	40	39.4	2.9	1.4	0.2	0.23	0.06	0.1	0.0	45	4
G1A_2.FIN2	Grt	2.9E+07	2.6E+06	612	24	234	11	4.7	**627**	**29**	2660	130	26.2	3.1	145.6	8.2	0.264	0.077	5.17	0.67	49.3	3.9	2.04	0.26	1.3	0.2	0.25	0.06	0.1	0.0	51.3	4
G1A_4d.FIN2	Grt	3.0E+07	2.4E+06	776	27	236	14	5.9	**628**	**37**	6390	320	33.5	5.4	288	18	0.296	0.066	9	1	809	70	25.9	2.6	0.5	0.1	0.26	0.06	0.0	0.0	14	1.4
G1A_4e.FIN2	Grt	3.1E+07	2.9E+06	795	33	254	12	4.7	**633**	**30**	6310	310	28.6	4.5	297	18	0.219	0.076	8.51	0.72	911	58	35.2	2.7	0.5	0.1	0.14	0.03	0.0	0.0	14.5	1
G1A_4c.FIN2	Grt	2.8E+07	2.6E+06	795	25	255	13	5.1	**634**	**32**	6480	310	31.6	5.1	287	17	0.264	0.082	9.02	0.87	862	65	32.2	2.2	0.3	0.1	0.15	0.04	0.0	0.0	16	1.5
G1A_1a.FIN2	Grt	3.0E+07	2.8E+06	670	24	267	15	5.6	**637**	**36**	5200	260	39.8	5.2	273	16	0.275	0.078	10.12	0.97	663	45	38.2	3.1	1.4	0.2	0.21	0.05	0.0	0.0	45.9	4
G1A_1c.FIN2	Grt	2.9E+07	2.8E+06	685	27	291	13	4.5	**644**	**29**	5470	250	37.6	5	301	15	0.197	0.068	10.74	0.98	718	50	32.8	2.6	1.3	0.2	0.23	0.05	0.0	0.0	48.1	4.1
G1A_4a.FIN2	Grt	2.8E+07	2.6E+06	753	29	319	17	5.3	**651**	**35**	6680	340	29.2	5.4	297	19	0.307	0.086	11.5	1.1	887	65	30.8	2.8	0.4	0.1	0.23	0.05	0.0	0.0	15	1.3
G1A_4b.FIN2	Grt	3.1E+07	3.0E+06	780	27	325	18	5.5	**652**	**36**	6300	330	25.9	5.4	287	17	0.323	0.085	13	1.1	1153	85	35.9	2.8	0.6	0.1	0.22	0.04	0.0	0.0	14.7	1.3
G1A_1d.FIN2	Grt	2.8E+07	2.6E+06	664	25	338	18	5.3	**655**	**35**	5450	240	34	5.4	288	16	0.166	0.086	13.3	1.3	952	81	50	4.4	1.6	0.2	0.24	0.06	0.1	0.0	52.4	5.3
G1A_9b.FIN2	Grt	2.7E+07	2.5E+06	769	30	431	21	4.9	**675**	**33**	11280	620	57.3	7.4	534	32	0.146	0.056	16.1	1.3	1450	100	65.8	5.3	1.6	0.2	0.27	0.06	0.0	0.0	61.3	5.2
G1A_8.FIN2	Grt	2.8E+07	2.5E+06	672	27	575	27	4.7	**700**	**33**	5280	250	28.4	4.6	244	14	0.241	0.075	19	1.5	760	55	33.6	2.9	0.7	0.1	0.23	0.05	0.0	0.0	20.1	1.8
G1A_16.FIN2	Grt	4.2E+07	5.0E+06	487	26	590	46	7.8	**702**	**55**	4860	370	36.7	6.5	339	39	0.231	0.071	15.6	2.2	241	28	32.6	3.8	2.8	0.4	0.13	0.05	0.0	0.0	117	14
G1A_9a.FIN2	Grt	2.8E+07	2.6E+06	818	31	600	29	4.8	**704**	**34**	12360	630	50.2	6.8	556	31	0.172	0.069	26.3	2.3	2340	160	83.4	6.4	1.6	0.2	0.25	0.06	0.0	0.0	64.9	5.6
G1A_7d.FIN2	Grt	2.8E+07	2.5E+06	734	28	808	43	5.3	**731**	**39**	8410	430	43.2	5.6	336	21	0.339	0.09	24.5	1.9	888	68	27.1	2.3	0.7	0.1	0.29	0.06	0.0	0.0	23.1	2.2
G1A_15a.FIN2	Grt	3.2E+07	2.7E+06	468	16	824	43	5.2	**732**	**38**	3370	210	30.9	3.8	264	14	0.311	0.074	20	1.5	248	17	31.4	2.2	2.7	0.3	0.03	0.02	0.0	0.0	126	10
G1A_7c.FIN2	Grt	2.9E+07	2.7E+06	751	30	845	49	5.8	**735**	**43**	9110	520	35.2	6	350	23	0.228	0.076	29.6	2.5	1197	87	29.9	2.6	0.9	0.1	0.23	0.06	0.8	0.3	27.8	2.5
G1A_12b.FIN2	Grt	3.9E+07	3.7E+06	578	31	850	54	6.4	**735**	**47**	5340	390	35.4	6.9	257	22	0.206	0.079	20.3	2.1	137	13	17.8	1.9	2.3	0.3	0.42	0.09	0.3	0.1	80.9	7.8
G1A_15c.FIN2	Grt	3.4E+07	2.8E+06	472	17	858	33	3.8	**736**	**28**	3350	160	37.4	3.1	277	17	0.307	0.076	19.7	1.6	333	22	46.7	3.3	4.4	0.5	1.12	0.16	0.0	0.0	141	10
G1A_15b.FIN2	Grt	2.8E+07	2.0E+06	492	21	859	44	5.1	**736**	**38**	3820	200	34.5	5.1	290	19	0.287	0.08	21.1	1.7	205	16	28.6	2.5	3.3	0.4	0.22	0.05	0.5	0.1	134	10
G1A_7b.FIN2	Grt	2.8E+07	2.6E+06	745	22	898	44	4.9	**740**	**36**	9000	440	39.1	5.3	371	20	0.231	0.077	28.8	2.4	1084	87	32.1	2.8	0.9	0.1	0.24	0.05	0.0	0.0	27.5	2.6
G1A_11.FIN2	Grt	2.8E+07	2.4E+06	495	15	1182	64	5.4	**767**	**42**	5620	280	41.7	5.2	269	16	0.175	0.069	32.8	2.3	844	58	64.1	4.2	2.6	0.3	0.19	0.05	0.0	0.0	99.6	7.4
G1A_7a.FIN2	Grt	2.7E+07	2.2E+06	911	35	1398	71	5.1	**784**	**40**	14020	720	39.4	5.4	636	38	0.3	0.077	51.3	4.4	2310	200	49	4.9	0.8	0.2	0.28	0.06	0.0	0.0	23.7	2.2
G1A_17.FIN2	Grt	2.0E+07	1.6E+06	358	20	2430	180	7.4	**845**	**63**	7150	590	83	12	249	21	0.32	0.12	59.5	5.5	541	54	190	19	4.6	0.5	0.06	0.03	0.1	0.0	191	19
G1A_12a.FIN2	Grt	2.6E+07	2.8E+06	494	20	2490	130	5.2	**848**	**44**	7170	340	83.1	6.1	286	17	0.206	0.076	91.9	6.9	732	52	129.8	9.8	2.7	0.3	0.27	0.05	0.1	0.0	107.1	9.1
G1A_7e.FIN2	Grt	2.7E+07	2.2E+06	988	34	3280	170	5.2	**880**	**46**	13890	730	29.3	5.1	633	36	0.234	0.083	125.8	8.6	6380	470	204	16	0.8	0.1	0.34	0.07	0.0	0.0	19.4	1.5
G1A_14.FIN2	Peak	3.3E+07	3.0E+06	511	16	6000	230	3.8	**960**	**37**	67100	3100	186	13	414	27	0.287	0.075	292	20	3050	230	896	69	11.7	2.9	5.40	2.60	0.0	0.0	216	16
G1A_13.FIN2	Peak	3.2E+07	2.6E+06	395	17	6860	320	4.7	**979**	**46**	50100	2300	218	12	406	23	0.291	0.079	319	20	2320	130	748	47	5.2	0.5	0.18	0.05	0.0	0.0	188	13
Retrogressed Granulite (GR11-1A)																																
GR11-1A-45.FIN2	Rextal	2.3E+07	1.9E+06	1809	71	2.26	0.43	19.0	**376**	**72**	635	42	0.99	0.33	26.8	2.6	0.021	0.041	0.142	0.081	76.2	7.1	0.29	0.11	0.0	0.0	0.08	0.07	0.0	0.0	bdl	-
GR11-1A-71.FIN2	Rextal	1.4E+07	1.6E+06	1589	53	3.64	0.57	15.7	**396**	**62**	478	19	1.99	0.49	39.4	2.4	0.005	0.042	0.44	0.16	27.9	1.5	2.62	0.39	0.1	0.1	-0.02	0.05	0.0	0.0	bdl	-
GR11-1A-58a.FIN2	Rextal	3.4E+07	3.3E+06	761	92	13.5	7.7	57.0	**454**	**259**	1390	600	2.1	1.3	46	14	0.06	0.1	3.1	1.1	261	99	16.8	5.6	0.0	0.0	-0.02	0.11	0.0	0.0	0.083	0.062
GR11-1A-76.FIN2	Rextal	2.6E+07	2.4E+06	933	53	15.8	1.9	12.0	**462**	**56**	1520	150	1.46	0.48	37.4	4.8	0.054	0.07	1.01	0.32	77	8.2	2.75	0.58	0.5	0.2	0.17	0.10	0.1	0.0	11.1	1.7
GR11-1A-62b.FIN2	Rextal	2.2E+07	1.8E+06	679	23	40.7	3.4	8.4	**513**	**43**	99	6.9	0.78	0.34	33.7	2.6	0.053	0.037	1.33	0.26	2.74	0.35	0.186	0.083	0.1	0.1	0.12	0.08	0.0	0.0	0.54	0.11
GR11-1A-64.FIN2	Rextal	2.7E+07	2.0E+06	1300	170	83	34	41.0	**556**	**228**	5200	1700	36	14	149	41	0.313	0.099	6	1.9	246	24	1050	100	0.9	0.3	0.11	0.06	0.1	0.0	41	16
GR11-1A-69.FIN2	Rextal	5.5E+07	3.9E+06	931	87	190	29	15.3	**612**	**93**	2600	310	19.7	6.4	124	13	0.67	0.21	8.7	2.4	114	35	41	16	0.8	0.2	0.15	0.08	0.0	0.0	45.4	6.9
GR11-1A-70.FIN2	Rextal	5.1E+07	3.4E+06	991	64	310	23	7.4	**649**	**48**	4250	430	20.3	6.3	239	25	0.73	0.21	14.9	1.1	92	15	12.1	1.8	1.0	0.4	0.02	0.06	0.0	0.0	59	10
GR11-1A-42.FIN2	Rextal	3.9E+07	2.6E+06	1810	68	322	22	6.8	**652**	**45**	1850	140	13.2	2	154	11	1.55	0.17	8.58	0.84	1.18	7	119.5	7	3.9	0.3	0.01	0.02	0.0	0.0	222	14
GR11-1A-60.FIN2	Rextal	5.0E+07	3.7E+06	1100	120	420	53	12.6	**673**	**85**	6330	640	109	15	356	49	1.11	0.26	20.8	2.1	169	22	289	67	1.4	0.3	0.01	0.03	0.0	0.0	75.8	8.8
GR11-1A-80.FIN2	Rextal	3.7E+07	3.0E+06	999	32	440	20	4.5	**677**	**31**	3750	170	34.4	2.6	348	20	1.01	0.13	20.8	1.5	176	11	119.1	6.6	2.3	0.2	0.01	0.02	0.0	0.0	114.1	7.6
GR11-1A-87.FIN2	Rextal	5.3E+07	5.6E+06	1052	73	440	49	11.1	**677**	**75**	2830	210	24.8	7.4	332	29	1.31	0.27	17	1.2	104.4	9.7	19	2.7	2.6	0.4	0.09	0.05	0.0	0.0	147	18
GR11-1A-17.FIN2	Rextal	4.0E+07	3.2E+06	799	23	463	17	3.7	**681**	**25**	3760	140	17	2.7	307	17	1.08	0.11	16.34	0.99	77.9	6.7	19.7	2.3	1.6	0.2	0.02	0.02	0.0	0.0	72.5	4.8
GR11-1A-22.FIN2	Rextal	4.2E+07	3.0E+06	723	23	470	22	4.7	**683**	**32**	3330	140	13.4	2.7	266	14	0.96	0.12	15.9	1.1	131.9	7.6	29.2	1.7	1.8	0.2	0.01	0.02	0.0	0.0	96.5	5.5
GR11-1A-20.FIN2	Rextal	6.0E+07	6.5E+06	887	93	475	39	8.2	**683**	**56**	3500	300	15	7.6	230	18	0.61	0.23	17.1	1.5	264	34	48.8	6.2	1.1	0.3	0.24	0.21	0.0	0.0	57.8	5.8
GR11-1A-73.FIN2	Rextal	5.4E+07	4.1E+06	1053	55	498	42	8.4	**687**	**58**	6210	530	29.8	3.5	308	25	0.92	0.16	25.7	2.3	230	17	183	13	2.3	0.4	0.00	0.02	0.0	0.0	149	14
GR11-1A-72.FIN2	Rextal	3.1E+07	2.0E+06	1009	38	517	26	5.0	**691**	**35**	6400	530	57.4	4.4	450	26	1.07	0.14	24.5	1.7	232	16	161	14	2.9	0.3	0.00	0.02	0.0	0.0	159	10
GR11-1A-44a.FIN2	Rextal	3.1E+07	2.4E+06	821	32	526	27	5.1	**692**	**36**	3320	180	15.7	2.7	332	20	1.22	0.15	20.4	1.5	124.5	7.8	33	2.6	3.4	0.3	-0.01	0.02	0.0	0.0	161.6	9.3
GR11-1A-75.FIN2	Rextal	4.7E+07	4.1E+06	1108	48	536	40	7.5	**694**	**52**	5250	420	51.2	5.3	371	31	1.2	0.18	23.7	2.2	137.8	9.5	95.6	7.8	2.4	0.3	-0.01	0.02	0.0	0.0	138	10
GR11-1A-53.FIN2	Rextal	3.6E+07	2.7E+06	915	31	556	31	5.6	**697**	**39**	5700	350	37.4	2.8	352	25	1.21	0.13	27	2	151	11	99.5	7.4	2.2	0.2	0.01	0.02	0.0	0.0	109.1	7.5
GR11-1A-48.FIN2	Rextal	3.2E+07	2.3E+06	769	28	560	28	5.0	**698**	**35**	4060	230	32.9	3.5	351	16	1.17	0.12	24.6	1.6	172	11	142.6	9	4.2	0.4	0.00	0.02	0.0	0.0	225	12
GR11-1A-57.FIN2	Rextal	4.7E+07	4.0E+06	1008	58	569	42	7.4	**699**	**52**	6000	480	57.5	6.1	432	38	1.38	0.27	22.2	2.4	175	13	90.8	6.9	3.7	0.5	-0.01	0.03	0.0	0.0	204	14
GR11-1A-55.FIN2	Rextal	3.8E+07	2.9E+06	1020	33	572	42	7.3	**699**	**51**	6060	340	41.4	5.1	402	29	1.33	0.16	28.3	2.1	504	34	253	18	4.9	0.4	0.00	0.02	0.0	0.0	229	17
GR11-1A-31.FIN2	Rextal	5.9E+07	4.1E+06	800	45	573	33	5.8	**700**	**40**	6200	480	22.5	5.7	220	21	0.64	0.13	24.6	2.3	231	21	355	40	2.5	0.3	0.03	0.03	0.0	0.0	141	20
GR11-1A-49.FIN2	Rextal	4.1E+07	3.8E+06	767	53	574	63	11.0	**700**	**77**	4190	360	34.2	4.6	362	30	1.1	0.28	23.6	2.7	79.1	9.5	89.2	9.7	4.0	0.5	0.00	0.03	0.0	0.0	203	20
GR11-1A-50.FIN2	Rextal	3.8E+07	2.8E+06	757	25	575	37	6.4	**700**	**45**	3990	250	32	3.1	315	23	1.11	0.13	23.5	1.8	151	15	118.7	8.3	4.3	0.4	0.01	0.02	0.0	0.0	217	14
GR11-1A-29.FIN2	Rextal	3.8E+07	2.2E+06	834	24	594	27	4.5	**703**	**32**	6200	310	27.1	3	289	18	1.04	0.13	25.6	1.9	188	14	210	16	3.2	0.3	0.00	0.02	0.0	0.0	164	10
GR11-1A-26.FIN2	Rextal	3.7E+07	2.8E+06	954	26	604	21	3.5	**704**	**24**	5830	250	12.2	2.7	284	13	1.024	0.095	22.8	1.3	339	19	67.5	4.6	3.3	0.2	0.00	0.02	0.0	0.0	163.9	8
GR11-1A-19.FIN2	Rextal	5.3E+07	3.0E+06	924	70	606	45	7.4	**704**	**52**	9270	820	21.9	4.9	291	20	0.66	0.19	30.4	2.1	697	71	149	16	2.2	0.4	0.01	0.03	0.0	0.0	150	16
GR11-1A-58b.FIN2	Rextal	3.3E+07	3.0E+06	1149	35	629	35	5.6	**708**	**39**	8650	520	63.7	4.9	394	21	1.47	0.19	29.8	1.9	378	19	350	23	3.5	0.3	-0.01	0.02	0.0	0.0	202	13
GR11-1A-36.FIN2	Rextal	4.5E+07	3.8E+06	740	28	630	38	6.0	**708**	**43**	4590	280	26.1	3.8	252	19	0.96	0.14	24.8	1.8	362	27	289	19	3.2	0.3	0.13	0.05	0.0	0.0	158	13
GR11-1A-56.FIN2	Rextal	3.7E+07	2.3E+06	1131	37	630	31	4.9	**708**	**35**	8030	340	48.2	3.8	395	19	1.31	0.15	27.8	1.8	535	30	470	31	4.8	0.3	0.00	0.02	0.0	0.0	230	13
GR11-1A-21.FIN2	Rextal	5.7E+07	4.6E+06	926	48	652	58	8.9	**711**	**63**	7970	620	20.6	3	258	23	0.83	0.13	21.8	1.7	355	28	84.6	5	1.1	0.2	0.09	0.06	0.0	0.0	53.8	3.5
GR11-1A-38b.FIN2	Rextal	4.6E+07	4.3E+06	762	33	653	37	5.7	**711**	**40**	5380	360	30.8	3.6	256	21	0.99	0.18	28.9	2.1	338	25	782	68	4.5	0.7	0.34	0.22	0.0	0.0	192	16
GR11-1A-44b.FIN2	Rextal	3.1E+07	2.3E+06	930	29	659	27	4.1	**712**	**29**	6010	290	26.8	3.7	352	20	1.05	0.13	25.1	1.4	306	17	141.7	8	3.5	0.3	0.01	0.02	0.0	0.0	174	8.2
GR11-1A-61.FIN2	Rextal	3.3E+07	2.9E+06	1199	42	660	30	4.5	**712**	**32**	7410	410	105.5	7	518	30	1.45	0.14	31.3	1.8	247	12	396	21	2.7	0.3	0.02	0.02	0.0	0.0	149.3	7.4
GR11-1A-66.FIN2	Rextal	4.5E+07	2.7E+06	2470	110	668	34	5.1	**713**	**36**	1687	97	7.7	1.7	96.7	9.1	1.3	0.21	16.1	1.7	113.4	8.7	103.6	9.1	2.6	0.3	0.02	0.02	0.0	0.0	134.9	8.9
GR11-1A-33.FIN2	Rextal	5.4E+07	4.4E+06	736	46	669	46	6.9	**713**	**49**	11950	840	101.9	9.2	253	24	0.69	0.15	35.1	3.4	578	49	2610	210	3.9	0.3	0.02	0.03	0.0	0.0	201	20
GR11-1A-24.FIN2	Rextal	4.7E+07	2.7E+06	1131	59	685	31	4.5	**715**	**32**	14400	1000	97.4	7.6	298	20	0.88	0.12	28.4	2	804	56	977	77	2.4	0.3	0.03	0.03	0.0	0.0	117.5	8.9
GR11-1A-4.FIN2	Rextal	5.3E+07	3.4E+06	806	31	688	38	5.5	**716**	**40**	4200	220	20.9	2	245	13	0.93	0.12	29.9	1.6	421	25	180	12	3.4	0.3	0.53	0.08	0.0	0.0	164.8	9.6

Sample and Analysis Number	Texture	Ti (cps)	± 2SE (cps)	V (ppm)	± 2SE (ppm)	Zr (ppm)	± 2SE (ppm)	± 2SE %	Zr-in-Rt T (°C)	± 2SE (°C)	Nb (ppm)	± 2SE (ppm)	Mo (ppm)	± 2SE (ppm)	Sn (ppm)	± 2SE (ppm)	Sb (ppm)	± 2SE (ppm)	Hf (ppm)	± 2SE (ppm)	Ta (ppm)	± 2SE (ppm)	W (ppm)	± 2SE (ppm)	206Pb (ppm)	± 2SE (ppm)	208Pb (ppm)	± 2SE (ppm)	Th (ppm)	± 2SE (ppm)	U (ppm)	± 2SE (ppm)
GR11-1A-52b.FIN2	Rextal	3.2E+07	2.4E+06	960	30	704	47	6.7	**718**	**48**	8370	530	32.3	4.7	363	22	1.25	0.12	31.3	1.8	585	33	706	42	5.6	0.4	-0.03	0.02	0.0	0.0	266	16
GR11-1A-12.FIN2	Rextal	4.3E+07	3.7E+06	850	33	709	27	3.8	**719**	**27**	4270	220	26.9	2.5	277	16	1.14	0.15	28.7	1.7	211	12	312	15	4.9	0.4	0.33	0.06	0.0	0.0	212.2	9.7
GR11-1A-46.FIN2	Rextal	3.7E+07	2.7E+06	950	33	718	35	4.9	**720**	**35**	7560	390	28.7	4.1	300	18	0.97	0.13	28.1	2	363	21	396	26	4.7	0.4	0.00	0.02	0.0	0.0	246	14
GR11-1A-85.FIN2	Grt	5.3E+07	5.0E+06	3860	510	732	45	6.1	**721**	**44**	9600	1000	102	21	378	54	1.95	0.42	61.6	9.2	569	89	900	140	7.8	0.9	0.03	0.04	0.0	0.0	458	60
GR11-1A-59a.FIN2	Rextal	3.8E+07	3.2E+06	1213	49	758	50	6.6	**725**	**48**	14330	930	96	9.3	438	33	1.6	0.2	49.3	4.1	726	54	3460	260	8.0	0.8	0.02	0.03	0.0	0.0	388	35
GR11-1A-82.FIN2	Rextal	3.7E+07	2.6E+06	1925	62	766	31	4.0	**726**	**29**	2760	120	22.1	2.5	322	17	1.95	0.17	21.2	1.3	167.7	9.3	138.1	8.7	6.9	0.5	0.00	0.02	0.0	0.0	353	22
GR11-1A-10.FIN2	Rextal	3.5E+07	3.4E+06	943	32	785	30	3.8	**728**	**28**	8450	340	35.3	3.9	313	17	1.25	0.12	34.8	1.8	462	22	915	45	5.2	0.4	0.09	0.03	0.0	0.0	251	12
GR11-1A-43b.FIN2	Rextal	3.5E+07	2.4E+06	700	25	801	33	4.1	**730**	**30**	4630	190	44.3	3.8	346	20	1.22	0.17	38.2	2.5	216	14	750	50	5.5	0.5	0.02	0.02	0.0	0.0	263	18
GR11-1A-38a.FIN2	Rextal	4.0E+07	2.8E+06	844	29	803	30	3.7	**730**	**27**	8470	370	37.2	2.9	261	14	0.94	0.12	38.2	2.3	465	29	1151	73	4.5	0.4	0.05	0.03	0.0	0.0	212	13
GR11-1A-11.FIN2	Rextal	3.1E+07	3.1E+06	1004	34	805	32	4.0	**730**	**29**	9920	360	25	3.4	328	16	1.23	0.14	32.9	1.7	912	43	550	28	4.3	0.3	0.20	0.05	0.0	0.0	196.3	9
GR11-1A-41.FIN2	Rextal	3.3E+07	2.4E+06	1164	36	809	32	4.0	**731**	**29**	17450	890	52.1	3.9	350	22	0.87	0.11	43.9	2.1	1312	60	1742	91	3.9	0.3	-0.02	0.01	0.0	0.0	197	10
GR11-1A-8.FIN2	Rextal	3.4E+07	2.9E+06	1054	34	871	38	4.4	**738**	**32**	9710	420	44.6	3.9	319	16	1.37	0.14	39	2.1	376	18	1424	67	6.2	0.4	0.07	0.03	0.0	0.0	288	16
GR11-1A-77.FIN2	Rextal	3.5E+07	2.5E+06	1372	41	886	30	3.4	**739**	**25**	15570	720	68.2	4.6	349	17	1.42	0.15	46.7	3.2	1043	68	3080	220	5.1	0.5	-0.01	0.02	0.0	0.0	233	17
GR11-1A-37a.FIN2	Rextal	3.6E+07	3.0E+06	902	30	890	40	4.5	**740**	**33**	10500	460	38.3	3.4	291	18	0.97	0.12	39.3	2.1	663	35	1172	61	4.2	0.3	0.01	0.02	0.0	0.0	208	12
GR11-1A-23b.FIN2	Rextal	4.6E+07	4.0E+06	779	29	894	47	5.3	**740**	**39**	5660	260	59.4	3.7	306	19	1.28	0.14	43.3	2.3	270	16	1431	87	6.5	0.4	0.00	0.02	0.0	0.0	337	21
GR11-1A-59b.FIN2	Rextal	3.8E+07	4.2E+06	1263	58	894	56	6.3	**740**	**46**	14000	1100	109	10	446	37	1.61	0.19	49.7	4.5	665	53	4360	330	8.5	0.9	0.01	0.03	0.0	0.0	369	30
GR11-1A-79a.FIN2	Rextal	3.4E+07	2.8E+06	1400	40	906	47	5.2	**741**	**38**	18950	950	63.4	5	395	22	1.4	0.13	43.7	2.7	1243	68	2480	140	6.4	0.5	0.01	0.02	0.0	0.0	299	16
GR11-1A-18.FIN2	Rextal	3.7E+07	3.6E+06	889	29	908	42	4.6	**742**	**34**	7690	330	37.6	3.2	343	20	1.01	0.11	38	2.2	258	15	501	24	4.2	0.4	-0.01	0.02	0.0	0.0	203	12
GR11-1A-38c.FIN2	Rextal	3.7E+07	2.6E+06	930	31	943	36	3.8	**745**	**28**	9200	390	44.9	3.9	287	16	1.05	0.13	43.4	2.5	370	17	1611	80	5.2	0.4	0.02	0.02	0.0	0.0	255	13
GR11-1A-59c.FIN2	Rextal	3.7E+07	2.8E+06	1253	37	987	56	5.7	**750**	**43**	15260	800	106.7	6	434	26	1.66	0.16	61.9	4	779	46	4200	250	8.2	0.6	-0.01	0.02	0.0	0.0	380	22
GR11-1A-1.FIN2	Rextal	4.4E+07	3.9E+06	1062	40	1003	43	4.3	**751**	**32**	6390	270	61	3.7	328	16	1.64	0.17	47.6	2.5	364	19	1308	63	9.5	0.6	0.50	0.06	0.0	0.0	414	21
GR11-1A-3.FIN2	Rextal	4.9E+07	3.5E+06	1263	59	1021	47	4.6	**753**	**35**	2129	99	23.1	1.9	309	18	1.29	0.14	26.1	1.5	124.1	6.1	188	10	6.6	0.5	0.56	0.07	0.0	0.0	281	18
GR11-1A-86.FIN2	Grt	5.2E+07	6.0E+06	2120	140	1040	120	11.5	**755**	**87**	2190	200	8.8	4.3	110	12	2.23	0.48	55	10	141	22	147	28	3.0	0.6	0.07	0.07	0.1	0.1	173	32
GR11-1A-78a.FIN2	Rextal	3.4E+07	2.6E+06	1457	50	1045	45	4.3	**755**	**33**	15030	600	56	4.6	379	20	1.43	0.14	52.2	3.1	1135	69	1780	100	5.5	0.5	0.00	0.02	0.0	0.0	254	15
GR11-1A-63.FIN2	Rextal	4.8E+07	3.3E+06	1165	85	1065	87	8.2	**757**	**62**	17800	1800	68.6	7.9	284	17	1.03	0.17	58.5	5.2	1052	99	2700	250	5.8	0.9	0.02	0.04	9.0	12.0	335	34
GR11-1A-25.FIN2	Rextal	3.7E+07	2.9E+06	971	32	1097	41	3.7	**760**	**28**	7970	290	76.7	3.9	361	18	1.81	0.17	59.3	3	356	16	1706	82	10.1	0.7	0.02	0.02	0.0	0.0	473	21
GR11-1A-34.FIN2	Rextal	3.3E+07	3.0E+06	664	23	1165	50	4.3	**766**	**33**	8320	370	120.2	7.4	321	17	1.07	0.11	56.5	3.2	458	25	1813	89	14.8	2.2	8.90	2.10	0.0	0.0	246	14
GR11-1A-37b.FIN2	Rextal	3.5E+07	3.0E+06	931	30	1175	49	4.2	**767**	**32**	11280	480	38	4.2	288	15	1.01	0.13	50.7	2.4	628	27	1074	46	5.1	0.4	-0.01	0.02	0.0	0.0	234	10
GR11-1A-65.FIN2	Rextal	3.5E+07	2.5E+06	1851	71	1212	61	5.0	**770**	**39**	2156	97	31.4	2.5	382	20	1.67	0.16	36.7	2.3	136	6.6	328	18	10.7	0.7	0.03	0.02	0.0	0.0	541	29
GR11-1A-23a.FIN2	Rextal	4.1E+07	3.7E+06	1126	51	1229	54	4.4	**771**	**34**	16000	780	53	4.6	324	19	1.12	0.15	58.2	3.3	899	55	1940	110	5.2	0.5	0.03	0.02	0.0	0.0	246	16
GR11-1A-54.FIN2	Rextal	4.5E+07	3.1E+06	2720	140	1253	86	6.9	**773**	**53**	1470	110	17.6	1.5	71.4	5.4	1.47	0.17	48.8	3.7	139.4	9.7	17.1	1.5	1.3	0.2	0.39	0.08	0.0	0.0	51.5	3
GR11-1A-40.FIN2	Rextal	3.7E+07	2.5E+06	831	27	1276	53	4.2	**775**	**32**	9770	410	64.9	4.8	308	20	1.04	0.14	62.5	3.7	351	18	1293	77	5.2	0.4	0.00	0.02	0.0	0.0	241	14
GR11-1A-83.FIN2	Rextal	4.4E+07	4.7E+06	2840	280	1330	170	12.8	**779**	**100**	1920	210	2.7	3	71.7	7.4	2.44	0.67	29.1	3.6	116	19	114	19	1.4	0.5	0.25	0.05	0.6	0.2	63.2	7.8
GR11-1A-78b.FIN2	Rextal	4.3E+07	3.5E+06	1278	61	1334	86	6.4	**779**	**50**	16600	1200	75.2	7.1	375	26	1.89	0.27	62.5	5.5	743	67	2800	210	7.7	0.9	0.03	0.03	0.0	0.0	345	30
GR11-1A-52a.FIN2	Rextal	3.6E+07	2.7E+06	906	32	1427	81	5.7	**786**	**45**	11450	740	91.3	8.2	344	24	1.14	0.14	82.9	5.5	471	33	3340	230	5.3	0.6	0.01	0.02	0.0	0.0	288	19
GR11-1A-31b.FIN2	Rextal	3.1E+07	2.7E+06	1954	67	1465	57	3.9	**789**	**31**	1858	68	14.6	1.5	166.6	9.1	1.63	0.14	38.5	2.2	119.9	5.5	171.6	7.3	5.2	0.4	0.03	0.03	0.6	0.2	247	11
GR11-1A-67b.FIN2	Rextal	4.4E+07	4.5E+06	2110	200	1470	130	8.8	**790**	**70**	1830	190	6.7	2.4	77	10	1.84	0.25	37	2.7	112	10	116	11	0.8	0.2	0.12	0.06	1.0	0.3	45.9	5.2
GR11-1A-43a.FIN2	Rextal	3.6E+07	2.4E+06	1253	44	1662	77	4.6	**802**	**37**	3510	160	21.2	3.1	298	16	0.635	0.09	42.1	1.9	197	9.8	320	17	11.5	0.6	0.01	0.02	0.0	0.0	577	26
GR11-1A-81.FIN2	Rextal	2.8E+07	2.2E+06	1336	47	1694	57	3.4	**805**	**27**	15010	520	74	5.5	407	18	1.13	0.13	75.3	3.1	812	33	2332	93	7.5	0.5	0.00	0.02	0.0	0.0	331	15
GR11-1A-27.FIN2	Rextal	2.9E+07	2.3E+06	856	28	1736	55	3.2	**807**	**26**	7440	320	65	4.9	350	14	1.21	0.13	80	3.8	315	14	1145	56	5.2	0.4	0.10	0.04	0.0	0.0	222.3	9.2
GR11-1A-32.FIN2	Rextal	3.9E+07	3.1E+06	1118	38	1842	86	4.7	**814**	**38**	15960	800	62.1	4.9	309	18	0.91	0.11	90.8	5.3	877	53	2120	140	3.9	0.3	-0.01	0.02	0.0	0.0	186	13
GR11-1A-28.FIN2	Rextal	4.6E+07	4.6E+06	750	42	1850	140	7.6	**814**	**62**	5310	430	68.4	7.7	297	23	1.17	0.19	84.5	8.3	232	20	1211	97	5.1	0.6	0.01	0.03	0.0	0.0	272	23
GR11-1A-79b.FIN2	Rextal	3.3E+07	2.9E+06	2043	69	1857	78	4.2	**814**	**34**	38300	1700	61.7	4.8	379	20	0.916	0.098	85.1	4.8	5480	330	1810	100	3.9	0.3	0.00	0.02	0.0	0.0	186	11
GR11-1A-67a.FIN2	Rextal	3.1E+07	2.6E+06	1885	62	2062	77	3.7	**826**	**31**	277	12	5.2	0.56	65.1	3.4	4.54	0.31	56.9	3	30.1	1.5	5.8	0.57	2.1	0.3	0.86	0.17	0.0	0.0	60.4	3.4
GR11-1A-35.FIN2	Rextal	5.3E+07	3.9E+06	881	44	2220	160	7.2	**834**	**60**	2990	240	38.6	4.7	233	21	1.28	0.19	56	5.1	146	11	293	28	6.3	0.7	0.31	0.17	0.0	0.0	336	23
GR11-1A-13.FIN2	Rextal	4.0E+07	3.4E+06	701	22	2660	110	4.1	**855**	**35**	3730	160	20	3.2	279	18	1.62	0.14	71.2	4	184	11	284	16	6.8	0.5	0.20	0.04	0.0	0.0	345	20
GR11-1A-2.FIN2	Rextal	3.7E+07	3.5E+06	1093	43	3200	110	3.4	**877**	**30**	7050	260	73.1	4.3	359	18	1.97	0.16	91.1	5.2	367	19	1744	88	11.7	0.8	0.46	0.07	0.0	0.0	508	28
GR11-1A-39.FIN2	Rextal	5.9E+07	6.5E+06	730	48	3480	360	10.3	**888**	**92**	18000	2000	101.4	7.9	267	34	0.67	0.17	108	13	990	130	1800	250	3.7	0.4	0.03	0.04	0.0	0.0	240	33
GR11-1A-84.FIN2	Rextal	3.3E+07	3.2E+06	2450	120	3540	180	5.1	**890**	**45**	1890	100	9.8	1.2	87	6.2	2.29	0.25	90.6	6.7	113.2	8.2	116.6	7.2	1.4	0.2	0.09	0.03	0.3	0.1	51.6	3.9
Retrogressed Granulite (GR 11-1C)																																
GR11-1C-17b.FIN2	Grt	3.1E+07	2.6E+06	395	14	190.3	8.8	4.6	**612**	**28**	4920	200	3.9	1.7	219	11	1.91	0.22	7.28	0.54	663	37	139	7.1	2.8	0.2	0.01	0.03	0.0	0.0	139.2	8.1
GR11-1C-11.FIN2	Grt	3.2E+07	3.8E+06	496	15	268	13	4.9	**637**	**31**	5080	250	11.3	2.6	329	25	3.78	0.38	7.59	0.66	739	39	162.2	9.8	4.1	0.4	0.17	0.06	0.0	0.0	181	11
GR11-1C-15.FIN2	Grt	2.6E+07	3.6E+06	533	20	329	13	4.0	**653**	**26**	5320	230	16.4	3.3	522	33	2.09	0.28	10.66	0.93	840	44	164	10	4.4	0.4	0.10	0.08	0.2	0.1	208	14
GR11-1C-4.FIN2	Grt	2.8E+07	2.2E+06	902	28	364	14	3.8	**661**	**25**	5740	250	12.3	3.6	659	34	1.97	0.18	9.98	0.81	865	50	179	11	4.2	0.4	0.04	0.03	0.0	0.0	203	13
GR11-1C-24.FIN2	Grt	3.3E+07	2.4E+06	470	16	726	49	6.7	**721**	**49**	6550	470	5.7	2.6	338	22	1.14	0.15	33.2	2.8	1091	76	47.9	3.9	6.4	0.6	-0.02	0.02	0.0	0.0	291	21
GR11-1C-9.FIN2	Grt	2.6E+07	2.3E+06	414	15	734	37	5.0	**722**	**36**	5630	280	10.7	3.6	375	22	0.82	0.14	22.8	1.7	767	43	184	11	7.8	0.9	4.21	0.61	0.8	0.1	164.3	9.3
GR11-1C-25.FIN2	Grt	3.3E+07	2.2E+06	360	13	794	62	7.8	**729**	**57**	5170	410	4.2	2.4	343	21	1.45	0.16	23.1	1.8	633	44	187	14	9.1	0.8	-0.02	0.02	0.0	0.0	418	26
GR11-1C-10.FIN2	Grt	3.8E+07	2.9E+06	566	20	798	32	4.0	**729**	**29**	5650	240	19.4	3.4	438	21	4.14	0.28	23	1.4	879	40	190	10	7.3	0.6	0.07	0.03	0.0	0.0	319	20
GR11-1C-6b.FIN2	Rextal	2.6E+07	3.2E+06	1000	26	799	31	3.9	**730**	**28**	3070	100	17.1	2.4	240	12	0.54	0.12	20	1.3	174.6	7.5	183.7	9	5.5	0.4	0.06	0.05	0.1	0.0	285	17
GR11-1C-23.FIN2	Grt	8.1E+06	3.7E+06	10800	3600	850	310	36.5	**735**	**268**	4640	550	-70	120	1560	410	96	72	6.1	3.1	470	86	283	76	-21.0	32.0	-57.00	34.00	0.3	0.2	269	49
GR11-1C-20.FIN2	Grt	1.3E+07	3.3E+06	1137	84	900	210	23.3	**741**	**173**	5460	600	18.7	5.3	1140	190	3.4	0.79	17.2	4.2	738	72	231	34	34.0	9.8	23.00	7.90	2.2	0.7	145	12
GR11-1C-13.FIN2	Grt	3.4E+07	4.1E+06	945	35	904	45	5.0	**741**	**37**	28500	1400	44.6	5.7	538	66	8.2	1	59.3	4.1	4130	250	1470	100	5.0	0.5	1.09	0.55	0.4	0.2	196	15
GR11-1C-3.FIN2	Grt	2.9E+07	2.0E+06	956	31	972	39	4.0	**748**	**30**	7480	320	7.1	2.9	767	36	2.09	0.21	28.4	1.9	1221	70	251	14	4.8	0.4	0.01	0.02	0.0	0.0	216	13
GR11-1C-17a.FIN2	Grt	3.6E+07	3.0E+06	704	20	1035	40	3.9	**754**	**29**	5450	230	4	2.1	543	26	3.53	0.25	36.7	2.2	909	51	165.6	9.8	4.1	0.4	0.00	0.02	0.0	0.0	209	13
GR11-1C-18c.FIN2	Grt	2.0E+07	4.5E+06	686	58	1140	100	8.8	**764**	**67**	18130	970	85	11	1290	160	5	0.9	58.6	7.6	3640	250	1250	110	13.0	2.8	7.20	2.10	0.3	0.2	180	20
GR11-1C-18a.FIN2	Grt	1.3E+07	2.7E+06	881	77	1293	52	4.0	**776**	**31**	19910	840	75	10	1035	76	4.06	0.59	65.5	3.8	2940	140	958	57	21.5	4.4	18.80	4.40	0.7	0.2	179	10
GR11-1C-5.FIN2	Grt	3.4E+07	2.4E+06	563	19	1297	77	5.9	**777**	**46**	7030	300	15.3	3.7	782	40	2.83	0.29	43.1	3.4	1098	63	234	15	5.0	0.4	0.12	0.06	2.5	1.1	246	14
GR11-1C-22.FIN2	Grt	3.4E+07	2.9E+06	482	17	1460	100	6.8	**789**	**54**	4420	330	10.6	3.3	359	27	3.27	0.28	49.3	3.9	537	46	153	14	23.6	2.1	-0.01	0.02	0.0	0.0	1047	86
GR11-1C-16a.FIN2	Grt	3.0E+07	3.7E+06	668	22	1606	55	3.4	**799**	**27**	3560	140	9.3	2.1	331	18	2.83	0.3	49.2	3.2	344	23	107.5	6.2	4.8	1.2	1.70	1.20	0.6	0.2	150.8	8.1
GR11-1C-18b.FIN2	Grt	2.9E+07	4.0E+06	641	27	1677	84	5.0	**803**	**40**	29900	1900	66	10	874	75	3.23	0.33	80.7	5.1	4410	450	992	61	5.3	0.5	0.21	0.11	0.5	0.2	266	21
GR11-1C-16b.FIN2	Grt	3.7E+07	2.2E+06	733	27	1816	82	4.5	**812**	**37**	4560	220	11.9	3.4	364	19	2.31	0.21	65.7	3.5	680	40	175	11	3.6	0.3	0.08	0.03	0.0	0.0	158	11
GR11-1C-8.FIN2	Rextal	3.3E+07	2.9E+06	913	25	2250	110	4.9	**836**	**41**	3650	160	12.5	2.4	292	18	0.49	0.1	65.1	3.4	214	11	197	12	6.4	0.5	0.19	0.07	0.1	0.0	280	17
GR11-1C-2.FIN2	Grt	2.5E+07	2.1E+06	324	12	2370	140	5.9	**842**	**50**	8870	550	26.9	5.1	634	50	2.92	0.3	130	10	1135	89	410	36	6.1	0.6	0.87	0.14	0.0	0.0	226	20

Sample and Analysis Number	Texture	Ti (cps)	± 2SE (cps)	V (ppm)	± 2SE (ppm)	Zr (ppm)	± 2SE (ppm)	± 2SE %	**Zr-in-Rt T (°C)**	**± 2SE (°C)**	Nb (ppm)	± 2SE (ppm)	Mo (ppm)	± 2SE (ppm)	Sn (ppm)	± 2SE (ppm)	Sb (ppm)	± 2SE (ppm)	Hf (ppm)	± 2SE (ppm)	Ta (ppm)	± 2SE (ppm)	W (ppm)	± 2SE (ppm)	206Pb (ppm)	± 2SE (ppm)	208Pb (ppm)	± 2SE (ppm)	Th (ppm)	± 2SE (ppm)	U (ppm)	± 2SE (ppm)
GR11-1C-7.FIN2	Rextal	3.1E+07	2.3E+06	978	32	2420	120	5.0	**844**	**42**	3390	170	15.3	2.3	291	16	0.79	0.13	64	4.2	183.7	9.9	237	16	7.9	0.6	0.13	0.05	0.1	0.1	369	24
GR11-1C-12.FIN2	Grt	2.9E+07	4.0E+06	368	12	2478	97	3.9	**847**	**33**	4800	210	10.8	2.7	335	26	0.375	0.097	78.6	4.3	647	33	160	11	3.8	0.9	3.05	0.93	0.6	0.2	39.2	2.4
GR11-1C-26.FIN2	Grt	3.7E+07	3.2E+06	527	22	2520	200	7.9	**849**	**67**	7110	640	14.3	3.6	430	31	2.75	0.32	90.5	7.2	1091	99	183	15	7.9	1.4	1.71	0.91	0.2	0.1	267	24
GR11-1C-1.FIN2	Grt	3.4E+07	2.6E+06	362	11	2810	120	4.3	**862**	**37**	20660	930	68.3	5.1	797	46	4.5	0.36	211	11	3580	200	672	39	5.8	0.4	0.02	0.03	0.0	0.0	277	18
GR11-1C-21.FIN2	Grt	9.4E+06	3.4E+06	1730	400	3150	270	8.6	**875**	**75**	6300	470	11	27	2250	780	24	16	60	13	880	85	660	130	15.0	13.0	-5.80	5.10	0.0	0.0	281	32
GR11-1C-14.FIN2	Grt	2.7E+07	3.2E+06	507	18	3550	170	4.8	**890**	**43**	6870	300	8.7	2.5	428	27	2.4	0.27	148.4	7.8	911	49	242	14	8.4	0.7	0.33	0.12	0.7	0.2	333	18
GR11-1C-27.FIN2	Grt	2.9E+07	4.0E+06	516	20	3590	250	7.0	**892**	**62**	9590	740	53.8	6.5	1020	100	4.97	0.64	119	9.5	1137	81	944	80	22.5	2.2	0.20	0.11	0.1	0.1	891	52
GR11-1C-19.FIN2	Grt	3.1E+07	2.3E+06	448	15	3690	170	4.6	**895**	**41**	10560	470	21.7	4.2	1122	57	3.52	0.29	201	10	1318	64	387	19	8.2	0.5	0.04	0.03	0.0	0.0	383	21
Leucogranulite (GR11-35)																																
GR11-35-26.FIN2	Peak	1.4E+07	1.4E+06	1342	37	8.9	1.4	15.7	**435**	**68**	3390	180	0.83	0.41	314	23	0.084	0.053	0.65	0.27	298	16	5.58	0.74	0.0	0.1	0.00	0.06	0.0	0.0	0.0062	0.0054
GR11-35-30.FIN2	Peak	1.8E+07	2.1E+06	2887	99	32.3	1.9	5.9	**500**	**29**	97.5	4.9	0.08	0.16	103.8	6.7	0.066	0.047	1.32	0.3	5.94	0.48	0.01	0.014	0.0	0.0	0.00	0.04	0.0	0.0	bdl	-
GR11-35-49B.FIN2	Peak	2.8E+07	2.9E+06	1047	66	38.9	7.1	18.3	**510**	**93**	2090	340	0.75	0.36	103	10	0.17	0.11	13.9	2	128	21	0.93	0.32	0.0	0.0	0.01	0.04	0.0	0.0	bdl	-
GR11-35-34A.FIN2	Peak	2.8E+07	2.2E+06	1890	130	41.9	7.1	16.9	**514**	**87**	7550	620	11.8	7.3	307	32	-0.023	0.016	14.4	1.3	531	57	10.4	1.5	0.0	0.0	0.07	0.04	0.0	0.0	0.026	0.018
GR11-35-34B.FIN2	Peak	2.4E+07	2.1E+06	2590	130	57.9	6.5	11.2	**533**	**60**	5650	410	2.5	2.6	378	37	0.045	0.047	12.7	1.6	363	30	11.9	1.4	6.8	1.3	6.00	1.10	4.5	1.2	4.14	0.83
GR11-35-47.FIN2	Peak	2.3E+07	2.3E+06	2350	150	60.2	5.1	8.5	**536**	**45**	894	62	1.22	0.4	144	17	0.011	0.033	14.9	1.8	27.4	2.3	2.81	0.55	1.2	0.3	1.37	0.27	0.3	0.2	0.023	0.016
GR11-35-44.FIN2	Peak	1.2E+07	1.1E+06	2302	94	106	18	17.0	**571**	**97**	1749	97	0.64	0.43	353	32	0.011	0.06	12.7	1.8	133	10	0.83	0.25	0.2	0.1	0.20	0.11	0.0	0.0	0.58	0.13
GR11-35-23.FIN2	Peak	4.6E+07	4.2E+06	504	17	1522	65	4.3	**793**	**34**	6620	280	0.51	0.84	1274	73	0.045	0.03	80.2	4.6	315	18	39.7	2.7	17.0	1.1	0.04	0.03	0.4	0.5	757	51
GR11-35-22.FIN2	Peak	4.8E+07	3.2E+06	1266	34	1917	77	4.0	**818**	**33**	10690	390	0.1	0.15	1119	60	0.028	0.02	103.7	5.6	1178	66	50.3	3.3	9.3	0.6	0.02	0.02	0.0	0.0	438	28
GR11-35-29.FIN2	Peak	2.9E+07	4.4E+06	986	36	1930	100	5.2	**819**	**42**	3740	220	1.42	0.57	1329	84	0.11	0.052	108.4	8.2	267	20	38.6	3	50.0	5.2	65.00	7.90	17500.0	2900.0	1510	200
GR11-35-2A.FIN2	Peak	3.8E+07	3.3E+06	957	29	2316	76	3.3	**839**	**28**	6350	240	2.9	1.7	832	44	0.028	0.019	78.4	4.2	584	26	57.8	2.8	13.4	0.8	0.02	0.02	0.0	0.0	543	30
GR11-35-21.FIN2	Peak	3.8E+07	3.1E+06	728	25	2334	98	4.2	**840**	**35**	4920	220	1.6	1.3	1258	70	0.082	0.034	109.7	6.8	264	15	29.2	2	13.1	0.9	0.02	0.02	0.0	0.0	549	39
GR11-35-25.FIN2	Peak	4.9E+07	3.8E+06	1039	33	2340	100	4.3	**840**	**36**	3930	180	0.89	0.71	694	33	0.13	0.042	77.5	4.8	241	16	53.6	3.8	24.9	2.0	2.75	0.80	16.4	5.8	960	75
GR11-35-2C.FIN2	Peak	4.4E+07	3.7E+06	1004	28	2476	86	3.5	**847**	**29**	6840	280	1.9	1.3	846	51	0.061	0.043	83.4	5.2	633	37	65.4	4.2	11.2	0.8	0.01	0.02	0.0	0.0	494	34
GR11-35-2B.FIN2	Peak	4.3E+07	4.2E+06	988	29	2580	110	4.3	**852**	**36**	7170	320	2.4	1.7	920	62	0.049	0.029	84.3	5.2	642	38	66.1	4.6	14.1	1.0	0.87	0.22	0.4	0.1	539	37
GR11-35-4.FIN2	Peak	4.5E+07	3.9E+06	1527	47	2690	110	4.1	**857**	**35**	6100	260	1.5	1.1	1122	85	0.1	0.039	120	8.1	260	15	36.3	2.4	19.2	1.5	0.01	0.02	0.0	0.0	792	54
GR11-35-2D.FIN2	Peak	3.9E+07	3.9E+06	1006	32	2720	130	4.8	**858**	**41**	7410	390	1.2	1.1	951	70	0.043	0.024	82.8	5.5	651	38	59.4	3.7	14.1	1.0	0.01	0.02	0.0	0.0	533	31
GR11-35-15.FIN2	Peak	4.4E+07	3.7E+06	3098	85	2893	89	3.1	**865**	**27**	1906	67	2.24	0.34	1089	42	0.122	0.036	97.4	4	63.4	2.5	26.9	1.1	19.0	0.8	0.34	0.06	0.0	0.0	823	26
GR11-35-6.FIN2	Peak	4.5E+07	3.3E+06	1311	40	2940	120	4.1	**867**	**35**	5710	240	2	1.2	906	73	0.082	0.03	94.1	5.2	359	20	81.6	4.4	14.2	0.9	-0.01	0.02	0.0	0.0	638	41
GR11-35-10.FIN2	Peak	4.5E+07	3.7E+06	2959	80	2980	140	4.7	**869**	**41**	4750	210	0.79	0.54	1085	73	0.146	0.04	94.8	6.3	477	33	42	3.1	12.3	1.0	0.01	0.02	0.0	0.0	512	38
GR11-35-42.FIN2	Peak	4.0E+07	2.9E+06	1375	42	3110	150	4.8	**874**	**42**	2670	140	1.27	0.57	1067	70	0.395	0.069	110.8	8.1	104.1	7.1	42.7	3.1	20.6	1.6	0.03	0.02	0.0	0.0	921	75
GR11-35-1.FIN2	Peak	4.4E+07	3.7E+06	1079	35	3170	140	4.4	**876**	**39**	7120	300	0.64	0.72	993	62	0.079	0.027	100.5	6.6	627	38	74.9	5.2	20.0	1.4	0.37	0.13	0.1	0.1	841	59
GR11-35-41.FIN2	Peak	3.9E+07	3.1E+06	2199	85	3180	160	5.0	**877**	**44**	4630	270	4	1.9	1570	100	0.306	0.09	99.9	6.2	116.9	8	64.4	4.4	35.5	2.3	0.17	0.07	0.1	0.1	1540	100
GR11-35-16.FIN2	Peak	4.4E+07	3.8E+06	3218	84	3270	140	4.3	**880**	**38**	1918	76	2.73	0.39	1225	73	0.142	0.037	111.6	7.9	58.5	4	30.9	2.2	25.9	1.9	0.11	0.03	0.0	0.0	1220	100
GR11-35-3.FIN2	Peak	5.1E+07	4.1E+06	652	19	3370	130	3.9	**884**	**34**	6240	250	1.26	0.87	864	48	0.048	0.021	102.6	5.8	774	42	50.9	3.2	12.6	0.8	0.00	0.02	0.0	0.0	542	38
GR11-35-32.FIN2	Peak	5.9E+07	5.1E+06	2150	100	3920	250	6.4	**903**	**58**	5210	440	5.1	2.5	1126	82	0.216	0.076	134	12	277	26	55.4	5.5	15.5	1.8	0.49	0.39	0.1	0.1	717	60
GR11-35-40.FIN2	Peak	3.9E+07	3.2E+06	2013	56	3990	160	4.0	**905**	**36**	4380	180	0.34	0.39	1166	67	0.167	0.049	131.4	8.9	265	17	46.8	2.6	21.2	1.6	0.01	0.02	0.0	0.0	823	55
GR11-35-28.FIN2	Peak	4.6E+07	3.0E+06	652	22	4010	160	4.0	**906**	**36**	3050	130	2.55	0.86	1145	56	0.077	0.028	137.3	8.4	106.9	6	39.7	2.7	6.0	0.5	0.00	0.01	0.0	0.0	282	18
GR11-35-20.FIN2	Peak	4.9E+07	3.6E+06	962	37	4100	180	4.4	**909**	**40**	4140	220	0.46	0.32	1346	83	0.06	0.04	152.8	9.5	250	16	56.8	3.7	14.4	1.2	0.33	0.17	0.2	0.1	630	46
GR11-35-33.FIN2	Peak	4.5E+07	3.2E+06	2107	65	4100	150	3.7	**909**	**33**	4090	150	2.05	0.8	1390	71	0.155	0.045	143.5	9.3	173.6	9.6	55.9	4	24.0	1.5	0.15	0.04	0.0	0.0	1121	64
GR11-35-37.FIN2	Peak	4.4E+07	3.4E+06	1745	55	4140	190	4.6	**910**	**42**	9860	470	1.82	0.86	1098	72	0.076	0.031	129.1	7.8	495	33	140	10	11.3	0.8	0.02	0.02	0.0	0.0	499	36
GR11-35-13.FIN2	Peak	5.4E+07	5.5E+06	2250	150	4170	440	10.6	**911**	**96**	6940	680	2.6	2.1	1320	140	0.156	0.097	188	21	477	42	206	24	7.7	1.1	0.03	0.04	0.4	0.1	342	49
GR11-35-24.FIN2	Peak	5.1E+07	3.7E+06	867	29	4340	170	3.9	**916**	**36**	4110	170	0.91	0.35	1129	60	0.046	0.025	168	10	282	17	37	2.3	8.3	0.7	0.35	0.17	0.2	0.1	362	25
GR11-35-18.FIN2	Peak	6.6E+07	6.3E+06	1191	59	4900	410	8.4	**932**	**78**	6610	390	-0.0236	0.0023	1121	92	0.036	0.032	185	14	382	32	53.8	4.7	17.0	1.9	0.51	0.16	0.3	0.3	804	68
GR11-35-38.FIN2	Peak	4.2E+07	3.2E+06	2149	75	4920	220	4.5	**933**	**42**	4840	240	2.4	1.2	1163	69	0.125	0.052	173	11	207	13	56.7	3.8	17.3	1.2	0.00	0.01	0.0	0.0	799	53
GR11-35-14.FIN2	Peak	4.4E+07	3.1E+06	2538	87	4950	250	5.1	**933**	**47**	12420	700	1.01	0.4	1389	88	0.68	0.14	145	10	1510	100	58.3	4.6	25.8	2.1	0.14	0.04	0.0	0.0	1157	87
GR11-35-19.FIN2	Peak	3.8E+07	4.4E+06	1169	44	5050	200	4.0	**936**	**37**	5830	270	9.4	3.7	1694	93	0.15	0.12	168	10	475	26	106.4	6.7	41.5	4.1	4.10	2.10	0.6	0.4	1488	96
GR11-35-36.FIN2	Peak	5.4E+07	5.1E+06	3790	150	5280	230	4.4	**942**	**41**	826	55	2.93	0.5	1015	85	0.172	0.07	145	11	15.7	1.5	24.7	1.7	23.3	2.0	0.32	0.24	0.1	0.1	1083	87
GR11-35-11.FIN2	Peak	4.5E+07	3.4E+06	3510	110	5860	250	4.3	**957**	**41**	17460	870	5.9	1.8	1398	91	0.094	0.031	260	18	2310	160	201	13	14.1	0.9	0.01	0.02	0.0	0.0	679	47
GR11-35-43.FIN2	Peak	2.9E+07	2.4E+06	616	23	5930	250	4.2	**958**	**40**	4880	220	1.3	1.1	1608	86	0.158	0.053	202	13	100.3	7.3	39	2.9	27.2	1.7	1.62	0.20	2.9	0.6	1074	81
GR11-35-17.FIN2	Peak	4.1E+07	3.6E+06	1252	41	6130	250	4.1	**963**	**99**	3940	160	2.15	0.92	1402	75	0.111	0.051	201.1	9.7	177	11	57.4	3.8	13.5	1.1	0.15	0.04	0.0	0.0	581	32
GR11-35-49A.FIN2	Peak	4.5E+07	3.2E+06	1178	39	6400	400	6.3	**969**	**61**	7160	430	1.8	1.1	941	49	0.179	0.048	250	19	413	31	43.4	4.1	18.9	1.5	0.13	0.09	0.0	0.0	781	52
GR11-35-50.FIN2	Peak	5.9E+07	4.1E+06	517	22	6440	730	11.3	**970**	**110**	12900	1300	2.7	2.4	1000	120	2.46	0.75	267	32	604	66	67.8	7.3	10.9	1.1	0.19	0.09	0.1	0.1	588	71
GR11-35-8.FIN2	Peak	4.6E+07	3.5E+06	1296	41	6710	250	3.7	**976**	**36**	8610	350	2.6	1.2	1117	66	0.104	0.035	198	12	585	35	159.6	9.6	15.1	1.0	0.01	0.02	0.0	0.0	634	45
GR11-35-31.FIN2	Peak	3.6E+07	3.4E+06	658	21	10160	440	4.3	**1039**	**45**	10250	370	5	2.3	1536	76	0.109	0.051	352	18	757	36	119.5	6.4	26.0	1.8	0.02	0.02	0.0	0.0	984	60
Charnockite (GR11-43)																																
GR11-43-42.FIN2	Peak	8.5E+06	1.2E+06	5760	650	4.22	0.92	21.8	**402**	**88**	827	43	53.6	6.2	606	81	0.14	0.11	0.091	0.09	76.1	4.5	0.7	0.27	1.6	0.5	1.74	0.39	0.0	1.0	0.0028	0.0055
GR11-43-13.FIN2	Peak	2.9E+07	2.8E+06	1436	52	70.6	5.2	7.4	**545**	**40**	126.3	9.5	23.3	2.2	288	22	1.76	0.24	5.42	0.71	9	0.89	0.31	0.12	0.3	0.1	0.29	0.08	0.0	1.0	0.216	0.042
GR11-43-27.FIN2	Peak	2.4E+07	2.0E+06	557	21	682	29	4.3	**715**	**30**	33100	1500	150.4	9.1	932	58	0.161	0.043	56.1	3.4	1212	68	2890	180	1.3	0.2	1.17	0.15	0.0	1.0	19.9	1.2
GR11-43-3.FIN2	Peak	3.0E+07	2.7E+06	1679	85	930	360	43.4	**733**	**318**	5210	310	157	12	1225	93	-0.0002	0.000019	51	18	193	21	234	26	7.3	0.9	5.51	0.75	0.1	0.1	87	10
GR11-43-19.FIN2	Peak	2.6E+07	2.4E+06	1964	77	1396	73	5.2	**784**	**41**	5850	330	179	13	1340	110	0.026	0.019	93.3	8.8	266	23	346	33	3.6	0.4	0.64	0.21	0.0	1.0	126	11
GR11-43-49.FIN2	Peak	2.1E+07	1.8E+06	1985	70	2040	100	4.9	**825**	**40**	6400	350	182	11	1480	110	0.041	0.023	117	9.1	255	18	331	26	5.4	0.5	1.65	0.40	0.0	0.0	143	11
GR11-43-41.FIN2	Peak	2.3E+07	1.8E+06	473	14	2460	120	4.9	**846**	**41**	6080	300	234	16	1267	84	0.99	0.2	131.7	8.1	175	11	386	24	2.9	0.4	0.00	0.01	0.0	1.0	128.8	8.9
GR11-43-36.FIN2	Peak	2.4E+07	1.8E+06	2151	72	2610	120	4.6	**853**	**39**	8690	420	136	9.9	1378	84	0.045	0.026	97.8	5.7	474	30	679	41	1.4	0.2	0.02	0.02	0.0	1.0	68.3	4.5
GR11-43-47.FIN2	Peak	2.5E+07	2.3E+06	2900	100	3310	160	4.8	**882**	**43**	6340	320	70.1	5.6	1231	80	0.56	0.11	112.6	7.9	268	19	344	27	1.1	0.2	0.05	0.03	0.0	1.0	45.1	3.4
GR11-43-6.FIN2	Peak	2.9E+07	2.8E+06	1831	59	3960	180	4.5	**904**	**41**	4500	270	151.5	9.3	1173	79	0.028	0.017	130.1	9.1	125	11	198	17	2.0	0.3	0.09	0.04	0.0	1.0	93.7	7.8
GR11-43-28.FIN2	Peak	2.9E+07	2.0E+06	1348	45	4170	170	4.1	**911**	**37**	9480	390	228	11	1281	67	0.036	0.023	165.3	9.9	533	30	839	52	2.6	0.3	0.44	0.13	0.0	1.0	96.2	5.8
GR11-43-50.FIN2	Peak	2.4E+07	2.0E+06	2805	94	4190	400	9.5	**911**	**87**	6730	660	141	14	1120	90	0.024	0.019	152	16	361	38	351	35	1.7	0.2	0.02	0.02	0.0	1.0	80.5	6.3
GR11-43-51.FIN2	Peak	2.4E+07	2.2E+06	1666	57	4230	170	4.0	**913**	**37**	23270	960	160	11	1544	97	0.055	0.027	119.5	7.1	1615	98	1760	110	1.2	0.2	0.01	0.02	0.0	1.0	55.1	3.5
GR11-43-48.FIN2	Peak	2.7E+07	2.2E+06	1888	62	4310	230	5.3	**915**	**49**	7240	410	139.5	9.5	1186	79	0.487	0.098	161	12	478	32	436	31	3.3	0.4	0.00	0.01	0.0	1.0	153	11
GR11-43-7.FIN2	Peak	2.5E+07	2.7E+06	1870	100	4350	260	6.0	**916**	**55**	4980	270	179	12	1225	74	0.053	0.03	156	12	177	15	254	23	9.3	1.7	7.50	1.70	0.0	0.0	119	12
GR11-43-1.FIN2	Peak	2.3E+07	2.1E+06	1858	68	4370	190	4.3	**917**	**40**	4070	200	235	13	1339	83	0.032	0.024	159	11	308	20	360	25	6.8	0.9	3.36	0.65	0.0	0.0	127.9	9.1
GR11-43-5.FIN2	Peak	2.1E+07	1.5E+06	2181	67	4390	160	3.6	**917**	**33**	4360	200	146.7	6.7	1332	62	0.018	0.015	150.6	8.8	120.3	5.9	207	12	8.5	0.8	6.80	0.61	0.0	0.0	83.9	5
GR11-43-8.FIN2	Peak	3.5E+07	2.5E+06	1456	56	4390	230	5.2	**917**	**48**	6790	480	195	15	1230	100	0.02	0.018	157	12	253	19	377	28	2.5	0.4	0.36	0.18	0.0	1.0	104	8.2

Sample and Analysis Number	Texture	Ti (cps)	± 2SE (cps)	V (ppm)	± 2SE (ppm)	Zr (ppm)	± 2SE (ppm)	± 2SE %	**Zr-in-Rt T (°C)**	**± 2SE (°C)**	Nb (ppm)	± 2SE (ppm)	Mo (ppm)	± 2SE (ppm)	Sn (ppm)	± 2SE (ppm)	Sb (ppm)	± 2SE (ppm)	Hf (ppm)	± 2SE (ppm)	Ta (ppm)	± 2SE (ppm)	W (ppm)	± 2SE (ppm)	206Pb (ppm)	± 2SE (ppm)	208Pb (ppm)	± 2SE (ppm)	Th (ppm)	± 2SE (ppm)	U (ppm)	± 2SE (ppm)
GR11-43-31.FIN2	Peak	2.9E+07	3.1E+06	1554	60	4390	190	4.3	**917**	**40**	10050	530	234	15	1355	88	0.019	0.017	166	12	496	36	640	57	5.4	0.6	3.11	0.50	0.0	0.0	115.3	9.2
GR11-43-35.FIN2	Peak	3.0E+07	2.2E+06	2254	66	4420	190	4.3	**918**	**39**	9870	530	161	11	1037	55	0.027	0.015	157	11	538	33	432	26	1.8	0.2	0.09	0.03	0.0	1.0	80.9	5.4
GR11-43-17.FIN2	Peak	2.2E+07	1.8E+06	1538	45	4440	190	4.3	**919**	**39**	6920	350	156	10	1300	76	0.042	0.031	159.9	9.7	207	14	380	28	7.4	0.6	3.84	0.39	0.0	1.0	128	11
GR11-43-43.FIN2	Peak	2.6E+07	2.4E+06	1483	61	4470	200	4.5	**920**	**41**	9870	550	269	17	1435	96	0.021	0.021	167	12	483	37	703	54	3.9	0.4	0.21	0.10	0.0	1.0	169	15
GR11-43-12.FIN2	Peak	2.7E+07	2.2E+06	1795	73	4490	250	5.6	**920**	**51**	6620	440	198	16	989	78	0.014	0.013	154.8	9.7	358	19	546	32	4.4	0.4	0.71	0.18	0.0	1.0	168.7	9.9
GR11-43-26.FIN2	Peak	2.6E+07	2.1E+06	1330	41	4490	160	3.6	**920**	**33**	8660	430	259	14	1444	87	0.033	0.022	182	11	484	30	629	40	3.8	0.4	0.04	0.02	0.0	1.0	158.7	9.2
GR11-43-2.FIN2	Peak	3.9E+07	3.2E+06	1615	88	4520	280	6.2	**921**	**57**	5840	370	269	24	1390	120	0.015	0.015	172	16	113	11	580	55	3.0	0.4	0.28	0.12	0.0	1.0	159	17
GR11-43-46.FIN2	Peak	2.8E+07	2.3E+06	1987	80	4520	310	6.9	**921**	**63**	7820	520	153	13	1223	84	1.63	0.25	166	11	374	24	404	25	7.1	0.7	3.58	0.55	0.0	0.0	153	10
GR11-43-14.FIN2	Peak	2.4E+07	1.7E+06	1606	55	4610	370	8.0	**924**	**74**	7940	690	228	22	1223	92	0.029	0.016	184	14	394	33	601	52	3.7	0.4	0.12	0.03	0.0	1.0	162	11
GR11-43-29.FIN2	Peak	2.2E+07	1.8E+06	1780	63	4650	220	4.7	**925**	**44**	6790	300	250	13	1337	68	0.01	0.01	174	11	447	27	669	44	3.0	0.3	0.20	0.05	0.0	1.0	119.6	8.2
GR11-43-45.FIN2	Peak	2.2E+07	2.4E+06	2320	100	4680	260	5.6	**926**	**51**	7740	460	160	15	1500	130	3.6	0.5	163	14	430	35	500	36	3.8	0.5	0.22	0.07	0.0	1.0	162	13
GR11-43-40.FIN2	Peak	2.4E+07	1.9E+06	1743	59	4710	250	5.3	**927**	**49**	9500	540	258	14	1429	97	0.084	0.041	165	11	1001	73	529	36	2.9	0.3	0.05	0.03	0.0	1.0	140	11
GR11-43-9.FIN2	Peak	2.6E+07	1.8E+06	1046	34	4750	200	4.2	**928**	**39**	14730	690	367	17	2030	100	0.021	0.016	204	13	812	50	1750	120	4.6	0.4	0.04	0.02	0.0	1.0	219	17
GR11-43-15.FIN2	Peak	2.8E+07	2.5E+06	1232	44	4760	290	6.1	**928**	**57**	7170	460	258	20	1340	110	0.042	0.03	197	14	252	16	507	35	4.1	0.6	0.70	0.32	0.0	1.0	167	13
GR11-43-44.FIN2	Peak	2.8E+07	2.0E+06	1628	50	4810	280	5.8	**930**	**54**	8040	490	211	14	1138	80	1.72	0.29	180	13	392	26	605	44	3.5	0.3	0.01	0.02	0.0	1.0	169	12
GR11-43-34.FIN2	Peak	3.2E+07	2.9E+06	1749	81	4820	310	6.4	**930**	**60**	6360	430	235	13	1280	110	0.019	0.016	167	17	292	26	474	43	6.7	2.1	4.00	1.80	0.0	0.0	109.5	9.9
GR11-43-18.FIN2	Peak	2.1E+07	1.8E+06	1775	59	4900	240	4.9	**932**	**46**	6610	360	252	17	1409	92	0.01	0.012	176	15	200	16	518	44	10.2	1.1	6.00	0.83	0.0	0.0	214	21
GR11-43-38.FIN2	Peak	2.9E+07	2.6E+06	1388	64	4930	300	6.1	**933**	**57**	7850	460	195	19	1120	110	0.019	0.02	175	16	255	19	490	38	27.0	10.0	23.50	9.60	0.9	0.7	128.3	9
GR11-43-32.FIN2	Peak	2.3E+07	1.9E+06	1425	46	5020	210	4.2	**935**	**39**	10060	400	266	12	1287	69	0.056	0.032	182	11	492	28	672	43	5.6	0.6	3.31	0.52	0.0	0.0	115.1	8.3
GR11-43-39.FIN2	Peak	2.4E+07	1.6E+06	1374	44	5080	300	5.9	**937**	**55**	7280	480	226	18	1246	92	0.0059	0.0084	190	14	236	16	556	42	2.5	0.2	0.03	0.02	0.0	1.0	129.1	9.5
GR11-43-21.FIN2	Peak	2.9E+07	2.2E+06	1518	69	5150	390	7.6	**939**	**71**	11430	770	243	20	1300	100	0.02	0.016	229	18	786	65	966	79	3.3	0.5	0.29	0.13	0.0	1.0	158	12
GR11-43-23.FIN2	Peak	3.1E+07	3.6E+06	1534	85	5220	490	9.4	**941**	**88**	21900	2000	294	35	1670	200	-9E-05	0.000015	209	25	1710	170	1101	98	3.8	0.7	1.01	0.44	0.0	1.0	150	14
GR11-43-30.FIN2	Peak	2.8E+07	2.3E+06	1681	62	5380	200	3.7	**945**	**35**	11120	460	246	12	1275	65	0.018	0.014	220	12	589	35	756	49	2.5	0.2	0.37	0.07	0.0	1.0	102.5	7.3
GR11-43-10.FIN2	Peak	2.4E+07	1.8E+06	1579	56	5450	230	4.2	**946**	**40**	13510	710	263	16	1268	76	0.01	0.011	237	15	767	46	1170	73	4.3	0.4	0.02	0.02	0.0	1.0	182	12
GR11-43-37.FIN2	Peak	2.6E+07	1.7E+06	1413	40	5480	340	6.2	**947**	**59**	25200	1700	331	27	1294	79	0.0046	0.0065	233	16	1425	89	1680	120	3.2	0.3	0.10	0.03	0.0	1.0	159.7	8.6
GR11-43-16.FIN2	Peak	2.6E+07	1.9E+06	1250	43	5520	330	6.0	**948**	**57**	20600	1300	214	16	1313	80	0.012	0.012	208	15	865	62	736	54	2.6	0.3	-0.01	0.01	0.0	1.0	127.3	8.9
GR11-43-33.FIN2	Peak	3.6E+07	2.4E+06	827	31	5900	340	5.8	**957**	**55**	15320	800	286	16	1113	68	0.0029	0.0059	238	12	651	34	1098	74	2.3	0.4	0.38	0.11	0.0	1.0	115.3	8.2
Stromatic Granulite (Bras10-5b-1)															nd	-																
Bras10Sb-37d	Grt	3.7E+06	2.0E+06	6770	530	62.4	5.6	9.0	**538**	**48**	656	23	4.4	1.4	nd	-	1.2	1.2	6.4	1.1	120.8	8.4	39.5	4.8	10.2	5.3	6.50	2.60	3.3	0.8	3.18	0.74
Bras10Sb-37f	Grt	4.1E+07	2.6E+06	881	33	74.1	3.9	5.3	**549**	**29**	1567	60	0.68	0.28	nd	-	1.188	0.082	3.49	0.47	94.5	2.9	394	24	0.4	0.2	0.22	0.14	4.2	1.3	14.3	1.3
Bras10Sb-35	Grt	3.4E+07	3.6E+06	1275	37	98.1	2.5	2.5	**566**	**14**	1452	48	2.67	0.28	nd	-	1.22	0.16	6.76	0.3	93.7	1.4	536	17	0.3	0.1	0.05	0.01	0.0	0.0	11.2	0.46
Bras10Sb-36b	Grt	3.2E+07	4.9E+06	900	30	99.2	3	3.0	**567**	**17**	1435	40	1.45	0.16	nd	-	0.89	0.14	5.09	0.32	91.6	3.6	513	21	0.4	0.1	0.18	0.04	0.2	0.0	12.43	0.64
Bras10Sb-37e	Grt	3.1E+07	4.3E+06	741	16	99.7	1.7	1.7	**567**	**10**	1477	35	0.56	0.11	nd	-	1.99	0.23	4.15	0.31	92.3	2.4	355	14	2.7	0.3	0.22	0.07	0.6	0.3	108.6	2.7
Bras10Sb-34a	Grt	2.9E+07	4.1E+06	1120	24	99.9	2.4	2.4	**568**	**14**	1395	48	2.54	0.49	nd	-	1.37	0.21	4.28	0.31	82.6	2.1	514	15	0.8	0.2	0.18	0.11	0.0	0.0	22.23	0.75
Bras10Sb-37a	Grt	3.3E+07	4.0E+06	995	29	103.7	2.8	2.7	**570**	**15**	1557	39	2.59	0.33	nd	-	2.14	0.17	4.16	0.39	93.5	2.3	392	13	3.9	0.3	0.02	0.02	0.4	0.1	181.5	4.4
Bras10Sb-37c	Grt	3.1E+07	4.5E+06	894	21	107.9	2.2	2.0	**573**	**12**	1683	51	0.92	0.15	nd	-	2.39	0.2	5.24	0.31	98.5	2.2	447	12	2.6	0.1	0.03	0.02	0.0	0.0	130.7	6.1
Bras10Sb-36a	Grt	2.9E+07	3.2E+06	1139	28	118.5	3.6	3.0	**579**	**18**	1428	41	2.8	0.3	nd	-	0.91	0.11	5.32	0.37	88.2	3.1	548	16	0.7	0.1	0.15	0.04	0.0	0.0	31.4	1.1
Bras10Sb-34c	Grt	4.2E+07	2.4E+06	1191	72	168	14	8.3	**603**	**50**	1386	45	2.24	0.16	nd	-	3.113	0.092	6.71	0.71	78.7	3.4	531.4	3.5	1.4	0.4	0.95	0.01	0.9	0.4	19.41	0.86
Bras10Sb-34d	Grt	3.1E+07	4.2E+06	1112	20	218.1	5.8	2.7	**622**	**17**	1481	46	2.77	0.31	nd	-	0.559	0.051	6.21	0.39	88.6	3.4	555	20	2.0	0.2	0.02	0.02	0.0	0.0	96.7	3.6
Bras10Sb-34b	Grt	3.4E+07	3.9E+06	800	21	226.6	5.4	2.4	**625**	**15**	1464	43	2.05	0.31	nd	-	0.846	0.088	5.87	0.35	81.8	2.7	565	19	1.8	0.2	0.05	0.03	0.0	0.0	82.1	2.8
Bras10Sb-37b	Grt	3.3E+07	5.6E+06	1123	28	268.7	6.4	2.4	**638**	**15**	1504	23	3.5	0.4	nd	-	3.14	0.32	9.95	0.41	92.3	2.3	516.2	8.6	8.4	1.4	0.88	0.74	0.0	0.0	329.5	7.6
Bras10Sb-26b	Rextal	4.2E+07	2.5E+06	2230	160	778	31	4.0	**727**	**29**	1950	66	20.5	3.2	nd	-	0.081	0.091	25.6	2.4	84.7	3.1	501	51	8.0	1.7	0.52	0.24	0.0	0.1	410	44
Bras10Sb-1t	Rextal	2.4E+07	1.5E+06	1359	29	951	33	3.5	**746**	**26**	2366	55	26.4	1.1	nd	-	0.164	0.076	31.3	1.2	137.9	5.7	1712	49	9.3	0.7	0.45	0.14	0.0	0.0	362.6	9.9
Bras10Sb-24a	Rextal	3.6E+07	4.3E+06	1889	37	951	18	1.9	**746**	**14**	2011	37	23.7	1.3	nd	-	0.214	0.037	33.02	0.7	77.3	2.2	703	15	10.8	0.4	1.28	0.20	0.0	0.0	463	13
Bras10Sb-26c	Rextal	3.0E+07	4.1E+06	2461	97	953	34	3.6	**746**	**27**	1951	38	19.36	0.89	nd	-	0.188	0.066	35.4	1.2	96.5	2.1	1008	26	9.4	0.5	0.13	0.04	0.0	0.0	418	11
Bras10Sb-26a	Rextal	2.8E+07	3.2E+06	2478	47	1009	24	2.4	**752**	**18**	2226	79	21.59	0.97	nd	-	0.199	0.058	36.2	1.3	140.2	3.7	1236	42	9.6	0.5	0.43	0.11	0.0	0.0	415	16
Bras10Sb-28b	Rextal	2.7E+07	3.8E+06	2572	79	1020	32	3.1	**753**	**24**	1801	49	22.3	1.4	nd	-	0.17	0.1	33.15	0.84	87.4	2.2	680	22	12.1	0.6	0.37	0.09	0.0	0.0	488	16
Bras10Sb-24b	Rextal	3.6E+07	4.7E+06	2055	41	1085	42	3.9	**759**	**29**	2186	62	24.3	1.2	nd	-	0.213	0.056	37	1.2	93.9	2.7	907	32	11.3	0.5	1.52	0.15	0.0	0.0	474	15
Bras10Sb-24c	Rextal	3.7E+07	5.0E+06	1926	42	1090	27	2.5	**759**	**19**	2128	41	23.78	0.69	nd	-	0.176	0.048	38.4	1.4	106.6	1.8	1053	37	11.4	0.4	0.98	0.13	0.0	0.0	485	15
Bras10Sb-28a	Rextal	2.8E+07	3.4E+06	2295	49	1126	31	2.8	**762**	**21**	1861	53	21.74	0.96	nd	-	0.183	0.083	37.1	1.6	40.9	1.2	167.4	7	9.2	0.4	0.01	0.02	0.0	0.0	417	17
Bras10Sb-24e	Rextal	3.8E+07	4.5E+06	2002	57	1178	34	2.9	**767**	**22**	2190	59	24.5	1.3	nd	-	0.15	0.063	41.7	1.6	121.5	3.1	1482	44	11.6	0.4	0.90	0.15	0.0	0.0	519	14
Bras10Sb-24d	Rextal	3.8E+07	5.0E+06	1983	48	1205	31	2.6	**769**	**20**	2240	44	24.7	1	nd	-	0.253	0.054	44.7	1.2	129.9	3.7	1531	41	11.3	0.5	0.80	0.11	0.0	0.0	510	13
Bras10Sb-28c	Rextal	2.8E+07	3.5E+06	2762	56	1257	34	2.7	**773**	**21**	2351	65	20.5	0.85	nd	-	0.182	0.078	53.8	1.3	105.2	4.1	915	30	9.3	0.7	0.16	0.05	0.0	0.0	394	22
Bras10Sb-2	Rextal	1.6E+07	1.1E+06	938	23	1277	67	5.2	**775**	**41**	4810	140	154.5	6	nd	-	0.64	0.13	35.7	2.4	84.8	3.5	13.58	0.74	7.4	0.6	0.10	0.05	0.0	0.0	293	14
Bras10Sb-30	Rextal	2.9E+07	3.9E+06	1971	46	1425	22	1.5	**786**	**12**	2262	48	29.6	1.4	nd	-	0.135	0.068	52.7	2.3	123.9	5	1638	57	7.1	0.4	0.18	0.04	0.0	0.0	318	11
Bras10Sb-27	Rextal	3.1E+07	4.6E+06	1481	43	1588	41	2.6	**798**	**21**	2230	70	18.6	0.58	nd	-	0.178	0.055	71.9	3.4	164.1	7	1202	54	11.8	0.5	1.50	0.25	0.0	0.0	501	20
Bras10Sb-25r	Rextal	3.1E+07	4.1E+06	2693	58	1857	65	3.5	**814**	**29**	2648	97	30.4	1.6	nd	-	0.157	0.092	66	3	161.4	6.4	2130	100	11.3	0.5	0.21	0.04	0.0	0.0	526	14
Bras10Sb-25c	Rextal	3.0E+07	3.6E+06	2652	63	1859	49	2.6	**815**	**21**	2648	65	31	1.4	nd	-	0.18	0.1	66.5	2.3	156.8	4.7	2050	66	11.2	0.6	0.03	0.02	0.0	0.0	523	24
Bras10Sb-29a	Rextal	2.4E+07	1.8E+06	961	25	1906	46	2.4	**817**	**20**	2808	92	36.9	1.6	nd	-	0.091	0.064	77.5	3.3	158.4	5.8	2315	91	9.0	0.3	0.42	0.09	0.0	0.0	389	10
Bras10Sb-29b	Rextal	2.6E+07	3.6E+06	914	21	2568	78	3.0	**851**	**26**	2901	81	38	1.7	nd	-	0.166	0.097	94.8	3.1	115.6	4.1	2840	110	8.7	0.4	0.75	0.10	0.0	0.0	390	12
Bras10Sb-32i	Peak	3.7E+07	4.5E+06	3166	65	4220	79	1.9	**912**	**17**	8770	170	30.6	1.2	nd	-	0.046	0.036	127.9	3	1521	52	524	14	1.8	0.2	0.02	0.01	0.0	0.0	89.6	2.4
Bras10Sb-33c	Peak	2.9E+07	3.7E+06	1216	23	4270	120	2.8	**914**	**26**	4370	120	57	2.4	nd	-	0.32	0.079	119.1	3.8	272.7	8.5	229.1	8.3	5.1	0.5	0.04	0.02	0.0	0.0	247.1	8.6
Bras10Sb-32r	Peak	3.7E+07	4.2E+06	3193	44	4290	110	2.6	**914**	**23**	8890	230	31.3	1.4	nd	-	0.079	0.045	130.9	4.1	1499	35	597	25	1.9	0.1	0.00	0.01	0.0	0.0	91	1.5
Bras10Sb-32c	Peak	3.6E+07	3.9E+06	3215	86	4304	94	2.2	**915**	**20**	8850	190	32.1	1.5	nd	-	0.08	0.052	129.4	2.1	1498	31	462	18	1.8	0.1	0.01	0.01	0.0	0.0	89.7	2.1
Bras10Sb-21	Peak	3.1E+07	4.0E+06	765	20	4412	98	2.2	**918**	**20**	2671	53	228.4	6.7	nd	-	0.386	0.045	98.6	2.2	34.1	1.1	3	0.24	7.7	0.3	0.40	0.11	0.0	0.0	342	10
Bras10Sb-6	Peak	2.7E+07	3.9E+06	1281	45	4610	120	2.6	**924**	**24**	6780	250	34.1	1.6	nd	-	0.056	0.069	142.9	3.1	1423	48	302	12	3.2	0.3	0.06	0.01	0.0	0.0	132.8	4.1
Bras10Sb-38c	Peak	1.8E+07	1.3E+06	2620	97	4720	160	3.4	**927**	**31**	2172	70	31.4	1.3	nd	-	0.235	0.071	126.9	6.5	167.6	7	235	11	3.1	0.5	0.05	0.03	0.0	0.0	109.7	6.2
Bras10Sb-4	Peak	1.9E+07	1.4E+06	2632	78	4760	150	3.2	**928**	**29**	2725	73	44.5	2	nd	-	0.11	0.11	128.7	4.4	198.9	5.8	122.5	4.6	2.9	0.2	0.06	0.03	0.0	0.0	107.2	4.2
Bras10Sb-11tb	Peak	3.0E+07	3.9E+06	2363	49	4781	95	2.0	**929**	**18**	2748	72	81.3	3	nd	-	-0.042	0.066	147.1	4.6	211.3	6.6	181.7	5.2	1.2	0.1	0.02	0.02	0.0	0.0	52.9	1.3
Bras10Sb-38r	Peak	1.9E+07	9.3E+05	2740	89	4970	190	3.8	**934**	**36**	2295	99	34.1	1.8	nd	-	0.228	0.097	131.7	7.7	190.2	8.1	286	14	2.6	0.3	0.04	0.03	0.0	0.0	118.6	5.3
Bras10Sb-33a	Peak	2.1E+07	2.3E+06	1503	33	5040	120	2.4	**936**	**22**	5240	86	80.1	2.9	nd	-	0.36	0.11	146.6	4.5	355.4	7.7	144.1	3.8	8.3	0.5	0.46	0.18	0.0	0.0	332.7	7.8
Bras10Sb-16	Peak	2.2E+07	3.9E+06	1404	24	5100	190	3.7	**937**	**35**	3400	65	69.5	3.5	nd	-	0.5	0.11	129.6	3.8	202.8	5.1	171.1	5.1	2.9	0.6	1.45	0.90	0.0	0.0	89.1	3
Bras10Sb-43a	Peak	4.6E+07	5.1E+06	2380	110	5120	380	7.4	**938**	**70**	1942	74	17.6	1.8	nd	-	0.052	0.07	171.7	7	180	10	80.4	5.2	3.5	1.0	2.07	0.98	0.0	0.0	74.4	3.5

Sample and Analysis Number	Texture	Ti (cps)	± 2SE (cps)	V (ppm)	± 2SE (ppm)	Zr (ppm)	± 2SE (ppm)	± 2SE %	Zr-in-Rt T (°C)	± 2SE (°C)	Nb (ppm)	± 2SE (ppm)	Mo (ppm)	± 2SE (ppm)	Sn (ppm)	± 2SE (ppm)	Sb (ppm)	± 2SE (ppm)	Hf (ppm)	± 2SE (ppm)	Ta (ppm)	± 2SE (ppm)	W (ppm)	± 2SE (ppm)	206Pb (ppm)	± 2SE (ppm)	208Pb (ppm)	± 2SE (ppm)	Th (ppm)	± 2SE (ppm)	U (ppm)	± 2SE (ppm)
Bras105b-3	Peak	1.6E+07	7.8E+05	1342	51	5390	120	2.2	**945**	**21**	6110	120	104.6	4.2	nd	-	0.641	0.093	150.2	6	860	21	387	17	9.9	0.8	0.09	0.04	0.0	0.0	380	15
Bras105b-19t	Peak	4.2E+07	1.6E+06	1650	68	5460	480	8.8	**947**	**83**	3100	120	151.8	6.6	nd	-	0.35	0.12	181	16	294	10	149.7	4.5	19.9	1.1	0.05	0.02	0.0	0.0	923	38
Bras105b-9ta	Peak	2.8E+07	3.2E+06	1561	30	5650	93	1.6	**951**	**16**	2740	100	70	2.1	nd	-	0.05	0.052	180.6	5.8	204.9	6.3	325	13	2.4	0.2	0.03	0.02	0.0	0.0	108.9	4.4
Bras105b-11ta	Peak	3.4E+07	4.9E+06	1923	60	5770	180	3.1	**954**	**30**	3072	84	63.7	1.8	nd	-	0.1	0.037	172.9	3.5	263.4	6.3	193.8	3.9	1.2	0.1	0.04	0.02	0.0	0.0	61.1	2
Bras105b-33b	Peak	2.4E+07	1.6E+06	1510	50	5810	140	2.4	**955**	**29**	5590	98	77.9	1.9	nd	-	0.28	0.1	178.3	4.6	566	17	380.6	8.6	7.8	0.5	0.07	0.03	0.0	0.0	353	11
Bras105b-31	Peak	2.9E+07	6.3E+06	1732	69	5840	250	4.3	**956**	**41**	3032	93	72.1	3.3	nd	-	0.035	0.061	161.6	5.7	232.5	7	234.6	8.4	2.0	0.2	0.06	0.03	0.0	0.0	88.1	3.3
Bras105b-9tb	Peak	2.3E+07	9.4E+05	1477	59	5950	140	2.4	**959**	**23**	3380	110	103.1	4.5	nd	-	0.24	0.11	130.3	4.4	102.9	2.9	99.2	3.5	2.6	0.2	0.02	0.02	0.0	0.0	110.9	4.3
Bras105b-43b	Peak	3.6E+07	5.0E+06	1962	36	6199	90	1.5	**964**	**14**	2272	38	45.4	1.4	nd	-	0.145	0.034	207.7	3.7	214.8	4.5	129	4.2	3.1	0.1	1.02	0.13	0.0	0.0	110.2	2.7
Bras105b-17t	Peak	2.4E+07	2.2E+06	799	24	7620	260	3.4	**994**	**34**	2759	68	130.5	5.1	nd	-	0.086	0.073	249.5	8.9	172.4	5.7	300.5	9.6	3.0	0.3	0.05	0.03	0.0	0.0	124.1	4.7
Bras105b-14t	Peak	3.5E+07	4.0E+06	1702	24	8290	170	2.1	**1007**	**21**	3364	39	135	3.7	nd	-	0.101	0.068	260.3	6.2	303.7	7.4	202.3	6.3	2.7	0.3	0.02	0.01	0.0	0.0	142.9	3.5
Bras105b-23tb	Peak	3.5E+07	4.7E+06	889	23	9110	320	3.5	**1021**	**36**	8390	200	479	17	nd	-	0.483	0.066	453	16	760	20	584	25	14.2	0.9	3.24	0.79	0.0	0.0	490	30
Bras105b-23ta	Peak	3.2E+07	4.0E+06	839.8	9.6	9250	180	1.9	**1024**	**20**	7250	120	447	11	nd	-	0.296	0.035	448	11	746	20	700	20	12.7	0.9	2.51	0.33	0.0	0.0	451	17
Bras105b-22	Peak	2.7E+07	2.2E+06	890	19	12590	230	1.8	**1074**	**20**	12290	260	767	22	nd	-	0.33	0.11	591	12	1161	31	1437	42	20.7	1.0	2.39	0.63	0.0	0.0	807	27
Stromatic Granulite (Bras10-Sb-2)																																
Br105b2-41.FIN2	Zrc	3.0E+07	2.7E+06	1635	71	663	32	4.8	**712**	**34**	4300	150	113	8.4	648	35	0.022	0.051	49.2	2.9	403	18	1012	50	3.4	0.4	0.06	0.03	0.0	1.0	151.3	6.6
Br105b2-39.FIN2	Peak	3.3E+07	1.9E+06	1694	62	744	28	3.8	**723**	**27**	4940	200	87	7.2	616	22	0.04	0.042	55.6	2.6	802	29	1385	56	3.0	0.2	0.02	0.01	0.0	1.0	132.1	5
Br105b2-62b.FIN2	Peak	3.4E+07	1.6E+06	1430	120	892	59	6.6	**740**	**49**	3100	180	88.1	5.2	533	30	0.18	0.11	55.4	4.4	257	17	248	16	3.9	0.5	0.06	0.04	0.0	1.0	190	11
Br105b2-51.FIN2	Peak	3.3E+07	1.9E+06	1240	38	991	32	3.2	**750**	**24**	2324	78	128.9	5.6	683	24	0.025	0.041	64.9	2.7	136	4.5	404	12	6.9	0.4	1.05	0.13	0.0	1.0	203	5.9
Br105b2-38.FIN2	Peak	4.3E+07	2.8E+06	1517	46	1131	35	3.1	**763**	**24**	3130	100	68	4	497	18	0.041	0.034	72.9	2.4	196.3	6.3	371	12	2.2	0.2	0.00	0.01	0.0	1.0	101	3
Br105b2-37.FIN2	Peak	4.1E+07	2.7E+06	1530	44	1164	36	3.1	**766**	**24**	3211	91	77.2	6.1	554	21	0.034	0.033	75.1	2.7	269	7.2	533	18	2.4	0.2	0.01	0.01	0.0	1.0	111.2	3.4
Br105b2-34.FIN2	Peak	3.1E+07	2.3E+06	1599	61	1417	54	3.8	**786**	**30**	4870	180	87.8	6.9	498	20	0.03	0.046	88.4	3.6	442	16	803	30	3.3	0.3	0.03	0.02	0.0	1.0	135.1	4.8
Br105b2-62a.FIN2	Peak	2.2E+07	2.6E+06	1449	95	1600	120	7.5	**798**	**60**	2980	260	104	12	551	45	0.043	0.098	84.4	8.5	190	16	186	11	4.7	0.6	0.05	0.04	0.0	1.0	192	11
Br105b2-1.FIN2	Peak	2.4E+07	1.9E+06	990	47	1723	90	5.2	**806**	**42**	11870	560	279	18	942	48	0.056	0.064	141.3	7.8	1168	53	3420	160	8.2	0.7	0.06	0.03	0.0	1.0	299	14
Br105b2-14.FIN2	Peak	3.9E+07	2.5E+06	987	27	2130	62	2.9	**830**	**24**	4930	140	101.6	6.1	521	18	0.036	0.042	117.9	3.9	226.5	6.6	886	24	2.5	0.2	0.04	0.01	0.0	1.0	112.6	3.7
Br105b2-21.FIN2	Peak	2.4E+07	1.7E+06	1446	50	2239	99	4.4	**835**	**37**	3900	130	129.2	7.1	595	22	0.111	0.076	106.4	4.9	358	14	674	28	11.9	0.7	5.14	0.34	0.1	0.0	174.8	6.4
Br105b2-11.FIN2	Peak	1.0E+07	1.5E+06	1743	91	2290	230	10.0	**838**	**84**	4780	440	116	13	578	43	0.11	0.21	145	17	576	48	1470	150	2.9	0.7	0.07	0.11	0.0	1.0	101.5	9.8
Br105b2-10.FIN2	Peak	3.0E+07	2.2E+06	921	34	2570	110	4.3	**851**	**36**	5620	180	209	13	740	29	0.092	0.061	149.8	6.4	332	12	1053	38	4.9	0.4	0.02	0.02	0.0	1.0	162.5	5.8
Br105b2-77.FIN2	Peak	2.3E+07	2.5E+06	1354	59	3360	150	4.5	**883**	**39**	4920	250	144.7	9.3	632	35	0.027	0.075	141.3	7.4	374	19	1005	42	5.1	0.5	0.04	0.03	0.0	1.0	178.8	8.5
Br105b2-73.FIN2	Peak	1.4E+07	2.5E+06	1560	110	3390	260	7.7	**885**	**68**	3360	250	122	11	605	51	0.11	0.31	122.9	9.3	241	13	784	50	3.3	0.7	0.03	0.03	0.0	1.0	122.6	6.9
Br105b2-42.FIN2	Peak	2.7E+07	2.4E+06	1564	69	3900	160	4.1	**902**	**37**	3320	140	94.1	6.3	461	23	0.021	0.049	145.2	7.7	317	14	610	26	3.5	0.3	0.05	0.02	0.0	1.0	133.6	5.4
Br105b2-20.FIN2	Peak	2.5E+07	2.1E+06	1512	65	4140	180	4.3	**910**	**40**	4120	180	164.4	9.1	681	29	0.108	0.073	191.8	8.2	503	20	1174	53	5.7	0.4	0.14	0.04	0.0	1.0	239.2	9.1
Br105b2-8.FIN2	Peak	3.1E+07	2.3E+06	1463	47	4160	170	4.1	**910**	**37**	3300	140	92.6	6.8	484	21	0.049	0.049	153.1	7.6	250	11	654	30	3.3	0.3	0.06	0.03	0.0	1.0	119.2	4.3
Br105b2-78.FIN2	Peak	2.6E+07	2.0E+06	1515	58	4180	140	3.3	**911**	**31**	5570	230	146	10	621	28	0.111	0.065	159.9	7.2	585	24	1218	59	4.7	0.4	0.02	0.01	0.0	1.0	178	7.1
Br105b2-67a.FIN2	Peak	2.6E+07	1.8E+06	1553	61	4200	200	4.8	**912**	**43**	3420	130	93.3	5.8	490	22	0.097	0.052	158.2	6.8	229.5	8.2	1074	42	3.1	0.3	0.02	0.01	0.0	1.0	134.4	5.6
Br105b2-75.FIN2	Peak	3.5E+07	2.7E+06	1335	42	4220	170	4.0	**912**	**37**	3410	100	104.8	5.1	457	18	0.034	0.044	159.7	6.1	229	7.5	824	28	3.1	0.3	0.02	0.01	0.0	1.0	129.6	4.4
Br105b2-33.FIN2	Peak	2.8E+07	2.1E+06	1538	54	4230	170	4.0	**913**	**37**	4010	160	92.3	7.2	531	26	0	0.04	167.7	6.6	441	16	802	30	3.3	0.3	0.02	0.02	0.0	1.0	135.6	5.9
Br105b2-67c.FIN2	Peak	2.3E+07	2.1E+06	1274	55	4250	220	5.2	**913**	**47**	3420	150	103.2	7.3	506	21	0.043	0.06	155.3	7.9	204.7	8.7	908	37	3.0	0.3	0.04	0.02	0.0	1.0	131.9	6.2
Br105b2-35.FIN2	Peak	3.0E+07	1.9E+06	1552	49	4300	160	3.7	**915**	**34**	4040	140	102.8	6.4	575	21	0.034	0.042	169.5	7.5	390	14	821	28	3.8	0.3	0.03	0.02	0.0	0.0	147.5	5.1
Br105b2-47.FIN2	Peak	8.2E+06	1.2E+06	1720	190	4400	380	8.6	**918**	**79**	5390	580	148	19	795	79	0.14	0.22	139	15	498	42	1047	93	7.1	1.5	0.22	0.17	0.0	1.0	216	16
Br105b2-71.FIN2	Peak	3.2E+06	4.2E+05	1480	200	4440	590	13.3	**919**	**122**	3130	590	112	21	690	100	1.4	1.5	160	32	195	34	1000	150	4.7	2.1	0.97	0.46	0.0	1.0	152	37
Br105b2-25.FIN2	Peak	3.3E+07	2.6E+06	1533	55	4470	170	3.8	**920**	**35**	3250	130	94.9	5.9	584	22	0.07	0.054	175	6.3	322	12	484	20	5.6	0.7	1.78	0.49	0.0	1.0	146.7	4.9
Br105b2-4.FIN2	Peak	3.3E+07	2.3E+06	1641	55	4470	160	3.6	**920**	**33**	3630	130	83.2	6.2	520	22	-0.003	0.036	171.7	7.3	376	14	647	23	2.7	0.2	0.04	0.02	0.0	1.0	105.1	3.7
Br105b2-60.FIN2	Peak	3.3E+07	2.2E+06	1339	60	4510	190	4.2	**921**	**39**	3430	160	145.7	5.8	545	25	0.077	0.051	167.7	8.3	247	12	753	35	5.9	0.4	0.05	0.02	0.0	1.0	240.1	8.6
Br105b2-7c.FIN2	Peak	3.4E+07	2.6E+06	1549	61	4520	150	3.3	**921**	**31**	4150	170	132.8	7.7	605	27	0.019	0.04	190.6	7.9	441	18	1080	42	5.0	0.4	0.38	0.06	0.0	1.0	187.2	6.9
Br105b2-52.FIN2	Peak	3.6E+07	2.4E+06	1383	38	4560	130	2.9	**922**	**26**	3880	120	109.5	6.2	599	23	0.012	0.034	160.2	5.5	207.2	5.4	709	22	4.2	0.3	0.37	0.06	0.0	1.0	133.5	3.7
Br105b2-61.FIN2	Peak	4.4E+07	3.0E+06	1450	110	4560	320	7.0	**922**	**65**	3290	250	83.1	4.8	469	33	0.022	0.047	181	11	221	17	651	46	3.0	0.4	0.07	0.03	0.0	1.0	150.4	9.1
Br105b2-30.FIN2	Peak	2.6E+07	2.0E+06	1371	82	4570	250	5.5	**923**	**50**	5290	270	126	9.3	719	32	0.042	0.067	187	12	457	23	798	40	3.9	0.4	0.08	0.03	0.0	1.0	159.4	8.5
Br105b2-46.FIN2	Peak	1.4E+07	2.1E+06	1740	100	4570	250	5.5	**923**	**50**	5450	320	132.7	9.8	773	46	0.1	0.15	171	12	543	31	1234	70	7.1	0.6	0.16	0.07	0.0	1.0	255	16
Br105b2-70.FIN2	Peak	2.3E+07	1.7E+06	1541	72	4590	210	4.6	**923**	**42**	2850	100	83.5	6.3	534	23	0.024	0.05	165.5	7.4	169.1	7.2	780	31	2.9	0.3	0.14	0.04	0.0	1.0	111.9	4.7
Br105b2-7d.FIN2	Peak	3.3E+07	2.5E+06	1434	46	4600	160	3.5	**924**	**32**	4060	120	129.9	7.1	606	25	0.056	0.046	172.5	6.5	375	12	730	25	5.6	0.4	0.39	0.07	0.0	0.0	184.7	6
Br105b2-48a.FIN2	Peak	5.3E+07	3.2E+06	1463	76	4610	220	4.8	**924**	**44**	5110	260	128.2	9.8	497	27	0.018	0.032	193	12	551	25	1108	55	4.1	0.4	0.01	0.01	0.0	1.0	183	10
Br105b2-64a.FIN2	Peak	3.4E+07	2.3E+06	1562	52	4610	130	2.8	**924**	**26**	4370	140	25	5.3	398	14	0.069	0.044	154.1	5.9	219	7.7	30	1.2	3.9	0.2	0.02	0.01	0.0	1.0	146.5	5.3
Br105b2-36.FIN2	Peak	3.2E+07	2.2E+06	1575	54	4650	190	4.1	**925**	**38**	4400	140	87.9	6	563	23	0.009	0.036	177.8	7.3	440	15	907	34	3.3	0.3	0.05	0.02	0.0	1.0	139.7	5.4
Br105b2-45.FIN2	Peak	3.1E+07	1.7E+06	1230	43	4650	180	3.9	**925**	**36**	7110	270	156.6	7.9	667	24	0.081	0.048	190.6	7.1	713	30	1880	69	4.7	0.3	0.02	0.01	0.0	1.0	194.5	6
Br105b2-17.FIN2	Peak	3.1E+07	2.1E+06	1547	56	4700	210	4.5	**926**	**41**	4660	170	111.2	7	560	24	0.053	0.053	183.5	7.3	473	16	1256	43	3.9	0.3	0.15	0.04	0.0	1.0	159.3	6.2
Br105b2-64b.FIN2	Peak	3.9E+07	2.3E+06	1664	74	4700	210	4.5	**926**	**41**	4900	190	22.1	4.8	396	19	0.074	0.045	163.1	7.4	244	10	30.1	1.5	2.2	0.2	0.05	0.02	0.0	1.0	95.3	3.8
Br105b2-12a.FIN2	Peak	2.9E+07	2.1E+06	1488	54	4720	190	4.0	**927**	**37**	2920	100	92.5	5.5	548	21	0.016	0.051	179.8	7.8	164	5.8	539	21	3.5	0.3	0.05	0.03	0.0	1.0	117.3	3.5
Br105b2-23a.FIN2	Peak	3.8E+07	3.0E+06	1332	42	4790	150	3.1	**929**	**29**	3290	120	116.7	6.3	572	23	0.006	0.033	184.4	6.3	346	12	498	19	4.6	0.3	0.09	0.03	0.0	1.0	184.8	5.3
Br105b2-27.FIN2	Peak	3.9E+07	2.6E+06	1425	36	4810	160	3.3	**930**	**31**	3120	100	81.6	4	521	19	0.037	0.039	169.7	5.9	339	10	611	20	3.3	0.3	0.00	0.01	0.0	1.0	138.2	4.5
Br105b2-43b.FIN2	Peak	4.5E+07	2.2E+06	1246	61	4810	300	6.2	**930**	**58**	4790	260	121.9	8.6	601	31	0.07	0.05	208	12	412	21	960	35	3.8	0.4	0.00	0.01	0.0	1.0	169.8	8.9
Br105b2-31.FIN2	Peak	3.1E+07	2.5E+06	1519	61	4850	210	4.3	**931**	**40**	4840	180	117.9	8	565	23	0.048	0.041	185.8	9	519	20	1064	41	3.5	0.3	0.04	0.02	0.0	1.0	150.6	5.1
Br105b2-67b.FIN2	Peak	3.6E+07	2.1E+06	1368	69	4910	320	6.5	**932**	**61**	3540	230	106.8	8.8	490	22	0.078	0.069	174	12	241	15	840	42	3.1	0.4	0.04	0.03	0.0	1.0	122.4	7.4
Br105b2-48b.FIN2	Peak	4.0E+07	2.4E+06	1424	38	4930	150	3.0	**933**	**28**	5020	140	150.3	5.7	588	23	0.121	0.05	206.7	5.4	604	16	1323	37	4.7	0.3	0.01	0.01	0.0	1.0	189.5	4.8
Br105b2-44.FIN2	Peak	3.6E+07	2.3E+06	1596	51	5030	180	3.6	**936**	**33**	2808	92	26.2	3.4	519	20	-0.008	0.03	170.5	7.8	261.6	8.4	114	4	1.2	0.1	-0.01	0.01	0.0	1.0	59.3	2
Br105b2-23b.FIN2	Peak	4.0E+07	2.8E+06	1427	51	5100	210	4.1	**937**	**39**	3490	110	120.5	6.2	589	24	0.033	0.042	197.7	8.7	334	12	459	18	4.2	0.3	0.05	0.02	0.0	1.0	189.6	6.2
Br105b2-16.FIN2	Peak	3.8E+07	2.7E+06	1433	47	5110	160	3.1	**938**	**29**	2817	98	77.7	4	484	19	0.021	0.037	187.3	5.4	123.3	4.2	615	19	2.1	0.2	0.02	0.01	0.0	1.0	98.3	3.1
Br105b2-29.FIN2	Peak	3.6E+07	2.5E+06	1599	55	5120	190	3.7	**938**	**35**	3300	110	78.4	5.1	560	23	0.027	0.042	178.2	7.7	317	12	515	19	3.6	0.3	0.02	0.01	0.0	1.0	155.2	5.7
Br105b2-43a.FIN2	Peak	3.2E+07	2.2E+06	1208	40	5120	180	3.5	**938**	**33**	4410	140	133.4	6.8	588	23	0.016	0.036	183.3	7	370	13	918	30	4.3	0.4	0.02	0.01	0.0	1.0	183.5	5.5
Br105b2-66.FIN2	Peak	2.5E+07	1.9E+06	1581	68	5130	220	4.3	**938**	**40**	1399	65	36.6	2.1	559	25	0.009	0.04	154.3	7.4	41.9	1.9	49.1	2.3	2.8	0.3	0.07	0.03	0.0	1.0	117.7	5.6
Br105b2-26.FIN2	Peak	3.6E+07	2.3E+06	1490	57	5150	210	4.1	**939**	**38**	3370	110	107.6	5.9	624	23	0.028	0.031	189.6	8.4	360	14	550	19	4.3	0.3	0.02	0.01	0.0	1.0	188.6	6.9
Br105b2-12b.FIN2	Peak	4.4E+07	2.7E+06	1615	78	5190	220	4.2	**940**	**40**	2460	130	74.6	4.4	513	26	0.013	0.039	181	11	121.4	5.1	341	16	2.7	0.3	0.05	0.02	0.0	1.0	113.7	5.2
Br105b2-49.FIN2	Peak	4.0E+07	2.6E+06	1360	36	5300	160	3.0	**943**	**28**	4970	150	143.4	7.7	584	21	0.047	0.041	195.5	5.9	551	16	1037	32	4.3	0.3	0.02	0.01	0.0	1.0	171.9	5.1
Br105b2-72.FIN2	Peak	2.7E+07	2.1E+06	1461	57	5310	240	4.5	**943**	**43**	3950	160	119.1	6.9	617	25	0.136	0.074	206.1	9.6	252	11	988	45	3.3	0.3	0.29	0.05	0.0	1.0	131.4	6.2

Sample and Analysis Number	Texture	Ti (cps)	± 2SE (cps)	V (ppm)	± 2SE (ppm)	Zr (ppm)	± 2SE (ppm)	± 2SE %	**Zr-in-Rt T (°C)**	**± 2SE (°C)**	Nb (ppm)	± 2SE (ppm)	Mo (ppm)	± 2SE (ppm)	Sn (ppm)	± 2SE (ppm)	Sb (ppm)	± 2SE (ppm)	Hf (ppm)	± 2SE (ppm)	Ta (ppm)	± 2SE (ppm)	W (ppm)	± 2SE (ppm)	206Pb (ppm)	± 2SE (ppm)	208Pb (ppm)	± 2SE (ppm)	Th (ppm)	± 2SE (ppm)	U (ppm)	± 2SE (ppm)
Br105b2-74.FIN2	Peak	4.0E+07	3.4E+06	1382	53	5310	210	4.0	**943**	**37**	4820	160	123.3	7.6	501	24	-0.004	0.034	200	7.7	329	13	961	38	3.1	0.3	0.03	0.02	0.0	1.0	138.1	5.7
Br105b2-58.FIN2	Peak	4.1E+07	2.5E+06	1540	48	5360	190	3.5	**944**	**33**	2583	71	35	2.5	388	15	0.076	0.04	177.1	6.4	443	14	47.8	1.9	2.0	0.2	0.07	0.02	0.0	1.0	88.4	2.7
Br105b2-19t.FIN2	Peak	3.4E+07	2.5E+06	1312	39	5400	190	3.5	**945**	**33**	8090	220	173.1	7.7	682	26	0.037	0.043	227.1	7.4	810	24	1972	69	6.4	0.4	0.92	0.13	0.0	1.0	232.4	5.5
Br105b2-55.FIN2	Peak	3.8E+07	3.0E+06	1382	41	5450	160	2.9	**946**	**28**	1714	59	28.3	1.7	528	20	0.025	0.042	165.1	6.1	126.4	4.2	56.2	2.1	2.4	0.2	0.05	0.02	0.0	1.0	74	2.4
Br105b2-76.FIN2	Peak	3.0E+07	2.0E+06	1415	53	5500	220	4.0	**948**	**38**	4150	140	140	10	656	26	0.021	0.041	201.1	7.4	259.7	9.1	1252	39	4.7	0.4	0.01	0.01	0.0	1.0	161.1	5.7
Br105b2-32.FIN2	Peak	3.4E+07	2.1E+06	1311	45	5620	220	3.9	**951**	**37**	3930	150	92.4	6.1	580	22	0.047	0.042	224.5	8	528	20	983	36	4.2	0.3	0.01	0.01	0.0	1.0	177.2	6.8
Br105b2-28.FIN2	Peak	3.5E+07	2.4E+06	1312	43	5860	180	3.1	**957**	**29**	4900	160	122.8	5.7	603	24	0.065	0.044	220.8	9.5	526	19	829	24	4.3	0.3	0.02	0.01	0.0	1.0	174.8	5.1
Br105b2-57.FIN2	Peak	3.6E+07	2.3E+06	1438	48	5950	210	3.5	**959**	**34**	6540	220	97.3	5.1	447	15	0.056	0.039	206	6.2	406	14	767	27	3.9	0.2	0.01	0.01	0.0	1.0	169.7	5.5
Br105b2-59.FIN2	Peak	3.7E+07	2.7E+06	1378	50	6070	210	3.5	**961**	**33**	2252	94	31.4	2.3	443	23	0.065	0.053	209.3	8	260.9	9.8	32.7	1.2	1.9	0.2	0.05	0.04	0.0	1.0	75.6	2.9
Br105b2-40.FIN2	Peak	3.8E+07	2.4E+06	1517	51	6090	190	3.1	**962**	**30**	3730	120	89.3	4.7	550	18	0.042	0.04	218.4	7.4	351	12	610	18	2.3	0.2	0.03	0.01	0.0	1.0	115	3.1
Br105b2-63.FIN2	Peak	3.2E+07	1.9E+06	1085	33	6220	200	3.2	**965**	**31**	6960	230	91.2	6.1	548	19	0.092	0.053	209.5	8.3	300	11	76.1	2.7	4.4	0.3	0.03	0.01	0.0	1.0	171.5	5.2
Br105b2-6.FIN2	Peak	3.6E+07	3.3E+06	1462	53	6320	250	4.0	**967**	**38**	3040	120	88.9	6.2	563	29	0.102	0.055	215	10	307	13	456	19	3.8	0.5	1.67	0.38	0.0	1.0	96.7	4
Br105b2-56.FIN2	Peak	3.7E+07	2.0E+06	1320	47	6590	250	3.8	**973**	**37**	6920	220	54.9	4.5	532	17	0.098	0.048	234.1	9.1	487	17	64.3	2.6	4.7	0.3	0.01	0.01	0.0	1.0	184.4	5.7
Br105b2-3.FIN2	Peak	3.1E+07	1.9E+06	1019	35	6750	250	3.7	**977**	**36**	5620	180	150.3	7.4	731	26	0.023	0.036	239.7	8.3	557	22	1108	33	4.9	0.3	0.02	0.01	0.0	1.0	192.4	6.5
Br105b2-24.FIN2	Peak	3.7E+07	2.4E+06	1122	40	7290	220	3.0	**988**	**30**	3490	120	69.5	4.5	608	23	0.089	0.045	211.7	7.8	276	11	110.7	4.6	2.3	0.2	0.03	0.01	0.0	1.0	109.5	3.7
Stromatic Granulite (Bras10-6-1)																																
71t	Grt	1.8E+07	5.0E+06	2758	90	110.2	4.1	3.7	**574**	**21**	1453	31	7.25	0.79	nd	-	0.4	0.12	9.41	0.98	78.3	2.8	91.6	5.4	1.2	0.2	0.48	0.14	0.4	0.1	30.6	1
72ta	Grt	1.2E+07	4.3E+06	1800	200	124	38	30.6	**582**	**178**	880	280	5	1.6	nd	-	0.55	0.27	6.4	1.6	51	15	57	15	2.8	0.8	0.10	0.06	11.3	2.9	83	22
72tb	Grt	2.6E+07	4.1E+06	1483	42	134.1	3.3	2.5	**587**	**14**	1494	20	6.41	0.49	nd	-	0.426	0.077	13.71	0.93	84.7	2.2	59.8	3.4	1.2	0.1	0.02	0.01	0.0	0.0	54.9	1.0
6	Peak	2.6E+07	3.5E+06	1500	34	847	23	2.7	**735**	**20**	10990	280	129.1	5.1	nd	-	0.138	0.065	56.3	2.8	1534	30	284.1	6.4	8.8	0.3	0.06	0.03	0.0	1.0	387	13
20t	Zrc	2.4E+07	2.5E+06	2645	61	1031	30	2.9	**754**	**22**	20280	640	109.2	3.9	nd	-	0.057	0.073	64.2	3.2	1903	60	574	19	5.0	0.4	0.03	0.01	0.0	1.0	212.2	7.6
14	Peak	3.0E+07	4.2E+06	1595	36	1123	30	2.7	**762**	**20**	13960	400	108	2.6	nd	-	0.13	0.056	74.2	3.3	1384	51	510	26	4.0	0.2	0.04	0.02	0.0	1.0	179.7	5.3
27t	Peak	2.5E+07	4.1E+06	2155	72	1145	36	3.1	**764**	**24**	18490	390	116.5	4.4	nd	-	0.062	0.074	72.6	2.6	1625	41	239	4.4	6.4	0.5	0.08	0.02	0.0	0.0	263.9	5.9
5d	Peak	2.6E+07	2.9E+06	2411	50	1161	18	1.6	**765**	**12**	16240	350	86.3	3	nd	-	0.13	0.1	93.1	2.7	1802	40	290.3	9.2	7.3	0.4	0.00	0.01	0.0	1.0	337.4	6.7
5a	Peak	2.0E+07	2.8E+06	2348	74	1190	31	2.6	**768**	**20**	14110	490	102.5	4.6	nd	-	0.27	0.12	77.7	3.7	1572	52	245.1	8.9	6.6	0.4	0.02	0.02	0.0	1.0	297.9	7.2
5b	Peak	2.6E+07	2.6E+06	2476	80	1590	66	4.2	**798**	**33**	16250	250	87.1	2.7	nd	-	0.116	0.085	106.1	4.8	1841	40	354.8	7.2	7.3	0.4	0.01	0.02	0.0	1.0	315	14
22	Peak	2.9E+07	4.2E+06	1950	44	2470	180	7.3	**847**	**62**	13810	310	94.5	3.4	nd	-	0.051	0.031	143.1	7	1138	19	320.2	9	5.0	0.3	0.02	0.02	0.0	1.0	228	8
32	Peak	3.0E+07	4.1E+06	2350	61	3790	170	4.5	**898**	**40**	16360	510	54.2	1.4	nd	-	0.048	0.051	145.7	4.4	1844	84	162.7	9.9	3.3	0.4	0.01	0.01	0.0	1.0	162.3	6
84	Peak	2.2E+07	2.5E+06	1671	32	3900	100	2.6	**902**	**23**	2053	45	65.9	2.5	nd	-	0.238	0.067	114.1	3.2	77.6	1.4	61.2	3	5.2	0.2	0.05	0.02	0.0	0.0	217.5	6.3
80	Peak	2.1E+07	2.1E+06	2822	77	3965	83	2.1	**904**	**19**	7260	170	53.1	2.2	nd	-	0.075	0.04	140.5	3.1	614	14	235.7	7.1	3.4	0.3	0.16	0.03	0.0	1.0	151.1	3.2
88t	Peak	2.3E+07	2.7E+06	2422	73	4020	96	2.4	**906**	**22**	2328	64	51.7	2.2	nd	-	0.262	0.047	122.6	4.1	95.5	3.4	50.3	1.8	5.5	0.4	0.11	0.04	0.0	1.0	238.2	7.7
87a	Peak	2.2E+07	2.5E+06	2147	56	4076	81	2.0	**908**	**18**	2282	51	49.6	1.9	nd	-	0.285	0.075	132.3	3.5	163.1	3.2	121.2	3.1	3.4	0.4	0.06	0.03	0.0	1.0	138.4	3.2
13a	Peak	3.2E+07	3.3E+06	1830	37	4503	95	2.1	**921**	**19**	9870	140	48.8	1.8	nd	-	0.031	0.063	152.4	2.6	1281	20	176.7	2.7	4.2	0.3	0.14	0.04	0.0	1.0	181.8	2.8
87t	Peak	2.2E+07	2.8E+06	2226	43	4797	97	2.0	**929**	**19**	2295	40	53.3	1.9	nd	-	0.312	0.06	168.9	5.2	190.7	3.6	142.5	4.4	3.2	0.4	0.09	0.02	0.0	1.0	144.6	2.2
86	Peak	2.1E+07	2.8E+06	2245	73	4910	130	2.6	**932**	**25**	2818	44	77.1	4.4	nd	-	0.142	0.076	163.2	4.1	157.9	4.3	141.3	6.3	4.7	0.5	0.24	0.06	0.0	1.0	194.7	5.9
35	Peak	2.2E+07	2.3E+06	2579	78	5100	110	2.2	**937**	**20**	19030	580	58.3	1.6	nd	-	-0.039	0.05	174.5	6.1	1626	49	250	10	2.6	0.2	0.05	0.03	0.7	0.3	110.3	3.1
2	Peak	1.7E+07	1.8E+06	3671	89	5120	160	3.1	**938**	**29**	15970	460	70.6	2.4	nd	-	0.32	0.14	177.4	6.2	1920	85	282.8	8.1	4.0	0.3	0.09	0.04	0.0	1.0	154.2	6.7
59	Peak	2.4E+07	3.5E+06	1749	57	5140	160	3.1	**938**	**29**	17090	440	58.7	3	nd	-	0.074	0.069	165.1	6.7	1879	54	207.9	5.6	2.9	0.3	0.03	0.02	0.0	1.0	126.2	3.9
44t	Peak	2.6E+07	4.0E+06	2494	40	5170	130	2.5	**939**	**24**	23350	710	68.3	2.2	nd	-	0.068	0.048	203.3	5.4	2951	68	292.7	6.9	4.3	0.2	0.02	0.02	0.0	1.0	191.2	3.1
44a	Peak	2.8E+07	3.8E+06	2503	54	5250	140	2.7	**941**	**25**	24030	570	72.7	3.3	nd	-	0.054	0.058	214.6	5.7	2919	81	296.2	9	3.7	0.2	0.03	0.02	0.0	1.0	180.9	3.3
1c	Peak	1.8E+07	1.9E+06	3422	78	5290	140	2.6	**942**	**25**	14520	210	73.6	3	nd	-	0.27	0.14	162.1	3.8	1712	65	264.5	8	3.3	0.2	0.09	0.05	0.0	1.0	133.9	5.6
34	Peak	2.6E+07	3.2E+06	2466	67	5290	210	4.0	**942**	**37**	18580	480	79.5	3.8	nd	-	-0.018	0.066	181	6.6	1101	45	273.9	6	3.6	0.3	0.03	0.03	0.0	1.0	170.8	7.9
43b	Peak	2.9E+07	4.4E+06	2221	51	5290	110	2.1	**942**	**20**	13410	310	57	1.9	nd	-	0.041	0.056	180.8	3.1	1613	26	206.3	6.6	3.8	0.3	0.08	0.01	0.0	1.0	180	4.1
1r	Peak	1.8E+07	2.1E+06	3456	84	5428	94	1.7	**946**	**16**	14380	330	70.9	1.9	nd	-	0.27	0.11	172.6	3.3	1678	53	278	10	3.6	0.3	0.04	0.04	0.0	1.0	145.7	6.2
82a	Peak	2.3E+07	2.9E+06	1714	43	5430	120	2.2	**946**	**21**	3670	120	70.1	3.1	nd	-	0.103	0.049	177.8	5	264.5	8.3	195.3	6.4	3.6	0.4	0.09	0.02	0.0	1.0	147.3	5.1
82t	Peak	2.2E+07	2.6E+06	1673	65	5430	140	2.6	**946**	**24**	3490	110	68.2	2.2	nd	-	0.173	0.052	171.7	5.7	249.2	8.1	192.6	8.7	4.1	0.3	0.09	0.03	0.0	1.0	172	5.8
82b	Peak	2.3E+07	2.7E+06	1696	52	5440	92	1.7	**946**	**16**	3526	60	66.8	1.6	nd	-	0.093	0.064	181	7.7	266.7	4.9	216.8	8.7	4.2	0.3	0.04	0.03	0.0	1.0	172.8	1.8
82c	Peak	2.1E+07	1.9E+06	1691	45	5570	120	2.2	**949**	**20**	3620	120	70.8	2.3	nd	-	0.149	0.067	181.8	5.3	295	11	231.3	7.3	5.0	0.3	0.04	0.02	0.0	1.0	218.8	7.7
18b	Peak	2.9E+07	3.5E+06	1997	44	5700	140	2.5	**953**	**23**	6750	160	62.7	1.8	nd	-	0.019	0.051	196	6.7	640	15	281	11	3.0	0.2	0.02	0.01	0.0	1.0	136.2	3.9
65t	Peak	2.2E+07	2.7E+06	1916	54	5700	130	2.3	**953**	**22**	13500	350	100	3.9	nd	-	0.233	0.091	195.3	4.9	1510	55	263.1	8.7	7.4	0.7	0.05	0.03	0.0	1.0	321.8	9.1
48dt	Peak	1.8E+07	2.1E+06	2417	85	5780	150	2.6	**955**	**25**	8760	200	96.1	3.5	nd	-	0.289	0.073	196.6	4.4	829	21	261	11	9.5	0.6	2.02	0.32	0.0	1.0	324	16
48a	Peak	1.9E+07	2.7E+06	1883	31	5940	140	2.4	**958**	**23**	9770	220	122	4.6	nd	-	0.14	0.096	216.6	9.6	869	32	262.4	8	10.4	0.7	1.50	0.27	0.0	1.0	366	13
4	Peak	1.8E+07	2.7E+06	2585	70	6150	220	3.6	**963**	**34**	14260	330	98.1	5.2	nd	-	0.2	0.14	199.9	3.5	1691	34	311.1	8.9	5.9	0.2	0.03	0.02	0.0	1.0	240.9	7.6
29a	Peak	2.6E+07	3.3E+06	1695	48	6170	140	2.3	**964**	**22**	14080	230	69.6	2.3	nd	-	0.102	0.056	214	4.8	1461	46	289	10	4.4	0.3	0.01	0.02	0.0	1.0	192.3	4.4
7	Peak	2.0E+07	5.6E+06	633	61	6280	210	3.3	**966**	**32**	5540	95	152	12	nd	-	0.29	0.22	179	8.5	282.9	5.9	227	12	13.0	1.4	0.07	0.05	0.0	0.0	529	19
17t	Peak	2.8E+07	5.5E+06	1781	49	6330	120	1.9	**967**	**18**	7420	170	69.9	2.8	nd	-	0.184	0.091	199.3	5.9	495	13	240.9	6.9	3.8	0.2	0.06	0.04	0.0	0.0	177.1	2.9
45	Peak	2.7E+07	3.9E+06	2758	79	6344	99	1.6	**968**	**15**	11610	310	91.6	3.2	nd	-	0.1	0.062	242.7	5.5	1401	32	248.4	7.4	5.7	0.5	0.04	0.02	0.0	1.0	259.7	5.2
77	Peak	2.5E+07	4.1E+06	1497	31	6380	120	1.9	**969**	**18**	3688	81	76.8	2.3	nd	-	0.118	0.054	210.5	8.2	225.5	6.6	170.9	4.3	3.4	0.2	0.19	0.07	0.0	1.0	145.2	2.4
3a	Peak	2.2E+07	3.1E+06	3313	85	6540	170	2.6	**972**	**25**	26340	670	83.7	2.2	nd	-	0.6	0.12	262.9	8.4	3920	130	443	15	3.4	0.3	0.02	0.02	0.0	1.0	145.6	3.6
57b	Peak	1.9E+07	2.4E+06	2543	58	6960	120	1.7	**981**	**17**	36000	1000	94.7	3.6	nd	-	0.109	0.075	247.9	7	3535	59	493	22	3.5	0.3	0.16	0.04	0.0	0.0	129.6	4.3
34b	Peak	2.1E+07	2.1E+06	2717	68	6980	190	2.7	**981**	**27**	24840	880	89.9	3.2	nd	-	0.1	0.08	237	6.1	2361	55	388.9	8	4.5	0.5	0.03	0.02	0.0	1.0	190.1	7
36	Peak	2.4E+07	3.7E+06	2646	59	7010	200	2.9	**982**	**28**	21260	510	77.1	1.8	nd	-	0.5	0.11	238.4	6.2	1396	33	330	12	3.6	0.3	0.06	0.04	0.0	0.0	153	3.4
75	Peak	2.9E+07	3.7E+06	1755	33	7040	150	2.1	**983**	**21**	3966	83	89.2	3.1	nd	-	0.175	0.07	227.9	5.9	349.9	7.5	246.9	7.6	4.5	0.3	0.03	0.02	0.0	1.0	212.7	3.4
23	Peak	2.7E+07	4.4E+06	2150	57	7120	170	2.4	**984**	**24**	10950	250	82.2	2.5	nd	-	0.063	0.069	242.5	4.8	1330	27	318	9.7	5.9	0.4	0.07	0.03	0.0	1.0	248.2	4.9
15t	Peak	3.5E+07	5.1E+06	544.3	5.7	7400	150	2.0	**990**	**20**	3267	54	140.9	4.9	nd	-	0.194	0.067	233	6.4	282.4	4.4	232.3	6.2	5.7	0.4	0.00	0.01	0.0	1.0	286.9	8.2
30	Peak	3.1E+07	4.4E+06	2174	32	7760	220	2.8	**997**	**28**	18850	300	76.9	2.5	nd	-	-0.016	0.047	268.9	5.1	3009	60	339	11	3.9	0.3	0.03	0.01	0.0	1.0	183.8	4
Stromatic Granulite (Bras10-6-2)																																
Br1062-3d	Grt	2.1E+07	1.7E+06	827	35	28.9	1.6	5.5	**494**	**27**	44	2.3	0.87	0.28	22.3	1.5	-0.052	0.06	1.98	0.32	1.71	0.16	1.9	1	0.0	0.0	0.06	0.03	0.0	1.0	0.127	0.084
Br1062-2a	Grt	1.9E+07	1.5E+06	930	39	34.6	2.2	6.4	**504**	**32**	54.9	3	1	0.37	15.5	1.3	0.022	0.092	2.35	0.53	1.93	0.2	1.23	0.35	0.2	0.1	0.22	0.10	0.0	1.0	0.034	0.027
Br1062-2c	Grt	1.6E+07	1.7E+06	885	37	35.5	2.5	7.0	**505**	**36**	51.9	2.9	1.62	0.57	15.9	1.4	0.01	0.11	2.47	0.47	2.51	0.3	0.61	0.21	0.1	0.1	0.07	0.04	0.0	0.0	0.045	0.019
Br1062-21g	Grt	1.8E+07	1.2E+06	471	23	40.8	2.5	6.1	**513**	**31**	427	23	1.07	0.4	37.6	2.5	0.007	0.088	5.44	0.71	19.6	1.3	4.03	0.62	0.7	0.2	0.81	0.13	0.0	1.0	bdl	-
Br1062-34c	Grt	2.4E+07	1.7E+06	1468	43	51.7	2	3.9	**527**	**20**	2850	92	2.93	0.59	95.4	4.2	0.03	0.066	7.62	0.64	225	6.6	12.26	0.73	0.0	0.0	0.01	0.01	0.0	1.0	bdl	-
Br1062-6h	Grt	3.6E+07	1.5E+06	1157	66	57.6	4	6.9	**533**	**37**	57.2	3.3	0.63	0.33	62.7	5.9	0.03	0.11	4.34	0.78	1.72	0.22	0.17	0.1	0.0	0.0	0.02	0.02	0.0	1.0	bdl	-

Sample and Analysis Number	Texture	Ti (cps)	± 2SE (cps)	V (ppm)	± 2SE (ppm)	Zr (ppm)	± 2SE (ppm)	± 2SE %	Zr-in-Rt T (°C)	± 2SE (°C)	Nb (ppm)	± 2SE (ppm)	Mo (ppm)	± 2SE (ppm)	Sn (ppm)	± 2SE (ppm)	Sb (ppm)	± 2SE (ppm)	Hf (ppm)	± 2SE (ppm)	Ta (ppm)	± 2SE (ppm)	W (ppm)	± 2SE (ppm)	206Pb (ppm)	± 2SE (ppm)	208Pb (ppm)	± 2SE (ppm)	Th (ppm)	± 2SE (ppm)	U (ppm)	± 2SE (ppm)
Br1062-4c	Grt	2.3E+07	1.8E+06	974	37	65.8	2.5	3.8	**541**	**21**	414	19	3.37	0.46	164.2	6.4	0.081	0.068	19.8	1.3	15.5	1.9	11.7	1.8	0.0	0.0	0.02	0.01	0.0	1.0	bdl	-
Br1062-3g	Grt	5.2E+07	3.3E+06	1363	42	77.1	3.1	4.0	**551**	**22**	1891	70	3.4	1.1	171.2	6.7	0.354	0.07	11.97	0.77	105.8	4.4	84.4	4.1	1.5	0.2	0.47	0.06	0.4	0.1	42.5	1.4
Br1062-3f	Grt	4.5E+07	3.1E+06	1384	45	80.3	2.8	3.5	**554**	**19**	1991	65	3.47	0.85	202.2	7.9	0.361	0.071	12.89	0.55	133.1	4.2	151.4	4.8	1.0	0.1	0.05	0.02	1.8	0.2	42.7	1.2
Br1062-17e	Grt	3.5E+07	2.2E+06	1023	46	83.2	7.4	8.9	**556**	**49**	1790	140	2.3	1	115.5	7.5	0.19	0.19	5.4	1.2	68.9	8.6	43.9	4.7	0.7	0.2	0.09	0.06	0.2	0.1	22.1	2.7
Br1062-6i	Grt	4.3E+07	3.1E+06	943	33	84.4	3.1	3.7	**557**	**20**	1985	56	4.9	1.3	118.2	4.2	0.399	0.071	11.58	0.65	91.5	3	57.1	1.9	1.1	0.1	0.04	0.01	0.6	0.1	55.7	1.7
Br1062-6m	Grt	3.6E+07	2.5E+06	2423	93	93.8	3.3	3.5	**563**	**20**	1841	58	4.8	1	187.8	7.7	1	0.15	11.85	0.62	80.6	2.5	59.3	2.6	1.3	0.1	0.46	0.07	1.8	0.3	34.4	1.1
Br1062-6j	Grt	4.5E+07	2.9E+06	1051	38	94.1	3.3	3.5	**564**	**20**	2011	69	4.9	1.4	143.5	5.5	0.326	0.064	9.33	0.53	95.4	3.1	62.3	2.2	0.9	0.1	0.01	0.01	0.2	0.0	42.6	1.4
Br1062-17b	Grt	3.7E+07	2.1E+06	1191	39	96.1	4.1	4.3	**565**	**24**	3260	130	2.8	1.6	159.5	5.7	0.525	0.083	10.07	0.58	118	4.4	59	2.1	1.3	0.2	0.26	0.06	0.1	0.0	42.5	1.5
Br1062-17d	Grt	1.7E+07	1.9E+06	1590	56	100	4.5	4.5	**568**	**26**	2900	110	3.71	0.71	93.4	5.8	0.15	0.14	10.3	1	128.5	4.7	42.6	2.7	19.0	6.4	21.10	6.70	1.4	0.5	0.51	0.15
Br1062-4a	Grt	3.7E+07	2.9E+06	988	37	102	4.1	4.0	**569**	**23**	2043	74	3.26	0.84	135.1	6.3	0.446	0.087	12.4	0.72	101.6	3.4	51.5	2.1	2.2	0.2	0.14	0.03	0.4	0.1	72.3	2.6
Br1062-17a	Grt	4.2E+07	2.8E+06	1145	36	107.6	4.3	4.0	**572**	**23**	3131	84	4.6	2.3	151	4.6	0.456	0.083	10.31	0.62	117	3.6	57.1	2	1.3	0.2	0.19	0.04	0.0	0.0	47.2	1.4
Br1062-19f	Grt	3.5E+07	2.7E+06	1184	40	113.8	4.7	4.1	**576**	**24**	3300	110	1.34	0.88	186.1	7.8	0.531	0.091	10.52	0.66	133.4	4.4	90.7	3.5	0.8	0.1	0.15	0.04	0.0	0.0	32.3	1.3
Br1062-16	Grt	4.0E+07	3.4E+06	1196	35	126.9	4.3	3.4	**583**	**20**	3203	92	5.5	2.6	178.1	7.4	0.6	0.1	14.9	0.72	124.5	3.3	83.4	3.2	2.3	0.4	1.41	0.30	0.4	0.1	35	1.2
Br1062-37a	Grt	3.3E+07	2.4E+06	1197	44	126.9	6	4.7	**583**	**28**	1966	62	6	1	161.4	6.5	0.531	0.099	11.43	0.76	94.2	3.5	75.3	3	3.9	0.3	0.04	0.02	0.6	0.2	160	5.7
Br1062-4b	Grt	3.8E+07	2.9E+06	890	32	127	4.7	3.7	**584**	**22**	2207	79	3.83	0.86	230.8	9.6	0.32	0.064	16.2	1	105.9	4.7	88.1	3.8	2.2	0.2	0.15	0.04	0.3	0.0	82.8	2.7
Br1062-35f	Grt	2.9E+07	1.9E+06	2041	83	128.6	5.8	4.5	**584**	**26**	3620	140	0.66	0.54	311	15	0.67	0.12	10.82	0.89	201.4	8.7	93.4	3.9	0.5	0.1	0.04	0.02	0.0	1.0	20.6	0.77
Br1062-35a	Grt	3.1E+07	4.1E+06	1740	120	129	10	7.8	**585**	**45**	3170	260	1.02	0.78	229	17	0.53	0.19	11	1.5	220	15	108.8	6.3	2.0	0.4	0.58	0.15	2.9	0.3	31.3	1.8
Br1062-19e	Grt	3.4E+07	2.3E+06	1152	39	130.7	5	3.8	**585**	**22**	3570	120	2.1	1.6	187.9	7.3	0.341	0.088	9.48	0.63	124.4	4	73.7	2.6	0.9	0.1	0.13	0.03	0.0	0.0	33.8	1.2
Br1062-15a	Grt	6.0E+07	2.5E+06	1079	55	137	10	7.3	**589**	**43**	3300	220	-0.0361	0.0017	133.6	7.5	0.66	0.18	12.8	1.2	147	12	73.4	4.1	1.2	0.3	0.07	0.06	0.9	0.2	48.7	2.9
Br1062-34d	Grt	4.2E+07	3.2E+06	1031	34	137.8	4.8	3.5	**589**	**21**	3750	120	2.8	2.2	163.2	7	0.401	0.071	14.63	0.73	222	6.4	74.8	2.6	0.8	0.1	0.02	0.01	0.0	0.0	34.9	1
Br1062-15b	Grt	2.2E+07	1.2E+06	1358	50	138	5.7	4.1	**589**	**24**	3022	97	3.88	0.67	124	6.6	0.035	0.064	10.1	0.65	141.7	5.4	39.2	1.7	0.0	0.0	0.05	0.02	0.1	0.1	1.26	0.58
Br1062-8t	Grt	6.9E+07	4.4E+06	923	45	139	9.7	7.0	**590**	**41**	3300	180	2.4	3.3	126	6.4	0.335	0.097	12.4	1.1	165	11	60.9	3.6	0.6	0.1	0.01	0.01	0.0	0.0	27.5	1.5
Br1062-18a	Grt	3.5E+07	2.2E+06	1118	43	140	5.6	4.0	**590**	**24**	3290	110	2.1	1.3	175.8	6.4	0.373	0.093	10.49	0.72	139.1	4.1	67.9	2.6	0.8	0.1	0.06	0.02	0.2	0.0	35.8	0.97
Br1062-3e	Grt	4.7E+07	3.3E+06	1920	65	150.7	5.9	3.9	**595**	**23**	4540	140	8.1	3.7	271	10	0.325	0.077	25.7	1.1	272	7.8	378	12	1.1	0.1	0.03	0.01	0.6	0.1	53.4	1.4
Br1062-19b	Grt	3.5E+07	4.3E+06	1481	68	155.8	7.4	4.7	**598**	**28**	3380	150	3.6	2	199	11	0.3	0.1	12.28	0.96	119.5	5	136.1	6.1	1.1	0.2	0.16	0.05	0.5	0.2	40.7	1.7
Br1062-19a	Grt	3.7E+07	2.5E+06	1431	40	159.5	6.8	4.3	**599**	**26**	3410	120	3.3	2.1	197.2	7.2	0.404	0.081	12.52	0.85	125.2	3.8	129.1	5.3	1.1	0.2	0.11	0.03	0.0	0.0	42.5	1.4
Br1062-4d	Grt	2.3E+07	2.0E+06	1746	50	162.4	5.7	3.5	**601**	**21**	1841	54	8.15	0.75	253	11	0.042	0.065	18.9	1	98.7	2.8	23.7	1	bdl	0.0	0.04	0.02	0.0	1.0	bdl	-
Br1062-6k	Grt	4.3E+07	3.1E+06	2120	55	167.9	5.6	3.3	**603**	**20**	1853	48	4.22	0.92	221.6	7.6	0.37	0.075	9.44	0.5	86.2	2.5	61.1	1.9	1.2	0.1	0.01	0.01	0.1	0.0	54.3	1.6
Br1062-34b	Grt	4.2E+07	2.7E+06	980	27	175.4	5.2	3.0	**606**	**18**	3860	110	1.4	1.5	165.9	6.3	0.335	0.074	13.76	0.77	231.2	6.4	66.6	2.4	0.7	0.1	0.04	0.02	0.2	0.1	25.67	0.82
Br1062-19c	Grt	3.4E+07	2.3E+06	1597	62	178.2	7.4	4.2	**607**	**25**	3410	130	1.9	1.3	224	7.9	0.425	0.086	10.74	0.71	134.4	4.6	84.9	3.2	1.6	0.1	0.31	0.05	1.4	0.3	46.7	1.7
Br1062-17c	Grt	4.4E+07	3.6E+06	1067	44	179.3	7.3	4.1	**608**	**25**	3350	120	3.1	2.6	163.9	7.1	0.58	0.14	14.18	0.95	117.1	4.2	74.1	3.1	1.7	0.2	0.27	0.08	1.2	0.6	57	1.8
Br1062-35g	Grt	3.9E+07	2.7E+06	2010	65	182.8	6.4	3.5	**609**	**21**	3740	130	1.3	1.5	296	13	0.473	0.086	12	0.79	200.2	7.1	82.3	3.4	1.4	0.3	0.52	0.27	0.0	0.0	33.7	1.3
Br1062-34a	Grt	2.9E+07	4.6E+06	1241	40	184.2	7.5	4.1	**610**	**25**	3580	140	3.1	1.3	250	13	0.55	0.19	9.34	0.85	208.4	7.5	69.5	3.1	0.9	0.2	0.16	0.06	0.6	0.1	29	0.95
Br1062-19h	Grt	3.3E+07	8.8E+06	1190	100	187	14	7.5	**611**	**46**	3440	250	1.7	1.4	201	19	0.34	0.17	13.1	1.8	112	11	79.3	6.9	1.5	0.5	0.25	0.14	1.6	0.5	35	3.4
Br1062-19d	Grt	3.7E+07	2.6E+06	1802	64	193.5	7.2	3.7	**613**	**23**	3410	130	5.5	2.6	252	11	0.49	0.099	11.79	0.76	128.5	4.7	80.7	3.3	1.8	0.2	0.47	0.07	0.9	0.1	47.9	1.8
Br1062-7b	Grt	3.6E+07	2.3E+06	1086	36	194.7	7.8	4.0	**614**	**25**	3540	120	5.4	3.1	189.9	8.4	0.428	0.083	11.92	0.7	189	5.8	60.9	2.3	0.6	0.1	0.11	0.03	0.1	0.0	17.38	0.63
Br1062-6l	Grt	4.6E+07	3.2E+06	2149	62	204.1	6.7	3.3	**617**	**20**	1926	59	3.61	0.95	226.8	9.4	0.365	0.076	10.5	0.58	80.7	2.5	55.9	1.8	1.4	0.1	0.02	0.01	0.1	0.0	56	1.4
Br1062-35d	Grt	3.6E+07	2.2E+06	1570	52	206.3	7.3	3.5	**618**	**22**	3940	130	0.23	0.35	286	11	0.403	0.086	13.18	0.79	216.5	6.7	112.1	4	0.8	0.1	0.02	0.01	0.0	0.0	35.5	1.5
Br1062-6a	Grt	5.2E+07	3.0E+06	1069	47	212.9	8	3.8	**620**	**23**	2094	75	1	0.82	152.6	6.8	0.48	0.1	19.1	1.3	108.2	4.4	55.5	1.9	3.5	0.3	0.02	0.01	0.0	1.0	152.4	4.9
Br1062-37e	Grt	3.6E+07	2.6E+06	1145	43	216.7	7	3.2	**621**	**20**	1967	61	7	1.2	185	7	0.411	0.095	11.63	0.78	89.2	2.4	101.4	3.5	4.3	0.3	0.05	0.02	0.1	0.0	176.3	6
Br1062-17f	Grt	4.4E+07	3.7E+06	1047	39	217	10	4.6	**621**	**29**	3360	120	5	3.9	180	10	0.37	0.12	11.9	0.93	129	7.4	75.9	3.5	1.0	0.3	0.12	0.06	0.9	0.6	32.4	1.7
Br1062-35c	Grt	3.7E+07	2.4E+06	1904	70	217.8	9.3	4.3	**622**	**27**	3770	130	2.9	2.4	281	10	0.402	0.082	13.13	0.68	226	7.7	81	2.8	0.8	0.1	0.06	0.02	0.3	0.0	26.72	0.77
Br1062-21f	Grt	3.2E+07	2.4E+06	703	25	227.4	8.9	3.9	**625**	**24**	3490	130	1.29	0.68	232	10	0.51	0.1	11.07	0.82	192.2	7.6	106.8	4.4	3.3	0.3	1.41	0.15	0.0	1.0	73.8	2.8
Br1062-37b	Grt	3.5E+07	2.3E+06	1080	36	237	10	4.2	**628**	**26**	2017	66	6.4	1	175.7	6.2	0.423	0.098	10.85	0.63	89.9	2.9	84.6	2.7	5.9	0.4	0.04	0.02	0.2	0.1	260	12
Br1062-18c	Grt	3.1E+07	2.3E+06	1197	47	239	11	4.6	**629**	**29**	3630	120	2.3	1.4	201.4	7.6	0.68	0.12	14.23	0.88	169.8	6.2	86.2	3.3	1.6	0.2	0.03	0.02	0.0	1.0	67.1	2.2
Br1062-3b	Grt	5.8E+07	3.1E+06	1254	54	239	14	5.9	**629**	**37**	2670	140	2	2.3	186	11	0.46	0.11	26.6	1.7	220.7	9.1	573	20	1.3	0.2	0.04	0.02	1.8	0.3	67.9	3.6
Br1062-18b	Grt	3.4E+07	2.1E+06	1196	38	249.9	9.2	3.7	**632**	**23**	3530	110	0.93	0.57	204.6	7.2	0.431	0.073	13.36	0.73	136.4	3.9	69.8	2.6	1.1	0.1	0.07	0.02	2.4	0.5	45.1	1.5
Br1062-17g	Grt	3.6E+07	3.8E+06	969	34	255	9.2	3.6	**634**	**23**	3290	100	4.6	2.3	197.7	8.3	0.41	0.11	13.14	0.76	129.4	4.6	64.3	2.8	0.8	0.2	0.15	0.05	0.6	0.3	26.51	0.83
Br1062-2e	Grt	4.2E+07	2.7E+06	1219	65	297	14	4.7	**645**	**30**	3290	160	12.7	6.5	219	9.7	0.74	0.13	23.3	1.3	175.4	6.8	645	34	2.0	0.3	0.08	0.03	0.0	1.0	94.2	4.7
Br1062-19g	Grt	3.4E+07	4.0E+06	1125	39	299	11	3.7	**646**	**24**	3760	130	2.8	1.1	245	12	0.252	0.098	17.2	1.2	141.4	6.3	130.6	5.8	2.5	0.4	1.40	0.38	2.3	0.6	48.8	1.7
Br1062-2d	Grt	3.1E+07	2.3E+06	1327	48	316	12	3.8	**650**	**25**	3740	160	4.6	2.4	247.1	9.8	0.85	0.12	27.2	1.2	206.1	8.9	687	29	2.6	0.3	0.01	0.01	0.0	1.0	97.8	3.8
Br1062-3a	Grt	5.1E+07	2.9E+06	1344	54	323	10	3.1	**652**	**20**	3166	85	7.4	3.7	221.2	8.4	0.53	0.097	30.9	1.3	213.5	7	584	21	1.4	0.2	0.04	0.02	0.0	1.0	69.4	2.3
Br1062-35b	Grt	4.0E+07	3.0E+06	1948	67	333	10	3.0	**654**	**20**	3920	140	3.6	2.5	303	14	0.5	0.082	15.71	0.81	222.3	8.7	116.7	4.4	1.5	0.2	0.01	0.01	0.0	1.0	65.8	2.4
Br1062-2f	Grt	3.3E+07	2.2E+06	1338	42	342	12	3.5	**656**	**23**	3910	150	1.7	1.3	260	11	0.91	0.14	28.5	1.5	230.5	8.5	868	27	2.4	0.2	0.13	0.03	0.2	0.1	96.4	3.3
Br1062-2g	Grt	3.0E+07	2.5E+06	1358	49	383	16	4.2	**666**	**28**	4060	150	10.1	4	279	12	0.99	0.18	30.5	1.7	228.8	9.4	654	24	3.0	0.3	0.29	0.05	0.0	0.0	107.3	3.6
Br1062-2i	Grt	4.7E+07	3.4E+06	1308	63	389	18	4.6	**667**	**31**	3670	180	3.7	3.1	238	11	0.82	0.12	30.4	1.7	200.5	9.4	545	24	2.5	0.2	0.05	0.02	0.0	0.0	105	4.1
Br1062-2b	Grt	3.3E+07	2.5E+06	1390	53	442	17	3.8	**677**	**26**	3930	150	5.1	2.6	286	12	0.7	0.12	35.3	1.7	250.1	9.1	1096	36	2.8	0.2	0.03	0.01	0.0	1.0	119.5	3.6
Br1062-2h	Grt	3.5E+07	2.3E+06	1480	54	479	19	4.0	**684**	**27**	5100	150	8.4	4.2	298	11	0.85	0.11	41.5	2.4	253.2	8.8	912	29	2.3	0.2	0.01	0.01	0.0	1.0	101.9	3.3
Br1062-6c	Grt	4.3E+07	3.1E+06	1005	35	521	16	3.1	**691**	**21**	2028	63	5	1.1	408	16	0.212	0.061	23.8	1.1	105.6	3	46	1.6	1.1	0.1	0.03	0.01	0.2	0.0	49.6	1.4
Br1062-6d	Grt	3.9E+07	2.8E+06	1839	60	553	20	3.6	**696**	**25**	2949	94	5.2	2.3	428	15	0.252	0.063	22.9	1.2	122.6	3.7	48.7	1.9	2.1	0.2	0.05	0.02	0.0	0.0	83.7	2.7
Br1062-3c	Grt	4.1E+07	3.0E+06	1370	44	573	21	3.7	**700**	**26**	3418	94	8	3.3	303	12	0.412	0.077	30.1	1.3	187.5	5.4	438	14	1.7	0.2	0.08	0.02	0.0	1.0	74.1	2.4
Br1062-35e	Grt	3.6E+07	2.8E+06	749	25	578	21	3.6	**700**	**25**	3980	150	0.31	0.39	214.3	8.9	1.5	0.17	21.94	0.97	229.2	8.5	99.3	3.6	1.2	0.1	0.04	0.02	0.1	0.0	52.8	1.8
Br1062-6b	Grt	4.4E+07	3.0E+06	1221	33	595	20	3.4	**703**	**24**	1900	56	5.4	1.2	445	18	0.083	0.039	18.66	0.88	98.4	3	63	2.4	1.2	0.1	0.03	0.01	0.0	1.0	54.7	1.7
Br1062-21d	Peak	4.2E+07	3.0E+06	1057	29	867	28	3.2	**737**	**24**	2910	110	4.6	2.5	608	23	0.209	0.059	19.3	1.1	153.8	5.5	67.7	2.5	3.3	0.2	0.45	0.06	0.1	0.0	125.7	3.5
Br1062-7a	Grt	3.9E+07	3.2E+06	463	14	957	33	3.4	**747**	**26**	3487	98	4.8	2.2	209.1	7.9	0.176	0.058	24.7	1.3	83.2	3	16.52	0.81	1.9	0.2	0.03	0.01	0.0	1.0	81.7	2
Br1062-10i	Grt	4.9E+07	3.2E+06	1200	32	1035	29	2.8	**754**	**21**	4430	120	3.2	2.2	409	15	0.192	0.055	58.3	2.2	427	12	47.1	1.4	1.6	0.2	0.01	0.01	0.0	1.0	68.9	1.7
Br1062-1t	Grt	4.6E+07	3.3E+06	1123	33	1083	35	3.2	**759**	**25**	3049	99	6.5	3.2	332	14	0.218	0.055	43.5	1.7	174.9	6	494	15	1.3	0.1	0.01	0.01	0.0	1.0	61.9	1.8
Br1062-21e	Peak	2.9E+07	4.2E+06	1040	36	1094	38	3.5	**760**	**26**	4100	150	4.3	1.6	618	28	0.142	0.086	30.5	1.7	228.5	6.9	135.1	5.4	4.1	0.4	1.19	0.21	0.6	0.2	127.5	4.9
Br1062-6g	Grt	4.7E+07	3.1E+06	932	26	1105	36	3.3	**761**	**25**	1895	51	8.2	1.9	466	17	0.175	0.051	30.3	1.1	94.4	2.9	52.4	2	1.8	0.2	0.05	0.02	0.0	0.1	78.3	2.5
Br1062-6e	Grt	4.9E+07	3.0E+06	2050	110	1389	52	3.7	**784**	**29**	1859	88	10.7	4.5	340	16	0.184	0.076	41.5	2.4	107.7	5.1	56.4	2.2	1.8	0.2	0.08	0.03	4.6	0.3	73	2.9
Br1062-12t	Grt	4.6E+07	3.3E+06	1043	31	1422	43	3.0	**786**	**24**	4030	120	3.8	2.6	167.1	6	0.368	0.075	83.9	3.1	219.4	6.1	101.3	3.3	1.3	0.2	0.08	0.03	0.5	0.1	56.7	1.4
Br1062-6f	Grt	3.8E+07	3.4E+06	1879	55	1551	54	3.5	**795**	**28**	2031	69	12.5	2.2	493	18	0.223	0.068	40.4	1.6	96.3	3.1	62.7	2.5	2.4	0.2	0.03	0.02	0.0	0.0	104.6	3.3
Br1062-20c	Peak	3.7E+07	2.4E+06	1412	46	2196	90	4.1	**833**	**34**	6080	230	37.8	6.7	581	21	0.131	0.048	89.1	3.8	191.1	7.2	21.2	1.2	3.4	0.2	0.08	0.03	0.0	1.0	142.5	4.6

Sample and Analysis Number	Texture	Ti (cps)	± 2SE (cps)	V (ppm)	± 2SE (ppm)	Zr (ppm)	± 2SE (ppm)	± 2SE %	Zr-in-Rt T (°C)	± 2SE (°C)	Nb (ppm)	± 2SE (ppm)	Mo (ppm)	± 2SE (ppm)	Sn (ppm)	± 2SE (ppm)	Sb (ppm)	± 2SE (ppm)	Hf (ppm)	± 2SE (ppm)	Ta (ppm)	± 2SE (ppm)	W (ppm)	± 2SE (ppm)	206Pb (ppm)	± 2SE (ppm)	208Pb (ppm)	± 2SE (ppm)	Th (ppm)	± 2SE (ppm)	U (ppm)	± 2SE (ppm)
Br1062-36b	Rextal	2.8E+07	3.0E+06	961	33	2980	110	3.7	**869**	**32**	2132	66	28.8	3.2	650	28	0.39	0.11	69.7	3.4	97.3	3.7	178.8	7	7.7	0.5	0.19	0.05	0.0	0.0	327.7	9.1
Br1062-36a	Rextal	3.3E+07	1.7E+06	903	23	3090	100	3.2	**873**	**28**	2180	66	30.5	2.3	588	21	0.235	0.069	84.6	2.8	107	4.2	140.3	4.8	7.8	0.5	0.42	0.07	0.0	1.0	303	11
Br1062-33a	Peak	3.8E+07	2.6E+06	547	17	3240	100	3.1	**879**	**27**	4400	130	23.8	5.2	432	15	0.152	0.068	106.8	3.9	277	11	97	3.1	2.8	0.2	0.06	0.02	0.0	0.0	118.1	3.7
Br1062-33b	Peak	3.9E+07	2.9E+06	553	17	3250	110	3.4	**879**	**30**	4410	120	15.1	4.2	439	14	0.195	0.058	100.2	3.5	274.7	7.9	114.3	3.9	3.1	0.2	0.02	0.01	0.0	1.0	119.2	3.7
Br1062-33c	Peak	4.2E+07	2.8E+06	899	24	3340	94	2.8	**883**	**25**	4070	110	37.1	4.8	497	18	0.351	0.083	117.6	4.1	236.9	6.9	112.1	3.6	3.1	0.2	0.02	0.01	0.0	1.0	134.8	4.1
Br1062-37d	Peak	3.6E+07	2.3E+06	1337	42	3380	140	4.1	**884**	**37**	3120	110	115.1	6.7	842	34	0.529	0.093	93.4	3.3	163.3	5.6	405	15	11.2	0.6	0.03	0.01	0.0	1.0	460	16
Br1062-21b	Peak	3.4E+07	2.2E+06	994	35	3630	120	3.3	**893**	**30**	4900	150	33.1	6.5	609	21	0.285	0.095	107.6	4.2	261.9	9.4	88.7	3.3	4.0	0.3	0.46	0.06	0.0	0.0	150.1	5.2
Br1062-20a	Peak	2.2E+07	2.8E+06	2260	100	3650	180	4.9	**894**	**44**	17300	720	25.8	8.7	738	32	0.18	0.11	144.6	6.3	1746	81	401	20	4.3	0.4	0.10	0.04	0.0	1.0	163.5	7.7
Br1062-20b	Peak	3.1E+07	5.8E+06	2400	180	4030	240	6.0	**906**	**54**	6050	280	44.4	9.8	700	55	0.27	0.13	133	10	562	37	170	14	5.3	0.7	0.28	0.10	0.4	0.2	180	13
Br1062-6n	Peak	4.2E+07	2.9E+06	1821	47	4140	160	3.9	**910**	**35**	1885	56	14.8	1.9	497	19	0.165	0.056	127.8	4	90.3	2.9	70.8	2.7	2.2	0.2	0.01	0.00	0.0	1.0	99.9	3.6
Br1062-10a	Peak	4.6E+07	3.5E+06	1099	27	4180	130	3.1	**911**	**28**	2985	81	5.3	1.2	298	12	0.117	0.045	123.6	3.8	332.7	8.5	46.7	1.6	1.2	0.1	0.01	0.01	0.0	1.0	51.1	1.4
Br1062-20d	Peak	4.0E+07	3.2E+06	1965	56	4180	120	2.9	**911**	**26**	15410	510	30.1	5.6	598	21	0.213	0.075	158.5	5.4	1139	40	220.2	6.4	3.0	0.2	0.13	0.03	0.0	1.0	124	3.5
Br1062-22b	Peak	2.7E+07	1.6E+06	1286	46	4400	180	4.1	**918**	**38**	5690	210	39.4	8.3	561	17	0.065	0.061	136	6.4	434	14	158.6	7.3	2.5	0.2	0.04	0.02	0.0	0.0	103.9	3.8
Br1062-22c	Peak	3.2E+07	2.3E+06	1372	58	4400	190	4.3	**918**	**40**	4800	200	41.8	7	568	24	0.199	0.081	123.1	4.5	307	11	143.9	7.2	3.0	0.2	0.09	0.03	0.0	1.0	119.4	5.1
Br1062-10d	Peak	5.1E+07	3.2E+06	1118	31	4410	110	2.5	**918**	**23**	2988	87	6.2	1.7	290	12	0.125	0.047	125.3	4.2	286.6	7.7	38.8	1.2	1.2	0.1	0.01	0.01	0.0	1.0	51.3	1.2
Br1062-20f	Peak	4.9E+07	4.5E+06	2251	96	4420	180	4.1	**918**	**37**	16700	530	27	5.7	595	34	0.118	0.057	164.9	6.5	2730	110	250	10	2.5	0.3	0.15	0.10	0.0	0.0	105.5	4.3
Br1062-10g	Peak	5.1E+07	3.3E+06	1104	38	4520	140	3.1	**921**	**29**	3460	110	7	1.8	284	11	0.154	0.048	128.7	3.6	292.5	8.7	51.7	1.8	1.3	0.1	0.00	0.00	0.0	1.0	57.3	1.7
Br1062-10b	Peak	4.4E+07	3.5E+06	1161	34	4670	150	3.2	**926**	**30**	3148	71	6.3	1.7	326	14	0.162	0.051	142.6	4.4	361	10	49.5	1.7	1.6	0.2	0.12	0.03	0.2	0.1	54.4	1.7
Br1062-9	Peak	4.9E+07	3.2E+06	1141	31	4810	140	2.9	**930**	**27**	3318	83	5.3	1.5	286	10	0.156	0.051	147	5	396.7	9.6	58.8	1.7	1.1	0.1	0.01	0.01	0.0	1.0	50	1.4
Br1062-5t	Peak	3.7E+07	2.2E+06	1545	59	4820	190	3.9	**930**	**37**	3060	110	46.1	5.7	479	17	0.234	0.071	150.4	6.8	195.3	7.6	145.5	5.6	3.5	0.3	0.04	0.02	0.0	1.0	138.7	5.7
Br1062-10f	Peak	5.2E+07	3.4E+06	1053	26	4840	130	2.7	**930**	**25**	3075	74	4.4	1.2	290.2	9.6	0.116	0.036	149.3	4.7	352	10	52.5	1.5	1.3	0.1	0.03	0.01	0.0	1.0	58.3	1.5
Br1062-21a	Peak	2.8E+07	1.4E+06	982	38	4930	200	4.1	**933**	**38**	6290	240	56.9	7.6	616	23	0.312	0.086	153	7	391	14	145.4	5.8	5.9	0.5	0.69	0.10	0.0	1.0	191.9	6.8
Br1062-38	Peak	4.2E+07	5.3E+06	452	15	5090	160	3.1	**937**	**29**	3470	120	186.6	8.3	1106	51	0.19	0.11	170.6	6.8	154.9	7.1	485	22	11.1	1.2	5.40	1.30	0.0	1.0	297	11
Br1062-24a	Peak	3.9E+07	2.6E+06	1841	62	5170	190	3.7	**939**	**35**	4360	140	65.8	4	500	19	0.105	0.054	172.2	5.1	293	10	206.1	7.5	3.3	0.2	0.65	0.07	0.0	1.0	114.8	3.6
Br1062-20e	Peak	4.3E+07	3.4E+06	2170	78	5210	150	2.9	**940**	**27**	17620	540	36.6	4.8	604	24	0.133	0.054	189.6	5.5	1498	42	254.6	8.5	3.3	0.2	0.06	0.02	0.0	1.0	136.4	4
Br1062-14b	Peak	5.3E+07	3.5E+06	1191	38	5250	150	2.9	**941**	**27**	3410	100	26.2	3.4	526	22	0.107	0.045	166.9	4.5	318	9.6	56.3	1.8	2.5	0.2	0.02	0.01	0.0	1.0	102.2	2.9
Br1062-14d	Peak	4.8E+07	3.3E+06	1175	35	5310	140	2.6	**943**	**25**	3513	92	30.3	1.9	535	19	0.145	0.048	162.2	4.5	315.9	8.6	57.2	1.7	2.0	0.2	0.00	0.00	0.0	1.0	78.6	2.2
Br1062-10e	Peak	4.9E+07	3.3E+06	1422	33	5360	150	2.8	**944**	**26**	3488	87	5.8	1.5	327	13	0.061	0.046	164.8	3.8	388	11	57.5	1.8	1.1	0.1	0.01	0.01	0.0	1.0	58.1	1.3
Br1062-14a	Peak	5.0E+07	3.1E+06	1169	32	5360	160	3.0	**944**	**28**	3520	87	26.4	3.5	542	19	0.159	0.049	168.6	5.1	312.1	8.7	58.1	1.8	2.0	0.2	0.01	0.01	0.0	1.0	77.8	2
Br1062-14c	Peak	4.8E+07	3.1E+06	1216	33	5450	130	2.4	**946**	**23**	3540	87	32.6	2.1	557	21	0.088	0.04	173.6	4.5	334	10	60.9	1.9	2.0	0.1	0.01	0.01	0.0	1.0	88	2.6
Br1062-37c	Peak	4.3E+07	5.2E+06	1424	92	5470	420	7.7	**947**	**73**	3080	170	168	13	814	55	0.37	0.14	165.7	9	178.9	9.3	388	27	10.9	1.1	0.61	0.39	0.1	0.0	427	21
Br1062-39	Peak	4.1E+07	3.6E+06	1906	95	5520	330	6.0	**948**	**57**	1573	57	72.9	4.3	939	42	0.16	0.086	170.5	8.9	70	3.6	142.2	5.4	2.1	0.3	0.04	0.02	0.0	0.0	108.1	4.5
Br1062-32	Peak	4.3E+07	2.7E+06	702	21	5530	150	2.7	**948**	**26**	5340	140	34.2	4	503	19	0.168	0.057	177.5	6.1	429	14	121.7	4	2.2	0.2	0.02	0.01	0.0	1.0	97.8	3.7
Br1062-13	Peak	5.6E+07	3.7E+06	1608	63	5550	230	4.1	**949**	**39**	3300	130	11	3.6	472	24	0.213	0.058	166.2	7.5	355	11	57.9	2.4	3.3	0.3	0.01	0.01	0.0	1.0	146.2	5.3
Br1062-22a	Peak	3.4E+07	2.3E+06	1177	43	5600	200	3.6	**950**	**34**	6320	210	45.7	6.1	690	21	0.154	0.065	177.6	7.9	491	16	135.8	4.9	3.5	0.2	0.56	0.08	0.0	1.0	133	4.3
Br1062-21c	Peak	3.2E+07	2.1E+06	1580	55	5640	240	4.3	**951**	**40**	7900	300	71.5	4	561	23	0.284	0.092	193	9	272	11	168.5	7.5	5.5	0.4	0.38	0.07	0.0	1.0	207.3	7.9
Br1062-24b	Peak	4.0E+07	2.7E+06	1844	61	5680	200	3.5	**952**	**34**	4770	150	63.3	4.3	528	22	0.046	0.045	189.5	6.8	326	11	192.2	7.2	3.9	0.3	0.90	0.12	0.0	0.0	120.5	4.4
Br1062-26	Peak	4.4E+07	2.9E+06	1229	30	5720	150	2.6	**953**	**25**	4590	130	62.7	3.9	472	19	0.072	0.045	187.2	4.8	172.6	4.9	58	2.1	2.7	0.2	0.05	0.02	0.0	1.0	117.6	2.8
Br1062-29	Peak	2.7E+07	3.3E+06	1617	68	5740	230	4.0	**954**	**38**	9050	350	83	11	795	36	0.083	0.09	186.4	8.1	840	32	289	13	5.5	0.4	0.10	0.03	0.1	0.0	193.3	7.3
Br1062-23a	Peak	3.4E+07	2.1E+06	1387	47	7370	300	4.1	**989**	**40**	11680	380	97.6	5.6	763	30	0.11	0.059	249	11	862	33	329	12	4.2	0.3	0.38	0.06	0.0	1.0	149.4	5.2
Br1062-23b	Peak	3.5E+07	2.1E+06	1374	48	7440	220	3.0	**991**	**29**	11600	430	90	6.3	742	29	0.037	0.051	244.6	8.1	794	25	290.7	9.9	4.6	0.3	0.60	0.09	0.0	1.0	157.1	5.1
Br1062-10h	Peak	5.0E+07	4.0E+06	1203	38	7510	230	3.1	**992**	**30**	4460	140	3	1.5	405	18	0.11	0.045	241.1	8	459	12	40.5	1.4	1.2	0.1	0.01	0.01	0.0	1.0	58.2	1.8
Br1062-31a	Peak	3.2E+07	2.1E+06	1644	62	7730	300	3.9	**996**	**39**	19600	790	112.1	8.1	979	39	0.274	0.085	266.9	8.9	2340	85	475	18	5.3	0.4	0.02	0.01	0.0	0.0	206.5	8.2
Br1062-30	Peak	3.4E+07	5.3E+06	2030	130	7750	490	6.3	**997**	**63**	16300	1000	84	10	867	53	0.15	0.14	268	20	1244	70	328	23	4.4	1.0	1.12	0.50	0.1	0.1	112.2	6.3
Br1062-31b	Peak	3.3E+07	2.2E+06	1630	65	7800	340	4.4	**998**	**43**	19230	710	103.8	6.5	946	42	0.128	0.057	270	11	2309	85	467	21	5.0	0.4	0.02	0.01	0.0	1.0	209.2	7.5
Br1062-10c	Peak	4.8E+07	3.1E+06	1248	36	8010	220	2.7	**1002**	**28**	4450	130	6.3	3	344	12	0.141	0.058	265.3	7.4	775	19	151.9	4	1.5	0.1	0.03	0.01	0.0	1.0	66	1.8

Notes:
Textures: Grt = rutile included in or in embayment in garnet; Peak = rutile in peak matrix assemblage; Rextal = rutile in recrystallized matrix; Zrc = rutile in contact with zircon
Zr-in-rutile T(°C): temperature calculated from Zr concentration using the equation of Tomkins et al. (2007) at 9 kbar
nd = not determined
bdl = below detection limit

Table 2.4. Zr-in-rutile temperature and U-Pb dates for selected analyses.

Sample and Analysis Number	Texture	Zr-in-rutile T (°C)	206Pb/238U Date (Ma)	± 2SE (Ma)
Retrogressed Granulite (GR11-1A)				
GR11-1A-17.FIN2	Rextal	681	23.5	1.2
GR11-1A-22.FIN2	Rextal	683	24.4	1.9
GR11-1A-57.FIN2	Rextal	699	25.5	1.3
GR11-1A-50.FIN2	Rextal	700	25.8	3.1
GR11-1A-24.FIN2	Rextal	715	27.3	1.7
GR11-1A-59a.FIN2	Rextal	725	27.1	0.8
GR11-1A-41.FIN2	Rextal	731	24.8	2.5
GR11-1A-8.FIN2	Rextal	738	28.5	0.9
GR11-1A-37a.FIN2	Rextal	740	25.6	0.9
GR11-1A-23b.FIN2	Rextal	740	23.0	1.0
GR11-1A-59b.FIN2	Rextal	740	25.7	2.6
GR11-1A-18.FIN2	Rextal	742	27.3	1.0
GR11-1A-59c.FIN2	Rextal	750	25.8	2.0
GR11-1A-1.FIN2	Rextal	751	24.3	0.7
GR11-1A-25.FIN2	Rextal	760	25.2	1.3
GR11-1A-23a.FIN2	Rextal	771	26.8	1.0
GR11-1A-40.FIN2	Rextal	775	27.8	1.3
GR11-1A-52a.FIN2	Rextal	786	25.8	1.6
GR11-1A-43a.FIN2	Rextal	802	26.1	1.6
GR11-1A-81.FIN2	Rextal	805	19.8	0.9
GR11-1A-27.FIN2	Rextal	807	27.1	1.1
GR11-1A-32.FIN2	Rextal	814	26.2	1.9
GR11-1A-28.FIN2	Rextal	814	18.8	1.5
GR11-1A-79b.FIN2	Rextal	814	26.2	1.2
GR11-1A-35.FIN2	Rextal	834	27.2	1.4
GR11-1A-2.FIN2	Rextal	877	27.1	0.7
GR11-1A-39.FIN2	Rextal	888	26.5	2.3
Retrogressed Granulite (GR11-1C)				
GR11-1C-17b.FIN2	Grt	612	23.8	2.1
GR11-1C-11.FIN2	Grt	637	24.1	1.0
GR11-1C-15.FIN2	Grt	653	24.0	1.6
GR11-1C-24.FIN2	Grt	721	25.6	2.4
GR11-1C-9.FIN2	Grt	722	25.6	1.5
GR11-1C-25.FIN2	Grt	729	23.7	2.5
GR11-1C-23.FIN2	Grt	735	23.4	2.4
GR11-1C-3.FIN2	Grt	748	24.8	0.9
GR11-1C-17a.FIN2	Grt	754	22.4	2.6
GR11-1C-18a.FIN2	Grt	776	21.5	2.7
GR11-1C-22.FIN2	Grt	789	25.7	2.6
GR11-1C-16a.FIN2	Grt	799	24.8	1.5
GR11-1C-7.FIN2	Grt	844	23.0	2.5
GR11-1C-12.FIN2	Grt	847	25.6	1.6
GR11-1C-26.FIN2	Grt	849	25.1	1.7
GR11-1C-1.FIN2	Grt	862	23.5	3.0
GR11-1C-27.FIN2	Grt	892	26.7	1.8
Stromatic Granulite (Bras10-5b-1)				
Bras105b-6	Peak	924	27.4	0.8
Bras105b-4	Peak	928	23.5	0.9
Bras105b-9ta	Peak	951	19.6	1.0
Bras105b-11ta	Peak	954	26.2	0.9
Bras105b-17t	Peak	994	20.6	0.7

Table 2.4

Sample and Analysis Number	Texture	Zr-in-rutile T (°C)	206Pb/238U Date (Ma)	± 2SE (Ma)
Bras105b-14t	Peak	1007	19.8	0.7
Stromatic Granulite (Bras10-6-1)				
72ta	Grt	582	18.7	1.0
72tb	Grt	587	22.3	1.4
6	Rextal	735	23.9	0.7
20t	Rextal	754	24.1	0.6
14	Rextal	762	22.9	0.8
27t	Rextal	764	21.8	0.6
5d	Rextal	765	20.6	0.5
5a	Rextal	768	20.8	0.5
5b	Rextal	798	22.0	0.6
22	Rextal	847	21.1	0.5
32	Peak	898	21.0	0.7
84	Peak	902	24.4	0.8
80	Peak	904	22.0	0.9
87a	Peak	908	22.5	0.9
13a	Peak	921	25.3	0.9
86	Peak	932	24.9	1.0
35	Peak	937	21.8	0.8
2	Peak	938	22.1	0.6
59	Peak	938	20.6	0.7
44a	Peak	941	24.1	0.7
34	Peak	942	21.4	0.7
1c	Peak	942	18.7	0.7
43b	Peak	942	20.4	0.7
1r	Peak	946	20.7	0.8
82a	Peak	946	22.1	0.8
82b	Peak	946	22.4	0.8
82c	Peak	949	22.1	0.7
18b	Peak	953	24.7	0.9
65t	Peak	953	24.6	0.5
48dt	Peak	955	26.0	0.8
48a	Peak	958	27.5	0.6
4	Peak	963	21.3	0.6
29a	Peak	964	21.0	0.6
7	Peak	966	24.6	0.6
17t	Peak	967	26.6	1.1
45	Peak	968	21.7	0.6
77	Peak	969	21.9	0.7
3a	Peak	972	19.1	0.6
57b	Peak	981	23.7	0.7
34b	Peak	981	21.8	0.6
36	Peak	982	23.5	0.7
75	Peak	983	21.8	0.7
23	Peak	984	20.5	0.5
15t	Peak	990	21.7	0.6
30	Peak	997	22.3	0.7

Notes:

Textures: Grt = rutile included in garnet; Peak = rutile in peak matrix assemblage; Rextal = rutile in recrystallized matrix

Zr-in-rutile T(°C): temperature calculated from Zr concentration using the equation of Tomkins et al. (2007) at 9 kbar

CHAPTER 3

Constraining the timing of UHT metamorphism, melt crystallization, and deformation with zircon geochronology and trace element geochemistry: The Gruf Complex, Central Alps

Jeffrey Oalmann[1]

Andreas Möller[1]

Romain Bousquet[2]

Jessica Savage[1]*

[1]*The University of Kansas, Department of Geology, 1475 Jayhawk Blvd., Rm. 120, Lawrence, KS 66045 USA.*

[2]*Christian-Albrechts-Universität zu Kiel, Institute of Geosciences, Ludewig-Meyn-Straße 10, 24098 Kiel, Germany.*

** Currently at Northern Arizona University, School of Earth Sciences and Environmental Sustainability, 525 S. Beaver St., Flagstaff, AZ 86011 USA*

Abstract

The results of U-Pb geochronology and trace element geochemistry of zircon are used to constrain the timing of ultra-high temperature (UHT) metamorphism of granulites and charnockites, ductile deformation, and exhumation of the UHT rocks into the migmatitic middle crust. Titanium-in-zircon thermometry and rare earth element patterns of zircon reveal that zircon in the granulites was resorbed at UHT conditions, and featureless rims, which overgrew resorbed Permian–Cretaceous oscillatory-zoned cores, formed shortly after UHT garnet breakdown at 32.7 ± 0.7Ma. The UHT rocks were juxtaposed against upper amphibolite facies migmatites along mylonitic shear zones between 30 and 27 Ma. Ductile deformation ended by ca. 26 Ma, but felsic magmatism continued until ca. 24 Ma, culminating in the intrusion of the Novate leucogranite.

The most plausible geodynamic scenario is that UHT metamorphism occurred as a result of advection of asthenospheric material or magmas to the base of the crust at ca. 34 Ma after slab breakoff and partial exhumation of the (ultra)-high pressure nappes in the Central Alps. The lower crustal rocks were then exhumed to the middle crust, likely aided by the buoyant, intruding magmas of the Bergell intrusion.

Introduction

Ultra-high temperature (UHT) metamorphism, which is defined as temperature in excess of 900°C within the stability field of sillimanite (Harley, 1998; Brown, 2007; Harley, 2008), requires an elevated geothermal gradient (Kelsey, 2008) or advection of an external heat source (Collins, 2002; Sizova et al., 2010; Clark et al., 2011). Therefore, by understanding the timing of UHT metamorphism geodynamic processes and their rates and temperatures can be better constrained.

With applications in studies of igneous, metamorphic, and sedimentary systems, zircon is the most widely used U-Pb geochronometer (e.g. Hanchar and Hoskin, 2003; Harley and Kelly, 2007; Schoene, 2014). However, relating zircon dates to geological processes can be challenging, especially when dealing with rocks that have experienced multiple high temperature metamorphic or magmatic events (e.g. Möller et al., 2002; Harley et al., 2007). Combining zircon dates with trace element compositions of zircon and other minerals and their textural relationships can be used to help determine the pressure-temperature (P-T) conditions of zircon growth in metamorphic rocks (e.g. Rubatto, 2002; Möller et al., 2003; Whitehouse and Platt, 2003; Kelly and Harley, 2005), and thus help unravel the geodynamic evolution of terranes.

The Gruf Complex of the Central Alps, which is characterized by UHT granulites and charnockites juxtaposed against upper amphibolite facies migmatites, is enigmatic in that it is the

only occurrence of UHT rocks within the Central Alps (Bousquet et al., 2012a). Therefore, knowing the age of UHT metamorphism is important for reconstructions of the tectonometamorphic evolution of the Central Alpine orogeny, but this has been a matter of debate. Recent works by Galli *et al.* (2011; 2012; 2013) have concluded that UHT metamorphism occurred during Permian rifting of the European margin, whereas previous studies (Liati and Gebauer, 2003; Schmitz et al., 2009) interpreted the UHT sapphirine-forming reactions to occur during Alpine orogenesis.

In this study, we combine U-Pb zircon geochronology with Ti-in-zircon thermometry and zircon trace element geochemistry to constrain the timing of UHT metamorphism in the granulites of the Gruf Complex. Samples of different types of felsic dikes, which trend from less evolved and structurally earlier to more evolved and less deformed, were also collected for U-Pb zircon geochronology to establish the absolute timing of crystallization and deformation. We use these dike crystallization ages to bracket the timing of deformation and juxtaposition of the UHT rocks and migmatites, which lack evidence for ever experiencing UHT metamorphism.

Geologic Setting

The Central Alps (Figure 3.1) consist of several thrust-bound terranes that were amalgamated during the Alpine orogeny (e.g. Stampfli et al., 1998; Bousquet et al., 2012b). The nappes were originally part of either the pre-Alpine European margin or the Penninic units, which consist of the Piemont-Liguria and Valais oceans and the Briançonnais microcontinent (Figure 3.1). Many of the units in the Central Alps experienced (ultra)-high pressure ((U)HP) metamorphism during the continental subduction phase of the Alpine orogeny (e.g. Becker, 1993; Gebauer, 1996; Brouwer et al., 2005; Hermann et al., 2006). After amalgamation, a Barrovian metamorphic field gradient formed across a large part of the Central Alps (the Lepontine Dome),

resulting in greenschist facies metamorphism in the north and upper amphibolite facies migmatization in the south at the Southern Steep Belt (Niggli and Niggli, 1965; Trommsdorff, 1966; Todd and Engi, 1997; Frey and Ferreiro Mählmann, 1999; Burri et al., 2005; Berger et al., 2011). Migmatization in the Southern Steep Belt continued for ca. 10 m.y. between 32 and 22 Ma (Rubatto et al., 2009).

The Gruf Complex, which lies at the eastern extent of the Central Alps, is structurally overlain by the 32–30 Ma (von Blanckenburg, 1992; Samperton et al., 2015) Bergell intrusion (Berger et al., 1996; Davidson et al., 1996). To the north, the Gruf complex is bordered by the Chiavenna ophiolite and Tambo nappe, which are Penninic units. To the west, across Valle della Mera, is the Adula nappe, which experienced UHP metamorphism (Nimis and Trommsdorff, 2001). Originally the Gruf Complex was thought to be part of the Adula nappe , but more recent studies (Ciancaleoni and Marquer, 2006; Galli et al., 2013) have concluded that the normal sense Forcula fault separates the two units (Figure 3.1), which experienced different pressure-temperature histories. The 24 ± 1 Ma (Liati et al., 2000) Novate leucogranite intruded the southwest part of the Gruf Complex.

Based on the detailed map presented by Galli et al. (2013), the Gruf Complex primarily comprises upper amphibolite facies migmatitic ortho- and paragneisses (Figure 3.2) that underwent peak metamorphism at 700–750°C and ca. 6.5–7.5 kbar (Galli et al., 2013; Oalmann et al., in preparation-a). However, several charnockite units ranging from meter- to kilometer-wide layers are also present. The largest of these charnockite layers occur in the center of the Gruf Complex at the highest elevations (Figure 3.2). Scarce sapphirine-bearing granulites (Figure 3.3) occur within the charnockite bodies as meter-scale rafts and pods and finer-scale melanosomes. The granulites and charnockites underwent UHT metamorphism as garnet was breaking down

along a decompression P-T path at 900–960°C and 8–10 kbar (Guevara and Caddick, 2016; Oalmann et al., in preparation-a). Mylonitic shear zones (up to 50 cm wide) separate the charnockite/granulite units from the migmatite units (Figure 3.3A).

Felsic dikes are common throughout the Gruf Complex and range from biotite granite to muscovite ± garnet ± tourmaline ± beryl-bearing pegmatites. The dikes show different degrees of deformation (Figure 3.4). The most mineralogically primitive (i.e. muscovite-free and muscovite-poor) dikes are ductily deformed or deformed within the mylonitic shear zones (Figure 3.4A) that separate the UHT rocks from the migmatites. The most mineralogically evolved (i.e. muscovite-rich) dikes are not deformed within the mylonitic shear zones (Figure 3.4B) and crosscut some of the less evolved dikes (Figure 3.4D, E) and foliations in the migmatites and UHT rocks. This observed correlation provides a relative time–composition framework of melt crystallization within the Gruf complex that will be explored using U-Pb zircon dating.

Sample Descriptions

Leucogranulite

Sample GR11-37 is a leucogranulite (Figure 3.3B) consisting mainly of quartz + K-feldspar + plagioclase leucosome. Minor mafic minerals (biotite + orthopyroxene + garnet + sapphirine + spinel) and very scarce, elongate sillimanite laths (Figure 3.5A) typically occur in thin layers (Figure 3.A1A). Biotite commonly fringes orthopyroxene, and thus likely grew during retrograde rehydration. Garnet prophyroblasts are subhedral to anhedral and commonly have embayments filled with orthopyroxene, biotite, plagioclase, sapphirine, spinel, and/or oxide minerals. These garnet-breakdown textures are interpreted to have formed during UHT decompression (Guevara and Caddick, 2016; Oalmann et al., in preparation-a).

Zircon occurs mainly in the leucosome of the leucogranulite sample (Figure 3.5A, B), but some grains occur within garnet breakdown textures (Figure 3.A1A). The grains typically have rounded to square shapes and reach 300 μm length (Figure 3.5A, B).

Residual Granulite

The residual granulite sample (GR11-12b) is characterized by large garnet porphyroblasts (up to 1 cm) and abundant orthopyroxene and sapphirine porphyroblasts (Figure 3.3C). Garnet, orthopyroxene, and sapphirine are commonly separated from one another by cordierite moats. Garnet is fringed by orthopyroxene + sapphirine ± cordierite intergrowths or symplectites of cordierite + orthopyroxene (Figure 3.5C). Elongate sillimanite porphyrobasts are commonly fringed by sapphirine ± spinel symplectites, which are surrounded by cordierite moats in some cases. Elongate bands of subrounded quartz grains occur mostly in close proximity to the sillimanite prophyroblasts. Quartz and sapphirine that are fringing sillimanite, are in contact in some rare cases. Biotite occurs as aggregates (up to 3 mm) that are commonly in contact with the other mafic minerals. Leucosomes are present as pods or bands of quartz + K-feldspar + plagioclase.

Zircon grains range from equant (square or round) to elongate (up to 300 μm long) and occur mostly as inclusions in biotite or cordierite or in the leucosomes (Figure 3.A1B). One large, elongate grain (grain 6) emanates from the largest garnet porphyroblast into an othropyroxene + cordierite symplectite (Figure 3.5C, A1B).

Stromatic Granulite

Stromatic granulite sample Bras10-6-2 is characterized by alternating leucosome and melanosome zones (Figure 3.3D). The thin section used in this study is from a melanosome that

contains two large, subhedral garnet porphyroblasts surrounded by orthopyroxene, biotite, and sapphirine plus leucosomes of quartz + K-feldspar + plagioclase (Figure 3.A1C). The garnets have inclusion rich cores and inclusion poor rims, indicating resorption of the cores. The center of one garnet surrounds an orthopyroxene + sapphirine intergrowth (Figure 3.A1C), which is interpreted to have formed at the expense of garnet.

Of all studied granulite samples, this thin section contains the fewest zircon grains, which are typically anhedral. Zircon occurs as inclusions in garnet (Figure 3.5D) and within the leucosome (Figure 3.A1C).

Leucosomes and Dikes

The most deformed dike/leucosome sample (GR11-55) is a biotite-granite leucosome that forms the matrix of a magmatic breccia containing clasts of altered mafic and ultramafic rock (Figure 3.4C). The overall fabric within the breccia and the orientation of the breccia itself are subparallel to the foliation in the migmatitic orthogneiss that hosts it (Figure 3.2; 4C).

Sample GR11-54 is a biotite-bearing granitic pegmatite that is folded and boudinaged within a migmatitic biotite orthogneiss (Figure 3.4D). The width of the pegmatite changes in a wave-like pattern along strike, which is parallel to the foliation in the host migmatites. We interpret this geometry to indicate that the pegmatite intruded the migmatite while the migmatite was undergoing ductile deformation and possibly still contained melt.

Sample GR11-27 is a biotite granite pod that crosscuts the foliation in the charnockite it intruded (Figure 3.4E). This relationship indicates that the charnockite was not ductily deforming when the granitic mass intruded and crystallized. Two generations of aplitic dikes crosscut the contact between the granite and the charnockite.

Sample GR11-32 is a medium-grained biotite-granite dike that contains <1 volume percent muscovite and crosscuts the foliation in the charnockite (Figure 3.4F). This dike is mineralogically similar to the largest deformed muscovite-poor dike in the mylonite zone shown in Figure 3.4A, indicating that it intruded prior to or coeval with the juxtaposition of the charnockite/granulite and migmatitic gneiss units. This dike is crosscut by muscovite-rich pegmatitic dikelets (Figure 3.4F).

Sample GR11-34 is a garnet-biotite-muscovite granitic pegmatite dike that crosscuts the foliation in ultramafic rocks included in the charnockite (Figure 3.4G). This dike is mineralogically similar to the dikelets that crosscut the biotite-granite dike sample GR11-32 (Figure 3.4F) and the dike that is not deformed within the mylonite zone (Figure 3.4B). Therefore, we interpret that this muscovite-rich dike intruded later than the muscovite-poor dike (sample GR11-32) and subsequent to the juxtaposition of the charnockite/granulite and migmatitic gneiss units.

Sample VER11-1 is a pegmatitic two mica dike that crosscuts the foliation in migmatitic orthogneisses (Figure 3.4H). The sample was collected south of the Novate intrusion, but this dike is similar in mineralogy to dikes that crosscut the migmatites within the Gruf Complex proper. Therefore, we interpret that this dike intruded at approximately the same time as the most evolved pegmatites, which crosscut the Gruf charnockites and migmatites (e.g. sample GR11-34).

Two samples of the Novate leucogranite were collected from a quarry ca. 1 km north of the town of Novate Mezzola along highway SS36 (Via Spluga). The samples (NOV11-1A and -1B) look similar in hand sample, with sample A containing a slightly higher proportion of biotite than sample B. Both samples are leucocratic and also contain muscovite, biotite, and garnet.

Analytical Methods

For the UHT granulites, zircon grains were analyzed directly within thin sections to preserve textural context (*in situ*). Color cathodoluminescence (CL) images were collected using

a microscope CL system in the Geology Department at the University of Kansas. Black and white CL images were collected using a FEI Versa 3D dual beam scanning electron micsoscope (SEM) coupled to a Gatan CL detector at the University of Kansas Microscopy and Analytical Imaging (MAI) Laboratory. To acquire the images, an accelerating voltage of 15kV, a beam current of 45 nA, and a working distance of 6 mm were used in low vacuum mode.

Leucosome and dike samples underwent standard mineral separation procedures to extract zircon grains. For most samples, the grains were then picked and mounted in epoxy. CL imaging was performed at the University of Kansas MAI Laboratory using a Zeiss LEO SEM with a Gatan CL detector. Core and rim domains were targeted using the LA-ICP-MS system at the University of Kansas Isotope Geochemistry Laboratory to assess both inheritance and last crystallization of the zircon grains. For two samples, grains were simply mounted on double sided tape mounts and ablated from the outside of the grain in order to target the youngest overgrowths by depth-profiling.

For the granulites, the U-Pb and trace element data were collected simultaneously by laser ablation (LA) coupled with a Thermo-Scientific Element 2 (single collector) sector field inductively coupled plasma mass spectrometer (ICP-MS) to ensure that the U-Pb isotopic and compositional data came from the same volume of zircon. This resulted in shorter counting times on U and Pb isotopes than standard U-Pb analyses, increasing the reproducibility uncertainty of U-Pb ratios from 1–2% to 3–4%. These analyses were carried out at the University of Kansas Isotope Geochemistry Laboratory. The U-Pb data for the granulite and dike samples were reduced using the VizualAge data reduction scheme (Petrus and Kamber, 2011) for Iolite (Paton et al., 2011). The software ET_Redux (McLean et al., 2016) was used to construct concordia plots and calculate ages. Trace element data from the granulite zircons were reduced using the TraceElementsIS data reduction scheme of Iolite. GJ-1 zircon (Jackson et al., 2004) was the

calibration standard used for U-Pb data reduction, and NIST612 glass (Jochum et al., 2005) was used as the calibration standard for trace element data reduction. Plešovice (Sláma et al., 2008) and GJ-1 zircon were the validation reference materials for trace element compositions, and only Plešovice zircon was used as a validation reference material for the dating. The specific analytical parameters used for the granulite and dike samples are shown in Tables 1 and 2, respectively. The Ti-in-zircon temperatures were calculated using the calibration of Watson et al. (2006).

Whole-rock major element compositions of leucosome and dike samples were obtained by x-ray fluorescence (XRF) with a Thermo-ARL automated XRF spectrometer at the Peter Hooper GeoAnalytical Lab at Washington State University. These data were used for calculating zircon saturation temperatures with the equation of Watson and Harrison (1983). The compositional data and calculated temperatures are shown in Table 3.

Zircon CL Textures

Granulites

Zircon grains in the granulites range in morphology from equant to prismatic, and show a wide variety of complex zoning patterns visible in the CL images (Figure 3.6). Zircon crystals from leucogranulite GR11-37 and stromatic granulite Bras10-6-2 (Figure 3.6A, C) have one or more bluish or CL-dark, featureless, patchy zoned, or more rarely strong to weak oscillatory-zoned interior domains and at least one yellowish, featureless overgrowth domain. Most of the grains from the residual granulite sample GR11-12B (Figure 3.6B) have at least one interior domain that exhibits strong oscillatory zoning and featureless exterior domains. The largest grains have up to 6 distinct domains based on their CL characteristics (e.g. the two largest grains from sample GR11-12B, Figure 3.6B grains 6 and 24), but only 2 or 3 domains are visible in most grains (Figure 3.6). The majority of the outermost domains have euhedral boundaries with the matrix minerals,

whereas internal domains are typically irregular, indicating some resorption. However, most of the grains from the stromatic granulite sample Bras10-6-2 have irregular outer grain boundaries (Figure 3.6C). Some grains have bright yellow curvilinear features, which crosscut domain boundaries (e.g. Figure 3.6A grain D2-3), that are interpreted as the result of recrystallization along fractures or fracture fills.

Leucosomes and Dikes

Zircon separated from the leucosome of the magmatic breccia (sample GR11-55) comprises mostly CL-dark or -bright, equant (soccer ball) grains (Figure 3.7A). However, some grains are characterized by a CL-bright or -dark, weakly to strongly oscillatory-zoned interior domain surrounded by a CL-dark, featureless domain with a very thin (<5 μm), CL-bright rim (Figure 3.7A).

The biotite leucogranite dike sample GR11-32 contains zircons dominated by oscillatory zoning, but sector-zoned and featureless domains are also observed (Figure 3.7B). Most grains exhibit two or three domains with distinct zoning patterns and CL brightness. The zoning patterns of interior domains are commonly truncated by the zoning patterns of the outer domains, and in some cases, interior domains have a mottled appearance (e.g. grain 7e).

Zircon grains from the garnet-biotite-muscovite pegmatite sample GR11-34 commonly consist of oscillatory-zoned or mottled, CL-dark interior domains with featureless, CL-bright exteriors (Figure 3.7C). Zoning patterns of the interior domains are commonly truncated by the exterior domains. Some of the featureless outer domains have irregular (anhedral) outer grain boundaries (grains 4c, 10b). Scarce prismatic, featureless or sector-zoned grains are also observed.

The biotite-muscovite pegmatite sample VER11-1 yielded mostly euhedral (prismatic), oscillatory- or sector-zoned zircon grains (Figure 3.7D). A variety of core-rim relationships are

observed, including CL-dark interiors with CL-bright exteriors and vice versa, as well as grains with homogenous CL (Figure 3.7D).

The zircons from the Novate leucogranite sample NOV11-1B almost invariably exhibit oscillatory zoning patterns (Figure 3.7E). The zoning patterns of some interior domains are truncated by the zoning patterns of exterior domains. Scarce mottled domains are also present.

U-Pb Ages

Granulites

Zircon domains from the granulites fall into three main age populations: (1) Oscillatory-zoned cores and intermediate zones, which have the largest range of dates spreading along concordia from 200 to 350 Ma (Figure 3.6, 8A-C; Table 4). (2) Oscillatory-zoned and featureless domains ranging from 75–175 Ma (Figure 3.6, 8A-C). (3) Featureless overgrowths and scarce whole grains with dates from 29–35 Ma (Figure 3.6, 8D-E).

Leucogranulite sample GR11-37 (47 analyses from 18 grains) yielded one concordant analysis at ca. 350 Ma and a tight cluster of concordant analyses between 250 and 300 Ma (Figure 3.8A). Three concordant and two discordant analyses have dates between 200 and 250 Ma (Figure 3.8A). Three analyses are concordant or slightly discordant at ca. 130 Ma, and there is one discordant analysis at 75 Ma (Figure 3.8A). The largest number of grains with young (<40 Ma) overgrowths (Figure 3.6A, 8A, D; Table 4) occur in this sample. Most of the overgrowths have dates that overlap with one another (Figure 3.8D). The weighted mean $^{206}Pb/^{238}U$ age of the analyses that are <10% discordant with $^{206}Pb/^{238}U$ dates between 31.0 and 33.5 (Figure 3.8D; Table 5) is 32.7 ± 0.7 Ma (MSWD = 0.65, n = 8). One grain (Figure 3.5B, 6A grain D3-11) has a CL-dark, featureless core with a $^{206}Pb/^{238}U$ date of 32.5 ± 1.5 Ma. The overgrowth, characterized by alternating dark and bright-yellow CL bands, has $^{206}Pb/^{238}U$ dates of 29.1 ± 0.6 and 29.1 ± 0.9 Ma

with a weighted mean $^{206}Pb/^{238}U$ age of 29.1 ± 0.5 (MSWD = 0.001, n = 2). One bright yellow CL rim has an intermediate $^{206}Pb/^{238}U$ date of 30.9 ± 1.1 Ma but is more than 10% discordant and not used for further interpretations.

From oldest to youngest, the results from residual granulite sample GR11-12B (48 analyses from 16 grains) include analyses that spread along concordia from 220–330 Ma (Figure 3.8B). Three analyses are concordant at 150 Ma, and four discordant analyses define a discordia that intersects these concordant analyses (Figure 3.8B). One domain is concordant at 75 Ma. Several grains with featureless (CL dark or bright) overgrowths (Figure 3.6B) occur in this sample. However, only one of these grains (Figure 3.6B grain 14, 8D) yielded Oligocene dates. The core and rim domains from this young grain gave overlapping dates (Figure 3.6B grain 14) with a weighted mean $^{206}Pb/^{238}U$ age of 34.8 ± 1.1 Ma (MSWD = 0.16, n = 5) (Figure 3.8D).

The zircon analyses from a thin section of a melanosome in the stromatic granulite sample Bras10-6-2 (22 analyses from 7 grains) yielded clusters of concordant analyses at 310 Ma, 290 Ma, and 255 Ma. One discordant analysis occurs at 200 Ma, and one analysis is concordant at 160 Ma, albeit with large uncertainty. This sample did not yield any grains with overgrowths younger than ca. 45 Ma (Figure 3.6C, 8C; Table 4). Based on their discordance, two analyses that are younger than 100 Ma (Figure 3.8C) probably represent mixing, due to analyzing different age zones, of older and younger domains. One grain with a 65.5 ± 2.6 Ma exterior domain (Figure 3.5D, 6C grain 2) is included in a garnet core (analysis 02-3r in Table 4; grain 2 in Figure 3.A1C). The zircon grains from this sample have the most irregular grain boundaries (Figure 3.6C), which may be interpreted as indicating late resorption.

Leucosomes and Dikes

All of the dike and leucosome samples contain inherited zircon (Figure 3.7, 9). Most samples do not contain grains with domains older than 300 Ma, however, some samples contain a few grains (up 17% of the analyzed population) as old as 1800 Ma (Figure 3.7; Table 5), with the most compositionally evolved dikes containing the most >300 Ma inherited domains. The concordia plots in Figure 3.9 only show results up to 400 Ma for clarity.

The leucosome of the magmatic breccia (sample GR11-55; 85 analyses from 29 grains) contains inherited zircon cores and scarce whole grains with concordant dates of 300–260 Ma, ca. 200 Ma, and ca. 150 Ma (Figure 3.9A). However, the vast majority of the grains (68 of 85) from this sample form a well-defined, concordant population with a weighted mean $^{206}Pb/^{238}U$ age of 32.4 ± 0.1 Ma (MSWD = 0.91, n = 68) (Figure 3.9I; Table 5). Most of these young grains have equant (soccer ball) shapes (Figure 3.7A). However, some CL-dark interior domains also yielded <35 Ma dates (Figure 3.7A, grain 7e).

The boudinaged biotite pegmatite dike sample GR11-54 (42 analyses from 42 grains) yielded two analyses with nearly concordant dates of ca. 1800 Ma (Table 5) and one nearly concordant date of ca. 600 Ma. Several analyses from interior and exterior domains spread along concordia from 250 to 350 Ma (Figure 3.9B). The youngest population has a lower intercept age of 29.2 +1.0/-1.1 Ma (MSWD = 1.2, n = 22) with a common-Pb upper intercept (Figure 3.9J), excluding four nearly concordant analyses that have $^{206}Pb/^{238}U$ dates >33.5 Ma and one young discordant analysis that lie off the discordia.

Sample GR11-27 (66 analyses from 66 grains), the biotite granite pod, contains one inherited zircon with a concordant date of ca. 450 Ma (Table 5; not shown in the concordia diagram). Several concordant analyses have dates between 240 and 310 Ma, and several analyses form a discordia between ca. 250 Ma and the youngest population (Figure 3.9C). The youngest,

concordant (<10% discordance; Table 5) analyses with $^{206}Pb/^{238}U$ dates <31 Ma give a weighted mean $^{206}Pb/^{238}U$ age of 29.8 ± 0.4 Ma (MSWD = 0.53, n = 14) (Figure 3.9K).

Sample GR11-32 (36 analyses from 36 grains) is a biotite-bearing leucogranite dike that crosscuts the main foliation in the charnockites it intrudes. Excluding two analyses, which are nearly concordant at ca. 75 Ma and ca. 310 Ma (Figure 3.7B, 9D), most of the analyses form a discordia with a lower intercept of 27.2 +0.5/-0.6 Ma (MSWD = 0.93, n = 31) and upper intercept of ca. 1200 Ma. This young population consists of analyses of oscillatory-zoned overgrowths and homogenous grains (Figure 3.7B). Three analyses that are >15% discordant and do not plot with the main discordia trend (Figure 3.9L; Table 5) were not included in the age calculation. We prefer the lower intercept age to the weighted mean age for this sample because of the well-defined discordia formed by the analyses.

Garnet-biotite-muscovite pegmatite sample GR11-34 (33 analyses from 32 grains) contains inherited zircon spreading along concordia from ca. 230 to 280 Ma, two analyses at ca. 180 Ma, and a few younger discordant analyses at ca. 70 Ma and 43 Ma (Figure 3.9E). Most of these older dates come from oscillatory-zoned interior domains, but some of the featureless overgrowths have dates as old as 276±10 Ma (Figure 3.7C grain 4b). The youngest zircon population, which exclusively comprises analyses from featureless overgrowths and prismatic grains (Figure 3.7C), has a lower intercept age of 29.6 +0.3/-0.3 Ma (MSWD = 1.2, n = 18) with a common-Pb upper intercept (Figure 3.9M). Based on this dike's crosscutting nature and highly evolved composition, however, we do not interpret this to be the crystallization age of the pegmatite itself (see '*Zircon saturation in the dike samples'* below).

Inherited zircon, consisting of oscillatory-zoned interior and scarce exterior domains (Figure 3.7D), is abundant in the biotite-muscovite pegmatite sample (VER11-1; 50 analyses from

36 grains). Clusters of concordant analyses occur at 600 Ma, 500 Ma, 250–300 Ma, and ca. 175–200 Ma (Table 5, Figure 3.9F). One analysis is concordant, albeit with large uncertainty at ca. 34 Ma, and there is one near-concordant grain at ca. 27 Ma. The weighted mean $^{206}Pb/^{238}U$ age of the youngest concordant population ($^{206}Pb/^{238}U$ dates between 24 and 27 Ma and <10% discordance) is 25.6 ± 0.3 Ma (MSWD = 0.54, n = 19) (Figure 3.9N). These analyses are from oscillatory-zoned, sector-zoned, and featureless whole grains and exterior domains (Figure 3.7D).

Although the two samples of the Novate leucogranite (NOV11-1A and B) look very similar in hand sample, they have distinct zircon populations (Figure 3.9G-H, O). The youngest zircon grains found in sample A (131 analyses from 60 grains) are >250 Ma (Figure 3.9G), whereas abundant Mesozoic and Cenozoic and some Proterozoic grains were found in sample B (170 analyses from 64 grains) (Figure 3.9H). Both samples yielded concordant dates between 370 and 600 Ma, and >90% of analyses from sample A and <10% of analyses from sample B have concordant dates between 250 and 300 Ma (Figure 3.9G-H). Sample B also contains zircons with concordant dates between 200 and 250 Ma, and there are Jurassic and Cretaceous populations with lower intercept ages of ca. 150 Ma and ca. 75 Ma, respectively (Figure 3.9H). One grain (Figure 3.7E) consists of a featureless, dark-CL core with a $^{206}Pb/^{238}U$ date of 33.5 ±2.1 Ma and an oscillatory-zoned rim with a $^{206}Pb/^{238}U$ date of 27.4 ± 1.0 Ma, both of which are concordant. Of the 170 spots analyzed in sample B, 111 analyses have $^{206}Pb/^{238}U$ dates between 21.6 and 27.4 Ma (Table 5; Figure 3.9O, P). There are two separate discordia trends with lower intercepts between 26 and 22 Ma (Figure 3.9O). The youngest of these trends has a lower intercept age of 23.8 +0.1/-0.1 Ma (MSWD = 1.2, n = 93) with a common-Pb upper intercept. This age excludes the data that define the slightly older lower intercept age and two analyses, one of which is concordant, that define a discordia with a lower intercept of 21.5 Ma.

Granulite Zircon Trace Element Compositions

Zircon Rare Earth Element Patterns

Figure 3.10 shows chondrite-normalized rare earth element (REE) plots colored by $^{206}Pb/^{238}U$ date and grouped by sample. Most analyses have similar REE patterns with enrichment of heavy REE (HREE) relative to light REE (LREE), positive Ce anomalies, and negative Eu anomalies. The slopes of the HREE patterns (shown also as chondrite-normalized Yb/Dy ratios - YbN/DyN - in Figure 3.11A-C) vary with date and from sample to sample (Figure 3.10 and 11A-C). This will be discussed in more detail below.

In leucogranulite sample GR11-37, the youngest zircon domains are depleted in LREE and middle REE (MREE) compared to the older domains (Figure 3.10A), and the HREE patterns of the youngest zircon domains have steeper positive slopes than the older domains (Figure 3.10A and 11A). The normalized Yb/Dy ratios (YbN/DyN) of the young (29.1–43.5 Ma) domains range from 9.1–32.2, and domains between 45.3 and 135 Ma have YbN/DyN values between 9.3 and 15.1 (Table 4; Figure 3.11A). Domains older than 194 Ma exhibit two distinct HREE slopes (Figure 3.10A, 11A): moderately positive (YbN/Dy = 3.1–13.5) and nearly flat (YbN/DyN = 1.0–2.1) (Table 4; Figure 3.10A, 11A). All except 2 of these 13 domains with YbN/DyN = 3.1–13.5 are older than 240 Ma (Table 4; Figure 3.10A, 11A).

The younger domains in the residual granulite sample (GR11-12b) are enriched in LREE and MREE compared to most of the older domains, and the younger domains have shallower (negative in one case) HREE slopes than the older domains (Table 4; Figure 3.10B, 11B). The YbN/DyN values for the young (34.5–43.9 Ma) domains range from 0.3–4.0, whereas YbN/DyN values for >135 Ma domains range from 4.8–12.1 (Table 4; Figure 3.10B, 11B). One Cretaceous

zircon domain ($^{206}Pb/^{238}U$ date = 75.2 ± 5.9 Ma) has a YbN/DyN value of 4.9 (Figure 3.11B), which is intermediate between that of most of the older grains and the younger domains.

All domains from the stromatic granulite sample Bras10-6-2 have very small Eu anomalies (Eu/Eu* = 0.28–0.68) and YbN/DyN between 5.9 and 12.9 (except for one ca. 285 Ma domain with YbN/DyN = 32.9, which is also more depleted in MREE compared to all other domains) (Table 4; Figure 3.10C, 11C). The younger zircon domains in this sample are depleted in all REE compared to most of the older domains (Table 4; Figure 3.11C).

Ti-in-zircon Thermometry

Figure 3.11D-F shows that there is no simple relationship between $^{206}Pb/^{238}U$ dates and Ti-in-zircon temperatures (TiZrcT). However, there is a general increase in TiZrcT with decreasing date from 350–150 Ma and decrease in TiZrcT with decreasing date from 150–30 Ma. Most of the analyzed domains give nominal Ti-in-zircon temperatures between 542 and 870°C, with most of those again ranging from 650–750°C (Figure 3.11D–F). Several analyses (3 from the residual granulite sample GR11-12B and 1 from the stromatic granulite sample Bras10-6-2) have Ti-in-zircon temperatures between 1040°C and 1275°C (>140 ppm Ti; Table 4), but based on the sharp increases (spikiness) of Ti intensity in the time resolved signals, these results are likely the result of ablating sub-micron Ti-rich inclusions (Chapman et al., 2016). Two of these high Ti analyses are from the tips of zircon grain G12b-14 in the residual granulite sample (Table 4; Figure 3.6D grain 14). This grain is included in high-Ti biotite, and thus inclusions or intergrowths of biotite or rutile or ilmenite needles exsolved from the biotite may have been inadvertently ablated and analyzed. The apparent Ti concentration of one analysis from the residual granulite sample GR11-12B is 0.6 ± 1.6 ppm, corresponding to a Ti-in-zircon temperature of 542 ± 299°C (Table 4), which

is at the detection limit of Ti with this method. Because of the extremely high uncertainty, this analysis will not be considered further.

Th-U Ratios

There is no simple correlation between Th-U ratios and the calculated dates (Figure 3.11G–I; Table 4). Overall, the Th-U ratios range from 0.001 to 1.4, and the >200 Ma domains have the widest ranges. The Th-U ratios of domains older than 75 Ma from the leucogranulite sample GR11-37 range from 0.01 to 0.68, and the youngest domains (29–36 Ma) have the lowest Th-U ratios of all the analyses, ranging from 0.001–0.009 (Table 4; Figure 3.11F). In the residual granulite sample (GR11-12B), domains older than 135 Ma have Th-U ratios between 0.1 and 1.0, and younger domains have Th/U values ranging from 0.1 to 0.31 (Table 4; Figure 3.11E). The domains from the stromatic granulite sample Bras10-6-2 have the most diverse Th-U ratios; Th-U ratios range from 0.07–1.4 and 0.03–0.4, respectively for domains older and younger than 250 Ma (Table 4; Figure 3.11F).

Correlations Between REE and Ti

Figure 3.11J shows that there is a slight negative correlation between TiZrcT and YbN/DyN. In general, domains with the highest YbN/DyN, which are also the youngest domains, have the lowest TiZrcT. However, there is no correlation between TiZrcT and YbN/DyN in the residual and stromatic granulite samples (Figure 3.11K–L).

Discussion

Validity of Ti-in-zircon Temperature Estimates

Rutile is present in all the investigated samples, but it is unlikely that rutile was always present throughout the history of these rocks. Rutile, which records UHT conditions, is abundant in the matrices and leucosomes of the leucogranulite and stromatic granulite samples (Oalmann et al., submitted). However, it is very unlikely that rutile was present prior to metamorphism of these samples. Thus, it cannot be assumed that the activity of TiO_2 (a_{TiO2}) was unity throughout the history of the granulites, especially at the time the inherited zircon domains first crystallized from their magmas, which rarely precipitate rutile. Therefore, it could be argued that the apparent Ti-in-zircon temperature estimates from zircon domains that crystallized from melts prior to UHT metamorphism may not represent true zircon crystallization temperatures (Watson and Harrison, 2005; Watson et al., 2006). For non-rutile-saturated systems, TiZrcT are minimum estimates of zircon crystallization temperature (Watson et al., 2006). Decreasing a_{TiO2} to 0.6, which is a minimum estimate of a_{TiO2} in basic rocks (Ghent and Stout, 1984), would increase the temperature estimates by ca. 40–50°C in most cases (Table 4), resulting in only one >900°C (930°C) temperature estimate from a 155 Ma domain in the stromatic granulite (Table 4). However, the granulites are Mg-Al-rich metapelites (Galli et al., 2011; Oalmann et al., in preparation-a), and a_{TiO2} in most pelitic systems is between 0.9 and 1.0 (Ghent and Stout, 1984; Watson et al., 2006), indicating that it is unlikely that a_{TiO2} was as low as 0.6 in these aluminous samples. Therefore, we interpret the TiZrcT estimates presented here to be robust indicators of zircon crystallization temperatures within analytical uncertainty, which ranges from ±14°C to ±55°C (2SE) and is shown as vertical error bars in Figure 3.11D–F.

Conditions of zircon growth and timing of UHT metamorphism in the Granulites

Although there is strong petrologic evidence that the Gruf granulites underwent metamorphism in excess of 900°C (Galli et al., 2011; Guevara and Caddick, 2016; Oalmann et al.,

in preparation-a; Oalmann et al., submitted), none of the robust Ti-in-zircon temperature estimates are higher than 850°C (Figure 3.11G-I), excluding the four analyses that are considered to be erroneous measurements due to ablation of Ti-rich microinclusions (see *Ti-in-zircon Thermometry* section above). We therefore interpret the lack of >850°C zircon domains combined with the observed irregular grain and domain boundaries (Figure 3.6) to indicate that zircon was not (re)crystallizing but resorbing during UHT metamorphism. Domains ranging from 140–300 Ma commonly exhibit irregular grain boundaries (Figure 3.6), and in some cases, <34 Ma euhedral rims overgrow older domains along anhedral interfaces (e.g. Figure 3.6A). Based on the more euhedral nature of the younger domains (e.g. Figure 3.6A), it is likely that resorption of zircon and thus UHT metamorphism occurred sometime after ca. 140 Ma but prior to ca. 33 Ma. At UHT conditions, Zr may have been sequestered in rutile, melt, and garnet.

Petrographic evidence (e.g. orthopyroxene + sapphirine symplectites replacing garnet) and results from Zr-in-rutile thermometry (Oalmann et al., submitted) and thermobarometric modeling of whole-rock samples and microdomains (Galli et al., 2011; Guevara and Caddick, 2016; Oalmann et al., in preparation-a) indicate that UHT metamorphism of the Gruf granulites occurred during decompression, resulting in the formation of orthopyroxene, sapphirine, and cordierite at the expense of garnet. The steep HREE patterns (YbN/DyN ≥ 15) of the 29.1–33.5 Ma zircon domains in leucogranulite sample GR11-37 (Figure 3.10A, 11A) indicate that these domains grew after or coeval with garnet breakdown (Rubatto, 2002) and thus after or coeval with UHT metamorphism. The shallower HREE slopes in the older zircon domains from this sample (Figure 3.10A, 11A) indicate that garnet was stable prior to ca. 33.5 Ma (date of oldest concordant zircon overgrowth with YbN/DyN >15) (Rubatto, 2002). Some of the 210–280 Ma zircon domains from the leucogranulite sample GR11-39 have nearly flat HREE patterns (YbN/DyN = 1.0–2.1),

possibly indicating that at least some garnet was present during Permo-Triassic time (Rubatto, 2002). We interpret the extremely low Th/U values (<0.01) of the <34 Ma zircon domains from this sample to indicate that monazite, which formed at near-UHT, post-peak conditions (Oalmann et al., in preparation-b), grew before or concurrently with these domains, outcompeting zircon for Th.

In contrast to the leucogranulite, the youngest zircon grain from residual granulite sample GR11-12B has YbN/DyN values of ≤4.0 (Table 4; Figure 3.10B, 11B). We interpret these very shallow HREE patterns to indicate that this grain crystallized while garnet was stable (Rubatto, 2002). Therefore, UHT garnet breakdown must have occurred after (re)crystallization of the youngest zircon in the residual granulite sample (weighted mean $^{206}Pb/^{238}U$ age = 34.8 ± 1.1 Ma) and prior to (re)crystallization of the 32.7 ± 0.7 Ma zircon population in the leucogranulite sample. We interpret the relatively high YbN/DyN values of the >135 Ma zircon domains in the residual granulite sample (4.8–12.1 compared to <4.0 for the younger domains; Table 4, Figure 3.10B, 11B) to indicate that this sample did not experience significant garnet growth or high-grade metamorphism during the Permian through Cretaceous zircon-producing events.

Therefore, we interpret UHT metamorphism to have occurred between 34.8 ± 1.1 Ma (age of zircon in equilibrium with garnet from residual granulite) and ca. 32.7 ± 0.7 Ma (age of zircon that grew during/after garnet breakdown). The corroded nature of Permian through Mesozoic zircon domains (Figure 3.6) also supports the UHT event to be younger than Mesozoic. The presence of a zircon grain with a 65.5 ± 2.6 Ma (albeit discordant) exterior domain included in a garnet core, which was breaking down during UHT metamorphism (Oalmann et al., in preparation-a), in the stromatic granulite sample Bras10-6-2 (analysis 02-3r in Table 4; grain 2 in Figure 3.A1C) provides further evidence for a young (<65 Ma) UHT event. We interpret the ca. 29 Ma

zircon rim surrounding a ca. 32.5 Ma core (Figure 3.6B grain D3-11) in the leucogranulite sample GR11-37 to indicate that there was melt infiltration into the granulites at ca. 29 Ma, coeval with emplacement of the deformed dikes (see '*Dating deformation using crystallization ages of leucosomes and felsic dikes*' below).

Independent evidence, including preservation of complex major element zoning profiles in garnet (Oalmann et al., in preparation-a) and preservation of UHT Zr-in-rutile temperatures (Oalmann et al., submitted), indicates that the UHT event was short-lived (≤1 m.y.). In a recent review, Harley (2016) noted that zircon only forms at UHT conditions in long-lived (30–100 m.y.) UHT terranes when trapped melt interacts with the surrounding rock, leading to zircon crystallization. The lack of zircon crystallizing at UHT conditions in the Gruf Complex is therefore consistent with the short-lived UHT event inferred from the zircon ages.

Our interpretation of an Alpine UHT event is in contrast to that of Galli et al. (2012) who concluded that UHT metamorphism of the Gruf Complex occurred during late Variscan (Permian) rifting of the European margin. These authors based their conclusion in part on the presence of scarce orthopyroxene inclusions (with up to 8 wt. % Al_2O_3) in Permian zircon domains from the charnockites. However, the images of the inclusion textures provided show clearly that the minerals interpreted as inclusions are aligned along cracks in the zircon grains, which show undated recrystallization textures along their edges. The zircon domains yielding the Permian ages are distant from the cracks and have oscillatory zoning patterns, placing doubt on the interpretation as true inclusions. Additionally, orthopyroxene porphyroblasts in the granulites have up to 12 weight percent Al_2O_3 (Oalmann et al., in preparation-a). This may either indicate that the plutonic protoliths of the charnockites originally crystallized orthopyroxene, but at a lower temperature than UHT conditions, which are recorded by the sapphirine- and orthopyroxene-forming garnet-

breakdown reactions in the granulites, or it indicates that the orthopyroxene "inclusions" were incorporated during a later metamorphic stage. Galli et al. (2012) also used zircon saturation temperatures of the charnockites to interpret that the presence of abundant Permian zircon indicates the UHT event could not have occurred during Alpine orogenesis. However, a short-lived UHT event would not have resulted in complete dissolution of zircon in dry melts because of kinetic factors (Harrison and Watson, 1983; Watson and Harrison, 1983). (Ultra)-high temperature rocks commonly contain zircon inherited from lower temperature magmatic and metamorphic events (see review by Taylor et al., 2016).

All zircon grains with <34 Ma domains (e.g. Figure 3.6A) occur within the leucosome-rich leucogranulite sample GR11-37. We interpret this to indicate that most of the zircon produced during the Alpine event formed while melts crystallized. The lack of young, concordant zircon domains in the residual and stromatic granulite samples, with the exception of the single ca. 35 Ma grain in the residual granulite and undateable microzircon growing on rutile in the stromatic granulites (Oalmann et al., submitted), indicate that solid-state reactions did not play a major role in producing zircon in the Gruf granulites. This has also been observed in other UHT granulite terranes (e.g. Kelsey and Hand, 2015; Harley, 2016; Taylor et al., 2016). This is exemplified by the elongate, oscillatory zoned grain within the garnet breakdown texture in the residual granulite sample that lacks overgrowths younger than ca. 200 Ma (Figure 3.5C, grain 6 in Figure 3.6E, A1B). The shape and type of zoning leads us to interpret this to be an inherited (igneous) grain, indicating that it did not participate in the UHT garnet-breakdown reaction in any way. The lack of young zircons in the residual and stromatic granulite types also leads to the interpretation that these rocks lost melt prior to 33.5 Ma.

Zircon saturation in the leucosome and dike samples

The calculated zircon saturation temperatures (Table 3, Figure 3.12) are considered maximum melt temperatures because all of the dike samples contain inherited zircon (Miller et al., 2003). Therefore, it is likely that some of these evolved felsic magmas that intruded after the peak of Alpine metamorphism never reached their zircon saturation temperatures, and thus the zircon ages do not represent the timing of dike emplacement. For example, one of the Novate leucogranite samples (NOV11-1A) lacks zircon younger than ca. 250 Ma, but it is clear from the other sample (NOV11-1B) and from previous studies (Liati et al., 2000) that the intrusion crystallized at ca. 24 Ma. The lack of new zircon growth was likely the result of the very high calculated zircon saturation temperature (ca. 850°C) for sample NOV11-1A (Figure 3.9G), above the temperature of the Novate magma, which is constrained to be ≤700°C (zircon saturation temperature calculated from sample NOV11-1B; Table 3).

The age obtained for the youngest zircon domains in the garnet-biotite-muscovite pegmatite dike sample GR11-34 (29.6 ± 0.3 Ma) overlaps with the ages of deformed dike samples (GR11-27: 29.8 ± 0.4 Ma, and GR11-54: 29.2 +1.0/-1.1 Ma), but the pegmatite clearly crosscuts the foliation of its host rocks and has a more evolved mineralogy than the deformed dikes, which lack abundant muscovite and garnet. Therefore, we argue that this garnet-biotite-muscovite pegmatite did not crystallize new zircon at the time it was emplaced. The zircon saturation temperature calculated for this sample is ca. 730°C (Figure 3.12, Table 3). However, the mineralogy, which is similar to that of the Novate granite (zircon saturation temperature = 699°C), and pegmatitic texture likely indicate that it intruded at a lower temperature and was therefore unable to crystallize new zircon. We interpret the anhedral shape of some of the young (ca. 30 Ma) exterior zircon domains (Figure 3.7C), to have formed as a result of resorption. This may indicate that these grains were in contact with melt after ca. 30 Ma, and thus provides further evidence for

post 30 Ma emplacement of this pegmatite. Therefore, this evolved pegmatite was likely emplaced at approximately the same time as the biotite-muscovite pegmatite (VER11-1) and Novate leucogranite, between 26 and 24 Ma.

The most evolved pegmatite samples (GR11-34 and VER11-1) and the Novate leucogranite samples (NOV11-1A, -1B) contain 29–33 Ma zircon grains and domains (Figure 3.7, 9; Table 4). We interpret this zircon to have been inherited from the source of the melt that formed the dikes. Therefore, the source of the latest dikes must have been felsic material (e.g. migmatites, granulites, older dikes, and/or unexposed plutons) that crystallized zircon between 29 and 33 Ma.

Dating deformation using crystallization ages of leucosomes and felsic dikes

With the exception of the garnet-biotite-muscovite pegmatite (sample GR11-34) discussed above, there is a good correlation between degree of deformation and U-Pb zircon ages of the felsic dikes (Figure 3.4, 9) and a general decrease in age towards younger, more evolved compositions. Therefore, we can use the zircon crystallization ages of the dikes to constrain the timing of deformation and juxtaposition of the lower crustal UHT granulites and charnockites against the mid crustal migmatites. The biotite-granite dike sample GR11-32, which is mineralogically similar to a dike that is deformed within the mylonite zone shear zone separating the UHT rocks from the migmatitic gneisses (Figure 3.4A), has an age of 27.2 +0.5/-0.6 Ma, indicating that amalgamation of the Gruf Complex was not complete at this time. Undeformed muscovite-rich pegmatites (samples GR11-34 and VER11-1) and the Novate leucogranite, which are mineralogically similar to pegmatites that intruded a mylonite zone after mylonitization had ceased (Figure 3.4B) and crosscut the biotite-granite dike (Figure 3.4F), were emplaced between 24 and 26 Ma. This leads to the interpretation that juxtaposition of the lower crustal UHT rocks was completed by ca. 26 Ma. The overlapping ages of the biotite pegmatite dike (GR11-54: 29.2

+1.0/-1.1 Ma), which is deformed within the migmatites, and the bioite-granite pod (GR11-27: 29.8 ± 0.4 Ma), which crosscuts the foliation in the charnockite, indicates that internal ductile deformation was still occurring within the migmatite but had ceased within the charnockite/granulite unit by ca. 29 Ma.

The older (32.4–29.2 Ma) dike and leucosome samples completely lack muscovite, and the 27.2 +0.5/-0.6 Ma dike contains very little muscovite. These intrusions are deformed within the migmatites and mylonitic shear zones (Figure 3.4). In contrast, the younger (25.6–23.8 Ma) pegmatites and Novate leucogranite samples, which crosscut the mylonitic shear zones (Figure 3.4), contain abundant magmatic muscovite, and the biotite-muscovite pegmatite (VER11-1) and one of the Novate leucogranite samples (NOV11-1A) have the highest alumina saturation indices (ASI = molar Al/Na+K+Ca = 1.10 and 1.11, respectively; Table 3) of all the leucosome and dike samples, implying a predominately crustal source for these magmas (Chappell and White, 1974). This correlation between increasing crustal melt component (or decreasing mantle melt component) and decreasing contractional deformation suggests that the amalgamated Gruf Complex was undergoing extension and exhumation beginning at ca. 26 Ma. Further evidence for exhumation at this time includes extensional deformation along the normal-sense Forcola fault (Figure 3.1), which was coeval with emplacement of the Novate leucogranite (Ciancaleoni and Marquer, 2006) at 23.8 ± 0.1 Ma.

Temperature-deformation-time Implications

The results presented and discussed here provide constraints on several aspects of the temperature-deformation-time evolution of the Gruf Complex that are shown in Figure 3.13. Prior to UHT metamorphism there was minor zircon growth at 34.8 ± 1.1 Ma, in equilibrium with garnet during prograde metamorphism in the residual granulite sample. Based on the Ti-in-zircon

temperatures of the youngest rims in the leucogranulite sample GR11-37, the granulite/charnockite until had cooled from UHT conditions to ca. 700–800°C by 32.7 ± 0.7 Ma. Therefore, the age of UHT metamorphism is bracketed to ca. 34 Ma. The age of the youngest zircon population in the leucosome of the magmatic breccia (32.4 ± 0.1 Ma), which is deformed within the migmatitic orthogneiss unit, indicates that the migmatites began to crystallize zircon at nearly the same time as the zircon rims formed in the leucogranulite sample. The most primitive magmas within immediate vicinity of the Gruf Complex (the Bergell tonalite and granodiorite) were emplaced in the middle crust at 32–30 Ma (von Blanckenburg, 1992; Samperton et al., 2015). Based on the zircon crystallization ages of deformed and crosscutting dike samples studied here, the UHT granulite/charnockite unit was exhumed into the middle crust and juxtaposed against the upper amphibolite facies migmatites between 30 and 27 Ma. Between 26 and 24 Ma, highly evolved pegmatitic dikes and the Novate leucogranite intruded the Gruf complex during extensional deformation. Based on U-Pb rutile ages presented by Oalmann et al. (submitted), the Gruf Complex remained above ca. 400°C until about 19 Ma. This temperature-time scenario results in the following possible cooling rates: (a) ca. 60°C/m.y. between 34 and 30 Ma for the granulite/charnockite unit and either (b) 25°C/m.y. between 30 and 19 Ma or (c) ca. 8°C/m.y. between 30 and 24 Ma increasing to ca. 45°C/m.y. between 24 and 19 Ma for the amalgamated Gruf Complex (Figure 3.13).

Regional Geodynamic Implications

Although we cannot directly date the UHT metamorphism of the Gruf granulites because zircon did not crystallize during the short-lived UHT event, we can bracket the timing of UHT metamorphism to ca. 34 Ma (between the 34.8 ± 1.1 Ma age of zircon in equilibrium with garnet in residual granulite sample and the 32.7 + 0.7 Ma age of post-UHT zircon in leucogranulite

sample). In order to constrain the geodynamic mechanism responsible for UHT metamorphism, we compare the ages obtained from the Gruf Complex to the ages of other metamorphic and plutonic events in the Central Alps (Figure 3.14). Several nappes within the Central Alps, including the Adula nappe, experienced UHP metamorphism between 43 ± 2 and 35.4 ± 0.5 Ma (e.g. Gebauer, 1996). These units were exhumed beginning at 34.2 ± 0.2 Ma (Hermann et al., 2006) and underwent a high temperature (Barrovian) overprint between 32 and 22 Ma (Rubatto et al., 2009). The coinciding time of UHT metamorphism of the Gruf lower crustal rocks and the switch from UHP to Barrovian metamorphism in the other units likely implies that exhumation of the UHP units and UHT metamorphism are genetically linked. A possible scenario we favor is that UHT metamorphism occurred in the lower crust after the UHP units had been exhumed to the middle crust.

Obtaining UHT conditions at ca. 8–10 kbar requires a very high geothermal gradient (>>20°C/km (Kelsey et al., 2008)) or advection of hot material to the base of the crust (Collins, 2002; Sizova et al., 2010; Clark et al., 2011). Because there is no strong evidence for an extreme geothermal gradient in the Central Alps, we conclude that heat for UHT metamorphism came from advection of hot material to the base of the crust. Many authors agree that the exhumation of Alpine (U)HP units occurred as a result of slab breakoff (e.g. Davies and von Blanckenburg, 1995; von Blanckenburg and Davies, 1995; Handy et al., 2010). Therefore, we postulate that slab breakoff (von Blanckenburg and Davies, 1995) resulted in asthenospheric upwelling, which then provided the necessary heat for UHT metamorphism of the Gruf charnockites and granulites. The lithospheric thinning model related to slab rollback (Beltrando et al., 2010) is not favored because it cannot accurately explain the timing and location of Bergell magmatism. Shortly after UHT metamorphism, the charnockites and granulites were exhumed into the middle crust. This

exhumation may have been aided by the Bergell magmas, which were intruding the middle crust at the same time.

Conclusions

The zircon grains within the Gruf Complex granulites have multiple textural and age domains, but we conclude that during brief attainment of UHT conditions zircon was being resorbed and not growing. Therefore, the UHT event cannot be directly dated by U-Pb zircon geochronology. Based on the low HREE abundances in the youngest zircon grain from the residual granulite sample, we interpret that there was minor zircon growth in equilibrium with garnet during Alpine prograde metamorphism at 34.8 ± 1.1 Ma. However, based on the lack of UHT Ti-in-zircon temperatures, and enriched HREE contents found in the youngest zircon rims in the leucogranulite, we conclude that most of the Alpine zircon growth resumed during the retrograde stages of the UHT event, concurrent with crystallization of partial melts, between 29.1 and 33.5 Ma. The location of these domains in the leucosomes of the granulites and their extremely low Th-U ratios indicate that they crystallized from partial melts and not from solid-state reactions, concurrently with monazite. In summary, we conclude that the UHT event occurred at ca. 34 Ma. Heat for UHT metamorphism possibly came from advection of asthenosphere or mantle derived melts resulting from slab breakoff (Davies and von Blanckenburg, 1995; von Blanckenburg and Davies, 1995; Handy et al., 2010) and after exhumation of the (U)HP nappes in the Central Alps.

The U-Pb zircon ages of felsic dikes analyzed in this study indicate that the UHT granulites/charnockites and upper amphibolite facies migmatites were amalgamated, and contractional ductile deformation ended between 27.2 +0.5/-0.6 Ma and 25.6 ± 0.4 Ma. The lower crustal, UHT rocks and the Bergell magmas (von Blanckenburg, 1992; Samperton et al., 2015) were emplaced into the migmatitic middle crust at the same time, indicating a temporal and genetic

link between UHT metamorphism, large-scale plutonism, and exhumation in the Central Alps. Felsic magmatism resulting from crustal anatexis in and around the Gruf Complex continued until ca. 24 Ma. Future research on felsic dikes in the surrounding units (e.g. Adula and Chiavenna) could shed light on the timing of amalgamation of the Central Alps.

Acknowledgements

This research is supported by the American National Science Foundation under Grant No. EAR 0911633 to A. Möller. We would like to thank A. Galli for showing us around the Gruf Complex, the Biavaschi family at Rifugio Brasca for their hospitality and logistical help, P.G. Lippert for field assistance, C. Fischer at the University of Potsdam and W.C. Dickerson at the University of Kansas for preparing thin sections, and J.A. Wolff and the rest of the team at Washington State University's Peter Hooper GeoAnalytical Laboratory for XRF analyses.

Figure Captions

Figure 3.1: Tectonic map of the Central Alps color coded by paleogeographic affinity. Ages for the Bergell and Novate intrusions are from (von Blanckenburg, 1992) and Liati et al. (2000), respectively. Modified from Bousquet et al. (2012b).

Figure 3.2: Geologic map of the Gruf Complex and surrounding units with granulite and dike sample locations. Modified from (Galli., 2010).

Figure 3.3: Outcrop photos of the granulite types: (A) Mylonitic shear zones separating charnockite (bottom of photo) from migmatitic orthogneiss (top of photo). (B) Leucogranulite

sample GR11-37. (C) Residual granulite sample GR11-12b. (D) Stromatic granulite sample Bras10-6-2.

Figure 3.4: Photos of leucosome and dike samples: (A) Muscovite-poor biotite-granite dikes (mineralogically similar to sample GR11-32) that are deformed within a mylonitic shear zone, which separate charnockite from migmatitic orthogneiss. (B) Garnet-biotite-muscovite pegmatite (mineralogically similar to sample GR11-34) and quartzite that lack internal deformation within a mylonite zone, which separates charnockite from migmatitic orthogneiss (not shown in photo). (C) Magmatic breccia with biotite granite leucosome (sample GR11-55) and ultramafic and mafic clasts. (D) Biotite-bearing granite pegmatite dike (sample GR11-54) boudinaged within foliation of migmatitic host rocks. (E) Biotite-granite pod (sample GR11-27) crosscutting foliation in charnockite and crosscut by two small aplitic dikes. (F) Medium-grained biotite-granite dike (sample GR11-32) crosscutting foliation in charnockite and leucogranulite. (G) Garnet + muscovite + biotite granitic pegmatite dike (sample GR11-34) that crosscuts the foliation in the charnockite and entrains an ultramafic pod. (H) Muscovite + biotite granitic pegmatite dike (sample VER11-1) that crosscuts migmatitic orthogneiss.

Figure 3.5: Photomicrographs of selected zircon-bearing textures. (A) Zircon between sillimanite and leucosome in leucogranulite sample GR11-37. (B) Zircon in leucosome in leucogranulite sample GR11-37. (C) Zircon emanating from garnet into orthopyroxene + cordierite symplectite in residual granulite sample GR11-12B. (D) Zircon included in garnet in stromatic granulite sample Bras10-6-2.

Figure 3.6: CL images of representative zircon grains from each of the granulite samples showing grain/analyses numbers, location of laser ablation pits, and $^{206}Pb/^{238}U$ dates: (A) Leucogranulite sample GR11-37. (B) Residual granulite sample GR11-12b. (C) Stromatic granulite sample Bras10-6-2. All pit diameters are 15 μm. Italicized dates are >10% discordant and not used in the age calculations in Figure 3.8.

Figure 3.7: CL images of representative zircon grains from leucosome and dike samples showing grain/analysis number, location of laser ablation pits, and $^{206}Pb/^{238}U$ dates: (A) Biotite-bearing leucosome of magmatic breccia (sample GR11-55). (B) Medium-grained biotite-granite dike (sample GR11-32). (C) Garnet-biotite-muscovite granitic pegmatite dike (sample GR11-54). (D) Muscovite + biotite-bearing granititc pegmatite dike (sample VER11-1). (E) Garnet-biotite-muscovite leucogranite (sample NOV11-1B). There are no CL images of zircon from the other dike samples because these grains were analyzed on tape mounts. All pit diameters are 30 μm. Italicized dates are >10% discordant and not used in age calculations shown in Figure 3.9.

Figure 3.8: Wetherill concordia diagrams for granulite samples: (A-C) All analyses between 0 and 400 Ma for each of the samples. (D-E) Youngest populations from the leucogranulite GR11-37 and residual granulite GR11-12b samples with ages. Blue ellipses were used to calculate the ages.

Figure 3.9: Wetherill concordia diagrams for leucosome and dike samples: (A-H) All analyses between 0 and 400 Ma for all dike and leucosome samples. (I-O) Youngest populations with ages for all samples except NOV11-1A, which did not yield young zircon.

Figure 3.10: Chondrite-normalized REE plots for zircon from granulite samples color coded by $^{206}Pb/^{238}U$ date: (A) Leucogranulite (sample GR11-37). (B) Residual granulite sample GR11-12b. (C) Stromatic granulite sample Bras10-6-2. REE concentrations are normalized to the CI carbonaceous chondrite values of McDonough and Sun (1995).

Figure 3.11: Trace element plots for zircon from leucogranulite (GR11-37), residual granulite (GR11-12B), and stromatic granulite (Breas10-6-2) samples. (A–C) Chondrite normalized Yb-Dy ratio (YbN/DyN) versus $^{206}Pb/^{238}U$ date color coded by concordance. (D-F) Ti-in-zircon temperature versus $^{206}Pb/^{238}U$ date color coded by concordance. (G-I) Th/U versus $^{206}Pb/^{238}U$ date color coded by concordance. (M-O) Chondrite-normalized Yb-Dy ratio (YbN/DyN) versus Ti-in-zircon temperature color coded by $^{206}Pb/^{238}U$ date.

Figure 3.12: Zircon saturation temperature versus age plot for leucosome and dike samples.

Figure 3.13: Schematic temperature-time diagram showing the evolution of zircon, dike emplacement, deformation, and major mineral reactions in the Gruf granulites and dikes.

Figure 3.14: Age ranges of metamorphic and plutonic events in the Central Alps. The numbers refer to the following references: (1) U-Pb staurolite: ca. 28 Ma (Nagel, 2002), (2) U-Pb zircon (rims) 33–32 Ma (Liati et al., 2009), (3) Ar-Ar phengite: 33–30 Ma (Talerico, 2000), (4) U-Pb zircon: 37.1 ± 0.9 Ma (Liati et al., 2003), (5) U-Pb rutile: 30–19 Ma (Oalmann et al., in preparation-b), (6) U-Pb zircon: 24.0 ± 1.2 Ma (Liati et al., 2000), which envelopes our age of 23.8 ± 0.1 Ma, (7) U-Pb zircon (tonalite): 31.88 ± 0.09 Ma, U-Pb allanite (granodiorite): 30.1 ± 0.25 Ma (von

Blanckenburg, 1992), (8) U-Pb zircon: 32–22 Ma (Rubatto et al., 2009), (9) U-Pb zircon: 34.2 ± 0.2 and 32.9 ± 0.3 Ma (Hermann et al., 2006), (10) Lu-Hf garnet: 70–36 Ma (Brouwer et al., 2005), (11) U-Pb zircon: 43 ± 2 and 35.4 ± 0.5 Ma (Gebauer, 1996).

Appendix 3.A. Thin Section Scans

Figure 3.A1: Scans of thin sections showing location of analyzed zircon grains in the granulite samples. A) Leucogranulite sample GR11-37. (B) Residual granulite sample GR11-12b. (C) Stromatic granulite sample Bras10-6-2.

References

Becker, H., 1993. Garnet peridotite and eclogite Sm-Nd mineral ages from the Lepontine dome (Swiss Alps): New evidence for Eocene high-pressure metamorphism in the central Alps. Geology, 21(7): 599-602.

Beltrando, M., Lister, G.S., Rosenbaum, G., Richards, S., Forster, M.A., 2010. Recognizing episodic lithospheric thinning along a convergent plate margin: The example of the Early Oligocene Alps. Earth-Science Reviews, 103(3): 81-98.

Berger, A., Rosenberg, C., Schmid, S., 1996. Ascent, emplacement and exhumation of the Bergell pluton within the Southern Steep Belt of the Central Alps. Schweizerische mineralogische und petrographische Mitteilungen, 76(3): 357-382.

Berger, A., Schmid, S.M., Engi, M., Bousquet, R., Wiederkehr, M., 2011. Mechanisms of mass and heat transport during Barrovian metamorphism: A discussion based on field evidence from the Central Alps (Switzerland/northern Italy). Tectonics, 30(1): TC1007.

Bousquet, R. et al., 2012a. Metamorphic Framework of the Alps, Commission for the Geological Map of the World, CCGM/CGMW.

Bousquet, R. et al., 2012b. Tectonic framework of the Alps, Commission for the Geological Map of the World, CCGM/CGMW.

Brouwer, F., Burri, T., Engi, M., Berger, A., 2005. Eclogite relics in the Central Alps: PT-evolution, Lu-Hf ages, and implications for formation of tectonic mélange zones. Schweizerische mineralogische und petrographische Mitteilungen, 85: 147-174.

Brown, M., 2007. Metamorphic conditions in orogenic belts: a record of secular change. International Geology Review, 49(3): 193-234.

Burri, T., Berger, A., Engi, M., 2005. Tertiary migmatites in the Central Alps: Regional distribution, field relations, conditions of formation, and tectonic implications. Schweizerische mineralogische und petrographische Mitteilungen, 85(2-3): 215-232.

Chapman, J.B., Gehrels, G.E., Ducea, M.N., Giesler, N., Pullen, A., 2016. A new method for estimating parent rock trace element concentrations from zircon. Chemical Geology, 439: 59-70.

Chappell, B., White, A., 1974. Two contrasting granite types. Pacific geology, 8(2): 173-174.

Ciancaleoni, L., Marquer, D., 2006. Syn-extension leucogranite deformation during convergence in the Eastern Central Alps: example of the Novate intrusion. Terra Nova, 18(3): 170-180.

Clark, C., Fitzsimons, I.C., Healy, D., Harley, S.L., 2011. How does the continental crust get really hot? Elements, 7(4): 235-240.

Collins, W., 2002. Hot orogens, tectonic switching, and creation of continental crust. Geology, 30(6): 535-538.

Davidson, C., Rosenberg, C., Schmid, S., 1996. Symmagmatic folding of the base of the Bergell pluton, Central Alps. Tectonophysics, 265(3): 213-238.

Davies, J.H., von Blanckenburg, F., 1995. Slab breakoff: a model of lithosphere detachment and its test in the magmatism and deformation of collisional orogens. Earth and Planetary Science Letters, 129(1-4): 85-102.

Frey, M., Ferreiro Mählmann, R., 1999. Alpine metamorphism of the Central Alps. Schweizerische mineralogische und petrographische Mitteilungen, 79(1): 135-154.

Galli, A. et al., 2011. Granulites and charnockites of the Gruf Complex: Evidence for Permian ultra-high temperature metamorphism in the Central Alps. Lithos, 124(1-2): 17-45.

Galli, A. et al., 2012. U–Pb zircon dating of the Gruf Complex: disclosing the late Variscan granulitic lower crust of Europe stranded in the Central Alps. Contributions to Mineralogy and Petrology, 163: 353-378.

Galli, A., Le Bayon, B., Schmidt, M.W., Burg, J.-P., Reusser, E., 2013. Tectonometamorphic history of the Gruf complex (Central Alps): exhumation of a granulite–migmatite complex with the Bergell pluton. Swiss Journal of Geosciences, 106(1): 33-62.

Galli., A., 2010. Tectonometamorphic evolution of the Gruf Complex (Swiss and Italian Central Alps). PhD Thesis Thesis, ETH Zurich, 164 pp.

Gebauer, D., 1996. A P-T-t path for an (Ultra?-) High-pressure ultramafic/mafic rock-association and its felsic country-rocks based on SHRIMP-dating of magmatic and metamorphic zircon domains. Example: Alpe Arami (Central Swiss Alps), Earth Processes: Reading the Isotopic Code. Geophys. Monogr. Ser. AGU, Washington, DC, pp. 307-329.

Ghent, E.D., Stout, M.Z., 1984. TiO2 activity in metamorphosed pelitic and basic rocks: principles and applications to metamorphism in southeastern Canadian Cordillera. Contributions to Mineralogy and Petrology, 86(3): 248-255.

Guevara, V., Caddick, M., 2016. Shooting at a moving target: phase equilibria modelling of high-temperature metamorphism. Journal of Metamorphic Geology, 34: 209-235.

Hanchar, J.M., Hoskin, P.W., 2003. Zircon. Reviews in Mineralogy and Geochemistry, 153. The Mineralogical Society of America, Washington, DC.

Handy, M.R., Schmid, S.M., Bousquet, R., Kissling, E., Bernoulli, D., 2010. Reconciling plate-tectonic reconstructions of Alpine Tethys with the geological–geophysical record of spreading and subduction in the Alps. Earth-Science Reviews, 102(3): 121-158.

Harley, S., 2008. Refining the P–T records of UHT crustal metamorphism. Journal of Metamorphic Geology, 26(2): 125-154.

Harley, S.L., 1998. On the occurrence and characterization of ultrahigh-temperature crustal metamorphism. Geological Society, London, Special Publications, 138(1): 81-107.

Harley, S.L., 2016. A matter of time: The importance of the duration of UHT metamorphism. Journal of Mineralogical and Petrological Sciences, 111(2): 50-72.

Harley, S.L., Kelly, N.M., 2007. Zircon tiny but timely. Elements, 3(1): 13-18.

Harley, S.L., Kelly, N.M., Möller, A., 2007. Zircon behaviour and the thermal histories of mountain chains. Elements, 3(1): 25-30.

Harrison, T.M., Watson, E.B., 1983. Kinetics of zircon dissolution and zirconium diffusion in granitic melts of variable water content. Contributions to Mineralogy and Petrology, 84(1): 66-72.

Hermann, J., Rubatto, D., Trommsdorff, V., 2006. Sub-solidus Oligocene zircon formation in garnet peridotite during fast decompression and fluid infiltration (Duria, Central Alps). Mineralogy and Petrology, 88(1): 181-206.

Jackson, S.E., Pearson, N.J., Griffin, W.L., Belousova, E.A., 2004. The application of laser ablation-inductively coupled plasma-mass spectrometry to in situ U–Pb zircon geochronology. Chemical Geology, 211(1): 47-69.

Jochum, K.P. et al., 2005. GeoReM: a new geochemical database for reference materials and isotopic standards. Geostandards and Geoanalytical Research, 29(3): 333-338.

Kelly, N.M., Harley, S.L., 2005. An integrated microtextural and chemical approach to zircon geochronology: refining the Archaean history of the Napier Complex, east Antarctica. Contributions to Mineralogy and Petrology, 149(1): 57-84.

Kelsey, D., Clark, C., Hand, M., 2008. Thermobarometric modelling of zircon and monazite growth in melt-bearing systems: Examples using model metapelitic and metapsammitic granulites. Journal of Metamorphic Geology, 26(2): 199-212.

Kelsey, D.E., 2008. On ultrahigh-temperature crustal metamorphism. Gondwana Research, 13(1): 1-29.

Kelsey, D.E., Hand, M., 2015. On ultrahigh temperature crustal metamorphism: phase equilibria, trace element thermometry, bulk composition, heat sources, timescales and tectonic settings. Geoscience Frontiers, 6(3): 311-356.

Liati, A., Gebauer, D., 2003. Geochronological constraints for the time of metamorphism in the Gruf Complex (Central Alps) and implications for the Adula-Cima Lunga nappe system. Swiss Bulletin of Mineralogy and Petrology, 83(2): 159-172.

Liati, A., Gebauer, D., Fanning, C.M., 2003. The youngest basic oceanic magmatism in the Alps (Late Cretaceous; Chiavenna unit, Central Alps): geochronological constraints and geodynamic significance. Contributions to Mineralogy and Petrology, 146(2): 144-158.

Liati, A., Gebauer, D., Fanning, C.M., 2009. Geochronological evolution of HP metamorphic rocks of the Adula nappe, Central Alps, in pre-Alpine and Alpine subduction cycles. Journal of the Geological Society, 166(4): 797-810.

Liati, A., Gebauer, D., Fanning, M., 2000. U-PbSHRIMP dating of zircon from the Novate granite (Bergell, Central Alps): evidence for Oligocene-Miocene magmatism, Jurassic/Cretaceous continental rifting and opening of the Valais trough. Schweizerische mineralogische und petrographische Mitteilungen, 80(3): 305-316.

McDonough, W.F., Sun, S.-S., 1995. The composition of the Earth. Chemical geology, 120(3): 223-253.

McLean, N., Bowring, J., Gehrels, G., 2016. Algorithms and software for U-Pb geochronology by LA-ICPMS. Geochemistry, Geophysics, Geosystems.

Miller, C.F., McDowell, S.M., Mapes, R.W., 2003. Hot and cold granites? Implications of zircon saturation temperatures and preservation of inheritance. Geology, 31(6): 529-532.

Möller, A., O'Brien, P., Kennedy, A., Kröner, A., 2002. Polyphase zircon in ultrahigh-temperature granulites (Rogaland, SW Norway): constraints for Pb diffusion in zircon. Journal of Metamorphic Geology, 20(8): 727-740.

Möller, A., O'Brien, P.J., Kennedy, A., Kröner, A., 2003. Linking growth episodes of zircon and metamorphic textures to zircon chemistry: an example from the ultrahigh-temperature granulites of Rogaland (SW Norway). Geological Society, London, Special Publications, 220(1): 65-81.

Nagel, T., 2002. Metamorphic and structural history of the southern Adula Nappe (Grabünden, Switzerland), University of Basel, Basel.

Niggli, E., Niggli, C., 1965. Karten der Verbreitung einiger Mineralien der alpidischen Metamorphose in den Schweizer Alpen (Stilpnomelan, Alkali-Amphibol, Chloritoid, Staurolith, Disthen, Sillimanit). Eclogae Geologicae Helvetiae, 58: 335-368.

Nimis, P., Trommsdorff, V., 2001. Revised thermobarometry of Alpe Arami and other garnet peridotites from the Central Alps. Journal of Petrology, 42(1): 103-115.

Oalmann, J., Düsterhöft, E., Möller, A., Bousquet, R., in preparation-a. Constraining the pressure-temperature evolution and geodynamic setting of UHT granulites and migmatitic paragneisses of the Gruf Complex, Central Alps.

Oalmann, J., Möller, A., Bousquet, R., in preparation-b. Texturally controlled U-Pb monazite dating of sapphirine granulites from the Gruf Complex, Central Alps: Evidence for UHT metamorphism in a Cenozoic continent-continent collision.

Oalmann, J., Möller, A., Bousquet, R., submitted. Decoupling of Zr-thermometry and U-Pb thermochronology in rutile from the UHT granulites and charnockites of the Gruf Complex (Central Alps).

Paton, C., Hellstrom, J., Paul, B., Woodhead, J., Hergt, J., 2011. Iolite: Freeware for the visualisation and processing of mass spectrometric data. J. Anal. At. Spectrom., 26(12): 2508-2518.

Petrus, J.A., Kamber, B.S., 2011. VisualAge: A novel approach to U-Pb LA-ICP-MS geochronology. Mineralogical Magazine, 75: 1633.

Rubatto, D., 2002. Zircon trace element geochemistry: partitioning with garnet and the link between U-Pb ages and metamorphism. Chemical Geology, 184(1-2): 123-138.

Rubatto, D., Hermann, J., Berger, A., Engi, M., 2009. Protracted fluid-induced melting during Barrovian metamorphism in the Central Alps. Contributions to Mineralogy and Petrology, 158(6): 703-722.

Samperton, K.M. et al., 2015. Magma emplacement, differentiation and cooling in the middle crust: Integrated zircon geochronological–geochemical constraints from the Bergell Intrusion, Central Alps. Chemical Geology, 417: 322-340.

Schmitz, S. et al., 2009. Chemical U-Th-Pb dating of monazite by 3D-Micro X-ray fluorescence analysis with synchrotron radiation. European Journal of Mineralogy, 21(5): 927-945.

Schoene, B., 2014. U–Th–Pb Geochronology. In: Rudnick, R.L. (Ed.), The Crust. Treatise on Geochemistry. Elsevier, Amsterdam, pp. 341-378.

Sizova, E., Gerya, T., Brown, M., Perchuk, L., 2010. Subduction styles in the Precambrian: insight from numerical experiments. Lithos, 116(3): 209-229.

Sláma, J. et al., 2008. Plešovice zircon—a new natural reference material for U–Pb and Hf isotopic microanalysis. Chemical Geology, 249(1): 1-35.

Stampfli, G. et al., 1998. Subduction and obduction processes in the Swiss Alps. Tectonophysics, 296(1): 159-204.

Talerico, C., 2000. Petrological and chemical investigation of a metamorphosed oceanic crust-mantle section (Chiavenna, Bergell Alps), ETH Zürich, Zürich.

Taylor, R.J., Kirkland, C.L., Clark, C., 2016. Accessories after the facts: Constraining the timing, duration and conditions of high-temperature metamorphic processes. Lithos, 264: 239-257.

Todd, C.S., Engi, M., 1997. Metamorphic field gradients in the Central Alps. Journal of Metamorphic Geology, 15(4): 513-530.

Trommsdorff, V., 1966. Progressive Metamorphose kieseliger Karbonatgesteine in den Zentralalpen zwischen bernina und Simplon. Schweizerische mineralogische und petrographische Mitteilungen, 46: 431-460.

von Blanckenburg, F., 1992. Combined high-precision chronometry and geochemical tracing using accessory minerals: applied to the Central-Alpine Bergell intrusion (central Europe). Chemical Geology, 100(1-2): 19-40.

von Blanckenburg, F., Davies, J.H., 1995. Slab breakoff: a model for syncollisional magmatism and tectonics in the Alps. Tectonics, 14(1): 120-131.

Watson, E., Harrison, T., 2005. Zircon thermometer reveals minimum melting conditions on earliest Earth. Science, 308(5723): 841-844.

Watson, E., Wark, D., Thomas, J., 2006. Crystallization thermometers for zircon and rutile. Contributions to Mineralogy and Petrology, 151(4): 413-433.

Watson, E.B., Harrison, T.M., 1983. Zircon saturation revisited: temperature and composition effects in a variety of crustal magma types. Earth and Planetary Science Letters, 64(2): 295-304.

Whitehouse, M.J., Platt, J.P., 2003. Dating high-grade metamorphism--constraints from rare-earth elements in zircon and garnet. Contributions to Mineralogy and Petrology, 145(1): 61-74.

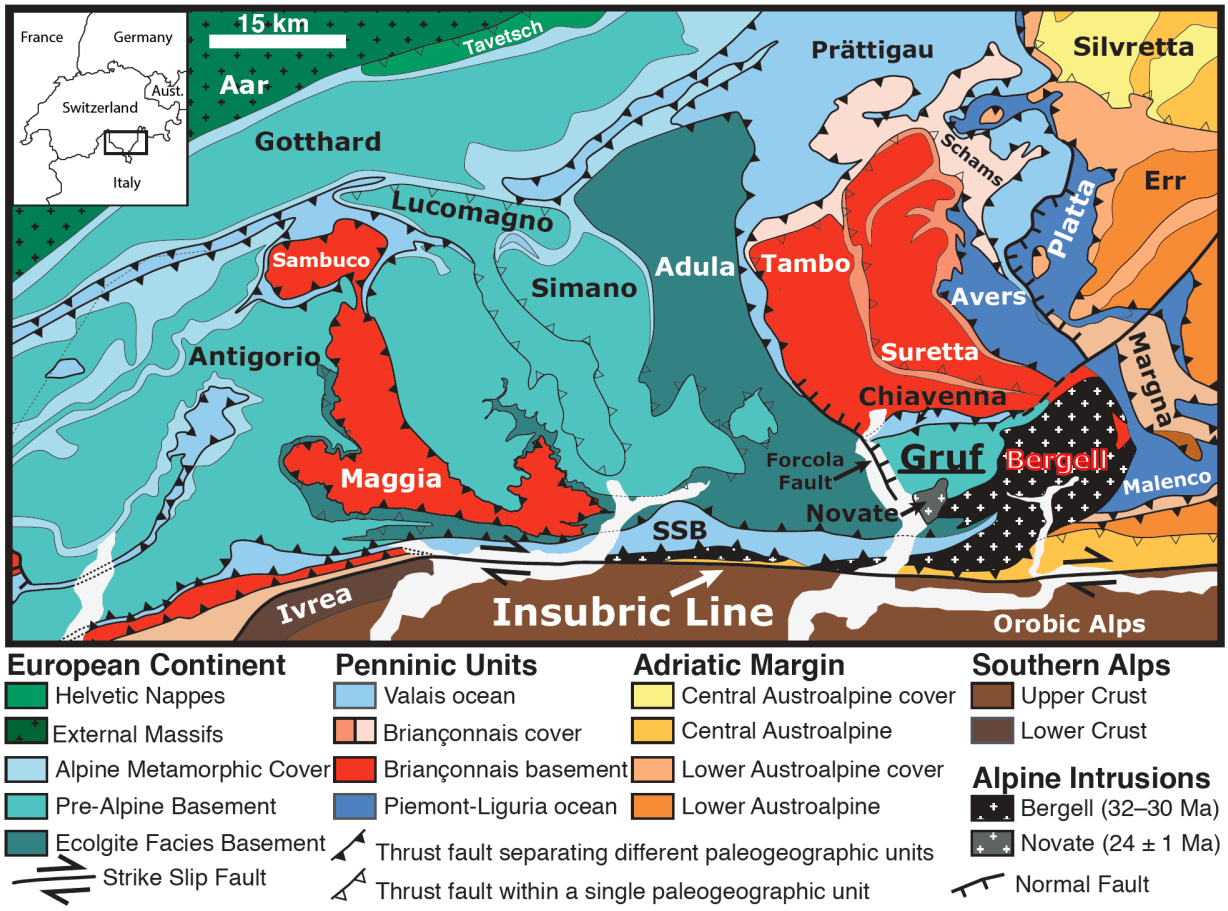
France
Germany
Aust.
Switzerland
Italy
15 km
Tavetsch
Aar
Gotthard
Lucomagno
Sambuco
Simano
Adula
Prättigau
Silvretta
Schams
Err
Platta
Tambo
Avers
Suretta
Margna
Antigorio
Chiavenna
Gruf
Bergell
Malenco
Forcola Fault
Maggia
Novate
SSB
Ivrea
Insubric Line
Orobic Alps
European Continent
Helvetic Nappes
External Massifs
Alpine Metamorphic Cover
Pre-Alpine Basement
Ecolgite Facies Basement
Strike Slip Fault
Penninic Units
Valais ocean
Briançonnais cover
Briançonnais basement
Piemont-Liguria ocean
Thrust fault separating different paleogeographic units
Thrust fault within a single paleogeographic unit
Adriatic Margin
Central Austroalpine cover
Central Austroalpine
Lower Austroalpine cover
Lower Austroalpine
Southern Alps
Upper Crust
Lower Crust
Alpine Intrusions
Bergell (32–30 Ma)
Novate (24 ± 1 Ma)
Normal Fault

Figure 3.1

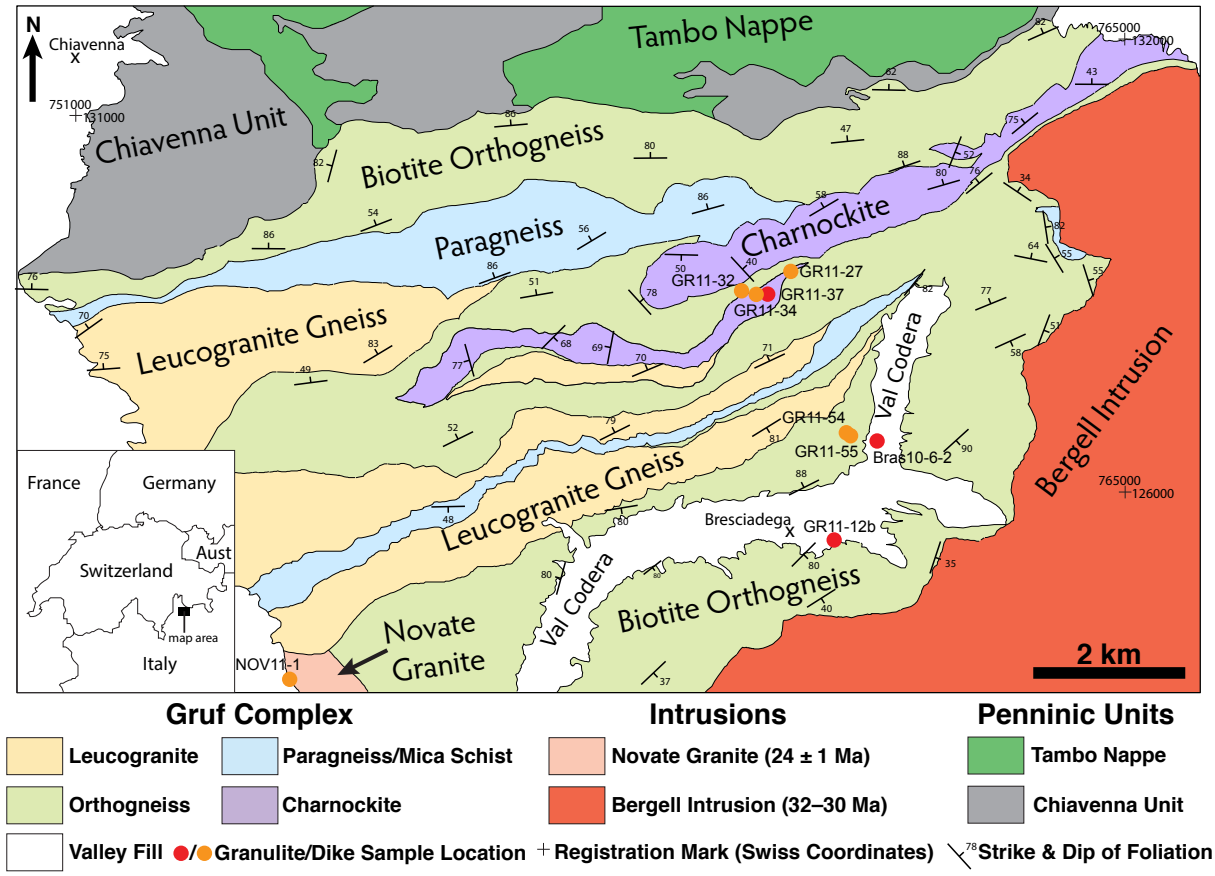
N
Chiavenna
751000
131000
Chiavenna Unit
Tambo Nappe
Biotite Orthogneiss
Paragneiss
Charnockite
Leucogranite Gneiss
GR11-32
GR11-27
GR11-37
GR11-34
Val Codera
GR11-54
GR11-55
Bras10-6-2
Bergell Intrusion
765000
132000
765000
126000
Bresciadega
GR11-12b
Leucogranite Gneiss
Biotite Orthogneiss
Val Codera
Novate Granite
NOV11-1
2 km
France
Germany
Switzerland
Aust
map area
Italy
Gruf Complex
Leucogranite
Paragneiss/Mica Schist
Orthogneiss
Charnockite
Valley Fill
Granulite/Dike Sample Location
Intrusions
Novate Granite (24 ± 1 Ma)
Bergell Intrusion (32–30 Ma)
Registration Mark (Swiss Coordinates)
Penninic Units
Tambo Nappe
Chiavenna Unit
Strike & Dip of Foliation

Figure 3.2

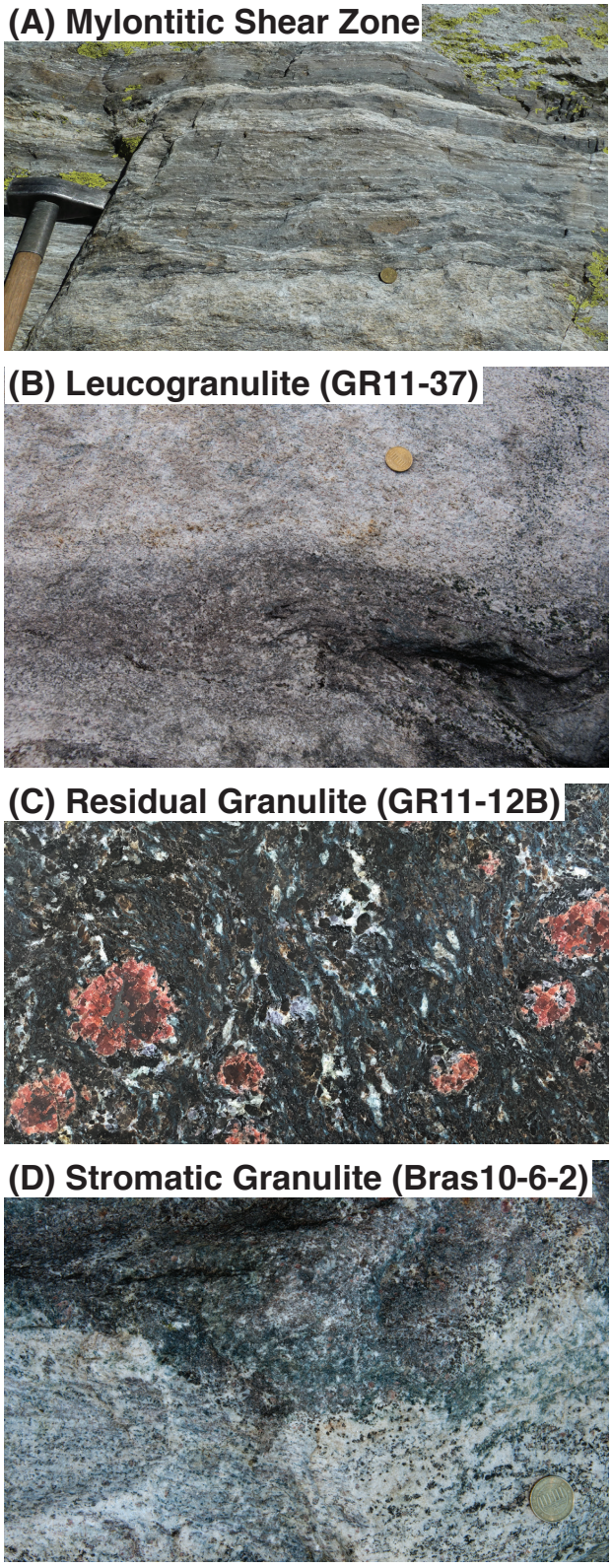
(A) Mylontitic Shear Zone
(B) Leucogranulite (GR11-37)
(C) Residual Granulite (GR11-12B)
(D) Stromatic Granulite (Bras10-6-2)

Figure 3.3

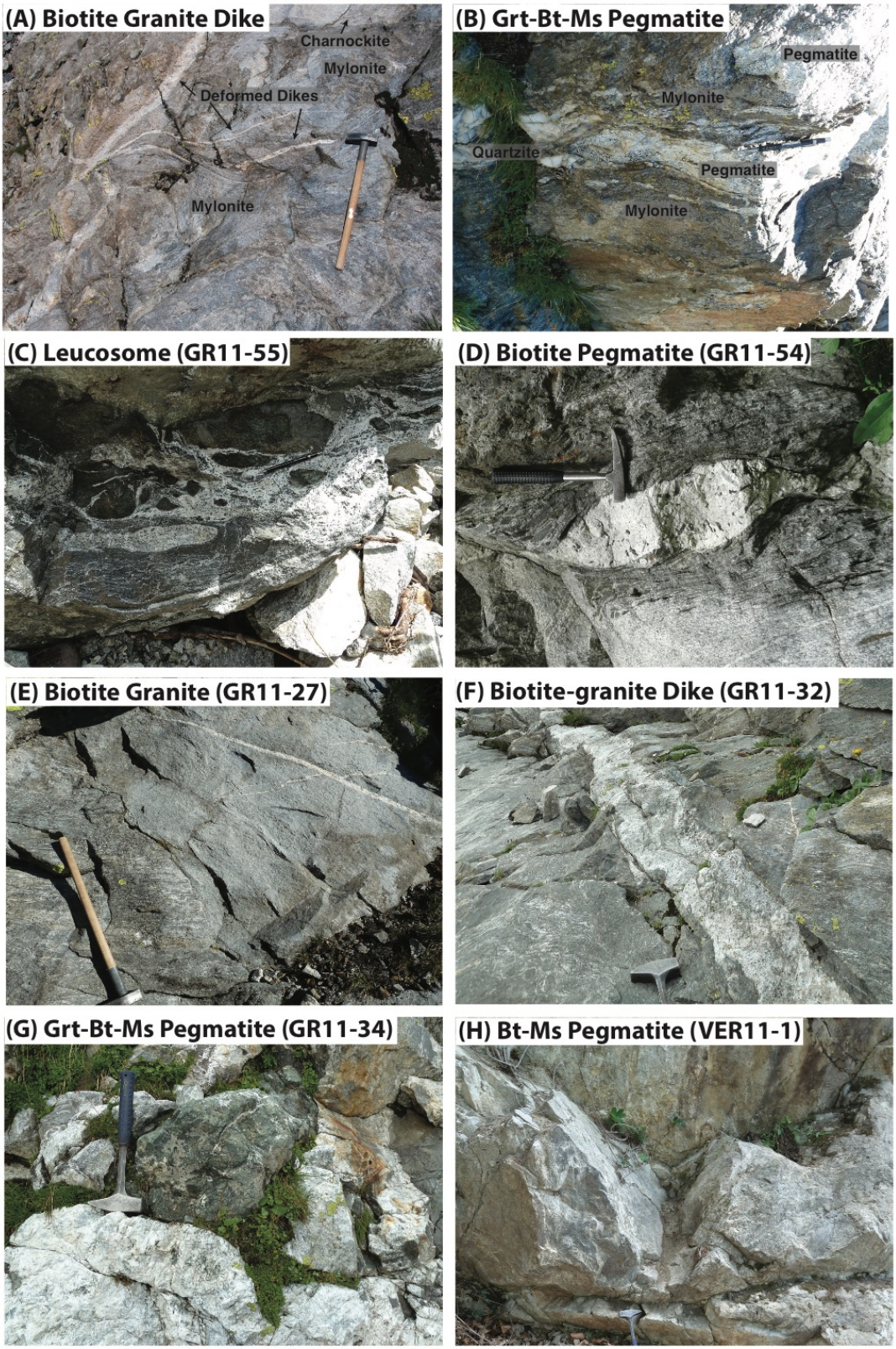
(A) Biotite Granite Dike
Charnockite
Mylonite
Deformed Dikes
Mylonite
(B) Grt-Bt-Ms Pegmatite
Pegmatite
Mylonite
Quartzite
Pegmatite
Mylonite
(C) Leucosome (GR11-55)
(D) Biotite Pegmatite (GR11-54)
(E) Biotite Granite (GR11-27)
(F) Biotite-granite Dike (GR11-32)
(G) Grt-Bt-Ms Pegmatite (GR11-34)
(H) Bt-Ms Pegmatite (VER11-1)

Figure 3.4

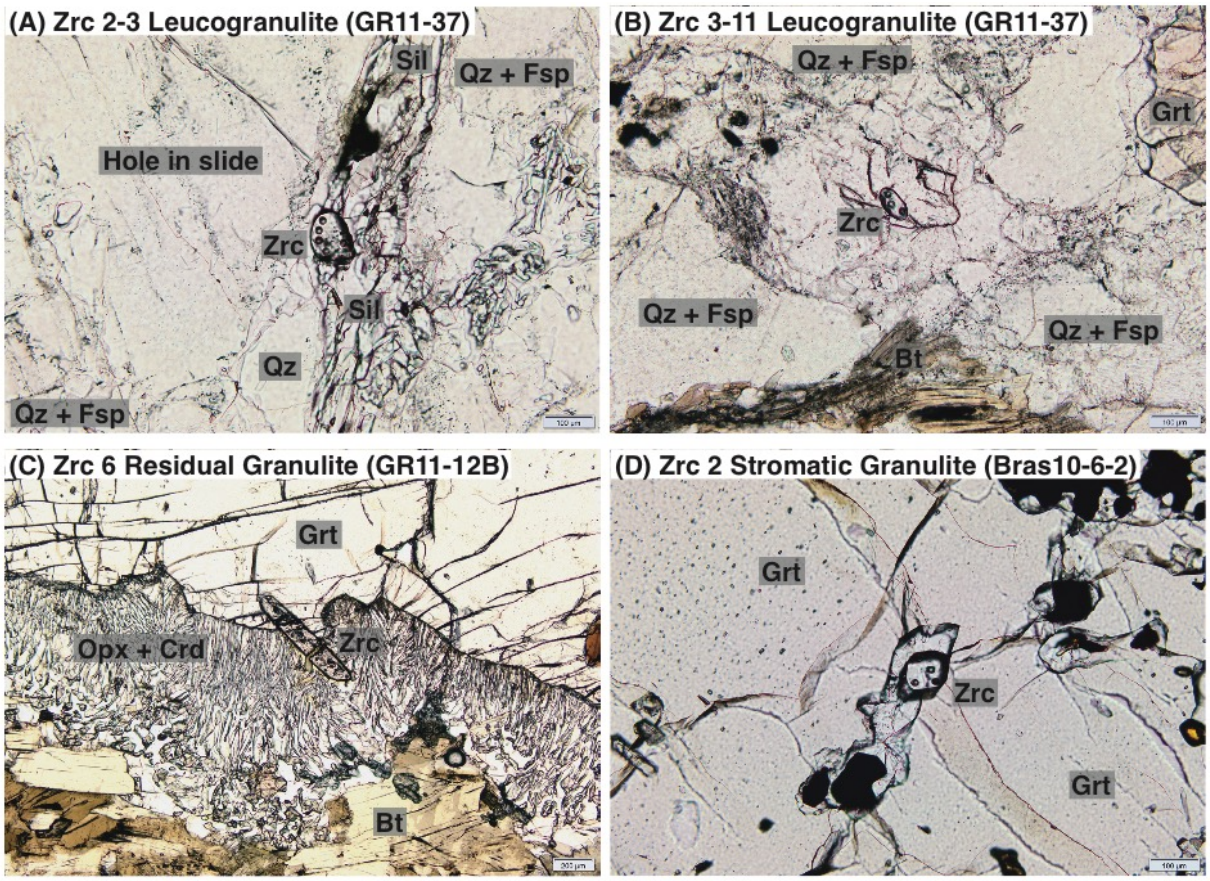
(A) Zrc 2-3 Leucogranulite (GR11-37)
Sil
Qz + Fsp
Hole in slide
Zrc
Sil
Qz
Qz + Fsp
(B) Zrc 3-11 Leucogranulite (GR11-37)
Qz + Fsp
Grt
Zrc
Qz + Fsp
Qz + Fsp
Bt
(C) Zrc 6 Residual Granulite (GR11-12B)
Grt
Opx + Crd
Zrc
Bt
(D) Zrc 2 Stromatic Granulite (Bras10-6-2)
Grt
Zrc
Grt

Figure 3.5

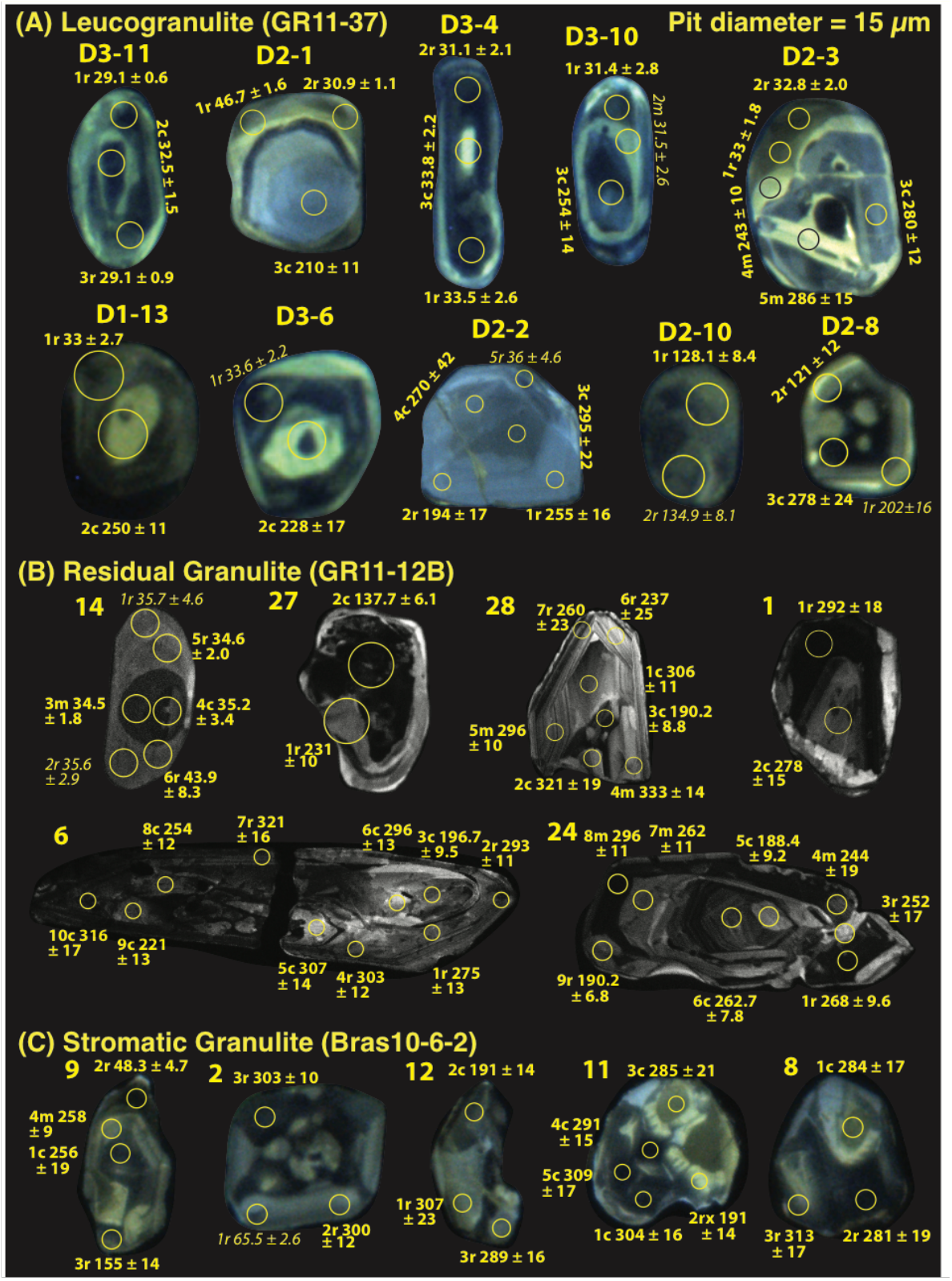
(A) Leucogranulite (GR11-37)
Pit diameter = 15 μm
D3-11
1r 29.1 ± 0.6
2c 32.5 ± 1.5
3r 29.1 ± 0.9
D2-1
1r 46.7 ± 1.6
2r 30.9 ± 1.1
3c 210 ± 11
D3-4
2r 31.1 ± 2.1
3c 33.8 ± 2.2
1r 33.5 ± 2.6
D3-10
1r 31.4 ± 2.8
2m 31.5 ± 2.6
3c 254 ± 14
D2-3
2r 32.8 ± 2.0
1r 33 ± 1.8
4m 243 ± 10
3c 280 ± 12
5m 286 ± 15
D1-13
1r 33 ± 2.7
2c 250 ± 11
D3-6
1r 33.6 ± 2.2
2c 228 ± 17
D2-2
5r 36 ± 4.6
4c 270 ± 42
3c 295 ± 22
2r 194 ± 17
1r 255 ± 16
D2-10
1r 128.1 ± 8.4
2r 134.9 ± 8.1
D2-8
2r 121 ± 12
3c 278 ± 24
1r 202±16
(B) Residual Granulite (GR11-12B)
14
1r 35.7 ± 4.6
5r 34.6 ± 2.0
3m 34.5 ± 1.8
4c 35.2 ± 3.4
2r 35.6 ± 2.9
6r 43.9 ± 8.3
27
2c 137.7 ± 6.1
1r 231 ± 10
28
7r 260 ± 23
6r 237 ± 25
1c 306 ± 11
3c 190.2 ± 8.8
5m 296 ± 10
2c 321 ± 19
4m 333 ± 14
1
1r 292 ± 18
2c 278 ± 15
6
8c 254 ± 12
7r 321 ± 16
6c 296 ± 13
3c 196.7 ± 9.5
2r 293 ± 11
10c 316 ± 17
9c 221 ± 13
5c 307 ± 14
4r 303 ± 12
1r 275 ± 13
24
8m 296 ± 11
7m 262 ± 11
5c 188.4 ± 9.2
4m 244 ± 19
3r 252 ± 17
9r 190.2 ± 6.8
6c 262.7 ± 7.8
1r 268 ± 9.6
(C) Stromatic Granulite (Bras10-6-2)
9
2r 48.3 ± 4.7
4m 258 ± 9
1c 256 ± 19
3r 155 ± 14
2
3r 303 ± 10
1r 65.5 ± 2.6
2r 300 ± 12
12
2c 191 ± 14
1r 307 ± 23
3r 289 ± 16
11
3c 285 ± 21
4c 291 ± 15
5c 309 ± 17
1c 304 ± 16
2rx 191 ± 14
8
1c 284 ± 17
3r 313 ± 17
2r 281 ± 19

Figure 3.6


(A) GR11-55
7j 32.2±1.1
8g 32.0±1.1
5d 32.9±1.1
5e 32.2±1.1
7e 32.2±1.0
7g 32.8±1.1
8h 31.6±1.0
7b 127±5
7c 33.0±1.1
7d 33.5±1.4
7f 31.6±1.2
7i 31.8±1.2
7h 49.0±2.4
8i 31.8±1.1
7a 32.6±1.1
8a 32.3±1.3
1n 32.2±1.1
1j 33.6±1.2
1k 32.5±1.1
5f 32.3±1.2
8b 31.9±1.0
5g 289±11
1l 32.7±1.1
1m 102±7
1i 32±1.1
8c 32.1±1.2
5h 33.7±1.2
2c 254±9
4a 33.0±1.4
7k 32.1±11
4c 273±10
7l 196±8
2e 287±9
2b 287±10
2d 198±8
4d 145±11
2a 146±10
4b 33.0±1.1
7m 32.5±1.1
(B) GR11-32
5d 27.2±1.0
5a 26.2±1.1
5c 27.5±1.2
7b 27.3±1.1
7d 30.2±1.7
5b 29.9±1.0
7e 70.9±3.2
2e 299±12
(C) GR11-34
6e 29.0±1.4
3e 29.4±1.2
10a 29.7±1.1
4d 28.8±1.0
6f 78.4±4.1
7b 182±8
10b 40.9±4.6
4a 152±7
4b 276±10
3d 280±11
4c 250±10
(D)VER11-1
3e 25±2
2b 26±2
1d 26±2
1a 26.1±1.3
4b 25±1.4
1e 26±2
1b 26±2
2a 26.7±1.3
6b 27±2
4e 26±2
5a 26±2
4c 27±3
3b 174±12
4f 25±1.6
4d 207±12
5b 554±36
3a 190±22
6d 258±16
6a 26±2
3d 455±43
3h 273±16
1c 298±17
6e 565±32
2e 558±29
(E) NOV11-1B
4i 23.3±0.9
11c 27.4±1
9r 25.1±1
10m 23.3±1
8a 81.4±3.4
4h 23.6±1
9s 24.8±1
10n 24.1±1
10o 239±0.9
8b 418±16
11d 33.5±2.1
4g 23.6±1
9t 24.2±1
7a 23.9±0.9
8r 24.9±1
9l 24.9±1
8c 24.3±1
9m 272±16
7b 171±8
10p 26.4±1
4a 24.2±2.3
8q 25.0±1.2
9n 23.8±1.1
7c 26.2±0.9
4b 546±24
5i 24.2±1
7h 23.9±0.9
7r 24.5±0.9
4c 377±17
5j 211±10
7j 252±10
7s 774±30
9o 68.2±5.0
7j 277±10
9p 1989±77
7t 138±6
9q 29.5±1.1
5k 24.0±0.9
7k 24.6±1.1

Figure 3.7

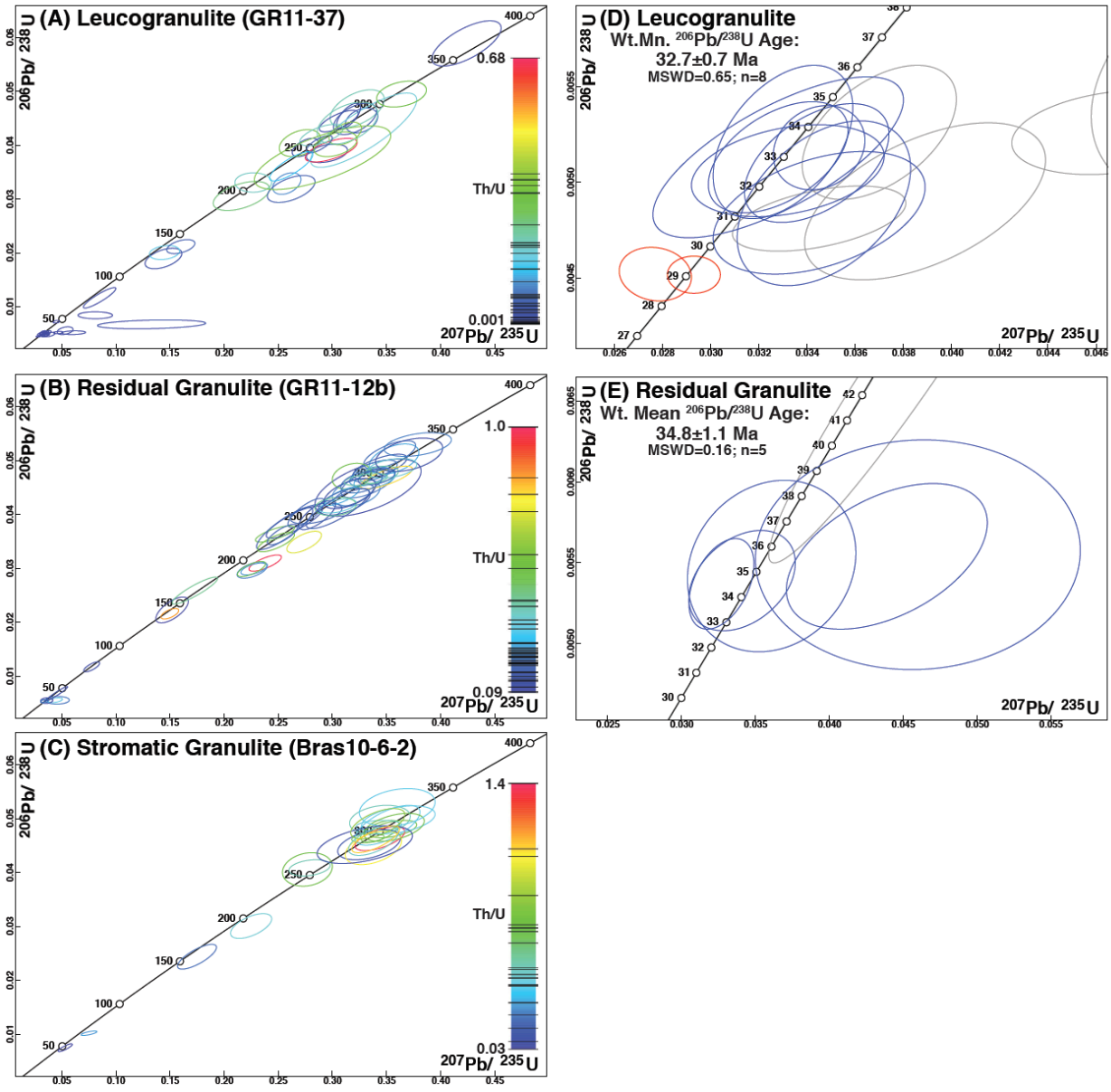
(A) Leucogranulite (GR11-37)
(B) Residual Granulite (GR11-12b)
(C) Stromatic Granulite (Bras10-6-2)
(D) Leucogranulite
Wt.Mn. 206Pb/238U Age:
32.7±0.7 Ma
MSWD=0.65; n=8
(E) Residual Granulite
Wt. Mean 206Pb/238U Age:
34.8±1.1 Ma
MSWD=0.16; n=5
Th/U
207Pb/ 235U
206Pb/ 238U

Figure 3.8

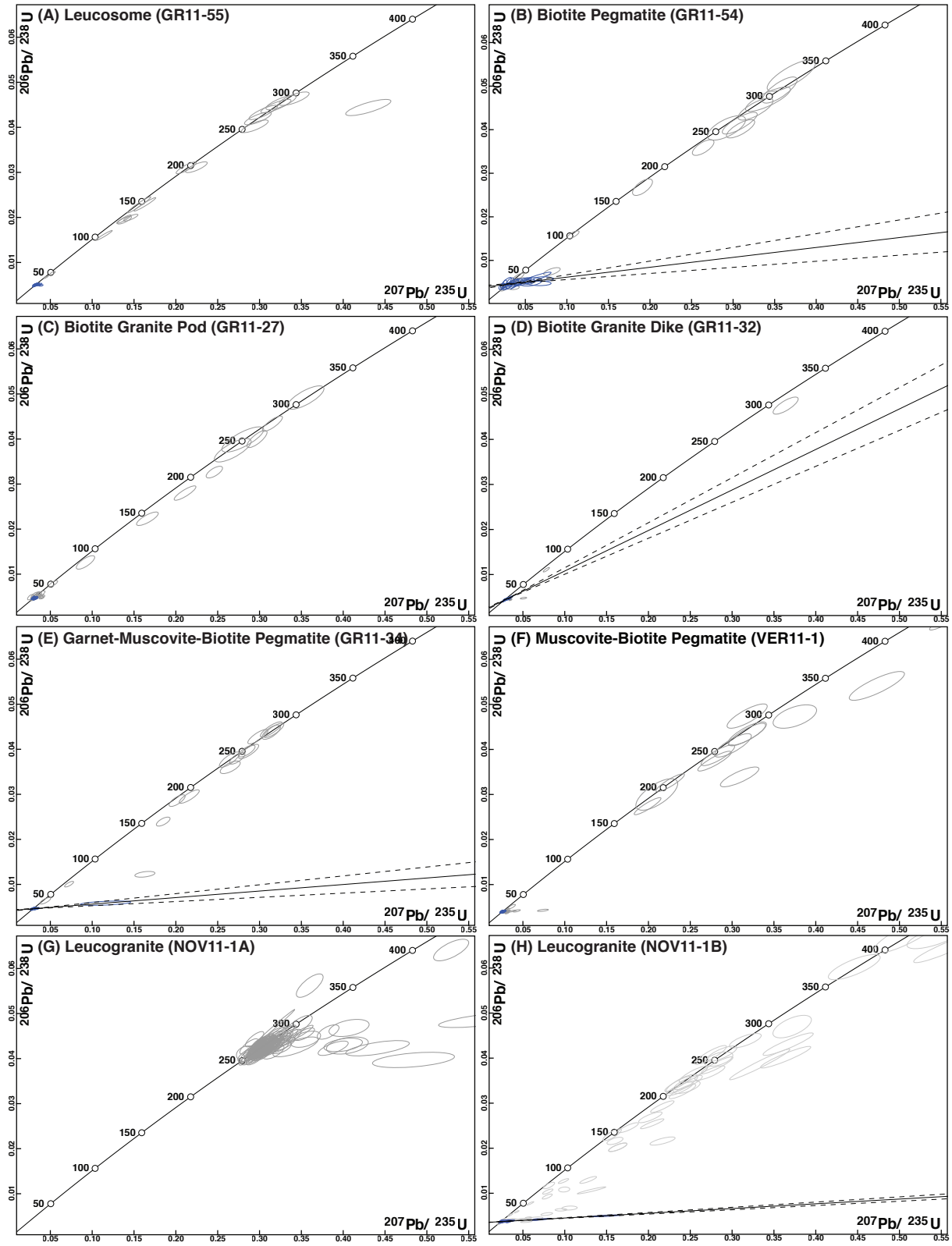
(A) Leucosome (GR11-55)
(B) Biotite Pegmatite (GR11-54)
(C) Biotite Granite Pod (GR11-27)
(D) Biotite Granite Dike (GR11-32)
(E) Garnet-Muscovite-Biotite Pegmatite (GR11-34)
(F) Muscovite-Biotite Pegmatite (VER11-1)
(G) Leucogranite (NOV11-1A)
(H) Leucogranite (NOV11-1B)
206Pb/ 238U
207Pb/ 235U

Figure 3.9

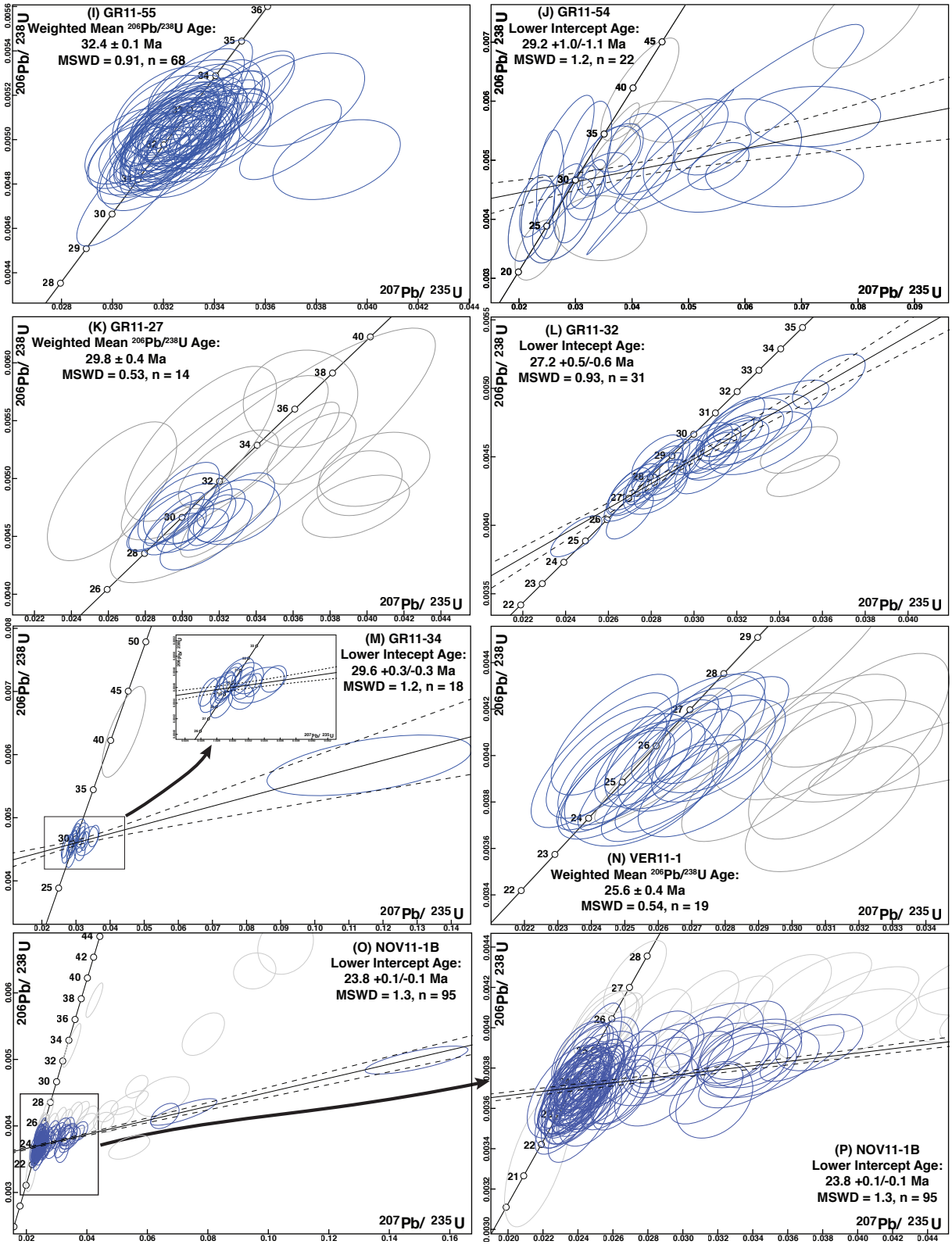

Figure 3.9 (continued)

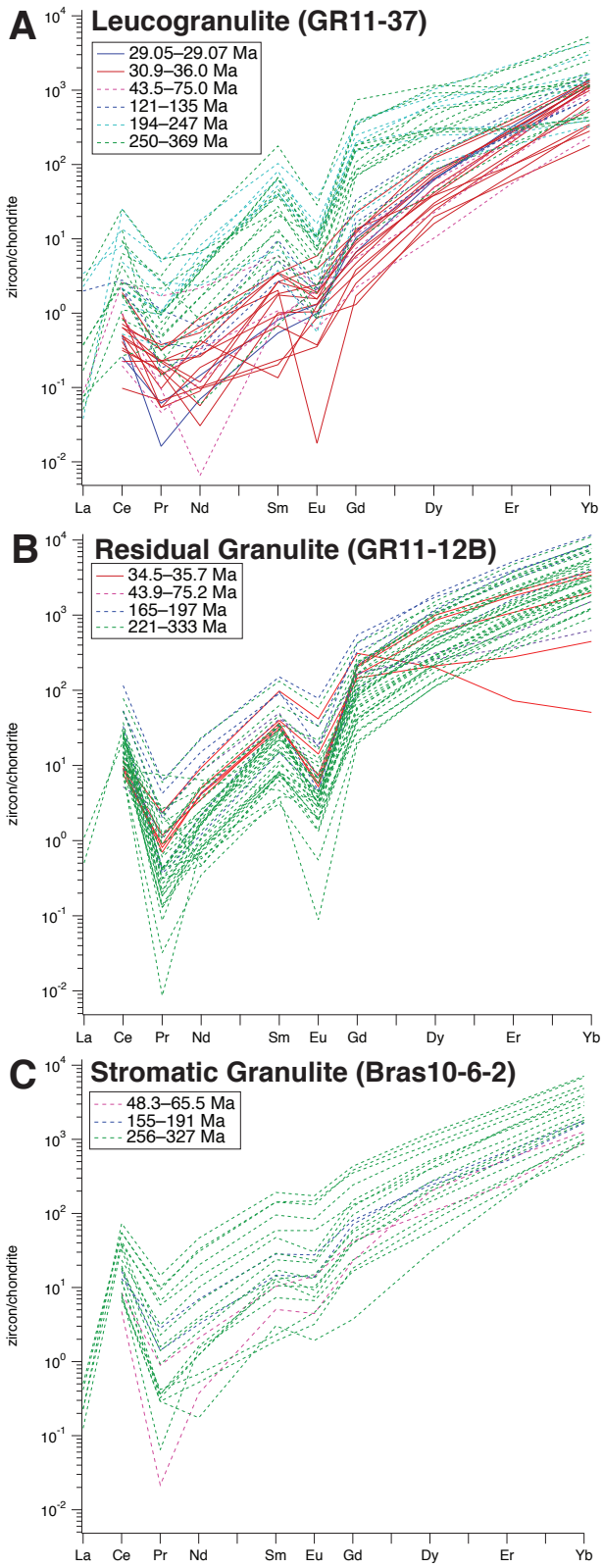
A
Leucogranulite (GR11-37)
29.05–29.07 Ma
30.9–36.0 Ma
43.5–75.0 Ma
121–135 Ma
194–247 Ma
250–369 Ma
zircon/chondrite
B
Residual Granulite (GR11-12B)
34.5–35.7 Ma
43.9–75.2 Ma
165–197 Ma
221–333 Ma
zircon/chondrite
C
Stromatic Granulite (Bras10-6-2)
48.3–65.5 Ma
155–191 Ma
256–327 Ma
zircon/chondrite
La Ce Pr Nd Sm Eu Gd Dy Er Yb

Figure 3.10

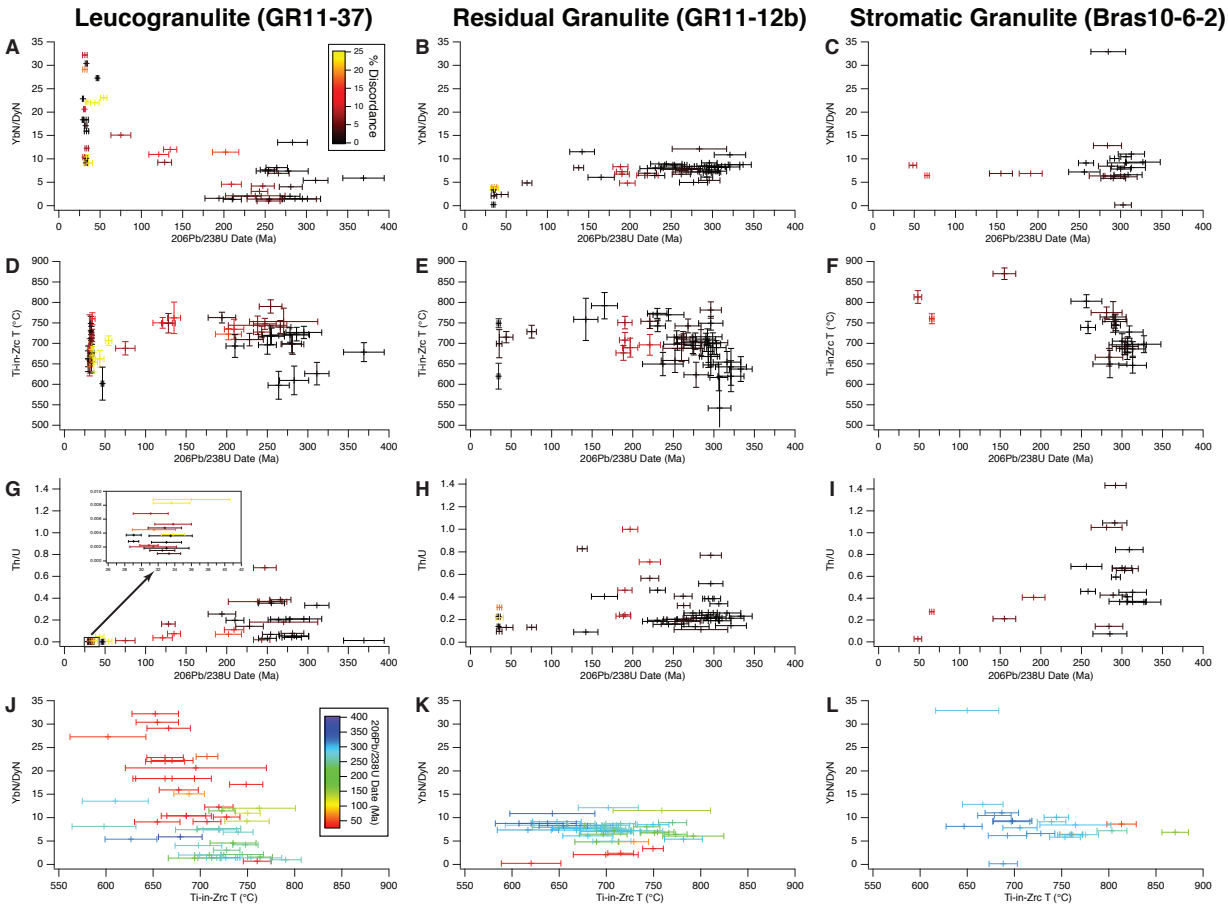
Leucogranulite (GR11-37)
Residual Granulite (GR11-12b)
Stromatic Granulite (Bras10-6-2)
A
B
C
D
E
F
G
H
I
J
K
L
% Discordance
206Pb/238U Date (Ma)
Ti-in-Zrc T (°C)
Th/U
Yb/Dy

Figure 3.11

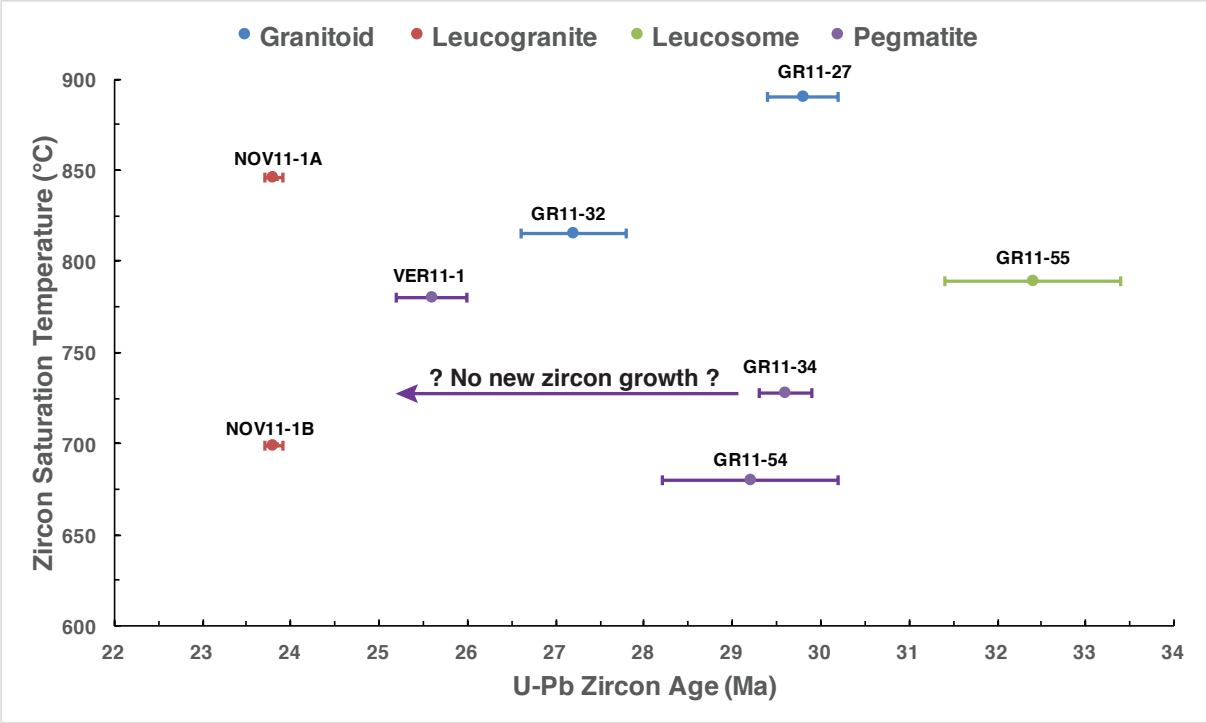
Granitoid
Leucogranite
Leucosome
Pegmatite
GR11-27
NOV11-1A
GR11-32
GR11-55
VER11-1
? No new zircon growth ?
GR11-34
NOV11-1B
GR11-54
Zircon Saturation Temperature (°C)
900
850
800
750
700
650
600
22
23
24
25
26
27
28
29
30
31
32
33
34
U-Pb Zircon Age (Ma)

Figure 3.12

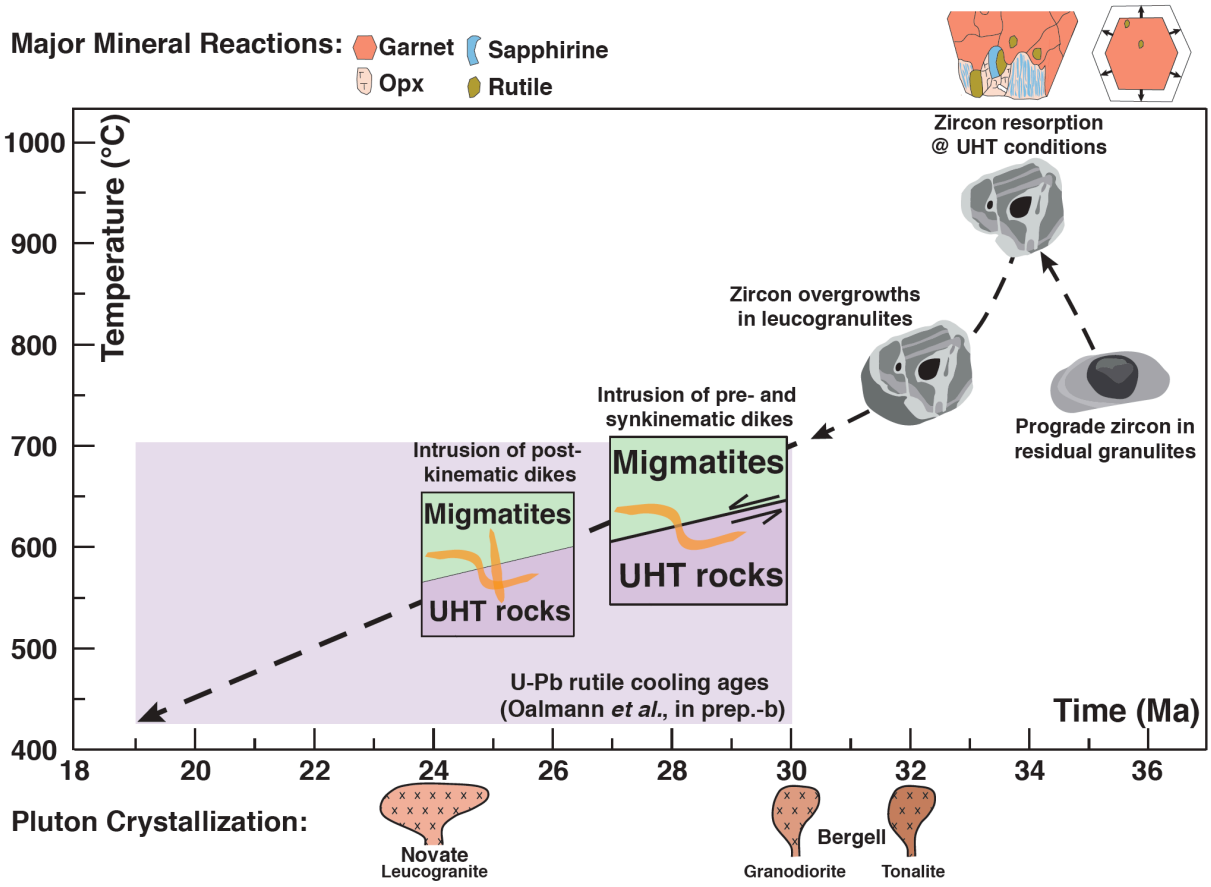
Major Mineral Reactions:
Garnet
Sapphirine
Opx
Rutile
Temperature (°C)
1000
900
800
700
600
500
400
Zircon resorption
@ UHT conditions
Zircon overgrowths
in leucogranulites
Prograde zircon in
residual granulites
Intrusion of pre- and
synkinematic dikes
Intrusion of post-
kinematic dikes
Migmatites
UHT rocks
Migmatites
UHT rocks
U-Pb rutile cooling ages
(Oalmann et al., in prep.-b)
Time (Ma)
18
20
22
24
26
28
30
32
34
36
Pluton Crystallization:
Novate
Leucogranite
Bergell
Granodiorite
Tonalite

Figure 3.13

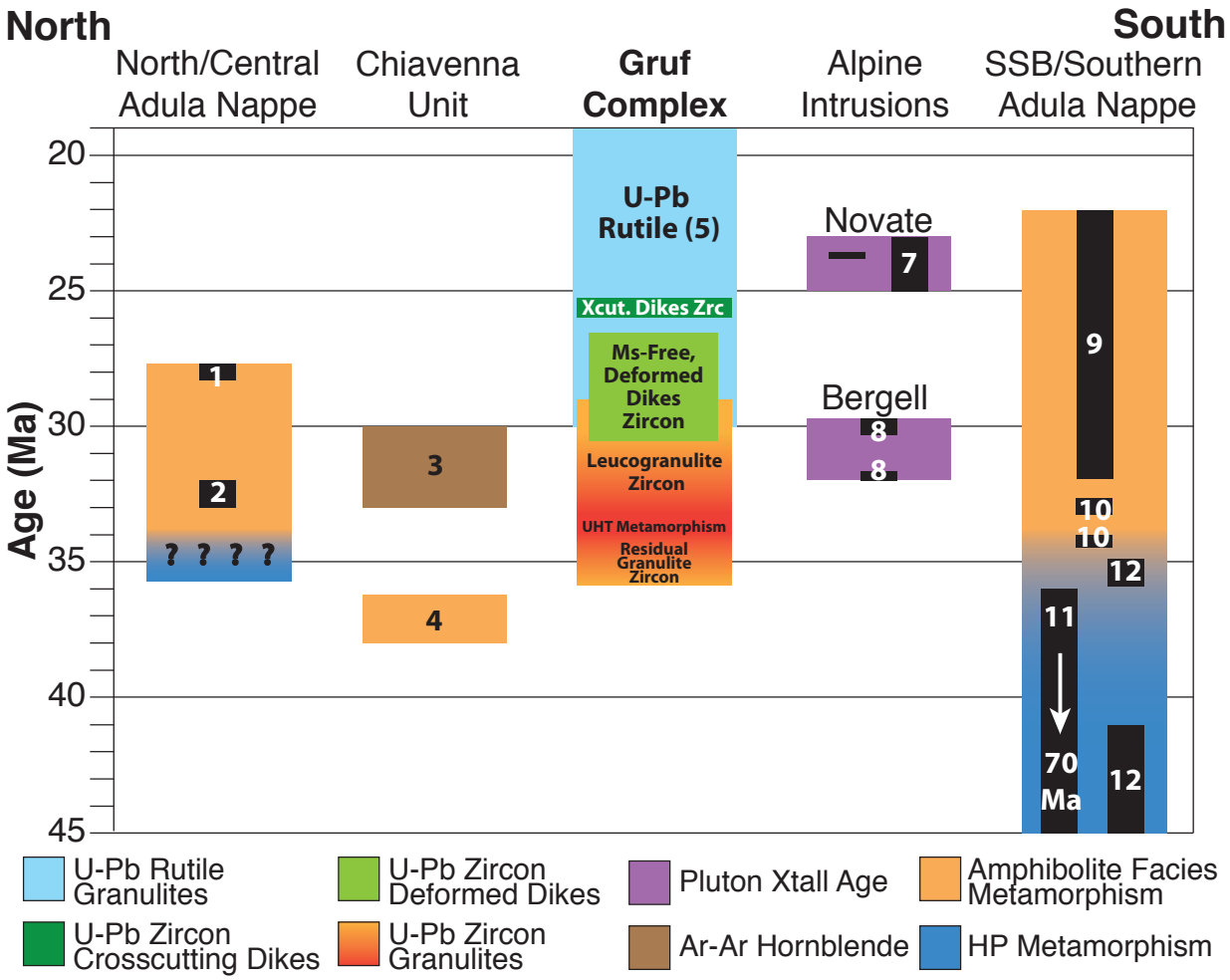
North
South
North/Central Adula Nappe
Chiavenna Unit
Gruf Complex
Alpine Intrusions
SSB/Southern Adula Nappe
Age (Ma)
20
25
30
35
40
45
U-Pb Rutile (5)
Xcut. Dikes Zrc
Ms-Free, Deformed Dikes Zircon
Leucogranulite Zircon
UHT Metamorphism
Residual Granulite Zircon
Novate
Bergell
1
2
? ? ? ?
3
4
7
8
8
9
10
10
12
11
70 Ma
12
U-Pb Rutile Granulites
U-Pb Zircon Deformed Dikes
Pluton Xtall Age
Amphibolite Facies Metamorphism
U-Pb Zircon Crosscutting Dikes
U-Pb Zircon Granulites
Ar-Ar Hornblende
HP Metamorphism

Figure 3.14


A
2500µm
3-11
3-10
3-9
3-4-6
3-3
3-2
2-11
2-10
2-9
2-7
2-8
2-6
2-5
2-4
2-3
13
11
10
9
8
3-12
2-2
2-1
1
2
3
5
6

Figure 3.A1

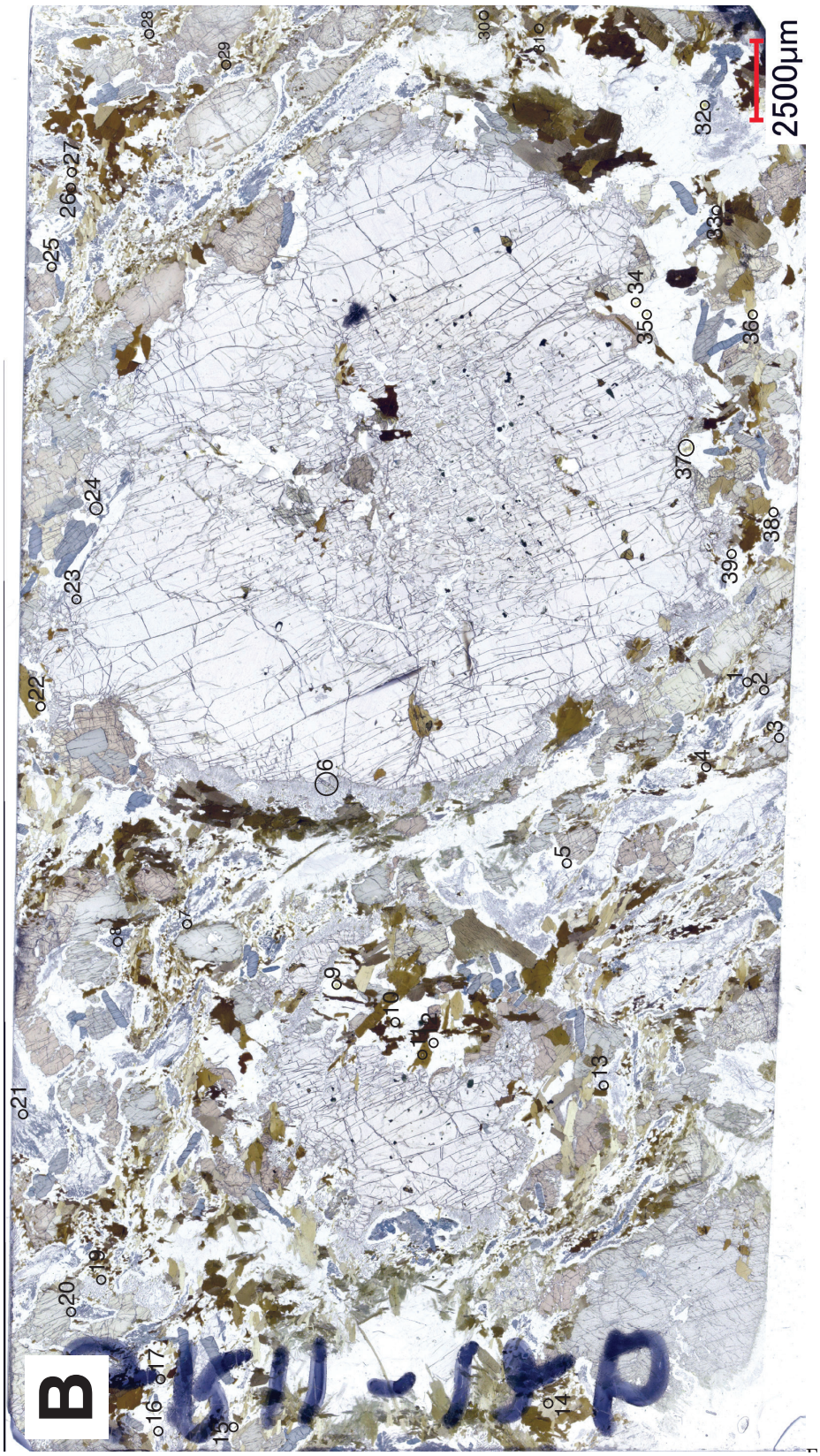

Figure 3.A1 (continued)

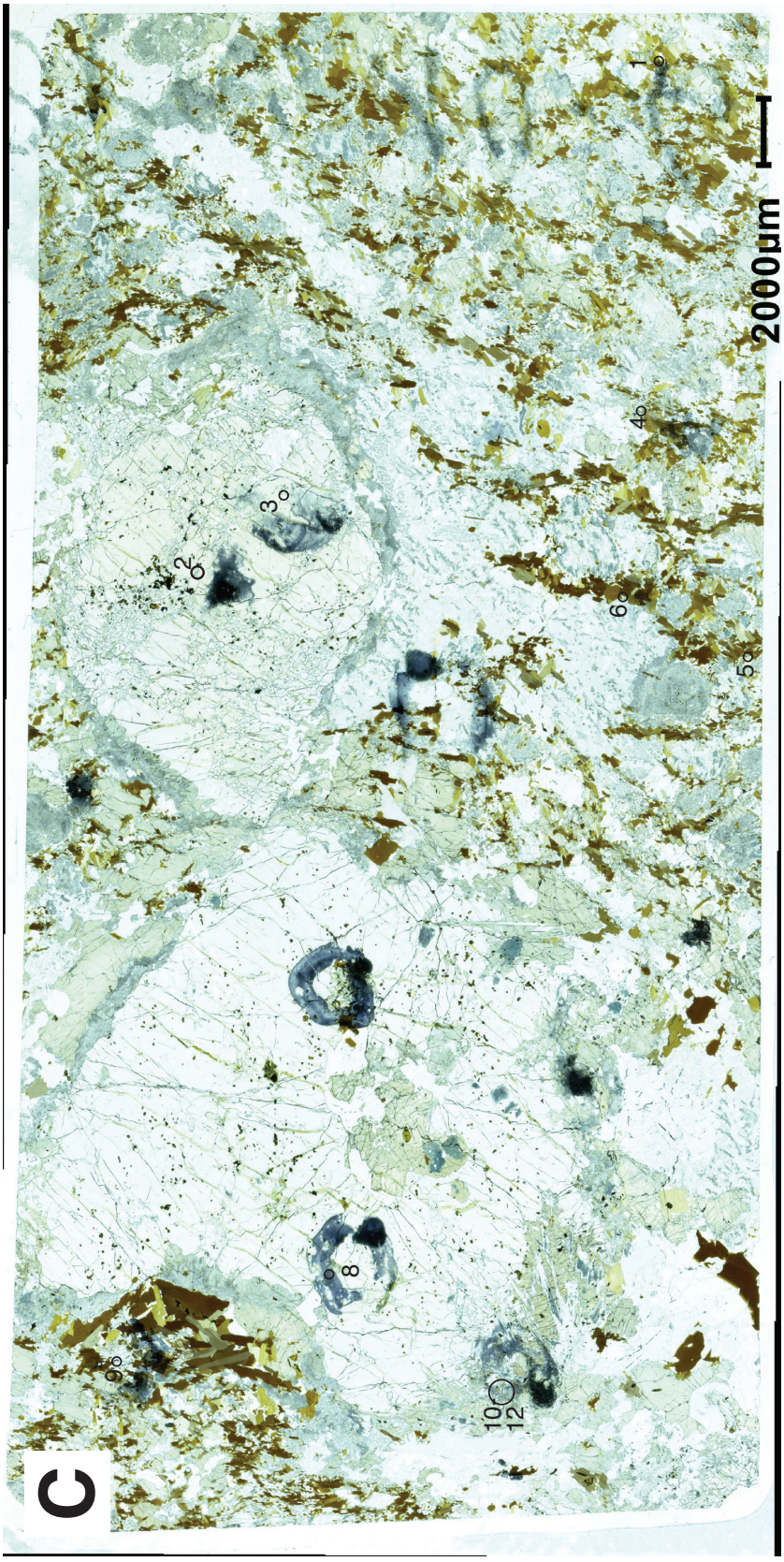

Figure 3.A1 (continued)

Table 3.1 LA-ICP-MS Parameters for Zircon Analyses from Granulite Samples

Laboratory & Sample Preparation	
Laboratory name	The University of Kansas, Dept. of Geology, Isotope Geochemistry Lab
Sample type/mineral	Zircon
Sample preparation	40 µm-thick, polished sections
Imaging	Microscope CL (color images) and SEM CL (black & white images)
Laser ablation system	
Make, model & type	ATL Arf excimer laser (193 nm), Photon Machines Analyte G2
Ablation cell & volume	HeLex
Laser wavelength	193 nm
Pulse width (ns)	5 ns
Fluence	2.5 J/cm^2
Repetition rate	10 Hz
Spot size (um)	15 µm
Sampling mode / pattern	Single spots
Carrier gas	He, 1.1 l/min, Ar, 1.1 l/min
Ablation duration	20 s
Cell carrier gas flow	He
ICP-MS Instrument	
Make, Model & type	Thermo Element2 magnetic sector field ICP-MS (single collector)
Sample introduction	Aerosol with sample + He was mixed with Ar using a T-connector 15 cm upstream from torch.
RF power	1400 W
Make-up gas flow	Ar, 16 l/min
Sampling depth	20 µm
Detection system	single detector (SEM), counting & analog modes
Elements/ isotopes analyzed	29Si, 49Ti, 89Y, 94Zr, 139La, 140Ce, 141Pr, 146Nd, 147Sm, 153Eu, 157Gd, 163Dy, 166Er, 172Yb, 178Hf, 206Pb, 207Pb, 208Pb, 232Th, 238U
Integration time per peak (Sample Time in miliseconds)	29Si=5, 49Ti=15, 89Y=5, 94Zr=3, 139La=10, 140Ce=10, 141Pr=10, 146Nd=10, 147Sm=10, 153Eu=10, 157Gd=5, 163Dy=5, 166Er=5, 172Yb=5, 178Hf=3, 206Pb=6, 207Pb=10, 208Pb=1, 232Th=1, 238U=2
Total integration time (Segment Duration in miliseconds)	29Si=40, 49Ti=60, 89Y=5, 94Zr=3, 139La=10, 140Ce=10, 141Pr=10, 146Nd=10, 147Sm=10, 153Eu=10, 157Gd=5, 163Dy=5, 166Er=5, 172Yb=5, 178Hf=3, 206Pb=24, 207Pb=40, 208Pb=4, 232Th=4, 238U=8

Table 3.1

Total method time	57 seconds (112 runs, 1 pass)
Sensitvity (cps/ppm)	29Si=21.5cps/ppm, 49Ti=62.3cps/ppm, 51V=1387cps/ppm, 53Cr=bdl, 90Zr=540cps/ppm, 93Nb=1391cps/ppm, 95Mo=348cps/ppm, 118Sn=1448cps/ppm, 120Sn=1992cps/ppm, 121Sb=1275cps/ppm, 178Hf= 563cps/ppm, 181Ta=1743cps/ppm, 184W=770cps/ppm, 206Pb=1064cps/ppm, 208Pb=2127cps/ppm, 232Th=2278cps/ppm, 238U=5099cps/ppm
ICP Dead time	4 ns
UO+/U+	≤0.2%
238U+/232Th+	≤1.6
Data Processing	
Gas blank	28 s
Calibration strategy	Trace elements: standard-sampling bracketing + internal standardization assuming 15% Si (stoichiometric); U-Pb: standard-sampling bracketing
Reference material info	Trace elements: GJ1 (Jackson et al., 2004); NIST612 (jochum et al., 2005)
Internal std for trace elements	29Si
Data processing package used / Correction for laser induced elemental fractionation (LIEF)	IGOR PRO, Iolite 2.5 (Patton et al. 2011): Trace elements: TraceElmentsIS data reduction scheme; U-Pb: U_Pb_Geochronology (Paton, et al. 2010) and VizualAge data reduction schemes (Petrus & Kamber, 2011), exponential LIEF correction for U-Pb ratios.
Common-Pb correction, composition and uncertainty	Not performed because of high Hg backgrounds
Uncertainty level & propagation	Trace elements: 2se internal uncertainty; U:Pb: 2se propogated uncertainty from VizualAge data reduction scheme. Concordia diagrams were plotted using ET_Redux (McLean et al. 2016) with 2s uncertainty ellipses.
Reproducibility	Trace elements: 5–7%. U-Pb ratios: 2–4%
Quality control / Validation	Plesovice zircon (Sláma et al., 2008) for U-Pb isotopes and trace elements; GJ1 (Jackson et al., 2004) for trace elements only

Table 3.2 LA-ICP-MS Parameters for Zircon Analyses from Dike and Leucosome Samples

Laboratory & Sample Preparation	
Laboratory name	The University of Kansas, Dept. of Geology, Isotope Geochemistry Lab
Sample type/mineral	Zircon
Sample preparation	Grain mounts and tape mounts
Imaging	Cathodoluminescence
Laser ablation system	
Make, model & type	ATL Arf excimer laser (193 nm), Photon Machines Analyte G1
Ablation cell & volume	Frames Cell with teardrop-shaped insert
Laser wavelength	193 nm
Pulse width (ns)	5 ns
Fluence	2.5 J/cm^2
Repetition rate	10 Hz
Spot size (um)	30 µm
Sampling mode / pattern	Single spots
Carrier gas	He, 0.4 l/min, Ar, 1.2 l/min
Ablation duration	30 s
Cell carrier gas flow	He, 0.4 l/min, Ar, 1.2 l/min
ICP-MS Instrument	
Make, Model & type	Thermo Element2 magnetic sector field ICP-MS (single collector)
Sample introduction	Aerosol with sample + He was mixed with Ar using a Y-connector 15 cm upstream from torch.
RF power	1200 W
Make-up gas flow	Ar, 16 l/min
Sampling depth	25 µm
Detection system	single detector (SEM), counting & analog modes
Elements/ isotopes analyzed	206Pb, 207Pb, 208Pb, 232Th, 235U, 238U
Integration time per peak (Sample Time in miliseconds)	206Pb=1, 207Pb=3, 208Pb=1, 232Th=1, 235U=2, 238U=1
Total integration time (Segment Duration in miliseconds)	206Pb=4, 207Pb=12, 208Pb=4, 232Th=4, 235U=8, 238U=4
Total method time	1 min 18 s (370 runs, 5 pass)
Sensitvity (cps/ppm)	232Th=14600cps/ppm, 235U=240cps/pppm, 238U=34300cps/ppm
ICP Dead time	22 ns
UO+/U+	0.25%
238U+/232Th+	≤1.7
Data Processing	
Gas blank	33 s

Table 3.2

Calibration strategy	Standard-sampling bracketing
Reference material info	GJ1 (Jackson et al., 2004)
Internal std for trace elements	n/a
Data processing package used / Correction for laser induced elemental fractionation (LIEF)	IGOR PRO, Iolite 2.5 (Patton et al. 2011): U_Pb_Geochronology (Paton, et al. 2010) and VizualAge data reduction schemes (Petrus & Kamber, 2011), exponential LIEF correction for U-Pb ratios.
Common-Pb correction, composition and uncertainty	Not performed because of high Hg backgrounds
Uncertainty level & propagation	2SE propogated uncertainty from VizualAge data reduction scheme. Concordia diagrams were plotted using ET_Redux (McLean et al. 2016) with 2s uncertainty ellipses.
Reproducibility	206Pb/238U=1.5-2.0%; 207Pb/235U=2.0-2.5%
Quality control / Validation	Plesovice zircon (Sláma et al., 2008)

Table 3.3. Whole rock compositional data and zircon saturation temperatures for dike and leucosome samples.

Sample	NOV11-1A	NOV11-1B	VER11-1	GR11-34	GR11-32	GR11-27	GR11-54	GR11-55
RockType	leucogranite	leucogranite	pegmatite	pegmatite	granitic dike	granitic pod	pegmatite	leucosome
SiO2	71.30	74.04	67.94	62.44	68.79	62.95	70.04	70.98
TiO2	0.40	0.04	0.21	0.40	0.30	0.67	0.20	0.28
Al2O3	14.42	14.70	17.37	17.28	16.18	17.94	16.45	14.11
FeO	2.81	0.48	1.25	3.65	2.00	3.86	1.65	2.40
MnO	0.04	0.03	0.03	0.08	0.04	0.06	0.04	0.06
MgO	0.64	0.07	0.36	3.64	0.76	1.34	0.67	1.56
CaO	1.64	1.41	2.26	5.30	2.36	2.93	2.20	1.91
Na2O	2.80	4.32	4.89	3.84	3.99	4.11	5.10	3.45
K2O	4.92	3.68	3.33	1.89	4.17	4.88	2.93	3.83
P2O5	0.17	0.05	0.08	0.44	0.20	0.26	0.18	0.16
LOI	0.50	0.39	0.67	0.70	0.49	0.32	0.67	0.42
Total	99.82	99.33	98.65	99.85	99.50	99.65	100.23	99.33
Na (mol)	0.045	0.070	0.079	0.062	0.064	0.066	0.082	0.056
K (mol)	0.052	0.039	0.035	0.020	0.044	0.052	0.031	0.041
Ca (mol)	0.029	0.025	0.040	0.095	0.042	0.052	0.039	0.034
Al (mol)	0.14	0.14	0.17	0.17	0.16	0.18	0.16	0.14
Si (mol)	1.19	1.23	1.13	1.04	1.14	1.05	1.17	1.18
Zr (ppm)	206	35	108	89	167	405	30	119
ASI	1.11	1.04	1.10	0.96	1.07	1.06	1.05	1.07
M	0.93	0.90	1.01	1.54	1.06	1.21	1.02	1.01
Zrc Sat T (°C)	846	699	780	728	815	890	680	789
Age (Ma)	23.9	23.9	25.6	29.5	27.2	29.9	29.2	32.4
Age ±2s (Ma)	0.1	0.1	0.3	0.3	0.6	0.4	1.0	0.1

Notes:

LOI = loss on ignition

ASI = alumina saturation index = molar Al/(Na+K+Ca)

M = (Na+K+2·Ca)/(Al·Si) (Watson and Harrison, 1983))

Zrc Sat T (°C) = zircon saturation temperature = 12,900/[2.95 + 0.85M + ln(496,000/Zr)] (Watson and Harrison, 1983)

Table 3.4: Isotopic ratios, dates, and trace elements of zircon from granulite samples.

Sample and Analysis Number	Isotopic Ratios 207Pb/235U	± 2SE (abs)	206Pb/238U	± 2SE (abs)	Rho: 206/238 vs 207/235	207Pb/206Pb	± 2SE (abs)	Rho: 238/206 vs 208Pb/232Th	208Pb/232Th	± 2SE (abs)	Dates (Ma) 206Pb/238U	± 2SE (abs)	207Pb/235U	± 2SE (abs)	% Discord. 6/38-7/35	207Pb/206Pb	± 2SE (abs)	208Pb/232Th	± 2SE (abs)	Trace Element Compositions 29Si (cps)	± 2SE (cps)	Ti (ppm)	± 2SE	T (°C) aTiO2=1	± 2SE (°C)	Ti (ppm) aTiO2=0.6	T (°C) aTiO2=0.6	Ti (ppm) aTiO2=0.7	T (°C) aTiO2=0.7	Y (ppm)	± 2SE (ppm)	Zr (ppm)	± 2SE (ppm)	La (ppm)	± 2SE (ppm)
Leucogranulite GR11-37																																			
G37D3-11-1r	0.0293	0.0011	0.00452	0.000097	-0.00082706	0.0481	0.0022	0.4285	-0.0002	0.0039	29.05	0.62	29.3	1.1	0.9	107	91	-5	78	1.9E+06	1.1E+05	3.8	1.1	663	19	6	702	5	690	292.3	5.9	328000	10000	b.d.l	-
G37D3-11-3r	0.0277	0.0015	0.00452	0.00014	-0.11.522	0.0446	0.0029	0.5862	0.0026	0.0043	29.07	0.9	27.8	1.5	-4.6	-40	120	51	87	2.2E+06	8.2E+04	3.8	1.9	663	31	6	702	5	690	268	14	362000	14000	b.d.l	-
G37D2-01-2r	0.0345	0.0036	0.00481	0.00017	0.47123	0.0526	0.0047	-0.1090	0.02	0.022	30.9	1.1	34.4	3.5	10.2	340	190	360	410	1.7E+06	9.2E+04	5.8	1.9	695	75	10	738	8	725	69.7	3.0	301000	10000	b.d.l	-
G37D3-04-2r	**0.0345**	**0.0044**	**0.00484**	**0.00032**	**0.47784**	**0.0515**	**0.0064**	**0.2657**	**0.0014**	**0.0034**	**31.1**	**2.1**	**34.4**	**4.3**	**9.6**	**230**	**250**	**28**	**69**	**1.5E+06**	**1.1E+05**	**5.1**	**2**	**685**	**27**	**9**	**727**	**7**	**714**	**-418**	**20**	**280000**	**21000**	**b.d.l**	**-**
G37D3-10-1r	**0.0347**	**0.0036**	**0.00489**	**0.00043**	**0.42263**	**0.0516**	**0.0082**	**0.4232**	**0.0003**	**0.0042**	**31.4**	**2.8**	**34.6**	**3.5**	**9.2**	**260**	**200**	**4**	**83**	**1.5E+06**	**1.2E+05**	**3.3**	**1.3**	**652**	**28**	**6**	**691**	**5**	**679**	**198**	**14**	**310000**	**23000**	**b.d.l**	**-**
G37D3-10-2m	0.0389	0.005	0.0049	0.00041	0.5254	0.0586	0.006	0.0720	0.008	0.01	31.5	2.6	38.6	4.9	18.4	550	210	150	200	1.8E+06	1.4E+05	4	1.4	666	23	7	707	6	694	174	13	315000	26000	b.d.l	-
G37D3-11-2c	**0.0332**	**0.004**	**0.00506**	**0.00024**	**0.31812**	**0.0467**	**0.0052**	**0.0417**	**-0.0059**	**0.0063**	**32.5**	**1.5**	**33.2**	**4**	**2.1**	**50**	**210**	**-120**	**130**	**1.6E+06**	**8.0E+04**	**10.9**	**2.3**	**749**	**18**	**18**	**796**	**16**	**781**	**302**	**5.1**	**314400**	**7300**	**b.d.l**	**-**
G37D2-03-2r	**0.0344**	**0.003**	**0.0051**	**0.00031**	**0.48929**	**0.0516**	**0.0041**	**0.1834**	**0.0001**	**0.0039**	**32.8**	**2**	**34.3**	**3**	**4.4**	**270**	**160**	**1**	**77**	**1.7E+06**	**1.1E+05**	**6.7**	**1.3**	**787**	**15**	**11**	**751**	**10**	**737**	**64.3**	**5.8**	**307000**	**13000**	**b.d.l**	**-**
G37D1-13-1r	**0.0328**	**0.0052**	**0.00513**	**0.00042**	**0.71324**	**0.0458**	**0.0056**	**-0.3893**	**-0.009**	**0.027**	**33.0**	**2.7**	**32.7**	**5.1**	**-0.9**	**170**	**200**	**-210**	**530**	**1.4E+06**	**6.8E+04**	**4.2**	**2.9**	**670**	**42**	**7**	**711**	**6**	**698**	**138**	**17**	**325000**	**19000**	**b.d.l**	**-**
G37D2-03-1r	**0.0328**	**0.0029**	**0.00513**	**0.00029**	**0.49081**	**0.0456**	**0.0034**	**0.0844**	**-0.0052**	**0.005**	**33.0**	**1.8**	**32.8**	**2.9**	**-0.6**	**20**	**140**	**-107**	**100**	**1.7E+06**	**9.4E+04**	**8.6**	**1.5**	**728**	**14**	**14**	**774**	**12**	**759**	**112.8**	**5.3**	**305000**	**17000**	**b.d.l**	**-**
G37D2-11-1c	**0.0345**	**0.0019**	**0.00518**	**0.00022**	**0.17327**	**0.0449**	**0.0031**	**0.4699**	**0.006**	**0.018**	**33.3**	**1.4**	**34.4**	**1.9**	**3.2**	**170**	**130**	**100**	**360**	**1.9E+06**	**1.2E+05**	**3.4**	**1.2**	**654**	**22**	**6**	**693**	**5**	**681**	**124**	**16**	**309000**	**10000**	**b.d.l**	**-**
G37D3-04-1r	**0.033**	**0.0029**	**0.00521**	**0.0004**	**0.44412**	**0.0488**	**0.0043**	**0.3610**	**0.0021**	**0.0022**	**33.5**	**2.6**	**33**	**2.8**	**-1.5**	**130**	**170**	**-42**	**45**	**1.9E+06**	**1.2E+05**	**4.6**	**1.4**	**677**	**21**	**8**	**718**	**7**	**705**	**288**	**20**	**287000**	**22000**	**b.d.l**	**-**
G37D3-06-1r	0.061	0.011	0.00523	0.00034	0.16116	0.085	0.015	0.1237	0.068	0.03	33.6	2.2	59	10	43.1	1160	340	1290	560	1.9E+06	1.1E+05	5.1	1.5	685	21	9	727	7	714	403	25	277000	24000	b.d.l	-
G37D2-11-2r	0.0468	0.0043	0.00526	0.00022	0.2527	0.0646	0.0037	0.2433	0.04	0.02	33.8	1.4	46.4	4.1	27.2	740	200	770	380	1.8E+06	1.1E+05	4.2	1.4	670	22	7	711	6	698	221	17	311000	14000	b.d.l	-
G37D3-04-3r	0.037	0.0032	0.00526	0.00035	0.49559	0.0501	0.0041	0.3191	0.001	0.0021	33.8	2.2	36.8	3.2	8.2	210	170	20	43	1.7E+06	1.1E+05	7.8	1.5	720	15	13	765	11	751	297	26	278000	15000	b.d.l	-
~~G37D3-09-1r~~	~~0.0404~~	~~0.0052~~	~~0.00529~~	~~0.00053~~	~~0.28561~~	~~0.0613~~	~~0.0078~~	~~0.2806~~	~~0.00211~~	~~0.00062~~	~~34.3~~	~~3.4~~	~~40.2~~	~~5.1~~	~~14.8~~	~~620~~	~~270~~	~~43~~	~~13~~	~~1.6E+06~~	~~9.2E+04~~	~~12.4~~	~~2.1~~	~~760~~	~~15~~	~~11~~	~~809~~	~~18~~	~~794~~	~~222~~	~~1.3~~	~~314000~~	~~26000~~	~~b.d.l~~	~~-~~
G37D2-02-5r	0.0531	0.0073	0.0056	0.00072	0.35733	0.0646	0.0096	0.3037	0.05	0.039	36.0	4.6	52.3	7	31.2	640	290	880	720	1.6E+06	8.5E+04	3.4	1.3	654	24	6	693	5	681	108	1.3	303000	17000	b.d.l	-
G37D3-05-1r	0.133	0.05	0.00677	0.00082	0.27238	0.139	0.046	-0.1242	0.026	0.011	43.5	5.2	124	44	64.9	1880	710	520	220	1.7E+06	7.9E+04	3.8	1.2	663	21	6	702	5	690	19.5	1.9	272000	26000	0.02	0.11
G37D2-01-1r	0.0451	0.0029	0.00726	0.00024	0.32784	0.0469	0.003	0.1971	0.038	0.034	46.7	1.6	44.8	2.8	-4.2	60	120	700	620	1.8E+06	1.2E+05	1.6	1.3	602	40	3	637	2	626	116	6.5	295000	17000	b.d.l	-
G37D2-04-1r	0.081	0.016	0.00846	0.00064	-0.010.552	0.07	0.012	0.2829	0.079	0.056	54.3	4.1	79	1.5	31.3	830	370	1.500	1100	1.7E+06	7.0E+04	6.7	1	707	12	11	751	10	737	50.3	4.5	314000	36000	b.d.l	-
G37D3-09-2r	0.085	0.015	0.0117	0.0019	0.90342	0.0503	0.0048	0.1662	0.0174	0.007	75	12	82	14	8.5	280	190	340	140	1.8E+06	1.1E+05	5.3	1.2	688	16	9	730	8	717	213.5	8.0	313000	10000	b.d.l	-
G37D2-08-2r	0.144	0.017	0.019	0.0019	0.49304	0.0551	0.0039	0.3439	0.0101	0.0033	121	12	136	1.5	11.0	410	220	203	66	1.9E+06	1.9E+05	11.1	1.7	730	13	19	798	16	783	486	29	297000	33000	0.47	0.9
G37D2-10-1r	0.145	0.014	0.0201	0.0013	0.24101	0.0505	0.0055	0.4809	0.011	0.0062	128.1	8.4	137	12	6.5	270	190	220	120	2.0E+06	9.6E+04	11	3.2	749	24	18	797	16	782	229	5.2	333000	36000	b.d.l	-
G37D2-10-2r	0.16	0.013	0.0212	0.0013	0.46764	0.057	0.0046	0.2768	0.0082	0.003	134.9	8.1	153	12	11.8	460	170	164	61	1.8E+06	1.0E+05	12.7	1.9	762	38	21	811	18	796	242	18	307000	15000	b.d.l	-
G37D2-02-2r	0.216	0.026	0.0306	0.0027	0.50216	0.0544	0.0053	0.0483	0.0122	0.0026	194	17	197	22	1.5	340	200	245	51	1.7E+06	1.4E+05	12.8	1.9	763	13	21	812	18	797	392	31	323000	28000	b.d.l	-
G37D2-08-1r	0.262	0.022	0.0319	0.0025	0.52984	0.0583	0.0044	0.3108	0.0247	0.0049	202	16	241	18	16.2	520	170	493	96	1.8E+06	1.5E+05	8.1	1.4	723	14	14	768	12	754	429	29	257000	14000	0.81	0.39
G37D1-09-2	0.258	0.013	0.0329	0.002	0.38492	0.0581	0.004	0.6495	0.0144	0.003	209	12	233	11	10.3	510	150	289	59	1.9E+06	9.8E+04	9.3	2.9	735	24	16	781	13	767	140.5	7.2	319000	14000	0.54	0.3
G37D2-01-3r	0.227	0.017	0.0331	0.0018	0.00910	0.0493	0.0051	0.6385	0.0124	0.0037	210	11	207	14	-1.4	190	210	249	73	1.5E+06	7.5E+04	5.7	2.3	694	28	10	736	8	723	490	17	309000	17000	b.d.l	-
G37D3-06-2r	0.262	0.02	0.0361	0.0027	0.80638	0.0551	0.0027	0.3714	0.0144	0.0026	228	17	235	16	3.0	410	100	289	52	1.8E+06	1.2E+05	6.9	1.4	709	15	12	753	10	740	1400	1.10	276000	15000	b.d.l	-
G37D3-10-4c	0.291	0.063	0.0377	0.0059	0.69364	0.0516	0.0094	0.0117	0.0116	0.0027	238	36	254	49	6.3	270	320	232	54	2.2E+06	3.3E+05	10.4	2.9	744	22	17	792	15	777	930	1.10	333000	62000	b.d.l	-
G37D2-03-4m	0.295	0.019	0.0383	0.0017	0.36756	0.0551	0.0041	0.3603	0.0167	0.0073	243	10	261	1.5	6.9	370	150	330	130	1.8E+06	1.2E+05	8.6	1.5	728	14	14	774	12	759	231	28	293000	12000	b.d.l	-
G37D2-04-4c	0.299	0.024	0.0391	0.0022	0.63453	0.054	0.0035	0.2346	0.0124	0.0022	247	14	264	19	6.4	360	140	249	43	1.8E+06	1.4E+05	10.8	1.7	748	13	18	795	15	781	2170	1.10	313000	21000	0.009	0.027
G37D1-13-2r	0.275	0.012	0.0396	0.0017	0.53775	0.0528	0.0021	0.5010	0.014	0.004	250	11	246.1	9.7	-1.6	306	89	281	80	1.6E+06	9.4E+04	5.9	1.9	697	23	10	739	8	726	1260	320	324000	14000	b.d.l	-
G37D3-02-1c	0.288	0.012	0.0402	0.0016	0.72348	0.0522	0.0018	0.3088	0.0133	0.0028	254	10	256.6	9.7	1.0	302	80	267	56	1.6E+06	7.4E+04	7.8	2.4	720	23	13	765	11	751	1900	2.50	287200	9200	0.04	0.029
G37D3-10-3c	0.303	0.02	0.0402	0.0023	0.40356	0.0528	0.0038	0.5658	0.01333	0.002	254	14	268	16	5.2	330	150	268	39	1.8E+06	1.2E+05	17.1	3	790	16	29	842	24	826	1690	140	311000	21000	0.015	0.024
G37D2-02-1r	0.27	0.019	0.0404	0.0025	0.37232	0.0513	0.0037	0.3630	0.0129	0.0025	255	16	242	1.5	-5.4	230	150	259	50	1.6E+06	1.1E+05	7.6	2	717	20	13	762	11	748	449	32	313000	22000	b.d.l	-
G37D2-06-1r	0.29	0.02	0.0419	0.002	0.61272	0.0493	0.0025	0.2663	0.0132	0.0027	264	13	258	16	-2.3	180	110	265	53	1.7E+06	8.2E+04	1.5	1	598	34	3	632	2	622	408	30	304000	15000	b.d.l	-
G37D2-06-1c	0.312	0.015	0.0422	0.0021	0.45288	0.0543	0.0027	0.3994	0.0148	0.0024	266	13	277	11	4.0	380	110	298	48	1.7E+06	1.1E+05	9.9	1.9	740	16	17	787	14	772	694	27	303000	12000	0.64	0.3
G37D2-02-4c	0.329	0.049	0.0428	0.0069	0.81469	0.0594	0.0054	0.2482	0.0143	0.0047	270	42	286	37	5.6	590	210	286	94	1.7E+06	1.1E+05	11.5	8.2	753	33	19	802	16	787	455	47	310000	51000	0.09	0.14
G37D2-08-3c	0.314	0.028	0.0441	0.0039	0.45803	0.051	0.0046	0.3725	0.0133	0.0021	278	24	276	22	-0.7	260	190	267	42	1.6E+06	1.2E+04	7.9	1.8	721	18	13	766	11	752	1140	240	307000	26000	b.d.l	-
G37D2-03-3c	0.306	0.018	0.0445	0.002	0.71967	0.0513	0.0019	0.0626	0.0139	0.0038	280	12	271	14	-3.3	248	80	278	76	1.8E+06	1.1E+05	6.1	1.9	699	22	10	742	9	729	966	24	312000	11000	b.d.l	-
G37D1-09-1	0.327	0.015	0.0446	0.0023	0.32128	0.0547	0.0039	0.6632	0.0182	0.0036	281	14	287	12	2.1	380	160	365	71	2.0E+06	1.2E+05	6	2.1	698	25	10	741	9	728	2280	130	301000	15000	0.088	0.094
G37D2-04-3r	0.321	0.02	0.0449	0.0029	0.52045	0.0536	0.0031	0.5592	0.0085	0.0035	283	18	282	16	-0.4	360	130	171	70	1.7E+06	9.6E+04	1.8	1.2	610	35	3	645	3	634	149	12	298000	21000	b.d.l	-
G37D2-05m	0.315	0.011	0.0454	0.0024	0.66573	0.0511	0.0019	0.6804	0.0148	0.0032	286	15	277.9	8.6	-2.9	252	86	297	64	1.7E+06	1.1E+05	8.1	1.7	723	16	14	768	12	754	1420	130	317000	12000	0.012	0.015
G37D2-02-3c	0.323	0.025	0.0468	0.0035	0.49633	0.0524	0.0028	0.3032	0.0133	0.0026	295	22	283	19	-4.2	310	120	268	53	1.6E+06	1.1E+05	8.5	1.6	727	15	14	773	12	758	462	26	321000	22000	b.d.l	-
G37D2-04-2c	0.364	0.023	0.0495	0.0024	0.32258	0.0535	0.004	0.4247	0.015	0.0028	311	15	314	17	1.0	310	150	302	56	1.8E+06	1.2E+05	2.3	1.1	626	27	4	663	3	652	650	34	290000	13000	b.d.l	-
G37D3-02-2r	0.434	0.032	0.0389	0.0042	0.67862	0.0513	0.0034	0.2584	0.031	0.026	369	25	358	23	-3.1	270	140	580	490	1.6E+06	7.9E+04	4.7	1.6	679	23	8	720	7	707	206	54	277000	15000	0.018	0.095
Residual Granulite GR11-12B																																			
G12b-14-3m	**0.0327**	**0.0022**	**0.00517**	**0.00028**	**0.43335**	**0.0459**	**0.0023**	**0.3739**	**0.0017**	**0.00046**	**34.5**	**1.8**	**33**	**2.3**	**-4.5**	**19**	**99**	**34.2**	**9.3**	**1.9E+06**	**1.2E+05**	**2.1**	**1.2**	**620**	**32**	**4**	**656**	**3**	**645**	**178.9**	**8.7**	**285000**	**14000**	**b.d.l**	**-**
G12b-14-5r	**0.0341**	**0.0036**	**0.00539**	**0.00031**	**0.35452**	**0.0445**	**0.0041**	**0.1983**	**0.00121**	**0.0005**	**34.6**	**2**	**34**	**3.5**	**-1.8**	**-10**	**170**	**24.5**	**10**	**1.7E+06**	**8.3E+04**	**11**	**1.4**	**749**	**11**	**18**	**797**	**16**	**782**	**1340**	**1.40**	**291000**	**12000**	**b.d.l**	**-**
G12b-14-4c	**0.0361**	**0.0057**	**0.00548**	**0.00053**	**0.1524**	**0.0475**	**0.0072**	**0.4266**	**0.00219**	**0.00088**	**35.2**	**3.4**	**36**	**5.6**	**2.2**	**80**	**290**	**-44**	**18**	**1.9E+06**	**1.8E+05**	**6.1**	**3.1**	**699**	**34**	**10**	**742**	**9**	**729**	**-400**	**5.8**	**284000**	**24000**	**b.d.l**	**-**
~~G12b-14-2r~~	**~~0.0438~~**	**~~0.0068~~**	**~~0.00554~~**	**~~0.00045~~**	**~~0.46363~~**	**~~0.0537~~**	**~~0.0076~~**	**~~0.1026~~**	**~~0.00191~~**	**~~0.00056~~**	**~~35.6~~**	**~~2.8~~**	**~~43.6~~**	**~~6.6~~**	**~~18.3~~**	**~~620~~**	**~~260~~**	**~~38.5~~**	**~~31~~**	**~~2.2E+06~~**	**~~3.2E+05~~**	**~~30.7~~**	**~~36~~**	**~~1169~~**	**~~24~~**	**~~5.12~~**	**~~1266~~**	**~~439~~**	**~~12.35~~**	**~~2000~~**	**~~80~~**	**~~276000~~**	**~~17000~~**	**~~b.d.l~~**	**~~-~~**
~~G12b-14-1r~~	**~~0.046~~**	**~~0.011~~**	**~~0.00555~~**	**~~0.00071~~**	**~~0.37597~~**	**~~0.049~~**	**~~0.013~~**	**~~0.4278~~**	**~~0.00281~~**	**~~0.00092~~**	**~~36.7~~**	**~~4.6~~**	**~~46~~**	**~~1.1~~**	**~~22.4~~**	**~~610~~**	**~~510~~**	**~~67~~**	**~~37~~**	**~~2.3E+06~~**	**~~2.0E+05~~**	**~~53.8~~**	**~~140.5~~**	**~~1276~~**	**~~40~~**	**~~897~~**	**~~1389~~**	**~~769~~**	**~~13.53~~**	**~~2690~~**	**~~3.10~~**	**~~284000~~**	**~~23000~~**	**~~b.d.l~~**	**~~-~~**
G12b-14-6r	0.0457	0.0098	0.0068	0.0013	0.96159	0.0485	0.0037	0.0016	0.00238	0.00068	43.9	8.3	45	9.3	2.4	120	150	48	14	1.7E+06	1.1E+05	7.4	1.3	715	14	12	760	11	746	47.5	5.4	301000	12000	b.d.l	-
G12b-15-1	0.0777	0.0073	0.01174	0.00092	0.74624	0.0503	0.0032	0.3539	0.0106	0.0025	75.2	5.9	77.3	7.3	2.7	200	130	213	50	2.2E+06	1.2E+05	8.7	1.7	729	16	15	775	12	760	638	53	298000	17000	b.d.l	-
~~G12b-27-2a~~	~~0.1499~~	~~0.0082~~	~~0.0216~~	~~0.00097~~	~~0.62193~~	~~0.0515~~	~~0.002~~	~~0.5690~~	~~0.0092~~	~~0.002~~	~~137.7~~	~~6.1~~	~~141.8~~	~~9.8~~	~~2.9~~	~~258~~	~~88~~	~~185~~	~~40~~	~~2.1E+06~~	~~3.9E+04~~	~~14.1~~	~~44~~	~~1043~~	~~44~~	~~235~~	~~1128~~	~~201~~	~~1098~~	~~2330~~	~~260~~	~~330000~~	~~26000~~	~~19~~	~~21~~
G12b-17-1	0.152	0.015	0.0223	0.0024	0.66571	0.051	0.0044	0.5263	0.0122	0.0026	142	15	143	13	0.7	240	180	244	52	2.0E+06	1.3E+05	12.2	3.1	739	32	20	807	17	792	950	82	310000	24000	71	62
G12b-20-2c	0.173	0.021	0.0239	0.0025	0.90114	0.0506	0.0026	0.0108	0.007	0.0016	155	16	162	18	-1.9	220	120	141	32	2.5E+06	1.9E+05	17.4	6.5	792	32	29	844	25	828	5250	710	329000	27000	b.d.l	-
G12b-24-5c	0.226	0.014	0.0297	0.0015	0.54968	0.0529	0.0024	0.4166	0.00963	0.0017	188.4	9.2	206.3	12	8.7	320	100	194	34	1.7E+06	1.1E+05	4.6	1.2	677	18	8	718	7	705	1520	1.50	309000	13000	b.d.l	-
G12b-24-9r	0.2275	0.012	0.0299	0.0011	0.57267	0.053	0.0018	0.3513	0.01061	0.0017	190.2	6.8	207.9	10	8.5	313	75	213.3	35	1.9E+06	1.2E+05	6.8	1.7	708	19	11	752	10	738	3630	210	317600	9400	b.d.l	-
G12b-28-3c	0.2253	0.013	0.0299	0.0014	0.7067	0.0522	0.0021	0.4951	0.0136	0.0024	190.2	8.8	206.2	10	7.8	281	90	273	48	2.0E+06	9.8E+04	11.2	2	751	15	19	799	16	784	2860	140	306000	13000	b.d.l	-
G12b-06-3c	0.238	0.015	0.031	0.0015	0.74096	0.0531	0.002	0.3850	0.01317	0.0022	196.7	9.5	216.8	12	9.3	330	86	264	44	1.8E+06	9.7E+04	5.4	1.3	690	23	9	732	8	719	4000	460	297000	14000	b.d.l	-
G12b-06-9c	0.274	0.016	0.0349	0.002	0.64286	0.0515	0.0024	0.3552	0.0121	0.0022	221	13	245.3	13	9.9	245	99	243	44	1.8E+06	9.1E+04	5.9	2.5	697	25	10	739	8	726	2350	690	312000	15000	b.d.l	-
G12b-33-2c	0.248	0.017	0.0349	0.0018	0.74409	0.0528	0.0019	0.1454	0.01	0.0019	221	11	229	12	3.5	315	84	202	59	2.0E+06	1.2E+05	11.6	2.4	754	18	19	802	17	787	1945	55	364200	6600	b.d.l	-
G12b-38-1	0.254	0.014	0.0363	0.0019	0.75742	0.052	0.002	0.3683	0.00992	0.0016	230	12	229.7	11	-0.1	277	84	199.5	33	1.6E+06	5.9E+04	14.3	1.9	773	12	24	834	20	808	2780	190	329000	17000	0.262	0.099
G12b-27-1r	0.247	0.018	0.0364	0.0015	0.73397	0.0518	0.0022	0.0312	0.0156	0.0027	230.6	9.6	223	14	-3.4	269	94	312	54	2.0E+06	1.1E+05	10.2	1.7	743	14	17	790	15	775	870	63	340000	12000	0.12	-
G12b-28-6r	0.256	0.026	0.0374	0.0039	0.85334	0.0501	0.0024	0.0807	0.0149	0.0029	237	25	231	21	-2.6	200	110	299	58	2.3E+06	2.4E+05	3.2	1.5	689	29	5	689	5	677	1430	100	326000	43000	b.d.l	-
G12b-24-4m	0.265	0.026	0.0386	0.003	0.83087	0.0517	0.0027	0.1468	0.01134	0.0019	244	19	238	20	-2.5	260	120	228	39	2.3E+06	1.4E+05	13.8	2.3	770	15	23	820	20	804	3100	260	345000	28000	b.d.l	-
G12b-24-3r	0.286	0.017	0.0399	0.0027	0.737	0.052	0.0025	0.5784	0.0154	0.0026	252	17	255	14	1.2	280	110	309	51	2.1E+06	1.5E+05	3.6	1.7	658	29	6	698	5	686	1203	94	292000	12000	b.d.l	-
G12b-06-8c	0.285	0.024	0.0402	0.0019	0.49244	0.053	0.0035	0.0816	0.0156	0.0034	254	12	254	19	0.0	300	140	312	67	1.8E+06	9.2E+04	7.4	1.5	715	16	12	760	11	746	404	16	306000	16000	b.d.l	-
G12b-19-1m	0.276	0.017	0.0403	0.0027	0.77524	0.0519	0.0021	0.6222	0.01207	0.002	255	17	247	14	-3.2	276	91	242	40	2.5E+06	8.2E+04	6	1.2	698	15	10	741	9	728	1960	160	309000	18000	0.063	0.064
G12b-28-7r	0.305	0.029	0.0411	0.0037	0.81975	0.0528	0.0017	0.0324	0.0151	0.0029	260	23	270	22	3.7	360	100	304	57	1.8E+06	1.0E+05	5.3	2.6	688	33	9	730	8	717	2060	180	320000	40000	0.006	0.047
G12b-24-7m	0.303	0.019	0.0415	0.0017	0.19813	0.0539	0.0032	0.5218	0.0133	0.0024	262	11	268	15	2.2	360	130	266	49	1.8E+06	1.1E+05	7.4	1.3	715	14	12	760	11	746	743	25	322000	11000	b.d.l	-
G12b-24-6c	0.305	0.017	0.0416

	Isotopic Ratios										Dates (Ma)										Trace Element Compositions																	
Sample and Analysis Number	207Pb/235U	± 2SE (abs)	206Pb/238U	± 2SE (abs)	Rho: 206/238 vs 207/235	207Pb/206Pb	± 2SE (abs)	Rho: 238/206 vs 208/232Th	208Pb/232Th	± 2SE (abs)	206Pb/238U	± 2SE (abs)	207Pb/235U	± 2SE (abs)	% Discord. 6/38-7/35	207Pb/206Pb	± 2SE (abs)	208Th/232Th	± 2SE (abs)	206Pb/238U	Ti (ppm)	± 2SE (ppm)	T(°C) aTiO2=1	± 2SE (°C)	Ti (ppm) aTiO2=0.6	T(°C) aTiO2=0.6	Ti (ppm) aTiO2=0.7	T(°C) aTiO2=0.7	Y (ppm)	± 2SE (ppm)	Zr (ppm)	± 2SE (ppm)	La (ppm)	± 2SE (ppm)
G12b-01-2c	0.322	0.022	0.0441	0.0025	0.33181	0.0513	0.0026	0.5842	0.0146	0.0028	278	15	282	17	1.4	240	100	292	55	2.0E+06	1.6E+05	2.2	1.2	623	31	4	660	3	649	626	32	339000	18000	b.d.l	-
G12b-06-11s	0.333	0.049	0.045	0.0053	0.58061	0.0557	0.0065	0.5654	0.0152	0.0039	284	33	290	37	2.1	390	230	304	77	2.1E+06	1.2E+05	6.3	2.9	702	32	11	745	9	732	541	39	340000	51000	b.d.l	-
G12b-36-2m	0.327	0.019	0.046	0.002	0.42918	0.0519	0.0025	0.4332	0.0138	0.0024	290	12	288	14	-0.7	260	100	277	49	1.9E+06	1.0E+05	7	1.3	711	14	12	755	10	741	887	64	361000	15000	b.d.l	-
G12b-01-1r	0.333	0.025	0.0459	0.0028	0.62294	0.0516	0.0028	0.3410	0.01475	0.0025	292	18	290	19	-0.7	290	120	296	50	2.0E+06	1.4E+05	7.5	1.9	716	19	13	761	11	747	3020	430	344000	24000	b.d.l	-
G12b-06-2r	0.339	0.019	0.0465	0.0017	0.47882	0.0534	0.0021	0.4846	0.016	0.0027	293	11	296	14	1.0	347	91	320	54	1.7E+06	8.1E+04	4.1	1.7	668	27	7	709	6	696	1141	39	308000	14000	0.008	0.021
G12b-33-1r	0.331	0.02	0.0465	0.0011	0.47544	0.0522	0.0017	0.3422	0.0135	0.0025	293.1	7.1	290	16	-1.1	286	73	271	50	1.5E+06	7.1E+04	4.8	1.9	680	27	8	722	7	709	1267	30	340100	7100	b.d.l	-
~~G12b-04-5r~~	~~0.35~~	~~0.024~~	~~0.0469~~	~~0.0021~~	~~0.75126~~	~~0.0537~~	~~0.0019~~	~~0.1185~~	~~0.017~~	~~0.0039~~	~~296~~	~~13~~	~~294~~	~~18~~	~~-1.6~~	~~348~~	~~81~~	~~341~~	~~68~~	~~1.7E+06~~	~~8.4E+04~~	~~15.6~~	~~5.5~~	~~783~~	~~30~~	~~26~~	~~888~~	22	817	~~3543~~	~~783~~	~~313000~~	~~11000~~	~~1.6~~	~~-~~
G12b-07-1r	0.318	0.018	0.0471	0.0024	0.29967	0.0514	0.0031	0.7012	0.0156	0.0029	296	15	280	14	-5.7	250	130	314	58	2.4E+06	5.1E+04	11	2.2	749	17	18	797	16	782	1091	89	330000	26000	b.d.l	-
G12b-24-8m	0.334	0.018	0.0471	0.0018	0.52082	0.0534	0.002	0.4830	0.01349	0.0022	296	11	292.5	13	-1.2	328	83	271	44	1.9E+06	1.3E+05	4.1	1.6	668	25	7	709	6	696	3550	120	317000	12000	b.d.l	-
G12b-28-5m	0.341	0.017	0.047	0.0015	0.47582	0.0521	0.0017	0.4142	0.0135	0.0025	296.1	9.5	297.3	13	0.4	280	72	270	50	1.9E+06	1.1E+05	3.1	1.3	648	26	5	686	4	674	746	21	302900	7900	b.d.l	-
G12b-26-1c	0.343	0.018	0.0474	0.0016	0.37478	0.0529	0.002	0.4673	0.01325	0.0023	298.4	9.7	299	14	0.2	329	89	266	46	1.8E+06	1.1E+05	6.1	2.3	699	27	10	742	9	729	1420	190	326000	10000	b.d.l	-
G12b-06-4r	0.339	0.021	0.0481	0.002	0.60736	0.0513	0.0022	0.1795	0.0168	0.0031	303	12	296	16	-2.4	239	94	336	61	1.7E+06	9.3E+04	5.4	1.3	690	17	9	732	8	719	858	34	321000	14000	b.d.l	-
G12b-28-1c	0.355	0.023	0.0486	0.0018	0.37124	0.0522	0.0031	0.3100	0.0148	0.0029	306	11	307	18	0.3	270	120	298	57	1.8E+06	1.3E+05	2	1.2	617	33	3	653	3	642	590	86	309000	12000	b.d.l	-
G12b-06-5c	0.344	0.025	0.0489	0.0023	0.68736	0.0522	0.0026	0.1077	0.0153	0.0038	307	14	300	19	-2.3	280	110	306	76	1.7E+06	9.2E+04	0.6	1.5	542	77	1	572	1	563	299	23	297000	13000	b.d.l	-
G12b-06-10c	0.357	0.023	0.0503	0.0028	0.44915	0.0528	0.0028	0.5067	0.0165	0.0034	316	17	309	17	-2.3	300	110	330	68	1.8E+06	1.0E+05	3.4	1.4	654	26	6	693	5	681	609	25	306000	15000	b.d.l	-
G12b-06-7r	0.353	0.024	0.0511	0.0026	0.66743	0.0515	0.0023	0.1077	0.0169	0.0032	321	16	306	18	-4.9	260	100	339	64	1.7E+06	8.5E+04	2.1	1.5	620	38	4	656	3	645	802	41	311000	14000	b.d.l	-
G12b-28-2c	0.371	0.031	0.0511	0.0031	0.41405	0.0538	0.004	0.3751	0.0177	0.0053	321	19	320	23	-0.3	340	160	353	110	2.2E+06	7.4E+04	2.9	2.4	643	45	5	681	4	669	339	17	318000	19000	b.d.l	-
G12b-28-4m	0.379	0.031	0.053	0.0022	0.3994	0.0497	0.0029	0.2719	0.0176	0.0037	333	14	324	22	-2.8	230	130	352	73	1.8E+06	8.4E+04	2.7	1.4	638	30	5	675	4	664	430	19	308000	10000	b.d.l	-
Stromatic Granulite Br10-6-2																																					
B62-09-2r	0.0332	0.0067	0.00752	0.00074	0.86991	0.0499	0.0032	0.2203	0.0083	0.0024	48.3	4.7	52.6	6.5	8.2	190	140	166	49	2.2E+06	9.0E+04	21.6	3.4	814	16	36	868	31	851	254	22	301000	18000	b.d.l	0.0018
B62-02-1r	0.0752	0.0073	0.01021	0.00041	0.71452	0.0519	0.0034	-0.1841	0.00353	0.00092	65.5	2.6	73.5	6.9	10.9	260	140	71	18	1.7E+06	1.0E+05	12.4	1.7	760	12	21	809	18	794	571	24	296300	7900	b.d.l	0.003
B62-09-3r	0.175	0.018	0.0244	0.0023	0.76073	0.054	0.0027	0.1991	0.0177	0.0035	155	14	163	16	4.9	360	110	354	69	2.1E+06	1.7E+05	36.9	4.5	870	14	62	930	53	912	525	67	298000	30000	b.d.l	0.0037
~~B62-12-2a~~	~~0.225~~	~~0.019~~	~~0.0301~~	~~0.0023~~	~~0.5837~~	~~0.054~~	~~0.0034~~	~~0.3656~~	~~0.0123~~	~~0.0024~~	~~191~~	~~14~~	~~206~~	~~16~~	~~7.3~~	~~350~~	~~130~~	~~247~~	~~42~~	~~1.6E+06~~	~~1.0E+05~~	~~150~~	~~110~~	~~1052~~	~~92~~	~~250~~	~~1139~~	214	1108	~~668~~	~~37~~	~~3.6E+00~~	~~21000~~	~~1.1~~	~~0.0037~~
B62-09-1c	0.277	0.023	0.0406	0.0031	0.1747	0.0496	0.0052	0.6536	0.0144	0.0028	256	19	248	18	-3.2	170	220	289	56	2.2E+06	1.4E+05	19.5	3.2	803	16	33	856	28	840	942	60	312000	16000	0.055	0.055
B62-09-4m	0.279	0.019	0.0409	0.0015	0.30324	0.0486	0.0026	0.4254	0.01309	0.0023	258.1	9.2	249	15	-3.7	120	110	263	45	1.8E+06	9.2E+04	9.8	1.8	739	15	16	786	14	771	582	45	330000	12000	b.d.l	0.0029
B62-08-2r	0.338	0.026	0.0446	0.0031	0.42383	0.0539	0.0045	0.5930	0.0139	0.0024	281	19	295	20	4.7	400	170	279	48	1.9E+06	1.3E+05	14.6	2.2	775	14	24	826	21	810	2770	170	340000	24000	0.099	0.052
B62-08-1c	0.334	0.029	0.0452	0.0028	0.44126	0.0549	0.0035	0.3396	0.0173	0.0035	284	17	295	22	3.7	380	140	346	70	1.8E+06	1.3E+05	4	1.3	666	21	7	707	6	694	253	20	325000	18000	b.d.l	0.0045
B62-11-3c	0.33	0.044	0.0452	0.0035	0.47412	0.0517	0.0055	0.0829	0.0118	0.003	285	21	287	33	0.7	290	230	237	60	2.1E+06	2.2E+05	3.2	1.8	650	33	5	689	5	677	135	12	312000	30000	b.d.l	0.005
B62-12-3r	0.338	0.023	0.0459	0.0027	0.3839	0.0554	0.0031	0.3936	0.0154	0.0027	289	16	295	18	2.0	390	120	309	54	1.8E+06	9.5E+04	13	6.2	765	38	22	814	19	798	755	36	338000	17000	b.d.l	0.0019
B62-11-4c	0.34	0.022	0.0462	0.0025	0.73045	0.0518	0.0019	0.4219	0.01412	0.0023	291	15	296	17	1.7	264	82	283	46	1.7E+06	9.3E+04	11.5	2.2	753	16	19	802	16	787	2920	170	350000	19000	0.054	0.034
B62-06-2c	0.344	0.023	0.0463	0.0022	0.60736	0.0519	0.0025	0.3600	0.01271	0.0021	292	13	299	17	2.3	280	110	255.2	41	1.8E+06	1.1E+05	12.2	1.8	739	13	20	807	17	792	2244	86	356000	17000	0.12	0.038
B62-04-2c	0.3329	0.015	0.04642	0.00089	0.28663	0.0524	0.0015	0.2710	0.01192	0.0021	292.5	5.5	293.6	13	0.4	309	70	240	42	1.9E+06	1.3E+05	10.4	1.6	744	13	17	792	15	777	1406	16	361700	6300	b.d.l	0.02
B62-02-2r	0.344	0.018	0.0477	0.002	0.60042	0.0529	0.002	0.6065	0.0141	0.0024	300	12	299	14	-0.3	308	83	283	48	1.6E+06	7.6E+04	6.6	1.6	706	18	11	749	9	736	1370	180	503000	14000	0.03	0.035
~~B62-02-3r~~	~~0.386~~	~~0.023~~	~~0.0481~~	~~0.0016~~	~~0.49869~~	~~0.0531~~	~~0.0032~~	~~0.3545~~	~~0.01491~~	~~0.0033~~	~~303~~	~~10~~	~~339~~	~~15~~	~~10~~	~~313~~	~~94~~	~~339~~	~~49~~	~~1.7E+06~~	~~9.6E+04~~	~~5.3~~	~~1.1~~	688	15	9	730	8	717	~~1314~~	~~37~~	~~360700~~	~~8500~~	~~1.1~~	~~0.02~~
B62-11-1c	0.357	0.028	0.0484	0.0026	0.45977	0.0541	0.0036	0.2539	0.01516	0.0025	304	16	312	22	2.6	330	140	304	50	1.7E+06	1.1E+05	5.6	1.6	692	20	9	735	8	722	1286	57	346000	20000	b.d.l	0.015
B62-04-1r	0.343	0.021	0.0487	0.001	0.17274	0.0516	0.0023	0.2415	0.0156	0.003	306.5	6.3	299	16	-2.5	255	95	313	60	1.8E+06	1.2E+05	4.7	1.2	679	18	8	720	7	707	548	17	339000	9200	b.d.l	0.0022
B62-12-1r	0.351	0.03	0.0488	0.0037	0.65902	0.0543	0.0033	0.4284	0.0141	0.0025	307	23	307	23	0.0	360	130	283	50	1.7E+06	1.1E+05	5.9	1.6	697	20	10	739	8	726	602	39	348000	24000	b.d.l	0.0037
B62-11-5c	0.342	0.025	0.0491	0.0028	0.59722	0.0509	0.0028	0.2966	0.01407	0.0023	309	17	304	20	-1.6	220	110	282	47	1.8E+06	9.4E+04	8.6	1.6	728	15	14	774	12	759	1872	99	343000	23000	0.143	0.045
B62-06-1r	0.361	0.034	0.0498	0.0026	0.40528	0.0522	0.0036	0.2094	0.0122	0.0035	313	16	315	25	0.6	260	140	245	70	1.8E+06	1.2E+05	5.2	1.3	687	18	9	729	7	716	187	13	352000	21000	b.d.l	0.0021
B62-08-3r	0.344	0.028	0.0498	0.0027	0.23173	0.051	0.0039	0.5801	0.0152	0.0028	313	17	299	21	-4.7	220	160	305	55	1.7E+06	1.1E+05	3.06	0.92	647	19	5	685	4	673	425	28	337000	17000	b.d.l	0.0033
B62-11-2m	0.36	0.035	0.0521	0.0035	0.27837	0.0499	0.0044	0.4229	0.0151	0.0033	327	21	310	26	-5.5	210	180	303	65	1.8E+06	1.2E+05	6	1.7	698	20	10	741	9	728	280	27	324000	19000	b.d.l	0.0028

Notes:

abs = absolute

rho = correlation coefficient between the ratios

% Discord. 6/38-7/35 = 100 - (100 * (206Pb/238U date) / (207Pb/235U date))

cps = counts per second

b.d.l = below detection limit

nd = not determined

Bold analyses are used in age calculations in Figure 8

~~Strikethrough~~ analyses – evidence for sibelating Ti-rich inclusions

Ce (ppm)	± 2SE (ppm)	Pr (ppm)	± 2SE (ppm)	Nd (ppm)	± 2SE (ppm)	Sm (ppm)	± 2SE (ppm)	Eu (ppm)	± 2SE (ppm)	Gd (ppm)	± 2SE (ppm)	Dy (ppm)	± 2SE (ppm)	Er (ppm)	± 2SE (ppm)	Yb (ppm)	± 2SE (ppm)	Hf (ppm)	± 2SE (ppm)	Th (ppm)	± 2SE (ppm)	U (ppm)	± 2SE (ppm)	Th/U	Chondrite-normalized REE values														Sample and Analysis Number
																									La	Ce	Pr	Nd	Pm	Sm	Eu	Eu/Eu*	Gd	Tb	Dy	Ho	Er	Tm	Yb	Lu	Yb/Dy	
Leucogranulite GR11-37																																							
0.158	0.032	0.0057	0.0057	b.d.l	-	0.12	0.18	0.074	0.032	1.31	0.35	15.24	0.99	51.4	1.6	228	4.7	14500	470	6.15	0.37	2189	76	0.003	b.d.l	0.26	0.061	-0.07	nd	0.8	1.31	0.36	6.6	nd	62.0	nd	321	nd	1416	nd	22.9	G37D3-11-1r
0.302	0.073	0.0015	0.008	0.032	0.052	0.08	0.27	0.056	0.034	2.06	0.5	15.8	1.9	45	2.8	190	10	15150	460	5.24	0.72	1410	180	0.004	b.d.l	0.49	0.016	0.07	nd	0.5	0.99	0.18	10.4	nd	64.2	nd	281	nd	1180	nd	18.4	G37D3-11-3r
0.44	0.11	0.03	0.016	0.3	0.15	0.3	0.33	0.001	0.018	0.34	0.21	3.93	0.49	11.62	0.99	53.1	2.7	15030	680	1.77	0.27	786	34	0.002	b.d.l	0.72	0.323	0.66	nd	2.0	0.02	0.01	1.7	nd	16.0	nd	73	nd	330	nd	20.6	G37D2-01-2r
0.6	**0.13**	**0.005**	**0.016**	**0.041**	**0.062**	**0.39**	**0.46**	**0.223**	**0.094**	**2.37**	**0.8**	**32.2**	**2.8**	**64**	**5.8**	**219**	**21**	**12500**	**1400**	**16**	**1.3**	**2300**	**220**	**0.007**	**b.d.l**	**0.98**	**0.1054**	**0.119**	**nd**	**2.6**	**3.96**	**0.54**	**11.9**	**nd**	**130.9**	**nd**	**400**	**nd**	**1360**	**nd**	**10.4**	**G37D3-04-2r**
0.194	**0.047**	**0.016**	**0.013**	**0.026**	**0.052**	**0.26**	**0.22**	**0.088**	**0.036**	**1.16**	**0.33**	**10.2**	**1.2**	**38**	**3.6**	**215**	**21**	**15400**	**1400**	**2.38**	**0.34**	**1170**	**100**	**0.002**	**b.d.l**	**0.32**	**0.172**	**0.06**	**nd**	**1.8**	**1.56**	**0.41**	**5.8**	**nd**	**41.5**	**nd**	**238**	**nd**	**1335**	**nd**	**32.2**	**G37D3-10-1r**
0.53	0.12	0.014	0.011	b.d.l	0.032	0.14	0.2	0.075	0.039	1.31	0.32	9.5	1	32.1	3.6	181	22	14600	1600	3	0.38	668	87	0.004	b.d.l	0.86	0.151	b.d.l	nd	0.9	1.33	0.35	6.6	nd	38.6	nd	201	nd	1124	nd	29.1	G37D3-10-2m
0.138	**0.044**	**0.021**	**0.014**	**0.17**	**0.11**	**0.52**	**0.25**	**0.107**	**0.058**	**1.72**	**0.41**	**16.7**	**2**	**48**	**12**	**187**	**67**	**18560**	**380**	**1.91**	**0.35**	**1270**	**280**	**0.002**	**b.d.l**	**0.23**	**0.226**	**0.37**	**nd**	**3.5**	**1.90**	**0.31**	**8.6**	**nd**	**67.9**	**nd**	**300**	**nd**	**1161**	**nd**	**17.1**	**G37D3-11-2r**
0.306	**0.051**	**b.d.l**	-	**0.044**	**0.062**	**0.03**	**0.22**	**0.049**	**0.027**	**0.26**	**0.19**	**4.85**	**0.74**	**9.7**	**1**	**29.1**	**3.2**	**16100**	**1100**	**2.5**	**0.32**	**527**	**53**	**0.005**	**b.d.l**	**0.50**	**b.d.l**	**0.10**	**nd**	**0.2**	**0.87**	**1.15**	**1.3**	**nd**	**19.7**	**nd**	**61**	**nd**	**181**	**nd**	**9.2**	**G37D2-03-2r**
0.21	**0.12**	**0.015**	**0.014**	**0.014**	**0.078**	**0.15**	**0.43**	**0.059**	**0.068**	**0.66**	**0.38**	**7.4**	**1.5**	**22.7**	**3.1**	**89**	**11**	**13940**	**900**	**1.23**	**0.41**	**670**	**59**	**0.002**	**b.d.l**	**0.34**	**0.162**	**0.03**	**nd**		**1.05**	**0.63**	**3.3**	**nd**	**30.1**	**nd**	**142**	**nd**	**553**	**nd**	**18.4**	**G37D1-13-1r**
0.254	**0.066**	**0.005**	**0.011**	**0.085**	**0.073**	**0.1**	**0.2**	**0.021**	**0.025**	**0.76**	**0.25**	**6.84**	**0.68**	**15.6**	**1.1**	**45.4**	**3.1**	**16070**	**900**	**1.62**	**0.25**	**604**	**38**	**0.003**	**b.d.l**	**0.41**	**0.054**	**0.19**	**nd**	**0.7**	**0.37**	**0.17**	**3.8**	**nd**	**27.8**	**nd**	**98**	**nd**	**282**	**nd**	**10.1**	**G37D2-03-1r**
0.06	**0.022**	**0.0062**	**0.0094**	**b.d.l**	-	**-0.22**	**0.2**	**0.02**	**0.023**	**0.5**	**0.22**	**5.88**	**0.76**	**20.9**	**2.9**	**117**	**14**	**10960**	**570**	**0.86**	**0.14**	**817**	**54**	**0.001**	**b.d.l**	**0.10**	**0.067**	**b.d.l**	**nd**	**b.d.l**	**0.36**	–	**2.5**	**nd**	**23.9**	**nd**	**131**	**nd**	**727**	**nd**	**30.4**	**G37D2-11-1c**
0.579	**0.047**	**b.d.l**	-	**0.064**	**0.056**	**0.39**	**0.27**	**0.103**	**0.046**	**1.86**	**0.51**	**18.3**	**1.7**	**46.7**	**4.1**	**191**	**22**	**12800**	**1300**	**8.52**	**0.97**	**2360**	**270**	**0.004**	**b.d.l**	**0.46**	**b.d.l**	**0.12**	**nd**	**2.6**	**1.83**	**0.31**	**9.3**	**nd**	**74.4**	**nd**	**292**	**nd**	**1186**	**nd**	**15.9**	**G37D3-04-1r**
1.16	0.19	0.029	0.018	0.4	0.13	0.51	0.33	0.333	0.065	4.49	0.74	29.9	2.8	57.3	6	204	19	13400	1000	16.7	2.2	2010	230	0.008	b.d.l	1.89	0.313	0.88	nd	3.4	5.91	0.45	22.6	nd	121.5	nd	538	nd	1267	nd	10.4	G37D3-06-1r
0.313	0.092	0.009	0.01	0.196	0.097	0.02	0.23	0.072	0.026	0.93	0.27	12.1	1	36.7	3.1	176	17	13620	480	2.61	0.5	688	44	0.004	b.d.l	0.51	0.097	0.43	nd	0.1	1.28	0.53	4.7	nd	49.2	nd	229	nd	1093	nd	22.2	G37D2-11-2r
0.397	0.057	0.021	0.012	0.119	0.071	0.27	0.25	0.135	0.034	2.52	0.53	19.9	2.7	43.4	4.7	160	16	12810	870	8.13	0.85	1540	120	0.005	b.d.l	0.65	0.226	0.26	nd	1.8	2.40	0.33	12.7	nd	80.9	nd	271	nd	994	nd	12.3	G37D3-04-3c
~~20.2~~	~~2.3~~	~~0.196~~	~~0.033~~	~~2.9~~	~~0.45~~	~~1.5~~	~~0.48~~	~~1.91~~	~~0.3~~	~~47.8~~	~~5~~	~~42~~	~~5.1~~	~~19.5~~	~~1.9~~	~~31.8~~	~~2.8~~	~~14000~~	~~1300~~	~~204~~	~~14~~	~~603~~	~~46~~	~~0.338~~	~~b.d.l~~	~~48.45~~	~~3.119~~	~~8.52~~	~~nd~~	~~57.8~~	~~22.92~~	0.21	~~340.2~~	~~nd~~	~~109.1~~	~~nd~~	~~120~~	~~nd~~	~~1.35~~	~~nd~~	~~0.7~~	~~G37D2-09-1c~~
0.39	0.12	0.035	0.018	0.25	0.11	0.5	0.34	0.087	0.048	2.7	1.2	9.4	2.8	15.6	1.7	56	4.6	13540	930	3.7	1.4	419	30	0.009	b.d.l	0.64	0.377	0.55	nd	3.4	1.55	0.18	13.6	nd	38.2	nd	98	nd	348	nd	9.1	G37D2-02-5r
1.58	0.51	0.158	0.065	0.99	0.4	0.87	0.51	0.13	0.1	1.47	0.7	11.8	1.1	33.6	4.5	170	30	11500	1000	25	10	520	100	0.048	0.084	2.58	1.703	2.17	nd	5.9	2.31	0.35	7.4	nd	48.0	nd	210	nd	1056	nd	22.0	G37D3-05-1r
0.12	0.044	0.0043	0.0094	b.d.l	-	b.d.l	-	1.1	0.34	5.51	0.53	20	1.5	98.4	6.5	1464.0	920	0.88	0.16	911	42	0.001	b.d.l	0.20	0.046	0.00	nd	-1.7	-0.78	-0.41	5.5	nd	22.4	nd	125	nd	611	nd	27.3	G37D2-01-1r
0.139	0.055	0.013	0.03	0.15	0.18	0.16	0.82	0.035	0.045	0.44	0.53	2.51	0.13	8.85	0.65	37.9	3.4	12500	1300	1.03	0.36	172	16	0.006	b.d.l	0.23	0.140	0.33	nd	1.1	0.62	0.38	2.2	nd	10.2	nd	5.5	nd	23.5	nd	23.1	G37D3-04-1r
0.61	0.12	0.0089	0.0082	0.003	0.034	0.13	0.13	0.113	0.041	2.27	0.46	1.5	1	35.5	1.8	148.3	8.4	13950	630	5.66	0.93	481	26	0.012	b.d.l	1.00	0.096	0.01	nd	0.9	2.01	0.33	11.4	nd	61.0	nd	222	nd	921	nd	15.1	G37D3-09-2r
1.71	0.25	0.103	0.051	0.3	0.17	1.42	0.67	0.123	0.054	6.7	1.2	38.2	3.7	79.4	9.5	274	36	13400	1500	28.4	4.9	752	93	0.038	1.983	2.79	1.110	0.66	nd	9.6	2.17	0.10	33.7	nd	155.3	nd	496	nd	1702	nd	11.0	G37D2-08-2r
1.31	0.48	0.017	0.012	0.13	0.15	0.41	0.31	0.048	0.051	3.3	1.3	20.3	3.8	40	10	123	33	11780	760	30	10	183	37	0.164	b.d.l	2.14	0.183	0.28	nd	2.8	0.85	0.09	16.6	nd	82.5	nd	230	nd	764	nd	9.3	G37D2-10-1r
1.34	0.16	0.037	0.017	0.15	0.12	0.75	0.24	0.113	0.039	2.56	0.56	15.6	1.4	42.5	3.5	122.8	7.9	10050	570	17.6	1.1	234	15	0.075	b.d.l	2.19	0.399	0.33	nd	5.1	2.01	0.22	12.9	nd	63.4	nd	266	nd	763	nd	12.0	G37D2-10-2r
1.31	0.18	0.099	0.03	2.08	0.31	6.18	0.9	0.45	0.1	30.1	3.4	60.9	4.8	42.1	4.3	63.6	7.4	9390	970	39	3.7	153	17	0.255	b.d.l	2.14	1.067	4.55	nd	41.8	7.99	0.08	151.3	nd	247.6	nd	263	nd	395	nd	1.6	G37D2-02-2r
5.01	0.82	0.242	0.086	1.08	0.42	1.05	0.39	0.172	0.067	4.69	0.62	31.1	2.4	72.2	5.5	233	18	12070	990	56.2	4.6	794	76	0.071	3.418	8.17	2.608	2.36	nd	7.1	3.06	0.20	23.6	nd	126.4	nd	451	nd	1447	nd	11.4	G37D2-08-1r
8.3	1.5	0.5	0.13	3.02	0.61	5.9	1	0.6	0.16	39.5	2.9	162.2	8.8	207	12	487	36	11050	710	93	8.6	837	50	0.111	2.278	13.54	5.388	6.61	nd	39.9	10.66	0.09	198.5	nd	659.3	nd	1294	nd	3025	nd	4.6	G37D1-09-2
0.804	0.087	0.087	0.024	1.83	0.39	7.69	0.77	0.54	0.13	39	3.4	75	3.9	52.3	3.2	67.3	4.6	9370	450	38.9	2.3	195.9	9.8	0.199	b.d.l	1.31	0.938	4.00	nd	52.0	9.59	0.08	196.0	nd	304.9	nd	327	nd	418	nd	1.4	G37D2-01-3r
1.31	0.16	0.095	0.024	2.84	0.4	12.1	1.5	0.635	0.085	76.7	7.9	201	15	160	13	265	18	11970	820	144	16	1009	80	0.143	b.d.l	2.14	1.024	6.21	nd	81.8	11.28	0.05	385.4	nd	817.1	nd	1000	nd	1646	nd	2.0	G37D3-06-2r
3	1.1	0.159	0.041	3.73	0.86	9.2	1.4	0.9	0.25	49.2	7.4	147	25	128	26	206	52	12800	3000	124	26	336	83	0.369	b.d.l	4.89	1.713	8.16	nd	62.2	15.99	0.10	247.2	nd	597.6	nd	800	nd	1280	nd	2.1	G37D3-10-4c
0.321	0.054	0.033	0.011	0.27	0.11	0.56	0.25	0.031	0.025	4.1	0.81	26.3	3.4	29.1	3.8	52.8	4.8	12510	720	4.48	0.51	227	18	0.020	b.d.l	0.52	0.356	0.59	nd	3.8	0.55	0.05	20.6	nd	106.9	nd	182	nd	326	nd	3.1	G37D2-03-4m
15.3	1.2	0.435	0.066	8.12	0.94	15.3	1	1.96	0.2	70	5.1	253	14	354	22	695	54	7830	500	231	17	369	26	0.680	0.038	24.96	4.903	17.77	nd	103.4	34.81	0.15	351.8	nd	1028.5	nd	2213	nd	4317	nd	4.2	G37D2-04-4c
1.09	0.32	0.02	0.023	0.45	0.22	2.01	0.64	0.128	0.061	1.68	4.1	11.3	28	204	49	5.50	120	13940	620	44	14	1300	220	0.033	b.d.l	1.78	0.216	0.98	nd	13.6	2.27	0.05	84.4	nd	459.3	nd	1275	nd	3416	nd	7.4	G37D1-13-2r
2.64	0.33	0.046	0.019	0.75	0.21	1.84	0.62	0.23	0.068	21.4	4.2	169	27	338	42	8.50	110	10900	540	84	12	1210	140	0.069	0.169	4.31	0.496	1.64	nd	12.4	4.09	0.07	107.5	nd	687.0	nd	2113	nd	5280	nd	7.7	G37D3-02-1c
3.92	0.58	0.295	0.049	7.01	0.59	26.4	2.5	1.6	0.16	147	15	286	30	173	17	187	22	11400	1200	416	47	1120	130	0.371	0.063	6.39	3.179	15.34	nd	178.4	28.42	0.06	738.7	nd	1162.6	nd	1081	nd	1161	nd	1.0	G37D3-10-3c
1.29	0.13	0.089	0.027	1.96	0.24	6.88	0.73	0.58	0.1	31.8	2.9	66.8	5.4	46.4	4.4	62.5	6.2	8790	660	47.2	3.5	133	10	0.355	b.d.l	2.10	0.959	4.29	nd	46.5	10.30	0.10	159.8	nd	271.5	nd	290	nd	388	nd	1.4	G37D2-02-1r
5.6	0.45	b.d.l	-	0.37	0.12	0.89	0.28	0.105	0.034	5.87	0.74	33.9	3.4	65.3	5	181	18	10990	730	53.8	5.3	265	27	0.203	b.d.l	9.14	b.d.l	0.81	nd	6.0	1.87	0.11	29.5	nd	137.8	nd	408	nd	1124	nd	8.2	G37D2-06-1r
15.5	1.9	0.49	0.25	3.1	1.3	3.41	0.83	0.321	0.051	14.4	1.3	62.5	3.4	114.5	6.8	283	18	8940	540	124.4	7.9	322	23	0.386	2.700	25.29	5.280	6.78	nd	23.0	5.70	0.12	72.4	nd	254.1	nd	716	nd	1738	nd	6.9	G37D2-06-1c
1.52	0.56	0.2	0.15	2.21	0.96	5.53	0.86	0.392	0.084	30.6	3.7	73.8	8.4	47.9	7	70	12	8800	1100	50.6	7.7	278	41	0.182	0.380	2.48	2.155	4.84	nd	37.4	6.96	0.07	153.8	nd	308.1	nd	299	nd	435	nd	1.4	G37D2-02-4c
8	1.4	0.013	0.017	0.21	0.1	1.35	0.5	0.052	0.043	1.36	3.4	84	19	168	33	408	67	11500	930	200	5.5	1100	210	0.209	b.d.l	13.05	0.140	0.46	nd	9.1	0.89	0.02	68.3	nd	341.5	nd	1050	nd	2534	nd	7.4	G37D2-08-3c
0.5	0.078	0.043	0.021	0.74	0.2	4.06	0.53	0.213	0.049	35.4	2.3	138	5.5	115.1	4.4	182	8.6	11030	490	26.4	2	651	22	0.041	b.d.l	0.82	0.463	1.62	nd	27.4	3.78	0.04	177.9	nd	561.0	nd	719	nd	1130	nd	2.0	G37D2-03-3c
1.65	0.27	0.094	0.042	1.66	0.3	9.93	0.85	0.6	0.1	67.3	5.4	271	17	318	22	718	61	9530	760	77	12	979	72	0.079	0.371	2.69	1.013	3.63	nd	67.1	10.66	0.05	338.2	nd	1101.6	nd	1988	nd	4460	nd	4.0	G37D1-09-1
1.03	0.088	b.d.l	-	0.027	0.039	b.d.l	-	0.133	0.047	1.94	0.42	10.6	1.1	26.9	2.3	93.9	8.9	8370	510	9.63	0.86	175	13	0.055	b.d.l	1.68	-0.041	0.06	nd	-0.7	2.36	0.52	9.7	nd	43.1	nd	168	nd	583	nd	13.5	G37D2-04-3r
0.674	0.064	0.091	0.027	1.63	0.31	9.7	1.2	0.396	0.067	75	6.8	225	18	154	15	222	16	10070	570	46.1	5.3	934	78	0.049	0.051	1.10	0.981	3.57	nd	65.5	7.03	0.03	376.9	nd	914.6	nd	963	nd	1379	nd	1.5	G37D2-05m
1.08	0.11	0.056	0.017	1.75	0.29	5.89	0.78	0.446	0.06	36.5	3.1	72.8	4.4	48.4	3.4	70.6	6.9	9210	730	54.6	3.9	259	21	0.211	b.d.l	1.76	0.603	3.83	nd	39.8	7.92	0.07	183.4	nd	295.9	nd	303	nd	439	nd	1.5	G37D2-02-3c
5.85	0.5	0.07	0.023	1.14	0.2	3.07	0.44	0.61	0.11	16.5	1.3	70.1	4.8	117.3	9.6	248	16	7710	500	60.3	4.3	180	15	0.335	b.d.l	9.54	0.754	2.49	nd	20.7	10.83	0.21	82.9	nd	285.0	nd	733	nd	1540	nd	5.4	G37D3-04-2r
0.164	0.091	0.033	0.021	0.19	0.12	0.77	0.4	0.046	0.033	2.9	1.2	21.2	7	30.6	8.9	82	17	12190	840	2.66	0.85	198	30	0.013	0.076	0.27	0.356	0.42	nd	5.2	0.82	0.08	14.6	nd	86.2	nd	191	nd	509	nd	5.9	G37D3-02-2r
Residual Granulite GR11-12B																																						
7.12	**0.5**	**0.219**	**0.036**	**4.28**	**0.48**	**14.5**	**1.1**	**2.35**	**0.22**	**61.8**	**4.4**	**49.5**	**2.7**	**11.6**	**1.2**	**8.2**	**1.3**	**10650**	**500**	**141**	**10**	**1015**	**53**	**0.139**	**b.d.l**	**11.62**	**2.360**	**9.37**	**nd**	**98.0**	**41.74**	**0.20**	**310.6**	**nd**	**201.2**	**nd**	**73**	**nd**	**51**	**nd**	**0.3**	**G12b-14-1m**
5.42	**0.3**	**0.075**	**0.023**	**1.9**	**0.27**	**4.54**	**0.72**	**0.416**	**0.077**	**32.1**	**2.1**	**145**	**14**	**174**	**19**	**323**	**33**	**10840**	**440**	**101.3**	**6.3**	**448**	**47**	**0.226**	**b.d.l**	**8.84**	**0.808**	**4.16**	**nd**	**30.7**	**7.39**	**0.08**	**161.3**	**nd**	**589.4**	**nd**	**1088**	**nd**	**2006**	**nd**	**3.4**	**G12b-14-6r**
4.67	**0.68**	**0.083**	**0.038**	**2.32**	**0.8**	**5.9**	**1.8**	**0.8**	**0.15**	**29**	**6**	**52.1**	**5.2**	**44.6**	**8**	**72**	**15**	**11000**	**1400**	**80**	**21**	**830**	**130**	**0.096**	**b.d.l**	**7.62**	**0.894**	**5.08**	**nd**	**39.9**	**14.21**	**0.15**	**145.7**	**nd**	**211.8**	**nd**	**279**	**nd**	**447**	**nd**	**2.1**	**G12b-14-4c**
~~6.03~~	~~0.42~~	~~0.108~~	~~0.045~~	~~1.63~~	~~0.27~~	~~5.47~~	~~0.62~~	~~0.293~~	~~0.083~~	~~40.8~~	~~3~~	~~21.1~~	~~3.4~~	~~288~~	~~14~~	~~5.48~~	~~32~~	~~30020~~	~~7.48~~	~~112.8~~	~~5.4~~	~~365~~	~~20~~	~~0.309~~	~~b.d.l~~	~~9.84~~	~~1.176~~	~~3.67~~	~~nd~~	~~27.9~~	~~6.29~~	~~0.04~~	~~208.5~~	~~nd~~	~~387.7~~	~~nd~~	~~1896~~	~~nd~~	~~2410~~	~~nd~~	~~4.0~~	~~G12b-14-2c~~
~~8.71~~	~~0.66~~	~~0.065~~	~~0.041~~	~~1.98~~	~~0.36~~	~~4.9~~	~~1.3~~	~~0.328~~	~~0.066~~	~~42.6~~	~~4.9~~	~~247~~	~~20~~	~~328~~	~~16~~	~~6.10~~	~~49~~	~~9770~~	~~9.30~~	~~108~~	~~11~~	~~496~~	~~44~~	~~0.218~~	~~b.d.l~~	~~9.21~~	~~0.700~~	~~4.23~~	~~nd~~	~~22.1~~	~~6.82~~	~~0.08~~	~~214.1~~	~~nd~~	~~380.1~~	~~nd~~	~~2050~~	~~nd~~	~~2780~~	~~nd~~	~~2.8~~	~~G12b-14-1r~~
5.53	0.35	0.103	0.027	1.93	0.21	6.19	0.65	1.06	0.12	34.1	2.6	64.1	5.5	59.4	8.9	101	19	11420	620	100.3	5.7	763	57	0.131	b.d.l	9.05	1.110	4.22	nd	41.8	18.83	0.18	171.4	nd	260.6	nd	371	nd	627	nd	2.4	G12b-14-6r
3.18	0.37	0.219	0.062	3.84	0.77	7.4	1.3	0.376	0.097	32.6	4.3	77.1	8.6	91	7.4	245	17	12040	720	101	1.5	762	60	0.133	b.d.l	5.19	2.360	8.40	nd	50.0	6.68	0.06	163.8	nd	313.4	nd	569	nd	1522	nd	4.9	G12b-11-5-1
~~16.5~~	~~7.1~~	~~10.2~~	~~8.7~~	~~3.5~~	~~3.2~~	~~20.3~~	~~8.7~~	~~2.83~~	~~0.4~~	~~49.6~~	~~7.3~~	~~20.1~~	~~2.4~~	~~40.8~~	~~5.2~~	~~107.0~~	~~14.0~~	~~8430~~	~~4.90~~	~~2210~~	~~59.0~~	~~2670~~	~~41.0~~	~~0.628~~	~~20.1.69~~	~~269.17~~	~~109.9.14~~	~~76.5.9~~	~~nd~~	~~127.3~~	~~59.37~~	0.26	~~244.3~~	~~nd~~	~~614.3~~	~~nd~~	~~23.50~~	~~nd~~	~~66.46~~	~~nd~~	~~3.1~~	~~G12b-27-2c~~
180	160	10	1.1	37	39	13	9.5	0.92	0.52	21.7	5.2	82.1	7.6	186	20	650	92	16500	1500	202	49	2220	280	0.091	299.578	293.64	107.7.59	80.86	nd	87.8	16.34	0.17	109.0	nd	333.7	nd	1163	nd	3851	nd	11.5	G12b-17-1
32.8	2.2	0.187	0.093	4.71	0.91	14.1	1.2	0.99	0.21	85.1	5.2	470	76	830	150	1870	330	10390	920	1090	260	2690	670	0.403	b.d.l	53.51	2.015	10.31	nd	95.3	17.58	0.07	427.6	nd	1910.6	nd	5188	nd	11615	nd	6.1	G12b-20-2c
9.3	1.2	0.034	0.02	0.55	0.17	2.21	0.63	0.233	0.069	20.8	2.5	119	14	265	28	649	76	10920	730	254	40	1100	170	0.231	b.d.l	15.17	0.366	1.20	nd	14.9	4.49	0.08	104.5	nd	483.7	nd	1656	nd	4031	nd	8.3	G12b-24-5c
20.4	2.6	0.039	0.019	1	0.23	5.06	0.65	0.26	0.065	42.6	3.7	295	18	607	39	1404	88	12320	510	831	78	3410	180	0.244	b.d.l	33.28	0.420	2.19	nd	34.2	4.62	0.04	214.1	nd	1199.2	nd	3794	nd	8720	nd	7.3	G12b-24-9r
32	1.5	0.394	0.05	6.97	0.7	13.4	1.2	1.85	0.19	65.6	4.7	268	17	474	23	1184	76	7810	350	560	35	1214	91	0.461	b.d.l	52.20	4.246	15.25	nd	90.5	32.86	0.16	329.6	nd	1089.4	nd	2963	nd	7354	nd	6.8	G12b-28-3c
71	10	0.58	0.1	10.4	1.5	22.3	3.4	4.39	0.59	109	13	429	52	630	74	1360	140	7990	410	1060	170	1060	120	1.000	b.d.l	115.82	6.250	22.76	nd	150.7	77.98	0.22	547.7	nd	1743.9	nd	3938	nd	8447	nd	4.8	G12b-06-3c
32.5	8.9	0.21	0.11	3.8	1.7	9.3	3.4	1.88	0.64	48	17	217	66	380	110	920	220	8700	610	420	130	590	140	0.712	b.d.l	53.02	2.263	8.32	nd	62.8	33.39	0.22	241.2	nd	882.1	nd	2375	nd	5714	nd	6.5	G12b-06-9c
15.36	0.9	0.108	0.039	2.27	0.42	5.2	1	1.23	0.14	33.4	2	172.5	8	334	15	785	39	7830	580	288	19	526	24	0.567	b.d.l	25.06	1.164	4.97	nd	35.1	21.85	0.22	167.8	n

Ce (ppm)	± 2SE (ppm)	Pr (ppm)	± 2SE (ppm)	Nd (ppm)	± 2SE (ppm)	Sm (ppm)	± 2SE (ppm)	Eu (ppm)	± 2SE (ppm)	Gd (ppm)	± 2SE (ppm)	Dy (ppm)	± 2SE (ppm)	Er (ppm)	± 2SE (ppm)	Yb (ppm)	± 2SE (ppm)	Hf (ppm)	± 2SE (ppm)	Th (ppm)	± 2SE (ppm)	U (ppm)	± 2SE (ppm)	Th/U	Chondrite-normalized REE values															Sample and Analysis Number
																									La	Ce	Pr	Nd	Pm	Sm	Eu	Eu/Eu*	Gd	Tb	Dy	Ho	Er	Tm	Yb	Lu	Yb/Dy	
6.97	0.45	0.012	0.015	0.48	0.14	1.2	0.4	0.104	0.046	8.1	1	54.6	3.9	107.2	6.9	300	24	11090	680	69	4.9	290	23	0.238	bdl	11.37	0.129	1.05	nd	8.1	1.85	0.08	40.7	nd	222.0	nd	670	nd	1863	nd	8.4	G12b-01-2c
5.37	0.79	bdl	-	bdl	-	0.69	0.41	0.114	0.084	7.4	1.5	43.7	5.7	98	10	347	48	11600	1400	85.8	8.3	763	98	0.112	bdl	8.76	bdl	bdl	nd	4.7	2.02	0.10	37.2	nd	177.6	nd	613	nd	2155	nd	12.1	G12b-06-11s
6.99	0.45	0.029	0.017	0.21	0.11	1.2	0.4	0.078	0.034	11.3	1.3	70.9	5.2	157	11	389	25	11090	390	131	12	622	38	0.211	bdl	11.40	0.313	0.46	nd	8.1	1.39	0.04	56.8	nd	288.2	nd	981	nd	2416	nd	8.4	G12b-3-62m
16.5	1.9	0.029	0.014	0.77	0.14	4.43	0.65	0.165	0.041	38.6	4.7	262	39	509	74	1240	190	13400	1200	470	78	2170	430	0.217	bdl	26.92	0.313	1.68	nd	29.9	2.93	0.03	194.0	nd	1065.0	nd	3181	nd	7702	nd	7.2	G12b-01-1r
12.06	0.79	0.038	0.021	0.61	0.19	2.23	0.42	0.256	0.054	16.9	1.9	105.2	6.4	196.9	9.3	507	32	10290	520	242	13	921	63	0.263	bdl	19.67	0.409	1.33	nd	15.1	4.55	0.09	84.9	nd	427.6	nd	1231	nd	3149	nd	7.4	G12b-062r
9.36	0.45	0.061	0.025	1.19	0.27	3.22	0.74	0.55	0.11	22.5	2	118.3	5.6	218	8.1	475	15	9200	340	123.6	4.1	320	11	0.386	bdl	15.27	0.657	2.60	nd	21.8	9.77	0.14	113.1	nd	480.9	nd	1363	nd	2950	nd	6.1	G12b-33-1r
~~48~~	~~11~~	~~0.65~~	~~0.15~~	~~10.8~~	~~3.9~~	~~19.6~~	~~4.9~~	~~3.96~~	~~0.82~~	~~9.8~~	~~2.5~~	~~33.3~~	~~8.3~~	~~68.5~~	~~9.7~~	~~148.9~~	~~18.5~~	~~6830~~	~~430~~	~~450~~	~~160~~	~~844~~	~~83~~	~~0.270~~	bdl	78.30	5.927	23.65	nd	13.2.4	59.68	0.21	~~427.1~~	nd	~~1353.7~~	nd	~~3175~~	nd	~~7329~~	nd	5.4	~~G12b-06-4e~~
16.9	2	0.116	0.04	1.61	0.32	4.3	1.1	0.7	0.16	19.3	2.7	95	10	170	16	329	35	9140	440	417	41	803	48	0.519	bdl	27.57	1.250	3.52	nd	29.1	12.43	0.20	97.0	nd	386.2	nd	1069	nd	3286	nd	8.5	G12b-074-1c
23	1.2	0.036	0.014	1.02	0.2	4.63	0.71	0.171	0.039	44.9	2.6	283	11	602	27	1420	75	12980	690	884	42	3640	190	0.243	bdl	37.52	0.388	2.23	nd	31.3	3.04	0.02	225.6	nd	1150.4	nd	3763	nd	8820	nd	7.7	G12b-24-8m
6.81	0.26	bdl	-	0.26	0.11	0.93	0.39	0.073	0.039	8.19	0.79	57.7	2.5	132.5	4.5	346	15	9970	370	88.7	3.7	461	21	0.192	bdl	11.11	0.000	0.57	nd	6.3	1.33	0.06	41.2	nd	234.6	nd	828	nd	2149	nd	9.2	G12b-28-5m
16.3	2	0.019	0.02	0.74	0.2	3.49	0.71	0.323	0.07	21	3.1	117	17	238	30	539	69	10230	280	313	63	810	150	0.386	bdl	26.59	0.205	1.62	nd	23.6	5.74	0.09	105.5	nd	475.6	nd	1488	nd	3348	nd	7.0	G12b-26-1c
7.97	0.56	0.012	0.013	0.32	0.12	1.12	0.41	0.159	0.05	12.2	1	73.4	4.4	149.1	7.7	403	23	10830	500	102.4	5.5	457	26	0.224	bdl	13.00	0.129	0.70	nd	7.6	2.82	0.08	61.3	nd	298.4	nd	932	nd	2503	nd	8.4	G12b-064r
11.4	2	0.029	0.015	0.41	0.14	1.19	0.62	0.232	0.063	8.6	2	50.3	8.1	99	14	243	32	10410	490	93	19	273	41	0.341	bdl	18.60	0.313	0.90	nd	8.0	4.12	0.16	43.2	nd	204.5	nd	619	nd	1509	nd	7.4	G12b-28-1c
5.16	0.43	0.04	0.024	0.28	0.13	0.46	0.49	0.031	0.037	4.18	0.69	27.8	2.8	55.4	5	149	10	10220	400	35.5	2.7	187	15	0.190	bdl	8.42	0.431	0.61	nd	3.1	0.55	0.05	21.0	nd	113.0	nd	346	nd	925	nd	8.2	G12b-065c
8.11	0.44	0.017	0.012	0.38	0.14	0.56	0.46	0.216	0.053	9.4	0.9	54.7	3.5	106.2	5.8	297	16	9890	580	69	4.4	266	17	0.259	bdl	13.23	0.183	0.83	nd	3.8	3.84	0.15	47.2	nd	222.4	nd	664	nd	1845	nd	8.3	G12b-0610c
7.14	0.39	0.013	0.014	0.37	0.12	1.23	0.49	0.188	0.054	11.5	1.4	64.2	3.3	135.4	6.7	369	24	9910	490	88.1	6	414	33	0.213	bdl	11.65	0.140	0.81	nd	8.3	3.34	0.10	57.8	nd	261.0	nd	846	nd	2292	nd	8.8	G12b-067r
4.67	0.27	0.003	0.012	0.16	0.15	0.56	0.44	0.005	0.034	3.89	0.94	28.1	1.8	63.1	4.5	200	14	9390	440	55.6	3.1	378	20	0.147	bdl	7.62	0.032	0.35	nd	3.8	0.09	0.01	19.5	nd	114.2	nd	394	nd	1242	nd	10.9	G12b-28-2c
6.1	0.32	bdl	-	0.216	0.099	1.14	0.6	0.109	0.047	5.38	0.8	34.3	2.1	72.1	4.1	197	12	10070	420	45.9	2.9	199	16	0.231	bdl	9.95	0.000	0.47	nd	7.7	1.94	0.11	28.0	nd	139.4	nd	451	nd	1224	nd	8.8	G12b-284m
																																									Stromatic Granulite Rr10-6-2
5.17	0.66	0.083	0.032	0.95	0.35	1.53	0.73	0.8	0.12	8.4	1.3	25.8	2.5	39.8	4.1	146	13	13400	1100	62.9	9.5	2220	230	0.028	bdl	8.43	0.894	2.08	nd	10.3	14.21	0.54	42.2	nd	104.9	nd	249	nd	907	nd	8.6	B62-09-2r
2.91	0.17	0.002	0.013	0.17	0.12	0.75	0.42	0.251	0.072	4.55	0.7	48.6	4.1	86.9	3	205	12	10220	2.50	140	11	507	35	0.276	bdl	4.75	0.022	0.37	nd	5.1	4.46	0.32	22.9	nd	197.6	nd	543	nd	1273	nd	6.4	B62-02-1r
8.1	1.4	0.262	0.039	3.18	0.68	4.2	1	1.55	0.21	16.1	4.4	59	11	82	10	266	37	9800	1100	170	36	800	110	0.213	bdl	13.21	2.823	6.96	nd	28.4	27.53	0.50	80.9	nd	239.8	nd	513	nd	1652	nd	6.9	B62-09-3r
~~10.18~~	~~0.98~~	~~0.132~~	~~0.04~~	~~1.46~~	~~0.36~~	~~2.18~~	~~0.74~~	~~0.78~~	~~0.11~~	~~14.2~~	~~1.9~~	~~64.4~~	~~4.5~~	~~110.1~~	~~7.6~~	~~290~~	~~23~~	~~10200~~	~~1000~~	~~161~~	~~12~~	~~395~~	~~42~~	~~0.408~~	~~bdl~~	~~16.61~~	~~1.420~~	~~3.19~~	~~nd~~	~~14.7~~	~~12.85~~	0.32	~~71.4~~	~~nd~~	~~261.8~~	~~nd~~	~~688~~	~~nd~~	~~1801~~	nd	~~6.9~~	~~B62-12-2e~~
25.6	4.2	0.54	0.11	6.39	0.95	8.7	1.5	3.31	0.28	26.1	2.1	97.4	8.8	1.58	9.8	460	51	6080	530	426	27	616	39	0.692	0.232	41.76	5.819	13.98	nd	58.8	58.79	0.62	131.2	nd	395.9	nd	988	nd	2857	nd	7.2	B62-09-1c
11.29	0.69	0.13	0.032	1.63	0.26	1.91	0.48	0.84	0.12	11.1	1.4	48.9	4.4	99.9	6.2	292	19	9800	510	209	16	451	21	0.463	bdl	18.42	1.401	3.57	nd	12.9	14.92	0.43	55.8	nd	198.8	nd	624	nd	1814	nd	9.1	B62-09-4m
33.4	2.4	0.94	0.11	13.9	1.1	21.1	1.3	7.35	0.4	76.4	6.5	265	21	425	34	1103	93	6800	530	914	72	871	67	1.049	0.418	54.49	10.129	30.42	nd	142.6	130.55	0.50	383.9	nd	1077.2	nd	2656	nd	6851	nd	6.4	B62-08-2r
4.76	0.43	0.027	0.016	0.24	0.14	0.28	0.39	0.18	0.051	3.63	0.68	18.9	2.2	43.9	3.3	1.59	14	8780	700	51	4.4	356	28	0.143	bdl	7.77	0.291	0.53	nd	1.9	3.20	0.32	18.2	nd	76.8	nd	274	nd	988	nd	12.9	B62-08-1c
4.56	0.78	0.027	0.02	0.08	0.14	0.45	0.72	0.109	0.065	0.74	0.37	7.33	0.76	27.4	3.6	1.58	21	9500	1500	47.9	6.6	650	100	0.074	bdl	7.44	0.291	0.18	nd	3.0	1.94	0.57	3.7	nd	29.8	nd	171	nd	981	nd	32.9	B62-11-3c
12.01	0.83	0.086	0.034	1.16	0.21	2.56	0.77	0.74	0.11	12	1.4	65.6	4.5	130.1	6.3	363	23	8660	470	188	10	438	24	0.429	bdl	19.59	0.927	2.54	nd	17.3	13.14	0.34	60.3	nd	266.7	nd	813	nd	2255	nd	8.5	B62-12-3r
45	3.3	1.34	0.13	21.2	1.7	28.4	2.3	9.74	0.57	86.2	6.2	300	17	457	25	11.50	72	7140	460	908	59	833	59	1.090	0.228	73.41	14.440	46.39	nd	191.9	173.00	0.55	433.2	nd	1219.5	nd	28.56	nd	7143	nd	5.9	B62-11-4c
34	1.9	0.867	0.082	1.5	1.1	21.1	1	8.33	0.4	70.2	4.7	210	10	344	19	873	45	7730	380	1002	49	699	38	1.433	0.506	55.46	9.343	32.82	nd	142.6	147.96	0.60	352.8	nd	853.7	nd	21.50	nd	5422	nd	6.4	B62-06-2c
19.71	0.74	0.147	0.04	1.8	0.25	3.51	0.68	1.208	0.091	19	1.8	98.8	3.7	229.1	6.1	6.52	20	8260	1.60	365	8	614	23	0.594	0.000	32.15	1.584	3.94	nd	23.7	21.46	0.36	95.5	nd	401.6	nd	1432	nd	4050	nd	10.1	B62-04-2c
22.3	2.1	0.212	0.049	3.02	0.74	4.29	0.83	1.32	0.23	24.7	3.8	118	16	225	27	607	56	8800	400	604	97	892	90	0.677	0.127	36.38	2.284	6.61	nd	29.0	23.45	0.31	124.1	nd	479.7	nd	1406	nd	3770	nd	7.9	B62-02-2r
~~17.88~~	~~0.87~~	~~0.149~~	~~0.035~~	~~2.56~~	~~0.35~~	~~5.15~~	~~0.66~~	~~1.69~~	~~0.15~~	~~36.8~~	~~1.6~~	~~108~~	~~4.8~~	~~188.9~~	~~7.8~~	~~510~~	~~35~~	~~9280~~	~~440~~	~~575~~	~~15~~	~~667~~	~~80~~	~~0.654~~	62.996	51.39	30.819	19.80	nd	11.8	21.67	3.24	1.6	nd	1.4	nd	1	nd	0	nd	0.2	~~B62-03-2e~~
14.4	1.2	0.29	0.049	4.57	0.43	7.01	0.72	1.7	0.16	30	2.2	127.4	6.5	2.12	13	5.15	39	8650	5.90	303	21	451	32	0.672	bdl	23.49	3.125	10.00	nd	47.4	30.20	0.30	150.8	nd	517.9	nd	1325	nd	3199	nd	6.2	B62-11-1c
7.52	0.43	0.033	0.017	0.74	0.18	1.57	0.51	0.57	0.086	7.88	0.93	40.2	2.1	88.5	3.3	275.3	9.9	9170	180	100.8	4.9	244	11	0.413	bdl	12.27	0.356	1.62	nd	10.6	10.12	0.40	39.6	nd	163.4	nd	533	nd	1710	nd	10.5	B62-04-1r
10.97	0.91	0.034	0.018	0.56	0.2	2.13	0.5	0.519	0.074	8.9	1.2	53.6	4.3	107.4	9	321	31	9810	930	145	12	390	37	0.372	bdl	17.90	0.366	1.23	nd	14.4	9.22	0.31	44.7	nd	217.9	nd	671	nd	1994	nd	9.2	B62-12-1r
23.4	1.4	0.616	0.064	9.2	0.7	14.1	1.3	4.74	0.42	48.2	3.6	182	11	298	20	787	49	7450	570	514	34	608	41	0.845	bdl	38.17	6.638	20.13	nd	95.3	84.19	0.50	242.2	nd	739.8	nd	1863	nd	4888	nd	6.6	B62-11-5c
4.11	0.39	0.039	0.016	0.31	0.14	0.34	0.43	0.259	0.053	3.3	0.76	14	1.6	32.9	2.5	101.3	8.1	9990	710	34.6	3.3	94.6	7.2	0.366	bdl	6.70	0.420	0.68	nd	2.3	4.60	0.49	16.6	nd	56.9	nd	206	nd	629	nd	11.1	B62-06-1r
7.4	0.62	0.03	0.017	0.56	0.14	1.83	0.42	0.42	0.095	8	1.2	35.4	3.1	67.3	4.9	189	17	9300	600	87.2	8.1	192	17	0.454	bdl	12.07	0.323	1.23	nd	12.4	7.46	0.28	40.2	nd	143.9	nd	421	nd	1174	nd	8.2	B62-08-3r
5.18	0.43	0.006	0.013	0.69	0.22	1.08	0.45	0.375	0.088	4.67	0.94	23.1	2.4	47.1	4.4	141	12	8240	6.50	38.2	3.6	104.9	9.1	0.364	bdl	8.45	0.065	1.51	nd	7.3	6.66	0.43	23.5	nd	93.9	nd	294	nd	876	nd	9.3	B62-11-2m

Table 3. 5. U-Pb Isotope Data for Dike and Leucosome Samples

	Isotopic Ratios							Dates (Ma)							Concentration	
Sample and Analysis Number	207Pb/ 235U	± 2SE (abs)	206Pb/ 238U	± 2SE (abs)	207Pb/ 206Pb	± 2SE (abs)	Rho: 206/238 vs 207/235	206Pb/ 238U	± 2SE (abs)	207Pb/ 235U	± 2SE (abs)	% Discord. 6/38-7/35	207Pb/ 206Pb	± 2SE (abs)	U (ppm)	Th/U
Leucosome of Magmatic Breccia (GR11-55)																
GR11-55-4g.FIN2	**0.031**	**0.002**	**0.0048**	**0.0003**	**0.0468**	**0.0022**	**0.82141**	**30.7**	**1.6**	**30.8**	**2.2**	**0.3**	**104**	**34**	**904**	**0.06**
GR11-55-1f.FIN2	**0.031**	**0.002**	**0.0049**	**0.0002**	**0.0472**	**0.0022**	**0.49062**	**31.34**	**1.2**	**31.39**	**1.8**	**0.2**	**166**	**30**	**236.6**	**0.32**
GR11-55-3e.FIN2	**0.033**	**0.002**	**0.0049**	**0.0002**	**0.0472**	**0.0022**	**0.40884**	**31.52**	**1**	**32.65**	**1.8**	**3.5**	**198**	**33**	**311**	**0.56**
GR11-55-7f.FIN2	0.039	0.003	0.0049	0.0002	0.057	0.0028	0.38373	31.55	1.2	38.6	2.4	18.3	473	47	233	0.54
GR11-55-8e.FIN2	**0.031**	**0.002**	**0.0049**	**0.0002**	**0.0454**	**0.0022**	**0.36051**	**31.58**	**1**	**30.85**	**1.7**	**-2.4**	**160**	**31**	**168**	**0.62**
GR11-55-8h.FIN2	**0.032**	**0.002**	**0.0049**	**0.0002**	**0.0461**	**0.0020**	**0.58466**	**31.6**	**1**	**31.54**	**1.8**	**-0.2**	**141**	**25**	**266.3**	**0.48**
GR11-55-8k.FIN2	**0.032**	**0.002**	**0.0049**	**0.0002**	**0.049**	**0.0022**	**0.52594**	**31.7**	**1**	**32.46**	**1.8**	**2.3**	**213**	**27**	**245.3**	**0.53**
GR11-55-7i.FIN2	**0.032**	**0.002**	**0.0049**	**0.0002**	**0.0478**	**0.0021**	**0.60017**	**31.78**	**1.2**	**31.68**	**1.7**	**-0.3**	**157**	**21**	**292**	**0.63**
GR11-55-4k.FIN2	**0.032**	**0.002**	**0.0049**	**0.0002**	**0.0472**	**0.0020**	**0.57197**	**31.79**	**1.1**	**31.82**	**1.8**	**0.1**	**159**	**24**	**319.2**	**0.34**
GR11-55-8i.FIN2	**0.033**	**0.002**	**0.0049**	**0.0002**	**0.0474**	**0.0021**	**0.61468**	**31.79**	**1.1**	**32.49**	**1.8**	**2.2**	**186**	**23**	**218.7**	**0.47**
GR11-55-3c.FIN2	**0.033**	**0.002**	**0.0049**	**0.0002**	**0.0478**	**0.0022**	**0.63652**	**31.8**	**1.3**	**32.6**	**2**	**2.5**	**174**	**43**	**314**	**0.59**
GR11-55-1e.FIN2	**0.032**	**0.002**	**0.005**	**0.0002**	**0.0465**	**0.0022**	**0.54625**	**31.84**	**1.1**	**32.1**	**1.9**	**0.8**	**167**	**30**	**245.7**	**0.40**
GR11-55-8b.FIN2	**0.033**	**0.002**	**0.005**	**0.0002**	**0.0475**	**0.0019**	**0.76351**	**31.86**	**1**	**32.63**	**1.7**	**2.4**	**143**	**20**	**2563**	**0.00**
GR11-55-5a.FIN2	**0.031**	**0.002**	**0.005**	**0.0002**	**0.0455**	**0.0020**	**0.63558**	**31.87**	**1.2**	**30.9**	**1.8**	**-3.1**	**138**	**29**	**289.4**	**0.34**
GR11-55-2h.FIN2	**0.032**	**0.002**	**0.005**	**0.0002**	**0.0458**	**0.0020**	**0.49433**	**31.88**	**1.1**	**32.08**	**1.8**	**0.6**	**151**	**28**	**263.3**	**0.36**
GR11-55-5c.FIN2	**0.031**	**0.002**	**0.005**	**0.0002**	**0.0456**	**0.0021**	**0.46275**	**31.9**	**1**	**31.26**	**1.8**	**-2.0**	**174**	**30**	**201.4**	**0.39**
GR11-55-1g.FIN2	**0.032**	**0.002**	**0.005**	**0.0002**	**0.0461**	**0.0020**	**0.62535**	**31.94**	**1.1**	**31.93**	**1.8**	**0.0**	**145**	**27**	**225.2**	**0.38**
GR11-55-8g.FIN2	**0.031**	**0.002**	**0.005**	**0.0002**	**0.0451**	**0.0020**	**0.50557**	**31.97**	**1.1**	**30.62**	**1.7**	**-4.4**	**114**	**30**	**223**	**0.46**
GR11-55-3b.FIN2	**0.032**	**0.002**	**0.005**	**0.0003**	**0.0463**	**0.0025**	**0.75353**	**32**	**1.6**	**31.8**	**2.3**	**-0.6**	**120**	**40**	**341**	**0.72**
GR11-55-5b.FIN2	**0.033**	**0.002**	**0.005**	**0.0002**	**0.048**	**0.0022**	**0.4105**	**32.01**	**1.1**	**32.71**	**1.8**	**2.1**	**182**	**25**	**223.8**	**0.34**
GR11-55-1i.FIN2	**0.033**	**0.002**	**0.005**	**0.0002**	**0.0473**	**0.0019**	**0.75469**	**32.05**	**1.1**	**32.88**	**1.7**	**2.5**	**116**	**15**	**4090**	**0.01**
GR11-55-8d.FIN2	**0.033**	**0.002**	**0.005**	**0.0002**	**0.0482**	**0.0027**	**0.24902**	**32.06**	**1.2**	**33.1**	**2**	**3.1**	**252**	**38**	**79.5**	**0.46**
GR11-55-7k.FIN2	**0.032**	**0.002**	**0.005**	**0.0002**	**0.0469**	**0.0019**	**0.78505**	**32.12**	**1.1**	**31.82**	**1.7**	**-0.9**	**115**	**19**	**2730**	**0.01**
GR11-55-8c.FIN2	0.037	0.002	0.005	0.0002	0.0528	0.0022	0.72674	32.12	1.2	36.88	2	12.9	345	26	1945	0.00
GR11-55-1n.FIN2	**0.032**	**0.002**	**0.005**	**0.0002**	**0.0465**	**0.0018**	**0.82794**	**32.15**	**1.1**	**32.22**	**1.7**	**0.2**	**91**	**16**	**3447**	**0.02**
GR11-55-3a.FIN2	**0.032**	**0.002**	**0.005**	**0.0002**	**0.0468**	**0.0021**	**0.61312**	**32.16**	**1.2**	**32.13**	**1.8**	**-0.1**	**181**	**31**	**262**	**0.69**
GR11-55-8j.FIN2	**0.032**	**0.002**	**0.005**	**0.0002**	**0.0478**	**0.0022**	**0.40981**	**32.16**	**1.1**	**32.19**	**1.9**	**0.1**	**164**	**31**	**219**	**0.53**
GR11-55-4e.FIN2	**0.032**	**0.002**	**0.005**	**0.0002**	**0.0468**	**0.0022**	**0.4478**	**32.18**	**1.2**	**31.77**	**1.8**	**-1.3**	**166**	**22**	**215.3**	**0.33**
GR11-55-7e.FIN2	**0.034**	**0.002**	**0.005**	**0.0002**	**0.0492**	**0.0021**	**0.56703**	**32.19**	**1**	**34.26**	**1.9**	**6.0**	**197**	**33**	**1321**	**0.06**
GR11-55-5e.FIN2	**0.032**	**0.002**	**0.005**	**0.0002**	**0.0463**	**0.0021**	**0.60576**	**32.21**	**1.1**	**32.46**	**1.9**	**0.8**	**145**	**28**	**189.4**	**0.73**
GR11-55-7j.FIN2	**0.033**	**0.002**	**0.005**	**0.0002**	**0.048**	**0.0021**	**0.6364**	**32.21**	**1.1**	**32.9**	**1.9**	**2.1**	**178**	**24**	**445**	**0.32**

	Isotopic Ratios							Dates (Ma)							Concentration	
Sample and Analysis Number	207Pb/ 235U	± 2SE (abs)	206Pb/ 238U	± 2SE (abs)	207Pb/ 206Pb	± 2SE (abs)	Rho: 206/238 vs 207/235	206Pb/ 238U	± 2SE (abs)	207Pb/ 235U	± 2SE (abs)	% Discord. 6/38-7/35	207Pb/ 206Pb	± 2SE (abs)	U (ppm)	Th/U
GR11-55-8a.FIN2	**0.033**	**0.002**	**0.005**	**0.0002**	**0.0476**	**0.0019**	**0.88715**	**32.27**	**1.3**	**32.89**	**1.8**	**1.9**	**100**	**16**	**2070**	**0.00**
GR11-55-5f.FIN2	**0.032**	**0.002**	**0.005**	**0.0002**	**0.0477**	**0.0022**	**0.55418**	**32.32**	**1.2**	**32.4**	**1.9**	**0.2**	**171**	**24**	**236**	**0.22**
GR11-55-2i.FIN2	**0.033**	**0.002**	**0.005**	**0.0002**	**0.0469**	**0.0021**	**0.52677**	**32.36**	**1.1**	**33.13**	**1.9**	**2.3**	**196**	**34**	**237.7**	**0.34**
GR11-55-2f.FIN2	**0.032**	**0.002**	**0.005**	**0.0002**	**0.0456**	**0.0023**	**0.32975**	**32.38**	**1.1**	**31.9**	**1.8**	**-1.5**	**196**	**30**	**123.8**	**0.43**
GR11-55-4j.FIN2	**0.032**	**0.002**	**0.005**	**0.0002**	**0.0469**	**0.0021**	**0.51214**	**32.38**	**1.1**	**32.33**	**1.9**	**-0.2**	**200**	**33**	**232.6**	**0.29**
GR11-55-2g.FIN2	**0.032**	**0.002**	**0.005**	**0.0002**	**0.0455**	**0.0019**	**0.76086**	**32.39**	**1.1**	**32.3**	**1.9**	**-0.3**	**127**	**25**	**384**	**0.61**
GR11-55-3d.FIN2	**0.034**	**0.002**	**0.005**	**0.0002**	**0.048**	**0.0021**	**0.53123**	**32.42**	**1.1**	**33.59**	**1.8**	**3.5**	**178**	**24**	**321**	**0.53**
GR11-55-5j.FIN2	**0.034**	**0.002**	**0.005**	**0.0002**	**0.0495**	**0.0022**	**0.55081**	**32.42**	**1.1**	**34.2**	**2**	**5.2**	**239**	**30**	**218**	**0.47**
GR11-55-7m.FIN2	**0.032**	**0.002**	**0.0051**	**0.0002**	**0.0464**	**0.0019**	**0.76996**	**32.48**	**1.1**	**31.96**	**1.7**	**-1.6**	**91**	**14**	**1570**	**0.02**
GR11-55-6a.FIN2	**0.033**	**0.002**	**0.0051**	**0.0002**	**0.0471**	**0.0019**	**0.72697**	**32.5**	**1.1**	**33.12**	**1.8**	**1.9**	**113**	**21**	**1403**	**0.03**
GR11-55-1k.FIN2	**0.034**	**0.002**	**0.0051**	**0.0002**	**0.0493**	**0.0020**	**0.68879**	**32.52**	**1.1**	**34.22**	**1.8**	**5.0**	**180**	**19**	**3240**	**0.03**
GR11-55-1a.FIN2	**0.032**	**0.002**	**0.0051**	**0.0002**	**0.0466**	**0.0019**	**0.80506**	**32.54**	**1.2**	**32.22**	**1.8**	**-1.0**	**90**	**16**	**5110**	**0.02**
GR11-55-7a.FIN2	**0.034**	**0.002**	**0.0051**	**0.0002**	**0.0492**	**0.0023**	**0.48728**	**32.58**	**1.1**	**34.1**	**2**	**4.5**	**260**	**30**	**112.9**	**0.65**
GR11-55-9a.FIN2	**0.033**	**0.002**	**0.0051**	**0.0002**	**0.0483**	**0.0021**	**0.57467**	**32.62**	**1.1**	**32.83**	**1.8**	**0.6**	**181**	**24**	**268.8**	**0.50**
GR11-55-5i.FIN2	**0.033**	**0.002**	**0.0051**	**0.0002**	**0.0475**	**0.0023**	**0.49048**	**32.62**	**1.1**	**32.9**	**2**	**0.9**	**245**	**32**	**188.1**	**0.42**
GR11-55-1b.FIN2	**0.033**	**0.002**	**0.0051**	**0.0002**	**0.0472**	**0.0019**	**0.81419**	**32.62**	**1.2**	**33.1**	**1.8**	**1.5**	**125**	**16**	**4630**	**0.01**
GR11-55-4f.FIN2	**0.033**	**0.002**	**0.0051**	**0.0002**	**0.0479**	**0.0022**	**0.57968**	**32.65**	**1.1**	**33.32**	**1.9**	**2.0**	**205**	**35**	**253.5**	**0.43**
GR11-55-1l.FIN2	**0.033**	**0.002**	**0.0051**	**0.0002**	**0.0476**	**0.0019**	**0.69215**	**32.67**	**1.1**	**33.43**	**1.8**	**2.3**	**126**	**18**	**3270**	**0.02**
GR11-55-4i.FIN2	**0.033**	**0.002**	**0.0051**	**0.0002**	**0.0477**	**0.0021**	**0.67903**	**32.7**	**1.3**	**33.2**	**1.9**	**1.5**	**96**	**22**	**926**	**0.05**
GR11-55-9b.FIN2	**0.033**	**0.002**	**0.0051**	**0.0002**	**0.0467**	**0.0020**	**0.62661**	**32.74**	**1.1**	**32.64**	**1.8**	**-0.3**	**155**	**24**	**237**	**0.38**
GR11-55-1d.FIN2	**0.033**	**0.002**	**0.0051**	**0.0002**	**0.0467**	**0.0019**	**0.75331**	**32.74**	**1.1**	**32.85**	**1.7**	**0.3**	**106**	**19**	**6760**	**0.02**
GR11-55-3h.FIN2	**0.034**	**0.002**	**0.0051**	**0.0002**	**0.0481**	**0.0020**	**0.71621**	**32.77**	**1.1**	**34**	**1.8**	**3.6**	**148**	**20**	**1282**	**0.00**
GR11-55-4h.FIN2	**0.032**	**0.002**	**0.0051**	**0.0002**	**0.0463**	**0.0028**	**0.42141**	**32.8**	**1.4**	**32.2**	**2.1**	**-1.9**	**163**	**53**	**236.3**	**0.71**
GR11-55-7g.FIN2	**0.033**	**0.002**	**0.0051**	**0.0002**	**0.0466**	**0.0021**	**0.50913**	**32.8**	**1.1**	**32.5**	**1.9**	**-0.9**	**141**	**23**	**224**	**0.48**
GR11-55-3g.FIN2	**0.033**	**0.003**	**0.0051**	**0.0004**	**0.0475**	**0.0023**	**0.84479**	**32.8**	**2.3**	**32.9**	**2.6**	**0.3**	**139**	**63**	**3040**	**0.00**
GR11-55-5d.FIN2	**0.032**	**0.002**	**0.0051**	**0.0002**	**0.0469**	**0.0024**	**0.40338**	**32.85**	**1.1**	**32.2**	**1.9**	**-2.0**	**202**	**34**	**137.1**	**0.68**
GR11-55-4l.FIN2	**0.033**	**0.002**	**0.0051**	**0.0002**	**0.0461**	**0.0019**	**0.70144**	**32.92**	**1.1**	**32.54**	**1.8**	**-1.2**	**113**	**22**	**1040**	**0.03**
GR11-55-4a.FIN2	**0.034**	**0.002**	**0.0051**	**0.0002**	**0.0484**	**0.0022**	**0.58778**	**33**	**1.4**	**33.84**	**1.9**	**2.5**	**162**	**35**	**1084**	**0.05**
GR11-55-4b.FIN2	**0.033**	**0.002**	**0.0051**	**0.0002**	**0.0468**	**0.0019**	**0.73822**	**33.03**	**1.1**	**32.9**	**1.8**	**-0.4**	**115**	**20**	**2257**	**0.03**
GR11-55-7c.FIN2	**0.034**	**0.002**	**0.0051**	**0.0002**	**0.0477**	**0.0020**	**0.64394**	**33.03**	**1.1**	**34.2**	**1.9**	**3.4**	**155**	**24**	**480**	**0.18**
GR11-55-6c.FIN2	**0.034**	**0.002**	**0.0051**	**0.0002**	**0.0475**	**0.0019**	**0.67306**	**33.08**	**1.1**	**34.12**	**1.8**	**3.0**	**137**	**19**	**2221**	**0.01**
GR11-55-1h.FIN2	**0.033**	**0.002**	**0.0052**	**0.0002**	**0.0462**	**0.0020**	**0.55593**	**33.25**	**1.1**	**33.14**	**1.8**	**-0.3**	**137**	**28**	**293**	**0.35**
GR11-55-7d.FIN2	0.037	0.002	0.0052	0.0002	0.0505	0.0027	0.46123	33.3	1.4	37.3	2.4	10.7	341	67	213	0.53

	Isotopic Ratios							Dates (Ma)							Concentration	
Sample and Analysis Number	207Pb/ 235U	± 2SE (abs)	206Pb/ 238U	± 2SE (abs)	207Pb/ 206Pb	± 2SE (abs)	Rho: 206/238 vs 207/235	206Pb/ 238U	± 2SE (abs)	207Pb/ 235U	± 2SE (abs)	% Discord. 6/38-7/35	207Pb/ 206Pb	± 2SE (abs)	U (ppm)	Th/U
GR11-55-8f.FIN2	**0.034**	**0.002**	**0.0052**	**0.0002**	**0.0463**	**0.0024**	**0.28394**	**33.35**	**1.1**	**33.4**	**2**	**0.1**	**188**	**34**	**106.2**	**0.48**
GR11-55-3f.FIN2	**0.035**	**0.002**	**0.0052**	**0.0002**	**0.0495**	**0.0020**	**0.76558**	**33.37**	**1.2**	**35.07**	**1.9**	**4.8**	**190**	**21**	**1750**	**0.00**
GR11-55-1j.FIN2	**0.035**	**0.002**	**0.0052**	**0.0002**	**0.0487**	**0.0020**	**0.77873**	**33.59**	**1.2**	**35.05**	**1.9**	**4.2**	**152**	**20**	**2424**	**0.02**
GR11-55-5h.FIN2	**0.033**	**0.002**	**0.0052**	**0.0002**	**0.046**	**0.0020**	**0.64036**	**33.65**	**1.2**	**33.23**	**1.9**	**-1.3**	**175**	**33**	**254.7**	**0.35**
GR11-55-3i.FIN2	0.045	0.003	0.0067	0.0003	0.0491	0.0020	0.90172	43.3	2	44.6	2.7	2.9	177	19	640	0.02
GR11-55-7h.FIN2	0.053	0.003	0.0076	0.0004	0.0503	0.0025	0.74182	49	2.4	52	3.2	5.8	181	38	1805	0.09
GR11-55-1m.FIN2	0.114	0.010	0.016	0.0011	0.0521	0.0021	0.96663	102.1	7.2	109.8	9	7.0	294	23	1256	0.16
GR11-55-1c.FIN2	0.139	0.008	0.0194	0.0009	0.0524	0.0022	0.80069	123.7	5.4	131.7	7.5	6.1	308	31	2239	0.41
GR11-55-6b.FIN2	0.138	0.009	0.0196	0.0009	0.0511	0.0020	0.92023	125.1	6	130.9	7.7	4.4	250	25	1300	0.05
GR11-55-7b.FIN2	0.146	0.009	0.0199	0.0008	0.0529	0.0022	0.8263	127.3	4.8	138.3	7.6	8.0	317	23	1930	0.36
GR11-55-4d.FIN2	0.156	0.014	0.0228	0.0018	0.0492	0.0020	0.96708	145	11	145	12	0.0	188	22	512	0.11
GR11-55-2a.FIN2	0.163	0.013	0.0229	0.0015	0.0518	0.0021	0.96607	146	9.7	152.6	12	4.3	281	17	2407	0.00
GR11-55-7l.FIN2	0.212	0.012	0.031	0.0013	0.0511	0.0021	0.86277	196.4	7.9	195.2	10	-0.6	246	21	478	0.21
GR11-55-2d.FIN2	0.225	0.013	0.0312	0.0012	0.0524	0.0022	0.79582	197.7	7.8	205.4	11	3.7	303	30	614	0.06
GR11-55-2c.FIN2	0.294	0.016	0.0402	0.0014	0.0527	0.0021	0.79359	254.2	8.6	261.7	12	2.9	337	18	720	0.09
GR11-55-3k.FIN2	0.298	0.016	0.042	0.0014	0.0518	0.0021	0.77887	265	8.4	264.5	13	-0.2	272	18	308	0.14
GR11-55-4c.FIN2	0.304	0.017	0.0433	0.0016	0.051	0.0020	0.8448	273.2	10	269.4	13	-1.4	231	18	221	0.21
GR11-55-5g.FIN2	0.43	0.027	0.0444	0.0018	0.0708	0.0030	0.781	279.8	11	364	19	23.1	942	35	646	0.14
GR11-55-2e.FIN2	0.32	0.018	0.0447	0.0015	0.0513	0.0020	0.83746	281.9	9	281.2	13	-0.2	264	17	359	0.06
GR11-55-2b.FIN2	0.326	0.018	0.0455	0.0016	0.052	0.0021	0.79009	286.5	10	285.8	14	-0.2	303	20	242	0.09
GR11-55-3j.FIN2	0.341	0.018	0.0464	0.0015	0.0532	0.0021	0.75392	292.1	9	297.9	14	1.9	326	17	353	0.38
Deformed Biotite Pegmatite Dike (GR11-54)																
GR11-54-1.FIN2	0.035	0.008	0.0039	0.0005	0.067	0.0190	0.001	24.8	3.6	34.4	7.9	27.9	1350	580	143	0.25
GR11-54-26.FIN2	**0.024**	**0.004**	**0.004**	**0.0007**	**0.0487**	**0.0098**	**0.079843**	**25.5**	**4.5**	**24.4**	**3.9**	**-4.5**	**220**	**240**	**416**	**0.07**
GR11-54-29.FIN2	**0.028**	**0.006**	**0.004**	**0.0007**	**0.0504**	**0.0092**	**0.4819**	**25.8**	**4.5**	**28**	**5.5**	**7.9**	**530**	**360**	**384**	**0.09**
GR11-54-35.FIN2	**0.022**	**0.004**	**0.004**	**0.0007**	**0.0478**	**0.0056**	**0.50305**	**25.9**	**4.7**	**22.3**	**4.1**	**-16.1**	**156**	**80**	**319**	**0.05**
GR11-54-17.FIN2	**0.027**	**0.004**	**0.0044**	**0.0006**	**0.0468**	**0.0050**	**0.75876**	**28.2**	**3.6**	**26.9**	**4.3**	**-4.8**	**280**	**100**	**243**	**0.11**
GR11-54-33.FIN2	**0.032**	**0.003**	**0.0045**	**0.0003**	**0.0522**	**0.0043**	**0.47598**	**29**	**2.1**	**32.1**	**3.1**	**9.7**	**546**	**89**	**277**	**0.12**
GR11-54-37.FIN2	**0.031**	**0.003**	**0.0045**	**0.0004**	**0.0478**	**0.0028**	**0.69071**	**29.2**	**2.4**	**30.7**	**2.9**	**4.9**	**406**	**92**	**4350**	**0.02**
GR11-54-43.FIN2	**0.034**	**0.006**	**0.0046**	**0.0006**	**0.0579**	**0.0085**	**0.48021**	**29.3**	**3.7**	**34.1**	**5.6**	**14.1**	**820**	**230**	**274**	**0.10**
GR11-54-22.FIN2	**0.026**	**0.002**	**0.0046**	**0.0009**	**0.0418**	**0.0088**	**0.30396**	**29.5**	**5.9**	**25.6**	**2.4**	**-15.2**			**557**	**0.05**
GR11-54-31.FIN2	**0.033**	**0.002**	**0.0047**	**0.0003**	**0.0533**	**0.0029**	**0.53044**	**30.4**	**1.9**	**33.2**	**2.1**	**8.4**	**437**	**54**	**222.1**	**0.00**
GR11-54-19.FIN2	0.067	0.014	0.0047	0.0005	0.106	0.0300	0.001	30.4	3.3	66	13	53.9	1890	240	50.6	0.03

	Isotopic Ratios							Dates (Ma)							Concentration	
Sample and Analysis Number	207Pb/ 235U	± 2SE (abs)	206Pb/ 238U	± 2SE (abs)	207Pb/ 206Pb	± 2SE (abs)	Rho: 206/238 vs 207/235	206Pb/ 238U	± 2SE (abs)	207Pb/ 235U	± 2SE (abs)	% Discord. 6/38-7/35	207Pb/ 206Pb	± 2SE (abs)	U (ppm)	Th/U
GR11-54-39.FIN2	**0.031**	**0.005**	**0.0048**	**0.0012**	**0.0466**	**0.0072**	**0.62039**	**30.7**	**7.6**	**31.1**	**5.1**	**1.3**	**620**	**250**	**393**	**0.12**
GR11-54-11.FIN2	0.045	0.013	0.0048	0.0014	0.0704	0.0080	0.99796	31.1	9.3	45	13	30.9	830	170	290	0.10
GR11-54-4.FIN2	0.055	0.005	0.0049	0.0004	0.0815	0.0086	0.47929	31.5	2.6	55.6	4.9	43.3	1230	150	161	0.23
GR11-54-34.FIN2	**0.027**	**0.007**	**0.0049**	**0.0012**	**0.0397**	**0.0056**	**0.80792**	**31.7**	**7.6**	**26.7**	**6.5**	**-18.7**			**360**	**0.09**
GR11-54-21.FIN2	0.036	0.006	0.005	0.0006	0.0514	0.0067	0.58238	32.2	3.9	35.9	5.8	10.3	640	210	204	0.12
GR11-54-12.FIN2	0.042	0.006	0.0051	0.0007	0.062	0.0120	0.1329	32.5	4.7	41.2	5.8	21.1	660	150	175	0.21
GR11-54-8.FIN2	0.056	0.014	0.0051	0.0010	0.084	0.0190	0.30971	32.7	6.1	55	13	40.5	1500	190	55	0.10
GR11-54-13.FIN2	0.037	0.004	0.0052	0.0004	0.0518	0.0068	0.27676	33.4	2.5	37	4.2	9.7	520	100	191	0.20
GR11-54-40.FIN2	0.054	0.007	0.0052	0.0005	0.0788	0.0092	0.42016	33.4	2.9	53.6	6.5	37.7	1200	130	103	0.24
GR11-54-7.FIN2	0.037	0.004	0.0052	0.0004	0.0522	0.0034	0.80565	33.6	2.5	37	4	9.2	500	97	670	0.09
GR11-54-16.FIN2	0.046	0.011	0.0052	0.0008	0.062	0.0110	0.68516	33.6	5.2	46	10	27.0	660	150	251	0.13
GR11-54-14.FIN2	0.036	0.005	0.0053	0.0007	0.0498	0.0036	0.92384	33.9	4.5	35.9	5.2	5.6	215	54	939	0.01
GR11-54-3.FIN2	0.059	0.022	0.0057	0.0016	0.075	0.0130	0.93293	36	10	58	21	37.9	910	250	213	0.03
GR11-54-20.FIN2	0.046	0.007	0.0057	0.0003	0.0589	0.0074	0.001	36.3	2.2	45.7	6.3	20.6	720	170	114	0.18
GR11-54-18.FIN2	0.072	0.012	0.0057	0.0005	0.093	0.0180	0.040078	36.9	3.3	71	11	48.0	1480	190	219	0.15
GR11-54-32.FIN2	0.041	0.007	0.0062	0.0009	0.0509	0.0054	0.78126	39.9	5.6	41.1	6.8	2.9	310	94	292	0.15
GR11-54-27.FIN2	0.082	0.010	0.0075	0.0009	0.082	0.0100	0.63657	47.9	5.7	79.5	9.8	39.7	1290	160	168	0.21
GR11-54-25.FIN2	0.108	0.007	0.0159	0.0009	0.0487	0.0020	0.73821	101.6	5.6	103.3	6.5	1.6	363	53	375	0.23
GR11-54-15.FIN2	0.191	0.012	0.0268	0.0019	0.0524	0.0025	0.64937	171	12	176.8	10	3.3	470	72	164	0.32
GR11-54-30.FIN2	0.264	0.013	0.0359	0.0018	0.0529	0.0019	0.68547	227	11	238	11	4.6	393	48	134.7	0.37
GR11-54-6.FIN2	4.08	0.290	0.0399	0.0025	0.734	0.0350	0.69398	252	16	1646	61	84.7	4628	40	17.67	0.04
GR11-54-23.FIN2	0.309	0.017	0.0402	0.0021	0.0549	0.0019	0.74685	254	13	272	13	6.6	458	52	177	0.24
GR11-54-9.FIN2	0.292	0.023	0.0404	0.0028	0.0538	0.0034	0.65805	255	18	261	18	2.3	550	81	122.6	0.42
GR11-54-42.FIN2	0.308	0.021	0.0415	0.0025	0.0526	0.0021	0.81058	262	16	272	16	3.7	482	65	504	0.05
GR11-54-41.FIN2	0.327	0.021	0.0447	0.0025	0.0533	0.0020	0.75359	282	16	287	16	1.7	517	60	1780	0.06
GR11-54-2.FIN2	0.342	0.027	0.047	0.0028	0.0526	0.0025	0.80496	296	17	294	20	-0.7	581	68	600	0.22
GR11-54-24.FIN2	0.356	0.021	0.0491	0.0030	0.053	0.0020	0.77454	308	18	309	15	0.3	376	54	405	0.30
GR11-54-28.FIN2	0.37	0.029	0.0524	0.0036	0.0515	0.0025	0.77565	329	22	323	21	-1.9	342	61	227	0.31
GR11-54-5.FIN2	0.813	0.047	0.0935	0.0054	0.0629	0.0026	0.70013	575	32	600	26	4.2	724	70	154	1.34
GR11-54-36.FIN2	4.72	0.300	0.308	0.0170	0.1073	0.0041	0.74808	1722	84	1744	55	1.3	1775	64	220	0.89
GR11-54-10.FIN2	4.99	0.360	0.312	0.0190	0.115	0.0049	0.79034	1749	94	1803	64	3.0	1873	68	243	0.26
Biotite Granite Pod (GR11-27)																
GR11-27-9.FIN2	**0.031**	**0.002**	**0.0045**	**0.0003**	**0.0505**	**0.0029**	**0.68332**	**29.1**	**2**	**31.2**	**2.4**	**6.7**	**404**	**73**	**1108**	0.49

	Isotopic Ratios							Dates (Ma)							Concentration	
Sample and Analysis Number	207Pb/ 235U	± 2SE (abs)	206Pb/ 238U	± 2SE (abs)	207Pb/ 206Pb	± 2SE (abs)	Rho: 206/238 vs 207/235	206Pb/ 238U	± 2SE (abs)	207Pb/ 235U	± 2SE (abs)	% Discord. 6/38-7/35	207Pb/ 206Pb	± 2SE (abs)	U (ppm)	Th/U
GR11-27-13.FIN2	**0.03**	**0.001**	**0.0045**	**0.0002**	**0.0478**	**0.0017**	**0.55157**	**29.11**	**1.1**	**29.9**	**1.3**	**2.6**	**228**	**36**	**715**	0.17
GR11-27-5.FIN2	**0.031**	**0.002**	**0.0046**	**0.0002**	**0.0504**	**0.0021**	**0.48312**	**29.3**	**1.2**	**31.2**	**1.5**	**6.1**	**277**	**51**	**1250**	0.45
GR11-27-15.FIN2	**0.03**	**0.002**	**0.0046**	**0.0002**	**0.0475**	**0.0021**	**0.70369**	**29.5**	**1.6**	**29.8**	**1.9**	**1.0**	**334**	**59**	**787**	0.27
GR11-27-41.FIN2	**0.03**	**0.001**	**0.0046**	**0.0002**	**0.0476**	**0.0016**	**0.41239**	**29.63**	**1.1**	**30.08**	**1.1**	**1.5**	**210**	**32**	**473**	0.29
GR11-27-26.FIN2	**0.029**	**0.002**	**0.0046**	**0.0003**	**0.0455**	**0.0019**	**0.70938**	**29.8**	**1.6**	**28.8**	**1.7**	**-3.5**	**224**	**37**	**719**	0.23
GR11-27-32.FIN2	**0.032**	**0.001**	**0.0046**	**0.0002**	**0.0499**	**0.0016**	**0.6556**	**29.8**	**1.4**	**31.6**	**1.3**	**5.7**	**219**	**36**	**1357**	0.18
GR11-27-34.FIN2	**0.03**	**0.002**	**0.0047**	**0.0002**	**0.0459**	**0.0012**	**0.83078**	**29.9**	**1.5**	**29.6**	**1.6**	**-1.0**	**178**	**30**	**1970**	0.43
GR11-27-16.FIN2	**0.03**	**0.003**	**0.0047**	**0.0003**	**0.0454**	**0.0024**	**0.79664**	**30**	**1.8**	**29.5**	**2.5**	**-1.7**	**190**	**59**	**321**	0.08
GR11-27-43.FIN2	**0.033**	**0.002**	**0.0047**	**0.0003**	**0.0501**	**0.0038**	**0.2824**	**30.3**	**1.8**	**32.7**	**2.5**	**7.3**	**290**	**110**	**354**	0.30
GR11-27-3.FIN2	**0.033**	**0.002**	**0.0048**	**0.0003**	**0.0504**	**0.0024**	**0.62294**	**30.5**	**1.9**	**32.7**	**2.1**	**6.7**	**265**	**62**	**1260**	0.20
GR11-27-39.FIN2	**0.03**	**0.002**	**0.0047**	**0.0003**	**0.048**	**0.0037**	**0.4319**	**30.5**	**2**	**30.3**	**2.4**	**-0.7**	**200**	**130**	**2210**	0.14
GR11-27-44.FIN2	**0.032**	**0.001**	**0.0047**	**0.0002**	**0.0499**	**0.0016**	**0.55095**	**30.51**	**1.1**	**32**	**1.3**	**4.7**	**252**	**34**	**532**	0.45
GR11-27-36.FIN2	0.039	0.003	0.0048	0.0003	0.0633	0.0041	0.47503	30.6	1.8	39.2	2.8	21.9	781	83	256	0.01
GR11-27-35.FIN2	**0.03**	**0.002**	**0.0048**	**0.0004**	**0.0462**	**0.0026**	**0.68344**	**30.8**	**2.2**	**29.8**	**2.2**	**-3.4**	**218**	**48**	**439**	0.17
GR11-27-8.FIN2	0.026	0.004	0.0049	0.0006	0.0401	0.0042	0.65746	31.4	3.9	26.2	3.5	-19.8	160	190	259	0.13
GR11-27-25.FIN2	0.04	0.002	0.005	0.0003	0.0596	0.0042	0.25044	31.9	1.8	39.4	2.2	19.0	545	89	981	0.28
GR11-27-1.FIN2	0.034	0.004	0.005	0.0007	0.0487	0.0025	0.90554	32.1	4.3	34.1	4.2	5.9	193	96	1300	0.01
GR11-27-12.FIN2	0.04	0.003	0.0051	0.0003	0.0566	0.0036	0.35541	32.7	2	40.2	3	18.7	517	77	292	0.07
GR11-27-42.FIN2	0.033	0.003	0.0051	0.0003	0.0476	0.0028	0.65714	32.7	2.2	32.4	2.7	-0.9	226	59	566	0.07
GR11-27-23.FIN2	0.035	0.009	0.0052	0.0011	0.0512	0.0053	0.8651	33.3	7.1	34.8	8.6	4.3	490	150	750	0.16
GR11-27-6.FIN2	0.032	0.006	0.0052	0.0007	0.0445	0.0046	0.81704	33.3	4.5	32.2	5.4	-3.4	357	93	506	0.01
GR11-27-40.FIN2	0.037	0.002	0.0053	0.0003	0.0499	0.0024	0.64047	33.8	2	36.8	2.4	8.2	378	55	458	0.00
GR11-27-31.FIN2	0.031	0.004	0.0053	0.0007	0.0437	0.0042	0.71094	34.1	4.3	31	4	-10.0	302	55	253	0.10
GR11-27-17.FIN2	0.036	0.003	0.0057	0.0004	0.0468	0.0050	0.10761	36.6	2.7	36.3	3	-0.8	160	180	510	0.06
GR11-27-30.FIN2	0.053	0.005	0.0079	0.0007	0.0517	0.0035	0.77563	50.6	4.3	52.7	5.1	4.0	427	85	312	0.39
GR11-27-27.FIN2	0.092	0.011	0.0126	0.0015	0.0531	0.0030	0.75541	80.8	9.7	88.9	10	9.1	334	80	480	0.13
GR11-27-33.FIN2	0.166	0.013	0.0223	0.0015	0.0532	0.0023	0.78851	142.9	9.3	156	12	8.4	468	63	92.8	0.36
GR11-27-38.FIN2	0.211	0.013	0.028	0.0016	0.0542	0.0016	0.85753	178.7	9.8	194	11	7.9	420	41	319	0.12
GR11-27-18.FIN2	0.246	0.010	0.0327	0.0013	0.0552	0.0014	0.68268	207	7.9	222.8	8.1	7.1	405	35	450	0.31
GR11-27-7.FIN2	0.268	0.022	0.0375	0.0026	0.0514	0.0026	0.75175	237	16	239	17	0.8	428	87	433	0.33
GR11-27-10.FIN2	0.28	0.025	0.0399	0.0028	0.0507	0.0026	0.77635	252	18	251	20	-0.4	442	76	2130	0.12
GR11-27-37.FIN2	0.297	0.012	0.04	0.0019	0.0534	0.0014	0.77691	253	12	264.3	9	4.3	381	35	990	0.22
GR11-27-29.FIN2	0.315	0.012	0.0434	0.0017	0.053	0.0011	0.81564	273.5	11	277.7	9	1.5	324	26	354	0.25

	Isotopic Ratios							Dates (Ma)							Concentration	
Sample and Analysis Number	207Pb/ 235U	± 2SE (abs)	206Pb/ 238U	± 2SE (abs)	207Pb/ 206Pb	± 2SE (abs)	Rho: 206/238 vs 207/235	206Pb/ 238U	± 2SE (abs)	207Pb/ 235U	± 2SE (abs)	% Discord. 6/38-7/35	207Pb/ 206Pb	± 2SE (abs)	U (ppm)	Th/U
GR11-27-22.FIN2	0.355	0.022	0.0492	0.0026	0.0523	0.0020	0.75413	309	16	306	16	-1.0	421	50	460	0.32
GR11-27-20.FIN2	0.569	0.036	0.0716	0.0041	0.0566	0.0024	0.70899	445	25	452	23	1.5	499	57	168	0.24
Biotite Granite Dike (GR11-32)																
GR11-32_4_e.FIN2	**0.025**	**0.001**	**0.0039**	**0.0001**	**0.0448**	**0.0016**	**0.73204**	**25.22**	**0.96**	**24.5**	**1.2**	**-2.9**	**236**	**50**	**1910**	**0.02**
GR11-32_5_a.FIN2	**0.027**	**0.001**	**0.0041**	**0.0002**	**0.0478**	**0.0017**	**0.67075**	**26.2**	**1.1**	**27**	**1.1**	**3.0**	**231**	**41**	**4030**	**0.11**
GR11-32_6_d.FIN2	**0.027**	**0.001**	**0.0042**	**0.0002**	**0.0468**	**0.0014**	**0.75536**	**27**	**1.1**	**27.1**	**1.2**	**0.4**	**215**	**42**	**4140**	**0.12**
GR11-32_5_d.FIN2	**0.027**	**0.001**	**0.0042**	**0.0002**	**0.0467**	**0.0015**	**0.63761**	**27.2**	**1**	**27.1**	**1.2**	**-0.4**	**214**	**41**	**881**	**0.28**
GR11-32_7_b.FIN2	**0.027**	**0.001**	**0.0043**	**0.0002**	**0.0474**	**0.0015**	**0.6693**	**27.3**	**1.1**	**27**	**0.98**	**-1.1**	**173**	**28**	**1570**	**0.17**
GR11-32_5_c.FIN2	**0.028**	**0.002**	**0.0043**	**0.0002**	**0.0471**	**0.0024**	**0.49825**	**27.5**	**1.2**	**28.2**	**1.5**	**2.5**	**297**	**93**	**568**	**0.16**
GR11-32_4_a.FIN2	**0.027**	**0.001**	**0.0043**	**0.0002**	**0.0465**	**0.0015**	**0.71193**	**27.6**	**1.1**	**27.2**	**1.1**	**-1.5**	**194**	**33**	**730**	**0.17**
GR11-32_8_a.FIN2	**0.028**	**0.001**	**0.0043**	**0.0002**	**0.0477**	**0.0016**	**0.64746**	**27.6**	**1.2**	**28.6**	**1.2**	**3.5**	**221**	**51**	**7460**	**0.09**
GR11-32_7_a.FIN2	**0.029**	**0.001**	**0.0043**	**0.0001**	**0.0475**	**0.0016**	**0.52614**	**27.83**	**0.98**	**28.7**	**1.1**	**3.0**	**273**	**38**	**1178**	**0.15**
GR11-32_2_g.FIN2	**0.028**	**0.001**	**0.0044**	**0.0002**	**0.046**	**0.0013**	**0.76627**	**28**	**1.2**	**27.9**	**1.2**	**-0.4**	**172**	**35**	**2280**	**0.37**
GR11-32_7_c.FIN2	0.035	0.002	0.0044	0.0002	0.0582	0.0020	0.64927	28.03	0.99	35	1.6	19.9	574	59	1910	0.15
GR11-32_2_c.FIN2	**0.028**	**0.001**	**0.0044**	**0.0002**	**0.0461**	**0.0011**	**0.81587**	**28.09**	**1**	**28.3**	**1.2**	**0.7**	**152**	**30**	**5430**	**0.10**
GR11-32_6_b.FIN2	**0.028**	**0.001**	**0.0044**	**0.0002**	**0.047**	**0.0014**	**0.78912**	**28.2**	**1.5**	**28.4**	**1.5**	**0.7**	**128**	**33**	**4000**	**0.09**
GR11-32_6_e.FIN2	**0.028**	**0.001**	**0.0044**	**0.0002**	**0.046**	**0.0014**	**0.69759**	**28.4**	**1.1**	**28.3**	**1.2**	**-0.4**	**237**	**38**	**2600**	**0.05**
GR11-32_6_c.FIN2	**0.029**	**0.001**	**0.0044**	**0.0002**	**0.0483**	**0.0017**	**0.75169**	**28.4**	**1.3**	**29.1**	**1.3**	**2.4**	**310**	**43**	**1690**	**0.16**
GR11-32_3_a.FIN2	**0.031**	**0.001**	**0.0044**	**0.0002**	**0.0494**	**0.0019**	**0.635**	**28.5**	**1.3**	**30.7**	**1.5**	**7.2**	**327**	**47**	**1009**	**0.21**
GR11-32_4_c.FIN2	**0.029**	**0.001**	**0.0045**	**0.0002**	**0.0478**	**0.0015**	**0.69863**	**28.6**	**1.2**	**29.2**	**1.2**	**2.1**	**202**	**32**	**2520**	**0.14**
GR11-32_1_d.FIN2	**0.028**	**0.001**	**0.0045**	**0.0002**	**0.0459**	**0.0016**	**0.61012**	**28.85**	**1.1**	**28.4**	**1.1**	**-1.6**	**202**	**31**	**728**	**0.39**
GR11-32_4_f.FIN2	**0.031**	**0.001**	**0.0045**	**0.0002**	**0.049**	**0.0014**	**0.6833**	**29**	**1.1**	**30.8**	**1.2**	**5.8**	**227**	**31**	**3430**	**0.09**
GR11-32_1_e.FIN2	**0.031**	**0.001**	**0.0045**	**0.0002**	**0.0488**	**0.0014**	**0.69691**	**29.18**	**1**	**31**	**1.2**	**5.9**	**252**	**32**	**1474**	**0.02**
GR11-32_6_a.FIN2	**0.03**	**0.002**	**0.0046**	**0.0002**	**0.048**	**0.0019**	**0.64654**	**29.3**	**1.2**	**30.3**	**1.5**	**3.3**	**331**	**54**	**886**	**0.16**
GR11-32_2_b.FIN2	**0.032**	**0.002**	**0.0046**	**0.0002**	**0.0494**	**0.0023**	**0.64494**	**29.3**	**1.4**	**31.5**	**2**	**7.0**	**454**	**80**	**3810**	**0.09**
GR11-32_4_d.FIN2	0.035	0.002	0.0046	0.0002	0.056	0.0026	0.52002	29.3	1.1	34.8	1.8	15.8	513	54	456	0.32
GR11-32_4_g.FIN2	**0.031**	**0.001**	**0.0046**	**0.0002**	**0.048**	**0.0017**	**0.686**	**29.4**	**1.1**	**30.7**	**1.5**	**4.2**	**327**	**52**	**1262**	**0.01**
GR11-32_4_b.FIN2	**0.033**	**0.002**	**0.0046**	**0.0002**	**0.0513**	**0.0029**	**0.56148**	**29.6**	**1.5**	**33**	**2.3**	**10.3**	**480**	**91**	**913**	**0.27**
GR11-32_1_a.FIN2	**0.032**	**0.001**	**0.0046**	**0.0002**	**0.0492**	**0.0017**	**0.7015**	**29.78**	**1**	**31.7**	**1.5**	**6.1**	**280**	**38**	**1820**	**0.02**
GR11-32_2_d.FIN2	**0.032**	**0.002**	**0.0046**	**0.0002**	**0.0512**	**0.0026**	**0.66885**	**29.8**	**1.4**	**32**	**2.1**	**6.9**	**533**	**67**	**1274**	**0.32**
GR11-32_5_b.FIN2	**0.032**	**0.001**	**0.0047**	**0.0002**	**0.0494**	**0.0014**	**0.68289**	**29.91**	**0.95**	**31.6**	**1.2**	**5.3**	**256**	**34**	**3750**	**0.18**
GR11-32_7_d.FIN2	**0.033**	**0.003**	**0.0047**	**0.0003**	**0.0499**	**0.0034**	**0.58322**	**30.2**	**1.7**	**32.8**	**2.6**	**7.9**	**259**	**64**	**728**	**0.20**
GR11-32_2_f.FIN2	**0.032**	**0.001**	**0.0047**	**0.0002**	**0.0489**	**0.0015**	**0.72725**	**30.3**	**1.4**	**31.8**	**1.5**	**4.7**	**187**	**32**	**1460**	**0.18**

	Isotopic Ratios							Dates (Ma)							Concentration	
Sample and Analysis Number	207Pb/ 235U	± 2SE (abs)	206Pb/ 238U	± 2SE (abs)	207Pb/ 206Pb	± 2SE (abs)	Rho: 206/238 vs 207/235	206Pb/ 238U	± 2SE (abs)	207Pb/ 235U	± 2SE (abs)	% Discord. 6/38-7/35	207Pb/ 206Pb	± 2SE (abs)	U (ppm)	Th/U
GR11-32_2_a.FIN2	**0.033**	**0.002**	**0.0047**	**0.0002**	**0.0479**	**0.0023**	**0.41349**	**30.4**	**1.3**	**32.5**	**1.9**	**6.5**	**198**	**76**	**1561**	**0.02**
GR11-32_6_f.FIN2	0.051	0.004	0.0048	0.0002	0.0787	0.0053	0.48795	30.5	1.2	50	3.7	39.0	1120	110	392	0.26
GR11-32_1_b.FIN2	**0.034**	**0.003**	**0.0048**	**0.0002**	**0.0512**	**0.0029**	**0.73954**	**31.1**	**1.5**	**33.5**	**2.7**	**7.2**	**382**	**61**	**1490**	**0.08**
GR11-32_1_c.FIN2	**0.036**	**0.002**	**0.0051**	**0.0002**	**0.0508**	**0.0019**	**0.6155**	**32.5**	**1.3**	**36.2**	**1.7**	**10.2**	**391**	**45**	**1026**	**0.03**
GR11-32_7_e.FIN2	0.078	0.004	0.0111	0.0005	0.0506	0.0015	0.85187	70.9	3.2	76.2	3.5	7.0	263	41	3190	0.18
GR11-32_2_e.FIN2	0.364	0.015	0.0475	0.0019	0.0563	0.0016	0.77125	299	12	315	11	5.1	471	43	917	0.07
Garnet-Biotite-Muscovite Pegmatite Dike (GR11-34)																
GR11-34_7_a.FIN2	**0.029**	**0.001**	**0.0044**	**0.0002**	**0.047**	**0.0017**	**0.59435**	**28.2**	**1.1**	**28.6**	**1.4**	**1.4**	**207**	**34**	**578**	**0.09**
GR11-34_4_d.FIN2	**0.031**	**0.002**	**0.0045**	**0.0002**	**0.0498**	**0.0029**	**0.14557**	**28.82**	**1**	**31.3**	**1.6**	**7.9**	**404**	**57**	**220**	**0.01**
GR11-34_2_c.FIN2	**0.029**	**0.001**	**0.0045**	**0.0002**	**0.0457**	**0.0018**	**0.54587**	**28.99**	**1**	**28.5**	**1.2**	**-1.7**	**248**	**50**	**503**	**0.09**
GR11-34_6_e.FIN2	**0.028**	**0.002**	**0.0045**	**0.0002**	**0.0452**	**0.0023**	**0.62617**	**29**	**1.4**	**27.7**	**1.6**	**-4.7**	**159**	**38**	**637**	**0.11**
GR11-34_2_b.FIN2	**0.027**	**0.001**	**0.0045**	**0.0002**	**0.0443**	**0.0016**	**0.61295**	**29.2**	**1.1**	**26.9**	**1.1**	**-8.6**	**172**	**52**	**680**	**0.32**
GR11-34_3_e.FIN2	**0.029**	**0.001**	**0.0046**	**0.0002**	**0.0451**	**0.0014**	**0.7194**	**29.4**	**1.2**	**29.1**	**1.3**	**-1.0**	**181**	**39**	**1270**	**0.11**
GR11-34_3_b.FIN2	**0.032**	**0.001**	**0.0046**	**0.0002**	**0.0494**	**0.0018**	**0.55185**	**29.64**	**1**	**31.5**	**1.4**	**5.9**	**303**	**41**	**506**	**0.10**
GR11-34_5_b.FIN2	**0.029**	**0.001**	**0.0046**	**0.0002**	**0.0468**	**0.0019**	**0.51679**	**29.7**	**1.2**	**29**	**1.3**	**-2.4**	**196**	**36**	**429**	**0.09**
GR11-34_10_a.FIN2	**0.029**	**0.001**	**0.0046**	**0.0002**	**0.0459**	**0.0019**	**0.49661**	**29.7**	**1.1**	**29.1**	**1.3**	**-2.1**	**233**	**37**	**387**	**0.34**
GR11-34_2_a.FIN2	**0.033**	**0.001**	**0.0046**	**0.0001**	**0.0514**	**0.0017**	**0.48819**	**29.76**	**0.96**	**32.5**	**1.1**	**8.4**	**311**	**39**	**557**	**0.09**
GR11-34_10_c.FIN2	**0.033**	**0.003**	**0.0046**	**0.0002**	**0.048**	**0.0039**	**0.45613**	**29.8**	**1.5**	**33.1**	**3.3**	**10.0**	**258**	**84**	**257**	**0.09**
GR11-34_3_c.FIN2	**0.031**	**0.001**	**0.0047**	**0.0002**	**0.0479**	**0.0016**	**0.69789**	**30.1**	**1.2**	**31.1**	**1.5**	**3.2**	**265**	**44**	**1130**	**0.00**
GR11-34_9_d.FIN2	**0.03**	**0.001**	**0.0047**	**0.0002**	**0.0464**	**0.0017**	**0.45339**	**30.2**	**1.1**	**29.9**	**1.1**	**-1.0**	**197**	**43**	**584**	**0.10**
GR11-34_9_c.FIN2	**0.035**	**0.002**	**0.0047**	**0.0002**	**0.0548**	**0.0024**	**0.37894**	**30.31**	**1.1**	**35.1**	**1.6**	**13.6**	**449**	**48**	**316**	**0.08**
GR11-34_9_b.FIN2	**0.03**	**0.001**	**0.0047**	**0.0002**	**0.0457**	**0.0017**	**0.56071**	**30.4**	**1.1**	**30**	**1.2**	**-1.3**	**92**	**32**	**1917**	**0.12**
GR11-34_8_b.FIN2	**0.032**	**0.002**	**0.0047**	**0.0002**	**0.049**	**0.0030**	**0.26316**	**30.4**	**1.3**	**31.9**	**1.9**	**4.7**	**280**	**66**	**384**	**0.43**
GR11-34_8_a.FIN2	**0.031**	**0.002**	**0.0048**	**0.0002**	**0.0463**	**0.0025**	**0.59317**	**30.6**	**1.4**	**30.5**	**2.1**	**-0.3**	**257**	**59**	**314**	**0.53**
GR11-34_8_c.FIN2	**0.116**	**0.030**	**0.0058**	**0.0005**	**0.149**	**0.0360**	**0.51173**	**37.5**	**3.1**	**115**	**29**	**67.4**	**2170**	**500**	**253**	**0.08**
GR11-34_10_b.FIN2	0.044	0.006	0.0064	0.0007	0.0519	0.0049	0.74831	40.9	4.6	43.6	6.2	6.2	320	110	331	0.18
GR11-34_9_e.FIN2	0.072	0.005	0.0101	0.0006	0.0507	0.0022	0.77799	64.5	4	70.9	5.1	9.0	271	48	538	0.08
GR11-34_6_f.FIN2	0.163	0.012	0.0122	0.0006	0.0929	0.0069	0.41587	78.4	4.1	152	11	48.4	1480	130	299	0.44
GR11-34_4_a.FIN2	0.185	0.008	0.0239	0.0010	0.0539	0.0015	0.66669	152.4	6.5	171.8	7	11.3	361	34	1717	0.12
GR11-34_7_b.FIN2	0.202	0.010	0.0286	0.0013	0.0511	0.0017	0.74429	181.9	7.9	186	8.1	2.2	294	47	4410	0.08
GR11-34_5_a.FIN2	0.216	0.012	0.0295	0.0015	0.0509	0.0016	0.83488	187.1	9.5	197.8	10	5.4	291	47	883	0.77
GR11-34_3_a.FIN2	0.265	0.012	0.036	0.0014	0.0535	0.0019	0.67902	229	8.6	239.1	9.5	4.2	394	49	723	0.23
GR11-34_5_d.FIN2	0.264	0.012	0.0377	0.0017	0.0511	0.0015	0.78442	238.4	11	236.8	9.3	-0.7	265	32	1580	0.52

	Isotopic Ratios							Dates (Ma)							Concentration	
Sample and	207Pb/	± 2SE	206Pb/	± 2SE	207Pb/	± 2SE	Rho: 206/238	206Pb/	± 2SE	207Pb/	± 2SE	% Discord.	207Pb/	± 2SE	U	
Analysis Number	235U	(abs)	238U	(abs)	206Pb	(abs)	vs 207/235	238U	(abs)	235U	(abs)	6/38-7/35	206Pb	(abs)	(ppm)	Th/U
GR11-34_5_c.FIN2	0.273	0.009	0.038	0.0013	0.0528	0.0014	0.72408	240.3	8.3	245.6	7.3	2.2	362	30	944	0.28
GR11-34_4_c.FIN2	0.287	0.012	0.0395	0.0016	0.0526	0.0013	0.7999	249.6	10	256.6	8.9	2.7	328	39	1133	0.18
GR11-34_9_a.FIN2	0.285	0.010	0.0396	0.0013	0.0513	0.0013	0.73047	250.1	8.3	253.7	8.1	1.4	283	38	446	0.15
GR11-34_3_f.FIN2	0.298	0.012	0.0428	0.0016	0.0511	0.0013	0.80542	270.1	10	265.6	9.5	-1.7	273	37	297	0.29
GR11-34_4_b.FIN2	0.314	0.011	0.0438	0.0016	0.0511	0.0014	0.70479	275.9	9.7	276.8	8.5	0.3	285	39	1084	0.20
GR11-34_2_d.FIN2	0.317	0.012	0.0442	0.0016	0.0525	0.0013	0.80934	278.5	9.6	278.5	8.9	0.0	330	29	841	0.23
GR11-34_3_d.FIN2	0.314	0.013	0.0444	0.0017	0.0502	0.0012	0.83045	279.6	11	276.1	10	-1.3	284	37	444	0.27
Two-mica Pegmatite Dike (VER11-1)																
VER11-1_1_i.FIN2	0.031	0.003	0.0038	0.0003	0.0584	0.0039	0.60358	24.2	1.7	31.1	2.6	22.2	622	85	383	0.55
VER11-1_1_h.FIN2	**0.026**	**0.002**	**0.0038**	**0.0002**	**0.0477**	**0.0021**	**0.74653**	**24.68**	**1.4**	**26.24**	**1.8**	**5.9**	**223**	**31**	**634**	**0.37**
VER11-1_7_b.FIN2	**0.027**	**0.002**	**0.0039**	**0.0002**	**0.0508**	**0.0024**	**0.62377**	**24.86**	**1.4**	**27.4**	**1.9**	**9.3**	**272**	**33**	**181.8**	**0.44**
VER11-1_1_j.FIN2	**0.027**	**0.002**	**0.0039**	**0.0002**	**0.0478**	**0.0021**	**0.78338**	**24.94**	**1.4**	**26.65**	**1.8**	**6.4**	**224**	**28**	**5560**	**0.08**
VER11-1_3_g.FIN2	**0.025**	**0.002**	**0.0039**	**0.0002**	**0.0455**	**0.0020**	**0.73889**	**25**	**1.4**	**24.85**	**1.7**	**-0.6**	**99**	**22**	**361**	**0.13**
VER11-1_1_e.FIN2	**0.026**	**0.002**	**0.0039**	**0.0003**	**0.047**	**0.0033**	**0.44573**	**25**	**1.7**	**25.6**	**2.3**	**2.3**	**346**	**90**	**136**	**0.24**
VER11-1_3_e.FIN2	**0.025**	**0.002**	**0.0039**	**0.0003**	**0.0463**	**0.0025**	**0.73216**	**25.1**	**1.7**	**25.3**	**2.2**	**0.8**	**192**	**50**	**234.7**	**0.47**
VER11-1_4_b.FIN2	**0.025**	**0.002**	**0.0039**	**0.0002**	**0.0465**	**0.0020**	**0.78981**	**25.12**	**1.4**	**24.73**	**1.7**	**-1.6**	**186**	**30**	**892**	**0.11**
VER11-1_4_i.FIN2	0.029	0.003	0.0039	0.0003	0.0535	0.0032	0.74631	25.3	1.9	29.3	2.5	13.7	447	64	154.1	0.40
VER11-1_4_f.FIN2	**0.025**	**0.002**	**0.0039**	**0.0002**	**0.0446**	**0.0024**	**0.61329**	**25.4**	**1.6**	**25.1**	**2**	**-1.2**	**213**	**49**	**137.9**	**0.36**
VER11-1_3_c.FIN2	**0.024**	**0.002**	**0.004**	**0.0003**	**0.0448**	**0.0024**	**0.7572**	**25.6**	**1.9**	**24.4**	**2**	**-4.9**	**145**	**42**	**243**	**0.15**
VER11-1_1_b.FIN2	**0.024**	**0.002**	**0.004**	**0.0002**	**0.0458**	**0.0022**	**0.67358**	**25.6**	**1.5**	**24.52**	**1.7**	**-4.4**	**195**	**38**	**304**	**0.50**
VER11-1_5_a.FIN2	**0.026**	**0.002**	**0.004**	**0.0003**	**0.0469**	**0.0021**	**0.88578**	**25.6**	**1.9**	**25.8**	**2**	**0.8**	**163**	**28**	**4520**	**0.02**
VER11-1_6_h.FIN2	**0.027**	**0.002**	**0.004**	**0.0002**	**0.0477**	**0.0023**	**0.59556**	**25.61**	**1.4**	**26.7**	**1.9**	**4.1**	**229**	**42**	**245.1**	**0.31**
VER11-1_4_e.FIN2	**0.026**	**0.002**	**0.004**	**0.0002**	**0.0474**	**0.0024**	**0.67981**	**25.8**	**1.5**	**26**	**1.8**	**0.8**	**295**	**49**	**268**	**0.38**
VER11-1_2_c.FIN2	**0.028**	**0.002**	**0.004**	**0.0002**	**0.05**	**0.0024**	**0.64675**	**25.84**	**1.4**	**27.8**	**2**	**7.1**	**304**	**46**	**274.5**	**0.47**
VER11-1_4_j.FIN2	0.032	0.003	0.004	0.0002	0.0553	0.0033	0.43324	25.84	1.4	31.8	2.6	18.7	500	85	269.1	0.52
VER11-1_2_b.FIN2	0.03	0.002	0.004	0.0002	0.0545	0.0031	0.44808	25.96	1.5	30	2.4	13.5	512	70	250	0.50
VER11-1_6_c.FIN2	0.032	0.003	0.004	0.0004	0.0593	0.0040	0.71283	26	2.6	31.6	3	17.7	562	89	1011	0.01
VER11-1_1_a.FIN2	**0.028**	**0.002**	**0.0041**	**0.0002**	**0.0505**	**0.0026**	**0.4842**	**26.07**	**1.3**	**27.6**	**1.9**	**5.5**	**292**	**44**	**266.7**	**0.54**
VER11-1_1_k.FIN2	**0.026**	**0.002**	**0.0041**	**0.0002**	**0.0457**	**0.0020**	**0.80802**	**26.1**	**1.5**	**26.3**	**1.9**	**0.8**	**167**	**29**	**2390**	**0.11**
VER11-1_6_f.FIN2	**0.027**	**0.002**	**0.0041**	**0.0003**	**0.0464**	**0.0027**	**0.62436**	**26.1**	**1.9**	**26.8**	**2.3**	**2.6**	**222**	**32**	**107**	**0.32**
VER11-1_6_b.FIN2	0.036	0.006	0.0041	0.0002	0.0599	0.0059	0.85738	26.2	1.6	36	5.5	27.2	600	120	213	0.35
VER11-1_1_d.FIN2	**0.025**	**0.002**	**0.0041**	**0.0003**	**0.0453**	**0.0023**	**0.69494**	**26.3**	**1.7**	**24.8**	**1.9**	**-6.0**	**188**	**47**	**256**	**0.23**
VER11-1_4_a.FIN2	**0.028**	**0.002**	**0.0041**	**0.0002**	**0.0502**	**0.0022**	**0.74975**	**26.45**	**1.4**	**27.9**	**1.9**	**5.2**	**244**	**31**	**930**	**0.22**
VER11-1_3_f.FIN2	**0.027**	**0.002**	**0.0041**	**0.0002**	**0.047**	**0.0022**	**0.7668**	**26.5**	**1.5**	**27.2**	**2**	**2.6**	**160**	**32**	**397**	**0.17**

	Isotopic Ratios							Dates (Ma)							Concentration	
Sample and	207Pb/	± 2SE	206Pb/	± 2SE	207Pb/	± 2SE	Rho: 206/238	206Pb/	± 2SE	207Pb/	± 2SE	% Discord.	207Pb/	± 2SE	U	
Analysis Number	235U	(abs)	238U	(abs)	206Pb	(abs)	vs 207/235	238U	(abs)	235U	(abs)	6/38-7/35	206Pb	(abs)	(ppm)	Th/U
VER11-1_6_a.FIN2	0.043	0.004	0.0042	0.0003	0.073	0.0050	0.67552	26.7	1.7	42.2	4.1	36.7	960	110	560	0.13
VER11-1_2_a.FIN2	0.031	0.002	0.0042	0.0002	0.0548	0.0025	0.57196	26.72	1.3	31.3	2.1	14.6	402	41	276.3	0.61
VER11-1_4_c.FIN2	**0.028**	**0.004**	**0.0042**	**0.0005**	**0.048**	**0.0024**	**0.95351**	**26.9**	**3.1**	**28.4**	**4.3**	**5.3**	**149**	**58**	**1650**	**0.13**
VER11-1_4_g.FIN2	0.074	0.007	0.0043	0.0002	0.1238	0.0080	0.57228	27.5	1.6	72.2	6.1	61.9	1999	85	373	0.27
VER11-1_3_j.FIN2	0.037	0.004	0.0051	0.0005	0.0504	0.0039	0.76595	32.9	3.1	36.6	4.1	10.1	297	56	339	0.06
VER11-1_3_b.FIN2	0.199	0.016	0.0274	0.0019	0.0528	0.0022	0.9063	174.3	12	183.6	14	5.1	332	35	409	0.14
VER11-1_3_a.FIN2	0.21	0.025	0.03	0.0035	0.0505	0.0040	0.68816	190	22	192	21	1.0	350	160	1880	0.05
VER11-1_4_d.FIN2	0.226	0.017	0.0326	0.0020	0.0501	0.0020	0.89362	206.6	12	207.4	14	0.4	256	30	775	0.54
VER11-1_7_a.FIN2	0.309	0.023	0.0339	0.0022	0.0664	0.0030	0.80898	215	14	272	18	21.0	834	45	534	1.19
VER11-1_4_h.FIN2	0.279	0.020	0.0374	0.0022	0.0526	0.0021	0.88342	236.4	14	249.3	16	5.2	350	27	830	0.23
VER11-1_2_f.FIN2	0.283	0.020	0.0387	0.0023	0.0509	0.0021	0.83657	244.9	14	254.3	17	3.7	276	35	369	0.28
VER11-1_6_d.FIN2	0.301	0.022	0.0409	0.0026	0.0519	0.0023	0.80008	258	16	268	17	3.7	275	45	865	0.06
VER11-1_3_h.FIN2	0.318	0.022	0.0433	0.0025	0.0512	0.0021	0.83276	273	16	279.7	17	2.4	292	35	326	0.23
VER11-1_6_g.FIN2	0.318	0.023	0.0435	0.0026	0.0524	0.0023	0.799	275	16	282.4	17	2.6	356	34	930	0.00
VER11-1_1_c.FIN2	0.318	0.024	0.0474	0.0027	0.0494	0.0021	0.81034	298	17	279	18	-6.8	240	38	991	0.38
VER11-1_3_i.FIN2	0.375	0.026	0.0473	0.0026	0.0556	0.0027	0.53484	298	16	322.6	19	7.6	456	33	37.7	0.31
VER11-1_2_g.FIN2	0.473	0.033	0.0541	0.0032	0.0595	0.0024	0.83716	339	20	394	23	14.0	582	33	632	0.04
VER11-1_3_d.FIN2	0.602	0.066	0.0737	0.0072	0.0595	0.0024	0.97555	455	43	467	43	2.6	603	28	286	0.18
VER11-1_1_f.FIN2	0.605	0.041	0.0771	0.0041	0.0574	0.0025	0.68621	479	24	483	26	0.8	533	33	770	0.18
VER11-1_5_b.FIN2	0.736	0.056	0.0899	0.0061	0.0593	0.0027	0.83169	554	36	560	32	1.1	591	43	156	0.32
VER11-1_2_e.FIN2	0.797	0.056	0.0906	0.0049	0.0612	0.0025	0.77352	558	29	593	32	5.9	641	37	209	0.44
VER11-1_6_e.FIN2	0.745	0.053	0.0917	0.0053	0.0575	0.0023	0.88667	565	32	562	31	-0.5	518	27	365	0.34
VER11-1_1_g.FIN2	0.862	0.063	0.0979	0.0056	0.0642	0.0029	0.80977	601	33	633	33	5.1	763	37	162	0.69
VER11-1_2_d.FIN2	1.214	0.097	0.1357	0.0088	0.0641	0.0025	0.91385	820	50	803	44	-2.1	760	31	169.5	0.52
Leucogranite NOV11-1A																
NOV11-1A_6j.FIN2	0.484	0.049	0.0397	0.0017	0.09	0.0083	0.42854	250.9	10	395	33	36.5	1300	170	868	0.22
NOV11-1A_2d.FIN2	0.285	0.010	0.04	0.0014	0.052	0.0012	0.84219	252.5	8.6	255.2	8.2	1.1	283	16	563	0.67
NOV11-1A_5i.FIN2	0.295	0.011	0.0401	0.0015	0.0527	0.0014	0.75327	253.4	9.5	262.7	8.7	3.5	338	25	675	0.08
NOV11-1A_5r.FIN2	0.295	0.011	0.0403	0.0014	0.0523	0.0013	0.7611	254.5	8.7	262.6	8.8	3.1	313	22	577	0.08
NOV11-1A_4b.FIN2	0.289	0.011	0.0403	0.0017	0.0513	0.0015	0.67636	255.9	11	257.3	8.8	0.5	263	25	213	0.17
NOV11-1A_4d.FIN2	0.295	0.011	0.0406	0.0014	0.0518	0.0012	0.76832	256.5	8.5	262.4	8.4	2.2	268	18	389	0.63
NOV11-1A_7l.FIN2	0.286	0.012	0.0408	0.0016	0.0508	0.0015	0.65817	257.9	9.8	255.2	9.8	-1.1	221	30	1065	0.09
NOV11-1A_8b.FIN2	0.287	0.010	0.0409	0.0016	0.0516	0.0015	0.75353	258.5	9.8	255.9	8	-1.0	285	25	686	0.75
NOV11-1A_8d.FIN2	0.284	0.012	0.0411	0.0017	0.051	0.0015	0.18324	259.6	11	253.7	9.6	-2.3	256	27	162.1	0.33

	Isotopic Ratios							Dates (Ma)							Concentration	
Sample and	207Pb/	± 2SE	206Pb/	± 2SE	207Pb/	± 2SE	Rho: 206/238	206Pb/	± 2SE	207Pb/	± 2SE	% Discord.	207Pb/	± 2SE	U	
Analysis Number	235U	(abs)	238U	(abs)	206Pb	(abs)	vs 207/235	238U	(abs)	235U	(abs)	6/38-7/35	206Pb	(abs)	(ppm)	Th/U
NOV11-1A_6l.FIN2	0.302	0.013	0.0412	0.0017	0.0528	0.0018	0.64605	260	11	269.1	10	3.4	325	32	1400	0.08
NOV11-1A_4m.FIN2	0.299	0.011	0.0412	0.0015	0.0514	0.0013	0.75113	260.3	9.2	265.6	8.4	2.0	264	16	287.5	0.42
NOV11-1A_5q.FIN2	0.299	0.011	0.0412	0.0015	0.052	0.0013	0.82778	260.3	9.4	265.4	8.8	1.9	277	19	1004	0.08
NOV11-1A_7d.FIN2	0.293	0.011	0.0412	0.0016	0.0515	0.0013	0.80053	260.3	9.6	261.2	8.6	0.3	265	19	402	0.38
NOV11-1A_6h.FIN2	0.303	0.011	0.0413	0.0014	0.053	0.0013	0.73235	260.5	8.7	268.6	8.3	3.0	337	17	526	0.20
NOV11-1A_3l.FIN2	0.305	0.011	0.0413	0.0016	0.0528	0.0015	0.70048	260.6	9.8	270.2	8.8	3.6	313	22	515	0.06
NOV11-1A_1b.FIN2	0.298	0.012	0.0414	0.0016	0.0522	0.0014	0.73094	261.4	9.9	264.1	9.1	1.0	314	20	89	0.33
NOV11-1A_3m.FIN2	0.296	0.010	0.0414	0.0014	0.0518	0.0012	0.79599	261.4	8.6	263.1	8.1	0.6	283	16	632	0.07
NOV11-1A_3n.FIN2	0.302	0.011	0.0414	0.0015	0.0521	0.0013	0.78848	261.4	9	267.8	8.5	2.4	288	20	365	0.17
NOV11-1A_3g.FIN2	0.305	0.011	0.0414	0.0014	0.0521	0.0014	0.71545	261.5	8.9	270.4	8.7	3.3	293	21	371	0.44
NOV11-1A_3i.FIN2	0.297	0.011	0.0414	0.0014	0.0512	0.0013	0.69232	261.5	8.5	264	8.4	0.9	248	22	179.8	0.56
NOV11-1A_8j.FIN2	0.296	0.012	0.0414	0.0018	0.051	0.0015	0.80267	261.7	11	262.6	9.5	0.3	252	33	310.2	0.25
NOV11-1A_6d.FIN2	0.301	0.011	0.0415	0.0014	0.0526	0.0014	0.74674	261.9	8.8	266.8	9	1.8	309	21	420.3	0.45
NOV11-1A_6o.FIN2	0.316	0.013	0.0415	0.0016	0.0554	0.0015	0.62752	262.2	9.7	278.5	10	5.9	423	28	194.5	0.48
NOV11-1A_5d.FIN2	0.304	0.011	0.0416	0.0014	0.0522	0.0013	0.65099	262.4	8.8	269.8	8.3	2.7	294	20	218.4	0.32
NOV11-1A_8l.FIN2	0.304	0.014	0.0416	0.0017	0.0547	0.0015	0.7843	262.5	11	268.7	11	2.3	399	31	1864	0.55
NOV11-1A_3d.FIN2	0.299	0.011	0.0417	0.0015	0.0515	0.0013	0.78721	263.1	9	265.7	8.2	1.0	262	15	430	0.42
NOV11-1A_3a.FIN2	0.298	0.010	0.0417	0.0014	0.0512	0.0012	0.72426	263.5	8.5	264.4	8	0.3	254	17	1470	0.03
NOV11-1A_8e.FIN2	0.296	0.010	0.0418	0.0015	0.0524	0.0013	0.78224	263.6	9	263.4	8	-0.1	309	16	595	0.12
NOV11-1A_7o.FIN2	0.3	0.013	0.0418	0.0017	0.0528	0.0014	0.929	263.7	11	266	10	0.9	330	22	808	0.24
NOV11-1A_6q.FIN2	0.299	0.011	0.0418	0.0016	0.0516	0.0014	0.7302	263.8	9.7	265.6	8.7	0.7	272	25	551	0.28
NOV11-1A_1f.FIN2	0.292	0.011	0.0418	0.0015	0.0506	0.0014	0.65441	263.9	9.2	259.9	8.5	-1.5	236	26	823	0.08
NOV11-1A_4j.FIN2	0.301	0.011	0.0418	0.0015	0.0513	0.0013	0.7686	263.9	9.3	267	8.2	1.2	275	22	724	0.18
NOV11-1A_5c.FIN2	0.305	0.011	0.0418	0.0014	0.0526	0.0013	0.67482	264.2	8.6	270.6	8.6	2.4	319	20	277.9	0.50
NOV11-1A_3o.FIN2	0.665	0.054	0.0419	0.0018	0.1126	0.0076	0.58835	264.6	11	513	33	48.4	1850	110	281	0.60
NOV11-1A_5n.FIN2	0.299	0.013	0.0419	0.0018	0.051	0.0015	0.76928	264.7	11	265.5	10	0.3	247	29	331.3	0.43
NOV11-1A_7e.FIN2	0.301	0.011	0.0419	0.0015	0.0522	0.0013	0.72799	264.8	9.1	267.3	8.4	0.9	290	17	355	0.43
NOV11-1A_6t.FIN2	0.299	0.011	0.042	0.0015	0.0517	0.0012	0.81321	265.2	9.1	265	8.4	-0.1	284	17	602	0.16
NOV11-1A_8c.FIN2	0.296	0.011	0.042	0.0016	0.0512	0.0013	0.78584	265.2	9.8	263.2	8.5	-0.8	267	19	429	0.06
NOV11-1A_1g.FIN2	0.305	0.011	0.0421	0.0015	0.0532	0.0013	0.75702	265.5	9.2	270.3	8.3	1.8	334	21	842	0.06
NOV11-1A_3j.FIN2	0.303	0.011	0.0421	0.0015	0.0523	0.0013	0.7523	265.6	9	269.1	8.2	1.3	297	19	828	0.10
NOV11-1A_5j.FIN2	0.306	0.011	0.0421	0.0016	0.0531	0.0017	0.56699	265.6	9.9	270.8	8.4	1.9	334	34	436	0.16
NOV11-1A_6m.FIN2	0.3	0.011	0.0421	0.0015	0.0509	0.0012	0.80385	265.9	9.3	266.1	8.7	0.1	239	18	1097	0.09
NOV11-1A_3b.FIN2	0.303	0.010	0.0422	0.0015	0.0517	0.0014	0.6182	266.1	9.1	268.5	7.9	0.9	276	20	174.8	0.44

	Isotopic Ratios							Dates (Ma)							Concentration	
Sample and	207Pb/	± 2SE	206Pb/	± 2SE	207Pb/	± 2SE	Rho: 206/238	206Pb/	± 2SE	207Pb/	± 2SE	% Discord.	207Pb/	± 2SE	U	
Analysis Number	235U	(abs)	238U	(abs)	206Pb	(abs)	vs 207/235	238U	(abs)	235U	(abs)	6/38-7/35	206Pb	(abs)	(ppm)	Th/U
NOV11-1A_3p.FIN2	0.309	0.011	0.0422	0.0014	0.0525	0.0013	0.70876	266.4	8.7	273.1	8.2	2.5	302	23	336	0.28
NOV11-1A_5a.FIN2	0.306	0.012	0.0422	0.0015	0.0515	0.0013	0.77761	266.6	9.5	270.4	9.1	1.4	289	22	1310	0.12
NOV11-1A_5o.FIN2	0.313	0.011	0.0423	0.0017	0.0535	0.0014	0.73921	266.7	10	275.9	8.8	3.3	364	20	492	0.21
NOV11-1A_7a.FIN2	0.303	0.011	0.0423	0.0015	0.052	0.0013	0.73777	266.7	9.5	268.8	8.4	0.8	287	21	1240	0.06
NOV11-1A_6n.FIN2	0.306	0.012	0.0421	0.0017	0.0519	0.0014	0.80909	266.8	10	270.4	9.3	1.3	309	23	259	0.46
NOV11-1A_4n.FIN2	0.306	0.010	0.0423	0.0015	0.0517	0.0013	0.73518	266.9	9.2	271.1	8.1	1.5	276	17	486	0.15
NOV11-1A_6g.FIN2	0.315	0.013	0.0423	0.0017	0.0545	0.0016	0.72798	267	10	278	9.7	4.0	389	19	289	0.12
NOV11-1A_5e.FIN2	0.388	0.018	0.0423	0.0016	0.066	0.0023	0.70336	267.2	9.6	332.1	13	19.5	800	50	702	0.13
NOV11-1A_8h.FIN2	0.299	0.011	0.0423	0.0015	0.0523	0.0014	0.73252	267.2	9.4	265.6	8.7	-0.6	289	27	187.5	0.54
NOV11-1A_9j.FIN2	0.305	0.012	0.0423	0.0016	0.0525	0.0016	0.64887	267.2	9.7	269.8	9.5	1.0	308	26	195	0.49
NOV11-1A_5m.FIN2	0.441	0.038	0.0423	0.0017	0.0732	0.0051	0.63251	267.3	11	367	26	27.2	950	130	280	0.23
NOV11-1A_6c.FIN2	0.743	0.075	0.0424	0.0020	0.1234	0.0092	0.74606	267.5	12	547	41	51.1	2030	100	412	0.38
NOV11-1A_4f.FIN2	0.305	0.011	0.0424	0.0015	0.0514	0.0015	0.66058	267.7	9.2	269.8	8.7	0.8	267	22	469	0.24
NOV11-1A_5b.FIN2	0.312	0.012	0.0424	0.0017	0.0529	0.0014	0.82284	267.7	11	275.1	9.4	2.7	321	27	779	0.13
NOV11-1A_3f.FIN2	0.31	0.012	0.0425	0.0016	0.0525	0.0014	0.76451	268	9.8	273.6	9.2	2.0	300	26	493	0.45
NOV11-1A_4p.FIN2	0.312	0.014	0.0425	0.0019	0.0526	0.0013	0.90984	268	12	274.9	11	2.5	301	14	1008	0.08
NOV11-1A_2e.FIN2	0.306	0.011	0.0424	0.0015	0.0521	0.0013	0.76655	268.4	9.2	271.6	8.7	1.2	289	16	589	0.19
NOV11-1A_2a.FIN2	0.324	0.014	0.0426	0.0015	0.055	0.0019	0.4462	268.8	9	284.4	11	5.5	401	46	118	0.26
NOV11-1A_2c.FIN2	0.313	0.012	0.0426	0.0015	0.0536	0.0014	0.72773	268.8	9.5	276.6	8.9	2.8	352	20	750	0.13
NOV11-1A_5p.FIN2	0.303	0.011	0.0426	0.0015	0.0519	0.0015	0.59483	268.9	9.5	269.3	8.5	0.1	277	24	1670	0.07
NOV11-1A_9h.FIN2	0.343	0.027	0.0426	0.0022	0.0586	0.0035	0.73657	269	14	298	20	9.7	560	100	272	0.15
NOV11-1A_7b.FIN2	0.298	0.012	0.0427	0.0020	0.052	0.0016	0.76987	269.2	12	264.6	9.5	-1.7	284	34	943	0.09
NOV11-1A_8a.FIN2	0.316	0.010	0.0427	0.0014	0.0542	0.0014	0.55827	269.2	8.7	279.4	8	3.7	365	18	581	0.28
NOV11-1A_9d.FIN2	0.3	0.012	0.0427	0.0016	0.0525	0.0013	0.79629	269.2	9.8	265.6	9	-1.4	301	20	301	0.51
NOV11-1A_9e.FIN2	0.287	0.011	0.0427	0.0017	0.049	0.0013	0.76844	269.3	11	256.7	9	-4.9	178	22	2145	0.08
NOV11-1A_6r.FIN2	0.313	0.012	0.0428	0.0017	0.0532	0.0015	0.65728	269.9	10	277.4	9.3	2.7	329	28	1027	0.16
NOV11-1A_8f.FIN2	0.302	0.014	0.0427	0.0022	0.0521	0.0016	0.7232	270	14	269.4	11	-0.2	283	31	160.7	0.30
NOV11-1A_8k.FIN2	0.303	0.011	0.0428	0.0015	0.0521	0.0013	0.80586	270.2	9.2	268.4	8.6	-0.7	285	15	989	0.05
NOV11-1A_3c.FIN2	0.306	0.010	0.0428	0.0015	0.052	0.0013	0.72133	270.3	9.3	270.7	8.1	0.1	286	16	371	0.46
NOV11-1A_7s.FIN2	0.298	0.011	0.0427	0.0016	0.0509	0.0013	0.78434	270.3	9.9	264.6	8.9	-2.2	246	20	225	0.32
NOV11-1A_4g.FIN2	0.405	0.025	0.0429	0.0019	0.067	0.0034	0.36758	270.4	12	344	18	21.4	840	100	1036	0.19
NOV11-1A_6e.FIN2	0.304	0.011	0.0429	0.0014	0.0515	0.0014	0.67197	270.4	8.9	269.1	8.4	-0.5	261	24	163.4	0.38
NOV11-1A_8g.FIN2	0.304	0.011	0.0429	0.0015	0.0522	0.0013	0.78188	270.5	9.1	269.2	8.2	-0.5	290	18	528	0.26
NOV11-1A_2b.FIN2	0.322	0.013	0.0429	0.0015	0.0545	0.0016	0.4968	270.7	9	283.2	9.8	4.4	392	34	344	0.30

	Isotopic Ratios							Dates (Ma)							Concentration	
Sample and	207Pb/	± 2SE	206Pb/	± 2SE	207Pb/	± 2SE	Rho: 206/238	206Pb/	± 2SE	207Pb/	± 2SE	% Discord.	207Pb/	± 2SE	U	
Analysis Number	235U	(abs)	238U	(abs)	206Pb	(abs)	vs 207/235	238U	(abs)	235U	(abs)	6/38-7/35	206Pb	(abs)	(ppm)	Th/U
NOV11-1A_7n.FIN2	0.312	0.011	0.0429	0.0015	0.0528	0.0014	0.70648	270.7	9.6	275.6	8.6	1.8	323	22	445	0.23
NOV11-1A_5g.FIN2	0.315	0.011	0.043	0.0015	0.0531	0.0014	0.73167	271.2	9.4	278.3	8.7	2.6	334	20	1038	0.17
NOV11-1A_4l.FIN2	0.305	0.011	0.043	0.0017	0.0515	0.0013	0.77327	271.3	11	269.9	8.5	-0.5	268	18	476.6	0.24
NOV11-1A_7h.FIN2	0.304	0.011	0.043	0.0016	0.0513	0.0013	0.76733	271.5	10	269	8.8	-0.9	260	22	124	0.34
NOV11-1A_1e.FIN2	0.4	0.023	0.043	0.0015	0.066	0.0032	0.39781	271.6	9.3	339	16	19.9	798	79	581	0.01
NOV11-1A_1c.FIN2	0.318	0.012	0.0431	0.0016	0.0542	0.0015	0.72591	271.7	10	279.8	9.6	2.9	392	28	729	0.11
NOV11-1A_5h.FIN2	0.305	0.012	0.0431	0.0016	0.0508	0.0012	0.80472	271.9	10	271.1	8.9	-0.3	235	22	332.8	0.20
NOV11-1A_1h.FIN2	0.304	0.011	0.0431	0.0015	0.0514	0.0014	0.69965	272	9	269	8.5	-1.1	271	24	312	0.41
NOV11-1A_7g.FIN2	0.309	0.011	0.0432	0.0015	0.0523	0.0013	0.71164	272.2	9.2	273.4	8.4	0.4	308	21	731	0.18
NOV11-1A_4k.FIN2	0.317	0.012	0.0432	0.0016	0.0523	0.0014	0.92032	272.7	9.7	279.2	9.5	2.3	308	27	133.8	0.36
NOV11-1A_8i.FIN2	0.308	0.012	0.0432	0.0016	0.0515	0.0014	0.71257	272.8	10	272.1	9.2	-0.3	269	27	741	0.19
NOV11-1A_4c.FIN2	0.33	0.013	0.0433	0.0015	0.0545	0.0014	0.75788	273	9.4	289.5	9.8	5.7	393	24	697	0.16
NOV11-1A_6s.FIN2	0.31	0.011	0.0433	0.0016	0.0521	0.0013	0.75621	273	9.7	274.6	8.8	0.6	280	18	1676	0.05
NOV11-1A_9c.FIN2	0.31	0.011	0.0433	0.0015	0.0524	0.0014	0.72275	273.2	9.6	274.2	8.6	0.4	316	21	534	0.14
NOV11-1A_7m.FIN2	0.312	0.013	0.0434	0.0017	0.051	0.0014	0.77174	273.9	11	275.1	9.9	0.4	271	23	657	0.13
NOV11-1A_4h.FIN2	0.316	0.011	0.0434	0.0015	0.052	0.0013	0.74858	274	9.1	279.4	8.7	1.9	283	18	226	0.24
NOV11-1A_9f.FIN2	0.302	0.012	0.0434	0.0016	0.0514	0.0014	0.67145	274	9.8	267.9	9	-2.3	275	25	155.1	0.34
NOV11-1A_7k.FIN2	0.315	0.012	0.0435	0.0016	0.0527	0.0014	0.69734	274.4	9.8	278.1	9.3	1.3	316	20	205.9	0.37
NOV11-1A_1a.FIN2	0.308	0.012	0.0436	0.0015	0.052	0.0014	0.67677	274.9	9.3	272.6	8.9	-0.8	294	24	717	0.07
NOV11-1A_6f.FIN2	0.325	0.012	0.0436	0.0015	0.0536	0.0014	0.70404	274.9	9.2	285.4	9.1	3.7	355	27	272	0.35
NOV11-1A_9a.FIN2	0.311	0.011	0.0436	0.0015	0.0521	0.0013	0.71301	275	9.4	275.2	8.7	0.1	303	20	474	0.33
NOV11-1A_4i.FIN2	0.697	0.064	0.0437	0.0017	0.1109	0.0073	0.91669	275.8	11	523	34	47.3	1810	110	143	0.31
NOV11-1A_9b.FIN2	0.31	0.011	0.0438	0.0015	0.052	0.0014	0.58833	276.5	9.1	274.7	8.6	-0.7	303	23	130.8	0.68
NOV11-1A_9g.FIN2	0.306	0.011	0.0439	0.0016	0.051	0.0013	0.76718	277.2	9.9	270.8	8.7	-2.4	254	21	331	0.19
NOV11-1A_6a.FIN2	0.325	0.012	0.0442	0.0017	0.0529	0.0015	0.63482	278.6	10	285.4	8.9	2.4	319	30	1400	0.10
NOV11-1A_3e.FIN2	0.326	0.012	0.0442	0.0014	0.0528	0.0014	0.65305	278.7	8.8	286.3	8.8	2.7	319	20	460	0.24
NOV11-1A_7r.FIN2	0.294	0.011	0.0443	0.0017	0.0489	0.0013	0.78272	279.4	11	261.3	8.9	-6.9	176	24	2916	0.07
NOV11-1A_1i.FIN2	0.355	0.018	0.0443	0.0018	0.0585	0.0024	0.45861	279.5	11	308	14	9.3	578	53	1288	0.04
NOV11-1A_5s.FIN2	0.316	0.012	0.0444	0.0017	0.0512	0.0014	0.65517	279.9	11	279.1	9.2	-0.3	282	26	1810	0.06
NOV11-1A_4a.FIN2	0.328	0.012	0.0447	0.0015	0.0523	0.0013	0.72626	281.7	9.6	287.6	8.9	2.1	305	20	840	0.16
NOV11-1A_7f.FIN2	0.322	0.012	0.0447	0.0015	0.0526	0.0015	0.67771	281.7	9.4	283	9.5	0.5	302	23	1671	0.14
NOV11-1A_4r.FIN2	0.337	0.013	0.0447	0.0018	0.0541	0.0015	0.76738	282	11	295.5	9.9	4.6	377	23	1077	0.05
NOV11-1A_5k.FIN2	0.334	0.012	0.045	0.0016	0.0538	0.0014	0.77025	283.8	9.9	292	9	2.8	353	21	543.4	0.19
NOV11-1A_7j.FIN2	0.32	0.012	0.0452	0.0017	0.0512	0.0014	0.64748	284.9	11	281.3	8.9	-1.3	261	30	2220	0.06

	Isotopic Ratios							Dates (Ma)							Concentration	
Sample and	207Pb/	± 2SE	206Pb/	± 2SE	207Pb/	± 2SE	Rho: 206/238	206Pb/	± 2SE	207Pb/	± 2SE	% Discord.	207Pb/	± 2SE	U	
Analysis Number	235U	(abs)	238U	(abs)	206Pb	(abs)	vs 207/235	238U	(abs)	235U	(abs)	6/38-7/35	206Pb	(abs)	(ppm)	Th/U
NOV11-1A_6k.FIN2	0.322	0.012	0.0453	0.0018	0.0516	0.0013	0.80125	285.3	11	283.1	9.4	-0.8	269	21	1143	0.21
NOV11-1A_3h.FIN2	0.328	0.013	0.0453	0.0019	0.0509	0.0014	0.76776	285.6	12	287.5	10	0.7	264	23	244	0.27
NOV11-1A_4e.FIN2	0.354	0.012	0.0454	0.0014	0.0558	0.0013	0.71255	286.3	8.8	308	9.3	7.0	430	20	560	0.08
NOV11-1A_3k.FIN2	0.348	0.016	0.0456	0.0018	0.0546	0.0014	0.92264	287.3	11	302.6	12	5.1	397	25	871	0.07
NOV11-1A_9i.FIN2	0.382	0.013	0.0459	0.0016	0.0612	0.0017	0.60297	289.2	10	328.8	9.8	12.0	651	32	242.6	0.93
NOV11-1A_6i.FIN2	0.331	0.012	0.0459	0.0015	0.0518	0.0012	0.86188	289.4	9.4	290.4	9.1	0.3	287	12	775	0.24
NOV11-1A_1j.FIN2	1.42	0.260	0.0465	0.0031	0.204	0.0240	0.92279	293	19	799	87	63.3	2720	170	165.4	0.28
NOV11-1A_7i.FIN2	0.407	0.024	0.0468	0.0019	0.0623	0.0027	0.4014	294.8	12	344	16	14.3	678	70	290	0.29
NOV11-1A_6p.FIN2	0.346	0.017	0.0472	0.0024	0.0522	0.0020	0.75878	297	15	301.5	13	1.5	304	49	1253	0.11
NOV11-1A_7c.FIN2	0.319	0.023	0.0472	0.0037	0.0491	0.0014	0.99438	297	22	279	16	-6.5	182	25	2457	0.03
NOV11-1A_1d.FIN2	0.58	0.066	0.0488	0.0019	0.0831	0.0070	0.72362	307.3	12	436	34	29.5	1160	130	211	0.17
NOV11-1A_7q.FIN2	0.36	0.016	0.0562	0.0026	0.0473	0.0016	0.72764	352	16	312	12	-12.8	125	26	3410	0.17
NOV11-1A_5f.FIN2	0.529	0.021	0.0641	0.0024	0.0592	0.0016	0.68181	400	15	429.9	14	7.0	586	33	1541	0.11
NOV11-1A_6b.FIN2	0.647	0.035	0.0799	0.0045	0.0576	0.0016	0.90484	495	27	509	22	2.8	522	23	992	0.27
NOV11-1A_2f.FIN2	0.674	0.023	0.0811	0.0027	0.0597	0.0015	0.67271	503.9	16	522.5	14	3.6	586	18	439	0.34
NOV11-1A_4o.FIN2	0.777	0.027	0.0904	0.0030	0.0613	0.0015	0.78098	558	18	583.2	16	4.3	649	17	739	0.37
NOV11-1A_2g.FIN2	0.799	0.029	0.0946	0.0034	0.061	0.0015	0.84186	582	20	595.2	16	2.2	645	17	379	0.47
NOV11-1A_4q.FIN2	0.862	0.029	0.099	0.0032	0.0624	0.0015	0.7373	608.1	19	632.3	16	3.8	705	15	429	0.32
NOV11-1A_5l.FIN2	1.398	0.054	0.1369	0.0050	0.0716	0.0018	0.77768	827	28	885	23	6.6	983	19	433	0.39
NOV11-1A_7p.FIN2	3.62	0.160	0.2364	0.0100	0.1113	0.0031	0.84175	1371	53	1550	35	11.5	1832	23	416	0.07
Leucogranite NOV11-1B																
NOV11-1B_1f.FIN2	0.022	0.002	0.0034	0.0003	0.0462	0.0041	0.63172	21.6	2.2	21.8	1.9	0.9	219	71	886	0.12
NOV11-1B_4d.FIN2	**0.023**	**0.002**	**0.0035**	**0.0001**	**0.047**	**0.0022**	**0.68359**	**22.63**	**0.94**	**23.23**	**1.6**	**2.6**	**137**	**24**	**882**	**0.25**
NOV11-1B_9h.FIN2	**0.024**	**0.002**	**0.0035**	**0.0002**	**0.0495**	**0.0027**	**0.67689**	**22.68**	**1.2**	**24.2**	**1.8**	**6.3**	**315**	**50**	**3430**	**0.22**
NOV11-1B_9v.FIN2	**0.023**	**0.002**	**0.0036**	**0.0002**	**0.0481**	**0.0025**	**0.55679**	**22.93**	**1**	**23.33**	**1.7**	**1.7**	**294**	**59**	**433**	**0.12**
NOV11-1B_11s.FIN	**0.024**	**0.002**	**0.0036**	**0.0001**	**0.0494**	**0.0023**	**0.70536**	**22.99**	**0.99**	**24.26**	**1.5**	**5.2**	**231**	**30**	**547**	**0.23**
NOV11-1B_4e.FIN2	**0.024**	**0.002**	**0.0036**	**0.0001**	**0.0469**	**0.0024**	**0.55367**	**23**	**0.95**	**23.77**	**1.6**	**3.2**	**166**	**32**	**309**	**0.12**
NOV11-1B_10m.FI	**0.024**	**0.002**	**0.0036**	**0.0002**	**0.0487**	**0.0023**	**0.64711**	**23.02**	**1**	**23.75**	**1.6**	**3.1**	**201**	**40**	**1414**	**0.19**
NOV11-1B_1c.FIN2	**0.025**	**0.002**	**0.0036**	**0.0002**	**0.05**	**0.0027**	**0.48612**	**23.03**	**1.1**	**24.8**	**1.8**	**7.1**	**258**	**57**	**466**	**0.13**
NOV11-1B_2n.FIN2	**0.024**	**0.002**	**0.0036**	**0.0001**	**0.0489**	**0.0022**	**0.70312**	**23.15**	**0.92**	**24.46**	**1.6**	**5.4**	**193**	**29**	**1255**	**0.15**
NOV11-1B_2h.FIN2	**0.023**	**0.001**	**0.0036**	**0.0001**	**0.0457**	**0.0023**	**0.48604**	**23.16**	**0.9**	**23.29**	**1.5**	**0.6**	**143**	**37**	**462.7**	**0.14**
NOV11-1B_7g.FIN2	**0.023**	**0.002**	**0.0036**	**0.0001**	**0.0465**	**0.0023**	**0.52799**	**23.2**	**0.92**	**23.42**	**1.5**	**0.9**	**125**	**28**	**584**	**0.25**
NOV11-1B_2d.FIN2	**0.024**	**0.001**	**0.0036**	**0.0002**	**0.0472**	**0.0023**	**0.65953**	**23.24**	**1**	**23.66**	**1.5**	**1.8**	**161**	**25**	**550**	**0.16**
NOV11-1B_4i.FIN2	**0.024**	**0.002**	**0.0036**	**0.0001**	**0.0482**	**0.0022**	**0.75382**	**23.26**	**0.92**	**24.22**	**1.6**	**4.0**	**159**	**23**	**793**	**0.18**

	Isotopic Ratios							Dates (Ma)							Concentration	
Sample and	207Pb/	± 2SE	206Pb/	± 2SE	207Pb/	± 2SE	Rho: 206/238	206Pb/	± 2SE	207Pb/	± 2SE	% Discord.	207Pb/	± 2SE	U	
Analysis Number	235U	(abs)	238U	(abs)	206Pb	(abs)	vs 207/235	238U	(abs)	235U	(abs)	6/38-7/35	206Pb	(abs)	(ppm)	Th/U
NOV11-1B_6e.FIN2	**0.024**	**0.002**	**0.0036**	**0.0002**	**0.0492**	**0.0023**	**0.72006**	**23.27**	**1**	**24.28**	**1.6**	**4.2**	**167**	**22**	**1583**	**0.19**
NOV11-1B_6l.FIN2	**0.023**	**0.002**	**0.0036**	**0.0002**	**0.0469**	**0.0023**	**0.58338**	**23.32**	**0.95**	**23.26**	**1.5**	**-0.3**	**199**	**35**	**656**	**0.20**
NOV11-1B_2f.FIN2	**0.024**	**0.002**	**0.0036**	**0.0002**	**0.0483**	**0.0022**	**0.79874**	**23.38**	**1**	**23.77**	**1.5**	**1.6**	**166**	**26**	**1908**	**0.16**
NOV11-1B_7e.FIN2	**0.025**	**0.002**	**0.0036**	**0.0001**	**0.0471**	**0.0023**	**0.41264**	**23.39**	**0.9**	**24.64**	**1.5**	**5.1**	**210**	**36**	**482**	**0.27**
NOV11-1B_6i.FIN2	**0.032**	**0.002**	**0.0036**	**0.0002**	**0.065**	**0.0039**	**0.32655**	**23.41**	**1.2**	**31.8**	**2.2**	**26.4**	**779**	**77**	**1200**	**0.37**
NOV11-1B_4f.FIN2	**0.026**	**0.002**	**0.0036**	**0.0002**	**0.0507**	**0.0024**	**0.63377**	**23.43**	**0.95**	**25.96**	**1.7**	**9.7**	**271**	**30**	**692**	**0.24**
NOV11-1B_11n.FIN	**0.027**	**0.002**	**0.0037**	**0.0002**	**0.0514**	**0.0024**	**0.67673**	**23.47**	**1**	**26.7**	**1.7**	**12.1**	**306**	**31**	**1382**	**0.12**
NOV11-1B_8j.FIN2	**0.025**	**0.002**	**0.0037**	**0.0002**	**0.0498**	**0.0024**	**0.58325**	**23.49**	**1**	**24.69**	**1.7**	**4.9**	**229**	**32**	**518**	**0.27**
NOV11-1B_5h.FIN2	**0.024**	**0.002**	**0.0037**	**0.0001**	**0.0484**	**0.0025**	**0.53651**	**23.52**	**0.88**	**23.94**	**1.6**	**1.8**	**269**	**44**	**306.8**	**0.15**
NOV11-1B_9f.FIN2	**0.025**	**0.002**	**0.0037**	**0.0002**	**0.0492**	**0.0023**	**0.81018**	**23.53**	**1.2**	**25.4**	**1.8**	**7.4**	**246**	**39**	**3400**	**0.18**
NOV11-1B_10a.FIN	**0.023**	**0.002**	**0.0037**	**0.0002**	**0.0465**	**0.0022**	**0.66865**	**23.57**	**1**	**23.37**	**1.5**	**-0.9**	**175**	**26**	**440**	**0.15**
NOV11-1B_8n.FIN2	**0.024**	**0.002**	**0.0037**	**0.0001**	**0.0477**	**0.0027**	**0.40266**	**23.57**	**0.99**	**23.9**	**1.7**	**1.4**	**440**	**110**	**557**	**0.18**
NOV11-1B_4h.FIN2	**0.024**	**0.002**	**0.0037**	**0.0002**	**0.0474**	**0.0022**	**0.64107**	**23.58**	**1**	**24.34**	**1.6**	**3.1**	**186**	**37**	**918**	**0.19**
NOV11-1B_2b.FIN2	**0.031**	**0.002**	**0.0037**	**0.0001**	**0.0612**	**0.0029**	**0.58015**	**23.59**	**0.97**	**31.43**	**2**	**24.9**	**658**	**47**	**983**	**0.16**
NOV11-1B_7o.FIN2	**0.025**	**0.002**	**0.0037**	**0.0001**	**0.0514**	**0.0027**	**0.5264**	**23.6**	**0.99**	**25.5**	**1.8**	**7.5**	**380**	**61**	**731**	**0.23**
NOV11-1B_4g.FIN2	**0.024**	**0.002**	**0.0037**	**0.0002**	**0.0474**	**0.0026**	**0.42651**	**23.62**	**1**	**24.27**	**1.6**	**2.7**	**269**	**40**	**318**	**0.11**
NOV11-1B_8l.FIN2	**0.023**	**0.002**	**0.0037**	**0.0002**	**0.0472**	**0.0023**	**0.69206**	**23.63**	**1.2**	**23.2**	**1.6**	**-1.9**	**164**	**29**	**517**	**0.14**
NOV11-1B_1a.FIN2	**0.024**	**0.002**	**0.0037**	**0.0001**	**0.048**	**0.0024**	**0.67776**	**23.63**	**0.99**	**24.3**	**1.7**	**2.8**	**223**	**30**	**323.3**	**0.16**
NOV11-1B_2i.FIN2	**0.024**	**0.002**	**0.0037**	**0.0002**	**0.0474**	**0.0021**	**0.78983**	**23.63**	**1**	**24.3**	**1.6**	**2.8**	**151**	**26**	**2580**	**0.09**
NOV11-1B_1g.FIN2	**0.027**	**0.002**	**0.0037**	**0.0002**	**0.053**	**0.0026**	**0.64023**	**23.68**	**1**	**26.55**	**1.7**	**10.8**	**333**	**40**	**677**	**0.13**
NOV11-1B_1b.FIN2	**0.023**	**0.002**	**0.0037**	**0.0002**	**0.0464**	**0.0035**	**0.57203**	**23.7**	**1.5**	**23.4**	**2.2**	**-1.3**	**440**	**100**	**218**	**0.12**
NOV11-1B_7m.FIN	**0.024**	**0.002**	**0.0037**	**0.0002**	**0.0482**	**0.0030**	**0.60748**	**23.7**	**1.4**	**24**	**2**	**1.3**	**221**	**40**	**417**	**0.24**
NOV11-1B_7d.FIN2	0.054	0.007	0.0037	0.0002	0.1006	0.0100	0.54296	23.7	1.1	53.2	6.5	55.5	1570	170	681	0.43
NOV11-1B_2e.FIN2	**0.023**	**0.002**	**0.0037**	**0.0001**	**0.0467**	**0.0022**	**0.65722**	**23.71**	**0.96**	**23.57**	**1.5**	**-0.6**	**177**	**32**	**698**	**0.16**
NOV11-1B_2c.FIN2	**0.024**	**0.002**	**0.0037**	**0.0002**	**0.0471**	**0.0022**	**0.70013**	**23.72**	**1**	**23.96**	**1.6**	**1.0**	**187**	**28**	**536**	**0.15**
NOV11-1B_3d.FIN2	**0.029**	**0.002**	**0.0037**	**0.0002**	**0.0551**	**0.0038**	**0.463**	**23.75**	**1.2**	**28.5**	**2.4**	**16.7**	**481**	**95**	**318.3**	**0.11**
NOV11-1B_9n.FIN2	**0.027**	**0.002**	**0.0037**	**0.0002**	**0.0527**	**0.0027**	**0.54225**	**23.76**	**1.1**	**26.55**	**1.8**	**10.5**	**396**	**48**	**537**	**0.11**
NOV11-1B_7f.FIN2	**0.024**	**0.002**	**0.0037**	**0.0002**	**0.0465**	**0.0024**	**0.56734**	**23.81**	**1**	**24.04**	**1.6**	**1.0**	**121**	**25**	**552**	**0.24**
NOV11-1B_3g.FIN2	**0.024**	**0.002**	**0.0037**	**0.0002**	**0.0477**	**0.0026**	**0.54658**	**23.89**	**1.1**	**24.46**	**1.7**	**2.3**	**237**	**35**	**227**	**0.14**
NOV11-1B_10o.FIN	**0.025**	**0.002**	**0.0037**	**0.0002**	**0.0478**	**0.0022**	**0.64664**	**23.89**	**0.94**	**24.77**	**1.6**	**3.6**	**190**	**32**	**667**	**0.14**
NOV11-1B_7h.FIN2	**0.024**	**0.001**	**0.0037**	**0.0001**	**0.0467**	**0.0020**	**0.83325**	**23.9**	**0.93**	**23.89**	**1.5**	**0.0**	**95**	**16**	**1630**	**0.25**
NOV11-1B_2a.FIN2	**0.024**	**0.002**	**0.0037**	**0.0002**	**0.0487**	**0.0024**	**0.64967**	**23.91**	**1**	**24.43**	**1.6**	**2.1**	**217**	**31**	**416**	**0.21**
NOV11-1B_1e.FIN2	**0.025**	**0.002**	**0.0037**	**0.0002**	**0.0487**	**0.0023**	**0.72309**	**23.93**	**1**	**24.83**	**1.6**	**3.6**	**209**	**33**	**593**	**0.16**
NOV11-1B_7a.FIN2	**0.025**	**0.002**	**0.0037**	**0.0001**	**0.048**	**0.0022**	**0.66098**	**23.94**	**0.94**	**24.83**	**1.6**	**3.6**	**185**	**24**	**604**	**0.16**

	Isotopic Ratios							Dates (Ma)							Concentration	
Sample and	207Pb/	± 2SE	206Pb/	± 2SE	207Pb/	± 2SE	Rho: 206/238	206Pb/	± 2SE	207Pb/	± 2SE	% Discord.	207Pb/	± 2SE	U	
Analysis Number	235U	(abs)	238U	(abs)	206Pb	(abs)	vs 207/235	238U	(abs)	235U	(abs)	6/38-7/35	206Pb	(abs)	(ppm)	Th/U
NOV11-1B_1d.FIN2	0.024	0.002	0.0037	0.0002	0.0478	0.0024	0.59871	23.97	1	24.16	1.6	0.8	258	42	344	0.15
NOV11-1B_5k.FIN2	0.024	0.001	0.0037	0.0001	0.0455	0.0021	0.60251	23.98	0.92	23.65	1.5	-1.4	122	24	774	0.16
NOV11-1B_3i.FIN2	0.025	0.002	0.0037	0.0002	0.0486	0.0025	0.7441	24	1.4	24.99	1.7	4.0	190	37	544	0.14
NOV11-1B_11r.FIN	0.024	0.002	0.0037	0.0002	0.0469	0.0022	0.70465	24.04	0.99	24.49	1.6	1.8	160	27	711	0.28
NOV11-1B_2k.FIN2	0.024	0.002	0.0037	0.0002	0.0463	0.0024	0.60204	24.09	1.1	24.08	1.6	0.0	219	36	213.9	0.10
NOV11-1B_11h.FIN	0.024	0.001	0.0037	0.0002	0.0467	0.0021	0.74409	24.09	1	24.35	1.5	1.1	121	21	1616	0.27
NOV11-1B_6g.FIN2	0.025	0.002	0.0038	0.0002	0.0498	0.0023	0.79456	24.12	1	24.97	1.7	3.4	247	35	1121	0.21
NOV11-1B_10x.FIN	0.025	0.002	0.0038	0.0002	0.048	0.0024	0.54676	24.13	0.99	24.98	1.7	3.4	249	59	855	0.17
NOV11-1B_10n.FIN	0.024	0.002	0.0038	0.0002	0.0472	0.0022	0.70161	24.14	0.98	24.31	1.6	0.7	176	27	1234	0.16
NOV11-1B_5b.FIN2	0.025	0.002	0.0038	0.0002	0.0478	0.0026	0.54764	24.15	1	25.53	1.8	5.4	209	31	171	0.17
NOV11-1B_3e.FIN2	0.034	0.003	0.0038	0.0002	0.064	0.0039	0.61273	24.18	1	33.7	2.7	28.2	716	89	505	0.12
NOV11-1B_4a.FIN2	0.024	0.002	0.0038	0.0004	0.0462	0.0031	0.79942	24.2	2.3	24.3	2.3	0.4	255	31	2120	0.06
NOV11-1B_5c.FIN2	0.028	0.002	0.0038	0.0001	0.0533	0.0036	0.26335	24.2	0.94	27.6	2.1	12.3	343	56	188.1	0.17
NOV11-1B_5i.FIN2	0.024	0.002	0.0038	0.0001	0.0466	0.0021	0.7342	24.21	0.95	23.96	1.5	-1.0	126	26	1876	0.27
NOV11-1B_6f.FIN2	0.024	0.001	0.0038	0.0002	0.0475	0.0027	0.60558	24.21	1.2	24	1.4	-0.9	81	24	1038	0.04
NOV11-1B_10b.FIN	0.025	0.002	0.0038	0.0002	0.0495	0.0027	0.52181	24.21	1	25	1.8	3.2	263	39	236	0.19
NOV11-1B_9t.FIN2	0.024	0.002	0.0038	0.0002	0.0475	0.0023	0.68144	24.23	1	24.27	1.6	0.2	193	26	512	0.18
NOV11-1B_5a.FIN2	0.024	0.002	0.0038	0.0002	0.0467	0.0022	0.62526	24.26	0.99	24.47	1.5	0.9	160	30	645	0.24
NOV11-1B_8c.FIN2	0.025	0.002	0.0038	0.0001	0.0503	0.0022	0.78132	24.29	1	25.5	1.7	4.7	198	24	889	0.12
NOV11-1B_10v.FIN	0.025	0.002	0.0038	0.0001	0.0476	0.0022	0.67411	24.35	0.98	25.1	1.6	3.0	152	31	875	0.15
NOV11-1B_11k.FIN	0.025	0.002	0.0038	0.0002	0.0477	0.0025	0.45556	24.42	1.1	25.03	1.7	2.4	165	36	451	0.13
NOV11-1B_10g.FIN	0.027	0.002	0.0038	0.0002	0.0513	0.0026	0.7075	24.47	1.1	26.7	1.9	8.4	283	34	1181	0.15
NOV11-1B_10f.FIN	0.033	0.003	0.0038	0.0002	0.0636	0.0041	0.35093	24.51	1	33.4	2.6	26.6	733	98	595	0.12
NOV11-1B_7r.FIN2	0.029	0.002	0.0038	0.0001	0.0541	0.0025	0.53591	24.52	0.92	28.82	1.8	14.9	399	38	1664	0.20
NOV11-1B_9u.FIN2	0.035	0.003	0.0038	0.0002	0.0656	0.0049	0.49386	24.59	1.1	34.3	3.3	28.3	870	140	913	0.28
NOV11-1B_9a.FIN2	0.026	0.002	0.0038	0.0002	0.0471	0.0029	0.57112	24.6	1.5	25.5	2	3.5	253	74	315	0.12
NOV11-1B_11j.FIN	0.031	0.002	0.0038	0.0002	0.0579	0.0032	0.61669	24.6	1	30.6	2.2	19.6	559	75	1055	0.20
NOV11-1B_7k.FIN2	0.029	0.002	0.0038	0.0002	0.055	0.0032	0.35891	24.6	1.1	28.5	1.9	13.7	491	79	886	0.19
NOV11-1B_5e.FIN2	0.026	0.002	0.0038	0.0002	0.0491	0.0026	0.49166	24.64	0.99	25.68	1.7	4.0	302	53	419	0.15
NOV11-1B_9s.FIN2	0.025	0.002	0.0039	0.0002	0.046	0.0025	0.59436	24.77	1	24.6	1.7	-0.7	119	41	335	0.15
NOV11-1B_3f.FIN2	0.024	0.002	0.0039	0.0002	0.0463	0.0023	0.68465	24.79	1.1	24.39	1.7	-1.6	193	31	369	0.18
NOV11-1B_5f.FIN2	0.024	0.002	0.0039	0.0002	0.0451	0.0023	0.5526	24.83	1.1	24.18	1.6	-2.7	157	34	425	0.19
NOV11-1B_5d.FIN2	0.034	0.003	0.0039	0.0002	0.0629	0.0037	0.3629	24.83	1	34	2.6	27.0	674	68	382	0.14
NOV11-1B_9l.FIN2	0.025	0.002	0.0039	0.0002	0.0481	0.0026	0.50204	24.88	1	25.47	1.7	2.3	196	34	225	0.08

	Isotopic Ratios							Dates (Ma)							Concentration	
Sample and	207Pb/	± 2SE	206Pb/	± 2SE	207Pb/	± 2SE	Rho: 206/238	206Pb/	± 2SE	207Pb/	± 2SE	% Discord.	207Pb/	± 2SE	U	
Analysis Number	235U	(abs)	238U	(abs)	206Pb	(abs)	vs 207/235	238U	(abs)	235U	(abs)	6/38-7/35	206Pb	(abs)	(ppm)	Th/U
NOV11-1B_8r.FIN2	**0.024**	**0.002**	**0.0039**	**0.0002**	**0.0457**	**0.0023**	**0.62999**	**24.9**	**1**	**24.29**	**1.6**	**-2.5**	**158**	**34**	**269**	**0.18**
NOV11-1B_2l.FIN2	**0.033**	**0.002**	**0.0039**	**0.0001**	**0.0612**	**0.0033**	**0.3186**	**24.9**	**0.83**	**33.3**	**2.3**	**25.2**	**651**	**72**	**1069**	**0.13**
NOV11-1B_11p.FIN	**0.029**	**0.002**	**0.0039**	**0.0002**	**0.0533**	**0.0030**	**0.58748**	**24.91**	**0.97**	**29**	**2.2**	**14.1**	**393**	**80**	**804**	**0.17**
NOV11-1B_3b.FIN2	**0.033**	**0.002**	**0.0039**	**0.0002**	**0.0592**	**0.0032**	**0.32398**	**24.91**	**0.94**	**32.7**	**2.1**	**23.8**	**595**	**67**	**2450**	**0.24**
NOV11-1B_6k.FIN2	**0.037**	**0.002**	**0.0039**	**0.0001**	**0.0704**	**0.0031**	**0.70374**	**24.91**	**0.92**	**36.71**	**2.3**	**32.1**	**937**	**26**	**938**	**0.18**
NOV11-1B_7l.FIN2	**0.034**	**0.003**	**0.0039**	**0.0002**	**0.0633**	**0.0041**	**0.51364**	**24.91**	**1.1**	**33.7**	**2.9**	**26.1**	**684**	**96**	**723**	**0.21**
NOV11-1B_10y.FIN	0.025	0.002	0.0039	0.0003	0.0471	0.0031	0.66935	25	2	24.8	2	-0.8	146	57	488	0.14
NOV11-1B_8q.FIN2	**0.029**	**0.002**	**0.0039**	**0.0002**	**0.0548**	**0.0032**	**0.43169**	**25.02**	**1.2**	**28.8**	**2.1**	**13.1**	**402**	**65**	**674**	**0.24**
NOV11-1B_9r.FIN2	**0.031**	**0.002**	**0.0039**	**0.0001**	**0.0587**	**0.0033**	**0.61499**	**25.07**	**0.99**	**30.6**	**2.3**	**18.1**	**567**	**70**	**527**	**0.14**
NOV11-1B_8k.FIN2	0.024	0.002	0.0039	0.0002	0.046	0.0022	0.68666	25.16	1	24.43	1.6	-3.0	157	28	768	0.22
NOV11-1B_10i.FIN	**0.033**	**0.003**	**0.0039**	**0.0002**	**0.0616**	**0.0036**	**0.54606**	**25.2**	**1.4**	**33.4**	**2.5**	**24.6**	**709**	**79**	**417**	**0.12**
NOV11-1B_5g.FIN2	**0.038**	**0.003**	**0.0039**	**0.0001**	**0.0703**	**0.0035**	**0.44398**	**25.25**	**0.92**	**37.6**	**2.5**	**32.8**	**913**	**52**	**255.4**	**0.20**
NOV11-1B_8p.FIN2	**0.032**	**0.003**	**0.0039**	**0.0002**	**0.059**	**0.0039**	**0.49963**	**25.32**	**1.2**	**31.7**	**2.7**	**20.1**	**537**	**82**	**732**	**0.30**
NOV11-1B_10j.FIN2	0.031	0.003	0.004	0.0002	0.0585	0.0036	0.67374	25.49	1	30.7	2.5	17.0	592	92	795	0.30
NOV11-1B_10c.FIN	0.028	0.002	0.004	0.0002	0.0521	0.0031	0.5848	25.6	1.4	28.3	2.2	9.5	369	61	809	0.16
NOV11-1B_10z.FIN	0.026	0.002	0.004	0.0002	0.0476	0.0022	0.77702	25.65	1.1	26	1.8	1.3	245	35	4940	0.07
NOV11-1B_6a.FIN2	0.026	0.002	0.004	0.0002	0.0459	0.0025	0.51	25.77	1.1	25.6	1.9	-0.7	230	77	461	0.18
NOV11-1B_11e.FIN	0.026	0.002	0.004	0.0002	0.0471	0.0023	0.65409	25.79	1.1	25.62	1.7	-0.7	170	29	415	0.21
NOV11-1B_11q.FIN	0.039	0.004	0.004	0.0002	0.0703	0.0056	0.5861	25.82	1.1	39.1	3.8	34.0	930	130	530	0.24
NOV11-1B_7c.FIN2	0.046	0.003	0.0041	0.0001	0.0785	0.0046	0.27281	26.15	0.9	45.2	3.3	42.1	1155	87	509	0.26
NOV11-1B_8m.FIN2	0.031	0.002	0.0041	0.0002	0.0573	0.0031	0.66824	26.2	1.3	30.9	2.3	15.2	500	52	1462	0.28
NOV11-1B_10p.FIN	0.033	0.002	0.0041	0.0001	0.0586	0.0026	0.65504	26.4	0.95	33.01	2	20.0	555	30	1559	0.35
NOV11-1B_11m.FIN	0.05	0.005	0.0041	0.0002	0.0879	0.0072	0.64144	26.4	1.2	49.4	5.2	46.6	1320	140	876	0.18
NOV11-1B_11g.FIN	0.04	0.003	0.0041	0.0002	0.0704	0.0046	0.64162	26.55	1.1	40.1	3.4	33.8	940	100	848	0.33
NOV11-1B_8i.FIN2	**0.066**	**0.005**	**0.0042**	**0.0002**	**0.1183**	**0.0068**	**0.44023**	**26.68**	**1.2**	**64.6**	**4.5**	**58.7**	**1926**	**61**	**727**	**0.25**
NOV11-1B_10l.FIN2	0.036	0.002	0.0042	0.0002	0.0619	0.0033	0.55341	26.9	1.2	35.9	2.4	25.1	698	42	587	0.36
NOV11-1B_6c.FIN2	0.038	0.003	0.0042	0.0002	0.0676	0.0039	0.68581	26.97	1.2	37.6	3	28.3	815	67	643	0.30
NOV11-1B_9x.FIN2	**0.072**	**0.011**	**0.0042**	**0.0002**	**0.119**	**0.0140**	**0.79813**	**27.09**	**1.3**	**69**	**10**	**60.7**	**1720**	**210**	**168**	**0.14**
NOV11-1B_7q.FIN2	0.047	0.003	0.0042	0.0002	0.083	0.0047	0.46864	27.14	1	46.8	3.2	42.0	1272	52	422	0.24
NOV11-1B_11c.FIN	0.027	0.002	0.0043	0.0002	0.0462	0.0021	0.69387	27.35	1.1	27.3	1.8	-0.2	154	31	1062	0.04
NOV11-1B_3h.FIN2	0.054	0.006	0.0044	0.0002	0.0945	0.0088	0.70065	27.96	1.2	53.2	5.9	47.4	1530	150	616	0.23
NOV11-1B_10u.FIN	0.065	0.009	0.0044	0.0003	0.1014	0.0092	0.41108	28.5	1.9	63.8	8.3	55.3	1700	140	2050	0.23
NOV11-1B_9q.FIN2	0.057	0.004	0.0046	0.0002	0.0904	0.0045	0.49212	29.52	1.1	55.8	3.6	47.1	1440	43	204	0.19
NOV11-1B_10d.FIN	**0.149**	**0.017**	**0.005**	**0.0002**	**0.217**	**0.0190**	**0.74488**	**32.09**	**1.3**	**139**	**15**	**76.9**	**2900**	**130**	**1000**	**0.20**

	Isotopic Ratios							Dates (Ma)							Concentration	
Sample and Analysis Number	207Pb/ 235U	± 2SE (abs)	206Pb/ 238U	± 2SE (abs)	207Pb/ 206Pb	± 2SE (abs)	Rho: 206/238 vs 207/235	206Pb/ 238U	± 2SE (abs)	207Pb/ 235U	± 2SE (abs)	% Discord. 6/38-7/35	207Pb/ 206Pb	± 2SE (abs)	U (ppm)	Th/U
NOV11-1B_11d.FIN	0.035	0.003	0.0052	0.0003	0.0467	0.0023	0.88147	33.5	2.1	34.9	3	4.0	156	55	2520	0.01
NOV11-1B_10q.FIN	0.079	0.007	0.0054	0.0003	0.103	0.0072	0.50898	34.6	2.1	76.6	6.5	54.8	1709	55	229.4	0.28
NOV11-1B_2m.FIN2	0.043	0.003	0.0059	0.0003	0.0512	0.0023	0.85028	37.8	1.6	42.3	2.7	10.6	264	27	1309	0.11
NOV11-1B_11b.FIN	0.096	0.007	0.0063	0.0003	0.1074	0.0068	0.10004	40.6	1.8	92.4	6.4	56.1	1701	67	1820	0.09
NOV11-1B_10s.FIN	0.106	0.009	0.0067	0.0004	0.116	0.0096	0.16673	43.2	2.8	101.8	8.4	57.6	1860	130	1288	0.16
NOV11-1B_8g.FIN2	0.059	0.004	0.0078	0.0004	0.0564	0.0025	0.89512	49.8	2.4	57.9	4	14.0	463	23	1346	0.05
NOV11-1B_6b.FIN2	0.079	0.006	0.0093	0.0006	0.0616	0.0033	0.76782	59.5	3.6	77.2	5.6	22.9	616	63	349	0.15
NOV11-1B_3a.FIN2	0.08	0.006	0.0104	0.0006	0.0537	0.0026	0.79388	66.9	3.7	77.7	5.8	13.9	366	38	473	0.01
NOV11-1B_9o.FIN2	0.132	0.017	0.0106	0.0008	0.0831	0.0058	0.95193	68.2	5	124	15	45.0	1190	120	608	0.03
NOV11-1B_11a.FIN	0.099	0.007	0.0108	0.0006	0.0671	0.0042	0.15396	69.4	3.5	96	6.2	27.7	790	88	1073	0.12
NOV11-1B_8d.FIN2	0.081	0.007	0.0117	0.0007	0.0506	0.0028	0.73196	75.1	4.7	79	6.3	4.9	339	64	698	0.10
NOV11-1B_8a.FIN2	0.099	0.006	0.0127	0.0005	0.0564	0.0025	0.84216	81.4	3.4	95.3	5.7	14.6	470	22	781	0.06
NOV11-1B_7n.FIN2	0.128	0.010	0.013	0.0008	0.071	0.0034	0.84694	83	4.9	122	9.1	32.0	970	39	342	0.19
NOV11-1B_9c.FIN2	0.163	0.011	0.0202	0.0009	0.0586	0.0027	0.77683	129	6	153.5	9.6	16.0	555	35	2210	0.05
NOV11-1B_9c.FIN2	0.163	0.011	0.0202	0.0009	0.0586	0.0027	0.77683	129	6	153.5	9.6	16.0	555	35	2210	0.05
NOV11-1B_7t.FIN2	0.217	0.015	0.0216	0.0009	0.0723	0.0034	0.73325	137.7	5.8	200	12	31.2	990	36	333.7	0.06
NOV11-1B_9e.FIN2	0.16	0.010	0.0216	0.0008	0.0533	0.0023	0.60742	137.9	5.1	150.7	8.4	8.5	339	26	1095	0.10
NOV11-1B_6h.FIN2	0.157	0.011	0.023	0.0013	0.0512	0.0024	0.81118	146.8	8.1	148.8	9.9	1.3	269	25	1058	0.03
NOV11-1B_3j.FIN2	0.176	0.012	0.0246	0.0011	0.0533	0.0024	0.84302	156.4	7.1	164.3	10	4.8	347	22	1006	0.10
NOV11-1B_11o.FIN	0.205	0.014	0.0254	0.0011	0.0564	0.0025	0.90591	161.9	7	189.1	12	14.4	471	26	748	0.05
NOV11-1B_7b.FIN2	0.202	0.014	0.0269	0.0012	0.0542	0.0024	0.82075	170.8	7.6	186.6	12	8.5	384	32	753	0.08
NOV11-1B_9g.FIN2	0.217	0.014	0.0292	0.0013	0.0537	0.0023	0.88101	185.7	7.9	198.7	12	6.5	335	22	757	0.08
NOV11-1B_11f.FIN	0.241	0.016	0.0326	0.0016	0.0536	0.0024	0.86579	206.9	9.7	218.5	13	5.3	362	26	463	0.11
NOV11-1B_5j.FIN2	0.237	0.016	0.0332	0.0015	0.0515	0.0023	0.81252	210.6	9.7	217.3	13	3.1	270	26	1057	0.11
NOV11-1B_8e.FIN2	0.246	0.016	0.0336	0.0014	0.0541	0.0024	0.63317	212.7	8.5	223.7	13	4.9	366	27	1089	0.32
NOV11-1B_9w.FIN2	0.236	0.016	0.0343	0.0017	0.0508	0.0022	0.89941	217	11	214.4	13	-1.2	235	24	1524	0.13
NOV11-1B_10r.FIN	0.24	0.019	0.0343	0.0021	0.0506	0.0027	0.79555	217	13	218	15	0.5	290	47	2560	0.02
NOV11-1B_9b.FIN2	0.247	0.017	0.0346	0.0016	0.0515	0.0024	0.81012	219.3	10	223.8	14	2.0	278	31	2039	0.01
NOV11-1B_8f.FIN2	0.254	0.017	0.0364	0.0018	0.0519	0.0024	0.85662	230.4	11	229.3	14	-0.5	306	33	630	0.11
NOV11-1B_9i.FIN2	0.273	0.018	0.0367	0.0016	0.0531	0.0023	0.83417	232.3	9.9	244.9	14	5.1	331	30	1071	0.39
NOV11-1B_2j.FIN2	0.333	0.036	0.0386	0.0034	0.0621	0.0029	0.97098	243	21	290	28	16.2	674	37	883	0.04
NOV11-1B_9k.FIN2	0.282	0.019	0.0384	0.0019	0.0521	0.0022	0.91349	243.6	11	251.4	15	3.1	298	22	1215	0.16
NOV11-1B_7i.FIN2	0.284	0.017	0.0398	0.0016	0.0516	0.0024	0.51873	251.7	10	253.5	14	0.7	305	25	1774	0.05
NOV11-1B_8h.FIN2	0.364	0.030	0.0402	0.0024	0.0682	0.0030	0.92891	254	15	314	22	19.1	856	25	371	0.22

	Isotopic Ratios							Dates (Ma)							Concentration	
Sample and	207Pb/	± 2SE	206Pb/	± 2SE	207Pb/	± 2SE	Rho: 206/238	206Pb/	± 2SE	207Pb/	± 2SE	% Discord.	207Pb/	± 2SE	U	
Analysis Number	235U	(abs)	238U	(abs)	206Pb	(abs)	vs 207/235	238U	(abs)	235U	(abs)	6/38-7/35	206Pb	(abs)	(ppm)	Th/U
NOV11-1B_8o.FIN2	0.274	0.019	0.0407	0.0021	0.0493	0.0022	0.87901	257	13	246.7	15	-4.2	171	26	1082	0.09
NOV11-1B_9j.FIN2	0.288	0.018	0.041	0.0017	0.0503	0.0022	0.76186	259.1	11	256.3	14	-1.1	251	31	744	0.32
NOV11-1B_9m.FIN2	0.367	0.030	0.0431	0.0025	0.0601	0.0027	0.91973	272	16	314	23	13.4	618	29	459	0.13
NOV11-1B_7j.FIN2	0.316	0.019	0.0439	0.0016	0.0526	0.0023	0.70679	276.8	9.9	279	15	0.8	336	21	766	0.13
NOV11-1B_6d.FIN2	0.372	0.023	0.047	0.0025	0.0587	0.0031	0.60625	296	15	320.7	17	7.7	544	59	1544	0.06
NOV11-1B_4c.FIN2	0.446	0.031	0.0602	0.0028	0.0536	0.0025	0.77199	377	17	375	21	-0.5	334	35	1416	0.03
NOV11-1B_6m.FIN2	0.557	0.040	0.0645	0.0033	0.0631	0.0027	0.9269	402	20	448	27	10.3	705	22	345	0.11
NOV11-1B_8b.FIN2	0.543	0.034	0.067	0.0027	0.0589	0.0026	0.71186	418	16	439.6	22	4.9	577	32	650	0.07
NOV11-1B_6j.FIN2	0.509	0.040	0.0674	0.0041	0.0568	0.0028	0.84789	420	24	420	26	0.0	460	56	330	0.11
NOV11-1B_10w.FIN	0.568	0.035	0.0722	0.0031	0.0567	0.0025	0.70439	449	18	457.4	24	1.8	498	27	192	0.15
NOV11-1B_10t.FIN2	0.628	0.041	0.0761	0.0030	0.0604	0.0028	0.62	472	18	494	26	4.5	601	28	230	0.13
NOV11-1B_4b.FIN2	0.76	0.052	0.0884	0.0040	0.0626	0.0029	0.77098	546	24	575	30	5.0	687	35	286.7	0.07
NOV11-1B_7s.FIN2	1.135	0.072	0.1277	0.0053	0.0638	0.0028	0.83798	774	30	770	35	-0.5	744	20	99.2	0.56
NOV11-1B_10e.FIN	2.67	0.190	0.1535	0.0076	0.1274	0.0065	0.78364	919	43	1320	55	30.4	2073	41	276.9	0.20
NOV11-1B_7p.FIN2	2.762	0.190	0.167	0.0081	0.1216	0.0053	0.86361	993	45	1342	50	26.0	1979	23	128	0.24
NOV11-1B_11i.FIN2	2.61	0.180	0.1708	0.0081	0.11	0.0048	0.90809	1014	45	1306	51	22.4	1803	22	259	0.53
NOV11-1B_11l.FIN2	4.44	0.290	0.2855	0.0120	0.1102	0.0050	0.69713	1616	61	1718	57	5.9	1814	34	301	0.27
NOV11-1B_3c.FIN2	4.36	0.280	0.2858	0.0120	0.1078	0.0048	0.75453	1617	60	1708	51	5.3	1776	28	48	1.13
NOV11-1B_10h.FIN	7.4	0.520	0.298	0.0160	0.1806	0.0083	0.85506	1674	78	2153	62	22.2	2669	27	427	0.29
NOV11-1B_10k.FIN	6.28	0.440	0.326	0.0140	0.1379	0.0073	0.71073	1819	70	2010	63	9.5	2192	52	67.1	0.55
NOV11-1B_9p.FIN2	7.94	0.540	0.36	0.0160	0.161	0.0071	0.84213	1989	77	2224	60	10.6	2473	19	150.4	0.58

Notes:

abs = absolute

rho is the correlation coefficient between the ratios

% Discord. 6/38-7/35 = 100 - (100 * (206Pb/238U date) / (207Pb/235U date))

Bold analyses were used in age calculations.

CHAPTER 4

Texturally controlled U-Pb monazite dating of sapphirine granulites from the Gruf Complex, Central Alps: Evidence for UHT metamorphism in a Cenozoic continent-continent collision

Jeffrey Oalmann[1]*

Andreas Möller[1]

Romain Bousquet[2]

[1]*The University of Kansas, Department of Geology, 1475 Jayhawk Blvd., Rm. 120, Lawrence, KS 66045 USA.*

[2]*Christian-Albrechts-Universität zu Kiel, Institute of Geosciences, Ludewig-Meyn-Straße 10, 24098 Kiel, Germany.*

Abstract

Whether ultra-high temperature (UHT) metamorphism of the Gruf complex occurred during Permian rifting or Alpine orogenesis has been a matter of debate. Here we present texturally controlled U-Pb data of monazite from UHT mineral assemblages within the Gruf granulites. All monazite grains and domains have U-Pb dates between 34 and 30 Ma. We interpret the association of monazite with peak and post-peak UHT minerals and textures and the lack of inherited monazite to indicate that the UHT metamorphic event resulted in complete recrystallization of monazite and thus must have occurred during Cenozoic Alpine orogenesis. Monazite likely formed as garnet was breaking down to produce orthopyroxene, sapphirine, and cordierite in response to decompression at UHT conditions. The range of dates likely indicates that monazite growth

continued for ca. 4 m.y., and Alpine UHT metamorphism is consistent with a model in which advection of mantle heat and material to the lower crust occurred in response to slab breakoff.

Introduction

Ultra-high temperature (UHT) metamorphic rocks are the products of extreme thermal conditions within the lower crust (>900°C and 7–13 kbar; Harley, 1998; Brown, 2007; Harley, 2008). Attaining UHT conditions requires either a hotter-than-normal geothermal gradient (in excess of 20°C/km; Kelsey, 2008) or geodynamic processes that bring heat to the lower crust (e.g. Collins, 2002; Clark et al., 2011). Therefore, understanding when UHT metamorphism occurred in a particular geologic setting has important implications for the thermal, tectonic, and rheological evolution of that setting. The evolution of continent-continent orogens, such as the Alps, can influence surface processes such as volcanic activity, earthquakes, and erosion. Therefore, studies of rocks exhumed from the deep parts of orogens can be used to further understand the deep geodynamic processes.

The Gruf Complex contains the only known UHT rocks in the Central Alps (Bousquet et al., 2012a). The maximum pressure and temperature conditions these rocks experienced have been agreed upon by several researchers (Galli et al., 2011; Guevara and Caddick, 2016; Oalmann et al., in preparation-a), but there has not been a consensus as to the timing of the UHT event. The first geochronological studies on the UHT granulites from the Gruf Complex (Liati and Gebauer, 2003; Schmitz et al., 2009), concluded that peak metamorphism occurred during the Alpine orogeny, at ca. 32 Ma. However, based on U-Pb zircon dating of charnockites associated with the UHT granulites, Galli et al. (2012) concluded that UHT metamorphism occurred during a Permian rifting event and that metamorphic conditions only reached ca. 700–750°C and 6–8 kbar during the Alpine orogeny (Galli et al., 2011). Here we present texturally-controlled U-Pb dating of

monazite from the Gruf granulites, thus linking P-T estimates directly to dates, to constrain the timing of UHT metamorphism in the Gruf Complex.

Geologic Setting

Several units in the Central Alps, including the Adula nappe (Figure 4.1), underwent ultra-high pressure (UHP) metamorphism related to subduction until ca. 35 Ma (Becker, 1993; Gebauer, 1996; Brouwer et al., 2005; Hermann et al., 2006; Liati et al., 2009) followed by exhumation and a Barrovian (temperature-dominated) metamorphic overprint, which began at ca. 34 Ma (Gebauer, 1996; Hermann et al., 2006) and continued to ca. 22 Ma (Rubatto et al., 2009). The Barrovian overprint, which affected an area known as the Lepontine dome, is characterized by greenschist facies metamorphism in the northern Central Alps increasing to upper-amphibolite to lower-granulite facies migmatization in the Southern Steep Belt (Todd and Engi, 1997; Figure 4.1; Frey and Ferreiro Mählmann, 1999; Burri et al., 2005). Previously proposed causes of the switch from high-pressure to high-temperature metamorphism include convective heating within an orogenic wedge (Bousquet et al., 2008; Berger et al., 2011), slab breakoff (von Blanckenburg and Davies, 1995; Handy et al., 2010), and lithospheric thinning (Beltrando et al., 2010).

The Gruf Complex is bordered to the north by the Chiavenna ophiolite and Tambo nappe. The normal sense Forcola Fault separates the Gruf Complex from the Adula nappe, which has a different P-T history, to the west (Figure 4.1; Ciancaleoni and Marquer, 2006; Bousquet et al., 2012b; Galli et al., 2013). The 32–30 Ma (von Blanckenburg, 1992; Samperton et al., 2015) Bergell tonalite to granodiorite intrusion structurally overlies the Gruf Complex (Davidson et al., 1996) and crops out to the east and south. The Novate leucogranite intruded the Gruf Complex at 23.8± 0.1 Ma (Oalmann et al., in preparation-c).

Upper amphibolite facies migmatitic orthogneisses and minor paragneisses and leucogranites are the most common rock types in the Gruf Complex. However, several mappable units of charnockite also occur, which contain scarce schlieren, rafts, and pods of sapphirine-bearing granulites. The granulites underwent simultaneous decompression and heating from ca. 800°C and 10–14 kbar to UHT conditions of 900–1000°C and 7.5–9.5 kbar (Oalmann et al., in preparation-a). The ages of variably deformed felsic dikes indicate that the UHT granulite/charnockite units were juxtaposed against the migmatites along mylonitic shear zones between 30 and 26 Ma (Oalmann et al., in preparation-c).

Sample Descriptions

Residual granulite samples Br03-55-3 and Br03-56-2, which lack a structural fabric, are very similar in their mineralogy, grain size, and textures. These granulites are dominated by large (up to 1 cm) anhedral garnet porphyroblasts and subhedral to euhedral sapphirine and orthopyroxene porphyroblasts, some of which are intergrown. Cordierite occurs in corona-textures around garnet and forms moats separating sapphirine and orthopyroxene. Quartz + K-feldspar + plagioclase occur in pod-shaped leucosomes that are scattered throughout the samples. Biotite occurs as monomineralic aggregates or fringes garnet and orthopyroxene porphyroblasts. Embayments in garnet are filled with sapphirine + orthopyroxene porphyroblasts, cordierite ± sapphirine ± orthopyroxene symplectites, and/or quartzofeldspathic leucosomes. In the residual granulites, anhedral to subhedral monazite is intergrown with or included in sapphirine, orthopyroxene, cordierite and/or bioite or occurs within leucosomes (Figure 4.2A-D). Monazite most commonly occurs near embayments in garnet.

Retrogressed granulite sample Br03-56-4 is similar in texture and appearance to the residual granulite samples. However, most of the sapphirine, orthopyroxene, and cordierite has

been replaced by secondary chlorite and biotite. Muscovite is also present in this sample. Anhedral monazite grains occur mainly within the retrogressed parts of this sample (Figure 4.2E).

Leucogranulite sample GR11-39 is characterized by alternating light and dark bands that give the sample a gneissic texture. The dark bands are dominated by orthopyroxene, garnet, biotite, and sapphirine, and the light bands comprise deformed quartz, K-feldspar, and plagioclase. Garnet occurs as single, anhedral porphyroblasts and clusters of anhedral grains that were probably originally a single porphyroblast. Garnet embayments are commonly filled with plagioclase, orthopyroxene, sapphirine, biotite, spinel, and magnetite. Monazite occurs exclusively as small, irregular grains on the edge of larger apatite grains (Figure 4.2F), except for one grain located in a leucosome between plagioclase and K-feldspar (grain 2, Table 4.A-2).

Results of U-Pb Monazite Dating

Monazite grains within four granulite samples (two residual granulites, one leucogranulite, and one retrogressed granulite) were dated by laser ablation inductively coupled plasma mass spectrometry (LA-ICP-MS) at The University of Kansas (see Appendix A for complete analytical procedures). To preserve textural context, small areas were drilled out of thin sections and mounted in epoxy from the residual and retrogressed granulite samples, and monazite was analyzed directly within a thin section from the leucogranulite sample. Discordance is reported as uncertainty weighted age difference (UWAD) (Table 4.A2).

Backscattered electron (BSE) images of selected, representative monazite-bearing textures are shown in Figure 4.2. All analyses have $^{206}Pb/^{238}U$ dates between 34.5 and 30 Ma, and there is limited correlation between position within grain (e.g. cores or rims) and date (Figure 4.2A-D). Some of the highest, concordant $^{206}Pb/^{238}U$ dates come from monazite intergrown with high-Al orthopyroxene (two analyses from texture GRM2-2 at 33.6±0.8 and 33.2±0.8 Ma) and a euhedral

monazite grain included in plagioclase within a garnet-breakdown texture (33.6±0.7 Ma) (Figure 4.2C), and monazite inclusions in sapphirine have $^{206}Pb/^{238}U$ dates older than 32 Ma. In a texture that is typical for monazite textures in the leucogranulite sample, the youngest monazite grains (31–30 Ma) occur on the edge of apatite grains (e.g. Figure 4.2F).

Within the residual and retrogressed granulite samples, discordant analyses are scarce and trend toward common-Pb upper intercepts (Figure 4.3A, 3B). The most concordant grains spread along concordia from 34 to 31 Ma (Figure 4.3A-C). The $^{206}Pb/^{238}U$ dates of the analyses with UWAD < 1.2 from the residual granulite sample Br03-56-2 range from 31.06±0.77 to 32.99±0.86 Ma (Table 4.A2; Figure 4.3A). The seven oldest concordant analyses make up a population that has a weighted mean $^{206}Pb/^{238}U$ age of 32.5±0.3 Ma (MSWD=0.5, n=7), and the lower intercept age of the other analyses is 31.5 +0.2/-0.2 Ma (MSWD=0.4, n=17). Analyses with UWAD < 1.2 from residual granulite sample Br03-55-3 have $^{206}Pb/^{238}U$ dates between 31.15±0.59 and 33.61±0.71 Ma (Table 4.2; Figure 4.3B). Excluding the two oldest and one youngest analyses with UWAD < 1.2 and the more discordant analyses, the weighted mean $^{206}Pb/^{238}U$ age for this sample is 32.4±0.2 Ma (MSWD=1.0, n=14). The three small grains from retrogressed granulite sample Br03-56-4 have UWAD ≤ 0.7 and $^{206}Pb/^{238}U$ dates ranging from 32.15±0.62 to 34.10±0.77 Ma (Table 4.2; Figure 4.3C). These grains do not encompass a single age population, and therefore, no ages are interpreted from the retrogressed granulite sample. However, these dates agree with the age range of most monazite grains from the residual granulite samples.

All except one of the analyses from leucogranulite sample GR11-39 have UWAD values > 1.2 (Table 4.2; Figure 4.3D), and these grains have the highest U concentrations (4090–12,330 ppm; Table 4.A2) of all the monazite analyzed in this study. The $^{206}Pb/^{238}U$ dates of analyses with UWAD ≤ 3.2 range from 30.04±0.52 to 31.98±0.56 Ma, which is a younger age range than in the

residual and retrogressed granulites. There are two distinct discordia trends with common-Pb upper intercepts (Figure 4.3D). The older population has a lower intercept age of 31.7 +0.4/-0.5 Ma (MSWD=0.2, n=4), and the younger discordant population has a lower intercept age of 30.8 +0.3/-0.3 Ma (MSWD=0.4, n=6). Two analyses that do not plot along either of the discordia trends have a weighted mean $^{206}Pb/^{238}U$ age of 30.1±0.4 Ma (MSWD=0.2, n=2).

Discussion and Conclusions

Although many of the U-Pb monazite dates overlap within uncertainty of one another, analyses from single samples and even from single grains do not form age populations with n-appropriate MSWDs without excluding some analyses. This leads us to the interpretation that not all monazite crystallized at the same time. It is more likely that monazite (re)crystallized more or less continuously over the ca. 4 m.y. period recorded by the $^{206}Pb/^{238}U$ dates of the concordant analyses, which range from 30.04±0.52 to 34.10±0.77 Ma. This age range is consistent with early post-peak UHT crystallization of zircon in the same rock units (Oalmann et al., in preparation-c).

Based on the close vicinity of most monazite grains to garnet breakdown textures in the residual granulites (Figure 4.2A, C, D) and high Y content of the monazite (up to 4 wt. % Y_2O_3; Schmitz et al., 2009), the mostly likely trigger for monazite growth was a release of P and REE during the breakdown of garnet, which contains ca. 0.1 ppm Ce on average (Appendix B). To balance the LREE needed for monazite, it is likely that melt and apatite and xenotime, which is present in the residual granulites but not dated, were involved in the monazite producing reactions. Monazite also occurs in a variety of textures associated with UHT minerals (e.g. high-Al orthopyroxene, sapphirine, and cordierite) (Figure 4.2A–D). The sapphirine granulites underwent simultaneous decompression and heating from ca. 800°C and 9–12 kbar to 900–1000°C and 7.0–9.5 kbar, resulting in orthopyroxene and sapphirine (and later cordierite) growth at the expense of

garnet (Oalmann et al., in preparation-b). Some of the oldest (i.e. >32 Ma) domains are from monazite grains included in sapphirine (Figure 4.2B, D). The texture shown in Figure 4.2B (orthopyroxene + sapphirine + cordierite) equilibrated at 850–1100°C and 7.25–10.5 kbar (Oalmann et al., in preparation-a) and contains monazite with $^{206}Pb/^{238}U$ dates ranging from 32.0±0.8–33.0±0.9 Ma (weighted mean $^{206}Pb/^{238}U$ age = 32.5±0.5, MSWD=1.5, n=3). The euhedral monazite shown in Figure 4.2C has $^{206}Pb/^{238}U$ dates ranging from 32.0±0.8–33.6±0.7 Ma (weighted mean $^{206}Pb/^{238}U$ age = 32.7±0.4, MSWD=5.3, n=3) and is within a texture that equilibrated at ca. 962°C and 8.7 kbar (Appendix C). The garnet-breakdown texture shown in Figure 4.2A equilibrated at 910°C and 7.6 kbar (Appendix C) contains anhedral monazite ($^{206}Pb/^{238}U$ dates = 31.2±0.6–32.4±0.7 Ma) intergrown with high-Al orthopyroxene and plagioclase. Based on the association of monazite with these UHT to slightly post-UHT textural and mineralogical indicators, we conclude that UHT metamorphism occurred simultaneous with or slightly prior to crystallization of the oldest monazite (i.e. during the Alpine orogeny at ca. 34 Ma).

The textural relationships between monazite and apatite in the leucogranulite sample GR11-35 (Figure 4.2F) are interpreted as monazite growth as the result of either LREE expulsion from apatite during decompression (e.g. Finger and Krenn, 2007; Krenn et al., 2009; Rocha et al., 2016) or fluid-assisted dissolution-reprecipitation (Harlov and Förster, 2002; Harlov et al., 2005). The two relatively young ages interpreted from this sample (30.8 +0.3/-0.3 Ma and 30.1±0.4 Ma) compared to the >31.5 Ma ages from the residual granulites (Figure 4.3) and the lack of concordant >32 Ma grains (Table 4.2; Figure 4.3D) indicate that this was a late-stage process. Because there is no evidence in the leucogranulite sample for low temperature fluid infiltration (e.g. abundant hydrous minerals within fractures), we interpret that LREE expulsion from apatite during

decompression and/or cooling led to the monazite growth on apatite. The different age groups (Figure 4.3D, Table 4.A-2) indicate that this process occurred at least three different times in the leucogranulite. Analyses of two different monazite grains (analyses GR11-35-3-1, and 3-2) along the edge of the same apatite grain have $^{206}Pb/^{238}U$ dates of 31.3±0.7 Ma and 34.5±0.8 Ma (discordant) and are part of two different age groups shown in Figure 4.3D. We interpret this to indicate that LREE expulsion occurred at two different times from the same apatite grain and thus was a very localized process.

The few monazite dates obtained from the retrogressed granulite sample Br03-56-4, which range from 32.15±0.62–34.10±0.77 Ma, overlap with the oldest dates from the residual granulite samples (Table 4.2; Figure 4.3). Because this sample is likely a retrogressed residual granulite sample (see *'Sample Descriptions'* above), we interpret that (re)crystallization or modification of monazite did not occur during greenschist-facies, retrograde metamorphism.

Many (U)HT granulites from other areas contain complexly zoned monazite grains that preserve the ages of multiple plutonic, metamorphic, or metasomatic events (e.g. Kelly et al., 2006; Mahan et al., 2006; Kelly et al., 2012; Dumond et al., 2015; Rocha et al., 2016). However, the Gruf granulites lack inherited monazite (Figure 4.2, 3). Experimental studies have revealed that the closure temperature for Pb diffusion in monazite is similar to that of Pb in zircon (e.g. Cherniak et al., 2004), and thus U-Pb monazite dates should not be affected by post-crystallization diffusive resetting. Therefore, we interpret the lack of inherited monazite to indicate that the Gruf granulites lacked monazite prior to the Alpine metamorphic event or that the rocks completely recrystallized during or slightly earlier than the time monazite (re)crystallized. The lack of inherited monazite precludes an older (Permian) UHT event followed by a moderate temperature overprint during the Alpine orogeny as suggested by Galli et al. (2011; 2012; 2013).

Figure 4.4 summarizes the likely Alpine P-T-t path taken by the Gruf granulites, which is in part based on data and observations presented by Oalmann et al. (in preparation-a; in preparation-c; submitted): (1) Prograde metamorphism reached conditions of 800°C and 10–14 kbar. The exact timing and duration of this part of the P-T path is unknown, but minor zircon growth in equilibrium with garnet occurred at 34.8 +1.0/-1.1 (Oalmann et al., in preparation-c). (2) During decompression, the granulites were heated to UHT conditions, resulting in garnet breakdown and the crystallization of the oldest monazite domains in the residual granulites at ca. 34 Ma. (3) Monazite continued to crystallize in the residual granulites until ca. 31 Ma, and the first pulse of monazite growth on apatite in the leucogranulite occurred at 31.7 +0.4/-0.5 Ma. (4) Between 31 and 30 Ma, monazite in the leucogranulite continued to crystallize along the edge of apatite grains. (5) The lower crustal granulites (and charnockites) were exhumed into the mid-crustal migmatites between 30 and 26 Ma (Oalmann et al., in preparation-c).

Attainment of UHT conditions in the lower crust of a continent-continent collision requires an external source of heat. The most likely heat source is the asthenospheric mantle. We postulate that either of two geodynamic processes could have led to heat advection to the lower crust: (1) Slab breakoff resulted in asthenospheric upwelling and mantle melting (von Blanckenburg and Davies, 1995; Handy et al., 2010); or (2) Slab rollback lead to lithospheric thinning of the overthickened orogenic wedge and thus asthenospheric upwelling and magma generation (Beltrando et al., 2010). However, we prefer the slab breakoff model because heating in response to lithospheric thinning would have resulted in a long-lived UHT event and widespread magmatism, both of which are not observed in the Alps.

An Alpine age for UHT metamorphism indicates that the Gruf Complex hosts the second youngest occurrence of exposed UHT rocks in the world. The youngest known exposure of UHT

granulites occur as lenses within an active subduction zone in Indonesia (Pownall et al., 2014), and Hacker et al. (2000) reported young UHT xenoliths in lavas erupted on the Tibetan plateau. Cenozoic UHT metamorphism may have occurred in other regions, but the products have not been yet recognized due to non-exposure, retrogression, or lack of UHT indicator assemblages (e.g. sapphirine + quartz).

Acknowledgements

This research is supported by the American National Science Foundation under Grant No. EAR 0911633 to A. Möller. We are grateful to A. Galli for guiding us in the field area, the Biavaschi family at Rifugio Brasca for their hospitality and logistical help, and P.G. Lippert for field assistance. Samples Br03-56-2, -56-4, and -55-3 were collected by S. Schefer.

Appendix 4.A: Analytical Methods for U-Pb Monazite Dating

Monazite was analyzed *in situ* (i.e. directly within thin sections or drilled out parts of thin sections) by LA-ICP-MS at The University of Kansas, Department of Geology's Isotope Geochemistry Lab. Table 4.A1 shows the analytical protocols that were used for all measurements. Table 4.A2 shows the U-Pb isotopic data and calculated ages.

Appendix 4.B: Analytical Methods for Garnet Trace Element Analyses

Trace elements concentrations of garnet from one of the monazite bearing textures were measured by LA-ICP-MS at The University of Kansas, Department of Geology's Isotope Geochemistry Lab. Electron microprobe major element data were used for the internal standard values (Ca concentration) for each spot. Table 4.B1 shows the analytical protocols that were used for all measurements. Table 4.B2 shows the trace element concentrations that were measured.

Figure 4.B1 shows chondrite-normalized rare earth element patterns for all of the spots that were analyzed.

Appendix 4.C: Thermobarometry Calculations

Pressure and temperature conditions corrected for retrograde exchange were estimated for textures in the residual granulites using the computer program RCLC of Pattison et al. (2003). Major element compositions used for the input to the calculations were determined by electron probe microanalysis (EMPA) at the Christian-Albrechts-Universität zu Kiel Institute for Geosciences using the methods presented by Oalmann et al. (in preparation-b). The compositional data and results of the calculations are presented in Table 4.C1. These calculations assume equilibrium between garnet, orthopyroxene, and plagioclase.

The estimates obtained for textures GRMPx3 (910°C at 7.6 kbar) (Figure 4.2A) and GRM-27 (962°C at 8.7 kbar) (Figure 4.2C) with this method are consistent with the results of thermobarometric modeling (peak conditions = 900–1000°C and 7.5–9.5 kbar) presented by Oalmann et al. (in preparation-b), but the estimated temperature for texture GRM-37 (1040°C at 9.1 kbar) (Figure 4.2B) is higher than the peak temperature range modeled by Oalmann et al. (in preparation-b). The garnet in this texture occurs as inclusions in orthopyroxene (Figure 4.2B). We interpret this relationship to indicate that garnet is a left over product of a garnet-consuming reaction that produced orthopyroxene + sapphirine + cordierite (Oalmann et al., in preparation-b), and thus all the phases are not in equilibrium in this texture.

Figure Captions

Figure 4.1. Tectonic map of part of the Central Alps (modified from Bousquet et al., 2012b) showing the location of the Gruf Complex and surrounding units. Ages for the Bergell and Novate

intrusions are from von Blanckenburg (1992) and (Oalmann et al., in preparation-c), respectively. SSB = Southern Steep Belt.

Figure 4.2. Backscattered electron (BSE) images of representative monazite-bearing textures showing locations of analyses and $^{206}Pb/^{238}U$ dates with 2σ propogated uncertainty. (A–B) Textures from residual granulite sample Br03-56-2. (C–D) Textures from residual granulite sample Br03-55-3. (E) A texture from retrogressed granulite Br03-56-4. (F) A texture from leucogranulite sample GR11-39.

Figure 4.3. Wetherill concordia diagrams plotted with ET_Redux (McLean et al., 2016) showing analyses from the different samples and calculated ages (LI = lower intercept; WM = weighted mean). Ellipse areas represent 2σ propagated uncertainty. (A) Residual granulite sample Br03-56-2. (B) Residual granulite sample Br03-55-3. (C) Retrogressed granulite sample Br03-56-4. (D) Leucogranulite sample GR11-39. For panels A and C, the different colored ellipses were used to calculate the different ages with corresponding colored text. In panel B, blue ellipses were used in the age calculations, and grey ellipses were excluded.

Figure 4.4. P-T diagram showing P-T path taken by the Gruf granulites, schematic mineral reactions, conditions and timing of monazite growth, and conditions and timing of exhumation of the lower crustal UHT rocks into the middle crust.

Figure 4.B1. Chondrite-normalized REE patterns for garnet analyses from residual granulite sample Br03-56-2.

References

Becker, H., 1993. Garnet peridotite and eclogite Sm-Nd mineral ages from the Lepontine dome (Swiss Alps): New evidence for Eocene high-pressure metamorphism in the central Alps. Geology, 21(7): 599-602.

Beltrando, M., Lister, G.S., Rosenbaum, G., Richards, S., Forster, M.A., 2010. Recognizing episodic lithospheric thinning along a convergent plate margin: The example of the Early Oligocene Alps. Earth-Science Reviews, 103(3): 81-98.

Berger, A., Schmid, S.M., Engi, M., Bousquet, R., Wiederkehr, M., 2011. Mechanisms of mass and heat transport during Barrovian metamorphism: A discussion based on field evidence from the Central Alps (Switzerland/northern Italy). Tectonics, 30(1): TC1007.

Bousquet, R. et al., 2008. Metamorphism of metasediments at the scale of an orogen: a key to the Tertiary geodynamic evolution of the Alps. Geological Society, London, Special Publications, 298(1): 393-411.

Bousquet, R. et al., 2012a. Metamorphic Framework of the Alps, Commission for the Geological Map of the World, CCGM/CGMW.

Bousquet, R. et al., 2012b. Tectonic framework of the Alps, Commission for the Geological Map of the World, CCGM/CGMW.

Brouwer, F., Burri, T., Engi, M., Berger, A., 2005. Eclogite relics in the Central Alps: PT-evolution, Lu-Hf ages, and implications for formation of tectonic mélange zones. Schweizerische mineralogische und petrographische Mitteilungen, 85: 147-174.

Brown, M., 2007. Metamorphic conditions in orogenic belts: a record of secular change. International Geology Review, 49(3): 193-234.

Burri, T., Berger, A., Engi, M., 2005. Tertiary migmatites in the Central Alps: Regional distribution, field relations, conditions of formation, and tectonic implications. Schweizerische mineralogische und petrographische Mitteilungen, 85(2-3): 215-232.

Cherniak, D., Watson, E.B., Grove, M., Harrison, T.M., 2004. Pb diffusion in monazite: a combined RBS/SIMS study. Geochimica et Cosmochimica Acta, 68(4): 829-840.

Ciancaleoni, L., Marquer, D., 2006. Syn-extension leucogranite deformation during convergence in the Eastern Central Alps: example of the Novate intrusion. Terra Nova, 18(3): 170-180.

Clark, C., Fitzsimons, I.C., Healy, D., Harley, S.L., 2011. How does the continental crust get really hot? Elements, 7(4): 235-240.

Collins, W., 2002. Hot orogens, tectonic switching, and creation of continental crust. Geology, 30(6): 535-538.

Davidson, C., Rosenberg, C., Schmid, S., 1996. Symmagmatic folding of the base of the Bergell pluton, Central Alps. Tectonophysics, 265(3): 213-238.

Dumond, G., Goncalves, P., Williams, M., Jercinovic, M., 2015. Monazite as a monitor of melting, garnet growth and feldspar recrystallization in continental lower crust. Journal of Metamorphic Geology, 33(7): 735-762.

Finger, F., Krenn, E., 2007. Three metamorphic monazite generations in a high-pressure rock from the Bohemian Massif and the potentially important role of apatite in stimulating polyphase monazite growth along a PT loop. Lithos, 95(1): 103-115.

Frey, M., Ferreiro Mählmann, R., 1999. Alpine metamorphism of the Central Alps. Schweizerische mineralogische und petrographische Mitteilungen, 79(1): 135-154.

Galli, A. et al., 2011. Granulites and charnockites of the Gruf Complex: Evidence for Permian ultra-high temperature metamorphism in the Central Alps. Lithos, 124(1-2): 17-45.

Galli, A. et al., 2012. U–Pb zircon dating of the Gruf Complex: disclosing the late Variscan granulitic lower crust of Europe stranded in the Central Alps. Contributions to Mineralogy and Petrology, 163: 353-378.

Galli, A., Le Bayon, B., Schmidt, M.W., Burg, J.-P., Reusser, E., 2013. Tectonometamorphic history of the Gruf complex (Central Alps): exhumation of a granulite–migmatite complex with the Bergell pluton. Swiss Journal of Geosciences, 106(1): 33-62.

Gebauer, D., 1996. A P-T-t path for an (Ultra?-) High-pressure ultramafic/mafic rock-association and its felsic country-rocks based on SHRIMP-dating of magmatic and metamorphic zircon domains. Example: Alpe Arami (Central Swiss Alps), Earth Processes: Reading the Isotopic Code. Geophys. Monogr. Ser. AGU, Washington, DC, pp. 307-329.

Guevara, V., Caddick, M., 2016. Shooting at a moving target: phase equilibria modelling of high-temperature metamorphism. Journal of Metamorphic Geology, 34: 209-235.

Guillong, M., Hametner, K., Reusser, E., Wilson, S.A., Günther, D., 2005. Preliminary Characterisation of New Glass Reference Materials (GSA-1G, GSC-1G, GSD-1G and GSE-1G) by Laser Ablation-Inductively Coupled Plasma-Mass Spectrometry Using 193 nm, 213 nm and 266 nm Wavelengths. Geostandards and Geoanalytical Research, 29(3): 315-331.

Hacker, B.R. et al., 2000. Hot and dry deep crustal xenoliths from Tibet. Science, 287(5462): 2463-2466.

Handy, M.R., Schmid, S.M., Bousquet, R., Kissling, E., Bernoulli, D., 2010. Reconciling plate-tectonic reconstructions of Alpine Tethys with the geological–geophysical record of spreading and subduction in the Alps. Earth-Science Reviews, 102(3): 121-158.

Harley, S., 2008. Refining the P–T records of UHT crustal metamorphism. Journal of Metamorphic Geology, 26(2): 125-154.

Harley, S.L., 1998. On the occurrence and characterization of ultrahigh-temperature crustal metamorphism. Geological Society, London, Special Publications, 138(1): 81-107.

Harlov, D.E., Förster, H.-J., 2002. High-grade fluid metasomatism on both a local and a regional scale: the Seward peninsula, Alaska, and the Val Strona di Omegna, Ivrea–Verbano Zone, Northern Italy. Part I: petrography and silicate mineral chemistry. Journal of Petrology, 43(5): 769-799.

Harlov, D.E., Wirth, R., Förster, H.-J., 2005. An experimental study of dissolution–reprecipitation in fluorapatite: fluid infiltration and the formation of monazite. Contributions to Mineralogy and Petrology, 150(3): 268-286.

Hermann, J., Rubatto, D., Trommsdorff, V., 2006. Sub-solidus Oligocene zircon formation in garnet peridotite during fast decompression and fluid infiltration (Duria, Central Alps). Mineralogy and Petrology, 88(1): 181-206.

Jochum, K.P., Willbold, M., Raczek, I., Stoll, B., Herwig, K., 2005. Chemical Characterisation of the USGS Reference Glasses GSA-1G, GSC-1G, GSD-1G, GSE-1G, BCR-2G, BHVO-2G and BIR-1G Using EPMA, ID-TIMS, ID-ICP-MS and LA-ICP-MS. Geostandards and Geoanalytical Research, 29(3): 285-302.

Kelly, N.M., Clarke, G.L., Harley, S.L., 2006. Monazite behaviour and age significance in poly-metamorphic high-grade terrains: a case study from the western Musgrave Block, central Australia. Lithos, 88(1): 100-134.

Kelly, N.M., Harley, S.L., Möller, A., 2012. Complexity in the behavior and recrystallization of monazite during high-T metamorphism and fluid infiltration. Chemical geology, 322: 192-208.

Kelsey, D.E., 2008. On ultrahigh-temperature crustal metamorphism. Gondwana Research, 13(1): 1-29.

Krenn, E., Janák, M., Finger, F., Broska, I., Konečný, P., 2009. Two types of metamorphic monazite with contrasting La/Nd, Th, and Y signatures in an ultrahigh-pressure metapelite from the Pohorje Mountains, Slovenia: Indications for pressure-dependent REE exchange between apatite and monazite? American Mineralogist, 94(5-6): 801-815.

Liati, A., Gebauer, D., 2003. Geochronological constraints for the time of metamorphism in the Gruf Complex (Central Alps) and implications for the Adula-Cima Lunga nappe system. Swiss Bulletin of Mineralogy and Petrology, 83(2): 159-172.

Liati, A., Gebauer, D., Fanning, C.M., 2009. Geochronological evolution of HP metamorphic rocks of the Adula nappe, Central Alps, in pre-Alpine and Alpine subduction cycles. Journal of the Geological Society, 166(4): 797-810.

Mahan, K., Goncalves, P., Williams, M., Jercinovic, M., 2006. Dating metamorphic reactions and fluid flow: application to exhumation of high-P granulites in a crustal-scale shear zone, western Canadian Shield. Journal of Metamorphic Geology, 24(3): 193-217.

McLean, N., Bowring, J., Gehrels, G., 2016. Algorithms and software for U-Pb geochronology by LA-ICPMS. Geochemistry, Geophysics, Geosystems.

Oalmann, J., Düsterhöft, E., Möller, A., Bousquet, R., in preparation-a. Constraining the pressure-temperature evolution and geodynamic setting of UHT granulites and migmatitic paragneisses of the Gruf Complex, Central Alps.

Oalmann, J., Möller, A., Bousquet, R., in preparation-b. Constraining the pressure-temperature evolution and geodynamic setting of UHT granulites and migmatitic paragneisses of the Gruf Complex, Central Alps.

Oalmann, J., Möller, A., Bousquet, R., submitted. Decoupling of Zr-thermometry and U-Pb thermochronology in rutile from the UHT granulites and charnockites of the Gruf Complex (Central Alps).

Oalmann, J., Möller, A., Bousquet, R., Savage, J., in preparation-c. Constraining the timing of UHT metamorphism, melt crystallization, and deformation with zircon geochronology and trace element geochemistry: The Gruf Complex, Central Alps.

Paton, C., Hellstrom, J., Paul, B., Woodhead, J., Hergt, J., 2011. Iolite: Freeware for the visualisation and processing of mass spectrometric data. J. Anal. At. Spectrom., 26(12): 2508-2518.

Paton, C. et al., 2010. Improved laser ablation U-Pb zircon geochronology through robust downhole fractionation correction. Geochemistry, Geophysics, Geosystems, 11(3).

Pattison, D.R., Chacko, T., Farquhar, J., McFarlane, C.R., 2003. Temperatures of granulite-facies metamorphism: constraints from experimental phase equilibria and thermobarometry corrected for retrograde exchange. Journal of Petrology, 44(5): 867-900.

Petrus, J.A., Kamber, B.S., 2011. VisualAge: A novel approach to U-Pb LA-ICP-MS geochronology. Mineralogical Magazine, 75: 1633.

Pownall, J.M., Hall, R., Armstrong, R.A., Forster, M.A., 2014. Earth's youngest known ultrahigh-temperature granulites discovered on Seram, eastern Indonesia. Geology, 42(4): 279-282.

Rocha, B., Moraes, R., Möller, A., Cioffi, C., Jercinovic, M., 2016. Timing of anatexis and melt crystallization in the Socorro–Guaxupé Nappe, SE Brazil: Insights from trace element composition of zircon, monazite and garnet coupled to U Pb geochronology. Lithos.

Rubatto, D., Hermann, J., Berger, A., Engi, M., 2009. Protracted fluid-induced melting during Barrovian metamorphism in the Central Alps. Contributions to Mineralogy and Petrology, 158(6): 703-722.

Samperton, K.M. et al., 2015. Magma emplacement, differentiation and cooling in the middle crust: Integrated zircon geochronological–geochemical constraints from the Bergell Intrusion, Central Alps. Chemical Geology, 417: 322-340.

Schmitz, S. et al., 2009. Chemical U-Th-Pb dating of monazite by 3D-Micro X-ray fluorescence analysis with synchrotron radiation. European Journal of Mineralogy, 21(5): 927-945.

Seydoux-Guillaume, A.-M., Paquette, J.-L., Wiedenbeck, M., Montel, J.-M., Heinrich, W., 2002. Experimental resetting of the U–Th–Pb systems in monazite. Chemical geology, 191(1): 165-181.

Todd, C.S., Engi, M., 1997. Metamorphic field gradients in the Central Alps. Journal of Metamorphic Geology, 15(4): 513-530.

von Blanckenburg, F., 1992. Combined high-precision chronometry and geochemical tracing using accessory minerals: applied to the Central-Alpine Bergell intrusion (central Europe). Chemical Geology, 100(1-2): 19-40.

von Blanckenburg, F., Davies, J.H., 1995. Slab breakoff: a model for syncollisional magmatism and tectonics in the Alps. Tectonics, 14(1): 120-131.

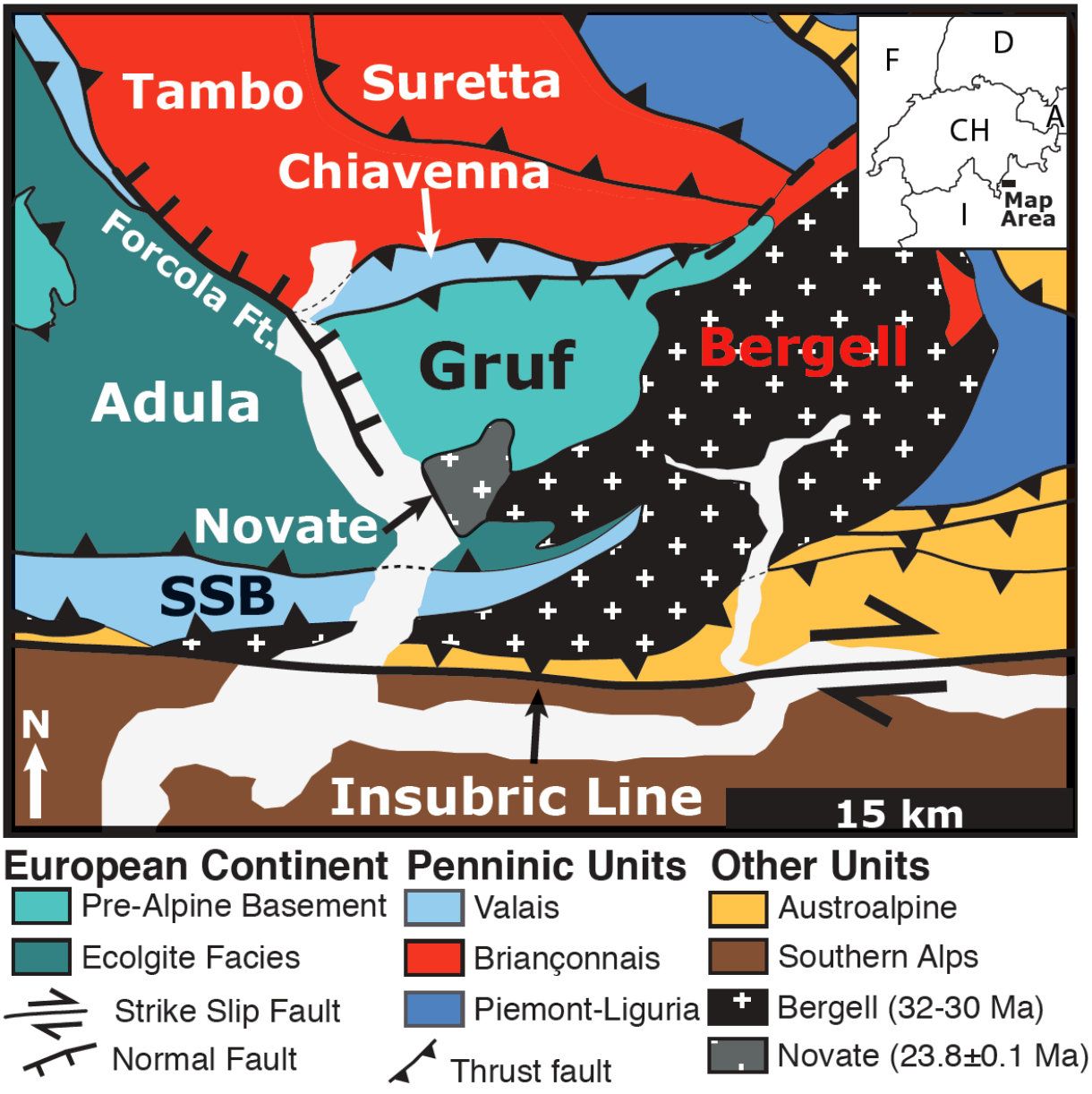
Tambo
Suretta
Chiavenna
Forcola Ft.
Gruf
Bergell
Adula
Novate
SSB
N
Insubric Line
15 km
F
D
CH
A
I
Map Area
European Continent
Pre-Alpine Basement
Ecolgite Facies
Strike Slip Fault
Normal Fault
Penninic Units
Valais
Briançonnais
Piemont-Liguria
Thrust fault
Other Units
Austroalpine
Southern Alps
Bergell (32-30 Ma)
Novate (23.8±0.1 Ma)

Figure 4.1

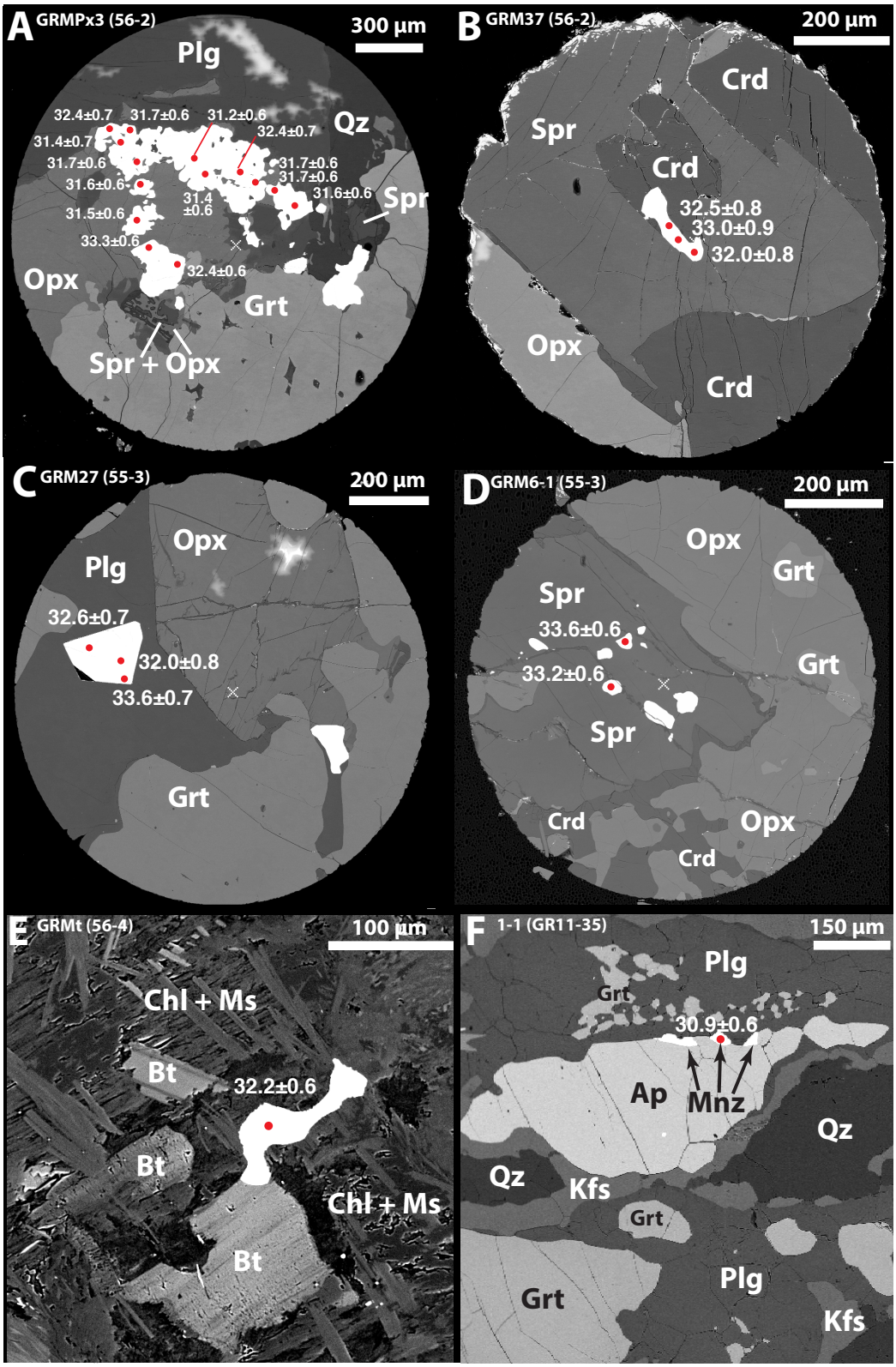
A GRMPx3 (56-2)
300 µm
Plg
Qz
Spr
Opx
Grt
Spr + Opx
32.4±0.7
31.7±0.6
31.2±0.6
31.4±0.7
32.4±0.7
31.7±0.6
31.7±0.6
31.6±0.6
31.7±0.6
31.6±0.6
31.4 ±0.6
31.5±0.6
33.3±0.6
32.4±0.6
B GRM37 (56-2)
200 µm
Crd
Spr
Crd
32.5±0.8
33.0±0.9
32.0±0.8
Opx
Crd
C GRM27 (55-3)
200 µm
Opx
Plg
32.6±0.7
32.0±0.8
33.6±0.7
Grt
D GRM6-1 (55-3)
200 µm
Opx
Grt
Spr
33.6±0.6
33.2±0.6
Grt
Spr
Crd
Opx
Crd
E GRMt (56-4)
100 µm
Chl + Ms
Bt
32.2±0.6
Bt
Chl + Ms
Bt
F 1-1 (GR11-35)
150 µm
Plg
Grt
30.9±0.6
Ap
Mnz
Qz
Qz
Kfs
Grt
Plg
Grt
Kfs

Figure 4.2

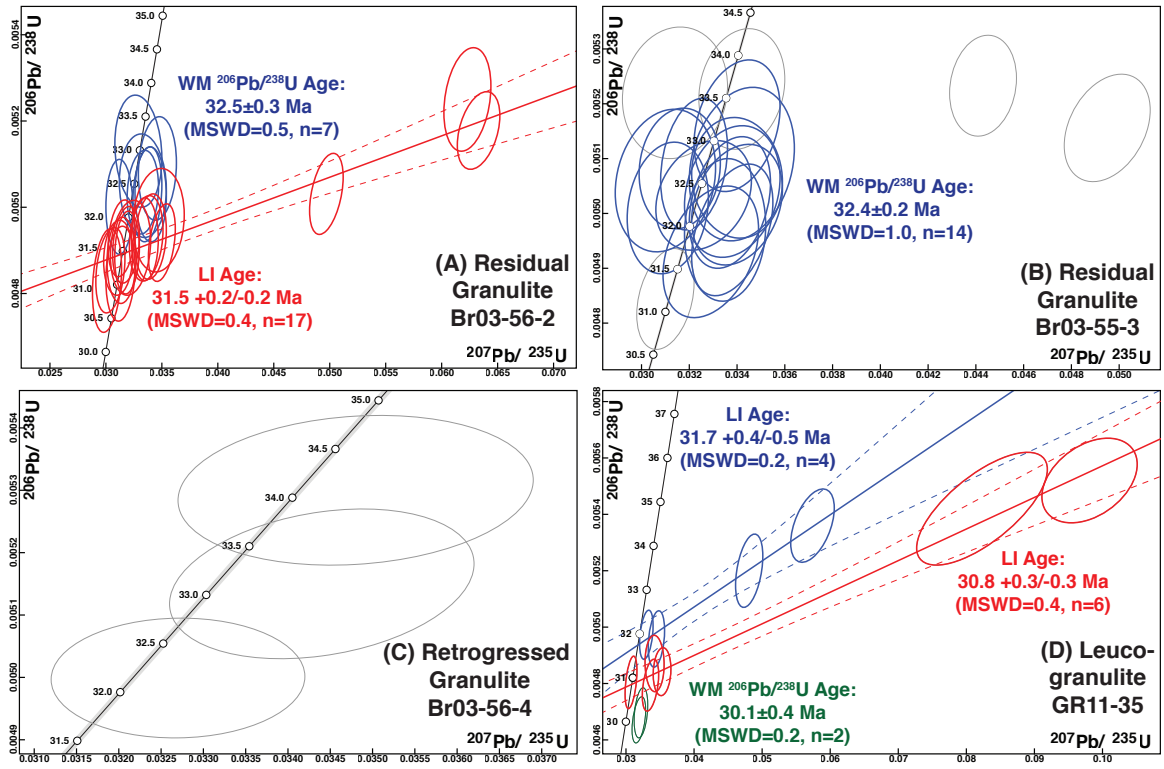
WM 206Pb/238U Age:
32.5±0.3 Ma
(MSWD=0.5, n=7)
LI Age:
31.5 +0.2/-0.2 Ma
(MSWD=0.4, n=17)
(A) Residual
Granulite
Br03-56-2
WM 206Pb/238U Age:
32.4±0.2 Ma
(MSWD=1.0, n=14)
(B) Residual
Granulite
Br03-55-3
(C) Retrogressed
Granulite
Br03-56-4
LI Age:
31.7 +0.4/-0.5 Ma
(MSWD=0.2, n=4)
LI Age:
30.8 +0.3/-0.3 Ma
(MSWD=0.4, n=6)
WM 206Pb/238U Age:
30.1±0.4 Ma
(MSWD=0.2, n=2)
(D) Leuco-
granulite
GR11-35
206Pb/ 238U
207Pb/ 235U

Figure 4.3

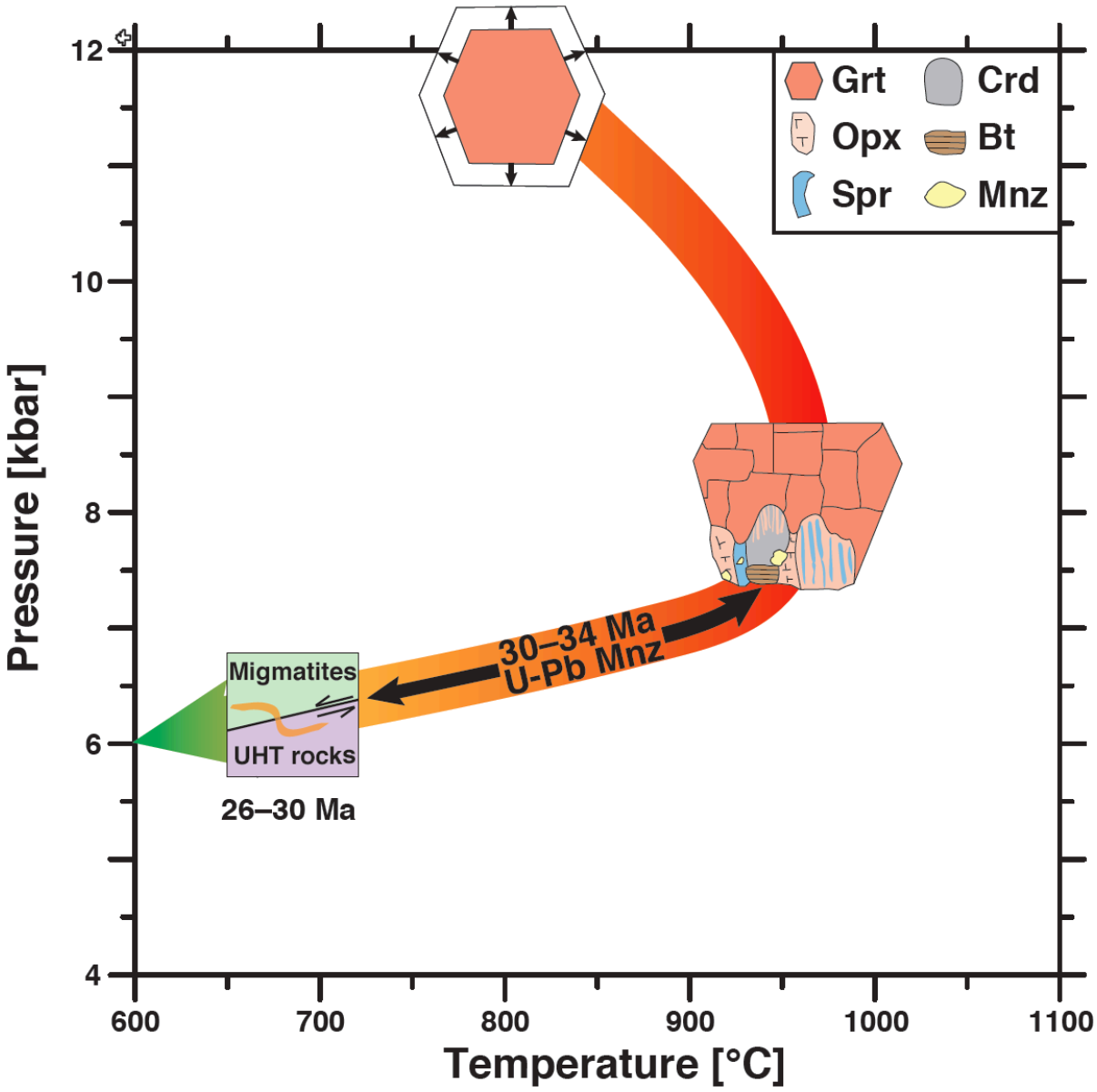
Grt
Crd
Opx
Bt
Spr
Mnz
Pressure [kbar]
12
10
8
6
4
600
700
800
900
1000
1100
Temperature [°C]
30–34 Ma
U-Pb Mnz
Migmatites
UHT rocks
26–30 Ma

Figure 4.4

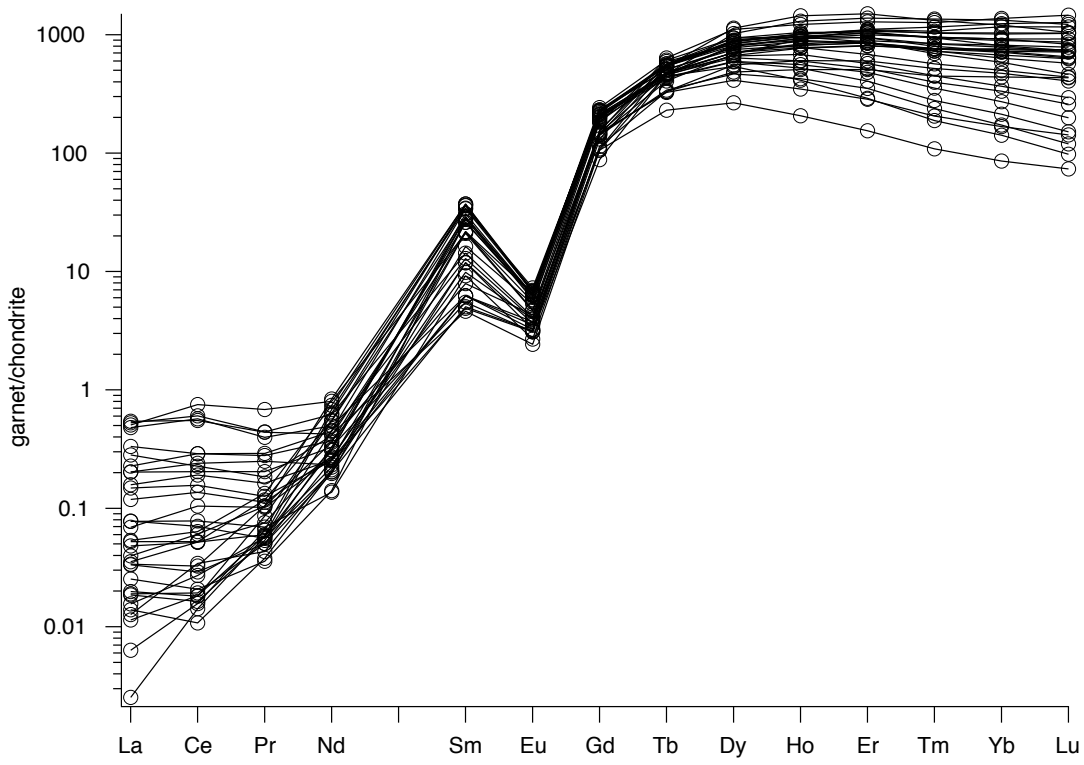
1000
100
10
1
0.1
0.01
garnet/chondrite
La
Ce
Pr
Nd
Sm
Eu
Gd
Tb
Dy
Ho
Er
Tm
Yb
Lu

Figure 4.B1

Table 4.A1. Monazite LA-ICP-MS Analytical Parameters.

Laboratory & Sample Preparation	
Laboratory name	The University of Kansas, Dept. of Geology, Isotope Geochemistry Lab
Sample type/mineral	Monazite
Sample preparation	40 µm-thick, polished sections
Imaging	BSE imaging on electron microprobe
Laser ablation system	
Make, model & type	ATL Arf excimer laser (193 nm), Photon Machines Analyte G2
Ablation cell & volume	HeLex
Laser wavelength	193 nm
Pulse width (ns)	5 ns
Fluence	2.4 J/cm^2
Repetition rate	5 Hz
Spot size (um)	15 µm
Sampling mode / pattern	Single spots
Carrier gas	He, 1.1 l/min, Ar, 1.095 l/min
Ablation duration	22 s
Cell carrier gas flow	He
ICP-MS Instrument	
Make, Model & type	Thermo Element2 magnetic sector field ICP-MS (single collector)
Sample introduction	Aerosol with sample + He was mixed with Ar using a T-connector 30 cm upstream from torch. A 'squid' device was used to attenuate the aerosol between the T-connector and the torch.
RF power	1095 W
Make-up gas flow	Ar, 16 l/min
Sampling depth	20 µm???
Detection system	single detector (SEM), counting & analog modes
Elements/ isotopes analyzed	206Pb, 207Pb, 238U
Integration time per peak (Sample Time in miliseconds)	206Pb = 4, 207Pb = 10, 238U = 2
Total integration time (Segment Duration in miliseconds)	206Pb = 12, 207Pb = 30, 238U = 6
Total method time	37 seconds (176 runs, 4 passes)
Sensitvity (cps/ppm)	238U = 1030 cps/ppm
ICP Dead time	2 ns
UO+/U+	0.10%
238U+/232Th+	1.1

Table 4.A1

Data Processing	
Gas blank	15 s
Calibration strategy	Standard-sampling bracketing
Reference material info	FG Manangotry pass, TIMS age 559.6±1.7 Ma (Möller, upubl.)
Internal std for trace elements	n/a
Data processing package used / Correction for laser induced elemental fractionation (LIEF)	IGOR PRO, Iolite 2.5 (Paton et al. 2011): U_Pb_Geochronology (Paton, et al. 2010) and VizualAge data reduction schemes (Petrus & Kamber, 2011), exponential LIEF correction for U-Pb ratios.
Common-Pb correction, composition and uncertainty	Not performed because of high Hg background
Uncertainty level & propagation	2se propogated uncertainty from VizualAge data reduction scheme. Concordia diagrams were plotted using ET_Redux (McLean et al. 2016) with 2σ uncertainty ellipses.
Reproducibility	206Pb/238U = 1.5-2.0%; 207Pb/235U = 2.5-3.0%
Quality control / Validation	Monazite: Moacyr (Seydoux-Guillaume et al. 2002) and JUP (Kennedy pers. comm)

Table 4.A2. Monazite U-Pb data.

		Isotopic Ratios							Dates (Ma)								
Sample and Analysis Number	Textural setting	207Pb/ 235U	±2σ %	206Pb/ 238U	±2σ %	Rho 6/38-7/35	207Pb/ 206Pb	±2σ %	206Pb/ 238U	±2σ abs	207Pb/ 235U	±2σ abs	207Pb/ 206Pb	±2σ abs	% disc a 6/38-7/35	% disc b 6/38-7/6	disc c unc. wt.	conc U (ppm)
Residual Granulite (Br03-56-2)																		
GRM28-1.FIN2	in Bt	0.0301	4.3	0.00483	2.5	0.24	0.0452	4.6	31.06	0.77	30.1	1.3	-8	85	-3.2	488.3	-0.7	4420
GRM28-2.FIN2	in Bt	0.0313	4.2	0.00485	2.3	0.14	0.0466	4.3	31.16	0.68	31.3	1.3	44	82	0.4	29.2	0.1	3690
GRM_Px3-6.FIN2	anhedral; with Opx (Fig. 2A)	0.0304	4.3	0.00485	2.0	0.28	0.0466	4.1	31.22	0.63	30.4	1.3	45	85	-2.7	30.6	-0.6	4750
GRM_Px3-8.FIN2	anhedral; with Opx (Fig. 2A)	0.0314	4.1	0.00488	2.1	0.05	0.0470	4.3	31.36	0.66	31.3	1.3	63	85	-0.2	50.2	0.0	4780
GRM_Px3-5.FIN2	anhedral; with Opx (Fig. 2A)	0.0311	4.2	0.00488	1.8	0.10	0.0459	4.4	31.40	0.56	31.1	1.3	18	83	-1.0	-74.4	-0.2	5310
GRM_Px3-12.FIN2	anhedral; with Opx (Fig. 2A)	0.0319	3.4	0.00490	2.0	0.12	0.0483	3.9	31.48	0.62	31.9	1.1	124	80	1.2	74.6	0.4	4550
GRM29bI-1.FIN2	in Bt	0.0322	5.6	0.00491	2.2	0.17	0.0485	5.6	31.55	0.72	32.2	1.7	120	110	2.0	73.7	0.4	2237
GRM_Px3-1.FIN2	anhedral; with Opx (Fig. 2A)	0.0318	3.8	0.00491	1.8	0.24	0.0475	4.0	31.59	0.57	31.8	1.2	83	81	0.7	61.9	0.2	4640
GRM_Px3-11.FIN2	anhedral; with Opx (Fig. 2A)	0.0350	3.4	0.00492	1.8	0.36	0.0515	3.5	31.63	0.58	34.9	1.2	251	75	9.4	87.4	2.7	6160
GRM_Px3-9.FIN2	anhedral; with Opx (Fig. 2A)	0.0335	3.6	0.00493	1.9	0.00	0.0501	3.8	31.68	0.62	33.4	1.2	189	81	5.2	83.2	1.5	5560
GRM_Px3-2.FIN2	anhedral; with Opx (Fig. 2A)	0.0336	4.5	0.00493	2.0	0.20	0.0492	4.5	31.69	0.64	33.6	1.5	163	91	5.7	80.6	1.3	4419
GRM_Px3-3.FIN2	anhedral; with Opx (Fig. 2A)	0.0314	3.8	0.00493	1.8	0.24	0.0461	3.7	31.69	0.57	31.4	1.2	28	72	-1.0	-13.2	-0.3	4910
GRM_Px3-7.FIN2	anhedral; with Opx (Fig. 2A)	0.0340	4.1	0.00493	2.0	0.15	0.0494	4.0	31.72	0.64	34.0	1.3	170	86	6.7	81.3	1.8	4190
GRM37I-1.FIN2	in Spr, Crd (Fig. 2B)	0.0347	6.6	0.00497	2.4	0.11	0.0516	6.8	31.96	0.80	34.6	2.2	240	140	7.6	86.7	1.2	1467
GRM28-3.FIN2	in Bt	0.0312	3.8	0.00500	2.2	0.00	0.0457	4.2	32.16	0.73	31.3	1.2	9	81	-2.7	-257.3	-0.7	4220
GRM_Px3-14.FIN2	anhedral; with Opx (Fig. 2A)	0.0497	3.0	0.00503	1.9	0.42	0.0714	2.8	32.35	0.60	49.3	1.5	969	58	34.4	96.7	11.3	9340
GRM_Px3-4.FIN2	anhedral; with Opx (Fig. 2A)	0.0337	3.9	0.00503	2.2	0.20	0.0481	4.0	32.35	0.72	33.6	1.3	120	83	3.7	73.0	1.0	3870
GRM_Px3-10.FIN2	anhedral; with Opx (Fig. 2A)	0.0340	4.1	0.00503	2.2	-0.03	0.0487	4.5	32.35	0.72	34.0	1.4	141	91	4.9	77.1	1.2	3760
GRM13-1.FIN2		0.0333	4.2	0.00504	1.9	0.13	0.0481	4.6	32.37	0.62	33.3	1.4	108	90	2.8	70.0	0.7	2903
GRM37I-3.FIN2	in Spr, Crd (Fig. 2B)	0.0333	6.3	0.00505	2.4	-0.07	0.0463	6.7	32.47	0.77	33.5	2.1	70	120	3.1	53.6	0.5	1559
GRM29bI-2.FIN2	in Bt	0.0346	4.9	0.00509	2.4	0.11	0.0492	4.9	32.70	0.74	34.5	1.7	178	100	5.2	81.6	1.1	2076
GRM37I-2.FIN2	in Spr, Crd (Fig. 2B)	0.0329	6.4	0.00513	2.5	-0.13	0.0465	6.7	32.99	0.86	32.8	2.1	40	120	-0.6	17.5	-0.1	1375
GRM_Px3-13.FIN2	anhedral; with Opx (Fig. 2A)	0.0633	3.0	0.00518	1.7	0.38	0.0889	2.8	33.29	0.58	62.3	1.8	1402	54	46.6	97.6	16.1	9910
GRM28-4.FIN2	in Bt	0.0623	3.4	0.00525	2.3	0.26	0.0870	3.3	33.78	0.79	61.3	2.0	1353	67	44.9	97.5	13.8	5740
Residual Granulite (Br03-55-3)																		
GRM16-4.FIN2	in Pl	0.0310	3.9	0.00484	1.9	0.31	0.0456	3.7	31.15	0.59	31.0	1.2	-5	72	-0.5	723.0	-0.1	6240
GRM17-2.FIN2	in Kfs	0.0329	6.1	0.00493	2.4	0.35	0.0488	5.7	31.70	0.77	32.9	2.0	150	110	3.6	78.9	0.6	1751
GRM27-3.FIN2	euhedral; in Pl (Fig. 2C)	0.0338	5.0	0.00497	2.4	0.42	0.0492	4.7	31.95	0.75	33.7	1.6	150	92	5.2	78.7	1.1	1971
GRM2_2-3.FIN2	intergrown with Opx	0.0335	5.1	0.00497	2.6	0.07	0.0491	5.5	31.99	0.82	33.4	1.7	150	110	4.2	78.7	0.8	2022
GRM16-1.FIN2	in Pl	0.0311	5.5	0.00501	2.4	0.16	0.0451	5.8	32.20	0.79	31.1	1.7	30	110	-3.5	-7.3	-0.6	2018
GRM2_2-4.FIN2	intergrown with Opx	0.0340	5.6	0.00502	2.2	0.26	0.0500	5.2	32.25	0.73	34.0	1.8	180	110	5.1	82.1	1.0	1612
GRM16-2.FIN2	in Pl	0.0337	5.0	0.00502	2.4	0.30	0.0489	4.9	32.26	0.78	33.6	1.7	151	100	4.0	78.6	0.8	2857
GRM2_1-2.FIN2	in Crd	0.0326	6.1	0.00503	2.0	0.26	0.0469	5.5	32.36	0.67	32.6	1.9	80	110	0.7	59.6	0.1	1862
GRM2_2-6.FIN2	intergrown with Opx	0.0338	5.9	0.00504	2.4	0.21	0.0489	5.7	32.46	0.80	33.8	1.9	160	110	4.0	79.7	0.7	2015
GRM2_1-1.FIN2	in Crd	0.0310	6.8	0.00506	2.6	0.17	0.0447	6.5	32.53	0.80	30.9	2.0	-30	120	-5.3	208.4	-0.8	1699
GRM27-2.FIN2	euhedral; in Pl (Fig. 2C)	0.0340	5.6	0.00507	2.2	-0.06	0.0488	6.1	32.57	0.72	34.0	1.9	150	120	4.2	78.3	0.8	1988
GRM2_2-2.FIN2	intergrown with Opx	0.0316	5.4	0.00508	2.2	0.09	0.0447	5.4	32.68	0.72	31.6	1.6	-39	99	-3.4	183.8	-0.7	2232
GRM17-1.FIN2	in Kfs	0.0342	6.4	0.00509	2.8	0.21	0.0488	6.4	32.73	0.87	34.1	2.1	160	120	4.0	79.5	0.7	1753
GRM16-3.FIN2	in Pl	0.0322	4.3	0.00509	2.4	0.25	0.0463	4.1	32.74	0.76	32.2	1.4	34	79	-1.7	3.7	-0.4	3510
GRM6_1-1.FIN2	in Spr (Fig. 2D)	0.0495	3.6	0.00516	1.9	0.33	0.0689	3.5	33.15	0.63	49.0	1.8	890	67	32.3	96.3	8.8	4390
GRM2_2-1.FIN2	intergrown with Opx	0.0340	5.3	0.00516	2.3	0.28	0.0471	5.1	33.20	0.75	33.9	1.7	67	97	2.1	50.4	0.4	1805
GRM2_2-5.FIN2	intergrown with Opx	0.0314	7.0	0.00522	2.3	0.10	0.0443	7.0	33.55	0.80	31.3	2.2	-30	130	-7.2	211.8	-1.0	1798
GRM27-1.FIN2	euhedral; in Pl (Fig. 2C)	0.0342	5.3	0.00523	2.1	0.16	0.0475	5.5	33.61	0.71	34.1	1.8	80	110	1.4	58.0	0.3	1949
GRM6_1-2.FIN2	in Spr (Fig. 2D)	0.0443	3.2	0.00523	1.8	0.15	0.0614	3.1	33.64	0.59	44.0	1.4	645	64	23.5	94.8	7.4	8010
Retrogressed Granulite (Br03-56-4)																		
GRMt-1.FIN2	with Chl, Bt, Ms	0.0327	4.6	0.00500	1.9	0.03	0.0470	4.7	32.15	0.62	32.6	1.5	72	92	1.4	55.3	0.3	3050
GRM33-1.FIN2	with Chl, Bt, Crd	0.0344	5.2	0.00515	2.3	0.27	0.0487	5.1	33.11	0.77	34.3	1.8	160	110	3.5	79.3	0.7	2066
GRM7-1.FIN2	in Crd	0.0348	6.0	0.00530	2.3	0.14	0.0491	6.1	34.10	0.77	34.7	2.0	140	120	1.7	75.6	0.3	1526
Leucogranulite (GR11-35)																		
GR1135_7-1.FIN2	On apatite	0.0319	3.1	0.00467	1.8	0.43	0.0495	2.8	30.04	0.52	31.9	1.0	550	66	5.7	94.5	1.8	12140
GR1135_9-1.FIN2	On apatite	0.0322	3.1	0.00470	1.9	0.31	0.0492	3.0	30.20	0.57	32.2	1.0	50	65	6.1	39.6	2.0	9840
GR1135_2-1.FIN2	Leucosome–b/t Pl and Kfs	0.0336	3.6	0.00479	1.9	0.41	0.0502	3.4	30.83	0.59	33.5	1.2	107	71	8.0	71.2	2.2	6420
GR1135_1-1.FIN2	On apatite (Fig. 2F)	0.0307	2.8	0.00480	1.9	0.44	0.0469	2.6	30.89	0.60	30.7	0.9	-	-	-0.5	-		12280
GR1135_2-2.FIN2	Leucosome–b/t Pl and Kfs	0.0353	3.7	0.00484	1.8	0.11	0.0532	3.9	31.14	0.54	35.3	1.3	-40	86	11.8	177.9	3.2	6680

		Isotopic Ratios							Dates (Ma)									
Sample and Analysis Number	Textural setting	207Pb/ 235U	±2σ %	206Pb/ 238U	±2σ %	Rho 6/38-7/35	207Pb/ 206Pb	±2σ %	206Pb/ 238U	±2σ abs	207Pb/ 235U	±2σ abs	207Pb/ 206Pb	±2σ abs	% disc a 6/38-7/35	% disc b 6/38-7/6	disc c unc. wt.	conc U (ppm)
GR1135_3-1.FIN2	On apatite	0.0342	4.1	0.00487	2.1	-0.04	0.0512	4.5	31.32	0.66	34.2	1.4	340	97	8.4	90.8	2.1	4240
GR1135_16-2.FIN2	On apatite	0.0823	11.7	0.00542	3.7	0.70	0.1100	9.1	34.90	1.30	80.0	9.0	170	190	56.4	79.5	5.0	4610
GR1135_16-3.FIN2	On apatite	0.0981	7.1	0.00552	2.7	0.38	0.1302	6.9	35.51	0.96	94.8	6.5	170	120	62.5	79.1	9.1	4090
GR1135_23-1.FIN2	On apatite	0.0345	3.5	0.00496	2.0	0.30	0.0512	3.5	31.88	0.64	34.5	1.2	210	76	7.7	84.8	2.2	7250
GR1135_18-1.FIN2	On apatite	0.0330	3.0	0.00497	1.7	0.36	0.0489	2.9	31.98	0.56	33.0	1.0	130	61	2.9	75.4	1.0	12330
GR1135_22-1.FIN2	On apatite, next to spinel	0.0481	4.2	0.00520	2.5	0.40	0.0686	4.1	33.46	0.82	47.6	2.0	1160	89	29.7	97.1	7.1	7660
GR1135_3-2.FIN2	On apatite	0.0574	5.6	0.00536	2.4	0.48	0.0767	4.8	34.46	0.82	56.6	3.1	230	96	39.1	85.0	7.1	2570
Calibration Standard F6																		
F6-1.FIN2		0.735	2.6	0.0899	2.2	0.53	0.0598	2.5	555	12	559	11	603	52	0.8	8.0	0.4	1240
F6-2.FIN2		0.734	2.9	0.0909	2.0	0.60	0.0580	2.4	561	11	558	12	526	55	-0.4	-6.6	-0.2	1246
F6-3.FIN2		0.736	2.7	0.0909	1.9	0.52	0.0582	2.4	561	10	559	12	530	51	-0.3	-5.8	-0.1	1225
F6-4.FIN2		0.723	2.6	0.0894	1.9	0.39	0.0586	2.6	552	10	552	11	558	56	0.0	1.1	0.0	1227
F6-5.FIN2		0.753	2.7	0.0922	2.0	0.57	0.0583	2.6	568	11	569	12	542	56	0.2	-4.9	0.1	1192
F6-6.FIN2		0.735	2.6	0.0901	2.3	0.41	0.0601	2.7	556	13	560	11	601	59	0.7	7.5	0.3	1222
F6-7.FIN2		0.718	2.6	0.0886	2.1	0.65	0.0582	2.4	547	11	549	11	537	53	0.3	-1.9	0.2	1237
F6-8.FIN2		0.733	2.6	0.0911	2.4	0.64	0.0595	2.4	562	13	559	11	579	52	-0.6	2.9	-0.3	1245
F6-9.FIN2		0.737	2.7	0.0911	2.1	0.55	0.0594	2.5	563	11	561	12	576	55	-0.4	2.3	-0.2	1215
F6-10.FIN2		0.722	2.8	0.0900	2.0	0.60	0.0585	2.4	555	11	552	12	555	52	-0.7	0.0	-0.3	1228
F6-13.FIN2		0.726	2.6	0.0915	2.3	0.50	0.0578	2.4	564	12	555	11	517	54	-1.7	-9.1	-0.8	1217
F6-14.FIN2		0.729	2.7	0.0919	2.2	0.47	0.0573	2.4	567	12	556	11	499	57	-2.1	-13.6	-1.0	1213
F6-15.FIN2		0.740	2.8	0.0911	2.2	0.57	0.0589	2.4	562	12	563	12	565	54	0.2	0.5	0.1	1198
F6-16.FIN2		0.737	2.7	0.0908	2.2	0.59	0.0587	2.6	560	12	560	12	566	53	0.0	1.1	0.0	1229
F6-17.FIN2		0.751	2.8	0.0911	2.1	0.54	0.0596	2.5	562	11	568	12	599	51	1.1	6.2	0.5	1220
F6-18.FIN2		0.757	2.6	0.0930	2.0	0.67	0.0594	2.2	573	11	572	12	578	48	-0.2	0.9	-0.1	1183
F6-19.FIN2		0.735	2.7	0.0905	2.2	0.51	0.0587	2.6	558	12	559	12	558	53	0.2	-	0.1	1230
F6-20.FIN2		0.739	2.8	0.0908	2.1	0.53	0.0585	2.6	560	11	561	12	552	51	0.2	-1.4	0.1	1210
F6-21.FIN2		0.739	2.7	0.0909	2.1	0.60	0.0592	2.2	561	11	562	12	575	50	0.3	2.5	0.1	1204
F6-22.FIN2		0.737	2.7	0.0909	2.1	0.58	0.0583	2.4	560	11	562	12	537	52	0.3	-4.4	0.1	1246
F6-23.FIN2		0.738	2.7	0.0901	2.0	0.52	0.0597	2.5	556	11	561	12	589	52	0.8	5.6	0.4	1230
F6-24.FIN2		0.743	2.7	0.0910	2.2	0.43	0.0592	2.5	561	12	566	12	577	57	0.8	2.8	0.4	1237
F6-25.FIN2		0.732	2.9	0.0908	2.1	0.63	0.0588	2.4	560	11	557	12	557	52	-0.6	-0.5	-0.3	1214
F6-26.FIN2		0.737	3.0	0.0905	2.1	0.49	0.0591	2.7	559	11	560	13	572	58	0.2	2.3	0.1	1229
F6-27.FIN2		0.732	2.9	0.0905	2.1	0.62	0.0581	2.6	558	11	558	12	535	55	0.0	-4.4	0.0	1229
F6-28.FIN2		0.729	2.7	0.0901	2.1	0.56	0.0589	2.5	556	11	556	12	565	54	0.1	1.6	0.0	1228
F6-29.FIN2		0.733	2.9	0.0897	2.2	0.64	0.0591	2.4	554	12	559	13	562	50	0.9	1.4	0.4	1211
Validation Reference Material JUP																		
JUP-1.FIN2		0.103	2.8	0.0158	1.6	0.48	0.0471	2.8	101	2	100	3	63	56	-1.3	-60.2	-0.5	5260
JUP-2.FIN2		0.103	2.5	0.0158	1.6	0.37	0.0474	2.5	101	2	100	2	66	51	-1.3	-53.2	-0.5	5360
JUP-3.FIN2		0.103	2.6	0.0158	1.7	0.35	0.0471	2.5	101	2	100	3	59	53	-1.7	-71.5	-0.7	5340
JUP-4.FIN2		0.103	2.6	0.0159	1.6	0.51	0.0477	2.3	101	2	100	3	86	50	-1.8	-17.9	-0.7	5280
JUP-5.FIN2		0.105	2.7	0.0158	1.7	0.22	0.0483	2.7	101	2	102	3	113	56	0.6	10.6	0.2	5340
JUP-6.FIN2		0.103	2.8	0.0159	1.7	0.41	0.0473	2.7	101	2	100	3	72	57	-1.9	-40.8	-0.7	5300
JUP-7.FIN2		0.103	2.6	0.0158	1.7	0.23	0.0479	2.5	101	2	99	3	94	55	-1.5	-7.3	-0.6	5450
JUP-8.FIN2		0.100	2.8	0.0157	1.7	0.28	0.0460	2.6	101	2	97	3	16	52	-3.5	-528.1	-1.3	5400
JUP-9.FIN2		0.103	2.8	0.0157	1.6	0.21	0.0479	2.7	101	2	100	3	99	60	-0.8	-1.6	-0.3	5270
JUP-10.FIN2		0.102	2.4	0.0158	1.6	0.17	0.0468	2.6	101	2	99	2	47	53	-2.2	-114.9	-1.0	5360
JUP-13.FIN2		0.105	2.9	0.0157	1.7	0.39	0.0481	2.5	100	2	101	3	107	57	1.2	6.4	0.4	5380
JUP-14.FIN2		0.106	2.6	0.0160	1.6	0.24	0.0482	2.5	102	2	102	3	101	55	-0.4	-1.3	-0.2	5260
JUP-15.FIN2		0.103	2.7	0.0158	1.5	0.25	0.0472	2.5	101	2	99	3	67	54	-1.7	-50.3	-0.7	5400
JUP-16.FIN2		0.103	2.8	0.0159	1.5	0.25	0.0479	2.7	101	2	100	3	88	58	-1.4	-15.2	-0.5	5240
JUP-17.FIN2		0.101	2.7	0.0158	1.6	0.44	0.0466	2.6	101	2	98	3	41	50	-3.5	-147.1	-1.4	5180
JUP-18.FIN2		0.103	2.5	0.0157	1.7	0.42	0.0478	2.5	101	2	99	2	89	53	-1.4	-12.9	-0.6	5330
JUP-19.FIN2		0.102	2.9	0.0159	1.6	0.31	0.0468	2.8	102	2	98	3	45	58	-3.4	-125.8	-1.2	5360
Validation Reference Material Moacyr																		
MCR-1.FIN2		0.687	2.9	0.0836	1.7	0.46	0.0591	2.7	518	9	530	12	562	59	2.4	7.9	1.0	1052

		Isotopic Ratios							Dates (Ma)									
Sample and Analysis Number	Textural setting	207Pb/ 235U	±2σ %	206Pb/ 238U	±2σ %	Rho 6/38-7/35	207Pb/ 206Pb	±2σ %	206Pb/ 238U	±2σ abs	207Pb/ 235U	±2σ abs	207Pb/ 206Pb	±2σ abs	% disc a 6/38-7/35	% disc b 6/38-7/6	disc c unc. wt.	conc U (ppm)
MCR-2.FIN2		0.669	2.8	0.0822	1.7	0.48	0.0591	2.5	509	8	520	12	586	57	2.1	13.2	0.9	1064
MCR-3.FIN2		0.683	2.8	0.0835	1.7	0.46	0.0595	2.4	517	9	528	11	586	52	2.1	11.8	1.0	1052
MCR-4.FIN2		0.674	2.7	0.0831	1.6	0.36	0.0589	2.4	515	8	523	11	565	51	1.6	8.9	0.8	1077
MCR-5.FIN2		0.671	2.7	0.0839	1.8	0.39	0.0579	2.4	520	9	521	11	526	55	0.3	1.2	0.1	1091
MCR-6.FIN2		0.675	2.8	0.0832	1.8	0.65	0.0586	2.4	515	9	523	11	550	50	1.5	6.4	0.7	1092
MCR-7.FIN2		0.658	2.4	0.0826	1.7	0.39	0.0581	2.2	512	9	513	10	537	50	0.2	4.7	0.1	1090
MCR-8.FIN2		0.672	2.8	0.0838	1.7	0.60	0.0582	2.4	519	8	524	11	541	49	1.0	4.1	0.5	1087
MCR-9.FIN2		0.674	2.5	0.0826	1.9	0.56	0.0589	2.2	512	10	523	10	566	49	2.1	9.6	1.1	1084
MCR-10.FIN2		0.673	2.7	0.0828	1.9	0.41	0.0592	2.4	513	10	523	11	571	55	1.9	10.2	0.9	1104
MCR-11.FIN2		0.658	2.7	0.0821	1.8	0.40	0.0582	2.6	509	9	514	11	539	55	1.0	5.6	0.5	1100
MCR-12.FIN2		0.675	3.0	0.0829	1.8	0.39	0.0590	2.5	513	9	523	12	561	58	1.9	8.5	0.8	1085
MCR-13.FIN2		0.661	2.6	0.0831	1.8	0.54	0.0573	2.4	515	9	515	11	501	54	0.0	-2.7	0.0	1084
MCR-14.FIN2		0.675	2.4	0.0838	1.8	0.42	0.0582	2.4	518	9	523	10	534	52	0.9	2.9	0.5	1077
MCR-15.FIN2		0.679	2.8	0.0835	1.8	0.50	0.0590	2.4	517	9	526	11	568	54	1.8	9.0	0.9	1072
MCR-16.FIN2		0.679	2.8	0.0837	1.7	0.22	0.0588	2.6	518	8	527	11	562	59	1.6	7.8	0.8	1073
MCR-17.FIN2		0.658	2.7	0.0821	1.8	0.43	0.0582	2.4	509	9	513	11	534	55	0.8	4.8	0.4	1053
MCR-18.FIN2		0.678	2.8	0.0829	1.8	0.55	0.0589	2.4	513	9	525	11	564	56	2.3	9.0	1.1	1052
MCR-19.FIN2		0.660	2.7	0.0830	1.9	0.59	0.0582	2.4	514	9	515	11	547	51	0.2	6.0	0.1	1064
MCR-20.FIN2		0.676	2.8	0.0836	1.8	0.38	0.0585	2.7	518	9	525	12	543	59	1.4	4.7	0.6	1048
MCR-21.FIN2		0.657	2.6	0.0832	1.7	0.26	0.0566	2.5	515	9	512	10	466	56	-0.6	-10.5	-0.3	1041

Notes:
Rho = correlation coeffecient between 206Pb/238U and 207Pb/235U ratios
% discordance a = 100 - (100 * (206Pb/238U date) / (207Pb/235U date))
% discordance b = 100 - (100 * (206Pb/238U date) / (207Pb/206Pb date))
discordance c = uncertainty weighted age difference (UWAD) = (206Pb/238U date - 207Pb/235U date)/207Pb/235U date uncertainty; red text indicates values >1.2
Colored text indicates analyses that were used in age calculations in Fig. 3. Text color corresponds to ellipse color.

Table 4.B1. Garnet LA-ICP-MS analytical methods.

Laboratory & Sample Preparation	
Laboratory name	The University of Kansas, Dept. of Geology, Isotope Geochemistry Lab
Sample type/mineral	Garnet
Sample preparation	40 µm-thick, polished sections
Imaging	BSE images and X-ray compositional maps
Laser ablation system	
Make, model & type	ATL ArF excimer laser (193 nm), Photon Machines Analyte G1
Ablation cell & volume	Frames Cell with teardrop-shaped insert
Laser wavelength	193 nm
Pulse width (ns)	5 ns
Fluence	3.2 J/cm^2
Repetition rate	10 Hz
Spot size (um)	35 µm circle
Sampling mode / pattern	Single spots
Carrier gas	He, 0.425 l/min, Ar, 1.24 l/min
Ablation duration	25 s
Cell carrier gas flow	He
ICP-MS Instrument	
Make, Model & type	Thermo Element2 magnetic sector field ICP-MS (single collector)
Sample introduction	Aerosol with sample + He was mixed with Ar using a Y-connector 15 cm upstream from torch.
RF power	1100 W
Make-up gas flow	Ar, 16 l/min
Sampling depth	20 µm
Detection system	Single detector (SEM), counting & analog modes
Elements/ isotopes analyzed	29Si, 43Ca, 44Ca, 45Sc, 49Ti, 89Y, 940Zr, 139La, 140Ce, 141Pr, 146Nd, 147Sm, 153Eu, 157Gd, 159Tb, 163Dy, 165Ho, 166Er, 169Tm, 172Yb, 175Lu
Integration time per peak (Sample Time in miliseconds)	29Si=10, 43Ca=10, 44Ca=10, 45Sc=10, 49Ti=10, 89Y=10, 94Zr=10, 139La=30, 140Ce=30, 141Pr=30, 146Nd=20, 147Sm=20, 153Eu=20, 157Gd=20, 159Tb=20, 163Dy=20, 165Ho=20, 166Er=10, 169Tm=10, 172Yb=10, 175Lu=10
Total integration time (Segment Duration in miliseconds)	29Si=10, 43Ca=10, 44Ca=10, 45Sc=10, 49Ti=10, 89Y=10, 94Zr=10, 139La=30, 140Ce=30, 141Pr=30, 146Nd=20, 147Sm=20, 153Eu=20, 157Gd=20, 159Tb=20, 163Dy=20, 165Ho=20, 166Er=10, 169Tm=10, 172Yb=10, 175Lu=10
Total method time	1 min 47 s (100 runs, 2 passes)

Table 4.B1

Sensitvity (cps/ppm)	29Si=122, 43Ca=12, 44Ca=199, 45Sc=5868, 49Ti=447, 89Y=7822, 94Zr=3915, 139La=13000, 140Ce=16723, 141Pr=16659, 146Nd=2615, 147Sm=2153, 153Eu=8914, 157Gd=1791, 159Tb=11996, 163Dy=2985, 165Ho=11585, 166Er=3939, 169Tm=12062, 172Yb=2655, 175Lu=10073
ICP Dead time	22 ns
UO+/U+	0.02%
238U+/232Th+	~1.5
Data Processing	
Gas blank	18 s
Calibration strategy	Standard-sampling bracketing + internal standardization using Ca concentration measured by electron microprobe for each spot
Reference material info	GSD-1G (Guillong et al., 2005; Jochum et al., 2005)
Internal std for trace elements	44Ca
Data processing package used	IGOR PRO, Iolite 2.5 (Patton et al. 2011): Trace elements: TraceElmentsIS data reduction scheme
Common-Pb correction, composition and uncertainty	n/a
Uncertainty level & propagation	2SE internal uncertainty
Reproducibility	3-8%
Quality control / Validation	GSE-1G (Guillong et al., 2005; Jochum et al., 2005)
Other information	

Table 4.B2. Garnet trace element data.

Analysis	Ca44 (cps)	±2SE (cps)	Si (ppm)	±2SE (ppm)	Ca (ppm)	±2SE (ppm)	Sc (ppm)	±2SE (ppm)	Ti (ppm)	±2SE (ppm)	Y (ppm)	±2SE (ppm)	Zr (ppm)	±2SE (ppm)	La (ppm)	±2SE (ppm)	Ce (ppm)	±2SE (ppm)	Pr (ppm)	±2SE (ppm)
GRMPx3-1.FIN2	8.5E+05	2.2E+04	2.5E+05	1.4E+04	8720	300	38.9	0.97	131	4.6	339	14	52.7	2.0	0.003	0.002	0.007	0.006	0.004	0.002
GRMPx3-3.FIN2	9.5E+05	4.5E+04	2.2E+05	1.2E+04	9990	620	38.4	2.4	123	9.7	753	89	50.9	4.2	0.125	0.072	0.370	0.210	0.042	0.020
GRMPx3-4.FIN2	1.2E+06	4.4E+04	2.2E+05	1.5E+04	10810	660	52.8	2.1	156	8.9	1522	80	75.5	3.6	0.006	0.005	0.013	0.002	0.003	0.001
GRMPx3-6.FIN2	1.3E+06	3.0E+04	2.4E+05	9.9E+03	12340	400	69.3	1.5	96.1	4.0	1739	48	53.8	1.6	0.008	0.002	0.018	0.003	0.005	0.002
GRMPx3-10.FIN2	1.2E+06	4.2E+04	2.5E+05	1.1E+04	12790	450	108	3.9	14.3	1.0	2400	120	30.9	1.2	0.035	0.006	0.096	0.014	0.012	0.003
GRMPx3-14.FIN2	1.2E+06	4.3E+04	2.5E+05	1.3E+04	13140	470	108	2.5	38.7	2.4	1842	63	51.3	1.4	0.028	0.004	0.084	0.007	0.011	0.002
GRMPx3-15.FIN2	1.2E+06	9.1E+04	2.6E+05	3.2E+04	12330	850	102	6.8	110	13	1840	130	86.4	5.9	0.067	0.048	0.139	0.089	0.018	0.008
GRMPx3-16.FIN2	1.2E+06	4.5E+04	2.2E+05	1.4E+04	10880	480	82.9	3.0	104	2.9	1214	46	72.8	2.5	0.008	0.002	0.032	0.008	0.006	0.002
GRMPx3-17.FIN2	1.3E+06	3.0E+04	2.2E+05	8.7E+03	10540	350	52.8	1.6	162	5.1	779	27	79.0	2.3	0.011	0.005	0.032	0.010	0.007	0.002
GRMPx3-18.FIN2	1.2E+06	4.3E+04	1.9E+05	1.3E+04	9020	470	53.4	2.1	73.4	4.0	920	52	43.9	2.3	0.079	0.025	0.177	0.039	0.028	0.007
GRMPx3-19.FIN2	1.3E+06	3.6E+04	1.7E+05	9.8E+03	8550	280	50.5	1.1	38.9	1.7	1112	36	31.7	0.95	0.018	0.005	0.048	0.011	0.007	0.001
GRMPx3-20.FIN2	1.2E+06	5.0E+04	2.6E+05	1.6E+04	12070	390	96.1	1.9	140	7.0	1387	68	62.0	2.9	0.009	0.007	0.037	0.012	0.010	0.003
GRMPx3-21.FIN2	1.2E+06	3.5E+04	2.6E+05	9.7E+03	12240	230	85.6	2.7	127	6.6	1510	68	56.0	4.5	0.004	0.002	0.010	0.003	0.005	0.002
GRMPx3-22.FIN2	1.2E+06	3.9E+04	2.6E+05	1.0E+04	12390	300	85.3	1.9	149	6.1	1437	35	55.1	1.3	0.012	0.007	0.032	0.016	0.011	0.004
GRMPx3-23.FIN2	1.3E+06	3.8E+04	2.5E+05	1.0E+04	12110	340	104	2.7	148	4.4	1766	67	74.6	2.6	0.003	0.001	0.011	0.002	0.006	0.002
GRMPx3-24.FIN2	1.3E+06	4.1E+04	2.6E+05	1.1E+04	12880	310	147	4.2	134	5.4	1896	81	59.9	2.1	0.013	0.003	0.039	0.005	0.013	0.002
GRMPx3-25.FIN2	1.4E+06	5.4E+04	2.4E+05	1.4E+04	12500	590	163	6.1	102	5.7	1962	87	67.0	2.1	0.008	0.003	0.020	0.004	0.010	0.003
GRMPx3-26.FIN2	1.3E+06	4.4E+04	2.4E+05	8.8E+03	12210	320	137	2.4	128	5.0	1425	39	44.8	1.4	0.005	0.002	0.011	0.003	0.008	0.002
GRMPx3-27.FIN2	1.3E+06	5.7E+04	2.5E+05	1.5E+04	12480	460	82.9	2.5	163	9.5	1488	82	75.0	4.6	0.001	0.002	0.009	0.004	0.006	0.002
GRMPx3-28.FIN2	1.3E+06	4.7E+04	2.2E+05	9.0E+03	10970	380	52.8	0.95	122	4.3	976	30	65.9	1.7	0.003	0.002	0.021	0.004	0.004	0.001
GRMPx3-29.FIN2	1.3E+06	4.4E+04	1.9E+05	1.1E+04	9250	290	39.1	1.1	167	7.2	916	35	67.0	2.3	0.005	0.002	0.012	0.005	0.005	0.002
GRMPx3-30.FIN2	1.3E+06	4.6E+04	2.5E+05	1.5E+04	12510	340	113	2.8	26.7	2.1	2550	100	44.3	1.6	0.019	0.004	0.043	0.005	0.005	0.002
GRMPx3-31.FIN2	1.3E+06	3.5E+04	2.5E+05	1.2E+04	12590	500	105	2.1	38.8	2.1	2148	83	59.6	2.0	0.038	0.007	0.117	0.020	0.016	0.003
GRMPx3-32.FIN2	1.3E+06	4.3E+04	2.3E+05	1.0E+04	10730	360	86.6	1.7	32.9	1.8	1798	70	42.4	1.4	0.048	0.010	0.125	0.028	0.019	0.005
GRMPx3-33.FIN2	1.4E+06	4.9E+04	1.9E+05	8.3E+03	9340	240	67.5	1.6	24.0	1.3	1582	64	29.3	1.1	0.129	0.015	0.338	0.035	0.042	0.005
GRMPx3-34.FIN2	1.3E+06	4.9E+04	1.9E+05	9.4E+03	9300	260	64.9	1.8	47.0	2.6	1105	40	49.7	2.1	0.048	0.005	0.147	0.017	0.024	0.005
GRMPx3-35.FIN2	1.4E+06	4.1E+04	2.4E+05	1.2E+04	11730	500	91.2	2.1	54.7	2.4	1377	60	69.1	2.4	0.054	0.015	0.177	0.041	0.027	0.007
GRMPx3-36.FIN2	1.4E+06	4.4E+04	2.4E+05	1.2E+04	12360	380	86.2	2.3	38.7	2.7	1703	58	46.8	1.7	0.114	0.031	0.349	0.058	0.038	0.006
GRMPx3-37.FIN2	1.3E+06	3.7E+04	2.3E+05	1.1E+04	11910	380	120	2.7	142	6.2	1689	74	61.7	2.4	0.002	0.002	0.010	0.002	0.006	0.001
GRMPx3-38.FIN2	1.3E+06	4.1E+04	2.4E+05	1.4E+04	12140	380	80.0	1.9	146	6.2	1763	69	70.7	3.1	0.004	0.002	0.017	0.006	0.005	0.002
GRMPx3-39.FIN2	1.3E+06	6.2E+04	2.2E+05	2.4E+04	10320	580	47.7	0.90	136	12.0	623	39	62.1	2.9	0.120	0.032	0.460	0.120	0.065	0.018
GRMPx3-40.FIN2	1.2E+06	5.6E+04	1.9E+05	1.0E+04	8840	480	48.0	1.8	123	9.9	1643	59	48.9	2.0	0.016	0.006	0.064	0.022	0.010	0.003

Nd (ppm)	±2SE (ppm)	Sm (ppm)	±2SE (ppm)	Eu (ppm)	±2SE (ppm)	Gd (ppm)	±2SE (ppm)	Tb (ppm)	±2SE (ppm)	Dy (ppm)	±2SE (ppm)	Ho (ppm)	±2SE (ppm)	Er (ppm)	±2SE (ppm)	Tm (ppm)	±2SE (ppm)	Yb (ppm)	±2SE (ppm)	Lu (ppm)	±2SE (ppm)
0.095	0.028	1.82	0.11	0.212	0.021	21.9	0.6	8.6	0.3	67.6	3.0	11.7	0.3	25.6	1.2	2.8	0.2	14.6	0.4	1.9	0.1
0.290	0.200	2.19	0.22	0.239	0.019	29.1	0.9	12.8	0.7	119	5.7	24.1	2.0	58.3	5.9	6.1	0.3	29.4	1.8	3.0	0.1
0.066	0.030	4.21	0.64	0.373	0.043	47.6	1.8	19.0	1.2	197	14.0	49.7	2.8	141	4.7	18.7	0.8	108	5.2	14.6	0.5
0.120	0.022	3.31	0.26	0.322	0.022	37.9	1.6	17.7	0.6	202	7.2	53.0	1.9	165	5.4	24.3	0.8	157	4.6	23.4	0.9
0.118	0.017	0.75	0.06	0.180	0.017	18.1	0.7	17.3	0.6	260	12.0	73.6	3.3	229	9.5	34.6	1.5	226	9.4	31.0	1.3
0.127	0.019	1.51	0.08	0.230	0.016	32.2	0.8	20.7	0.9	229	9.6	57.2	2.3	178	7.4	26.5	0.9	176	5.0	26.2	1.2
0.192	0.074	3.33	0.48	0.376	0.043	49.9	4.1	22.8	4.1	238	33.0	59.2	3.5	175	11	24.0	2.0	137	9.6	18.7	1.4
0.104	0.033	2.49	0.23	0.309	0.021	41.5	1.9	17.7	0.8	168	7.6	38.6	1.5	94.5	3.0	11.5	0.4	62.5	3.0	7.5	0.3
0.146	0.035	4.30	0.15	0.336	0.018	43.2	1.1	16.8	0.5	137	3.6	23.4	0.7	48.1	1.1	4.8	0.2	24.1	0.9	2.5	0.1
0.209	0.056	1.97	0.18	0.231	0.034	30.0	0.7	12.4	0.6	123	7.0	28.8	1.9	84.1	4.4	11.4	0.5	74.9	3.6	11.0	0.6
0.064	0.015	1.41	0.05	0.156	0.012	23.5	0.7	12.5	0.5	141	5.6	34.2	1.3	99.4	2.7	13.2	0.4	80.4	3.7	10.3	0.5
0.169	0.033	3.98	0.27	0.367	0.028	42.3	1.4	17.1	0.9	170	8.4	43.6	1.6	133	6.4	19.5	1.0	128	4.2	18.4	1.1
0.154	0.023	4.42	0.22	0.366	0.022	44.1	1.2	17.5	0.7	180	7.5	47.4	2.1	148	5.7	21.5	0.9	139	6.6	20.0	1.0
0.259	0.042	5.55	0.21	0.391	0.023	43.5	1.2	17.9	0.6	180	7.0	46.2	1.4	141	3.2	19.4	0.5	121	3.8	16.2	0.6
0.297	0.041	5.51	0.22	0.396	0.025	47.0	1.3	20.4	0.8	215	6.9	54.2	1.9	172	5.6	24.0	0.8	152	4.3	22.0	0.9
0.346	0.035	5.69	0.23	0.402	0.021	46.2	1.7	21.3	1.0	223	9.5	57.4	2.5	181	6.7	26.3	0.9	172	6.5	26.1	1.3
0.392	0.045	5.70	0.42	0.385	0.024	47.6	1.5	20.7	1.1	221	13.0	57.3	2.9	183	6.8	27.3	1.1	199	8.0	29.6	1.0
0.255	0.043	4.45	0.18	0.362	0.019	40.4	1.4	18.0	0.7	180	7.3	43.9	1.5	135	3.5	19.2	0.5	129	3.6	19.0	0.7
0.144	0.041	4.71	0.31	0.369	0.034	46.7	1.0	19.1	0.5	191	3.8	46.0	2.2	142	5.3	19.5	0.8	124	4.3	18.1	0.9
0.099	0.019	3.99	0.19	0.351	0.023	41.4	1.3	16.4	0.5	151	6.2	31.7	1.2	79.8	2.2	9.0	0.2	46.3	1.7	5.1	0.2
0.092	0.018	3.31	0.18	0.275	0.020	39.4	1.3	16.1	0.7	150	5.8	29.6	1.0	67.2	2.7	7.1	0.3	36.2	1.4	3.8	0.2
0.095	0.018	0.77	0.09	0.183	0.016	22.4	0.8	20.2	0.7	289	11.0	81.8	3.2	249	7.9	33.7	1.0	205	7.9	26.6	1.0
0.120	0.024	0.96	0.07	0.219	0.019	31.2	0.6	23.8	0.8	282	11.0	69.1	2.6	213	5.5	32.3	0.7	234	6.9	37.2	1.4
0.154	0.052	0.84	0.09	0.180	0.017	27.1	1.3	20.2	0.9	226	9.2	55.2	1.9	156	5.2	20.4	0.6	123	3.6	16.5	0.7
0.198	0.029	0.71	0.07	0.141	0.010	21.8	0.9	17.3	0.7	208	8.3	50.7	1.5	141	5.0	18.6	0.5	115	3.6	15.9	0.7
0.109	0.020	0.95	0.05	0.205	0.015	30.6	1.1	17.3	0.7	162	8.0	34.0	1.3	85.9	2.7	10.1	0.5	56.7	2.6	6.6	0.3
0.174	0.037	1.21	0.10	0.250	0.016	37.6	1.2	22.2	1.1	213	9.4	44.2	2.0	113	2.4	14.5	0.3	85.0	2.4	11.1	0.4
0.232	0.051	0.96	0.08	0.188	0.010	29.6	1.1	21.3	0.9	238	8.4	54.2	1.9	144	5.5	17.7	0.5	100	3.7	11.8	0.5
0.319	0.031	5.25	0.20	0.422	0.020	45.2	1.3	20.3	0.9	206	8.4	52.5	2.0	157	5.4	21.4	0.7	134	4.0	18.3	0.7
0.213	0.025	5.18	0.24	0.391	0.021	46.6	1.6	20.5	0.7	215	8.0	55.1	2.2	172	6.1	24.3	0.9	157	6.0	21.1	1.0
0.374	0.095	3.22	0.28	0.271	0.021	30.6	1.3	12.2	0.2	105	6.5	19.7	1.1	47.2	2.5	5.3	0.4	28.5	1.4	3.6	0.3
0.124	0.040	1.81	0.08	0.189	0.030	29.3	1.3	15.2	0.6	174	8.9	51.7	2.4	184	7.3	29.6	0.8	211	11	32.3	2.0

Table 4.C1: Results of EPMA analyses and thermobarometry calculations

Sample/Analysis	GRM_Px3: Grt7, Opx16, Pl1			GRM27: Grt7, Opx11, Pl1			GRM6-1: Grt2, Opx2, Pl27-1		
Mineral	garnet	orthopyroxene	plagioclase	garnet	orthopyroxene	plagioclase	garnet	orthopyroxene	plagioclase
Wt. % Oxides									
SiO2	39.74	50.15	47.09	38.92	49.89	54.02	39.47	48.89	54.02
TiO2	0	0.064	0.024	0.015	0.087	0	0	0.064	0
Al2O3	22.721	7.598	33.779	22.541	7.643	28.663	22.832	10.13	28.663
FeO Total	21.119	16.707	0.331	21.993	17.806	0.15	22.071	16.83	0.15
MnO	0.841	0.23	0.012	0.84	0.183	0.035	0.674	0.201	0.035
MgO	13.32	24.213	0.053	12.878	23.283	0	13.397	23.509	0
CaO	1.584	0.097	16.887	1.525	0.11	11.102	1.328	0.081	11.102
Na2O	0	0.013	1.828	0.013	0.017	5.3	0.004	0.001	5.3
K2O	0.005	0.006	0.206	0	0.003	0.316	0	0.007	0.316
Total	99.33	99.08	100.21	98.72	99.02	99.59	99.78	99.72	99.59
Cations									
Oxygens	12	6	8	12	6	8	12	6	8
Si	2.988	1.832	2.161	2.962	1.833	2.454	2.965	1.776	2.454
Ti	0.000	0.002	0.001	0.001	0.002	0.000	0.000	0.002	0.000
Al	2.014	0.327	1.827	2.022	0.331	1.535	2.022	0.434	1.535
Fe (all ferrous)	1.328	0.510	0.013	1.400	0.547	0.006	1.387	0.511	0.006
Mn	0.054	0.007	0.000	0.054	0.006	0.001	0.043	0.006	0.001
Mg	1.493	1.319	0.004	1.461	1.275	0.000	1.501	1.273	0.000
Ca	0.128	0.004	0.830	0.124	0.004	0.540	0.107	0.003	0.540
Na	0.000	0.001	0.163	0.002	0.001	0.467	0.001	0.000	0.467
K	0.000	0.000	0.012	0.000	0.000	0.018	0.000	0.000	0.018
Total	8.005	4.003	5.011	8.027	4.000	5.021	8.024	4.006	5.021
Thermobarometry results:									
Converged		910°C, 7.6 kbar			962°C, 8.7 kbar			1040°C, 9.1 kbar	
Initial		858°C, 7.9 kbar			904°C, 8.9 kbar			936°C, 9.4 kbar	

CHAPTER 5

Constraining the pressure-temperature evolution and geodynamic setting of UHT granulites and migmatitic paragneisses of the Gruf Complex, Central Alps

Jeffrey Oalmann[1]

Erik Düsterhöft[2]

Andreas Möller[1]

Romain Bousquet[2]

[1]*The University of Kansas, Department of Geology, 1475 Jayhawk Blvd., Rm. 120, Lawrence, KS 66045 USA.*

[2]*Christian-Albrechts-Universität zu Kiel, Institute of Geosciences, Ludewig-Meyn-Straße 10, 24098 Kiel, Germany.*

Abstract

Thermodynamic modeling of microdomains and whole-rock compositions is used to constrain the pressure-temperature (P-T) evolution of sapphirine granulites and migmatitic paragneisses from the Gruf Complex of the Central Alps. The P-T paths and conditions estimated from granulite microtextures and whole-rock compositions are consistent with one another, indicating that the estimates from both approaches are accurate. The sapphirine granulites were heated to ultra-high temperature (UHT) conditions of 900–1000°C and 7.0–9.5 kbar as they decompressed from ca. 800°C and 9–12 kbar, resulting in garnet breakdown. Nearly isothermal decompression led to the development of cordierite-bearing coronae and symplectites. By ca. 27 Ma, the lower crustal granulites and charnockites had been exhumed to the midcrustal level of migmatitic gneisses, which were undergoing peak metamorphism at ca. 675–750°C and 5–7 kbar. These results are consistent with a geodynamic model that invokes heat advection to the lower

crust closely following the continental-subduction (ultra-high pressure) stage of the Alpine orogeny. The most plausible geodynamic model consistent with the results of this study is breakoff of a southward subducting lithospheric slab, resulting in asthenospheric upwelling.

Introduction

Collisional orogens like the Alps affect global and regional climate and host major earthquakes and magmatism. Deep geodynamic processes that occur in these settings have some control on the surface dynamics such as earthquakes. The thermal structure of orogens also regulates the volume and type of magmatism produced. Metamorphic rocks that resided in the deep crust during orogenesis and were subsequently exhumed to the surface can provide important records of the thermal and geodynamic history of the orogens in which they are found.

Ultra-high temperature (UHT) metamorphism is of particular interest in understanding the thermal evolution of orogens because of the extreme crustal conditions it requires (ca. 900–1100°C and 7–13 kbar; Harley, 1998; Brown, 2007; Harley, 2008). During the Archean and Proterozoic eons, UHT metamorphism was more widespread than it has been during Phanerozoic time due to secular cooling of the Earth (Brown, 2006; Brown, 2007). Therefore, attaining UHT conditions within the Phanerozoic eon requires geodynamic processes that result in either a high geotherm (Kelsey, 2008), advection of heat to the crust from the mantle (Collins, 2002; Sizova et al., 2010; Clark et al., 2011), radiogenic heating (Clark et al., 2011; Kelsey and Hand, 2015), or shear heating (Kelsey, 2008). Constraining the pressure-temperature-time (P-T-t) history of Phanerozoic UHT rocks can be used to elucidate the nature, timing, and intensity of these geodynamic processes. However, determining the peak metamorphic conditions experienced by UHT rocks can be challenging because of retrograde elemental exchange and overprinting (e.g. Carswell and O'Brien, 1993; Fitzsimons and Harley, 1994; Harley, 1998; Pattison et al., 2003). Therefore,

techniques such as equilibrium phase diagram ("pseudosection") modeling (e.g. Pattison et al., 2003; O'Brien, 2008) and accessory mineral thermometry (e.g. Watson et al., 2006; Luvizotto et al., 2009; Blackburn et al., 2012; Kooijman et al., 2012) must be employed to constrain the P-T evolution of high-grade rocks.

The Gruf Complex is enigmatic in that it hosts the only occurrence of UHT rocks in the Central Alps (Figure 5.1) (Bousquet et al., 2012a). Therefore, understanding whether UHT metamorphism occurred during the Alpine orogeny and what processes led to it has important implications for the geodynamic history of the Central Alps. In this study, we summarize geochronological data and present the results of thermodynamic modeling to constrain the P-T-t history of UHT granulites and upper amphibolite facies migmatites from the Gruf Complex. The granulites are well suited for this study because they contain abundant reaction textures, which are used to constrain the P-T path. These results are used to propose a model for the geodynamic evolution of the Central Alps.

Geological Setting

The European Central Alps comprise nappes that were thrust together during the Alpine orogeny (Figure 5.1), which culminated in the collision of the European and Apulian plates, which began at ca. 40 Ma (Schmid et al., 1996; Pfiffner, 2016). The units that make up the Central Alps were derived from the European continental margin (Adula Nappe and Gruf Complex) and the Penninic units, which comprise the Valais (Chiavenna Ophiolite and Misox Zone) and Piemont-Liguria (Malenco unit) ocean basins and the Briançonnais (Tambo and Suretta Nappes) microcontinent (Figure 5.1). Part of the Central Alps (i.e. the Southern Steep Belt; SSB in Figure 5.1) has been referred to as a lithospheric mélange (Trommsdorff, 1990) or tectonic accretion channel (Engi et al., 2001) in which slivers of crust (nappes) with different paleogeographic

affinities and metamorphic histories were amalgamated along shear zones during the late stages of the Alpine orogeny. Prior to the collisional event and nappe stacking, the Adula nappe and parts of the Penninic units underwent high pressure metamorphism, ranging from blueschist facies conditions in the north to ultra-high pressure (UHP) conditions in the southern Adula nappe (e.g. Gebauer, 1996; Bousquet et al., 2002; Dobrzhinetskaya et al., 2002; Hermann et al., 2006; Berger and Bousquet, 2008), between ca. 45 and 35 Ma (e.g. Becker, 1993; Gebauer, 1996; Brouwer et al., 2005; Hermann et al., 2006; Berger and Bousquet, 2008). This was a result of subduction of the ocean basins, Briançonnais microcontinent, and edge of the European continental margin (e.g. Stampfli et al., 1998; Berger and Bousquet, 2008). After exhumation of the (U)HP units, a large part of the Central Alps (the Lepontine Dome) experienced Barrovian metamorphism between 32 and 22 Ma (Rubatto et al., 2009), ranging from greenschist facies in the north to sillimanite-zone migmatization in the south (Todd and Engi, 1997; Frey and Ferreiro Mählmann, 1999; Burri et al., 2005). In the southeastern Central Alps, the granodiorite to tonalite Bergell Intrusion was emplaced along the Insubric line, which is part of the Periadriatic fault system that represents the suture between the European and Apulian (or Adriatic) plates, between 32 and 30 Ma (von Blanckenburg, 1992; Samperton et al., 2015) (Figure 5.1). Magmatism in the Central Alps waned after the intrusion of the Novate leucogranite at 23.8 ± 0.1 Ma (Oalmann et al., in preparation-b).

The Gruf Complex occurs at the eastern extent of the Central Alps (Figure 5.1) where it is bordered to the north by the Chiavenna ophiolite (Valais) and Tambo nappes (Briançonnais). In the south and east, it is structurally overlain by the Bergell Intrusion (Berger et al., 1996; Davidson et al., 1996). The normal-sense Forcola fault separates the Gruf Complex from the Adula nappe, which experienced UHP metamorphism (Heinrich, 1986; Gebauer, 1996; Dobrzhinetskaya et al., 2002; Krogh Ravna and Terry, 2004), in the west (Ciancaleoni and Marquer, 2006; Bousquet et

al., 2012b; Galli et al., 2013). The Novate leucogranite intruded the southwestern part of the Gruf Complex along the Forcola fault at 24 ± 1 Ma (Liati et al., 2000; Oalmann et al., in preparation-b).

The Gruf Complex comprises mostly migmatitic biotite-bearing felsic orthogneisses with more scarce garnet + sillimanite + biotite ± muscovite metapelitic paragneisses and leucogranite gneisses (detailed mapping by Galli et al., 2013; Figure 5.2). Charnockitic sheets are separated from the migmatites by local, up to 50 cm-wide, mylonitic shear zones with reverse-sinistral shear sense (Galli et al., 2013). The two largest of these charnockite bodies outcrop along a high ridge at the center of the Gruf Complex (Figure 5.2). Scarce Mg- and Al-rich, residual sapphirine-bearing granulites occur as pods, rafts, and schlieren within the charnockites. Variably deformed felsic dikes, ranging from biotite-granite to beryl + garnet + biotite + muscovite pegmatite, occur throughout the Gruf Complex, and the older, muscovite-free and muscovite-poor dikes are deformed whereas the younger, muscovite-rich dikes are undeformed (Oalmann et al., in preparation-b).

In Oalmann et al. (in preparation-a), we used texturally-controlled U-Pb monazite dating to conclude that UHT metamorphism of the granulites occurred during Alpine orogenesis, with monazite dates constraining the timing of peak to post-peak metamorphism to between 34 and 30 Ma. In (Oalmann et al., in preparation-b), we used texturally-controlled zircon petrochronology to conclude that there was minor zircon growth in equilibrium with garnet at 34.8 ± 1.1 Ma, zircon was resorbing during UHT metamorphism, and zircon rims crystallized during early retrograde metamorphism and melt crystallization (ca. 700–800°C) at 32.7 ± 0.7 Ma. We used the U-Pb zircon ages of variably deformed felsic dikes to conclude that the UHT granulite/charnockite units were juxtaposed against the migmatitic ortho- and paragneisses along mylonitic shear zones between 30

and 27 Ma, that contractional deformation ended by 25.6 ± 0.3 Ma, and that decompression led to crustal melting between 26 and 24 Ma (Oalmann et al., in preparation-b). In another study (Oalmann et al., submitted), we determined that the granulites and charnockites cooled from 700 to 420°C between ca. 30 and 19 Ma using U-Pb rutile thermochronology.

Sample Descriptions

Leucogranulite (GR11-39)

Leucogranulite sample GR11-39 is a felsic granulite characterized by alternating light and dark bands, which define a gneissocity (Figure 5.3A, 4A). Quartz within the leucosomes (light bands) is characterized by a bimodal grain size distribution. Large quartz ribbons (up to 1 cm long) exhibit undulose extinction and are elongate subparallel to the gneissocity. Smaller quartz grains are equant and have lobate grain boundaries. Blocky plagioclase grains are elongate subparallel to the gneissocity and lineation defined by the large quartz porphyroclasts. Lens-like K-feldspar porphyroclasts are also elongate subparallel to the gneissocity.

The melanosomes consist of biotite, garnet, orthopyroxene, sapphirine, and minor spinel and rutile. Biotite occurs as elongate blades that are oriented subparallel to the gneissocity. Anhedral to subhedral garnet porphyroblasts (up to 1 mm in diameter) commonly have embayments filled with individual grains or symplectites of plagioclase ± orthopyroxene ± biotite ± sapphirine ± spinel (Figure 5.5A). Outside of the garnet embayments, blocky orthopyroxene occurs as isolated porphyroblasts. Up to 3 mm-long aggregates of sapphirine (± spinel) are aligned subparallel to the gneissocity and are typically isolated from the other mafic minerals except for biotite and occur within the leucosomes in some cases (Figure 5.4A). The relative proportion of the phases varies from layer to layer. Some melanosome layers consist mainly of elongate biotite with or without sapphirine ± spinel aggregates, whereas other layers are dominated by blocky

orthopyroxene. Garnet occurs as isolated porphyroblasts within the melanosomes and more scarcely within the leucosomes.

In this study, a garnet embayment filled with symplectites of orthopyroxene, plagioclase, sapphirine, and spinel (Figure 5.5A) is investigated. This garnet-breakdown texture is surrounded by quartz + K-feldspar, which represent crystallized melt. This type of texture is common in the leucogranulite samples and, to a lesser extent, in the charnockites.

Residual Granulite (Gruf100)

Residual granulite sample Gruf100 is a garnet-rich orthopyroxene + sapphirine + biotite + sillimanite + cordierite granulite that lacks a definite fabric (Figure 5.3B, 4B). The distribution of the constituent minerals at hand sample scale is homogeneous (Figure 5.3B).

Garnet porphyroblasts are subhedral and range from 3 mm to 2 cm in diameter (Figure 5.3B). The largest of these porphyroblasts are characterized by inclusion-rich cores and inclusion-poor rims (Figure 5.3B). Embayments in garnet are invariably filled with crystallized leucosome (quartz + feldspar), blocky orthopyroxene porphyroblasts, bladed sapphirine, biotite, cordierite, and/or symplectites consisting of orthopyroxene ± sapphirine ± cordierite (Figure 5.5B, C).

Subhedral orthopyroxene porphyroblasts range from 1–8 mm. In many cases, orthopyroxene and bladed sapphirine are intergrown (Figure 5.5C). In the more biotite-rich parts of the sample, biotite occurs along the edge and within cracks of orthopyroxene (Figure 5.5D).

Bladed sapphirine porphyroblasts range from <1 mm to 5 mm in length. These porphyroblasts are most common near garnet and orthopyroxene (Figure 5.5B, C), but also occur within leucosomes. There are no inclusions of sapphirine within the garnet.

Prismatic sillimanite porphyroblasts reach ca. 3 mm in length and are invariably (at least partly) surrounded by sapphirine + cordierite + minor spinel symplectites, which are separated

from orthopyroxene by cordierite coronae (Figure 5.5D). These textures likely formed from a reaction such as sillimanite + orthopyroxene = sapphirine + cordierite + spinel. In some cases, sillimanite occurs as aggregates made up of numerous small prisms that together form a blade-like shape (Figure 5.5D). This may be the result of sillimanite pseudomorphing kyanite.

Cordierite occurs in orthopyroxene-bearing symplectites or as coronae around and between garnet, orthopyroxene, sapphirine (Figure 5.5B, C) and sillimanite porphyroblasts (Figure 5.5D). In some areas of the thin section, cordierite is so abundant that the other mafic and aluminosilicate phases (garnet, orthopyroxene, sapphirine, and sillimanite) do not touch one another. We interpret these relationships to indicate that cordierite formed slightly after orthopyroxene and sapphirine.

Biotite mostly consists of small masses that surround orthopyroxene and garnet (Figure 5.5D). However, large aggregates of biotite are also present. Based on the relationship of biotite to the other phases, we interpret biotite to be a retrograde phase.

Leucosomes occur as discrete, ≤2 cm, white to gray pods comprising quartz + K-feldspar + plagioclase (Figure 5.3B, 4B). The feldspars in these leucosomes lack perthitic texture, and plagioclase and K-feldspar occur in roughly equal proportions. Minor blocky plagioclase also occurs outside of the leucosomes in garnet embayments.

Residual Granulite (Br03-56-2)

Another residual granulite sample with a slightly different bulk composition and mineral assemblage was also modeled. The whole-rock composition that was used for the input of this sample was taken from the Diplom Thesis of Schefer (2005). This residual granulite has a very similar appearance to the other residual granulite sample (Gruf100) in terms of its constituent minerals and their grain sizes, habits, and relationships to one another (Figure 5.4C). The main petrographic differences are that this sample lacks sillimanite (except for sillimanite exsolution

lamellae in orthopyroxene) and contains a higher proportion of spinel and biotite than sample Gruf100. Spinel occurs either as inclusions in or at the fringes of garnet or as fine-grained aggregates that fringe sapphirine (Figure 5.5E).

Residual granulite (GRM-37)

A monazite-bearing texture, which was extracted from a thin section of residual granulite sample Br03-56-2, contains orthopyroxene, sapphirine, and cordierite (Figure 5.5F). The monazite grain occurs with cordierite as part of a two-phase inclusion in sapphirine (Figure 5.5F). This monazite grain was dated by Oalmann et al. (in preparation-a) using Laser Ablation Inductively Coupled Plasma Mass Spectrometry (LA-ICP-MS) and yields a weighted mean $^{206}Pb/^{238}U$ age of 32.5 ± 0.5 Ma based on three analyses.

Migmatitic paragneiss (GR11-23)

Sample GR11-23 is a garnet + sillimanite + biotite + muscovite gneiss has well-developed gneissic banding, defined by segregations of quartzofeldspathic and garnet-sillimanite-biotite-muscovite-rich layers (Figure 5.3C, 4D). This sample exhibits a well-developed crenulation cleavage defined by folding of the gneissic banding and folds within the mica-rich layers (Figure 5.3C, 4D). Muscovite, biotite, and fibrolitic sillimanite are the most abundant mineral in the dark layers, whereas garnet is scarcer (Figure 5.5G). Euhedral garnet porphyroblasts are elongate subparallel to the gneissocity in some cases, but in most cases garnet is equant (Figure 5.5G). Quartz has a bimodal size distribution in which the largest grains have chessboard-type undulose extinction and are elongate subparallel to the gneissocity. Smaller quartz grains have lobate grain boundaries typically have similar extinction angles. K-feldspar occurs as augen within the leucosome, and plagioclase typically has a blocky habit.

Migmatitic paragneiss (GR11-25)

Sample GR11-25 is a migmatitic garnet + sillimanite + biotite gneiss that has well-developed gneissocity, which is defined by segregation of quartzofeldspathic and garnet-, sillimanite-, and biotite-rich layers (Figure 5.3D, 4E). This sample consists of a higher proportion of leucosome than sample GR11-23 (Figure 5.4D, E). Aggregates of biotite and sillimanite are elongate subparallel to the gneissocity (Figure 5.5H). Euhedral garnet porphyroblasts are mainly restricted to the melanosome layers and are elongate subparallel to the gneissocity in some cases (Figure 5.5H). Quartz has a similar bimodal size distribution and microstructural attributes as the quartz in the other paragneiss sample. The leucosomes of this sample comprise a higher proportion of plagioclase and a lower proportion of K-feldspar than the leucosomes in sample GR11-23.

Methods

Electron Probe Microanalysis (EPMA)

Quantitative major element compositions were collected with a JEOL Superprobe JXA-8900R electron microprobe at Christian Albrechts Universität zu Kiel (Table 5.1). An accelerating voltage of 15–20 kV and a beam current of 20 nA were used for the analyses, and the CITZAF method of Armstrong (1995) was used to correct the data. X-ray compositional maps were obtained using a 15 kV accelerating voltage, 10–40 nA beam current, and 80–200 ms dwell time. Backscattered electron (BSE) images were used with the JEOL Image-Archive software to determine the area percent of the phases comprising reaction textures. The bulk compositions of these textures were then calculated by comparing the intensity (counts) of X-ray compositional maps with using the quantitative EPMA spot analyses (weight percent) (Table 5.2).

X-ray Fluorescence (XRF)

Between 5 and 10 kg of sample (excluding weathered exteriors) were crushed and powdered using a steel plated jaw crusher and ball mill at the University of Kansas, Department of Geology. Splits of the powder were sent to the GeoAnalytical Lab at Washington State University for major and trace element analyses (Table 5.2). Further powdering of the samples, fusing into glass beads, and analysis by XRF were carried out following the methods of Johnson et al. (1999).

LA-ICP-MS

Garnet trace element compositions were measured using laser ablation inductively coupled mass spectrometry (LA-ICP-MS) at the University of Kansas, Department of Geology's Isotope Geochemistry Lab. The analytical protocols that were used for the measurements are shown in Table 5.3.

Pressure-Temperature Modeling

Equilibrium phase diagrams (commonly referred to as pseudosections) were calculated for whole-rock samples (granulites and migmatitic paragneisses; Table 5.2) and microtextural domains (Table 5.2) of the granulites using Theriak-Domino version 04.02.2017 (De Capitani, 1994; De Capitani and Petrakakis, 2010). The whole-rock compositions of the residual granulite samples (Gruf-100 and Br03-56-2) were used as the input for the phase diagram calculations because of the homogeneous distribution of phases in these samples.

In the leucogranulite sample (GR11-39), the effective compositions of reaction textures are not represented by the whole-rock composition because the subsolidus reactions are separated from one another by melt. Therefore, the input compositions for these reaction textures were calculated by combining the BSE image, X-ray composition maps, and EPMA spot analyses of

the area comprising the reaction texture as described above. This method was also used to calculate the composition of a monazite-bearing texture (GRM-37), which was drilled from a thin section of residual granulite sample Br03-56-2.

The Theriak-Domino database tcds55_p07 (downloaded from dtinkham.net/peq.html), which consists of thermodynamic data from Holland and Powell (1998), was used for all calculations. The following mineral solution models were used: talc, epidote, staurolite, chlorite, chloritoid, and cordierite (Holland and Powell, 1998); white mica (Coggon and Holland, 2002); orthopyroxene and spinel (White et al., 2002); feldspar (Holland and Powell, 2003); sapphirine and osumilite (Kelsey et al., 2004); biotite, garnet, and ilmenite (White et al., 2005); melt for metapelitic compositions (White et al., 2007); amphibole and clinopyroxene (Diener and Powell, 2012).

The H_2O content of all compositions was estimated using temperature versus mole fraction H_2O (M_{H2O}) binary phase diagrams (Figure 5.A1). See Appendix A for details.

Garnet Compositional Zoning

Leucogranulite

The major element zoning patterns of the garnet from the modeled reaction texture in the leucogranulite sample are shown in the X-ray compositional maps in Figure 5.6 (quantitative data in Table 5.1). The grossular component of this garnet is strongly zoned (Figure 5.6A). Mole fraction grossular ($X_{grossular}$) decreases from 0.1 in the core to 0.03 in the rim. There is a lack of zoning with respect to the other major cations (Mg, Fe, and Mn; Figure 5.6B, C, D) except for a decrease in Mg (X_{pyrope} = 0.36, whereas average X_{pyrope} = 0.41) (Figure 5.6B) and an increase in Fe ($X_{almandine}$ = 0.62, whereas average $X_{almandine}$ = 0.51) (Figure 5.6C) along one edge, which is in contact with orthopyroxene.

Residual Granulite

Figure 5.7 shows a profile of compositional zoning in a large garnet porphyroblast from residual granulite sample Gruf100. This garnet is typical of the residual granulite samples with an inclusion-rich core surrounded by an inclusion-poor rim (Figure 5.4B). The major and trace element zoning profiles described here are typical of garnet porphyroblasts in both residual granulite samples investigated in this study.

There is a sharp contrast in the major element zoning profiles between the core and rim (Figure 5.7). The almandine and grossular components ($X_{almandine}$ and $X_{grossular}$, respectively) gradually increase from the center of the inclusion-rich zone toward the contact with the inclusion-poor zone, whereas the pyrope component (X_{pyrope}) decreases. The spessartine ($X_{spesartine}$) component is invariable across the inclusion-rich zone.

Within the inclusion-poor rim, $X_{almandine}$ and $X_{grossular}$ decrease, whereas X_{pyrope} increases, from the core-rim contact toward the edge of the garnet. However, within ca. 0.3 mm of the garnet edge, $X_{almandine}$ and $X_{grossular}$ increase, and X_{pyrope} decreases. $X_{spesartine}$ gradually decreases from the core-rim contact toward the edge of the garnet.

Zoning of trace elements (REE, Y, and HFSE) is markedly different than that of the major elements. The Y concentration decreases from ca. 3500 ppm in the center of the inclusion-rich zone to ca. 400 ppm near the contact with the inclusion-poor zone (Figure 5.7). There is a sharp drop in Y concentration across the core-rim contact, and the Y concentration decreases from ca. 90 ppm to 30 ppm toward the edge of the garnet across the inclusion-poor domain. Zirconium concentration is much higher (ca. 50 ppm Zr on average; Table 5.1) in the inclusion-rich core than in the inclusion-poor rim (decreasing from ca. 7 ppm to 1 ppm; Table 5.1).

Pressure-Temperature Estimates

Leucogranulites

A garnet-breakdown texture (Figure 5.5A), which is representative of garnet textures in the leucogranulite samples, was targeted in sample GR11-39. The observed assemblage of garnet + orthopyroxene + plagioclase + sapphirine + spinel + melt (represented by quartz + K-feldspar) is stable at ca. 900–1050°C and 6–9 kbar on the calculated phase diagram (Figure 5.8A). The garnet compositional isopleths that correspond to the measured composition of the garnet core ($X_{grossular}$ = 0.05–0.10 and X_{pyrope} = 0.4) intersect at ca. 800°C and 9–12 kbar, which is well outside the stability field of the observed assemblage (Figure 5.8E). The calculated isopleths of garnet volume decrease sharply between the intersection of the garnet compositional isopleths and the stability field of the observed assemblage (Figure 5.8F), indicating that orthopyroxene, plagioclase, sapphirine, and spinel formed at the expense of garnet. The relative positions of the stability fields of sapphirine and orthopyroxene indicate that sapphirine grew earlier than orthopyroxene. This is consistent with the textural relationships between the phases and the anhedral shape of the garnet. Therefore, we interpret that the rock underwent heating to UHT conditions during decompression from near-eclogite facies conditions along the P-T path shown in Figure 5.8F.

Residual Granulites

The peak assemblage of residual granulite sample Gruf100 is interpreted to be K-feldspar + garnet + orthopyroxene + sapphirine + sillimanite + rutile + melt. This assemblage is stable at 925–975°C and 8.25–10.25 kbar on the calculated phase diagram (Figure 5.8B). The presence of sapphirine + orthopyroxene symplectites and coronae around garnet (Figure 5.5B, C) suggest that garnet was breaking down at peak conditions. Cordierite was stable at lower pressure than the interpreted peak assemblage (Figure 5.8B), suggesting that moats of cordierite around garnet, orthopyroxene, sapphirine, and sillimanite formed during continued decompression. Sapphirine +

cordierite symplectites around sillimanite porphyroblasts also suggest decompression to less than ca. 8.5 kbar (the edge of the sillimanite stability field) occurred prior to significant cooling (Figure 5.8B, G). The biotite-out reaction occurs very close to the stability field of the peak assemblage. Therefore, it is likely that some of the biotite did not react out completely at peak conditions and resumed growth shortly after cooling commenced. Garnet-volume percent isopleths (Figure 5.8G) indicate that garnet volume was highest at higher pressures and lower temperatures than the stability field of the peak assemblage, indicating that peak conditions were reached during decompression. Based on these observations, we interpret that this sample followed the P-T path shown in Figure 5.8G in which heating to UHT conditions occurred during decompression, and nearly isothermal decompression continued to <8.5 kbar.

The interpreted peak assemblage of residual granulite sample Br03-56-2 (garnet + othropyroxene + biotite + sapphirine + spinel + melt) is stable over a large area (925–1075°C and 6 to >11 kbar) of the P-T phase diagram (Figure 5.8C). This sample also shows textural evidence for garnet breaking down to form orthopyroxene, sapphirine, and cordierite (Figure 5.4C) similar to those in residual granulite sample Gruf100, and garnet-volume percent isopleths (Figure 5.8H) also indicate a higher garnet volume percent at higher pressure and lower temperature than the stability field of the peak assemblage. The beginning of the P-T path shown in Figure 5.8H represents a combination of the P-T paths determined for the leucogranulite garnet-breakdown texture (Figure 5.8F) and other residual granulite sample (Figure 5.8G). However, in contrast to sample Gruf100, the cordierite moats in sample Br03-56-2 probably formed in response to cooling rather than decompression according to the phase diagram (Figure 5.8C), indicating a that the slope of the P-T path became shallower (i.e. cooling became more dominant than decompression) at ca. 7 kbar.

Based on the straight grain boundaries between phases and intergrown nature of sapphirine and cordierite (Figure 5.5F), we interpret the texture within microdomain GRM-37 to represent equilibrium. The observed assemblage of orthopyroxene + sapphirine + cordierite was stable at 850–1100°C and 7.25–10.5 kbar (Figure 5.8D). This texture is from the residual granulite sample Br03-56-2 and the P-T estimates obtained using both the whole rock composition and the microdomain composition overlap considerably (Figure 5.8D, C).

Migmatitic paragneisses

The calculated phase diagram for the garnet + sillimanite + biotite + muscovite paragneiss (sample GR11-23) indicates that the observed peak assemblage (plagioclase + garnet + biotite + muscovite +quartz + sillimanite + ilmenite + melt) was stable at ca. 650–750°C and 4.0–7.5 kbar (Figure 5.9A). Sample GR11-25 is mineralogically and texturally similar to sample GR11-23, but it lacks muscovite and has a higher proportion of leucosome. However, the stability field of the observed peak assemblage (675–750°C and 5–7 kbar) overlaps considerably with that of the muscovite-bearing sample (Figure 5.9A, B). We interpret this to indicate that the difference in mineralogy reflects the slight difference in the bulk rock composition of these samples and not differences in peak P-T conditions.

Discussion

Accuracy of P-T Estimates

Determining the effective or equilibrium composition for a rock volume is probably the most challenging part of using thermodynamic software programs like Theriak-Domino to estimate P-T conditions. This is especially true for rocks that have undergone partial melting, which can result in significant changes of the effective composition during prograde and retrograde

metamorphism. However, we believe that our peak P-T estimates for the granulite samples are robust and accurate, because there is considerable overlap in peak P-T estimates and derived P-T paths, whether we used whole rock compositions determined by XRF or compositions of microdomains determined by EPMA (Figure 5.10). The starting point of the P-T paths shown in Figure 5.8E, F, and G is based on the composition of the garnet core in the microtexture from leucogranulite GR11-39. However, the effective bulk composition in which the garnet core formed may been different than the measured composition. Therefore, the starting point of the P-T path may not be accurate, but we believe that it is a close approximation because textural evidence (i.e. sapphirine + orthopyroxene growth at the expense of garnet followed by formation of cordierite coronae) indicates that the residual granulite samples followed similar decompression-heating P-T paths (Figure 5.8G, H) as the one derived from the garnet compositional isopleths for the leucogranulite shown in Figure 5.8E.

For the migmatitic paragneiss samples, we used whole rock compositions to model peak P-T conditions, which have the risk of not representing the equilibrium composition. However, other studies (e.g. Hamilton and Pattison, 2010; Hamilton and Pattison, 2017) have shown that in rocks in which melt segregated from solids, using a non-equilibrium (whole rock) composition only affects the position of the melt-related quartz-, plagioclase-, and K-feldspar-out lines and not the boundaries of the remnant solid phases. Therefore, we did not consider the stability of quartz or feldspars in estimating the peak P-T conditions, and the presented peak P-T estimates should be accurate.

Protoliths of Paragneisses and Granulites

Based on the presence of Al-rich phases such as sillimanite and garnet (and muscovite in sample GR11-23), it is likely that the protoliths of the migmatitic paragneisses were pelitic

sedimentary rocks with various amounts of quartz. The protoliths of the granulites, however, are not as easily discerned. Based on the low abundances of quartz and feldspars and high Al and low Si concentrations (Table 5.2), it is evident that the residual granulites lost melt at some point. All of the granulites contain Permian–Cretaceous, oscillatory-zoned zircon, which is interpreted to have crystallized from melt (Oalmann et al., in preparation-b), indicating that there was a higher proportion of melt in the residual granulites prior to Cenozoic time. Therefore, the residual granulites and melanosomes in the leucogranulites likely developed their restitic character, at least in part, prior to UHT metamorphism. The earlier melt-loss events preconditioned the granulites for the subsolidus reactions that took place at UHT conditions as described by Kelsey and Hand (2015). The presence of abundant high-Al phases (e.g. sillimanite, sapphirine, and garnet) and lack of high-Ca phases (e.g. orthopyroxene instead of clinopyroxene or amphibole) leads us to postulate the protoliths of the granulites and charnockites were also pelitic sedimentary rocks.

Composite Pressure-Temperature Path

The conditions of a pre-peak high-pressure stage (ca. 800°C and 9–12 kbar) are constrained by the garnet compositional isopleths from the leucogranulite sample GR11-39 (Figure 5.8E). The enrichment of X_{pyrope} in the inclusion-poor rims of the garnet from the residual granulite sample Gruf 100 (Figure 5.7) is consistent with a high-pressure stage preceding UHT metamorphism. The garnet volume percent isopleths from the leucogranulite and residual granulite samples imply that the granulite/charnockite units were decompressed/exhumed to ca. 7 kbar while being heated to UHT conditions (Figure 5.8F, G), resulting in sapphirine + orthopyroxene growth at the expense of garnet. Qualitatively, the symplectite textures that replace garnet are also suggestive of a decompression P-T path. The rocks were further decompressed into the stability field of cordierite + orthopyroxene for the residual granulites (less than ca. 8.5 kbar at 800–1000°C) (Figure 5.8H).

The lower crustal granulite/charnockite units were then juxtaposed against the mid crustal migmatites, which were undergoing peak metamorphism at ca. 700–750°C and 5–8 kbar. This implies a composite P-T path for the granulites and charnockites characterized by early decompression and heating, an intermediate, nearly isothermal decompression stage at UHT conditions, and finally cooling and decompression to the conditions recorded by the mid crustal migmatites (Figure 5.10).

Figure 5.11 shows the change in modal abundances of minerals in the granulites along the P-T path in Figure 5.10 calculated with the P-T loop function of Theriak-Domino. For the garnet-breakdown texture from leucogranulite sample GR11-39, sapphirine was the first of the symplectite-forming minerals to grow at 950°C and 9.2 kbar as the modal abundance of garnet was decreasing. At ca. 940°C and 7.25 kbar, there was a sharp increase in the modes of orthopyroxene and spinel and decrease in sapphirine, indicating that sapphirine was partially consumed to form orthopyroxene + spinel. Residual granulite sample Gruf100 and Br03-56-2 behaved similarly with orthopyroxene and sapphirine modes increasing and garnet mode decreasing beginning at 950°C and 9.2 kbar. In addition, the modal abundance of sillimanite decreased as cordierite and sapphirine modes increased in the residual granulite sample. These patterns are consistent with the petrographic observations that orthopyroxene + sapphirine (+ cordierite in the residual granulites) grew at the expense of garnet at UHT conditions, indicating that the proposed P-T path is accurate.

The conditions of garnet breakdown and symplectite formation determined in this study contrast the estimates presented by Galli et al. (2011) of 700–750°C and 6–8 kbar. Based in part on these results, the authors concluded that UHT metamorphism did not occur during Alpine orogenesis. However, we interpret our results to indicate that UHT conditions were reached during

the latest metamorphic event, which occurred during Alpine orogenesis, at ca. 34 Ma (Oalmann et al., in preparation-b). Furthermore, Galli *et al.* (2011; 2012) attributed UHT metamorphism to post-Variscan, Permian rifting of the European margin. However, isobaric cooling P-T paths are derived for UHT rocks from rift zones in most cases, whereas UHT decompression is more common in orogenic accretion and collision settings (Kelsey and Hand, 2015). Therefore, we interpret the decompression-heating P-T path derived for the Gruf granulites in this study to indicate that UHT conditions were obtained in an orogenic setting (i.e. the Alpine orogeny).

Relating the P-T Path to Ages

Figure 5.12 shows a pressure-temperature-time path for the Gruf Complex based on the U-Pb ages presented by Oalmann et al. (in preparation-a); Oalmann et al. (in preparation-b); Oalmann et al. (submitted) and assuming that UHT metamorphism occurred during a single, Alpine P-T loop as discussed above. Rare earth element patterns of 34.8 ± 1.1 Ma zircon domains in the residual granulite indicate that this zircon grew in equilibrium with garnet and thus prior to garnet breakdown (Oalmann et al., in preparation-b). Therefore, we interpret this age to constrain the timing of the pre-peak, high-pressure stage (Figure 5.12). The next youngest zircon population crystallized from post-UHT melts in the leucogranulite at 32.7 ± 0.7 Ma (Oalmann et al., in preparation-b), after garnet breakdown as indicated by steep REE-patterns with high HREE concentrations. This leads to the interpretation that UHT metamorphism likely occurred between 34.8 ± 1.1 Ma and 32.7 ± 0.7 Ma (Figure 5.12). A ca. 34 Ma age for UHT metamorphism is consistent with the 32.5 ± 0.5 Ma age (Oalmann et al., in preparation-a) of a monazite inclusion in a slightly post-peak sapphirine- + cordierite-bearing texture, which equilibrated at >850°C and >7 kbar (Figure 5.8D).

Because the migmatites were undergoing ductile deformation when the lower crustal charnockites and granulites were exhumed into the middle crust between 30 and 27 Ma (Oalmann et al., in preparation-b), we interpret that the P-T conditions estimated for the paragneiss samples (675–750°C and 5–7 kbar) (Figure 5.9) represent the conditions of the middle crust into which the lower crustal rocks were exhumed. The ages of undeformed, muscovite-rich dikes and plutons indicate that contractional deformation ended and the amalgamated Gruf Complex was being exhumed between 26 and 24 Ma (Oalmann et al., in preparation-b). U-Pb rutile ages indicate that the Gruf granulites and charnockites underwent cooling from 700–420°C between 30 and 19 Ma (Oalmann et al., submitted).

Geodynamic Model for the Central Alps

Any valid tectonometamorphic model for the Gruf Complex must consider the P-T-t path shown in Figure 5.12. One such scenario is that the lower crustal granulites and charnockites were subducted or buried to depths equivalent to 9–12 kbar (ca. 32–42 km) and subsequently exhumed to 7.5–9.5 kbar (ca. 25–33 km depth) while being heated by advected mantle or mantle-derived melts. The switch from nearly isothermal decompression to decompression + cooling (Figure 5.8, 10, 12) may have been the result of the granulites and charnockites retaining heat while being exhumed to depths equivalent to less than 7 kbar within the crust.

The tectonometamorphic evolution of the Gruf Complex discussed above, (U)HP metamorphism at 40–35 Ma (Gebauer, 1996; Brouwer et al., 2005; Hermann et al., 2006) followed by Barrovian metamorphism (beginning at ca. 32 Ma; Rubatto et al., 2009) of the Adula nappe and other units of the Lepontine Dome, and petrogenesis of the magmas that formed the Periadriatic intrusions (e.g. the Biella, Bergell, Adamello, Riesenferner, and Pohorje intrusions), which intruded the Western, Central and Eastern Alps between 34 and 28 Ma (von Blanckenburg and

Davies, 1995; Rosenberg, 2004), (e.g. Bergell and Adamello Intrusions in the Central Alps) must be represented in viable geodynamic models for the Central Alps. Based on U-Pb geochronological constraints, a valid model must also account for partial exhumation of the (U)HP units prior to ca. 34 Ma (Gebauer, 1996; Hermann et al., 2006). Two previously published geodynamic models could possibly produce the observations noted here: 1) Slab breakoff (e.g. von Blanckenburg and Davies, 1995; Handy et al., 2010) lead to buoyant exhumation of the (U)HP units (subducted Penninic units and European margin, i.e. the Adula Nappe) followed by infiltration of asthenospheric mantle into the gap, UHT metamorphism, exhumation of the Gruf lower crustal units, and emplacement of the Bergell magmas. 2) Slab rollback of either the Valaisian or African slabs lead to lithospheric thinning (Beltrando et al., 2010), resulting in exhumation of the (U)HP units along lithospheric-scale faults followed by upwelling of the asthenosphere, which lead to adiabatic melting in the lithospheric mantle and UHT metamorphism in the lower crust, and finally a switch back to contractional deformation. However, we prefer the slab breakoff model because the lithospheric thinning model of Beltrando et al. (2010) does not accurately portray the timing of the Bergell intrusion, and there is no evidence for large scale extension within the Central Alps.

Figure 5.13 schematically shows our proposed model for the geodynamic evolution of the Central Alps based on the results of this study and models presented by Schmid et al. (1996), Bousquet et al. (2002), Handy et al. (2010), and Pfiffner (2016). Figure 5.13A shows the subduction stage of the Alpine orogeny that resulted in (U)HP metamorphism of the Adula and Penninic nappes between 45 and 35 Ma (e.g. Becker, 1993; Gebauer, 1996; Bousquet et al., 2002; Hermann et al., 2006). During this time period the Gruf Complex, interpreted to be of European margin affinity (Bousquet et al., 2012b; Galli et al., 2012), was likely being thrust beneath the Austroalpine nappe stack and became part of the Penninic nappes.

At ca. 34 Ma, the results presented here indicate that the lower crustal part of the Gruf Complex was undergoing UHT metamorphism at 900–1000°C and 7.5–9.5 kbar (25–33 km depth) following decompression from 800°C and 10–13 kbar (35–45 km depth) at ca. 35 Ma (Figure 5.12, 13B). The position of the Gruf Complex at ca. 35 Ma is shown as the transparent unit with dashed outline in Figure 5.13B.

The lack of a UHT overprint on the Adula and Penninic units implies that these units had been exhumed above the European margin and thus slab breakoff had occurred prior to 34 Ma (Figure 5.13B). Between 30 and 27 Ma, the Gruf lower crustal granulites and charnockites were exhumed into the middle crust migmatites (Oalmann et al., in preparation-b) (Figure 5.13C). We envisage this to be the result of part of the lower crust of the European margin detaching and exhuming. Amalgamation of the Gruf Complex was coeval with the last stages of crystallization of the Bergell intrusion, indicating that exhumation of the lower crust may have been assisted by the buoyantly intruding Bergell magmas.

Between 26 and 24 Ma, contractional deformation had ceased, and the crustally-derived Novate leucogranite and associated muscovite-rich dikes intruded the Gruf Complex (Oalmann et al., in preparation-b). We interpret this to indicate that exhumation of the amalgamated Gruf Complex along the Insubric line occurred then and was likely a result of underplating of Apulian lower crust (Figure 5.13D) at the onset of continent-continent collision, which also cut the supply of mantle-derived magmas to the Gruf Complex. Slip along the normal sense Forcola Fault occurred coevally with intrusion of the Novate leucogranite at ca. 24 Ma, exhuming the Adula nappe relative to the Gruf Complex (Ciancaleoni and Marquer, 2006).

Comparison of the Central Alps with Cenozoic Contractional Settings

Ultra-high temperature rocks have been discovered in other Cenozoic convergent tectonic settings. For example, UHT xenoliths were entrained in lavas that erupted on the Pamir (Gordon et al., 2012) and Tibetan (Hacker et al., 2000) Plateaus, and UHT granulites outcrop on Seram Island within the Banda Arc in Indonesia (Pownall et al., 2014). The Pamir xenoliths were subjected to higher pressures (≥15–20 kbar) (Gordon et al., 2012) than the Gruf granulites, whereas the Tibetan xenoliths underwent UHT metamorphism at 8–12 kbar (Hacker et al., 2000). Proposed geodynamic models for UHT metamorphism of the Tibetan lower crust include lithospheric thinning, slab breakoff, and intracontinental subduction. Pownall et al. (2014) concluded that UHT metamorphism in eastern Indonesia resulted from exhumation of lithospheric mantle into the lower crust during a period of extreme extension driven by slab rollback in the Banda Arc. The Alpine orogeny is different from the Pamir-Tibet and Indonesian examples in that the oceanic subduction stage was not long-lived in the Alps.

All these models invoke advection of hot, mantle material into the crust resulting in UHT metamorphism. Therefore, UHT metamorphism can occur in contractional settings if there are episodes of lithospheric-scale extension or mantle upwelling. This may imply that UHT metamorphism is more common in Phanerozoic collisional orogens than previously thought. The products of these extreme thermal processes may not be exposed or not recognized as UHT rocks due to retrograde overprinting or bulk compositions that do not produce obvious UHT assemblages (e.g. sapphirine + quartz).

Conclusions

Thermodynamic modeling of whole-rock and microdomain (reaction texture) compositions from leucocratic as well as restitic granulites yields petrologically reasonable results if the effective reaction composition is determined. The modeled P-T path indicates that the

granulite/charnockite units of the Gruf Complex reached UHT conditions (ca. 900–1000°C and 7.0–9.5 kbar) during decompression from 9–12 kbar and ca. 800°C at ca. 34 Ma, leading to sapphirine + orthopyroxene growth at the expense of garnet in all granulite types. The lower crustal UHT rocks were further decompressed to <7 kbar at (near) UHT temperatures and subsequently juxtaposed against midcrustal migmatitic gneisses, which underwent peak metamorphism at 700–750°C and 5–8 kbar, by between 30 and 27 Ma.

The decompression-heating P-T path experienced by the granulites and charnockites likely was the result of a switch from subduction of oceanic and continental lithosphere to pre-collisional mantle upwelling at ca. 34 Ma within the Central Alps, likely resulting from slab breakoff. The Gruf UHT rocks are most likely somewhat analogous to UHT rocks from other Cenozoic convergent settings including the Tibetan plateau and the Banda Arc in Indonesia.

Acknowledgements

This research is supported by the American National Science Foundation under Grant No. EAR 0911633 to A. Möller. We would like to thank A. Galli for guiding us in the field area, the Biavaschi family at Rifugio Brasca for their hospitality and logistical help, P.G. Lippert for field assistance, and C. Fischer (University of Potsdam) and W.C. Dickerson (University of Kansas) for preparing thin sections. P. Appel and B. Mader (University of Kiel) and C. Gunther and M. Konrad-Schmolke (University of Potsdam) assisted with the EPMA work. We are also grateful to A. Galli, V. Guevara, M. Caddick, and several others for fruitful discussions about the Gruf Complex.

Appendix 5.A

The H_2O content of samples and reaction textures were estimated using temperature versus mole fraction hydrogen (M_H) diagrams. Pressure was fixed at 9 kbar for the granulite samples and textures therein (Figure 5.A1A–D) and 6 kbar for the paragneisses (Figure 5.A1E–F) based on the previously published P-T estimates of Galli et al. (2011) and Guevara and Caddick (2016). For all samples, M_H values ranging from 0 (dry conditions) to 20 (H_2O-saturated conditions) were used in the binary plots.

For the garnet breakdown texture from leucogranulite GR11-39 (Figure 5.A1A), the observed peak assemblage consists of plagioclase + garnet + sapphirine + orthopyroxene + spinel + melt ± K-feldspar (red shaded fields in Figure 5.A1A). The presence of coexisting plagioclase, sapphirine, orthopyroxene, and spinel in the garnet-breakdown texture limit M_H to less than 16. It is unclear whether K-feldspar was stable as a solid phase at peak conditions. Therefore, we used a M_H value of 8 to calculate the P-T diagram (Figure 5.8A).

For the residual granulite Gruf100 (Figure 5.A1B), the observed peak assemblage (red-shaded field in Figure 5.A1B) comprises plagioclase + garnet + orthopyroxene + sapphirine + sillimanite + rutile + melt. The sillimanite-out reaction (purple line in Figure 5.A1B) is nearly vertical in the calculated diagram, indicating that the presence or absence of sillimanite is strongly affected by H_2O content for this bulk composition. In this sample, the coexistence of sapphirine, and sillimanite restrict M_H to less than 11 (Figure 5.A1B). Therefore, we used an M_H value of 4, which crosses the field of the observed peak assemblage, to calculate the P-T diagram for this sample.

The field of the observed peak assemblage (garnet + orthopyroxene + sapphirine + biotite + melt) in residual granulite Br03-56-2 is stable over a wide range of M_H values, ranging from 7–19 (Figure 5.A1C). The minerals that were stable at peak conditions (garnet, sapphirine,

orthopyroxene) do not tightly constrain the H_2O content. Therefore, we chose a M_H value of 10, which intersects near the center of field of the observed peak assemblage (Figure 5.A1C).

The observed assemblage in the monazite bearing texture (GRM-37) from residual granulite sample Br03-56-2 is stable over a narrow range of M_H values, ranging from 3–5 (Figure 5.A1D). Assuming that neither free H_2O nor melt were present at peak conditions in this microdomain, we used a M_H value of 5 to calculate the P-T diagram (Figure 5.8D).

The stabilities of quartz and feldspars are not used to estimate the P-T conditions experienced by migmatitic paragneiss samples (see *Accuracy of P-T Estimates* above), and thus are not used to constrain the H_2O contents of these samples. Therefore, the only constraint for H_2O content in the muscovite-bearing paragneiss sample GR11-23 is the presence of muscovite and melt, which coexist at M_H values ranging from 9 to >20 (Figure 5.A1E). The presence of sillimanite and melt and absence of cordierite at peak conditions in the muscovite-free paragneiss sample GR11-25 indicates that M_H was >5.5 at peak conditions (Figure 5.A1F). We used a M_H value of 15 to calculate the P-T diagrams (Figure 5.9) for both paragneiss samples because this value intersects the field of the observed peak assemblage in sample GR11-23 and intersects fields that contain and lack free H_2O for sample GR11-25 (red shaded fields in Figure 5.A1F).

Figure Captions

Figure 5.1. Tectonic Map of the Central Alps (modified from Bousquet et al., 2012b). Ages from Bergell and Novate intrusions are from von Blanckenburg (1992) and Liati et al. (2000), respectively.

Figure 5.2. Geologic map of the Gruf Complex showing locations of samples used in this study (modified from Galli, 2010).

Figure 5.3. Sample photos: (A) Leucogranulite sample GR11-39. (B) Resdiual granulite sample Gruf100. (C) Muscovite-bearing migmatitic paragneiss sample GR11-23. (D) Muscovite-free migmatitic paragneiss sample GR11-25.

Figure 5.4. Scans of thin sections that were used in this study: (A) Leucogranulite sample GR11-39. (B) Resdiual granulite sample Gruf100, showing the location of the electron microprobe traverse used in Figure 5.7. (C) Residual granulite sample Br03-56-2. (D) Muscovite-bearing migmatitic paragneiss sample GR11-23. (E) Muscovite-free migmatitic paragneiss sample GR11-25.

Figure 5.5. Photomicrographs (colored) and backscattered electron (BSE) (black and white) images of textures in the granulites and paragneisses: (A) BSE image of garnet breakdown texture from leucogranulite sample GR11-39. (B) Photomicrograph from residual granulite sample Gruf100 showing embayment in garnet filled with prismatic sapphirine, sapphirine + orthopyroxene symplectites and quartz + feldspar, which represents crystallized melt. (C) Photomicrograph from residual granulite sample Gruf100 showing intergrown sapphirine and orthopyroxene porphyroblast separated from garnet by cordierite moat. Garnet is also fringed with orthopyroxene + cordierite symplectites. (D) Photomicrograph from residual granulite sample Gruf100 showing large sillimanite porphyroblast rimmed by sapphirine + spinel + cordierite symplectite, which is separated from orthopyroxene and biotite by a cordierite corona. (E) Photomicrograph from residual granulite sample Br03-56-2 showing a large sapphirine porphyroblast fringed by fine-grained spinel aggregates surrounded by cordierite, biotite, and

orthopyroxene. (F) BSE image of texture GRM-37 from residual granulite sample showing orthopyroxene, sapphirine, cordierite, and monazite. (G) Photomicrograph from muscovite-bearing migmatitic paragneiss sample GR11-23 showing typical leucosomes and melanosome, which consists of biotite, muscovite, sillimanite, and garnet. (H) Photomicrograph from muscovite-free migmatitic paragneiss sample GR11-25 showing typical leucosomes and melanosome, which consists of biotite, sillimanite, and aggregate of garnet porphyroblasts that are aligned subparallel to the foliation/gneissocity.

Figure 5.6. X-ray composition maps of the modeled reaction texture in the leucogranulite sample: (A) Relative Ca concentration. (B) Relative Mg concentration. (C) Relative Fe concentration. (D) Relative Mn concentration.

Figure 5.7. Chemical zoning profile of a large garnet porphyroblast from residual granulite sample Gruf100. The traverse location is shown in Figure 5.4B.

Figure 5.8. (A-D): Equilibrium phase diagrams calculated for granulite samples and reaction textures. (E) P-T diagram showing peak field and garnet compositional isopleths (X_{pyrope} and $X_{grossular}$) calculated for the garnet breakdown texture in leucogranulite sample GR11-39. The orange bar represents the range of measured compositions in the garnet. (F) P-T diagram with peak field and garnet volume percent isopleths for the garnet breakdown texture in leucogranulite sample GR11-39. The P-T path is drawn from the garnet compositional range from Figure 5.8E to the peak field, indicating a decrease of garnet volume during decompression and heating. (G) P-T diagram with peak field and garnet volume percent isopleths for the residual granulite sample

Gruf100. The starting point of the P-T path coincides with the maximum pressure starting point in Figure 5.8F, and the path is drawn to indicate a decrease in garnet volume during decompression and heating and continued nearly isothermal decompression through the stability field of the peak assemblage into the cordierite stability field. (H) P-T diagram with peak field and garnet volume percent isopleths for the residual granulite sample Br03-56-2. The P-T paths is drawn to indicate a decrease in garnet volume during decompression and heating to peak conditions. The starting point coincides with the maximum pressure starting point in Figure 5.8F. The P-T path also considers the growth of spinel after sapphirine and crosses into the cordierite stability field (see Figure 5.8C).

Figure 5.9. Equilibrium phase diagrams calculated for migmatitic paragneiss samples: (A) Muscovite-bearing paragneiss sample GR11-23. (B) Muscovite-free paragneiss sample GR11-25.

Figure 5.10. P-T diagram showing estimates of peak metamorphic conditions for the granulites and paragneisses and a composite P-T path for the granulites.

Figure 5.11. Diagrams showing modal abundance changes of selected minerals along the P-T path shown in Figure 5.10. (A) Leucogranulite GR11-39. (B) Residual granulite Gruf100. (C) Residual granulite Br03-56-2.

Figure 5.12. Pressure-temperature diagram showing the pressure-temperature-time evolution of the Gruf granulites and migmatitic paragneisses with schematic mineral reactions and structural events. Zr-in-rutile temperatures and U-Pb rutile age are from Oalmann et al. (submitted).

Monazite and zircon ages are from Oalmann et al. (in preparation-a) and Oalmann et al. (in preparation-b), respectively.

Figure 5.13. Schematic model for the geodynamic evolution of the Central Alps. (A) 40–36 Ma: subduction of Penninic units and Adula nappe. (B) ca. 34 Ma: UHT metamorphism of the Gruf lower crustal rocks following slab breakoff and exhumation of (U)HP Adula and Penninic nappes. (C) 30–27 Ma: amalgamation of the Gruf Complex closely following intrusion of the Bergell tonalite and granodiorite. (D) ca. 24 Ma: exhumation of the amalgamated Gruf Complex along the Insubric line, intrusion of the Novate leucogranite, slip along the Forcola Fault, and onset of continent-continent collision. The black harpoon symbols represent active slip on thrust faults, and the yellow harpoon symbol in panel D represents active slip along the normal-sense Forcola Fault.

Figure 5.A1: Temperature versus mole fraction hydrogen (M_H) phase diagrams calculated at 9 kbar pressure for granulite microtextures and samples (A–D) and at 6 kbar pressure for migmatitic paragneiss samples (E–F). The red-shaded fields correspond to the observed peak assemblages, and the thick, dashed lines correspond to the M_H values used to compute the P-T diagrams (Figure 8, 9).

References

Armstrong, J.T., 1995. CITZAF-a package of correction programs for the quantitative Electron Microbeam X-Ray-Analysis of thick polished materials, thin-films, and particles. Microbeam Analysis, 4(3): 177-200.

Becker, H., 1993. Garnet peridotite and eclogite Sm-Nd mineral ages from the Lepontine dome (Swiss Alps): New evidence for Eocene high-pressure metamorphism in the central Alps. Geology, 21(7): 599-602.

Beltrando, M., Lister, G.S., Rosenbaum, G., Richards, S., Forster, M.A., 2010. Recognizing episodic lithospheric thinning along a convergent plate margin: The example of the Early Oligocene Alps. Earth-Science Reviews, 103(3): 81-98.

Berger, A., Bousquet, R., 2008. Subduction-related metamorphism in the Alps: review of isotopic ages based on petrology and their geodynamic consequences. Geological Society, London, Special Publications, 298(1): 117-144.

Berger, A., Rosenberg, C., Schmid, S., 1996. Ascent, emplacement and exhumation of the Bergell pluton within the Southern Steep Belt of the Central Alps. Schweizerische mineralogische und petrographische Mitteilungen, 76(3): 357-382.

Blackburn, T., Shimizu, N., Bowring, S.A., Schoene, B., Mahan, K.H., 2012. Zirconium in rutile speedometry: New constraints on lower crustal cooling rates and residence temperatures. Earth and Planetary Science Letters, 317: 231-240.

Bousquet, R., Goffé, B., Vidal, O., Oberhänsli, R., Patriat, M., 2002. The tectono-metamorphic history of the Valaisan domain from the Western to the Central Alps: New constraints on the evolution of the Alps. Geological Society of America Bulletin, 114(2): 207-225.

Bousquet, R. et al., 2012a. Metamorphic Framework of the Alps, Commission for the Geological Map of the World, CCGM/CGMW.

Bousquet, R. et al., 2012b. Tectonic framework of the Alps, Commission for the Geological Map of the World, CCGM/CGMW.

Brouwer, F., Burri, T., Engi, M., Berger, A., 2005. Eclogite relics in the Central Alps: PT-evolution, Lu-Hf ages, and implications for formation of tectonic mélange zones. Schweizerische mineralogische und petrographische Mitteilungen, 85: 147-174.

Brown, M., 2006. Duality of thermal regimes is the distinctive characteristic of plate tectonics since the Neoarchean. Geology, 34(11): 961-964.

Brown, M., 2007. Metamorphic conditions in orogenic belts: a record of secular change. International Geology Review, 49(3): 193-234.

Burri, T., Berger, A., Engi, M., 2005. Tertiary migmatites in the Central Alps: Regional distribution, field relations, conditions of formation, and tectonic implications. Schweizerische mineralogische und petrographische Mitteilungen, 85(2-3): 215-232.

Carswell, D., O'Brien, P., 1993. Thermobarometry and geotectonic significance of high-pressure granulites: examples from the Moldanubian Zone of the Bohemian Massif in Lower Austria. Journal of Petrology, 34(3): 427-459.

Ciancaleoni, L., Marquer, D., 2006. Syn-extension leucogranite deformation during convergence in the Eastern Central Alps: example of the Novate intrusion. Terra Nova, 18(3): 170-180.

Clark, C., Fitzsimons, I.C., Healy, D., Harley, S.L., 2011. How does the continental crust get really hot? Elements, 7(4): 235-240.

Coggon, R., Holland, T., 2002. Mixing properties of phengitic micas and revised garnet-phengite thermobarometers. Journal of Metamorphic Geology, 20(7): 683-696.

Collins, W., 2002. Hot orogens, tectonic switching, and creation of continental crust. Geology, 30(6): 535-538.

Davidson, C., Rosenberg, C., Schmid, S., 1996. Symmagmatic folding of the base of the Bergell pluton, Central Alps. Tectonophysics, 265(3): 213-238.

De Capitani, C., 1994. Gleichgewichts-Phasendiagramme: Theorie und Software. Beiheft zun Deutschen Mineralogischen Gesellschaft, 6: 1-48.

De Capitani, C., Petrakakis, K., 2010. The computation of equilibrium assemblage diagrams with Theriak/Domino software. American Mineralogist, 95(7): 1006-1016.

Diener, J., Powell, R., 2012. Revised activity–composition models for clinopyroxene and amphibole. Journal of Metamorphic Geology, 30(2): 131-142.

Dobrzhinetskaya, L., Schweinehage, R., Massonne, H.J., Green, H., 2002. Silica precipitates in omphacite from eclogite at Alpe Arami, Switzerland: evidence of deep subduction. Journal of Metamorphic Geology, 20(5): 481-492.

Engi, M., Berger, A., Roselle, G.T., 2001. Role of the tectonic accretion channel in collisional orogeny. Geology, 29(12): 1143-1146.

Fitzsimons, I., Harley, S., 1994. The influence of retrograde cation exchange on granulite PT estimates and a convergence technique for the recovery of peak metamorphic conditions. Journal of Petrology, 35(2): 543-576.

Frey, M., Ferreiro Mählmann, R., 1999. Alpine metamorphism of the Central Alps. Schweizerische mineralogische und petrographische Mitteilungen, 79(1): 135-154.

Galli, A., 2010. Tectonometamorphic evolution of the Gruf Complex (Swiss and Italian Central Alps). PhD Thesis Thesis, ETH Zürich, Zürich, 164 pp.

Galli, A. et al., 2011. Granulites and charnockites of the Gruf Complex: Evidence for Permian ultra-high temperature metamorphism in the Central Alps. Lithos, 124(1-2): 17-45.

Galli, A. et al., 2012. U–Pb zircon dating of the Gruf Complex: disclosing the late Variscan granulitic lower crust of Europe stranded in the Central Alps. Contributions to Mineralogy and Petrology, 163: 353-378.

Galli, A., Le Bayon, B., Schmidt, M.W., Burg, J.-P., Reusser, E., 2013. Tectonometamorphic history of the Gruf complex (Central Alps): exhumation of a granulite–migmatite complex with the Bergell pluton. Swiss Journal of Geosciences, 106(1): 33-62.

Gebauer, D., 1996. A P-T-t path for an (Ultra?-) High-pressure ultramafic/mafic rock-association and its felsic country-rocks based on SHRIMP-dating of magmatic and metamorphic zircon domains. Example: Alpe Arami (Central Swiss Alps), Earth Processes: Reading the Isotopic Code. Geophys. Monogr. Ser. AGU, Washington, DC, pp. 307-329.

Gordon, S. et al., 2012. The thermal structure of continental crust in active orogens: insight from Miocene eclogite and granulite xenoliths of the Pamir Mountains. Journal of Metamorphic Geology, 30(4): 413-434.

Guevara, V., Caddick, M., 2016. Shooting at a moving target: phase equilibria modelling of high-temperature metamorphism. Journal of Metamorphic Geology, 34: 209-235.

Guillong, M., Hametner, K., Reusser, E., Wilson, S.A., Günther, D., 2005. Preliminary Characterisation of New Glass Reference Materials (GSA-1G, GSC-1G, GSD-1G and GSE-1G) by Laser Ablation-Inductively Coupled Plasma-Mass Spectrometry Using 193 nm, 213 nm and 266 nm Wavelengths. Geostandards and Geoanalytical Research, 29(3): 315-331.

Hacker, B.R. et al., 2000. Hot and dry deep crustal xenoliths from Tibet. Science, 287(5462): 2463-2466.

Hamilton, B.M., Pattison, D.R., 2010. Thermodynamic modelling of open-system behaviour for anatectic metapelites, GeoCanada 2010 – Working with the Earth.

Hamilton, B.M., Pattison, D.R., 2017. Crystallization of heterogeneous pelitic migmatites: insights from thermodynamic modelling. Journal of Petrology, in press.

Handy, M.R., Schmid, S.M., Bousquet, R., Kissling, E., Bernoulli, D., 2010. Reconciling plate-tectonic reconstructions of Alpine Tethys with the geological–geophysical record of spreading and subduction in the Alps. Earth-Science Reviews, 102(3): 121-158.

Harley, S., 2008. Refining the P–T records of UHT crustal metamorphism. Journal of Metamorphic Geology, 26(2): 125-154.

Harley, S.L., 1998. On the occurrence and characterization of ultrahigh-temperature crustal metamorphism. Geological Society, London, Special Publications, 138(1): 81-107.

Heinrich, C.A., 1986. Eclogite facies regional metamorphism of hydrous mafic rocks in the Central Alpine Adula Nappe. Journal of Petrology, 27(1): 123-154.

Hermann, J., Rubatto, D., Trommsdorff, V., 2006. Sub-solidus Oligocene zircon formation in garnet peridotite during fast decompression and fluid infiltration (Duria, Central Alps). Mineralogy and Petrology, 88(1): 181-206.

Holland, T., Powell, R., 1998. An internally consistent thermodynamic data set for phases of petrological interest. Journal of Metamorphic Geology, 16(3): 309-343.

Holland, T., Powell, R., 2003. Activity–composition relations for phases in petrological calculations: an asymmetric multicomponent formulation. Contributions to Mineralogy and Petrology, 145(4): 492-501.

Jochum, K.P., Willbold, M., Raczek, I., Stoll, B., Herwig, K., 2005. Chemical Characterisation of the USGS Reference Glasses GSA-1G, GSC-1G, GSD-1G, GSE-1G, BCR-2G, BHVO-2G and BIR-1G Using EPMA, ID-TIMS, ID-ICP-MS and LA-ICP-MS. Geostandards and Geoanalytical Research, 29(3): 285-302.

Johnson, D., Hooper, P., Conrey, R., 1999. XRF analysis of rocks and minerals for major and trace elements on a single low dilution Li-tetraborate fused bead. In: Le Bas, M. (Editor), Advances in X-ray Analysis, pp. 843–867.

Kelsey, D., White, R., Holland, T., Powell, R., 2004. Calculated phase equilibria in K2O-FeO-MgO-Al2O3-SiO2-H2O for sapphirine-quartz-bearing mineral assemblages. Journal of Metamorphic Geology, 22(6): 559-578.

Kelsey, D.E., 2008. On ultrahigh-temperature crustal metamorphism. Gondwana Research, 13(1): 1-29.

Kelsey, D.E., Hand, M., 2015. On ultrahigh temperature crustal metamorphism: phase equilibria, trace element thermometry, bulk composition, heat sources, timescales and tectonic settings. Geoscience Frontiers, 6(3): 311-356.

Kooijman, E., Smit, M., Mezger, K., Berndt, J., 2012. Trace element systematics in granulite facies rutile: implications for Zr geothermometry and provenance studies. Journal of Metamorphic Geology.

Krogh Ravna, E., Terry, M.P., 2004. Geothermobarometry of UHP and HP eclogites and schists–an evaluation of equilibria among garnet–clinopyroxene–kyanite–phengite–coesite/quartz. Journal of metamorphic Geology, 22(6): 579-592.

Liati, A., Gebauer, D., Fanning, M., 2000. U-PbSHRIMP dating of zircon from the Novate granite (Bergell, Central Alps): evidence for Oligocene-Miocene magmatism, Jurassic/Cretaceous continental rifting and opening of the Valais trough. Schweizerische mineralogische und petrographische Mitteilungen, 80(3): 305-316.

Luvizotto, G. et al., 2009. Rutile crystals as potential trace element and isotope mineral standards for microanalysis. Chemical Geology, 261(3): 346-369.

O'Brien, P., 2008. Challenges in high-pressure granulite metamorphism in the era of pseudosections: reaction textures, compositional zoning and tectonic interpretation with examples from the Bohemian Massif. Journal of Metamorphic Geology, 26(2): 235-251.

Oalmann, J., Möller, A., Bousquet, R., in preparation-a. Texturally controlled U-Pb monazite dating of sapphirine granulites from the Gruf Complex, Central Alps: Evidence for UHT metamorphism in a Cenozoic continent-continent collision.

Oalmann, J., Möller, A., Bousquet, R., submitted. Decoupling of Zr-thermometry and U-Pb thermochronology in rutile from the UHT granulites and charnockites of the Gruf Complex (Central Alps).

Oalmann, J., Möller, A., Bousquet, R., Savage, J., in preparation-b. Constraining the timing of UHT metamorphism, melt crystallization, and deformation with zircon geochronology and trace element geochemistry: The Gruf Complex, Central Alps.

Paton, C., Hellstrom, J., Paul, B., Woodhead, J., Hergt, J., 2011. Iolite: Freeware for the visualisation and processing of mass spectrometric data. J. Anal. At. Spectrom., 26(12): 2508-2518.

Pattison, D.R., Chacko, T., Farquhar, J., McFarlane, C.R., 2003. Temperatures of granulite-facies metamorphism: constraints from experimental phase equilibria and thermobarometry corrected for retrograde exchange. Journal of Petrology, 44(5): 867-900.

Pfiffner, O.A., 2016. Basement-involved thin-skinned and thick-skinned tectonics in the Alps. Geological Magazine: 1-25.

Pownall, J.M., Hall, R., Armstrong, R.A., Forster, M.A., 2014. Earth's youngest known ultrahigh-temperature granulites discovered on Seram, eastern Indonesia. Geology, 42(4): 279-282.

Rosenberg, C., 2004. Shear zones and magma ascent: a model based on a review of the Tertiary magmatism in the Alps. Tectonics, 23(3).

Rubatto, D., Hermann, J., Berger, A., Engi, M., 2009. Protracted fluid-induced melting during Barrovian metamorphism in the Central Alps. Contributions to Mineralogy and Petrology, 158(6): 703-722.

Samperton, K.M. et al., 2015. Magma emplacement, differentiation and cooling in the middle crust: Integrated zircon geochronological–geochemical constraints from the Bergell Intrusion, Central Alps. Chemical Geology, 417: 322-340.

Schefer, S., 2005. Metamorphose und Deformation im Gruf-Komplex, Val Codera, Italien, University of Basel, Basel.

Schmid, S.M., Pfiffner, O.-A., Froitzheim, N., Schönborn, G., Kissling, E., 1996. Geophysical-geological transect and tectonic evolution of the Swiss-Italian Alps. Tectonics, 15(5): 1036-1064.

Sizova, E., Gerya, T., Brown, M., Perchuk, L., 2010. Subduction styles in the Precambrian: insight from numerical experiments. Lithos, 116(3): 209-229.

Stampfli, G. et al., 1998. Subduction and obduction processes in the Swiss Alps. Tectonophysics, 296(1): 159-204.

Todd, C.S., Engi, M., 1997. Metamorphic field gradients in the Central Alps. Journal of Metamorphic Geology, 15(4): 513-530.

Trommsdorff, V., 1990. Metamorphism and tectonics in the Central Alps: The Alpine lithospheric mélange of Cima Lunga and Adula. Memorie della Società Geologica Italiana, 45: 39-49.

von Blanckenburg, F., 1992. Combined high-precision chronometry and geochemical tracing using accessory minerals: applied to the Central-Alpine Bergell intrusion (central Europe). Chemical Geology, 100(1-2): 19-40.

von Blanckenburg, F., Davies, J.H., 1995. Slab breakoff: a model for syncollisional magmatism and tectonics in the Alps. Tectonics, 14(1): 120-131.

Watson, E., Wark, D., Thomas, J., 2006. Crystallization thermometers for zircon and rutile. Contributions to Mineralogy and Petrology, 151(4): 413-433.

White, R., Pomroy, N., Powell, R., 2005. An in situ metatexite–diatexite transition in upper amphibolite facies rocks from Broken Hill, Australia. Journal of Metamorphic Geology, 23(7): 579-602.

White, R., Powell, R., Clarke, G., 2002. The interpretation of reaction textures in Fe-rich metapelitic granulites of the Musgrave Block, central Australia: constraints from mineral equilibria calculations in the system K2O–FeO–MgO–Al2O3–SiO2–H2O–TiO2–Fe2O3. Journal of metamorphic Geology, 20(1): 41-55.

White, R., Powell, R., Holland, T., 2007. Progress relating to calculation of partial melting equilibria for metapelites. Journal of Metamorphic Geology, 25(5): 511-527.

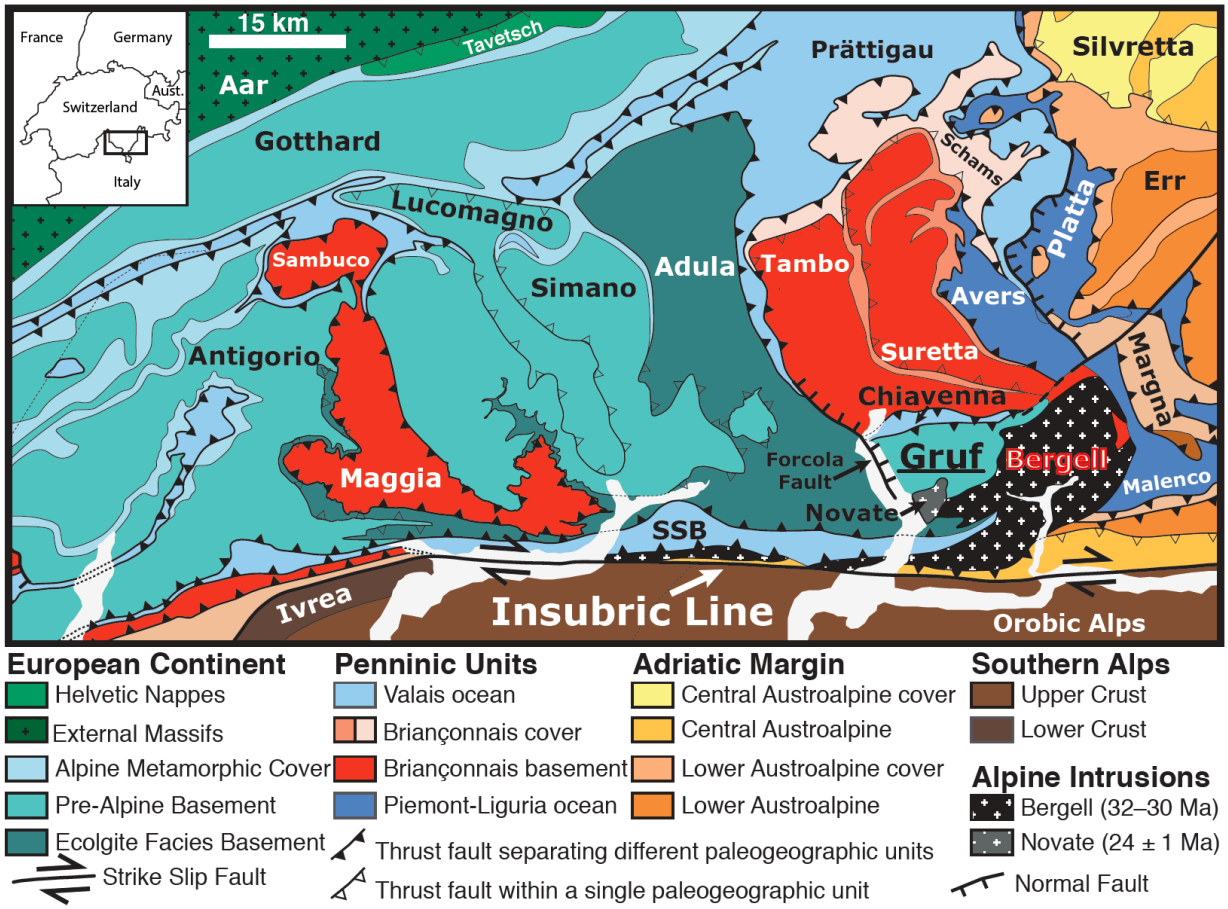
France
Germany
Aust.
Switzerland
Italy
15 km
Tavetsch
Aar
Gotthard
Lucomagno
Sambuco
Simano
Adula
Prättigau
Silvretta
Schams
Err
Platta
Tambo
Avers
Suretta
Margna
Antigorio
Chiavenna
Gruf
Bergell
Malenco
Forcola Fault
Maggia
Novate
SSB
Ivrea
Insubric Line
Orobic Alps
European Continent
Helvetic Nappes
External Massifs
Alpine Metamorphic Cover
Pre-Alpine Basement
Ecolgite Facies Basement
Strike Slip Fault
Penninic Units
Valais ocean
Briançonnais cover
Briançonnais basement
Piemont-Liguria ocean
Thrust fault separating different paleogeographic units
Thrust fault within a single paleogeographic unit
Adriatic Margin
Central Austroalpine cover
Central Austroalpine
Lower Austroalpine cover
Lower Austroalpine
Southern Alps
Upper Crust
Lower Crust
Alpine Intrusions
Bergell (32–30 Ma)
Novate (24 ± 1 Ma)
Normal Fault

Figure 5.1

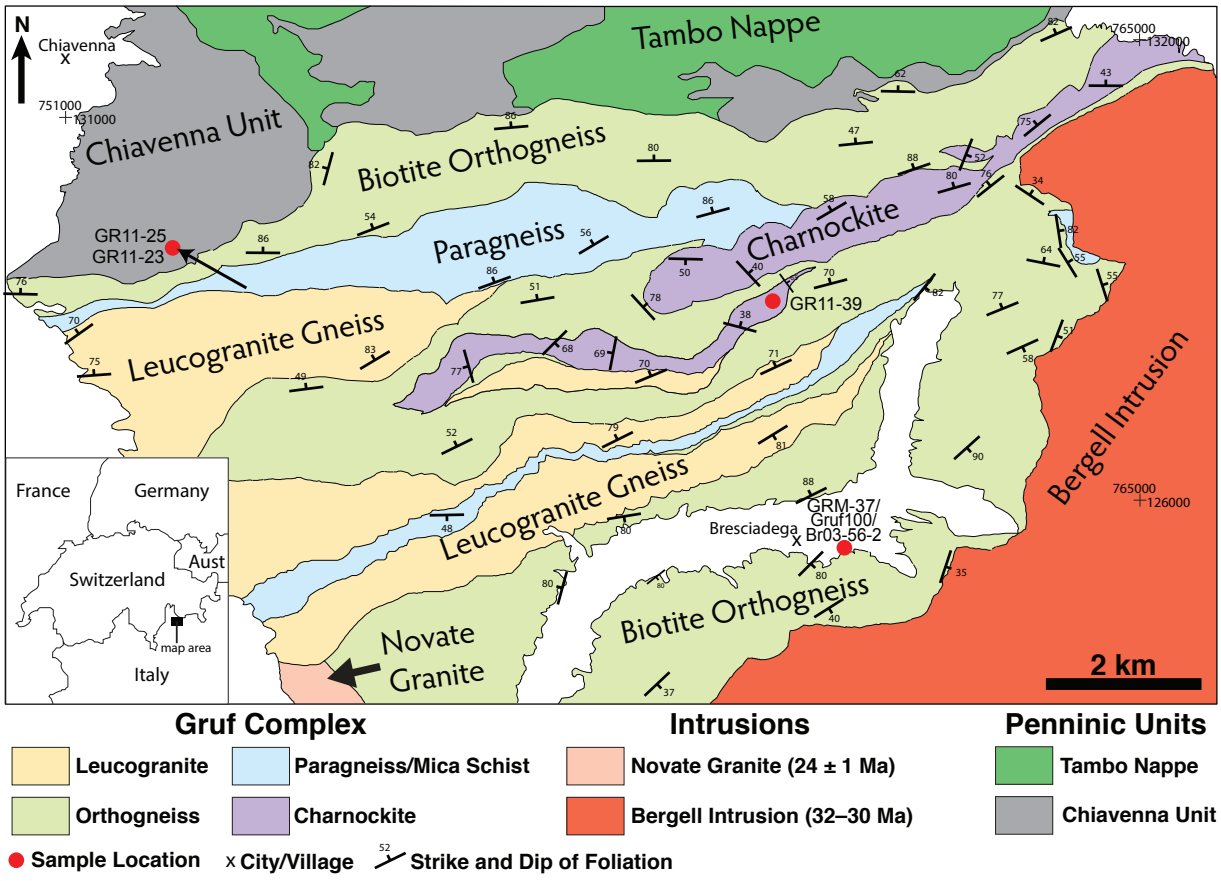
N
Chiavenna
751000
131000
Tambo Nappe
765000
132000
Chiavenna Unit
Biotite Orthogneiss
Paragneiss
Charnockite
GR11-25
GR11-23
GR11-39
Leucogranite Gneiss
Bergell Intrusion
765000
126000
France
Germany
Switzerland
Aust
map area
Italy
Leucogranite Gneiss
GRM-37/
Gruf100/
Br03-56-2
Bresciadega
Biotite Orthogneiss
Novate
Granite
2 km
Gruf Complex
Leucogranite
Paragneiss/Mica Schist
Orthogneiss
Charnockite
Sample Location
City/Village
Strike and Dip of Foliation
Intrusions
Novate Granite (24 ± 1 Ma)
Bergell Intrusion (32–30 Ma)
Penninic Units
Tambo Nappe
Chiavenna Unit

Figure 5.2

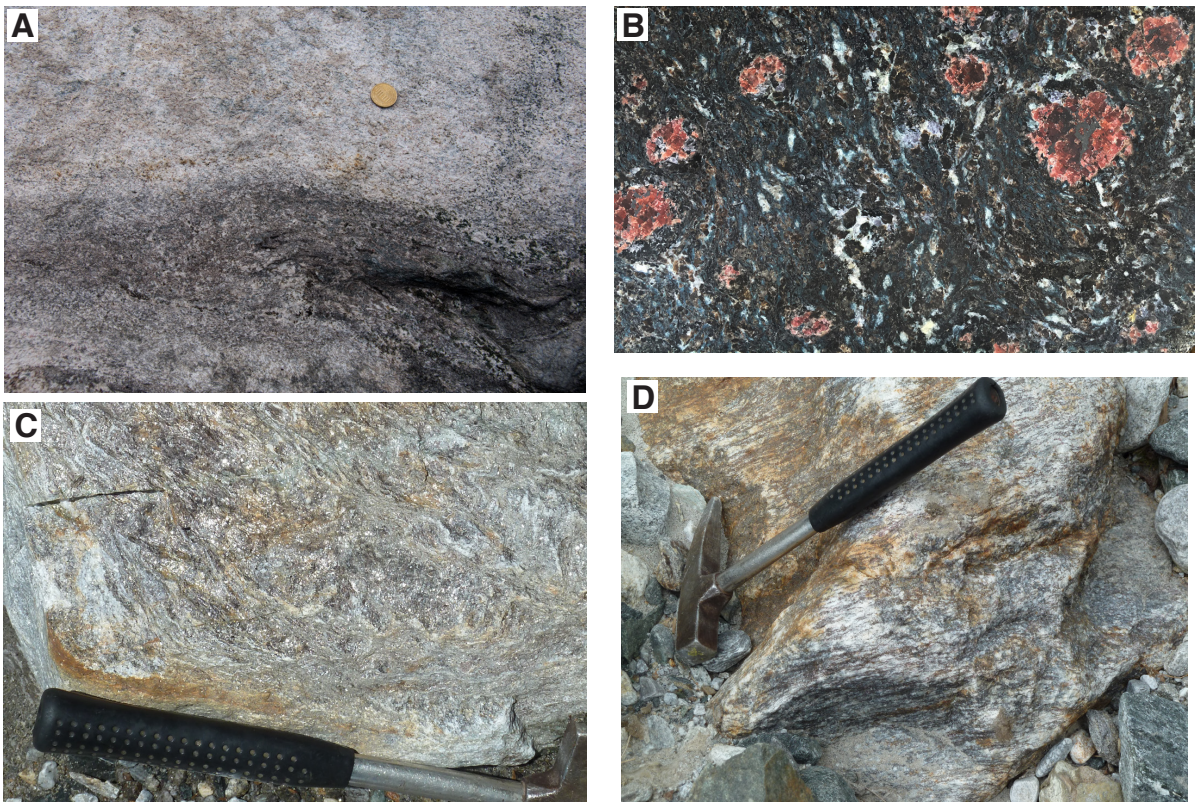

Figure 5.3

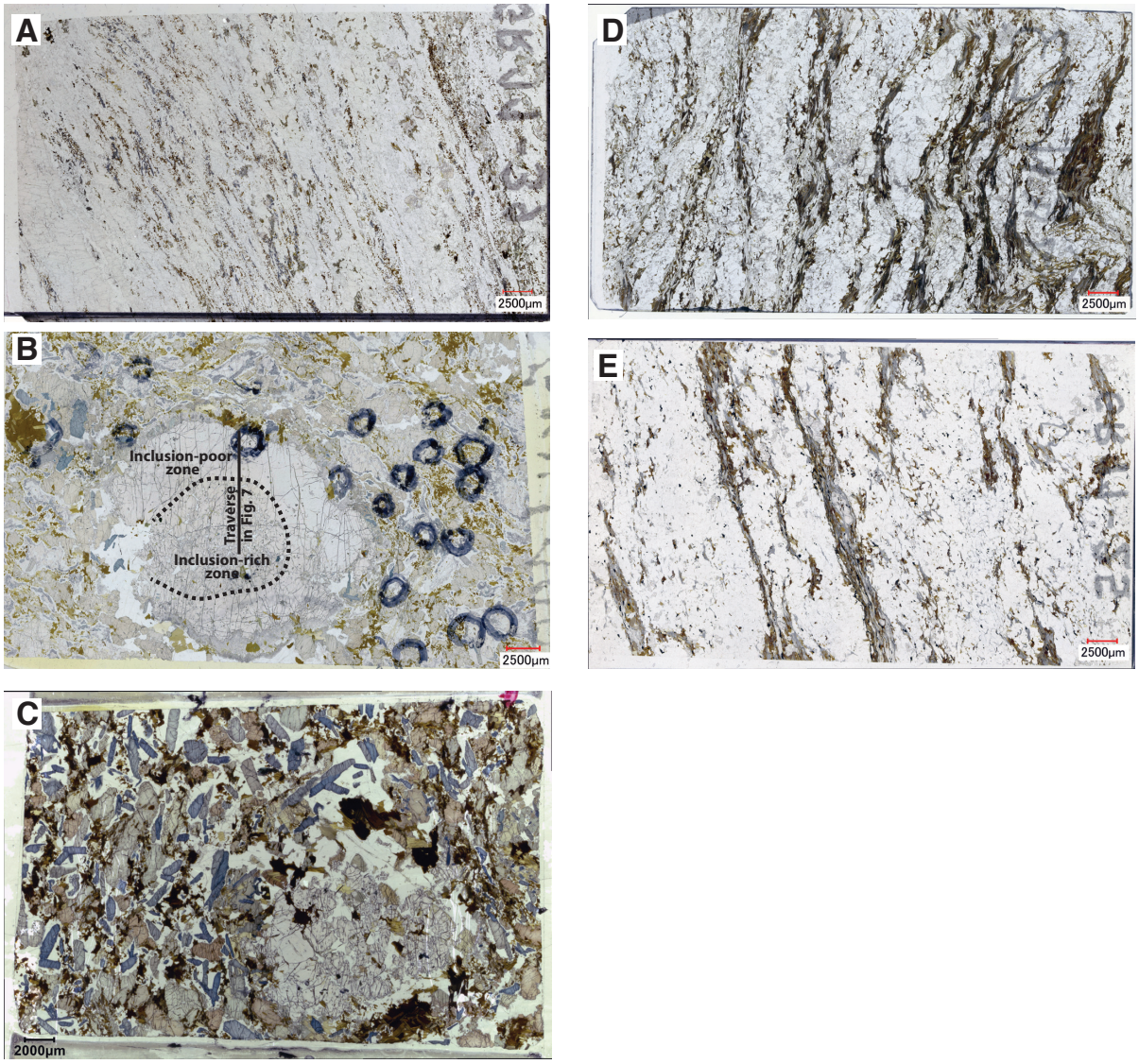
A
2500µm
D
2500µm
B
Inclusion-poor zone
Traverse in Fig. 7
Inclusion-rich zone
2500µm
E
2500µm
C
2000µm

Figure 5.4

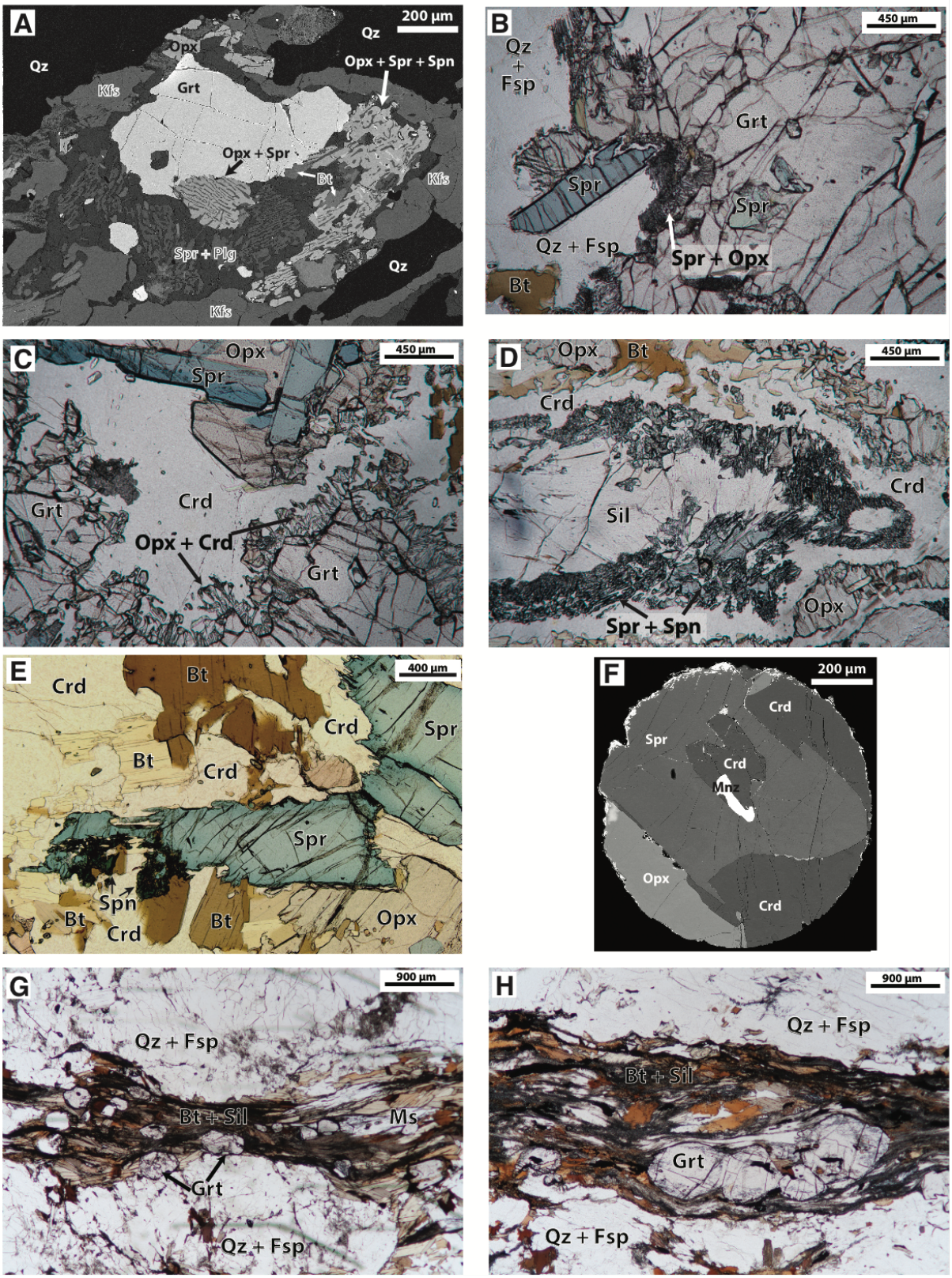
A
200 µm
Qz
Opx
Qz
Opx + Spr + Spn
Kfs
Grt
Opx + Spr
Bt
Kfs
Spr + Plg
Qz
Kfs
B
450 µm
Qz
+
Fsp
Grt
Spr
Spr
Qz + Fsp
Spr + Opx
Bt
C
450 µm
Opx
Spr
Grt
Crd
Opx + Crd
Grt
D
450 µm
Opx
Bt
Crd
Crd
Sil
Spr + Spn
Opx
E
400 µm
Crd
Bt
Crd
Spr
Bt
Crd
Spr
Spn
Bt
Crd
Bt
Opx
F
200 µm
Crd
Spr
Crd
Mnz
Opx
Crd
G
900 µm
Qz + Fsp
Bt + Sil
Ms
Grt
Qz + Fsp
H
900 µm
Qz + Fsp
Bt + Sil
Grt
Qz + Fsp

Figure 5.5

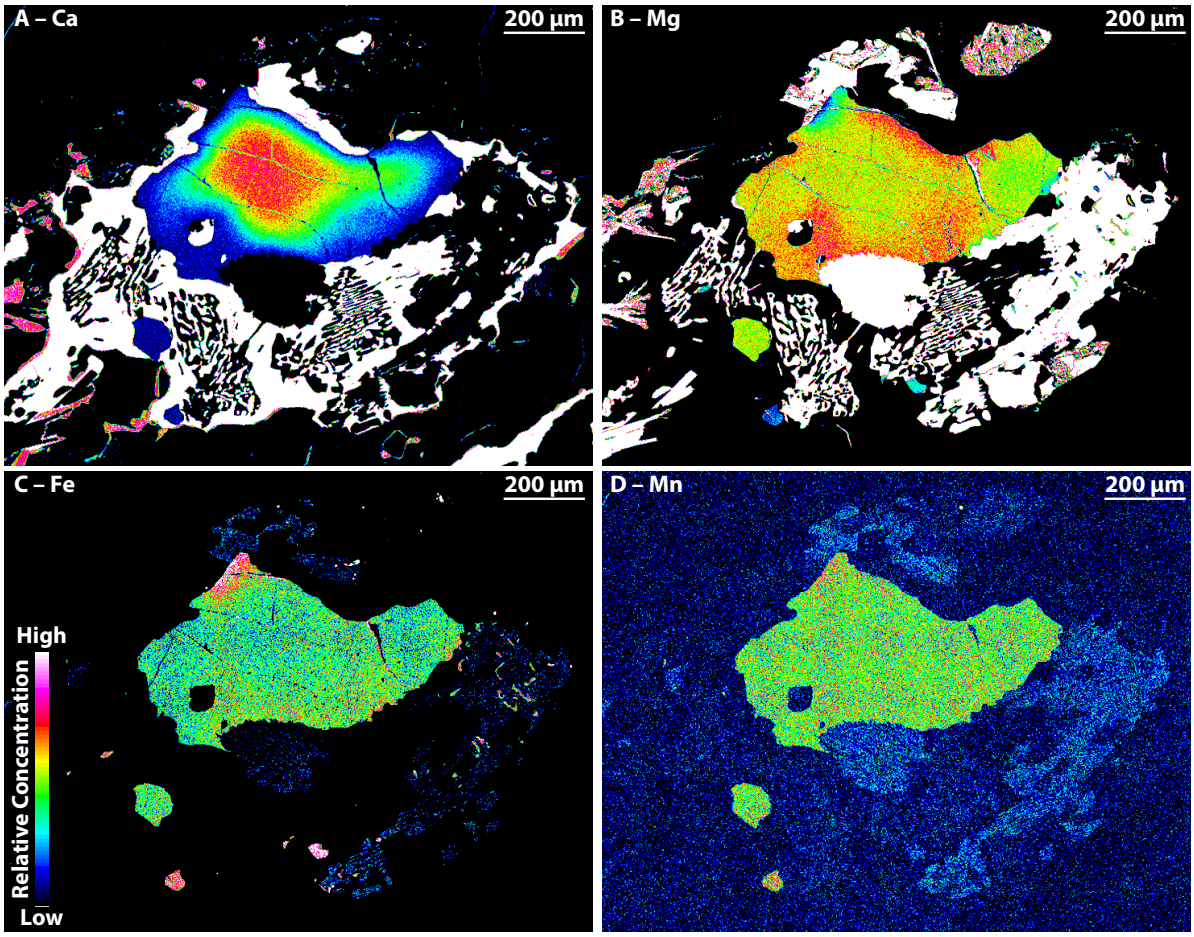
A – Ca
200 µm
B – Mg
200 µm
C – Fe
200 µm
High
Relative Concentration
Low
D – Mn
200 µm

Figure 5.6

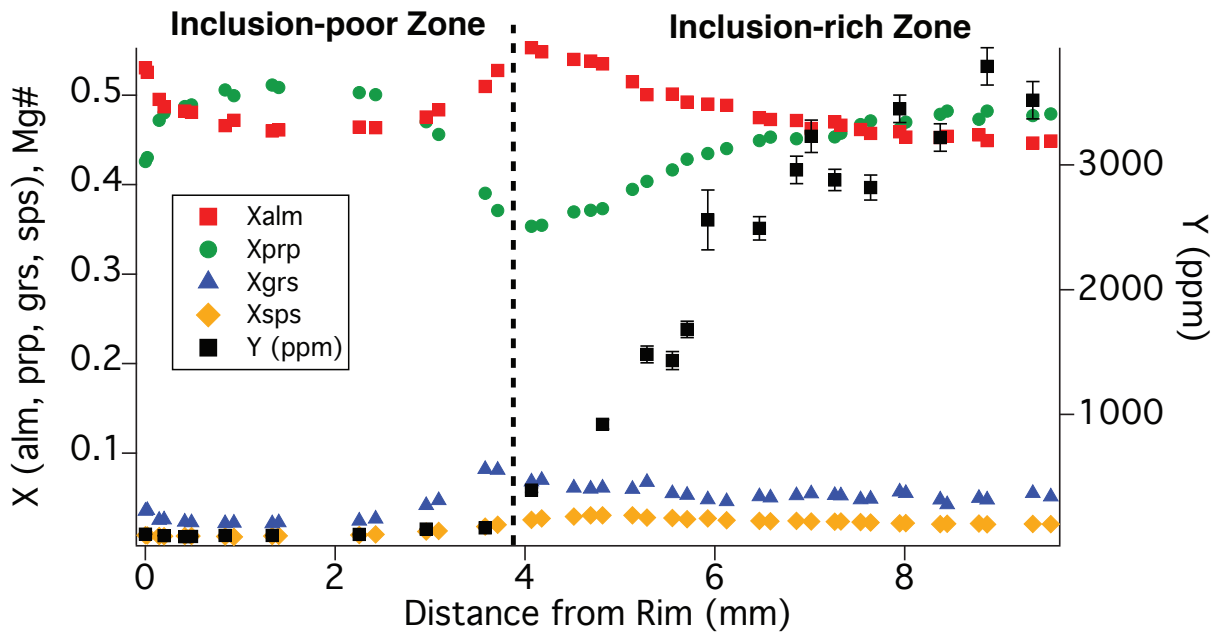
Inclusion-poor Zone
Inclusion-rich Zone
X (alm, prp, grs, sps), Mg#
Y (ppm)
Xalm
Xprp
Xgrs
Xsps
Y (ppm)
0.5
0.4
0.3
0.2
0.1
3000
2000
1000
0
2
4
6
8
Distance from Rim (mm)

Figure 5.7

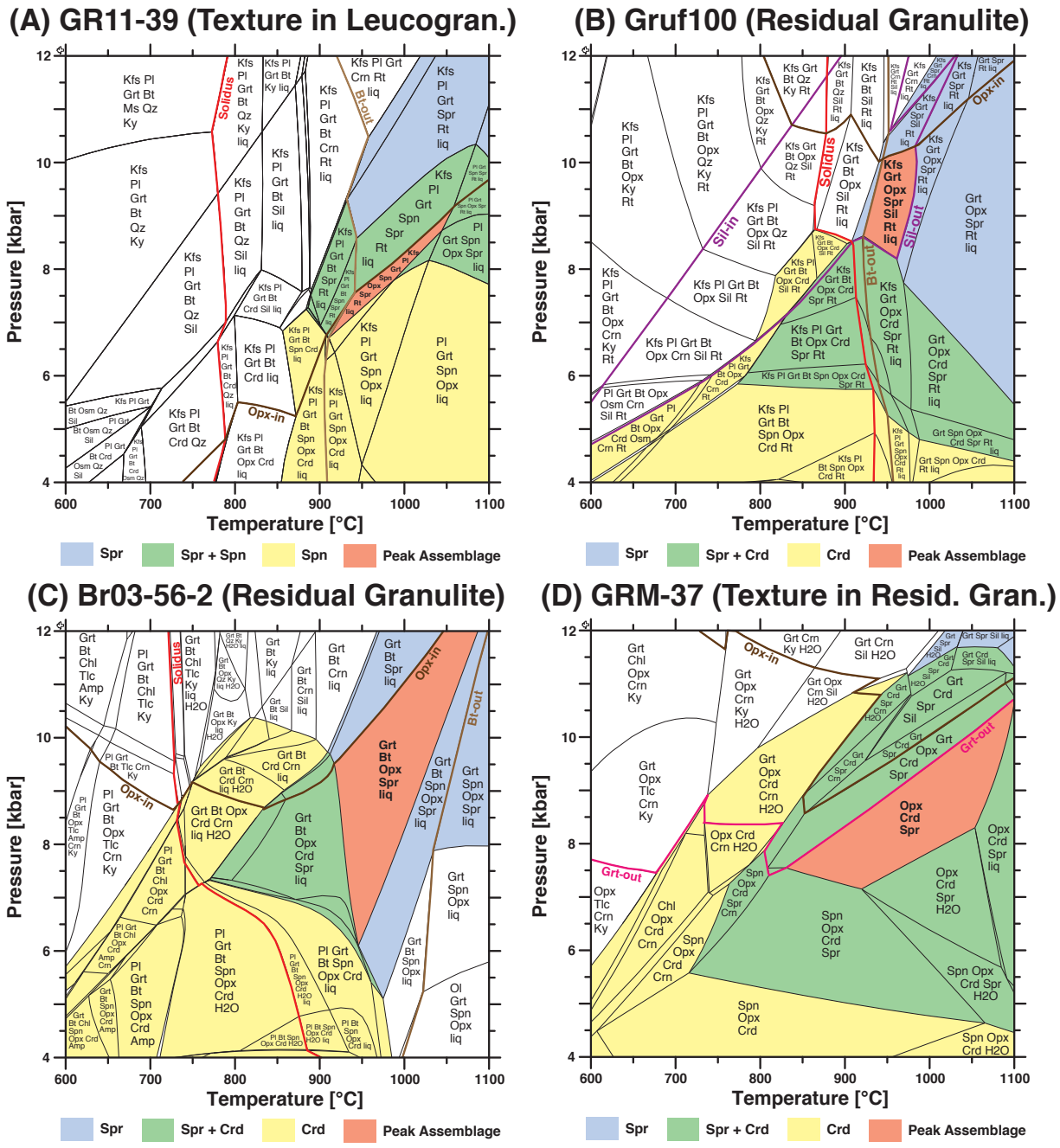
(A) GR11-39 (Texture in Leucogran.)
(B) Gruf100 (Residual Granulite)
(C) Br03-56-2 (Residual Granulite)
(D) GRM-37 (Texture in Resid. Gran.)
Pressure [kbar]
Temperature [°C]
Solidus
Bt-out
Opx-in
Sil-in
Sil-out
Grt-out
Spr
Spr + Spn
Spn
Spr + Crd
Crd
Peak Assemblage

Figure 5.8

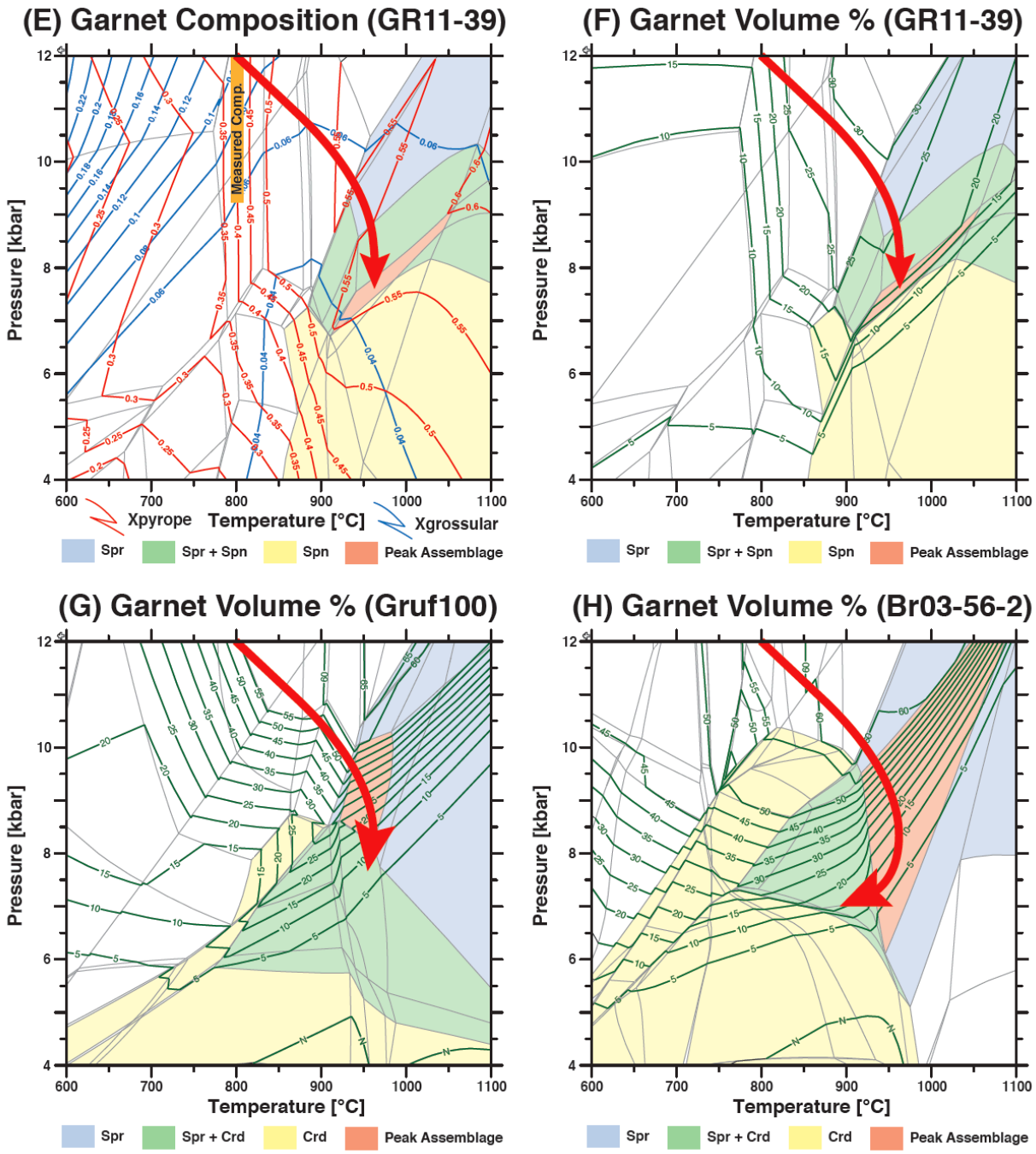

Figure 5.8 (continued)

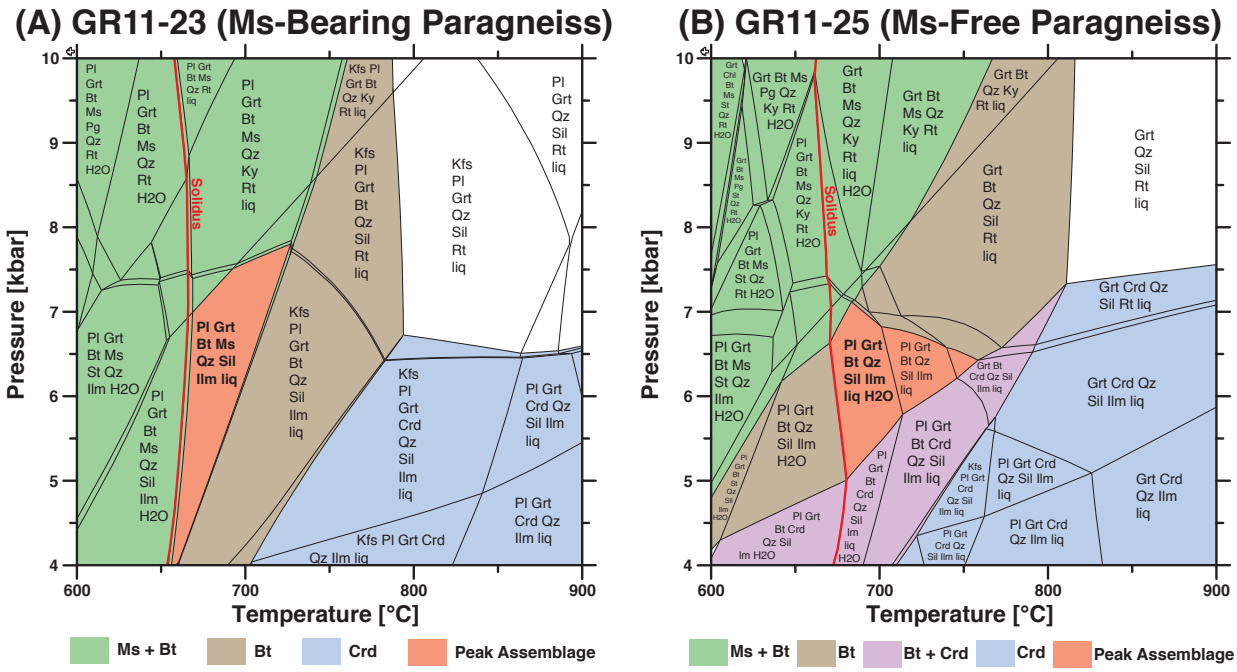
(A) GR11-23 (Ms-Bearing Paragneiss)
(B) GR11-25 (Ms-Free Paragneiss)
Pressure [kbar]
Temperature [°C]
Solidus
Pl Grt Bt Ms St Qz Ilm H2O
Pl Grt Bt Ms Qz Sil Ilm liq
Kfs Pl Grt Bt Qz Sil Ilm liq
Kfs Pl Grt Crd Qz Sil Ilm liq
Pl Grt Crd Qz Ilm liq
Kfs Pl Grt Crd Qz Ilm liq
Pl Grt Bt Qz Sil Ilm H2O
Pl Grt Bt Qz Sil Ilm liq H2O
Grt Crd Qz Sil Rt liq
Grt Crd Qz Sil Ilm liq
Grt Crd Qz Ilm liq
Ms + Bt
Bt
Bt + Crd
Crd
Peak Assemblage

Figure 5.9

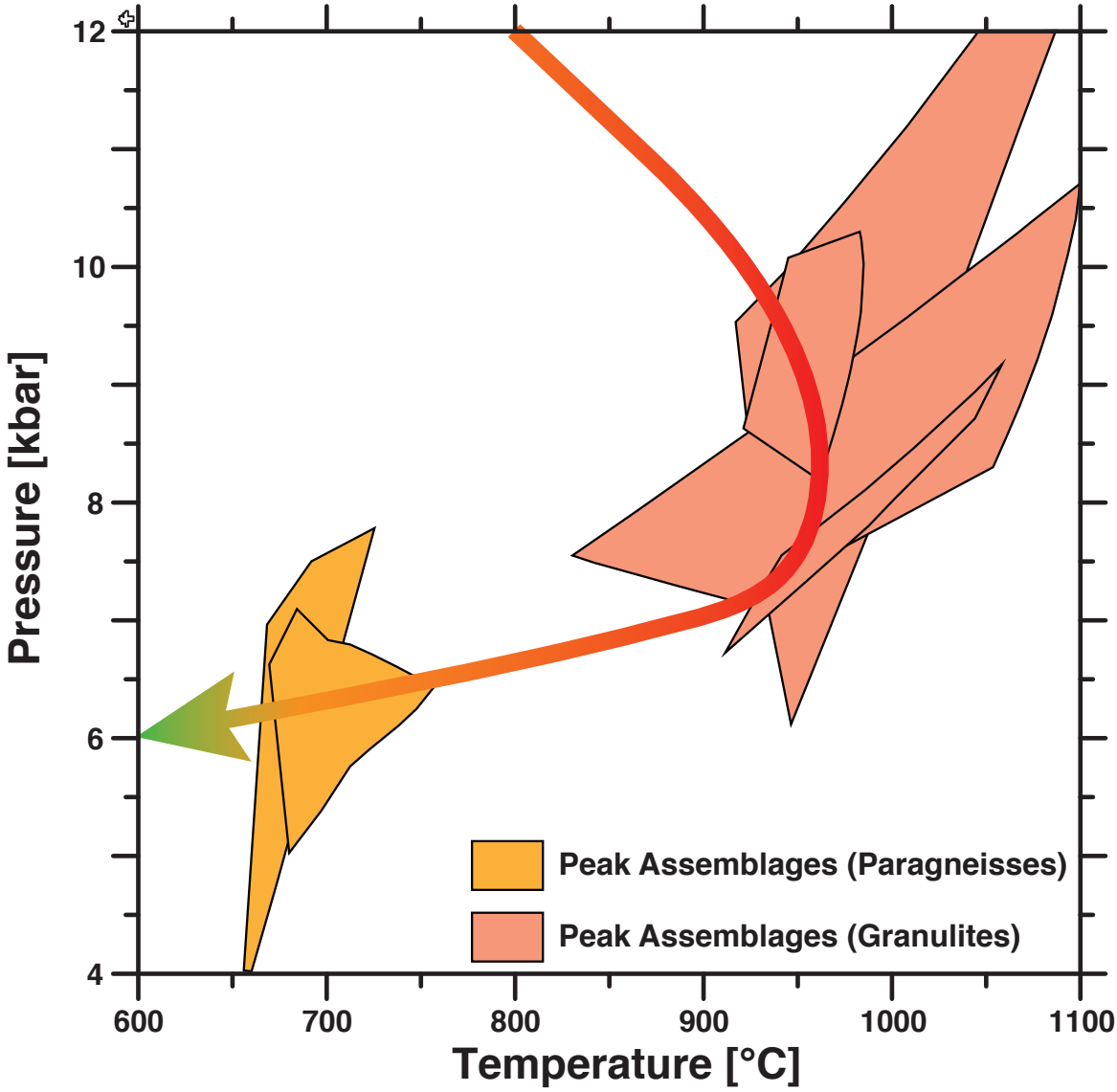
Pressure [kbar]
12
10
8
6
4
600
700
800
900
1000
1100
Temperature [°C]
Peak Assemblages (Paragneisses)
Peak Assemblages (Granulites)

Figure 5.10

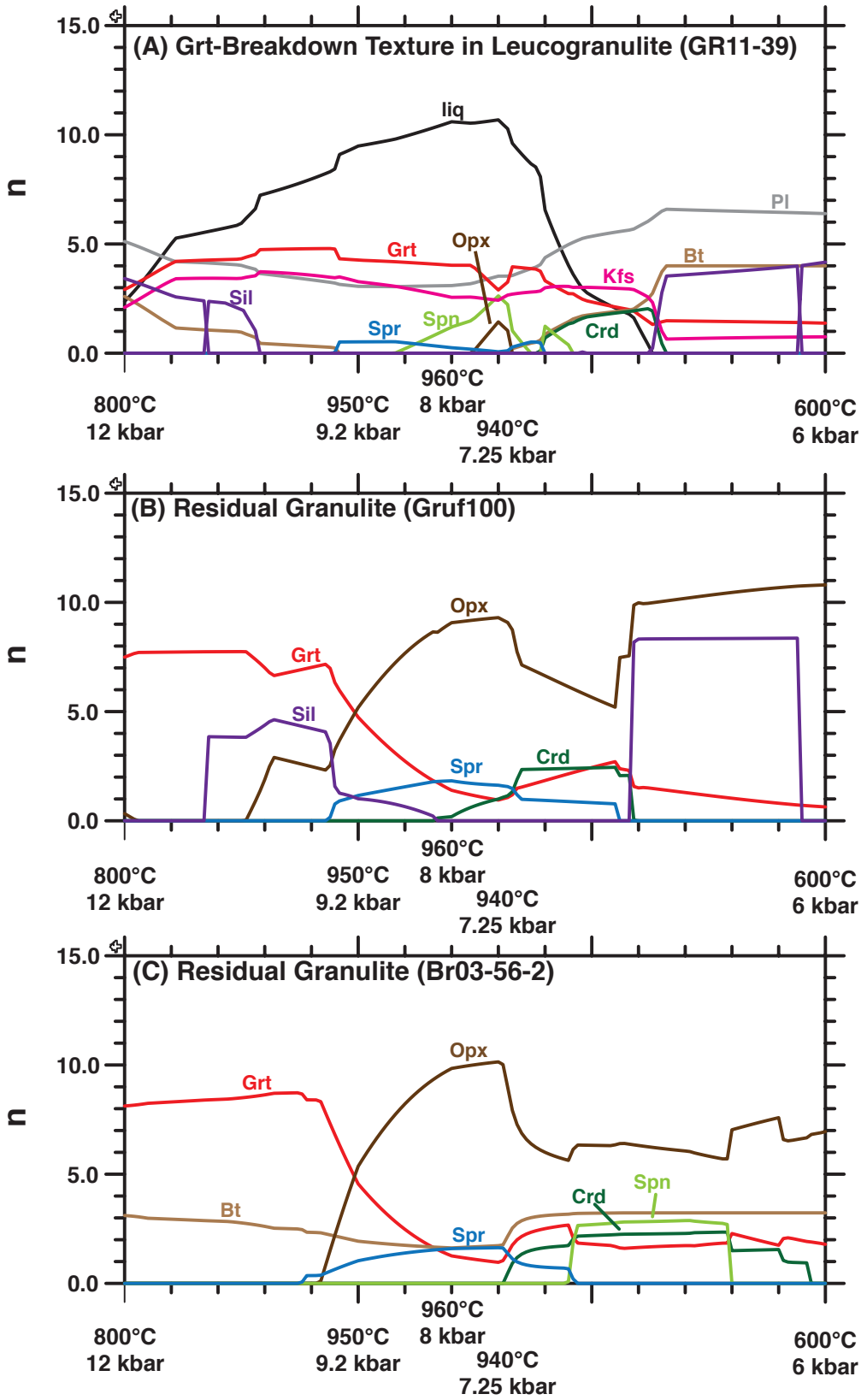
(A) Grt-Breakdown Texture in Leucogranulite (GR11-39)
n
15.0
10.0
5.0
0.0
liq
Pl
Grt
Opx
Bt
Kfs
Sil
Spr
Spn
Crd
800°C
12 kbar
950°C
9.2 kbar
960°C
8 kbar
940°C
7.25 kbar
600°C
6 kbar
(B) Residual Granulite (Gruf100)
Opx
Grt
Sil
Spr
Crd
(C) Residual Granulite (Br03-56-2)
Opx
Grt
Bt
Spr
Crd
Spn

Figure 5.11

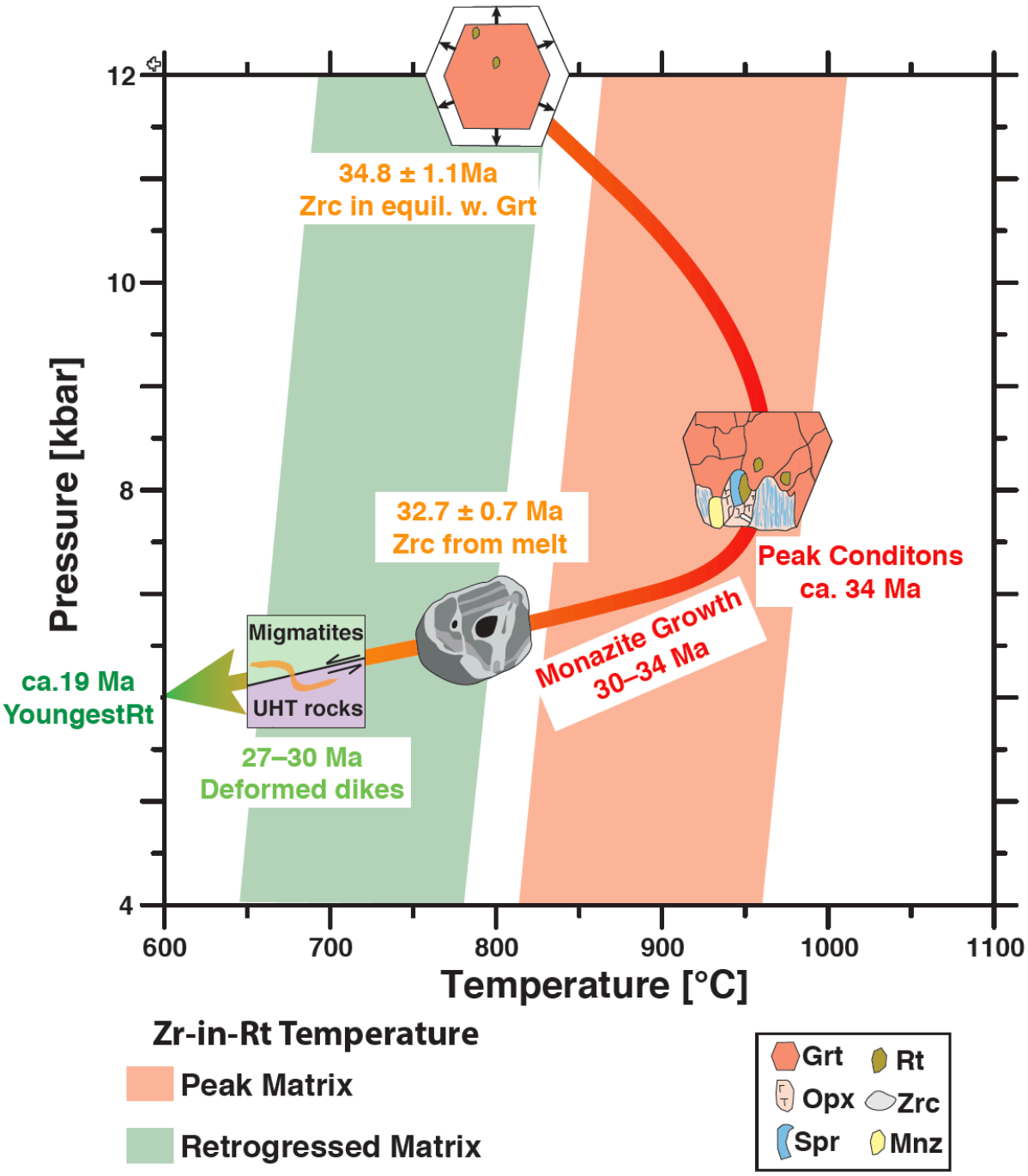
12
10
8
4
Pressure [kbar]
600
700
800
900
1000
1100
Temperature [°C]
34.8 ± 1.1Ma
Zrc in equil. w. Grt
32.7 ± 0.7 Ma
Zrc from melt
Peak Conditons
ca. 34 Ma
Monazite Growth
30–34 Ma
Migmatites
UHT rocks
ca.19 Ma
YoungestRt
27–30 Ma
Deformed dikes
Zr-in-Rt Temperature
Peak Matrix
Retrogressed Matrix
Grt
Rt
Opx
Zrc
Spr
Mnz

Figure 5.12

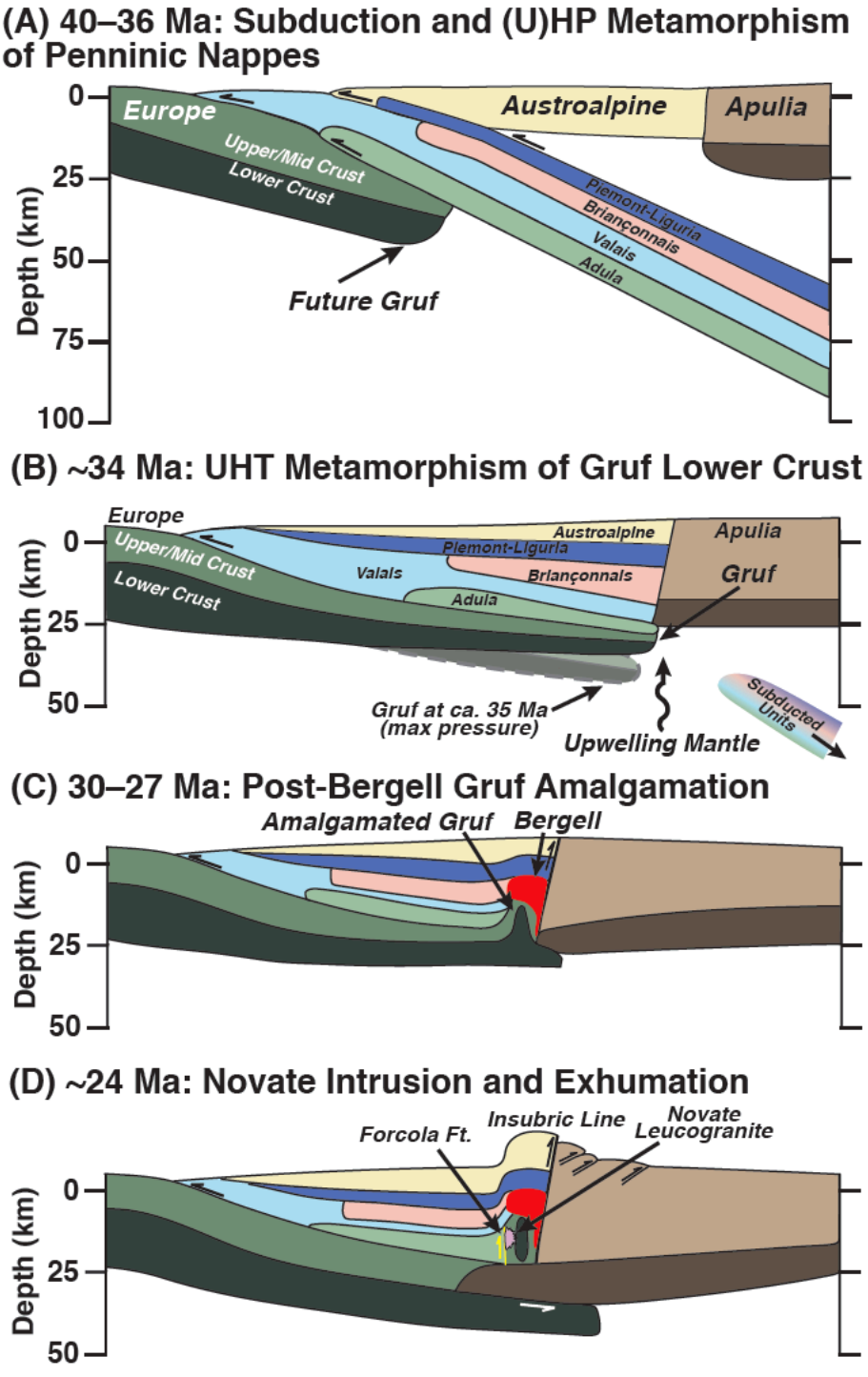
(A) 40–36 Ma: Subduction and (U)HP Metamorphism of Penninic Nappes
Depth (km)
0
25
50
75
100
Europe
Upper/Mid Crust
Lower Crust
Austroalpine
Apulia
Piemont-Liguria
Briançonnais
Valais
Adula
Future Gruf
(B) ~34 Ma: UHT Metamorphism of Gruf Lower Crust
Depth (km)
0
25
50
Europe
Upper/Mid Crust
Lower Crust
Valais
Austroalpine
Piemont-Liguria
Briançonnais
Adula
Apulia
Gruf
Gruf at ca. 35 Ma
(max pressure)
Upwelling Mantle
Subducted Units
(C) 30–27 Ma: Post-Bergell Gruf Amalgamation
Amalgamated Gruf
Bergell
Depth (km)
0
25
50
(D) ~24 Ma: Novate Intrusion and Exhumation
Forcola Ft.
Insubric Line
Novate Leucogranite
Depth (km)
0
25
50

Figure 5.13

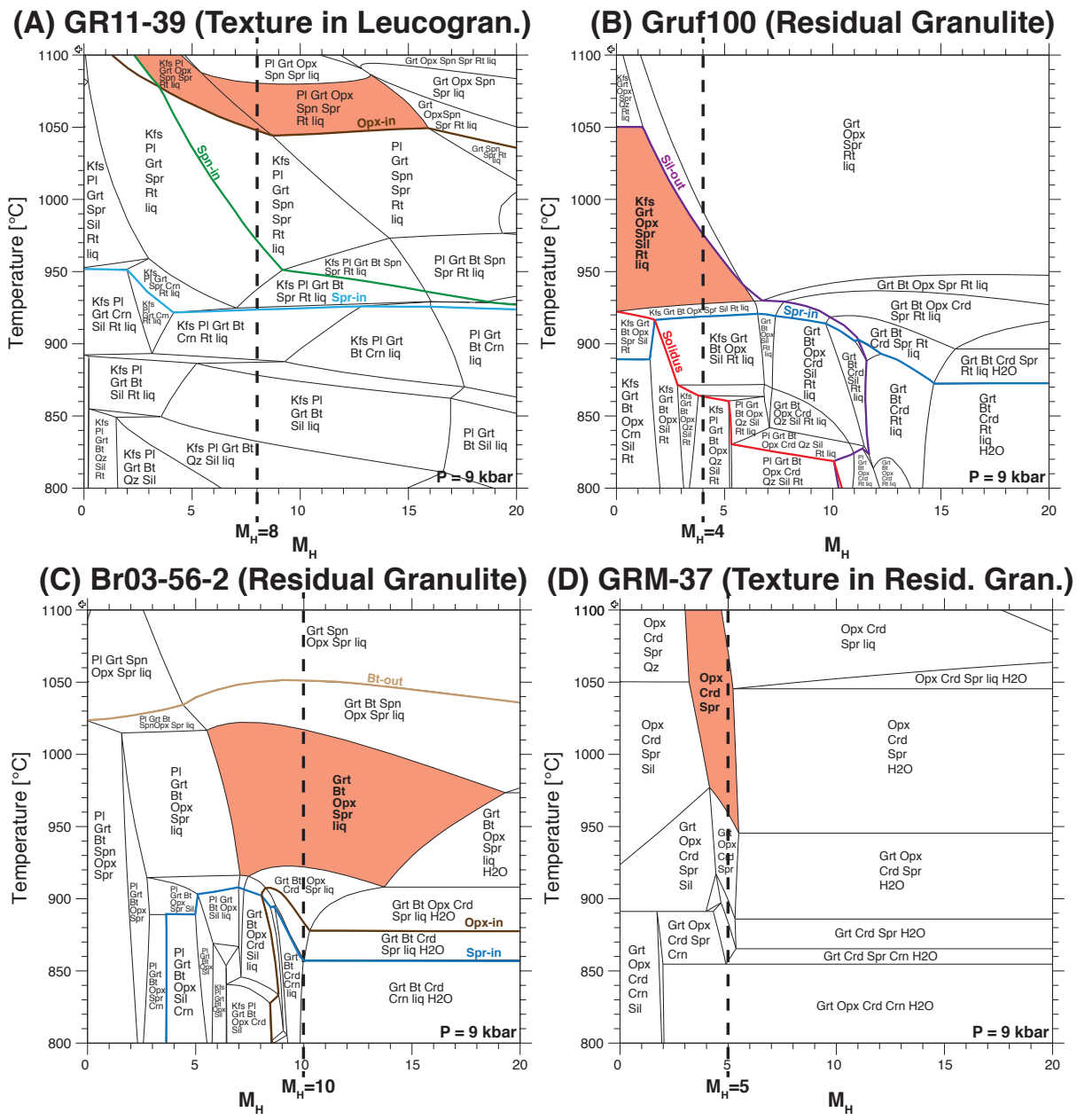
(A) GR11-39 (Texture in Leucogran.)
(B) Gruf100 (Residual Granulite)
(C) Br03-56-2 (Residual Granulite)
(D) GRM-37 (Texture in Resid. Gran.)
Temperature [°C]
M_H
M_H=8
M_H=4
M_H=10
M_H=5
P = 9 kbar
Spn-in
Opx-in
Spr-in
Sil-out
Solidus
Bt-out

Figure 5.A1

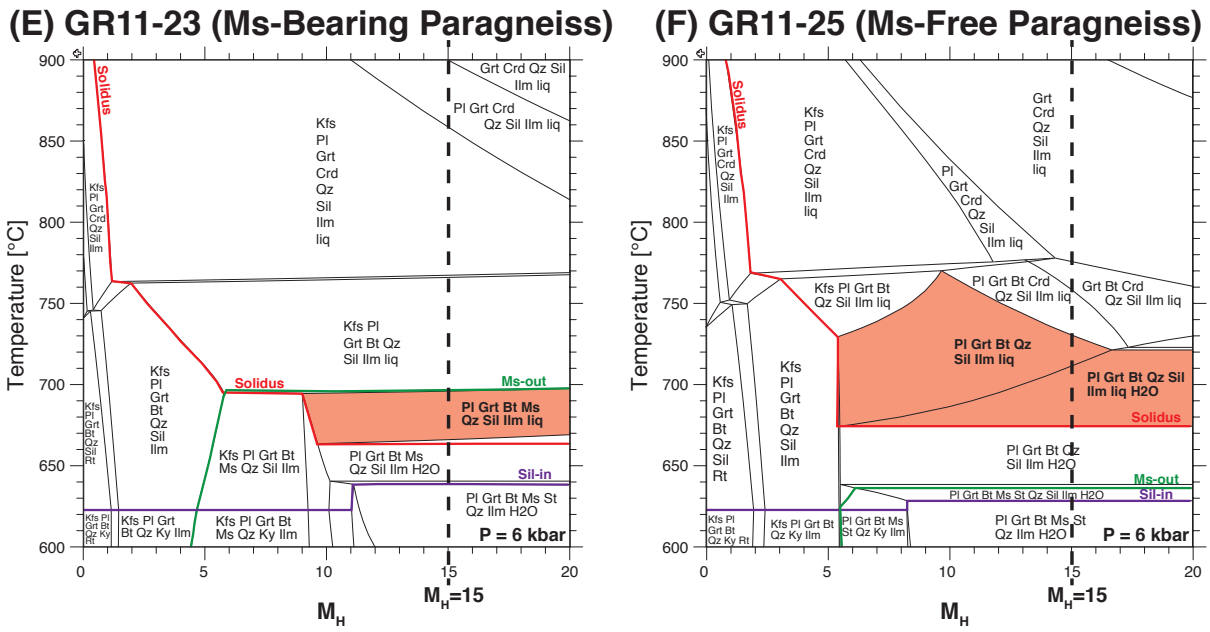

Figure 5.A1 (continued)

Table 5.1: Major and trace element data from minerals.

Sample and Analysis Number	Al2O3	TiO2	K2O	Na2O	Cr2O3	SiO2	FeO	CaO	MgO	MnO	Total	Al (mol)	Fe (mol)	Mg (mol)	Ca (mol)	Mn (mol)	Na (mol)	K (mol)	Grt Xal	Grt Xpr	Grt Xgr	Grt Xsp	Grt Xgs	Pig Xan	Opx Xmgts	Mg No.	Zr (ppm)	±2SE (ppm)	Y (ppm)	± 2SE (ppm)
Garnet-breakdown Texture from Leucogranulite (GR11-39)																														
Garnet																														
GR11-39_Grt1A-1	22.26	0.00	0.00	0.01	0.00	38.61	28.24	1.03	8.83	0.52	99.50	0.22	0.39	0.22	0.02	0.01	0.00	0.00	0.62	0.34	0.03	0.01	-	-	0.36	-	-	-	-
GR11-39_Grt1A-2	22.26	0.09	0.00	0.03	0.03	39.08	26.67	1.36	9.72	0.44	99.69	0.22	0.37	0.24	0.02	0.01	0.00	0.00	0.58	0.38	0.04	0.01	-	-	0.39	-	-	-	-
GR11-39_Grt1A-3	22.09	0.14	0.00	0.00	0.02	39.61	24.69	2.71	10.55	0.37	100.18	0.22	0.34	0.26	0.05	0.01	0.00	0.00	0.52	0.40	0.07	0.01	-	-	0.43	-	-	-	-
GR11-39_Grt1A-4	22.07	0.18	0.00	0.03	0.00	39.70	23.15	3.99	10.69	0.40	100.21	0.22	0.32	0.27	0.07	0.01	0.00	0.00	0.49	0.40	0.11	0.01	-	-	0.45	-	-	-	-
GR11-39_Grt1A-5	22.35	0.26	0.00	0.02	0.02	39.87	23.06	4.04	10.66	0.35	100.63	0.22	0.32	0.26	0.07	0.00	0.00	0.00	0.48	0.40	0.11	0.01	-	-	0.45	-	-	-	-
GR11-39_Grt1A-6	22.35	0.08	0.00	0.03	0.02	39.69	23.58	3.39	10.54	0.41	100.08	0.22	0.33	0.26	0.06	0.01	0.00	0.00	0.50	0.40	0.09	0.01	-	-	0.44	-	-	-	-
GR11-39_Grt1A-7	22.24	0.04	0.01	0.01	0.02	39.85	24.04	2.22	11.01	0.40	99.84	0.22	0.33	0.27	0.04	0.01	0.00	0.00	0.51	0.42	0.06	0.01	-	-	0.45	-	-	-	-
GR11-39_Grt1A-8	22.65	0.08	0.00	0.01	0.00	39.80	24.97	1.26	11.58	0.43	100.78	0.22	0.35	0.29	0.02	0.01	0.00	0.00	0.52	0.43	0.03	0.01	-	-	0.45	-	-	-	-
GR11-39_Grt1A-9	22.53	0.00	0.00	0.02	0.02	39.54	24.64	1.04	11.49	0.41	99.70	0.22	0.34	0.29	0.02	0.01	0.00	0.00	0.53	0.44	0.03	0.01	-	-	0.45	-	-	-	-
GR11-39_Grt1A-10	22.46	0.03	0.01	0.01	0.00	39.85	23.94	1.43	11.60	0.41	99.73	0.22	0.33	0.29	0.03	0.01	0.00	0.00	0.51	0.44	0.04	0.01	-	-	0.46	-	-	-	-
GR11-39_Grt1A-11	22.53	0.08	0.00	0.02	0.02	39.81	24.35	2.18	11.37	0.41	100.77	0.22	0.34	0.28	0.04	0.01	0.00	0.00	0.51	0.42	0.06	0.01	-	-	0.45	-	-	-	-
GR11-39_Grt1A-12	22.32	0.07	0.00	0.04	0.03	39.54	23.38	3.80	10.62	0.40	100.19	0.22	0.33	0.26	0.07	0.01	0.00	0.00	0.49	0.40	0.10	0.01	-	-	0.45	-	-	-	-
GR11-39_Grt1A-13	22.28	0.10	0.00	0.03	0.00	39.74	23.35	3.92	10.63	0.43	100.48	0.22	0.33	0.26	0.07	0.01	0.00	0.00	0.49	0.40	0.11	0.01	-	-	0.45	-	-	-	-
GR11-39_Grt1A-14	22.28	0.09	0.00	0.02	0.02	39.89	23.62	3.28	10.94	0.35	100.50	0.22	0.33	0.27	0.06	0.00	0.00	0.00	0.50	0.41	0.09	0.01	-	-	0.45	-	-	-	-
GR11-39_Grt1A-15	22.79	0.00	0.00	0.04	0.02	39.61	23.99	2.27	11.26	0.42	100.38	0.22	0.33	0.28	0.04	0.01	0.00	0.00	0.51	0.42	0.06	0.01	-	-	0.46	-	-	-	-
GR11-39_Grt1A-16	22.58	0.00	0.00	0.02	0.00	39.89	24.79	1.92	11.27	0.43	100.90	0.22	0.35	0.28	0.03	0.01	0.00	0.00	0.52	0.42	0.05	0.01	-	-	0.45	-	-	-	-
GR11-39_Grt1A-17	22.33	0.02	0.00	0.01	0.01	39.66	24.70	2.05	11.58	0.45	100.80	0.22	0.35	0.29	0.04	0.01	0.00	0.00	0.53	0.41	0.06	0.01	-	-	0.44	-	-	-	-
GR11-39_Grt1A-18	22.48	0.02	0.00	0.00	0.00	39.73	25.05	2.08	11.86	0.39	101.60	0.22	0.35	0.27	0.04	0.01	0.00	0.00	0.53	0.41	0.06	0.01	-	-	0.44	-	-	-	-
GR11-39_Grt1A-19	22.31	0.05	0.02	0.04	0.01	39.81	25.43	1.47	10.87	0.43	100.39	0.22	0.35	0.27	0.03	0.01	0.00	0.00	0.54	0.41	0.04	0.01	-	-	0.43	-	-	-	-
GR11-39_Grt1A-20	22.54	0.00	0.01	0.00	0.00	39.74	25.56	1.08	10.96	0.42	100.31	0.22	0.36	0.27	0.02	0.01	0.00	0.00	0.54	0.42	0.03	0.01	-	-	0.43	-	-	-	-
GR11-39_Grt1A-21	22.77	0.00	0.00	0.02	0.01	40.07	25.10	1.05	10.87	0.48	100.37	0.22	0.35	0.27	0.02	0.01	0.00	0.00	0.54	0.42	0.03	0.01	-	-	0.44	-	-	-	-
Orthopyroxene																														
GR11-39_Opx1A-1	8.69	0.20	0.00	0.02	0.00	49.49	18.29	0.05	23.14	0.08	99.96	0.09	0.25	0.57	0.00	0.00	0.00	0.00	-	-	-	-	-	-	0.72	0.69	-	-	-	-
GR11-39_Opx1A-2	8.93	0.25	0.00	0.01	0.03	49.01	19.26	0.05	22.45	0.08	100.07	0.09	0.27	0.56	0.00	0.00	0.00	0.00	-	-	-	-	-	-	0.71	0.68	-	-	-	-
GR11-39_Opx1A-3	8.58	0.13	0.00	0.00	0.00	48.88	19.52	0.04	22.18	0.11	99.44	0.08	0.27	0.55	0.00	0.00	0.00	0.00	-	-	-	-	-	-	0.70	0.67	-	-	-	-
GR11-39_Opx1A-4	9.13	0.13	0.00	0.00	0.00	48.38	19.35	0.09	21.56	0.11	98.75	0.09	0.27	0.53	0.00	0.00	0.00	0.00	-	-	-	-	-	-	0.70	0.67	-	-	-	-
GR11-39_Opx1A-5	9.36	0.12	0.00	0.02	0.01	48.38	19.45	0.07	21.96	0.06	99.43	0.09	0.27	0.54	0.00	0.00	0.00	0.00	-	-	-	-	-	-	0.70	0.67	-	-	-	-
GR11-39_Opx1A-6	8.67	0.09	0.00	0.01	0.00	48.56	20.22	0.04	21.65	0.08	99.31	0.09	0.28	0.54	0.00	0.00	0.00	0.00	-	-	-	-	-	-	0.69	0.66	-	-	-	-
GR11-39_Opx1A-7	9.71	0.18	0.00	0.00	0.00	48.15	20.12	0.05	21.26	0.07	99.54	0.10	0.28	0.53	0.00	0.00	0.00	0.00	-	-	-	-	-	-	0.69	0.65	-	-	-	-
GR11-39_Opx1A-8	9.48	0.00	0.00	0.02	0.00	48.26	20.32	0.05	21.57	0.06	99.75	0.09	0.28	0.54	0.00	0.00	0.00	0.00	-	-	-	-	-	-	0.69	0.65	-	-	-	-
GR11-39_Opx1A-9	9.16	0.13	0.00	0.01	0.00	48.60	20.01	0.06	22.19	0.09	100.25	0.09	0.28	0.55	0.00	0.00	0.00	0.00	-	-	-	-	-	-	0.70	0.66	-	-	-	-
GR11-39_Opx1A-10	9.29	0.00	0.00	0.02	0.00	48.33	19.84	0.04	21.37	0.08	99.00	0.09	0.28	0.53	0.00	0.00	0.00	0.00	-	-	-	-	-	-	0.69	0.66	-	-	-	-
GR11-39_Opx1A-11	9.09	0.14	0.00	0.03	0.01	48.31	20.43	0.09	21.18	0.14	99.42	0.09	0.28	0.53	0.00	0.00	0.00	0.00	-	-	-	-	-	-	0.68	0.65	-	-	-	-
GR11-39_Opx1A-12	9.24	0.02	0.00	0.00	0.00	49.46	20.63	0.06	21.54	0.07	100.02	0.08	0.29	0.53	0.00	0.00	0.00	0.00	-	-	-	-	-	-	0.68	0.65	-	-	-	-
GR11-39_Opx1A-13	9.20	0.06	0.00	0.02	0.01	48.99	20.32	0.06	21.49	0.13	99.62	0.09	0.29	0.53	0.00	0.00	0.00	0.00	-	-	-	-	-	-	0.68	0.65	-	-	-	-
GR11-39_Opx1A-14	8.81	0.01	0.00	0.02	0.00	48.90	20.28	0.04	21.67	0.12	99.80	0.09	0.28	0.54	0.00	0.00	0.00	0.00	-	-	-	-	-	-	0.69	0.66	-	-	-	-
GR11-39_Opx1A-15	9.63	0.16	0.00	0.02	0.00	47.96	21.27	0.06	20.66	0.12	99.88	0.09	0.30	0.51	0.00	0.00	0.00	0.00	-	-	-	-	-	-	0.67	0.63	-	-	-	-
GR11-39_Opx1A-16	7.22	0.08	0.02	0.02	0.00	50.00	20.70	0.05	21.72	0.15	99.96	0.07	0.29	0.54	0.00	0.00	0.00	0.00	-	-	-	-	-	-	0.68	0.65	-	-	-	-
GR11-39_Opx1A-17	8.21	0.07	0.02	0.01	0.00	49.19	20.67	0.07	21.02	0.15	99.61	0.08	0.29	0.52	0.00	0.00	0.00	0.00	-	-	-	-	-	-	0.67	0.64	-	-	-	-
GR11-39_Opx1A-18	9.06	0.08	0.00	0.03	0.00	48.35	20.93	0.06	21.10	0.08	99.70	0.09	0.29	0.52	0.00	0.00	0.00	0.00	-	-	-	-	-	-	0.68	0.64	-	-	-	-
GR11-39_Opx1A-19	9.49	0.03	0.00	0.03	0.00	48.23	21.57	0.10	20.66	0.10	100.20	0.09	0.30	0.51	0.00	0.00	0.00	0.00	-	-	-	-	-	-	0.67	0.63	-	-	-	-
GR11-39_Opx1A-20	6.97	0.22	0.00	0.02	0.01	49.71	21.47	0.07	21.47	0.13	100.06	0.07	0.30	0.53	0.00	0.00	0.00	0.00	-	-	-	-	-	-	0.67	0.64	-	-	-	-
GR11-39_Opx1A-21	9.58	0.06	0.00	0.00	0.01	48.53	20.06	0.04	21.83	0.12	100.24	0.09	0.28	0.54	0.00	0.00	0.00	0.00	-	-	-	-	-	-	0.69	0.66	-	-	-	-
GR11-39_Opx1A-22	10.41	0.13	0.00	0.01	0.00	47.48	20.33	0.08	21.50	0.07	100.00	0.10	0.28	0.53	0.00	0.00	0.00	0.00	-	-	-	-	-	-	0.69	0.65	-	-	-	-
GR11-39_Opx1A-23	7.13	0.20	0.00	0.01	0.00	50.00	20.47	0.08	22.32	0.09	100.31	0.07	0.28	0.55	0.00	0.00	0.00	0.00	-	-	-	-	-	-	0.69	0.66	-	-	-	-
GR11-39_Opx1A-24	9.52	0.25	0.01	0.01	0.01	47.80	20.44	0.09	21.49	0.12	99.73	0.09	0.28	0.53	0.00	0.00	0.00	0.00	-	-	-	-	-	-	0.69	0.65	-	-	-	-
GR11-39_Opx1A-25	10.49	0.17	0.00	0.02	0.00	47.69	20.20	0.08	21.32	0.07	100.05	0.10	0.28	0.53	0.00	0.00	0.00	0.00	-	-	-	-	-	-	0.69	0.65	-	-	-	-
GR11-39_Opx1A-26	7.94	0.20	0.00	0.00	0.02	49.81	19.74	0.06	22.43	0.13	100.32	0.08	0.27	0.56	0.00	0.00	0.00	0.00	-	-	-	-	-	-	0.70	0.67	-	-	-	-
GR11-39_Opx1A-27	6.89	0.13	0.00	0.02	0.01	50.73	20.07	0.07	22.98	0.14	101.04	0.07	0.28	0.57	0.00	0.00	0.00	0.00	-	-	-	-	-	-	0.70	0.67	-	-	-	-
Sapphirine																														
GR11-39_Spr1A-1	60.94	0.06	0.01	0.02	0.00	13.21	10.19	0.03	15.27	0.05	99.78	0.60	0.14	0.38	0.00	0.00	0.00	0.00	-	-	-	-	-	-	-	-	-	-	-	-
GR11-39_Spr1A-2	60.86	0.08	0.00	0.01	0.02	13.19	10.47	0.03	15.14	0.07	99.77	0.60	0.15	0.38	0.00	0.00	0.00	0.00	-	-	-	-	-	-	-	-	-	-	-	-
GR11-39_Spr1A-3	59.52	0.08	0.00	0.01	0.01	12.96	10.21	0.04	15.38	0.07	98.72	0.59	0.14	0.38	0.00	0.00	0.00	0.00	-	-	-	-	-	-	-	-	-	-	-	-
GR11-39_Spr1A-4	60.17	0.00	0.00	0.02	0.00	13.09	10.67	0.05	15.36	0.06	99.28	0.59	0.15	0.38	0.00	0.00	0.00	0.00	-	-	-	-	-	-	-	-	-	-	-	-
GR11-39_Spr1A-5	60.46	0.02	0.00	0.02	0.02	13.09	11.19	0.02	15.22	0.08	100.12	0.59	0.16	0.38	0.00	0.00	0.00	0.00	-	-	-	-	-	-	-	-	-	-	-	-
GR11-39_Spr1A-6	60.85	0.04	0.00	0.02	0.01	13.11	10.61	0.02	15.25	0.03	99.93	0.60	0.15	0.38	0.00	0.00	0.00	0.00	-	-	-	-	-	-	-	-	-	-	-	-
GR11-39_Spr1A-7	59.84	0.07	0.00	0.02	0.01	13.29	10.91	0.05	15.27	0.02	99.47	0.59	0.15	0.38	0.00	0.00	0.00	0.00	-	-	-	-	-	-	-	-	-	-	-	-
GR11-39_Spr1A-8	60.22	0.00	0.00	0.01	0.00	13.24	10.36	0.04	15.24	0.04	99.16	0.59	0.14	0.38	0.00	0.00	0.00	0.00	-	-	-	-	-	-	-	-	-	-	-	-
GR11-39_Spr1A-9	60.62	0.06	0.00	0.03	0.00	13.04	10.64	0.05	15.18	0.05	99.67	0.59	0.15	0.38	0.00	0.00	0.00	0.00	-	-	-	-	-	-	-	-	-	-	-	-
GR11-39_Spr1A-10	59.71	0.03	0.00	0.02	0.01	13.68	11.33	0.04	15.01	0.07	99.90	0.59	0.16	0.37	0.00	0.00	0.00	0.00	-	-	-	-	-	-	-	-	-	-	-	-
GR11-39_Spr1A-11	59.25	0.04	0.00	0.02	0.02	13.66	11.61	0.02	15.14	0.05	99.82	0.58	0.16	0.38	0.00	0.00	0.00	0.00	-	-	-	-	-	-	-	-	-	-	-	-
GR11-39_Spr1A-12	59.32	0.07	0.01	0.00	0.00	13.19	10.96	0.05	15.05	0.08	98.72	0.58	0.15	0.37	0.00	0.00	0.00	0.00	-	-	-	-	-	-	-	-	-	-	-	-
GR11-39_Spr1A-13	59.91	0.00	0.00	0.02	0.00	13.23	11.29	0.03	15.13	0.05	99.65	0.59	0.16	0.38	0.00	0.00	0.00	0.00	-	-	-	-	-	-	-	-	-	-	-	-
GR11-39_Spr1A-14	59.39	0.08	0.00	0.05	0.03	13.61	11.82	0.03	15.02	0.06	100.10	0.58	0.16	0.37	0.00	0.00	0.00	0.00	-	-	-	-	-	-	-	-	-	-	-	-
GR11-39_Spr1A-15	59.10	0.02	0.01	0.00	0.01	13.48	10.94	0.04	14.72	0.05	98.36	0.58	0.15	0.37	0.00	0.00	0.00	0.00	-	-	-	-	-	-	-	-	-	-	-	-
GR11-39_Spr1A-16	58.96	0.09	0.00	0.03	0.03	13.82	11.89	0.03	15.13	0.06	100.03	0.58	0.17	0.38	0.00	0.00	0.00	0.00	-	-	-	-	-	-	-	-	-	-	-	-
GR11-39_Spn1A-17	61.40	0.00	0.00	0.02	0.02	13.05	11.33	0.02	15.19	0.04	101.07	0.60	0.16	0.38	0.00	0.00	0.00	0.00	-	-	-	-	-	-	-	-	-	-	-	-
GR11-39_Spn1A-18	60.24	0.03	0.00	0.02	0.00	13.21	11.77	0.05	15.06	0.06	100.43	0.59	0.16	0.37	0.00	0.00	0.00	0.00	-	-	-	-	-	-	-	-	-	-	-	-
GR11-39_Spn1A-19	60.06	0.02	0.00	0.02	0.00	13.52	12.07	0.04	14.92	0.07	100.71	0.59	0.17	0.37	0.00	0.00	0.00	0.00	-	-	-	-	-	-	-	-	-	-	-	-

Table 5.1

Sample and Analysis Number	Al2O3	TiO2	K2O	Na2O	Cr2O3	SiO2	FeO	CaO	MgO	MnO	Total	Al (mol)	Fe (mol)	Mg (mol)	Ca (mol)	Mn (mol)	Na (mol)	K (mol)	Grt Xal	Grt Xpr	Grt Xgr	Grt Xsp	Plg Xan	Opx Xmgts	Mg No.	Zr (ppm)	±2SE (ppm)	Y (ppm)	± 2SE (ppm)
Plagioclase																													
GR11-39_Fsp1A-10	26.98	0.00	0.09	6.88	0.00	57.43	0.51	8.84	0.00	0.01	100.74	0.26	0.01	0.00	0.16	0.00	0.11	0.00	–	–	–	–	0.58	–	–	–	–	–	–
GR11-39_Fsp1A-14	26.87	0.00	0.12	6.88	0.03	57.31	0.15	9.02	0.01	0.00	100.39	0.26	0.00	0.00	0.16	0.00	0.11	0.00	–	–	–	–	0.59	–	–	–	–	–	–
GR11-39_Fsp1A-9	27.16	0.00	0.12	6.97	0.00	57.39	0.36	8.78	0.03	0.02	100.82	0.27	0.00	0.00	0.16	0.00	0.11	0.00	–	–	–	–	0.58	–	–	–	–	–	–
GR11-39_Fsp1A-12	26.66	0.10	0.13	6.95	0.01	57.19	0.23	8.94	0.02	0.04	100.26	0.26	0.00	0.00	0.16	0.00	0.11	0.00	–	–	–	–	0.58	–	–	–	–	–	–
GR11-39_Fsp1A-16	26.69	0.00	0.13	6.89	0.00	57.58	0.05	9.03	0.01	0.02	100.40	0.26	0.00	0.00	0.16	0.00	0.11	0.00	–	–	–	–	0.59	–	–	–	–	–	–
GR11-39_Fsp1A-7	26.71	0.02	0.13	6.96	0.01	57.75	0.24	8.63	0.01	0.01	100.47	0.26	0.00	0.00	0.15	0.00	0.11	0.00	–	–	–	–	0.58	–	–	–	–	–	–
GR11-39_Fsp1A-29	26.35	0.00	0.14	7.33	0.02	58.05	0.03	8.28	0.01	0.01	100.22	0.26	0.00	0.00	0.15	0.00	0.12	0.00	–	–	–	–	0.55	–	–	–	–	–	–
GR11-39_Fsp1A-11	27.06	0.00	0.15	6.68	0.00	56.71	0.19	9.28	0.00	0.01	100.08	0.27	0.00	0.00	0.17	0.00	0.11	0.00	–	–	–	–	0.60	–	–	–	–	–	–
GR11-39_Fsp1A-28	26.52	0.00	0.16	6.88	0.02	57.54	0.08	8.87	0.01	0.02	100.10	0.26	0.00	0.00	0.16	0.00	0.11	0.00	–	–	–	–	0.58	–	–	–	–	–	–
GR11-39_Fsp1A-13	27.05	0.04	0.17	7.00	0.00	57.31	0.09	8.90	0.01	0.03	100.59	0.27	0.00	0.00	0.16	0.00	0.11	0.00	–	–	–	–	0.58	–	–	–	–	–	–
GR11-39_Fsp1A-15	26.69	0.00	0.17	7.05	0.00	58.00	0.11	8.66	0.01	0.00	100.69	0.26	0.00	0.00	0.15	0.00	0.11	0.00	–	–	–	–	0.57	–	–	–	–	–	–
GR11-39_Fsp1A-5	26.85	0.02	0.18	7.02	0.00	57.48	0.31	8.72	0.03	0.00	100.60	0.26	0.00	0.00	0.16	0.00	0.11	0.00	–	–	–	–	0.57	–	–	–	–	–	–
GR11-39_Fsp1A-1	26.69	0.03	0.18	6.79	0.00	56.39	0.29	8.65	0.02	0.06	99.10	0.26	0.00	0.00	0.15	0.00	0.11	0.00	–	–	–	–	0.58	–	–	–	–	–	–
GR11-39_Fsp1A-8	26.87	0.00	0.18	7.14	0.02	58.13	0.28	8.54	0.01	0.02	101.19	0.26	0.00	0.00	0.15	0.00	0.12	0.00	–	–	–	–	0.57	–	–	–	–	–	–
GR11-39_Fsp1A-6	26.83	0.04	0.19	7.01	0.00	57.74	0.43	8.43	0.02	0.00	100.69	0.26	0.01	0.00	0.15	0.00	0.11	0.00	–	–	–	–	0.57	–	–	–	–	–	–
GR11-39_Fsp1A-3	26.71	0.04	0.19	7.07	0.00	57.55	0.16	8.53	0.02	0.02	100.30	0.26	0.00	0.00	0.15	0.00	0.11	0.00	–	–	–	–	0.57	–	–	–	–	–	–
GR11-39_Fsp1A-4	26.58	0.00	0.19	7.17	0.03	57.87	0.37	8.69	0.01	0.02	100.94	0.26	0.01	0.00	0.15	0.00	0.12	0.00	–	–	–	–	0.57	–	–	–	–	–	–
GR11-39_Fsp1A-2	26.83	0.00	0.21	6.94	0.00	57.63	0.25	8.67	0.02	0.02	100.57	0.26	0.00	0.00	0.15	0.00	0.11	0.00	–	–	–	–	0.58	–	–	–	–	–	–
GR11-39_Spn1A-20	27.00	0.00	0.09	6.98	0.01	57.81	0.36	8.64	0.03	0.05	100.96	0.26	0.01	0.00	0.15	0.00	0.11	0.00	–	–	–	–	0.58	–	–	–	–	–	–
GR11-39_Spn1A-21	27.10	0.02	0.07	7.10	0.00	57.51	0.54	8.69	0.03	0.01	101.07	0.27	0.01	0.00	0.15	0.00	0.11	0.00	–	–	–	–	0.57	–	–	–	–	–	–
K Feldspar																													
GR11-39_Fsp1A-24	18.69	0.03	14.05	2.16	0.01	64.77	0.01	0.17	0.00	0.00	99.90	0.18	0.00	0.00	0.00	0.00	0.03	0.15	–	–	–	–	–	–	–	–	–	–	–
GR11-39_Fsp1A-18	18.92	0.02	14.11	2.06	0.02	64.87	0.06	0.15	0.00	0.01	100.21	0.19	0.00	0.00	0.00	0.00	0.03	0.15	–	–	–	–	–	–	–	–	–	–	–
GR11-39_Fsp1A-25	18.84	0.00	14.23	1.99	0.00	64.73	0.05	0.12	0.01	0.01	99.99	0.18	0.00	0.00	0.00	0.00	0.03	0.15	–	–	–	–	–	–	–	–	–	–	–
GR11-39_Fsp1A-21	18.90	0.11	14.34	1.80	0.00	64.45	0.06	0.13	0.00	0.02	99.81	0.19	0.00	0.00	0.00	0.00	0.03	0.15	–	–	–	–	–	–	–	–	–	–	–
GR11-39_Fsp1A-20	18.83	0.06	14.38	1.66	0.00	64.60	0.02	0.10	0.00	0.02	99.67	0.18	0.00	0.00	0.00	0.00	0.03	0.15	–	–	–	–	–	–	–	–	–	–	–
GR11-39_Fsp1A-17	18.75	0.00	14.54	1.76	0.00	65.06	0.07	0.15	0.01	0.02	100.36	0.18	0.00	0.00	0.00	0.00	0.03	0.15	–	–	–	–	–	–	–	–	–	–	–
GR11-39_Fsp1A-26	18.95	0.00	14.60	1.63	0.00	64.92	0.00	0.10	0.01	0.03	100.24	0.19	0.00	0.00	0.00	0.00	0.03	0.15	–	–	–	–	–	–	–	–	–	–	–
GR11-39_Fsp1A-22	18.84	0.03	14.61	1.64	0.04	64.68	0.05	0.07	0.02	0.01	99.97	0.18	0.00	0.00	0.00	0.00	0.03	0.16	–	–	–	–	–	–	–	–	–	–	–
GR11-39_Fsp1A-19	19.02	0.05	14.66	1.76	0.00	64.90	0.00	0.11	0.01	0.01	100.53	0.19	0.00	0.00	0.00	0.00	0.03	0.16	–	–	–	–	–	–	–	–	–	–	–
GR11-39_Fsp1A-23	18.87	0.06	14.74	1.76	0.00	64.85	0.11	0.08	0.02	0.01	100.50	0.19	0.00	0.00	0.00	0.00	0.03	0.16	–	–	–	–	–	–	–	–	–	–	–
GR11-39_Fsp1A-27	18.88	0.00	14.97	1.45	0.00	64.63	0.04	0.09	0.00	0.00	100.06	0.19	0.00	0.00	0.00	0.00	0.02	0.16	–	–	–	–	–	–	–	–	–	–	–
Biotite																										–	–	–	–
GR11-39_Bt1A-1	17.49	2.13	10.20	0.13	0.01	38.84	6.87	0.01	20.24	0.01	95.94	0.17	0.10	0.50	0.00	0.00	0.00	0.11	–	–	–	–	–	–	0.84	–	–	–	–
GR11-39_Bt1A-2	17.42	1.53	10.23	0.16	0.00	39.43	6.47	0.01	20.37	0.00	95.63	0.17	0.09	0.51	0.00	0.00	0.00	0.11	–	–	–	–	–	–	0.85	–	–	–	–
GR11-39_Bt1A-3	17.42	1.75	10.14	0.14	0.01	38.64	9.16	0.01	18.48	0.07	95.83	0.17	0.13	0.46	0.00	0.00	0.00	0.11	–	–	–	–	–	–	0.78	–	–	–	–
GR11-39_Bt1A-4	17.33	1.87	10.05	0.11	0.00	38.92	9.63	0.04	18.75	0.00	96.70	0.17	0.13	0.47	0.00	0.00	0.00	0.11	–	–	–	–	–	–	0.78	–	–	–	–
GR11-39_Bt1A-5	17.30	1.90	10.26	0.13	0.00	38.95	9.62	0.03	18.13	0.02	96.34	0.17	0.13	0.45	0.00	0.00	0.00	0.11	–	–	–	–	–	–	0.77	–	–	–	–
GR11-39_Bt1A-6	17.23	1.82	10.24	0.11	0.00	39.14	9.51	0.02	18.03	0.04	96.14	0.17	0.13	0.45	0.00	0.00	0.00	0.11	–	–	–	–	–	–	0.77	–	–	–	–
Spinel																										–	–	–	–
GR11-39_Spn1A-1	61.29	0.00	0.00	0.00	0.00	0.01	28.48	0.02	9.68	0.07	99.55	0.60	0.40	0.24	0.00	0.00	0.00	0.00	–	–	–	–	–	–	0.38	–	–	–	–
GR11-39_Spn1A-2	60.44	0.00	0.00	0.00	0.02	0.04	30.22	0.02	8.72	0.05	99.50	0.59	0.42	0.22	0.00	0.00	0.00	0.00	–	–	–	–	–	–	0.34	–	–	–	–
GR11-39_Spn1A-3	61.46	0.01	0.00	0.14	0.02	1.18	26.92	0.14	11.03	0.06	100.97	0.60	0.37	0.27	0.00	0.00	0.00	0.00	–	–	–	–	–	–	0.42	–	–	–	–
GR11-39_Spn1A-4	59.57	0.00	0.00	0.00	0.00	0.25	31.02	0.12	8.15	0.10	99.21	0.58	0.43	0.20	0.00	0.00	0.00	0.00	–	–	–	–	–	–	0.32	–	–	–	–
GR11-39_Spn1A-5	62.00	0.03	0.01	0.00	0.00	0.04	27.58	0.00	10.54	0.03	100.22	0.61	0.38	0.26	0.00	0.00	0.00	0.00	–	–	–	–	–	–	0.41	–	–	–	–
GR11-39_Spn1A-6	61.57	0.00	0.00	0.00	0.01	0.03	28.59	0.05	9.10	0.13	99.48	0.60	0.40	0.23	0.00	0.00	0.00	0.00	–	–	–	–	–	–	0.36	–	–	–	–
Monazite-Bearing Texture in Residual Granulite (GRM-37)																													
Sapphirine																													
GRM-37I_Spr-1	61.62	0.05	0.00	0.02	0.01	13.86	7.76	0.01	16.50	0.02	99.84	0.60	0.11	0.41	0.00	0.00	0.00	0.00	–	–	–	–	–	–	0.79	–	–	–	–
GRM-37I_Spr-2	61.80	0.05	0.01	0.00	0.00	13.78	7.68	0.01	16.61	0.06	100.00	0.61	0.11	0.41	0.00	0.00	0.00	0.00	–	–	–	–	–	–	0.79	–	–	–	–
GRM-37I_Spr-3	61.71	0.04	0.00	0.00	0.00	13.90	7.50	0.02	16.79	0.03	99.97	0.61	0.10	0.42	0.00	0.00	0.00	0.00	–	–	–	–	–	–	0.80	–	–	–	–
GRM-37I_Spr-4	61.48	0.07	0.01	0.02	0.00	13.97	7.67	0.01	16.53	0.02	99.78	0.60	0.11	0.41	0.00	0.00	0.00	0.00	–	–	–	–	–	–	0.79	–	–	–	–
GRM-37I_Spr-5	61.13	0.05	0.00	0.03	0.01	13.78	7.97	0.02	16.52	0.02	99.51	0.60	0.11	0.41	0.00	0.00	0.00	0.00	–	–	–	–	–	–	0.79	–	–	–	–
GRM-37I_Spr-6	61.52	0.06	0.00	0.00	0.02	13.92	8.56	0.01	16.25	0.02	100.37	0.60	0.12	0.40	0.00	0.00	0.00	0.00	–	–	–	–	–	–	0.77	–	–	–	–
GRM-37I_Spr-7	61.18	0.09	0.00	0.01	0.03	13.87	8.98	0.02	16.22	0.03	100.42	0.60	0.12	0.40	0.00	0.00	0.00	0.00	–	–	–	–	–	–	0.76	–	–	–	–
GRM-37I_Spr-8	61.46	0.07	0.00	0.02	0.00	13.75	8.69	0.01	15.82	0.01	99.84	0.60	0.12	0.39	0.00	0.00	0.00	0.00	–	–	–	–	–	–	0.76	–	–	–	–
GRM-37I_Spr-9	61.96	0.07	0.00	0.00	0.02	13.31	8.47	0.02	15.64	0.06	99.54	0.61	0.12	0.39	0.00	0.00	0.00	0.00	–	–	–	–	–	–	0.77	–	–	–	–
GRM-37I_Spr-10	61.17	0.08	0.00	0.01	0.00	13.89	9.17	0.02	16.13	0.05	100.52	0.60	0.13	0.40	0.00	0.00	0.00	0.00	–	–	–	–	–	–	0.76	–	–	–	–
GRM-37I_Spr-11	60.60	0.07	0.00	0.02	0.00	13.91	8.84	0.01	16.09	0.08	99.62	0.59	0.12	0.40	0.00	0.00	0.00	0.00	–	–	–	–	–	–	0.76	–	–	–	–
GRM-37I_Spr-12	61.20	0.08	0.00	0.00	0.00	13.90	9.35	0.02	16.07	0.05	100.66	0.60	0.13	0.40	0.00	0.00	0.00	0.00	–	–	–	–	–	–	0.75	–	–	–	–
GRM-37I_Spr-13	61.49	0.08	0.01	0.01	0.00	13.75	9.30	0.02	15.71	0.05	100.41	0.60	0.13	0.39	0.00	0.00	0.00	0.00	–	–	–	–	–	–	0.75	–	–	–	–
Orthopyroxene																										–	–	–	–
GRM-37I_Opx-1	9.94	0.15	0.00	0.02	0.00	49.50	15.87	0.15	24.32	0.15	100.09	0.10	0.22	0.60	0.00	0.00	0.00	0.00	–	–	–	–	–	0.76	0.73	–	–	–	–
GRM-37I_Opx-2	10.07	0.11	0.00	0.00	0.01	49.07	15.83	0.15	23.99	0.13	99.36	0.10	0.22	0.60	0.00	0.00	0.00	0.00	–	–	–	–	–	0.76	0.73	–	–	–	–
GRM-37I_Opx-3	9.76	0.10	0.00	0.02	0.00	49.55	15.98	0.09	24.20	0.14	99.84	0.10	0.22	0.60	0.00	0.00	0.00	0.00	–	–	–	–	–	0.76	0.73	–	–	–	–
GRM-37I_Opx-4	9.11	0.11	0.01	0.00	0.01	49.35	16.04	0.09	24.15	0.13	99.00	0.09	0.22	0.60	0.00	0.00	0.00	0.00	–	–	–	–	–	0.76	0.73	–	–	–	–
Cordierite																										–	–	–	–
GRM-37I_Crd-1	34.57	0.00	0.01	0.07	0.00	49.61	2.82	0.01	11.63	0.03	98.75	0.34	0.04	0.29	0.00	0.00	0.00	0.00	–	–	–	–	–	–	0.88	–	–	–	–
GRM-37I_Crd-2	34.27	0.00	0.01	0.09	0.00	49.73	2.72	0.01	11.41	0.02	98.25	0.34	0.04	0.28	0.00	0.00	0.00	0.00	–	–	–	–	–	–	0.88	–	–	–	–
GRM-37I_Crd-3	34.36	0.00	0.00	0.13	0.02	49.58	2.83	0.01	11.51	0.03	98.47	0.34	0.04	0.29	0.00	0.00	0.00	0.00	–	–	–	–	–	–	0.88	–	–	–	–
GRM-37I_Crd-4	34.38	0.00	0.00	0.12	0.00	49.60	2.87	0.02	11.47	0.02	98.50	0.34	0.04	0.28	0.00	0.00	0.00	0.00	–	–	–	–	–	–	0.88	–	–	–	–
GRM-37I_Crd-5	34.16	0.02	0.00	0.09	0.00	49.68	2.95	0.02	11.34	0.02	98.28	0.33	0.04	0.28	0.00	0.00	0.00	0.00	–	–	–	–	–	–	0.87	–	–	–	–
GRM-37I_Crd-6	34.22	0.00	0.01	0.12	0.01	49.93	2.78	0.01	11.46	0.03	98.57	0.34	0.04	0.28	0.00	0.00	0.00	0.00	–	–	–	–	–	–	0.88	–	–	–	–
GRM-37I_Crd-7	34.21	0.02	0.00	0.10	0.01	49.77	2.79	0.02	11.50	0.02	98.43	0.34	0.04	0.29	0.00	0.00	0.00	0.00	–	–	–	–	–	–	0.88	–	–	–	–

Sample and Analysis Number	Al2O3	TiO2	K2O	Na2O	Cr2O3	SiO2	FeO	CaO	MgO	MnO	Total	Al (mol)	Fe (mol)	Mg (mol)	Ca (mol)	Mn (mol)	Na (mol)	K (mol)	Grt Xal	Grt Xpr	Grt Xgr	Grt Xsp	Plg Xan	Opx Xmgts	Mg No.	Zr (ppm)	±2SE (ppm)	Y (ppm)	± 2SE (ppm)
GRM-37I_Crd-8	34.54	0.00	0.00	0.11	0.01	49.75	2.80	0.01	11.55	0.04	98.79	0.34	0.04	0.29	0.00	0.00	0.00	0.00	–	–	–	–	–	–	0.88	–	–	–	–
Residual Granulite (Gruf100)																													
Garnet																													
Gruf100_Grt1	22.62	0.00	0.02	0.03	0.01	39.72	24.57	1.27	11.06	0.38	99.68	0.22	0.34	0.27	0.02	0.01	0.00	0.00	0.53	0.43	0.04	0.01	–	–	0.45	2.3	0.4	41	2
Gruf100_Grt2	22.85	0.00	0.01	0.02	0.00	39.99	24.63	1.32	11.31	0.37	100.49	0.22	0.34	0.28	0.02	0.01	0.00	0.00	0.53	0.43	0.04	0.01	–	–	0.45	–	–	–	–
Gruf100_Grt3	23.07	0.01	0.00	0.04	0.00	40.14	23.32	0.93	12.46	0.34	100.32	0.23	0.32	0.31	0.02	0.00	0.00	0.00	0.50	0.47	0.03	0.01	–	–	0.49	–	–	–	–
Gruf100_Grt4	22.77	0.00	0.04	0.10	0.00	40.14	23.11	0.95	12.78	0.34	100.23	0.22	0.32	0.32	0.02	0.00	0.00	0.00	0.49	0.48	0.03	0.01	–	–	0.50	1.9	0.2	29	1
Gruf100_Grt5	23.08	0.00	0.00	0.05	0.05	40.30	22.70	0.85	12.87	0.35	100.23	0.23	0.32	0.32	0.02	0.00	0.00	0.00	0.48	0.49	0.02	0.01	–	–	0.50	1.5	0.2	21	1
Gruf100_Grt6	22.93	0.01	0.01	0.04	0.00	40.12	22.93	0.84	13.09	0.34	100.32	0.22	0.32	0.32	0.01	0.00	0.00	0.00	0.48	0.49	0.02	0.01	–	–	0.50	2.2	0.2	23	1
Gruf100_Grt7	23.18	0.01	0.00	0.06	0.00	40.28	22.15	0.80	13.49	0.32	100.30	0.23	0.31	0.33	0.01	0.00	0.00	0.00	0.47	0.51	0.02	0.01	–	–	0.52	1.8	0.2	32	3
Gruf100_Grt8	23.25	0.00	0.00	0.04	0.01	40.42	22.35	0.82	13.27	0.30	100.46	0.23	0.31	0.33	0.01	0.00	0.00	0.00	0.47	0.50	0.02	0.01	–	–	0.51	–	–	–	–
Gruf100_Grt9	23.07	0.01	0.01	0.04	0.04	40.38	21.81	0.79	13.60	0.34	100.09	0.23	0.30	0.34	0.01	0.00	0.00	0.00	0.46	0.51	0.02	0.01	–	–	0.53	0.8	0.1	32	2
Gruf100_Grt10	22.86	0.01	0.04	0.12	0.01	39.99	21.84	0.83	13.51	0.36	99.57	0.22	0.30	0.34	0.01	0.01	0.00	0.00	0.46	0.51	0.02	0.01	–	–	0.52	–	–	–	–
Gruf100_Grt11	23.17	0.01	0.01	0.09	0.01	40.28	21.97	0.90	13.35	0.40	100.17	0.23	0.31	0.33	0.02	0.01	0.00	0.00	0.46	0.50	0.02	0.01	–	–	0.52	1.3	0.3	40	3
Gruf100_Grt12	23.20	0.00	0.01	0.05	0.00	40.31	22.06	0.99	13.36	0.43	100.41	0.23	0.31	0.33	0.02	0.01	0.00	0.00	0.46	0.50	0.03	0.01	–	–	0.52	–	–	–	–
Gruf100_Grt13	23.08	0.01	0.01	0.06	0.02	39.89	22.42	1.54	12.44	0.58	100.04	0.23	0.31	0.31	0.03	0.01	0.00	0.00	0.48	0.47	0.04	0.01	–	–	0.50	5.0	0.2	82	3
Gruf100_Grt14	22.69	0.05	0.00	0.02	0.00	40.07	22.94	1.75	12.14	0.62	100.28	0.22	0.32	0.30	0.03	0.01	0.00	0.00	0.48	0.46	0.05	0.01	–	–	0.49	–	–	–	–
Gruf100_Grt15	22.42	0.01	0.01	0.03	0.00	39.47	24.21	3.04	10.40	0.84	100.41	0.22	0.34	0.26	0.05	0.01	0.00	0.00	0.51	0.39	0.08	0.02	–	–	0.43	7.1	0.4	92	4
Gruf100_Grt16	22.47	0.06	0.01	0.01	0.00	39.52	24.68	2.96	9.74	0.93	100.37	0.22	0.34	0.24	0.05	0.01	0.00	0.00	0.53	0.37	0.08	0.02	–	–	0.41	–	–	–	–
Gruf100_Grt17	22.31	0.06	0.00	0.01	0.00	39.68	25.64	2.46	9.19	1.17	100.51	0.22	0.36	0.23	0.04	0.02	0.00	0.00	0.55	0.35	0.07	0.03	–	–	0.39	11.0	0.4	395	18
Gruf100_Grt18	22.65	0.03	0.00	0.00	0.00	39.28	25.63	2.55	9.30	1.25	100.68	0.22	0.36	0.23	0.05	0.02	0.00	0.00	0.55	0.35	0.07	0.03	–	–	0.39	–	–	–	–
Gruf100_Grt19	22.60	0.09	0.00	0.03	0.00	39.50	25.06	2.22	9.62	1.34	100.45	0.22	0.35	0.24	0.04	0.02	0.00	0.00	0.54	0.37	0.06	0.03	–	–	0.41	–	–	–	–
Gruf100_Grt20	22.47	0.13	0.00	0.01	0.04	39.24	24.77	2.16	9.59	1.38	99.80	0.22	0.34	0.24	0.04	0.02	0.00	0.00	0.54	0.37	0.06	0.03	–	–	0.41	–	–	–	–
Gruf100_Grt21	22.67	0.09	0.01	0.03	0.00	39.42	24.68	2.20	9.66	1.39	100.15	0.22	0.34	0.24	0.04	0.02	0.00	0.00	0.54	0.37	0.06	0.03	–	–	0.41	68.9	3.5	922	37
Gruf100_Grt22	22.58	0.06	0.00	0.00	0.00	39.51	24.05	2.18	10.34	1.41	100.13	0.22	0.33	0.26	0.04	0.02	0.00	0.00	0.52	0.39	0.06	0.03	–	–	0.43	–	–	–	–
Gruf100_Grt23	22.64	0.07	0.01	0.01	0.00	39.66	23.37	2.47	10.58	1.29	100.08	0.22	0.33	0.26	0.04	0.02	0.00	0.00	0.50	0.40	0.07	0.03	–	–	0.45	122.3	3.6	1482	68
Gruf100_Grt24	22.74	0.13	0.01	0.01	0.00	39.50	23.38	2.00	10.90	1.26	99.94	0.22	0.33	0.27	0.04	0.02	0.00	0.00	0.50	0.42	0.05	0.03	–	–	0.45	46.9	2.0	1433	73
Gruf100_Grt25	22.96	0.05	0.00	0.01	0.00	39.88	23.09	1.94	11.27	1.21	100.42	0.23	0.32	0.28	0.03	0.02	0.00	0.00	0.49	0.43	0.05	0.03	–	–	0.47	61.3	2.5	1683	66
Gruf100_Grt26	22.81	0.04	0.00	0.02	0.00	40.02	22.90	1.76	11.40	1.25	100.20	0.22	0.32	0.28	0.03	0.02	0.00	0.00	0.49	0.43	0.05	0.03	–	–	0.47	53.9	6.3	2560	240
Gruf100_Grt27	22.76	0.05	0.00	0.02	0.03	39.90	22.81	1.68	11.53	1.15	99.91	0.22	0.32	0.29	0.03	0.02	0.00	0.00	0.49	0.44	0.05	0.02	–	–	0.47	–	–	–	–
Gruf100_Grt28	22.93	0.07	0.01	0.03	0.03	39.57	22.11	1.88	11.74	1.12	99.47	0.22	0.31	0.29	0.03	0.02	0.00	0.00	0.47	0.45	0.05	0.02	–	–	0.49	49.5	1.5	2492	94
Gruf100_Grt29	22.84	0.05	0.00	0.00	0.00	39.92	22.18	1.84	11.92	1.10	99.84	0.22	0.31	0.30	0.03	0.02	0.00	0.00	0.47	0.45	0.05	0.02	–	–	0.49	–	–	–	–
Gruf100_Grt30	22.91	0.05	0.00	0.02	0.03	39.82	22.13	1.93	11.88	1.12	99.90	0.22	0.31	0.29	0.03	0.02	0.00	0.00	0.47	0.45	0.05	0.02	–	–	0.49	48.2	2.1	2960	110
Gruf100_Grt31	22.95	0.04	0.00	0.00	0.00	39.91	21.75	2.01	12.10	1.10	99.86	0.23	0.30	0.30	0.04	0.02	0.00	0.00	0.46	0.46	0.05	0.02	–	–	0.50	46.6	1.8	3230	130
Gruf100_Grt32	23.02	0.07	0.00	0.01	0.00	39.90	21.85	1.92	11.82	1.07	99.67	0.23	0.30	0.29	0.03	0.02	0.00	0.00	0.47	0.45	0.05	0.02	–	–	0.49	62.2	2.6	2881	85
Gruf100_Grt33	22.85	0.04	0.01	0.02	0.00	40.06	22.04	1.94	12.13	1.10	100.19	0.22	0.31	0.30	0.03	0.02	0.00	0.00	0.47	0.46	0.05	0.02	–	–	0.50	–	–	–	–
Gruf100_Grt34	22.85	0.03	0.00	0.00	0.00	40.04	21.78	1.78	12.37	1.07	99.92	0.22	0.30	0.31	0.03	0.02	0.00	0.00	0.46	0.47	0.05	0.02	–	–	0.50	–	–	–	–
Gruf100_Grt35	23.06	0.03	0.01	0.00	0.00	40.07	21.56	1.80	12.46	1.05	100.04	0.23	0.30	0.31	0.03	0.01	0.00	0.00	0.46	0.47	0.05	0.02	–	–	0.51	47.9	2.0	2820	100
Gruf100_Grt36	22.60	0.05	0.00	0.02	0.02	39.97	21.55	2.08	12.19	1.00	99.47	0.22	0.30	0.30	0.04	0.01	0.00	0.00	0.46	0.46	0.06	0.02	–	–	0.50	46.3	1.2	3450	110
Gruf100_Grt37	22.92	0.08	0.00	0.03	0.00	39.83	21.57	2.05	12.55	1.02	100.03	0.22	0.30	0.31	0.04	0.01	0.00	0.00	0.45	0.47	0.06	0.02	–	–	0.51	–	–	–	–
Gruf100_Grt38	23.14	0.06	0.01	0.00	0.03	40.01	21.43	1.77	12.71	0.97	100.11	0.23	0.30	0.32	0.03	0.01	0.00	0.00	0.45	0.48	0.05	0.02	–	–	0.51	56.5	2.6	3220	110
Gruf100_Grt39	22.94	0.00	0.00	0.02	0.00	40.31	21.36	1.56	12.73	0.98	99.90	0.22	0.30	0.32	0.03	0.01	0.00	0.00	0.45	0.48	0.04	0.02	–	–	0.52	–	–	–	–
Gruf100_Grt40	22.82	0.05	0.01	0.02	0.00	39.98	21.20	1.80	12.34	0.98	99.20	0.22	0.30	0.31	0.03	0.01	0.00	0.00	0.46	0.47	0.05	0.02	–	–	0.51	–	–	–	–
Gruf100_Grt41	22.97	0.05	0.00	0.02	0.01	40.15	21.08	1.76	12.70	0.95	99.68	0.23	0.29	0.32	0.03	0.01	0.00	0.00	0.45	0.48	0.05	0.02	–	–	0.52	62.7	2.2	3790	150
Gruf100_Grt42	22.87	0.04	0.00	0.04	0.00	40.18	21.02	2.03	12.60	0.97	99.73	0.22	0.29	0.31	0.04	0.01	0.00	0.00	0.45	0.48	0.06	0.02	–	–	0.52	61.8	3.1	3520	150
Gruf100_Grt43	23.22	0.00	0.01	0.03	0.02	39.98	21.22	1.90	12.70	0.96	100.03	0.23	0.30	0.32	0.03	0.01	0.00	0.00	0.45	0.48	0.05	0.02	–	–	0.52	–	–	–	–
Gruf100_Grt44	22.75	0.00	0.03	0.02	0.00	39.20	24.70	1.30	10.37	0.80	99.18	0.22	0.34	0.26	0.02	0.01	0.00	0.00	0.54	0.40	0.04	0.02	–	–	0.43	–	–	–	–
Gruf100_Grt45	22.88	0.01	0.02	0.06	0.00	39.56	24.19	0.98	11.15	0.76	99.61	0.22	0.34	0.28	0.02	0.01	0.00	0.00	0.52	0.43	0.03	0.02	–	–	0.45	–	–	–	–
Gruf100_Grt46	22.82	0.02	0.00	0.03	0.00	39.90	23.46	0.95	12.15	0.71	100.03	0.22	0.33	0.30	0.02	0.01	0.00	0.00	0.50	0.46	0.03	0.02	–	–	0.48	–	–	–	–
Gruf100_Grt47	22.90	0.00	0.00	0.02	0.00	40.10	22.94	0.91	12.56	0.66	100.09	0.22	0.32	0.31	0.02	0.01	0.00	0.00	0.49	0.47	0.02	0.01	–	–	0.49	–	–	–	–
Gruf100_Grt48	23.10	0.00	0.01	0.06	0.02	40.67	22.40	0.90	12.68	0.64	100.47	0.23	0.31	0.31	0.02	0.01	0.00	0.00	0.48	0.48	0.02	0.01	–	–	0.50	–	–	–	–
Gruf100_Grt49	22.98	0.01	0.01	0.06	0.03	40.40	21.99	0.90	13.27	0.61	100.27	0.23	0.31	0.33	0.02	0.01	0.00	0.00	0.46	0.50	0.02	0.01	–	–	0.52	–	–	–	–
Gruf100_Grt50	23.05	0.00	0.01	0.02	0.00	40.28	21.70	0.92	13.54	0.62	100.13	0.23	0.30	0.34	0.02	0.01	0.00	0.00	0.46	0.51	0.02	0.01	–	–	0.53	–	–	–	–
Gruf100_Grt51	23.26	0.03	0.01	0.12	0.00	40.08	21.70	0.90	13.56	0.60	100.26	0.23	0.30	0.34	0.02	0.01	0.00	0.00	0.46	0.51	0.02	0.01	–	–	0.53	–	–	–	–
Gruf100_Grt52	23.16	0.00	0.01	0.01	0.01	40.45	20.10	1.31	14.14	0.55	99.72	0.23	0.28	0.35	0.02	0.01	0.00	0.00	0.42	0.53	0.04	0.01	–	–	0.56	–	–	–	–
Gruf100_Grt53	23.29	0.05	0.01	0.02	0.00	40.92	19.99	1.22	14.26	0.58	100.33	0.23	0.28	0.35	0.02	0.01	0.00	0.00	0.42	0.53	0.03	0.01	–	–	0.56	–	–	–	–
Gruf100_Grt54	23.06	0.01	0.00	0.02	0.03	40.78	19.75	1.15	14.65	0.53	99.97	0.23	0.27	0.36	0.02	0.01	0.00	0.00	0.41	0.55	0.03	0.01	–	–	0.57	–	–	–	–
Gruf100_Grt55	23.39	0.00	0.00	0.02	0.00	40.71	20.06	1.13	14.50	0.63	100.45	0.23	0.28	0.36	0.02	0.01	0.00	0.00	0.42	0.54	0.03	0.01	–	–	0.56	–	–	–	–
Gruf100_Grt56	23.22	0.00	0.00	0.01	0.01	40.80	19.86	1.14	14.56	0.60	100.19	0.23	0.28	0.36	0.02	0.01	0.00	0.00	0.41	0.54	0.03	0.01	–	–	0.57	–	–	–	–
Gruf100_Grt57	23.35	0.03	0.01	0.01	0.00	40.80	19.71	1.20	14.66	0.57	100.33	0.23	0.27	0.36	0.02	0.01	0.00	0.00	0.41	0.54	0.03	0.01	–	–	0.57	–	–	–	–
Gruf100_Grt58	23.44	0.00	0.00	0.02	0.00	40.98	19.74	1.22	14.75	0.56	100.72	0.23	0.27	0.37	0.02	0.01	0.00	0.00	0.41	0.55	0.03	0.01	–	–	0.57	–	–	–	–
Gruf100_Grt59	23.40	0.00	0.00	0.01	0.00	40.73	19.31	1.21	14.76	0.55	99.97	0.23	0.27	0.37	0.02	0.01	0.00	0.00	0.40	0.55	0.03	0.01	–	–	0.58	–	–	–	–
Gruf100_Grt60	23.43	0.01	0.01	0.00	0.00	40.78	19.20	1.25	14.70	0.51	99.88	0.23	0.27	0.36	0.02	0.01	0.00	0.00	0.40	0.55	0.03	0.01	–	–	0.58	–	–	–	–
Gruf100_Grt61	23.28	0.01	0.01	0.01	0.02	40.77	19.32	1.24	14.76	0.55	99.97	0.23	0.27	0.37	0.02	0.01	0.00	0.00	0.40	0.55	0.03	0.01	–	–	0.58	–	–	–	–
Gruf100_Grt62	23.30	0.02	0.00	0.01	0.00	40.55	19.32	1.17	14.83	0.51	99.71	0.23	0.27	0.37	0.02	0.01	0.00	0.00	0.40	0.55	0.03	0.01	–	–	0.58	–	–	–	–

Notes:
Total Fe reported as FeO
Grt Xal, Xpr, Xgr, Xsp = almandine, pyrope, grossular, and spessartine components of garnet, respectively
Plg Xan = anorthite component of plagioclase
Opx Xmgts = Mg-Tschermakite (Mg, Al) component of orthopyroxene
Mg No. = Mg (mol)/[Mg (mol)+ Fe (mol)]

Table 5.2. Bulk compositions used for input to Theriak-Domino.

Rock Type	Residual Granulites			Leucogranulite	Paragneisses	
Analysis Type	XRF	XRF	EPMA	EPMA	XRF	XRF
Sample	Gruf100	Br03-56-2*	GRM-37	GR11-39	GR11-23	GR11-25
SiO2	44.85	n.d.	33.17	51.78	62.86	66.88
TiO2	0.63	n.d.	0.05	0.11	0.81	1.18
Al2O3	25.85	n.d.	43.41	24.80	19.35	16.74
FeO_T	8.65	n.d.	7.20	7.76	6.44	7.12
MnO	0.11	n.d.	0.05	0.09	0.10	0.10
MgO	15.74	n.d.	15.39	6.37	1.86	2.33
CaO	0.356	n.d.	0.03	2.694	0.829	0.501
Na2O	0.28	n.d.	0.05	2.28	1.72	0.54
K2O	2.33	n.d.	0.00	4.09	3.73	2.21
P2O5	0.07	n.d.	n.d.	n.d.	0.11	0.05
LOI (%)	0.82	n.d.	0.61	0.16	1.68	0.85
Sum (w. LOI)	99.69	n.d.	99.96	100.15	99.50	98.49
Mole %:						
Si	40.57	37.63	29.22	47.21	60.68	65.93
Ti	0.43	–	–	0.08	0.59	0.87
Al	27.56	25.81	45.07	26.65	22.02	19.45
Fe	6.54	7.53	5.30	5.92	5.20	5.87
Mn	0.08	0.08	0.08	0.07	0.08	0.08
Mg	21.23	24.73	20.21	8.66	2.67	3.42
Ca	0.34	0.54	–	2.63	0.86	0.53
Na	0.49	0.18	–	4.03	3.22	1.03
K	2.69	3.23	–	4.76	4.60	2.78
H	4.00	10.00	5.00	8.00	15.00	15.00
Excess Si	–	–	–	–	20.00	20.00

Notes:
Analysis type indicates whether the composition was obtained by XRF of whole-rock powders or by EPMA of microdomains.
*Whole-rock oxide data were not reported in the thesis of Schefer (2005).
LOI = loss on ignition
FeO_T = total iron reported as FeO
n.d. = not determined
Excess Si was added to the quartz-rich paragneiss samples to stabalize quartz in the phase diagrams

Table 5.3. LA-ICP-MS parameters for garnet trace element analyses.

Laboratory & Sample Preparation	
Laboratory name	The University of Kansas, Dept. of Geology, Isotope Geochemistry Lab
Sample type/mineral	Garnet
Sample preparation	40 µm-thick, polished sections
Imaging	BSE images and X-ray compositional maps
Laser ablation system	
Make, model & type	ATL ArF excimer laser (193 nm), Photon Machines Analyte G1
Ablation cell & volume	Frames Cell with teardrop-shaped insert
Laser wavelength	193 nm
Pulse width (ns)	5 ns
Fluence	3.2 J/cm^2
Repetition rate	10 Hz
Spot size (um)	35 µm circle
Sampling mode / pattern	Single spots
Carrier gas	He, 0.425 l/min, Ar, 1.24 l/min
Ablation duration	25 s
Cell carrier gas flow	He
ICP-MS Instrument	
Make, Model & type	Thermo Element2 magnetic sector field ICP-MS (single collector)
Sample introduction	Aerosol with sample + He was mixed with Ar using a Y-connector 15 cm upstream from torch.
RF power	1100 W
Make-up gas flow	Ar, 16 l/min
Sampling depth	20 µm
Detection system	Single detector (SEM), counting & analog modes
Elements/ isotopes analyzed	29Si, 43Ca, 44Ca, 45Sc, 49Ti, 89Y, 940Zr, 139La, 140Ce, 141Pr, 146Nd, 147Sm, 153Eu, 157Gd, 159Tb, 163Dy, 165Ho, 166Er, 169Tm, 172Yb, 175Lu
Integration time per peak (Sample Time in miliseconds)	29Si=10, 43Ca=10, 44Ca=10, 45Sc=10, 49Ti=10, 89Y=10, 94Zr=10, 139La=30, 140Ce=30, 141Pr=30, 146Nd=20, 147Sm=20, 153Eu=20, 157Gd=20, 159Tb=20, 163Dy=20, 165Ho=20, 166Er=10, 169Tm=10, 172Yb=10, 175Lu=10
Total integration time (Segment Duration in miliseconds)	29Si=10, 43Ca=10, 44Ca=10, 45Sc=10, 49Ti=10, 89Y=10, 94Zr=10, 139La=30, 140Ce=30, 141Pr=30, 146Nd=20, 147Sm=20, 153Eu=20, 157Gd=20, 159Tb=20, 163Dy=20, 165Ho=20, 166Er=10, 169Tm=10, 172Yb=10, 175Lu=10
Total method time	1 min 47 s (100 runs, 2 passes)

Table 5.3

Sensitvity (cps/ppm)	29Si=122, 43Ca=12, 44Ca=199, 45Sc=5868, 49Ti=447, 89Y=7822, 94Zr=3915, 139La=13000, 140Ce=16723, 141Pr=16659, 146Nd=2615, 147Sm=2153, 153Eu=8914, 157Gd=1791, 159Tb=11996, 163Dy=2985, 165Ho=11585, 166Er=3939, 169Tm=12062, 172Yb=2655, 175Lu=10073
ICP Dead time	22 ns
UO+/U+	0.02%
238U+/232Th+	~1.5
Data Processing	
Gas blank	18 s
Calibration strategy	Standard-sampling bracketing + internal standardization using Ca concentration measured by electron microprobe for each spot
Reference material info	GSD-1G (Guillong et al., 2005; Jochum et al., 2005)
Internal std for trace elements	44Ca
Data processing package used	IGOR PRO, Iolite 2.5 (Patton et al. 2011): Trace elements: TraceElmentsIS data reduction scheme
Common-Pb correction, composition and uncertainty	n/a
Uncertainty level & propagation	2SE internal uncertainty
Reproducibility	3-8%
Quality control / Validation	GSE-1G (Guillong et al., 2005; Jochum et al., 2005)